Targeting Bacterial and Fungal Pathogens through Novel Glycoconjugate-based Anti-Virulence Strategies

Kyle Doherty, B.Sc.

A thesis submitted to Maynooth University in fulfilment of the requirements for the degree of

Doctor of Philosophy

Department of Chemistry,

Maynooth University,

Maynooth,

Co. Kildare,

Ireland

October 2023

Head of Department: Prof A. Denise Rooney

Research Supervisor: Dr Trinidad Velasco-Torrijos

Table of Contents

Acknowledgements

There is a number of people who I owe special thanks to for their help and support over the last four years. Firstly, I would like to thank my supervisor Dr Trinidad Velasco-Torrijos for all her support, guidance and encouragement through these years. It has been a great experience and privilege working and learning from you. I can safely say our group trips to the coffee mill every so often has helped keep me somewhat sane!

I would like to thank Maynooth University for the award of a John and Pat Hume scholarship which allowed me to complete my PhD. I'd like to thank the rest of the academic staff at Maynooth university for their help at various stages throughout my four years. I'd like to thank Prof Kevin Kavanagh and the members of his group who carried out the biological testing in his lab as well as to Prof Fiona Walsh and Marwa Alawi for their work. Also, I would like to thank the technical and administrative staff in our department for their generosity and assistance whenever needed.

Thanks to the EU COST Action 18132 for funding two research trips to Tallinn, Estonia and secondly to Seville, Spain. Thank you to Dr Kaja Kasements in the National Institute of Chemical Physics and Biophysics, Tallinn and everyone else who helped me in the institute during my time there. I'd also like to thank Prof Carmen Ortiz Mellet in the University of Seville for hosting me in her lab, for the kindness and patience she and other members of her research group showed me in my time there.

Thank you to all the postgrads in the department, both past and present. Thanks to Harlei, Stephen, Amanda and Luke for helping me settle and get my bearings in the lab, with special thanks to Harlei for helping me so much during my first year. A special mention to Eoin, an avid German manga connoisseur and aggressive advocate for the teaching studentship, who started out with me. I think we were very much in the struggles together and made it eventually, only majorly scarred for life, I really appreciate the friendship and support. Best of luck for the future, may it be filled with many Yu-Gi-Oh cards and free style coke.

To all the lads in the TVT group- Darren, Alessio, Keela. Thanks to Darren for being an endless source of chemistry knowledge, craic and having more interest in my project

than I myself had at any stage. Cheers to Alessio for taking to our group so well, you didn't find it hard at all (that's what she said) and adding to the craic we had. Thanks to Keela for being the lab enforcer, keeping us all in line at times plus I won't mention the George Foreman incident. Thanks to Adam for lightening the mood in the lab and keeping us entertained with your singing and dancing and congratulations on the baby in advance (due in about 95 weeks from now). Best of luck to the new TVT group members, Oliwier, Shane and Rachel, I'm sure you will all do great. Best of luck to all the other members of the Synth Lab- Conor W, Conor G, Luke B, Stephen Healy, Farhad, Xuanyang, Sinead and Clara. As well as other members of the department, Colm, Caytlin, Keelan, Andrea, Emily, and Keane and anyone else I haven't mentioned.

Most importantly thank you to my family for their support, both during my undergraduate studies and during my PhD, I would not have achieved this without your support. Thank you to my Mum and Dad for supporting and allowing me to do whatever I wanted always. Thank you to Cora, the best driver of us three, and Jay 'the glue that holds the family together'- cheers bror. Thank you to the extended Doherty and Boyle families as well. I'd also like to mention and thank my Granny Pat and Granda Owenie and also Granny Breid and Lala, who I wish were here today.

Declaration

This thesis has been prepared in accordance with the PhD regulations of Maynooth University and is subject to copyright. For more information see PhD Regulations (December 2022).

Signed: _____ Date: _____

Kyle Doherty, B.Sc. (Hons)

Abstract

Numerous strategies have been developed to treat both bacterial and fungal infections. Of these strategies, the anti-adhesion strategy is of particular relevance to this work. Novel approaches to treat these infections are of particular importance due to the rapidly increasing prevalence of both bacterial and fungal resistant strains. Anti-virulence strategies are of interest due to an inherently lower selective pressure for resistant strains.

This thesis builds on previous work in our group and presents the synthesis of novel derivatives of lead compounds developed through a combination of synthetic carbohydrate chemistry and Copper-catalysed Azide-Alkyne Cycloaddition (CuAAC). Chapter 2 describes the study of the structural requirements for an interesting intramolecular cyclisation reaction in *cis*-Norbornene compounds: this reaction can lead to the development of potential pH-responsive compounds. Novel anti-adhesion compounds designed to combine anti-adhesion and anti-biofilm activity based on this scaffold are discussed. Chapter 3 describes the development of glycoconjugates with covalent crosslinking abilities in combination with inherent anti-adhesion activity for *C. albicans*, along with toxicity testing against several *Candida spp.* Chapter 4 describes a structure-activity-relationship (SAR) study of our lead compound, which included replacements with heterocycles, aromatic substituents and sp^2-glycomimetic analogues. Some of these derivatives exhibit comparable activity to this lead compound and open the door to the use of glycomimetics as anti-adhesion compounds in fungal infections. Additionally, a derivative of the lead compound was functionalized for resin modification and identification of the target lectin. This will ultimately allow for more efficient design of high affinity analogues. Chapter 5 describes the synthesis of a number of glycoconjugates exhibiting exciting dual anti-conjugation and anti-biofilm activities. These compounds are promising due to the key roles bacterial conjugation plays in the spread of AMR through horizontal gene transfer (HGT). Currently, preparation of fluorescently-labelled derivatives of these compounds is underway and it is hoped that this may help elucidate the mechanism of action of these compounds.

Abbreviations

[α] = Specific rotation [expressed without units, the units are (deg.mL)/(g.dm)]

Ac = Acetyl

ACN = Acetonitrile

Ac_2O = Acetic anhydride

ALS = agglutinin-like sequence

AMR = Antimicrobial resistance

Aq = Aqueous

Ar = Aromatic

Atm = Atmospheric pressure

ATR = Attenuated Total Reflection

Boc = t-butyloxycarbonyl

°C = Degrees Celsius

$CDCl_3$ = Deuterated chloroform

COSY = Correlation Spectroscopy

CuAAC = Copper(I) catalysed azide-alkyne cycloaddition

CRD = Carbohydrate recognition domain

DCM = Dichloromethane

DEPT = Distortionless enhancement by polarization transfer

DMF = Dimethylformamide

DMSO = Dimethylsulfoxide

Equiv. = Equivalents

ESI = Electrospray ionisation

EtOAc = Ethyl acetate

EtOH = Ethanol

Fuc = Fucose

Fig. = Figure

FITC = Fluorescein Isothiocyanate

Gal = Galactose

Glc = Glucose

GlcNAc = *N*-acetyl-glucosamine

h = Hours

HCl = Hydrochloric acid

HGT = Horizontal Gene Transfer

HMBC = Heteronuclear Multiple Bond Correlation

HPLC = High Performance Liquid Chromatography

HR-MS = High Resolution Mass Spectrometry

Hsp = Heat Shock Protein

HSQC = Heteronuclear Single Quantum Coherence

i.e. = Id est (Latin for 'that is')

IR = Infrared spectroscopy

ITC = Isothermal titration calorimetry

Lac = lactose

K = Kelvin

Man = mannose

mAbs = monoclonal antibodies

MeOD = Deuterated methanol

MeOH = Methanol

mg = Milligram

MIC = Minimal Inhibitory Concentration

mins = Minutes

mL = Millilitre

mm = Millimetre

Msg = Major Surface Glycoproteins

Mtb = *Mycobacterium tuberculosis*

µm = Micrometre

NEt_3 = Triethylamine

nm = Nanometre

NMR = Nuclear Magnetic Resonance

N,N-DIPEA = Diisopropylethylamine

OAc = Acetoxy group

OH = Hydroxy group

Pd/C = Palladium on activated carbon

Pet Ether = Petroleum ether

R_f = Retention Factor

ROS = Reactive oxygen species

RT = Room temperature

Rt = Retention Time

PAMP = Pathogen-associated molecular pattern

Pet Ether = Petroleum Ether

PRR = Pattern recognition receptor

SAR = Structure Activity Relationship

sat. = Saturated

sec = Seconds

spp. = species

SPR = Surface Plasmon Resonance

TBTU = O-(Benzotriazol-1-yl)-N,N,N’,N’-tetramethyluronium tetrafluoroborate

TFA = Trifluoroacetic acid

THF = Tetrahydrofuran

TLC = Thin Layer Chromatography

TLR = Toll-like receptor

Triaz = Triazole

Chapter 1

Introduction

1.1 Fungal infections

Fungal infections pose major public health concerns. It is estimated that there are in excess of 1.5 million fungal species, of which more than 600 species are capable of causing both simple and fatal infections in humans and animals [1,2]. It is estimated that between 1.5-2 million people die of fungal infections each year, which surpasses the amount of people killed by either malaria or tuberculosis [3].

In particular, incidences of some of these infections have increased in immunocompromised patients with other diseases such as COVID-19. Fungal pathogens utilise direct contact and inhalation as their primary routes of transmission. Damaged skin presents an ideal route for transmission via direct contact, while spores and/or conidia provide effective means for transmission in many pulmonary pathogens. In response to this, the host immune system employs pattern recognition receptors (PRR) and toll-like receptor (TLR) which recognise pathogen-associated molecular patterns (PAMP). Common fungal PAMPs include chitin and β-1,3-glucan [4]. Subsequent signal transduction pathways lead to an immune response involving a number of key processes such as phagocytosis, respiratory burst through reactive oxygen species (ROS), reactive nitrogen species (RNS), the production of cytokines and chemokines which result in a strong inflammatory response for neutralising the invading fungal pathogens. In response to these processes, fungal pathogens employ a number of pathways to evade and survive in the host environment.

A good example of this is *Pneumocystis*, which lacks chitin in its cell wall. In addition, *Pneumocystis* has also been found to mask β-1,3-glucan with major surface glycoproteins (Msg), this helps this pathogen to evade native host cell immune responses [5]. Melanin is a high molecular weight hydrophobic pigment, in *C. neoformans* the presence of melanin reduces its susceptibility to phagocytosis [6]. β-1,3-glucan recognition by Dectin-1 on macrophages and monocytes leads to cytokine production and phagocytosis. However, in *C. albicans* β-1,3-glucan is only recognised by Dectin-1 in the yeast form. Therefore, upon switching from yeast cell to filamentous form, *C. albicans* can shield this PAMP from Dectin-1, avoiding phagocytosis and ROS production [7].

In addition to evasion of the host immune response via cell surface shielding, some fungal pathogens have demonstrated the ability to transition between different forms in different environments. For example, *Candida* spp. are capable of growing in their yeast form and can then quickly switch to their filamentous hyphal form, which is better suited in disease progression due to increased tissue invasion abilities and reduced susceptibility to phagocytosis [8]. *C. neoformans* may form titan cells (**Fig. 1.1**), which are extremely large yeast cells- typically ranging from 14 to 20 times larger than normal yeast cell size. These titan cells have been shown to be part of a defensive mechanism in *C. neoformans* when challenged by macrophages [9].

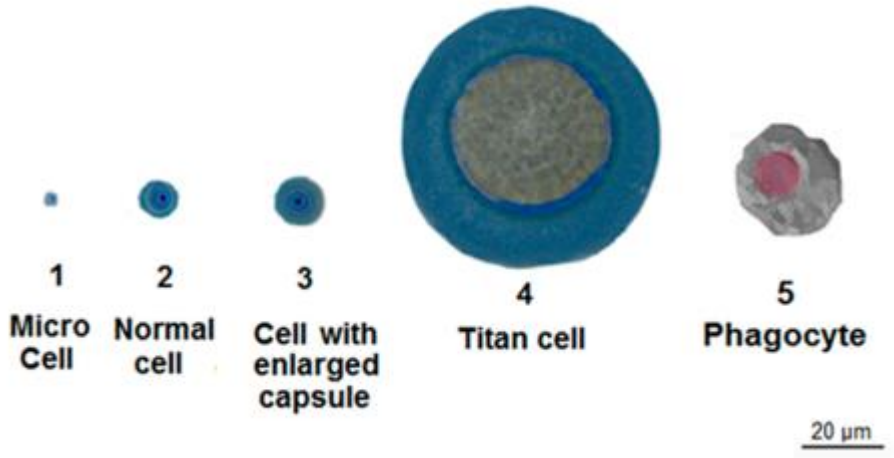

Figure 1.1: Size comparison of titan cells with other cell types [9].

In response to the production of antimicrobial peptides through the host humoral response, fungal pathogens have demonstrated the ability to secrete inactivating proteins. For example, *C. albicans* secretes aspartyl proteases Sap9 and Sap10 to cleave the antimicrobial peptide histatin 5, resulting in an inactivation of this peptide [10]. In addition, *C. albicans* can cleave the plasma membrane protein Msb2 to yield the Msb2 glycodomain which is secreted. The Msb2 glycodomain can bind to a number of antimicrobial peptides including LL-37, histatin 5, hNP-1 and hBD1, which inactivates these proteins [11,12].

Finally, biofilms are an important protective feature of fungal pathogens that have recently received more attention. These structures are heterogeneous three-dimensional matrices composed of microbes, extracellular polymeric molecules such

as polysaccharides and peptides, which aid in adherence to both biotic and abiotic surfaces. It is estimated that approximately 80% of microorganisms grow as biofilms as opposed to planktonic cells, due to the favourable protective and persistence properties conferred by biofilms in the hostile host environment [13,14]. Biofilms have been shown to confer protection against neutrophil attack due to the presence of β-glucans in the biofilm matrix and also do not induce reactive oxygen species (ROS) production [15]. In order to treat these biofilm-based infections combination therapies, involving the use of an anti-fungal compound and a non-anti-fungal compound known as a potentiator. These potentiators are used to enhance the efficacy of the anti-fungal compound in treating fungal biofilms [16]. An example of this type of treatment is the combination of Amphotericin (anti-fungal) and aspirin (potentiator). Zhou *et al.* found that this combination was capable of reducing the MIC of amphotericin B by up to 32-fold relative to a control, in the biofilm environment of *Candida* spp. This was attributed to aspirins ability to decrease biofilm formation in *Candida* and reduce the viability of biofilm cells at therapeutic concentrations [17].

1.1.1 Candida albicans

Though the genus *Candida* includes approximately 200 separate species, only a select number of these are opportunistic pathogens. *Candida albicans* is the most problematic and frequently encountered in a clinical setting [18]. Interestingly, *C. albicans* is a commensal component in humans and a normal component of the body's microbiota [19]. *C. albicans* and, to a lesser extent, other *Candida* species are present in the oral cavities of up to 75% of the population [20]. However, in the case of immunocompromised patients *C. albicans* can cause infections ranging from superficial to invasive infections. These fungal infections can be promoted by factors such as surgery, burns, stints in intensive care, diseases (such as cancer and HIV), previous treatment with antibiotics, chemotherapy and immunosuppression prior to organ transplantation [21].

C. albicans utilises a number of virulence factors to infect diverse host niches. These include polymorphism, adhesins, biofilm formation and secreted hydrolases. *C.*

albicans is a polymorphic fungus which is capable of growing as either an ovoid-shaped budding yeast, as ellipsoid cells with constrictions at the septa, known as pseudohyphae, or as true hyphae (**Fig. 1.2**) [22]. The transition between yeast and hyphal forms is called dimorphism and each form is important for different stages of the infection process. The yeast form is considered the primary form involved in dissemination, while the hyphal form is important for invasive processes [22,23]. Adhesins are also employed by *C. albicans* to mediate adherence to other microorganisms, abiotic surfaces and to host cells [24,25]. Adhesins are also a central focus in this thesis. As discussed in Chapter 3, Section 3.1.4, agglutinin-like sequence (ALS) are arguably the best studied class of adhesins in *C. albicans*. Interestingly, *C. albicans* is capable of invading host tissues via two mechanisms. These are induced endocytosis and active penetration [26,27]. Expression of specialised proteins by *C. albicans* on its cell surface called invasins mediate binding to different ligands on host cells. Such ligands include E-cadherin and N-cadherin; binding to these ligands leads to engulfment of the *C. albicans* cell into the host cell. Als3 and a heat shock protein 70 (Hsp70) family member, Ssa1, have been identified as invasins. Both Als3 and Ssa1 bind to E-cadherin and endocytosis is likely induced following this binding event [27,28]. Meanwhile, active penetration requires *C. albicans* hyphae. Secreted aspartic proteases (Saps) are believed to be important in the active penetration process [26,27]. Additionally, many adhesins in *C. albicans* are believed to be lectins, which bind to glycans on the surface of host cells [29]. Lectins have been proposed in *C. albicans* with specificities for fucose, *N*-acetyl-glucosamine (GlcNAc) and galactose [30,31].

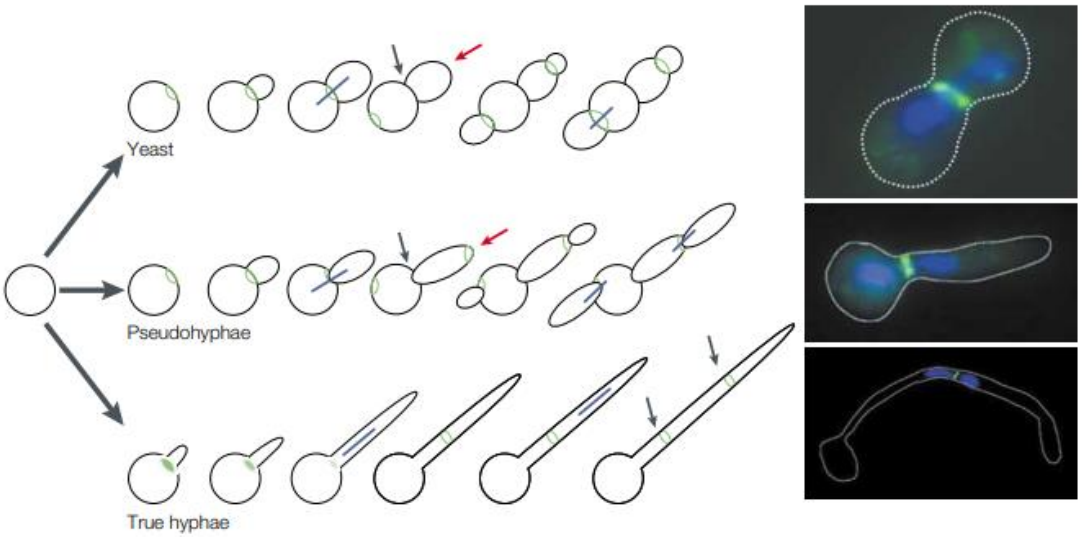

Figure 1.2: Yeast, Hyphal and True hyphal forms of *C. albicans* [22].

As mentioned earlier, biofilms are an important protective structure used by *C. albicans* to resist clearance by the host. Biofilms may be formed on both abiotic and biotic surfaces. Catheters and dentures (both abiotic) as well as mucosal cell surfaces are important sites for biofilm formation [32]. Mature biofilms are more resistant to antimicrobial agents and the host immune system in comparison to planktonic cells. Dispersion of yeast cells from biofilm structures has been attributed to enhanced virulence in mouse models [33]. Secreted hydrolases can be secreted following adhesion to host cell surfaces and hyphal growth and are thought to facilitate active penetration [34]. *C. albicans* is known to express three separate classes of secreted hydrolases which are proteases, phospholipases and lipases. Interestingly, there is a clear overexpression of Sap-encoding genes in *C. albicans* in comparison to other *Candida spp.*, this suggests that these proteases may have a role in virulence [34]. There are four classes of phospholipases (A, B, C and D) of which only five members of class B are extracellular and can contribute to pathogenicity through disruption of host cell membranes [35]. Finally, lipases are a family of secreted hydrolases consisting of 10 members (LIP1-10). A LIP8 mutant displayed reduced virulence in mouse models, indicating a role for this secreted hydrolase in *C. albicans* virulence [36].

1.2 Bacterial infections

Bacterial infections are another important and challenging threat to public health. Like fungal infections, this challenge is exacerbated by the increasing prevalence of antimicrobial resistance (AMR). According to the Lancet, in 2019 there were an estimated 4.95 million deaths associated with AMR, highlighting the danger of AMR which is becoming more widespread [37]. The six leading pathogens for deaths associated with AMR were *E. coli*, *S. aureus*, *K. pneumoniae*, *S. pneumoniae*, *A. baumannii* and *P. aeruginosa*. Similar to fungal virulence responses discussed above, bacteria possess a vast array of virulence factors used to persist and infect host tissues. These include strategies to evade host immune system and apoptosis regulation [38,39]. Another effective virulence factor used by many bacteria such as *P. aeruginosa* is quorum sensing. Quorum sensing allows for the coordinated expression of virulence genes in a population of pathogenic cells. Once the concentration of secreted acyl homoserine lactones (a quorum sensing molecule) reaches a certain level they enter the cytosol of these bacteria, binding to and subsequently activating transcriptional factor. This leads to the expression of key virulence genes that facilitate the persistence of *P. aeruginosa* [40].

Another key feature found in bacteria that is also found in fungal pathogens is biofilms [41]. Bacterial biofilms are particularly problematic in cases where they are adhered to catheters and/or implants in patients [42]. Persister cells are an important component in bacterial biofilms as they are resistant to many antibiotics and are also non-dividing. Persister cells also express toxin-antitoxin systems in which toxin modules block antibiotic targets [43]. Biofilm formation can be induced by quorum sensing (as mentioned above) and other molecules such as antibiotics and pigments [44]. Interestingly, at subinhibitory concentrations, antibiotics can induce alterations in gene expression. For example, subinhibitory concentrations of imipenem (antibiotic) in *P. aeruginosa* lead to increased expression of alginate which is a polysaccharide [45]. This leads to thicker biofilms, which require higher concentrations of antibiotics to be effective. A similar effect was observed when subinhibitory concentrations of tobramycin, an aminoglycoside antibiotic, were administered to treat *P. aeruginosa* and *E. coli* [46]. Work is ongoing to develop

effective treatments of bacterial biofilms. Organic acids, such as acetic acid, have been assessed as potential treatments for biofilms. Acetic acid has been found to both inhibit biofilm formation and eradicate mature biofilms [47]. Photo irradiation with blue light has also been studied as a means to treat wound infections, within which biofilms allow bacterial species to proliferate and cause further infection. Blue light irradiation has been shown to be effective against a number of problematic pathogens in their biofilm forms [48]. Blue light offers particular advantages as it promises to be relatively cheap and non-toxic treatment in comparison to Ultraviolet light. Ultraviolet light has mutagenic properties in humans, rendering it unsuitable for clinical use, however blue light lacks these properties [49].

1.2.1 Escherichia coli

Escherichia coli (*E. coli)* is a rod-shaped, gram-negative bacteria that is commensal and is found in the gastrointestinal tract in humans. However, in cases of immunocompromised patients and/or patients with breached gastrointestinal barriers it may cause infection [50]. Key virulence factors employed by *E. coli* include adhesins, toxins, iron acquisition factors and invasins [51]. In *E. coli*, adhesins typically form structures called fimbriae, also called pili, or fibrillae. Fimbriae are rod-like structures with diameters of 5-10 nm while fibrillae have diameters of 2-4 nm [52]. FimH is an important adhesin of uropathogenic *E. coli*, which binds to uroplakin 1A receptor on bladder epithelial cells, leading to invasion and formation of biofilm-like structures [53]. As discussed in Chapter 5, *E. coli* also utilises a number of toxin to enhance its virulence, including Shiga toxin 1 and 2 [54].

Resistance to the current crop of antibiotic drugs make treating *E. coli* infections especially challenging. *E. coli* is intrinsically resistant to therapeutic levels of penicillin G, which was the first β-lactam antibiotic used in clinical practice. This is due to its outer membrane, which confers resistance. Some strains of *E. coli* have also been observed to be resistant to a number of more recently developed classes of antibiotics [55,56]. As discussed in Chapter 5, β-lactamases are enzymes which cleave β-lactam and are the most important mediator of resistance to a range of β-lactam antibiotics in *E. coli*. β-lactamases are often encoded on plasmids, which allow for the

sharing of the required genetic information leading to widespread antibiotic resistance [57].

1.3 Anti-virulence strategies in different pathogens

Owing to the recent surge in resistant bacterial and fungal pathogens, there has been a renewed drive to identify novel strategies to treat the infections they cause. In particular, strategies/treatments that do not act by altering viability/killing the pathogen have received increased focus due to their presumed inherent lower risk of selecting for resistant strains. In addition, such anti-virulence drugs/treatments have the potential to be used in combination with existing antimicrobials, thus extending the life of these antimicrobials [58]. Many anti-virulence strategies have emerged in recent times including targeting toxins secreted by pathogens, adhesion inhibitors, inhibitors of bacterial secretory systems, inhibitors of virulence gene expression and inhibitors of cell-to-cell signalling [59].

Some of the earliest examples of targeting virulence traits in pathogens include targeting diphtheria toxin and tetanus toxin. These treatments involve the use of equine diphtheria antitoxin to combat diphtheria infections and human tetanus immunoglobulin to treat tetanus infections [60]. *C. difficile* is a gram-positive pathogen that produces toxins leading to diarrhoea and colitis. Though antibiotic resistance has not yet been observed for this pathogen, clearance of other illnesses via antibiotic use commonly leads to *C. difficile* infections which are recurrent and often difficult to treat. *C. difficile* produces two exotoxins, TcdA and TcdB, which have received much attention as potential anti-virulence targets to treat subsequent infections. Merck assessed two monoclonal antibodies (mAbs), actoxumab and bezlotoxumab, which can target TcdA and TcdB respectively. Eventually bezlotoxumab was found to be effective and was approved by the FDA to reduce *C. difficle* infection recurrence. This represents the first case of an FDA approved anti-virulence agent [61].

SortaseA is a membrane-localised enzyme that has recently been identified as an important virulence factor in a number of gram-negative pathogens, SortaseA is important for the assembly and anchoring of cell surface adhesins to the cell wall envelope. Interestingly, due to its ease of accessibility (position of cell membrane),

lack of homologous analogues in eukaryotes and that it is not essential for gram-positive bacterial growth, SortaseA constitutes a promising anti-virulence target [62,63]. A number of synthetic small molecule inhibitors of SortaseA have been described. In particular compounds **1.1** and **1.2** (**Fig. 1.3**) were found to inhibit SortaseA with IC_{50} values of 0.3 µM and 0.2 µM respectively against SortaseA isolated from *S. aureus*. These compounds were also found not to inhibit bacterial growth, which is important to limit selective pressure for resistant mutants [64].

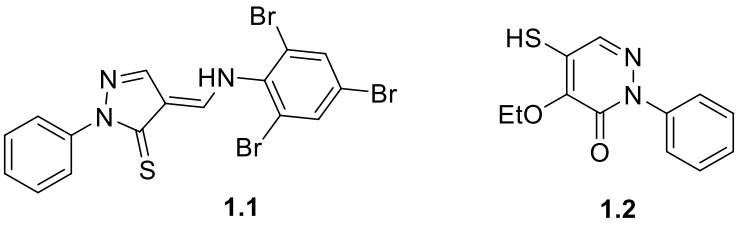

1.1 **1.2**

Figure 1.3: Structures of SortaseA inhibitors **1.1** and **1.2** [64].

1.4 'Click'/CuAAC chemistry in glycoconjugate synthesis and its medicinal applications

An important methodology commonly used to develop many novel anti-virulence compounds is 'Click'/CuAAC chemistry. Surprisingly, the application of the 'click reaction' or Cu(I)-catalyzed azide-alkyne 1,3-dipolar cycloaddition (CuAAC) in chemistry did not gain significant attention until the 1960s, despite its discovery at the start of the 20th century [65]. Sharpless defined a 'click' reaction as being modular and broad in scope, affording high to excellent yields with by-products that can be removed by non-chromatographic methods, and it must stereospecific though not necessarily enantioselective. CuAAC reactions involve organic azides and terminal alkynes in a regioselective reaction to yield the corresponding 1,4-disubstituted 1,2,3-triazoles (**Fig. 1.4**) [66]. Additionally, readily available starting materials and reagents, simple reaction conditions, the use of no solvent or a solvent that is easily removed and simple product isolation are required reaction characteristics [67]. Extensive use of this reaction has been employed in medicinal chemistry due to its compatibility with a range of functional groups, gentle reaction conditions, wide pH tolerance and compatibility with a variety of solvents to yield many biologically active molecules [68]. The triazolyl ring formed displays strong hydrolytic stability.

Additionally, triazoles are recognized as an isostere of amides, an important functional group in many biologically active molecules.

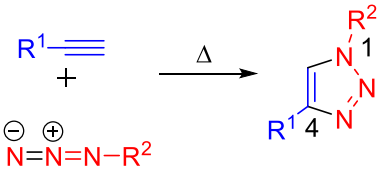

Figure 1.4: General synthesis of 1,4-disubstituted triazole using a terminal alkyne and an azide.

Carbohydrates and their mimetics are easily amenable to CuAAC reactions; the sugar moiety can be modified to contain the required alkyne or azide functionality through simple synthetic protocols. Through reaction of the sugar-azide/alkyne with the corresponding alkyne/azide, diverse mono- and multivalent presentations of carbohydrate containing a triazolyl ring have been reported; the triazole typically serves as (part of) a linker connecting the carbohydrate moiety to a scaffold or another biomolecule. In this way, many different scaffolds and biomolecules have been conjugated to carbohydrates through CuAAC chemistry to yield diverse glycoconjugates. These include glycoproteins, neoglycoconjugates, glycopolymers, glycoclusters, glycolipid conjugates macrocyclic glycoconjugates, calixarene glycoconjugates and oligonucleotides [65].

Carbohydrates have many important roles in biological systems beyond serving as an energy source, structural components of cell walls, or post-translational modifications of proteins. Of particular interest in the field of medicinal chemistry are carbohydrate recognition proteins (CRPs), also known as lectins, which interact with glycans on cell surfaces. This interaction is key to many biological events, such as adhesion of white blood cells to sites of infection or tissue damage, sperm-egg interactions during mammalian differentiation and the control of cell fate during differentiation [69]. Microbial pathogens commonly express CRPs that interact with glycan on host cell surfaces leading to inflammation, bacterial adhesion or viral invasion [70]. Due to the ubiquitous nature of carbohydrates in biological systems and the diverse, yet important roles they carry out, they represent viable targets for the treatment of disease, disease diagnosis and other biomedical applications. This section highlights the applications of a sub-category of triazole glycoconjugates,

anomeric triazole glycoconjugates, which contain a triazolyl ring linked to the anomeric carbon of the sugar moiety. These types of compounds are of particular interest as they can display higher stability to hydrolytic glycosidases.

1.4.1 Anti-bacterial and anti-fungal activity of triazolyl glycoconjugates

Many examples of anomeric triazolyl glycoconjugates evaluated as anti-infection agents in a wide range of diseases have been reported. For example, tuberculosis (TB), thought to have been mostly defeated as a disease in the last century, has reappeared in some parts of the world and has become one of the leading causes of death. In sub-Saharan Africa, where increased susceptibility to TB commonly arises from HIV infection, problems arise due to the incompatibility of antiviral and antitubercular drugs. Mycobacterium tuberculosis (Mtb), the etiological agent of TB, invades and colonizes macrophage cells. Its ability to survive within this inhospitable environment has been attributed to its robust cell wall. As such, an ideal target for novel TB drugs would be the biosynthesis of the mycobacterial cell envelope. Lo Conte *et al.* described the synthesis and biological evaluation of potential mycobacterial α-1,6-mannosyltransferases (α-(1,6)-ManT) inhibitors. The α-1,6-linked mannnoside core is commonly found in many cell wall components and thus compounds containing this core can potentially act as α-1,6-mannosyltransferases (α-(1,6)-ManT) inhibitors. The authors assayed the synthesised glycoconjugates against polyprenolphosphomannose (PPM)-dependent α-1,6-mannosyltransferases from membrane extracts of *Mycobacterium smegmatis*. All of the compounds developed (**Fig. 1.5**, **1.3**-**1.8**) displayed significant inhibition of the enzyme. Compounds **1.5** and **1.6** showed the highest activity, displaying approximately 95% inhibition. IC_{50} values were calculated for compounds **1.5** and **1.6** equal to 0.14 mM and 0.22 mM respectively [71].

Methicillin-resistant *Staphlococus aureus* (MRSA) accounts for 60-70% of *S. aureus* infections in hospitals and also causes the highest number of invasive infections amongst antibiotic-resistant bacteria. β-Lactam antibiotics are the most commonly used drugs in the treatment of bacterial infections. However, MRSA has developed several resistance mechanisms against such drugs. The main one involves

overexpression of penicillin binding protein 2a (PBP2a), since β-lactam antibiotics mainly associate with penicillin binding proteins leading to inhibition of cell wall biosynthesis. This ultimately leads to the renewal of bacterial cell wall biosynthesis and the effective inactivation of the corresponding β-lactam antibiotic(s). Hu *et al.* showed that a series of glycolipid derivatives (**Fig. 1.5**) can increase the susceptibility of MRSA to β-lactam antibiotics. The group found that these glycolipids could lower the minimum inhibitory concentration (MIC) of a number of conventional β-lactams. Alone, the glycolipids displayed only weak antimicrobial effects with an MIC of approx. 256 μg/mL against a MRSA strain. However, when tested in combination with oxacillin (β-lactam antibiotic), a synergistic effect was observed. Compound **1.9 (Fig. 1.5**) performed best, with a 128-256-fold reduction in the MIC of oxacillin. Compounds **1.10** and **1.11** (**Fig. 1.5**) displayed 64-fold reductions in the MIC of oxacillin. It was suggested by the group that each glycolipid forms micelles that increase internalization of the drug, as a result of the antibiotic being encapsulated. Compound **1.9** lowered the MIC of all 17 antibiotics tested in combination with **1.9** against an MRSA strain. Interestingly, using quantitative real-time PCR, it was determined that oxacillin, in combination with **58**, lowered the level of expression of the gene encoding PBP2a relative to oxacillin alone [72].

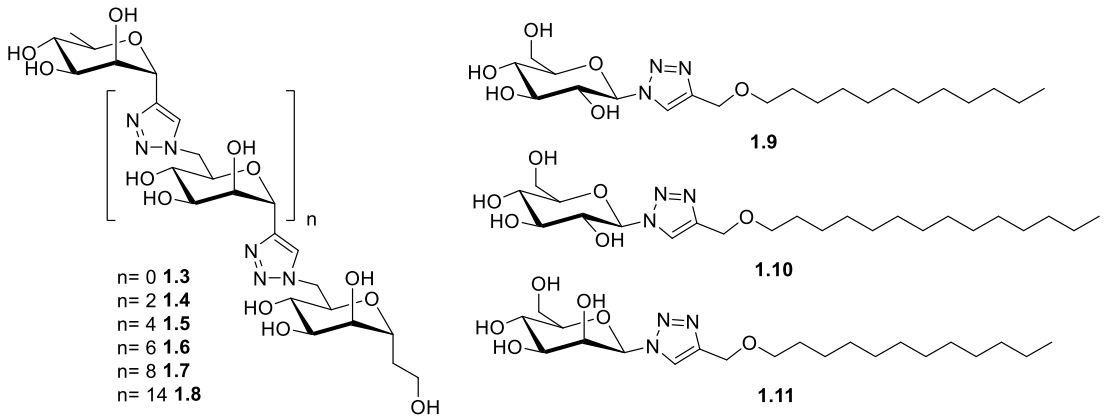

Figure 1.5: Structures of glycoconjugates **1.3**-**1.11** [71,72].

Many glycoconjugates have been reported with the ability to inhibit pathogen adhesion to host cells. This strategy poses an attractive advantage in that it does not apply as severe a selective pressure as conventional antibiotics. Hence, development

of resistance to these molecules should occur at a much slower pace than has occurred for antibiotics.

As mentioned earlier, *E. coli* is associated with a number of infectious diseases, such as urinary tract infections (UTIs), which affect millions of people each year. The most common adhesin expressed by uropathogenic *E. coli* is the lectin FimH which binds mannosides. Hence, Gouin and coworkers synthesised multiheptyl mannosides using CuAAC chemistry. In an inhibition of hemagglutination assay, heptyl mannoside (HepMan) was used as a positive control. It is well known that HepMan binds FimH with an affinity 650-fold better than mannose. In this assay compound **1.12** (**Fig. 1.6**) was found to inhibit FimH with the same potency as HepMan. However, in a bladder binding assay, compound **1.12** displayed an inhibition efficiency 13-fold better than HepMan [73].

Morsy and coworkers described the one-pot synthesis and biological evaluation of a number of 1,2,3-triazole nucleosides. Compounds **1.13**-**1.15** (**Fig. 1.6**) were tested in vitro against gram-positive bacteria (*Staphylococcus aureus* and *Micrococci luteus*), gram-negative bacteria (*Pseudomonas aeruginosa* and *Escherichia coli*) and fungi (*Candida albicans* and *Aspergillus niger*) using the agar diffusion method. These compounds produced zones of inhibition with diameters ranging from 21-35 and 29-34 mm against the assessed bacteria and fungi, respectively [74].

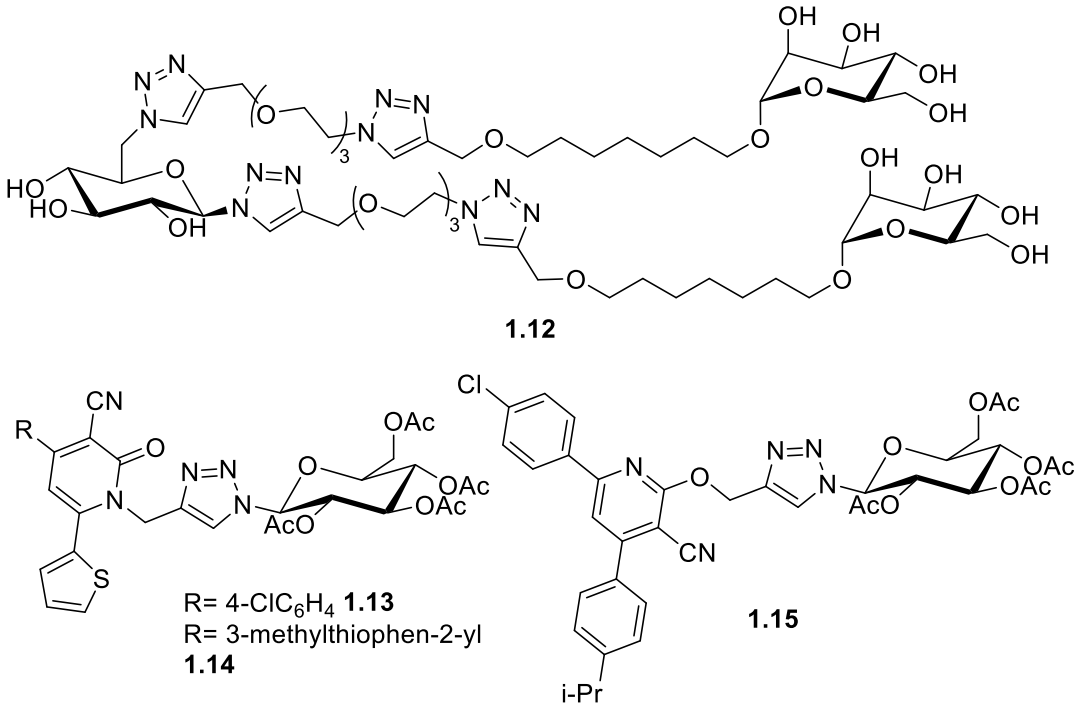

Figure 1.6: Structures of glycoconjugates **1.12**-**1.15** [73,74].

Chromene-containing compounds have been shown to display a wide range of biological activities such as anti-cancer, anti-microbial, anti-proliferative etc. Thanh *et al.* reported the synthesis and evaluation of a large library of chromene-containing glycoconjugates **1.16**-**1.31** (**Fig. 1.7**) against a range of bacterial and fungal species. Some of these glycoconjugates showed good activity against gram-positive and negative bacteria (**Table 1.1**). Next the group assessed the glycoconjugates activity against a number of fungi (**Table 1.2**). Thus, the library of compounds appeared to be more active against gram-negative than gram-positive bacteria (**Table 1.1**). This work provides further evidence of the advantages of the strategy involving conjugation of a carbohydrate moiety to a known active compound to improve its pharmacokinetic and/or pharmacodynamic properties [75].

Compound	Micro-organisms (Bacteria) MIC (µM)									
	Gram-positive			***Gram-negative***				***MRSA***		
	B.s	***S.a***	***S.e***	***E.c***	***K.p***	***P.a***	***S.t***	***MRSA198-1***	***MRSA198-2***	***MRSA198-3***
1.16	3.12								1.56	3.12
1.17	6.25	1.56						3.12		1.56
1.18	1.56		3.12	1.56						
1.19		3.12						1.56		3.12
1.20		1.56						1.56	1.56	
1.21			6.25							
1.22			1.56							
1.23			3.12							
1.24				1.56						
1.25					1.56					
1.26						1.56				
1.27							1.56			
1.28									1.56	1.56

B.s.: Bacillus subtilis; S.a.: Staphylococcus aureus; S.e.: Staphylococcus epidermidis; E.c.: Escherchia coli; K.p.: Klebsiella pneumoniae: P.a.: Pseudomonas aeruginosa: S.t.: Salmonella typhimurium.

Table 1.1: Notable observed MIC values for different Bacterial species [75].

Fungi				
Compound	**Micro-organisms (Fungi) MIC (µM)**			
	A.n	***A.f***	***C.a***	***S.c***
1.21	1.56			
1.24				1.56
1.27			1.56	
1.29				1.56
1.30		1.56		
1.31		1.56		

A.n.: Aspergillus niger; A.f.: Aspergillus niger; C.a.: Candida albicans; S.c.: Saccharomyces cerevisiae.

Table 1.2: Notable observed MIC values for different Fungal species [75].

Numerous nucleoside analogues have been extensively studied, showing a variety of anti-infection activities. Commercial drugs such as 5-fluorouracil and zidovudine are examples of uridine nucleoside drugs. Tachallait *et al.* reported the synthesis of a series of uridine nucleoside analogues and assessed the resulting biological activities against *S. aureus*, *L. monocytogenes*, *P. aeruginosa* and *E. coli*. The authors identified compound **1.32** (**Fig. 1.7**) as a potent inhibitor of *S. aureus* with a MIC = 6 µM. This compound also inhibited *L. monocytogenes* and *E. coli* (MIC = 23 µM for both). The group then studied bacterial growth kinetics using *S. aureus*. **1.32** was shown to have bactericidal activity, inducing nucleic acid leakage and significant membrane damage [76].

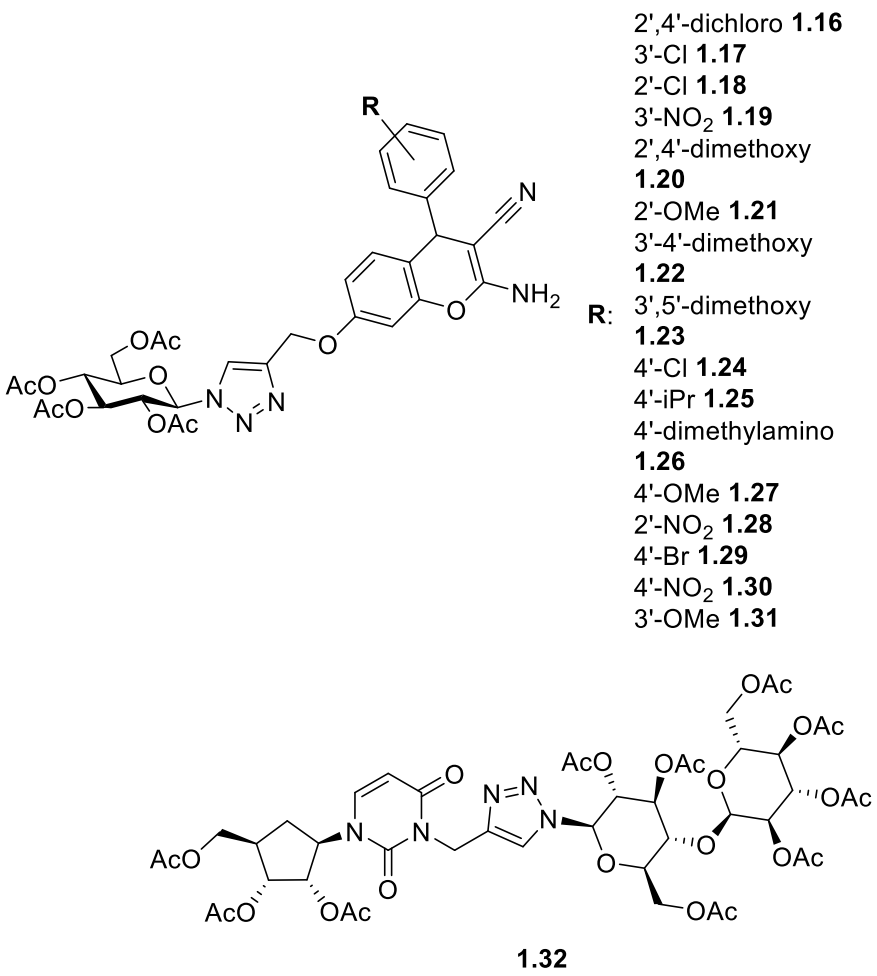

Figure 1.7: Structures of glycoconjugates **1.16**-**1.32** [75,76].

Mohammed *et al.* described the synthesis and evaluation of the anti-bacterial activity of glucose-based glycoconjugates, both protected and deprotected (**Fig. 1.8**), against *E. coli* and *S. aureus*. Compounds **1.33**, **1.34**, **1.35** and **1.36** were found to have lower activity than the antibiotic Kanamycin [77]. Ay *et al.* reported the synthesis and evaluation of a library of sulfanilamide glycoconjugates (**Fig. 1.8**) as potential novel anti-microbial agents. Of note, compounds **1.37** and **1.38** both produced MIC values of 0.08 mg/mL against *E. coli* [78].

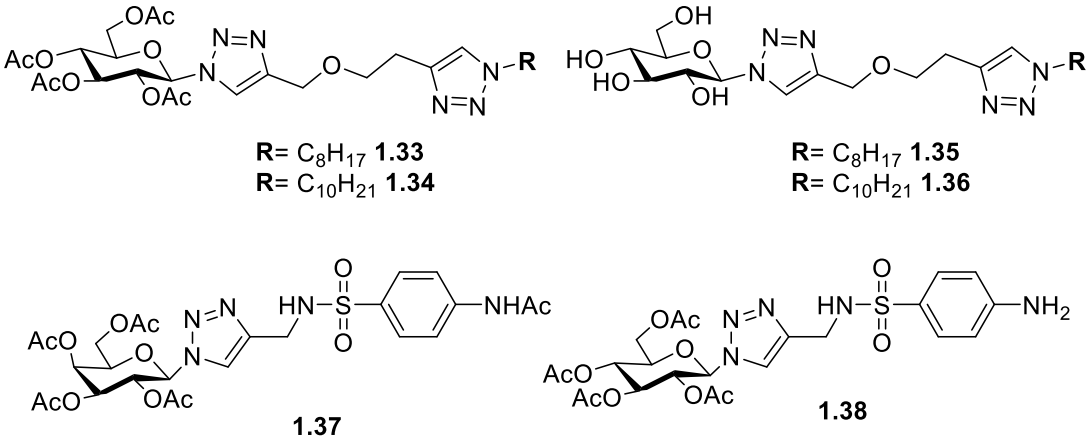

Figure 1.8: Structures of glycoconjugates **1.33**-**1.38** [77,78].

As discussed earlier, a key component to *C. albicans*' pathogenicity is its ability to adhere to a range of structures on the host cells surface such as proteins, glycans etc, as well as abiotic surfaces. Early studies on *C. albicans* suggest that host cell surface glycans play an important role in the adherence step of *C. albicans* to host tissues [79]. Previous work in our laboratory carried out by Martin *et al.* involved the synthesis of a series of aromatic-core glycoconjugates (AGC) and evaluation of their ability to inhibit the adherence of *C. albicans* to buccal epithelial cells (BECs). These compounds were evaluated in an exclusion assay, by incubating them with *C. albicans* and then exposing these yeast cells to BECs. Compound **1.39** (**Fig. 1.9**) was identified as the most potent inhibitor of *C. albicans* adhesion to BECs, with up to 80% decrease in adherence. Interestingly, in a displacement assay, which involved pre-incubation of *C. albicans* with BECs followed by incubation with **1.39**, compound **1.39** displaced up to 56% of *C. albicans* cells already adhered to BECs. Finally, the authors synthesised a fluorescently labelled derivative of **1.40**, compound **1.40** (**Fig. 1.9**) which showed a strong localized fluorescence at the yeast cell wall. This suggests that compound **1.39** appears to interact with a structural component of the cell surface of *C. albicans,* though the identity of the fungal adhesin involved in this interaction has yet to be determined. This work provides a good example of the utility of CuAAC chemistry for the synthesis of large libraries of glycoconjugates. In addition, the triazole ring at the anomeric position does not appear to adversely affect the binding of the glycoconjugate to the fungal adhesin [80].

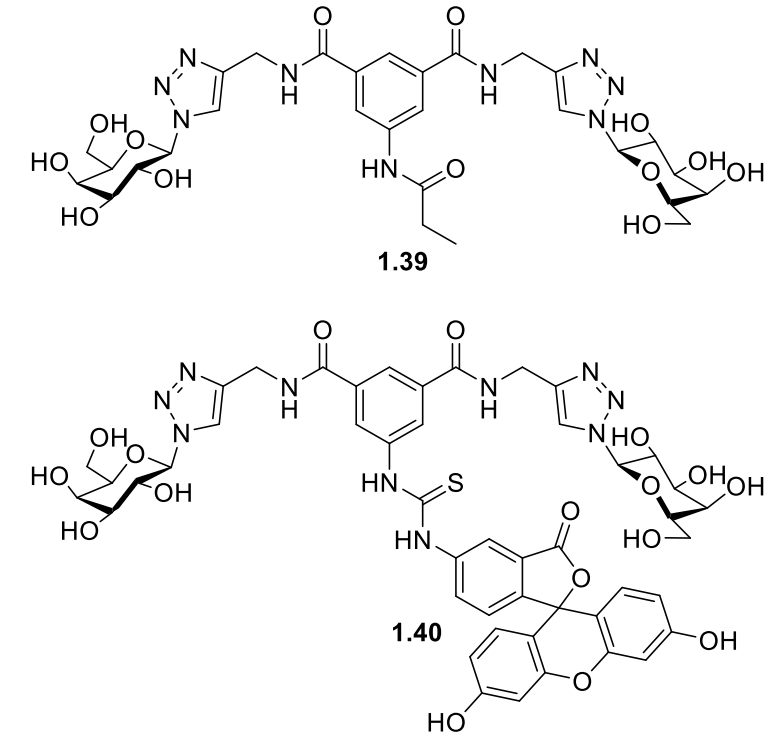

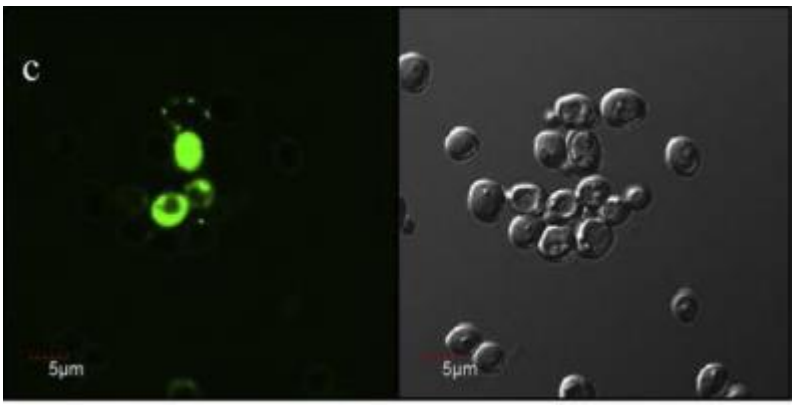

Figure 1.9: Structures of glycoconjugate **1.39**, fluorescently labelled derivative **1.40** and confocal image of **1.40** interacting with the cell surface of *C. albicans* [80].

1.4.2 Lectin ligand mimetics

When detailed structural information of the lectins involved in pathogen adhesion is available (though homology modelling or crystallography structures), it is possible to design high affinity ligands as inhibitors of adhesion. LecA is a virulence factor of the pathogen *Pseudomonas auruginosa* and is involved in bacterial adhesion and biofilm formation. This lectin is a tetramer, with 26 Å distance between neighbouring binding sites specific for galactose. Building on previous work, Pertici *et al.* synthesised and evaluated divalent galactosides containing rigid glucose-triazole spacers as LecA

inhibitors. Compounds **1.41, 1.42** and **1.43** (**Fig. 1.10**) displayed IC_{50} values of 160, 120 and 2.7 nM respectively. Using isothermal calorimetry (ITC), compound **1.43** was found to have a remarkable K_d value of 28 nM for LecA. Compounds **1.42** and **1.43** had approximately the same enthalpy change (Δ*H)*, whereas compound **1.43** showed a smaller change in entropy (Δ*S*) compared to compound **1.42** as it was less flexible [81,82]. Building on this work, the group prepared a series of derivatives of **1.43**, in order to ascertain which parts of the spacer units may be playing a role in the binding of the ligand **1.43** to LecA. Compounds **1.44** and **1.45** (**Fig. 1.10**) had improved binding for LecA, with K_d values of 12 and 13 nM, respectively. Replacement of the central glucose unit by a phenyl group (compound **1.44**) or an unconstrained central butyl unit (compound **1.45**) accounted for this enhanced affinity [83].

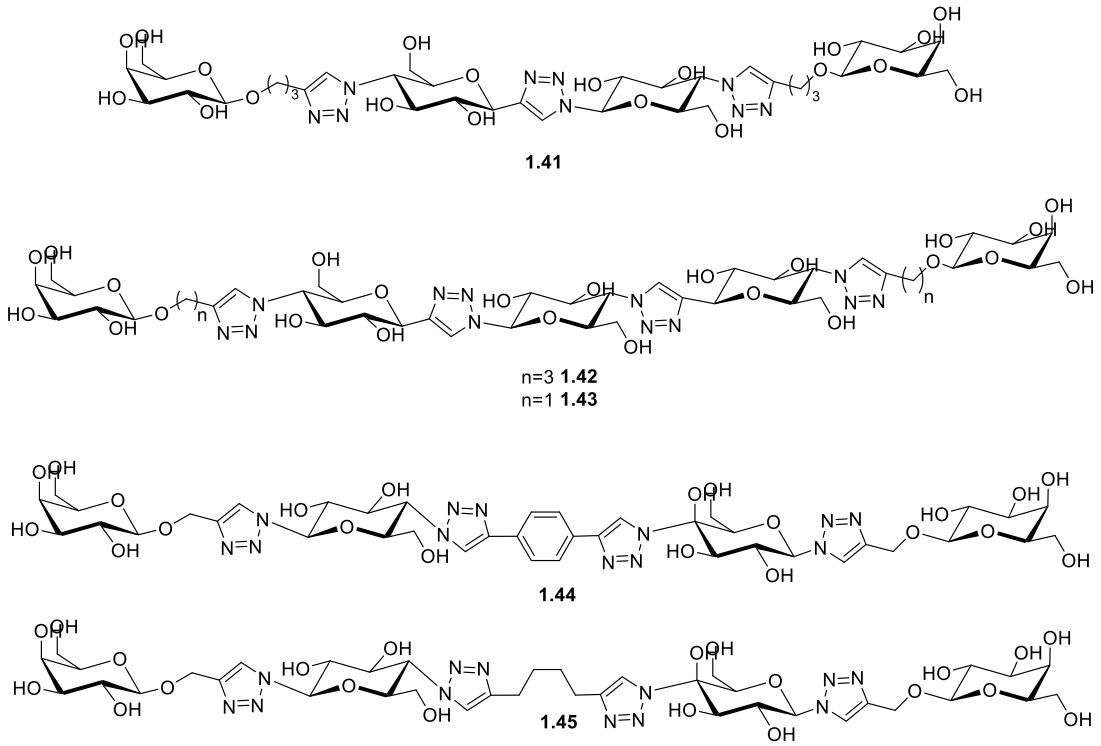

Figure 1.10: Structures of glycoconjugates **1.41**-**1.45** [81-83].

Galectins are β-D-galactoside binding lectins which show variation of expression during development, differentiation stages and under physiological/pathological conditions. For example, Galectin-3 (Gal-3) has been implicated in colon cancer, brain tumour progression and inhibition of metastasis-associated cancer cell adhesion. As such potential ligands that could modulate the activity and pathways associated with this important lectin could prove to be of substantial therapeutic importance.

Freichel *et al.* reported the synthesis and evaluation of a series of glycomacromolecules as potential ligands for Galectin-3. In an inhibition competition assay to assess the binding to galectin-3, compounds **1.46** and **1.47** (**Fig. 1.11**) had IC_{50} values of 29 and 16 µM, respectively. Interestingly, compound **1.46**, the smallest of the trivalent ligands, had the lowest IC_{50} value of this series of ligands. They hypothesised that this was, part at least, due to **1.46** achieving the correct distances/geometry to allow protein aggregation. Also, the group believed that the triazole ring in the linker may interact with the binding groove of Gal-3 via hydrophobic interactions. The authors noted work by Nilsson and coworkers, which found that the replacement of ester or amide bonds with triazole moieties impacted the affinity and specificity for Gal-3 ligands [84].

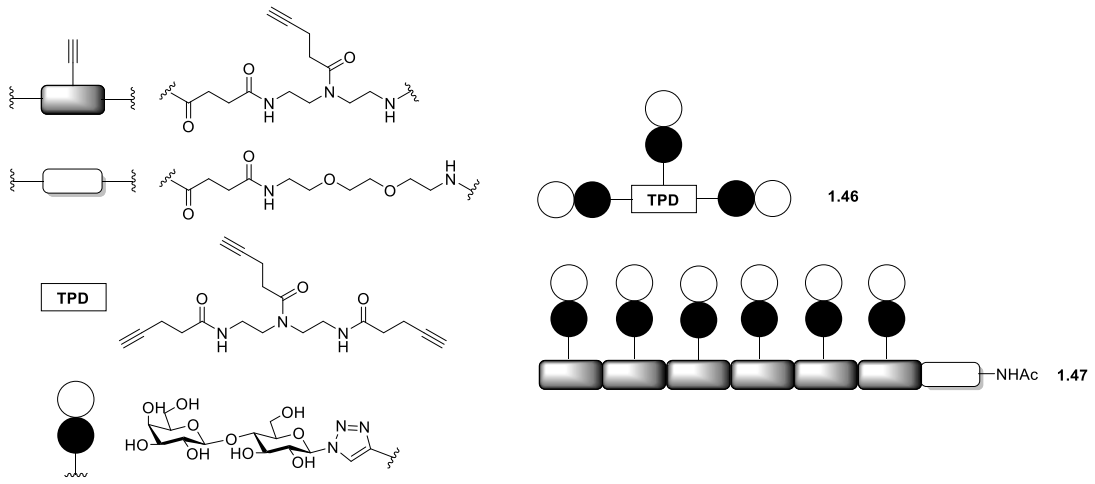

Figure 1.11: Structures of glycoconjugates **1.46** and **1.47** [84].

1.4.3 Triazolyl glycocopolymers

Nagao *et al.* reported the synthesis of a series of glucose glycopolymers via reversible addition fragmentation chain transfer (RAFT) polymerization. (**Fig. 1.12**) Plant lectin ConA contains four carbohydrate-binding domains, each with specificity for α-mannose and α-glucose. The evaluation of the binding of glycopolymers **1.48** and **1.49** to ConA, produced K_a values of 7.35×10^4 and 7.46×10^4 M^{-1}, respectively, in a fluorescence quenching assay. Glycopolymer **1.48** and **1.49** had similar hydrodynamic diameters (6.57 and 6.36 nm, respectively) matching the distance between two carbohydrate-binding domains in ConA, which suggests these glycocopolymers interact with this lectin in a two-site binding mode. This work

provides a good example of how carbohydrate moieties presented at the right geometry/ distances in a multivalent presentation can lead to significant interaction with a target lectin [85]. Similar work carried out by Otsubo *et al.* identified cellobiose derivative glycopolymer **1.50** (**Fig. 1.12**), with improved affinity for ConA ($K_a = 3.9x10^5$ M^{-1}) [86].

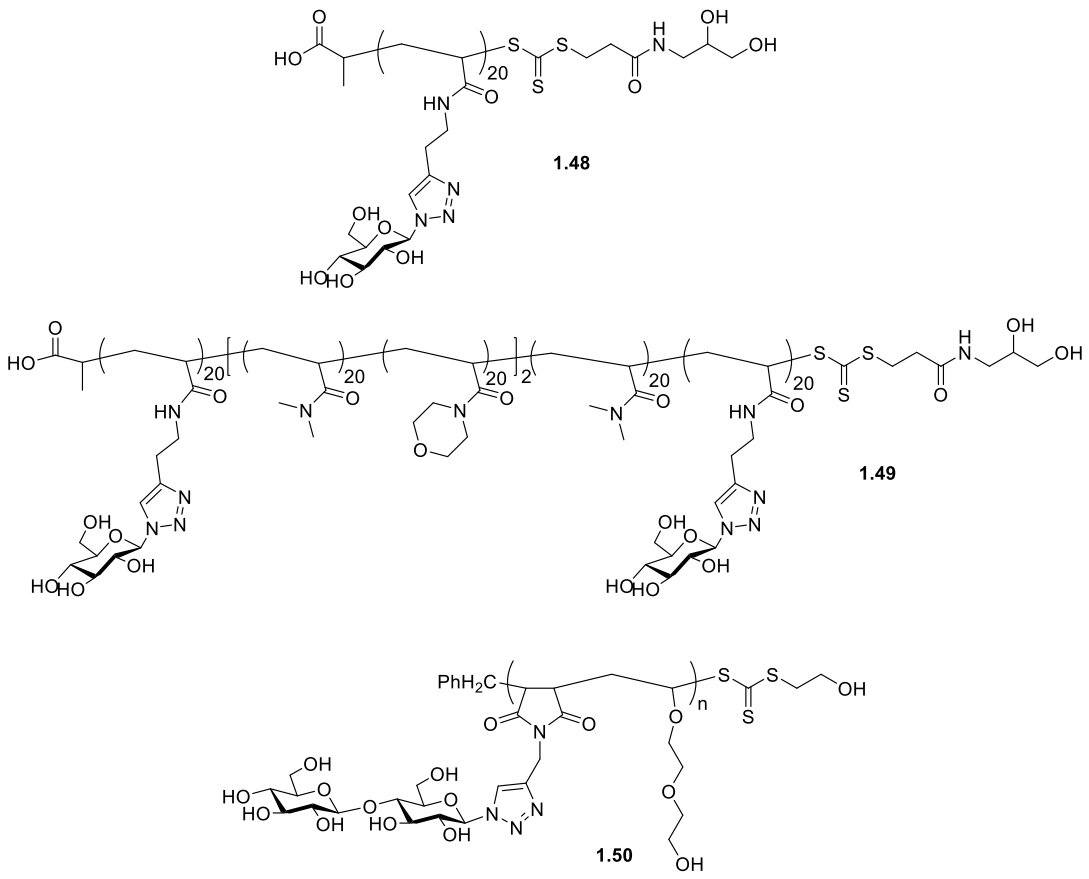

Figure 1.12: Structures of glycoconjugates **1.48**-**1.50** [85,86].

Liu *et al* have recently described the synthesis and evaluation of several heterogeneous glycopolymers; this class of glycopolymers has been reported sparingly in literature in comparison to homogeneous glycopolymers due to synthetic difficulties associated with their preparation. These glycopolymers were then assessed for binding to Con A using (ITC) in comparison to homoglycopolymers counterparts. The glycopolymers **1.51**, **1.52**, **1.53** and **1.54** displayed K_a values of 6.41, 2.05, 3.88 and 3.51 M^{-1} x10^6, respectively (**Fig. 1.13**). Heteroglycopolymers **1.53** and **1.54** displayed an approximate 1.7-1.9-fold increase in binding affinity in comparison to **1.52**, which suggested a possible synergistic effect for the respective

non-binding β-D-glucose and β-D-galactose in glycopolymers **1.53** and **1.54**, respectively [87].

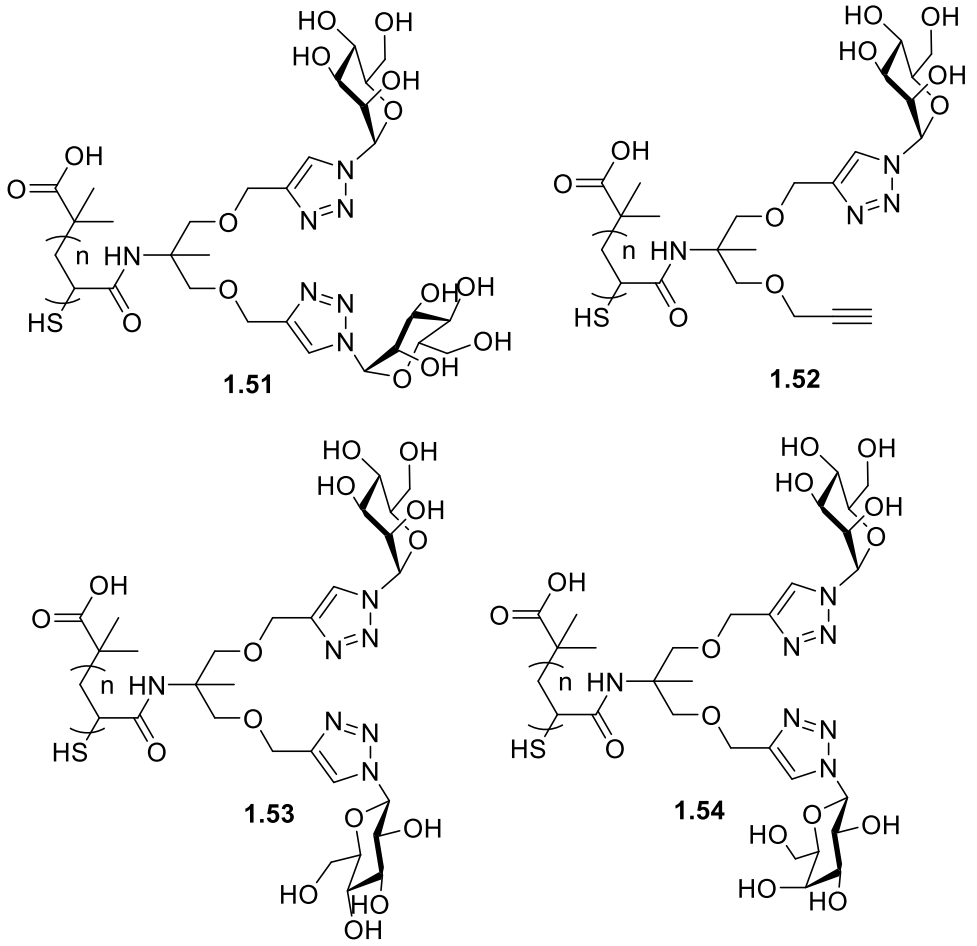

Figure 1.13: Structures of mannose glycoconjugates **1.51**-**1.54** [87].

Ehrmann *et al.* reported the synthesis and evaluation of a number of supramolecular glycoconjugates through encapsulation to β-cyclodextrin vesicles (CDVs) and evaluated their binding affinities to both ConA and FimH. Surface plasmon resonance (SPR) experiments with ConA, displayed K_d values of 50, 69 and 50 µM for compounds **1.55, 1.56 and 1.57** (**Fig. 1.14**), respectively. Functionalisation of these ligands onto CDVs decreased their corresponding K_d values to 7 µM (**1.55**), 13 µM (**1.56**) and 9 µM (**1.57**); this is attributed to the multivalent presentation of these supramolecular ensembles. Their ability to remove *E. coli* adhered to human uroepithelial cells was also assessed. Adherence of *E. coli* to these cells is mediated by the lectin FimH, which is specific for α-D-mannose. The CDVs functionalised with **1.56** and **1.57** proved to be

the best performing vesicles in the assay. The group also observed the binding of **1.57** to *E. coli* using cryo-transmission electron microscopy [88].

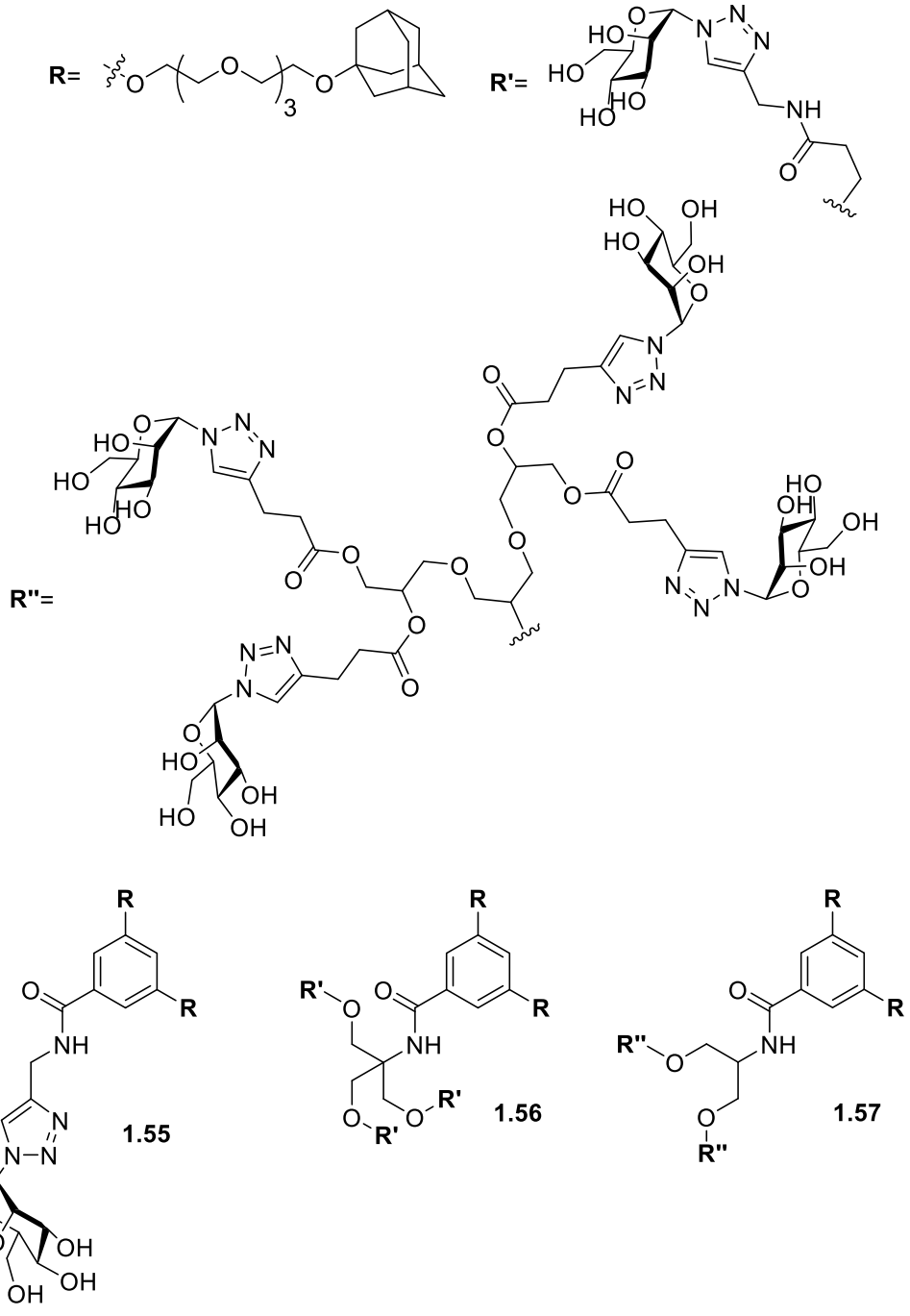

Figure 1.14: Structures of glycoconjugates **1.55**-**1.57** [88].

1.5 Aims and objectives

With the increasing prevalence of resistant strains of both fungal and bacterial pathogens, new antimicrobial treatments are of great importance. As discussed

earlier in this introduction, the adhesion of pathogens to host cell is a critical step to initiate infectious disease.

The central aims of the work described in this thesis revolves around the development of novel compounds that target the interactions between fungal and bacterial lectins and carbohydrates at the surface of the host cells to inhibit pathogen adhesion.

Most of the work in this thesis will focus on the opportunistic fungal pathogen *C. albicans* (Chapters 2-4). Building on work carried out in our research group, novel derivatives of previously identified lead compounds have been prepared and evaluated. Chapter 2 describes the synthesis of a series of *cis*-norbornene derivatives and the evaluation of their prodrug-like reactivity. In view of the recent reemergence of covalent inhibitors in the medicinal chemistry field, a series of potential covalent crosslinking glycoconjugates were prepared and evaluated against several Candida spps. pathogens (Chapter 3).

An extension of our ongoing Structural Activity Relationship (SAR) studies of lead compound **1.39** was carried out in Chapter 4. This includes the synthesis and evaluation of the anti-adhesion activity of several analogues, which feature cyclic glycomimetic moieties, heterocyclic systems and different substituents at the aromatic core.

Finally, we investigated the activity of glycoconjugates capable of inhibiting the transfer of genetic material which confers antimicrobial resistance (AMR), between bacterial cells, in this case *E. coli*. Previously reported high affinity ligands for *E. coli* fimbrial adhesin FimH were compared with novel compounds synthesised in our laboratory and tested as potential conjugation inhibitors in *E. coli* (Chapter 5).

Chapter 2

Norbornene-based compounds as potential stimuli-responsive anti-fungal agents

2.1 Introduction

2.1.1 Norbornene-based compounds in Biomedical applications

Norbornenes (NBs), also known as bicyclo[2.2.1]hept-2-ene, feature the generic structure seen below (**Fig. 2.1**). These compounds have been studied for a wide range of purposes such as catalysis, hydrogel formation and drug delivery systems [89-91].

Figure 2.1: General norbornene structure.

Sutthasupa *et al.* described the preparation of NB-based polymers **2.1** (**Fig. 2.2**) containing unprotected amino groups with an amino acid spacer between this amino group and the NB backbone of the polymer (**Fig. 2.2**). The authors achieved this synthesis via ring-opening metathesis polymerization (ROMP) using a Ruthenium catalyst and envisage the use of these polymers as biocompatible and pH responsive materials in future. In particular, the authors noted advantages of using Grubbs Ruthenium catalyst in these ROMP reactions as they allow for the incorporation of amines and nitriles into NB polymers. This work was the first successful example of the ROMP reaction of amino acid-derived NB monomers, such as **2.2** and **2.3** (**Fig. 2.2**) containing unprotected amino groups. Due to the stable nature of these polymers it is reasonable to view them as potential scaffolds for the preparation of different peptidomimetic products and perhaps biotherapeutics [92].

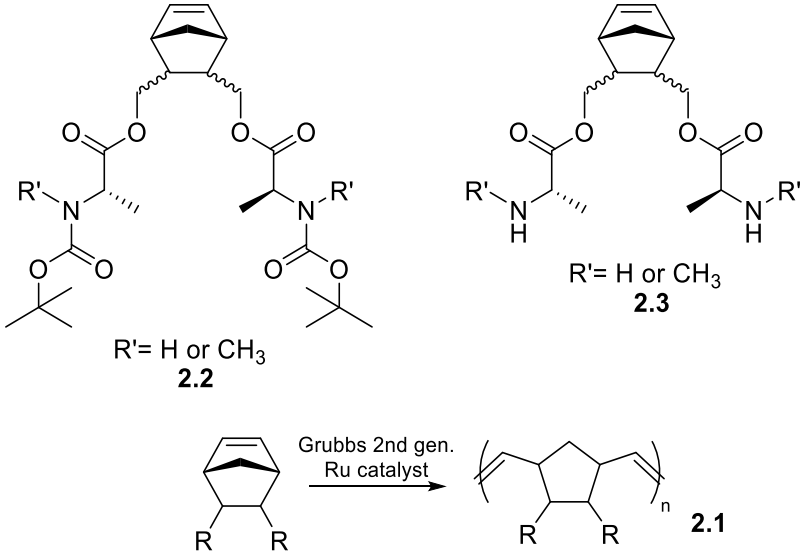

Figure 2.2: Structures of Norbornene monomers **2.2**, **2.3** and polymer **2.1** [92].

In work by Pfeffer *et al.*, the authors prepared polynorbornane scaffolds functionalised with different amino acids. This work is an excellent example of the chemical versatility of polynorbornyl scaffolds highlighted by the introduction of both alanine and glycine amino acids at different specific positions within the scaffold, as shown in compound **2.4** (**Fig. 2.3**). In addition, due to the compatibility of these scaffolds with peptide chemistry it is likely that they may play an important part in advances in the field of peptidomimetics [93].

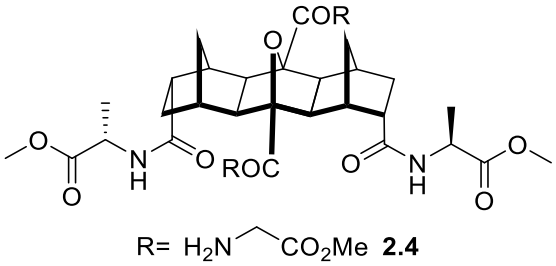

Figure 2.3: Structure of polnorbornane scaffold **2.4** [93].

Lin *et al.* reviewed some of the recent developments in the use of thiol-NB hydrogels (**Fig. 2.4**). These hydrogels have favourable conditions for photocrosslinking and have applications in terms of controlled delivery, 2D cell substrates and 3D cell encapsulation. These add to the potential value of these compounds in tissue engineering and regenerative medicine. A key advantage of such thiol-NB hydrogels,

in comparison to conventional poly(ethylene glycol) (PEGDA) hydrogels, is that they can deliver different proteins (e.g. BSA) to target sites in their bioactive form. This is in contrast to PEGDA hydrogels which, under the same UV light exposure conditions, were unable to deliver the same proteins in the bioactive state to the same extent. Hence, these thiol-NB hydrogels are superior to their PEGDA hydrogel equivalents in this regard. This is attributed to these hydrogels not being susceptible to oxygen inhibition during the thiol-NB photopolymerisation [91].

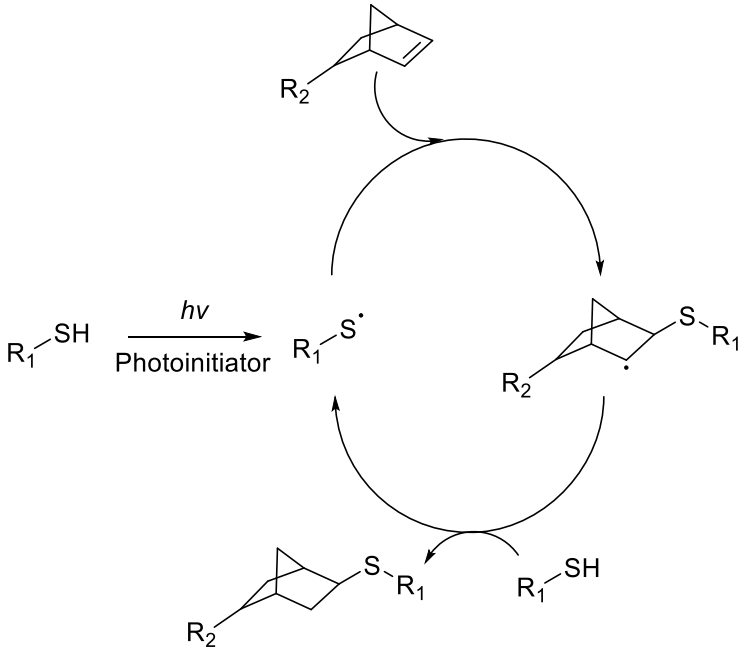

Figure 2.4: Photopolymerisation of thiol-norbornene hydrogels [91].

Miyamoto *et al.* reported the synthesis of two NB-glycopolymers **2.5** and **2.6** (**Fig. 2.5**) prepared by a ROMP reaction, in which they assessed the efficiency of three different catalysts in promoting this reaction. Yields of greater than 80% were achieved using three different catalysts, one molybdenum-based and two ruthenium-based. Polymers were prepared from NB monomers functionalized with either glucose or maltose. This work highlights the versatility of using NB scaffolds for presenting carbohydrate moieties. However, in this work the authors have not assessed any potential biological activity of the resulting glycoconjugates [94].

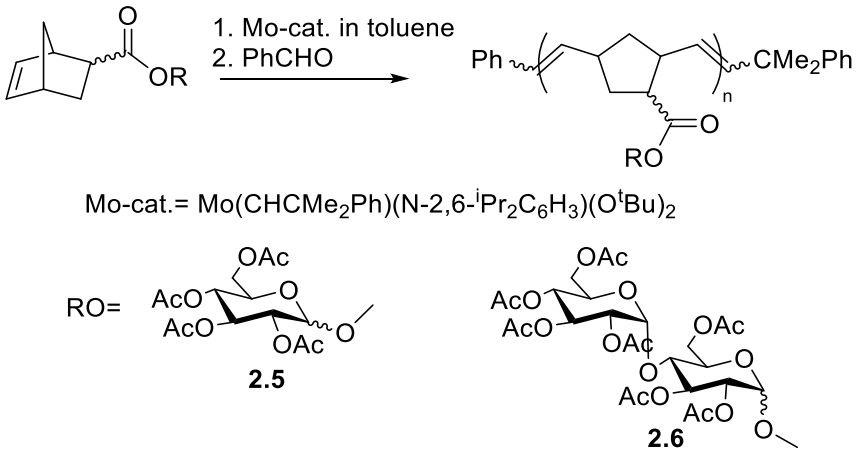

Figure 2.5: Structures of norbornene-glycopolymers **2.5** and **2.6** [94].

Mortell *et al.* have employed oxanorbornene scaffolds for the effective multivalent presentation of carbohydrate moieties to the lectin Concanavalin A (ConA), preparing these glycoconjugates via ROMP chemistry. Upon evaluation of a series of these glycopolymers as inhibitors of ConA, a mannoside-containing glycopolymer **2.7** (**Fig. 2.6**), showed a 50,000-fold increase in inhibition (inhibiting dose of $5x10^{-7}$ M) in comparison to an analogous monovalent derivative. A D-Glucose analogue of this glycopolymer, **2.8** (**Fig. 2.6**), displayed an inhibition dose of $5x10^{-5}$ M. This demonstrates the versatility of these scaffolds for suitable presentations of carbohydrate moieties with the aim of inhibiting lectin binding to native carbohydrate structures in human cells [95].

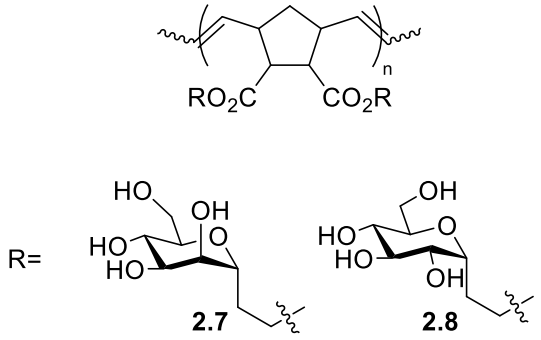

Figure 2.6: Structures of nobornene-glycopolymers **2.7** and **2.8** [95].

2.1.2 Stimuli-responsive bioactive compounds/drug delivery systems

Drug delivery systems/compounds with pH-responsive properties pose particular advantages for targeted delivery in the treatment of diseases in which the drug target

resides in a compartment with a differing pH to other compartments. Many examples of pH responsive systems have been reported. For example, Li *et al.* reported the preparation and evaluation of a hydrogel with pH-responsive properties, capable of releasing insulin over a sustained period of time (2 weeks) [96]. Reddy *et al.* demonstrated the pH-responsive release of doxorubicin (DOX) from two carboxymethyl chitosan (CMC) composite films [97]. Wang *et al.* utilised polymeric micelles containing DOX to treat melanoma. These examples effectively exploited the more acidic pH in the tumour microenvironment to release more DOX in tumour tissue [98].

Li *et al.* reported a doxorubicin-coumarin hybrid compound **2.9** (**Fig. 2.7**) which displayed both anti-cancer activity and real-time drug release in a pH-dependent manner. The group developed a pH-responsive prodrug containing three key parts; a tumour targeting moiety (GRGDS), a fluorescence reporter group (coumarin) and finally an anti-cancer drug, in this case DOX. GRGDS is an oligopeptide which can be specifically recognised by $\alpha_v\beta_3$ integrin which is overexpressed in a number of tumour cell lines. Coumarin was used to allow for the real-time monitoring of the release of DOX from the prodrug. DOX was used as the anti-cancer agent for two reasons; in addition to its anti-cancer activity, doxorubicin can act as a fluorescent quencher for different coumarin derivatives. In order to confer a pH-responsive character to the prodrug the authors linked DOX to the rest of the prodrug through a labile hydrazone bond, which would be selectively cleaved within the endo/lysosomes of cancer cells (pH of 5-6), thus releasing DOX within the cancer cell following targeting of these cells by $\alpha_v\beta_3$ integrin (**Fig. 2.7**). Lastly, release of DOX caused an increase in fluorescence as the contact-mediated quenching between DOX and coumarin is no longer possible and this allows real-time monitoring of the DOX release within acidic compartments of tumour cells. They found significant differences in the rate of release in pHs of 7.4 and 5, with 94% drug release after 11 h in pH 5 versus 41% drug release at pH 7.4 after the same time. A direct correlation between increasing fluorescence and DOX release provided further confirmation of this result [99].

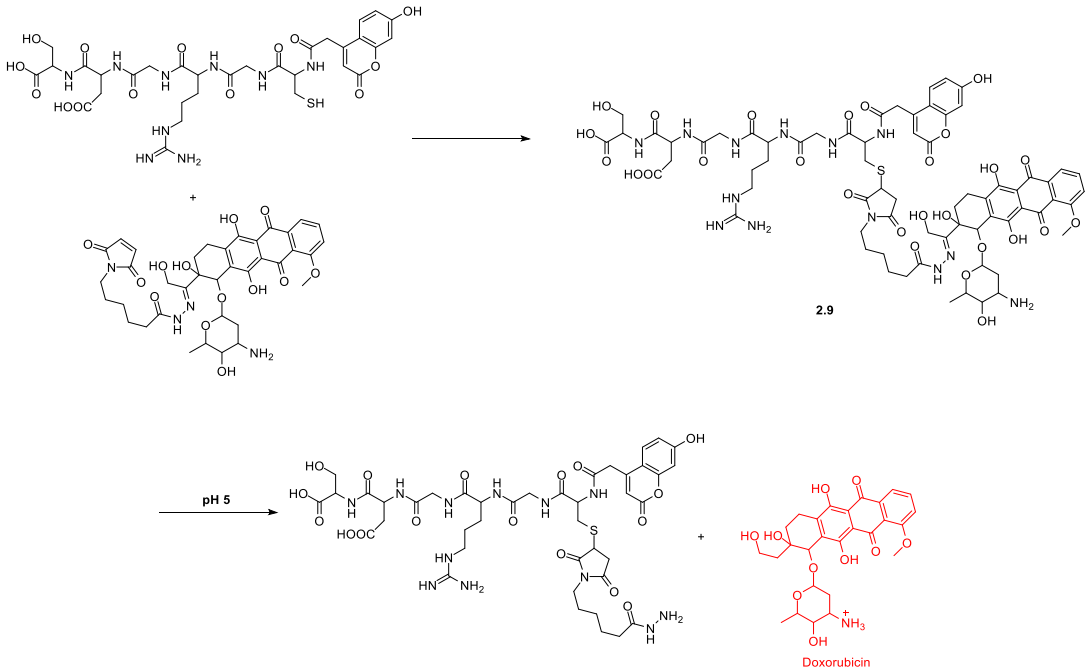

Figure 2.7: Structure of stimuli-responsive compound **2.9** and release of doxorubicin (anti-cancer agent) from this compound in acidic pH [99].

Saha *et al.* demonstrated the potential use of novel glycopolymeric nanoparticles composed of the glycopolymer **2.10** shown in Figure **2.8** as pH-responsive drug delivery systems. Notably, these glycopolymers were prepared from NB-containing glycomonomers through ROMP methodology. The authors found that changes in pH resulted in changes of the ionization state of the guanidiniocarbonyl pyrrole carboxylate (GCP) zwitterion. As a result of this the supramolecular binding motif of the GCP-zwitterion is destabilised, leading to an unfolding of the polymer to form large undefined aggregates. To further investigate the potential applications of these glycopolymers, the authors firstly demonstrated the targeting effect conferred by the lactose moieties in the glycopolymer. This allowed selective targeting of HepG2 cells, which express ASGPR receptors, over HeLa and HEK293T cell lines [89].

In another example, Chen *et al.* reported the synthesis and preparation of four polyion complex (PIC) micelles **2.11**, **2.12**, **2.13** and **2.14** (**Fig. 2.8**) loaded with DOX. Each of these complexes were made up of polymers terminated with NHCO-R-CO_2H, where R is a rigid 2-carbon linker as shown in Figure **2.8**. The presence of this structural motif makes the amide bond more susceptible to hydrolysis at acidic pH. Amide hydrolysis would release the lysisne side chains that, at acidic pH, would be

protonated leading to micelle disassembly and DOX release. The authors envisioned exploiting the differences in the pH sensitivity of the relevant amide bonds in each complex to afford a fine-tuned release profile of the encapsulated DOX. They observed a significant increase in the release of DOX when each complex was incubated at pH 7.4, 6.8 and 5.3, respectively. Additionally, the pH sensitivity of each complex could be correlated to the pH responsiveness of the relevant amide bonds in each complex, with more labile amide bonds corresponding to faster release of DOX [100].

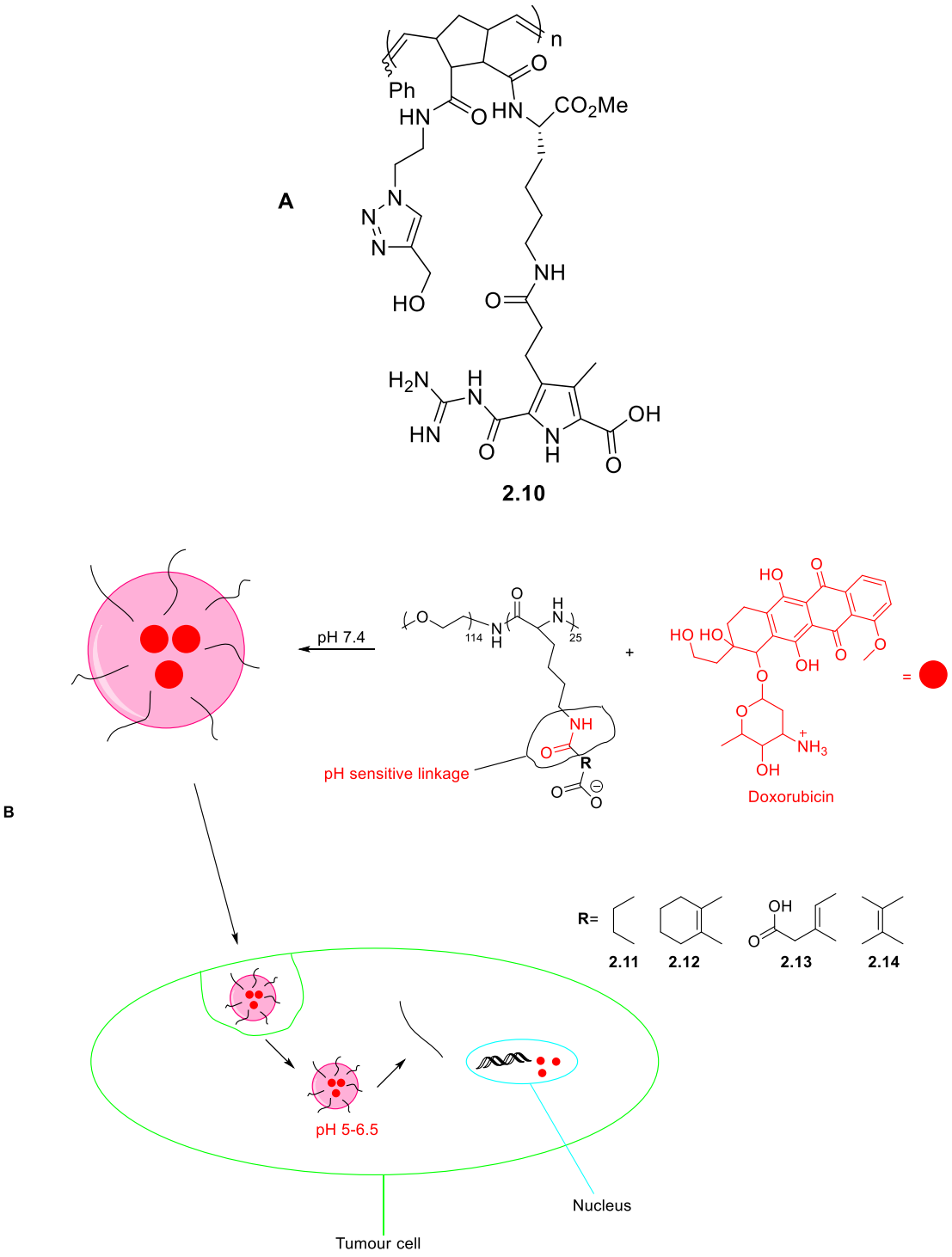

Figure 2.8: ***A.*** Structure of norbornene-glycopolymer **2.10** and ***B.*** Mechanism of action of pH-sensitive drug delivery system [89,100].

Similarly, Cheng *et al.* reported work in which exploitation of differences in pH between the tumour microenvironment and physiological pH allowed selective release of DOX following cleavage of a 2,3-dimethylmaleic anhydride (DMA) protecting group from their prodrug compound **2.15** (**Fig. 2.9**). The authors also used

an activatable cell-penetrating peptide (ACPP) called $CR_8G_3PK_6$ which confers rapid cellular uptake by tumour cells. The primary amines of the lysine residues in ACPP were protected using DMA to mask the cell penetrating function. Upon entering the tumour microenvironment, which has a pH of 6.8, hydrolysis of the amide functional groups formed between the DMA protecting group and the lysine residues in ACPP occurs, whereas this reaction does not occur at physiological pH (7.4). The selective nature of this approach is seen in the stability of the DMA protecting group with respect to cleavage at physiological pH and the rapid cleavage of this group when present in pH 6.8 (tumour microenvironment), thus allowing selective targeting of tumour cells by the ACPP and subsequent release of DOX within tumour cells [101].

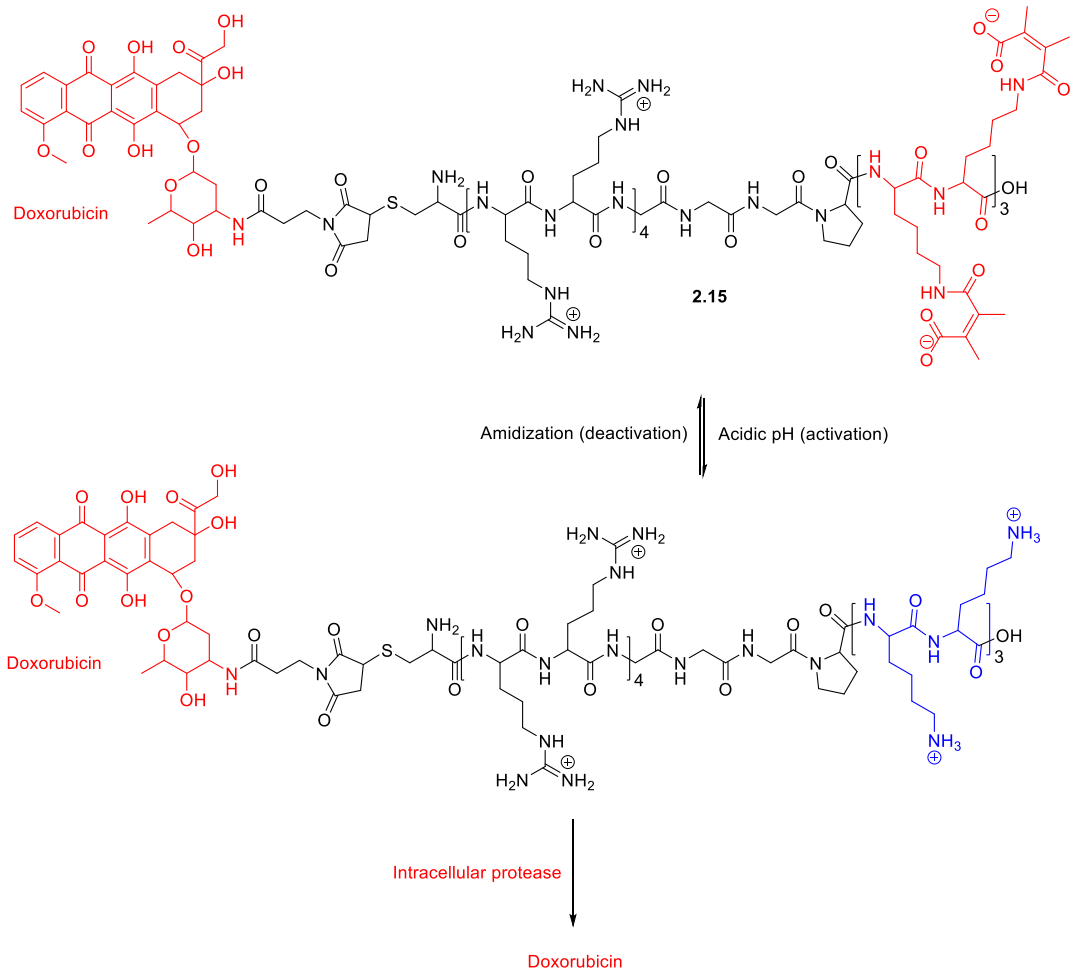

Figure 2.9: Structure of prodrug compound **2.15** and its mechanism of action [101].

A similar approach is presented in work by Zhou *et al.* who reported a charge-reversal drug conjugate **2.16** (**Fig. 2.10**) with targeted nuclear delivery of the active compound, camptothecin. The authors needed to balance and fine-tune the desired

nucleus-targeting properties of poly(L-lysine)(PLL), which is a cationic polymer, with its undesired toxic side-effects. To do this, they masked the amine functional groups with succinic acid derivatives, with the knowledge that the resulting amide groups would be acid-labile and could be deprotected within the cell lysosomes/endosomes (pH 4-5) or when it reaches the tumour extracellular environment (pH <7) revealing the targeting effect for the nucleus. Importantly, the authors noted the necessity of such acid-labile amide groups to have a neighbouring carboxylic acid in the β-position, which confers this acid-lability, this is of particular relevance to our work described in this chapter [102].

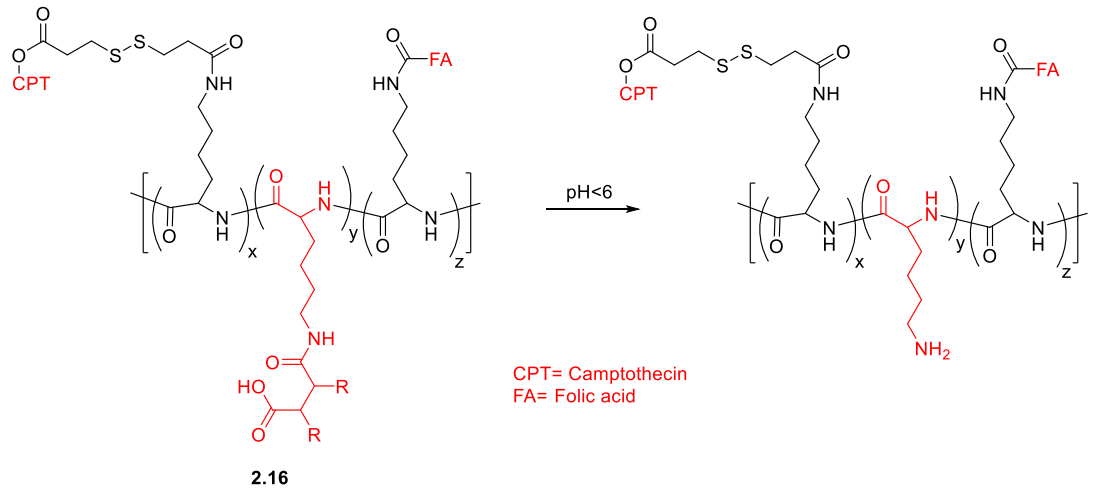

Figure 2.10: Glycopolymer **2.16** with pH-responsive properties [102].

2.1.3 Examples of pH-triggered Hydrolysis/cyclisation reactions and their structural requirements/reaction conditions

As mentioned previously in Section 2.1.2, amides with a β-carboxylic acid have a tendency to undergo hydrolysis reactions. An important factor that appears to influence the rate of such hydrolysis reactions is structural constraints which place the amide functional group in proximity to the carboxylic acid in the β-position relative to it. Zhou *et al.*, evaluated the tendency of each of the PLL scaffolds shown in Figure **2.11**, **2.17**, **2.18** and **2.19**, to undergo hydrolysis reaction to yield the corresponding free amine. The authors found that **2.18** was by far the most reactive one. The half hydrolysis times ($t_{1/2}$) of each PLL scaffold dropped as the pH was reduced from pH 7.4 to 5; for **2.18** it was reduced from 5 h to less than 5 minutes, for **2.17** from greater than 60 h to 30 minutes and for **2.19** from greater than 60 h to 2.4

h. This shows that structural constraints which place the amide and carboxylic acid functional groups in close proximity appear to accelerate the rate of hydrolysis in these scaffolds [102].

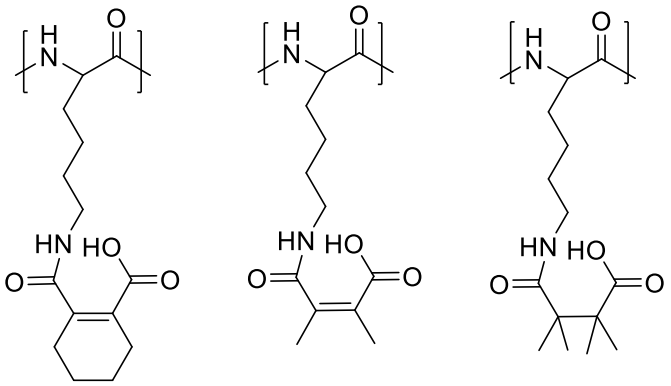

Figure 2.11: Structures of poly(L-lysine) polymers **2.17**, **2.18** and **2.19** [102].

In similar work carried out by Suh *et al.* the intramolecular catalysis of amide hydrolysis was studied as a model of Carboxypeptidase A (CPA). The three maleamic acid derivatives featuring different heterocycles used in this study are shown in Figure **2.12**. The effect on the rate of hydrolysis, if any, that the heterocycle had in each case was also examined. The rate of hydrolysis was measured at 65^{o}C over a range of pH values ranging from 1 to 6. The authors observed that both **2.20** and **2.21** underwent hydrolysis exclusively. However, for compound **2.22** above pH 2, it was observed that this compound underwent hydrolysis as well as another side reaction. Through colorimetric determination of the 2-aminomethylpyridine released in the hydrolysis reaction the authors determined that the amount released was only a fraction of the initial amount of **2.22** used, hence another reaction path must be available to this compound. They subsequently determined that the secondary reaction pathway used by **2.22** was an intramolecular conjugate addition reaction. This work provides further evidence of such compounds, containing amide and carboxylic acid functional groups in close proximity, that can undergo intramolecular hydrolysis and/or cyclisation reactions [103]. The authors have carried out further research into the structural requirements to successfully mimic the efficient catalysis of the hydrolysis of amides and esters by CPA [104].

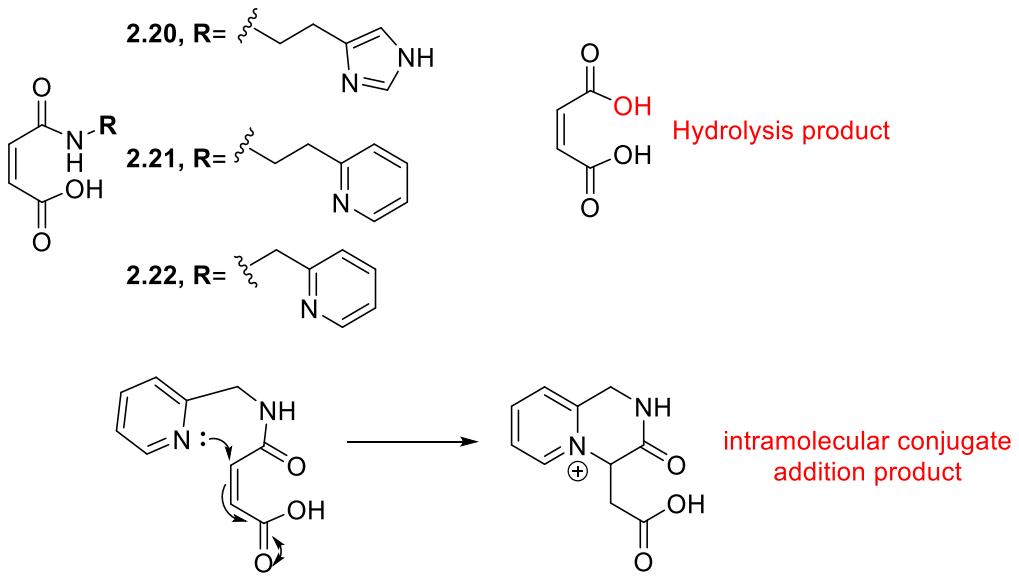

Figure 2.12: Structures of maleamic acid derivatives **2.20**, **2.21** and **2.22** [103].

Sim *et al.* studied the effects of different solvent mixtures on the rates of hydrolysis and the tendencies of each solvent mixture to promote either *O*-cyclisation (**Fig. 2.13**) or *N*-cyclisation in a number of phthalamic acid derivatives, such as **2.23**. These reactions were assessed in water/acetonitrile mixtures. The authors observed variations in the rates of hydrolysis of these derivatives, particularly as the % of acetonitrile was increased. The rate constants for *O*-cyclisation decreased non-linearly by approximately 20-fold with increasing acetonitrile concentrations. However, variation of the % acetonitrile had little effect on the preference of these compounds to undergo *O*-cyclisation over *N*-cyclisation. This work highlights the importance of considering solvent effects and other factors when designing stimuli-responsive compounds [105]. In similar work, Khan *et al.* assessed reaction kinetics for the hydrolysis of *o*-carboxybenzohydroxamic acid (OCBA) in water/acetonitrile mixtures by monitoring the formation of Phthalic anhydride spectrophotometrically. Again, it was found that the rate constants for hydrolysis of OCBA in this case are largely independent of the acetonitrile content of the solvent system. This suggests that as long as there is an appreciable percentage of water in the reaction system, addition of other solvents such as acetonitrile does not appear to prevent hydrolysis [106]. Further work by Cheong *et al.* added further evidence of this as in both water/acetonitrile and water/DMF mixtures decreasing the water content, thus

decreasing the overall polarity, has only a modest effect on the intramolecular hydrolysis reaction [107].

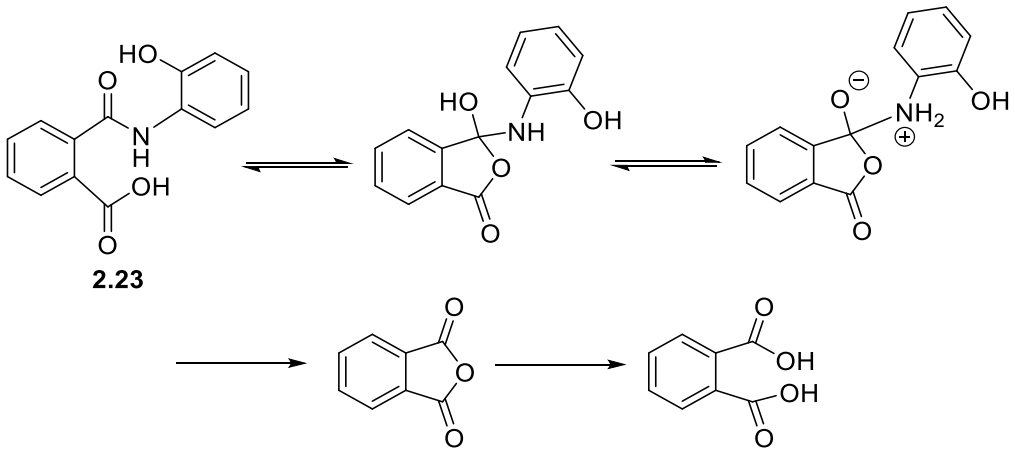

Figure 2.13: *O*-cyclisation and subsequent hydrolysis of phthalamic acid derivative **2.23** [105].

Whilst assessing the reactivities to undergo a Hoffman rearrangement reaction of a range of compounds, including NB and norbornadiene compounds, Moriconi *et al.* observed an unexpected intramolecular cyclisation reaction (**Fig. 2.14**) in compound **2.24**. However, this provides evidence that conformationally restricted compounds such as NB compounds with neighbouring amide/acid and in this case, an amide/ester groups may undergo such cyclisation reactions [108]. Through further investigation of the reaction pathway for the intramolecular hydrolysis of *N*-methylmaleamic acid, Park *et al.* found that the reaction proceeds through a concerted pathway. This reaction involves a simultaneous nucleophilic attack of the carboxyl oxygen on the amide carbonyl carbon and release of methylamine following intramolecular hydrogen transfer from the carboxyl group to the amide functional group [109]. Kim *et al.* demonstrated the utility of this reaction when they prepared mimics of Aspartic proteases by covering the surface of silica gel with carboxyl functional groups. This material hydrolysed the peptide/amide bonds in both hemoglobin and γ-globulin. This reaction involved the same concerted pathway as identified by Park *et al.* thus highlighting the biological relevance of this reaction [110].

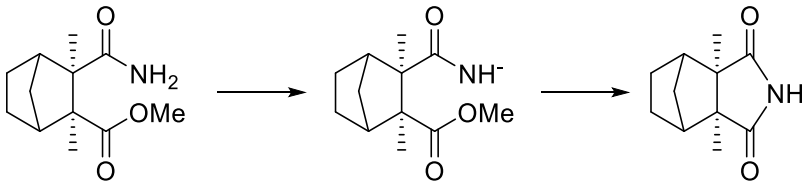

2.24

Figure 2.14: Intramolecular cyclisation reaction observed in compound **2.24** [108].

2.1.4 Norbornene/Norbornane compounds as anti-microbial compounds

There are few examples of NB/norbornane compounds displaying anti-microbial activity (**Fig. 2.15**). Hickey *et al.* prepared a series of cationic NB derivatives with the hope that these compounds could pose as mimics of naturally occurring cationic antimicrobial peptides. These peptides function by inserting themselves into the membrane of bacteria, which causes loss of the membrane's structural integrity, leading to cell lysis. The authors used a mixture of alkyl and mixed alkyl/aryl functionalities to mimic the lipophilic components found in many antimicrobial peptides. Secondly, amines and guanidine groups were used to mimic lysine and arginine residues found in many of the same peptides. Compounds **2.25**-**2.28** were found to have the best antimicrobial activity of the compounds tested. MIC values of less than or equal to 2 μg/mL against several Gram-positive bacterial isolates, including four *S. aureus* strains, *S. pneumoniae* and *E. faecalis,* were observed for these compounds. From these results it appeared that the dicationic species produced the best activity followed by monocationic compounds and then neutral compounds. This indicates that a higher charge density correlates with increased antimicrobial activity [111].

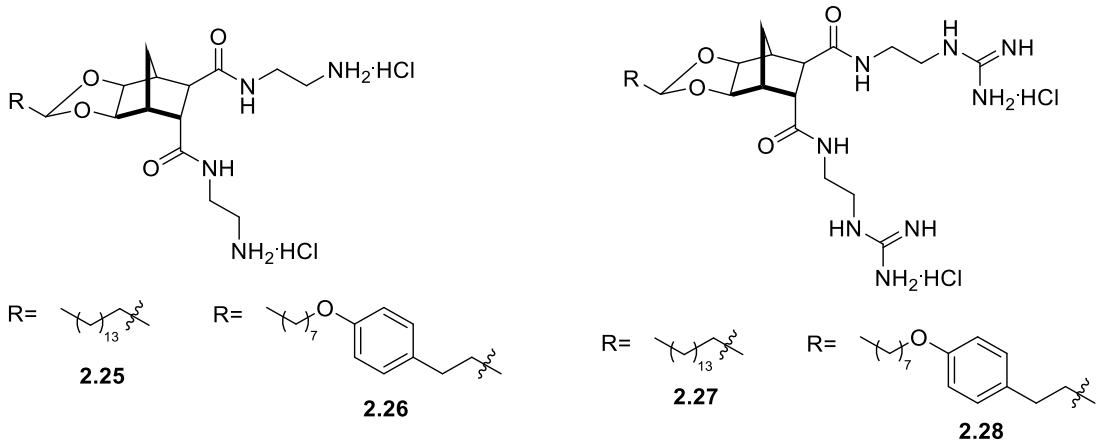

Figure 2.15: Cationic norbornane compounds **2.25**-**2.28** [111].

In further work, Hickey *et al.* reported the synthesis of a series of norbornane bisether diguandine compounds which displayed promising antibacterial activity. Compounds **2.29**, **2.30** and **2.31** (**Fig. 2.16**) were found to produce MIC values in the range of 8-32 µg/mL against a range of pathogens including *A. baumannii*, *P. aeruginosa*, *E. coli* and MRSA. This work provides further evidence that NB/norbornene scaffolds are attractive scaffolds upon which to functionalise different moieties to yield bioactive compounds [112].

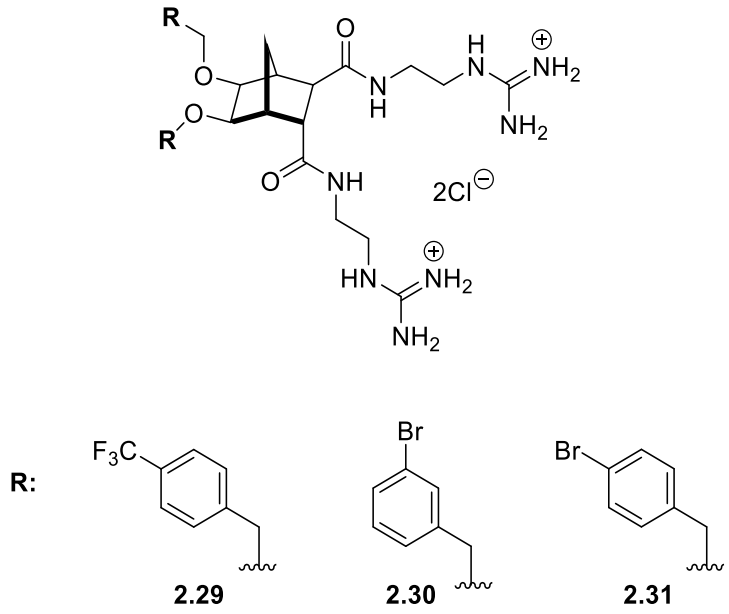

Figure 2.16: Structures of norbornane bisether diguandine compounds **2.29**-**2.31** [112].

Further work was carried out by Hickey *et al.* to improve on the antibacterial activity of the aforementioned norbornane compounds and to help elucidate their mode of action. Compound **2.32** (**Fig. 2.17**) showed excellent activity with MIC values ranging between 0.25-1 μg/mL against a number of *S. aureus* strains and *S. pneumoniae*. The authors also prepared two fluorescently labelled derivatives **2.33** and **2.34** (**Fig. 2.17**). Fluorescent microscopy showed the localization of these compounds at the periphery of both Gram-positive (*S. aureus*) and Gram-negative (*E. coli*) bacteria. This confirmed their hypothesis that the cationic nature of these compounds allows targeting of the bacterial cell membrane. In addition, fluorescence was only observed intracellularly in the case of *S. aureus* (Gram-positive). The authors believed that the increased antibacterial activity against Gram-positive bacteria could be attributed to this [113].

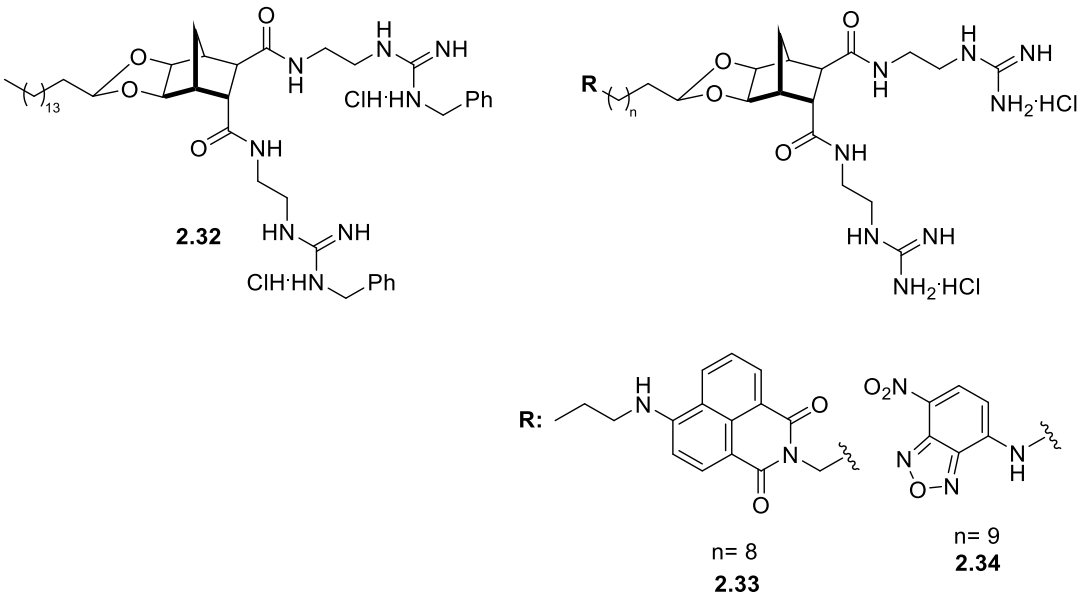

Figure 2.17: Cationic norbornane compounds **2.32**-**2.34** [113].

Previous work in our group resulted in the development of NB-based glycoconjugates with anti-adhesion activity against the fungal pathogen *C. albicans* (**Fig. 2.18**). Both *cis* and *trans* divalent galactosides **2.35** and **2.36** (**Fig. 2.18**), respectively were evaluated as non-aromatic core analogues of a previously reported lead compound **1.39**, discussed previously in Section **1.4.1** (**Fig. 1.9**) [114]. The synthesis of these compounds required, as a final step, the mild basic hydrolysis of the sugar acetyl protecting groups and subsequent treatment with acidic amberlite resin. However,

it was found that, upon treatment of the *cis*-NB compound **2.35** with Amberlite H^+ resin, a cyclisation reaction occurred, forming the cyclic imide product **2.37** shown in Figure **2.18**. Interestingly, this reaction was not observed for the corresponding *trans*-NB **2.36** [114]. These observations suggest that such *cis*-NB compounds have potential to act as pH-sensitive compounds. The proposed reaction mechanism for this cyclisation reaction is shown in Scheme **2.1**. Although 1,2,3-triazoles are weak bases (N-3 azolium pK_a ca. 1.3) this proposed mechanism suggests that N-3 nitrogen in the 1,2,3-triazole ring is acting as a general base catalyst [115]. Deprotonation of the amide nitrogen in a concerted manner increases its nucleophilicity as it attacks the carbonyl carbon of the neighbouring amide group. This is made possible by the *cis* relationship between the two amide groups. Another potential role of the N-3 nitrogen may be the formation of a hydrogen bond with the adjacent amide nitrogen.

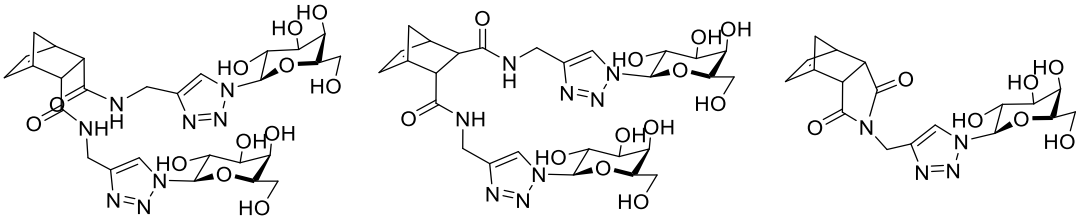

2.35 **2.36** **2.37**

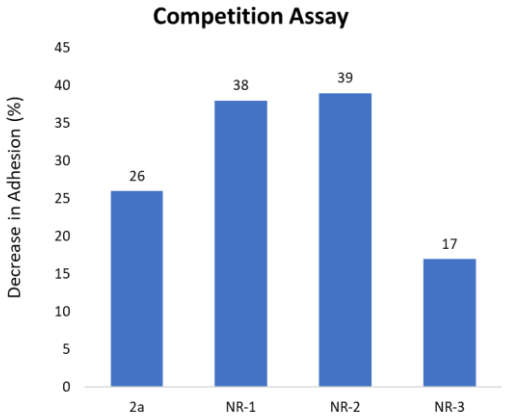

Figure 2.18: Anti-adhesion activity of Norbornene glycoconjugates **2.35**-**2.37** [114]. Note: 2a=**1.39** ,NR-1= **2.36**, NR-2= **2.35** and NR-3= **2.37**.

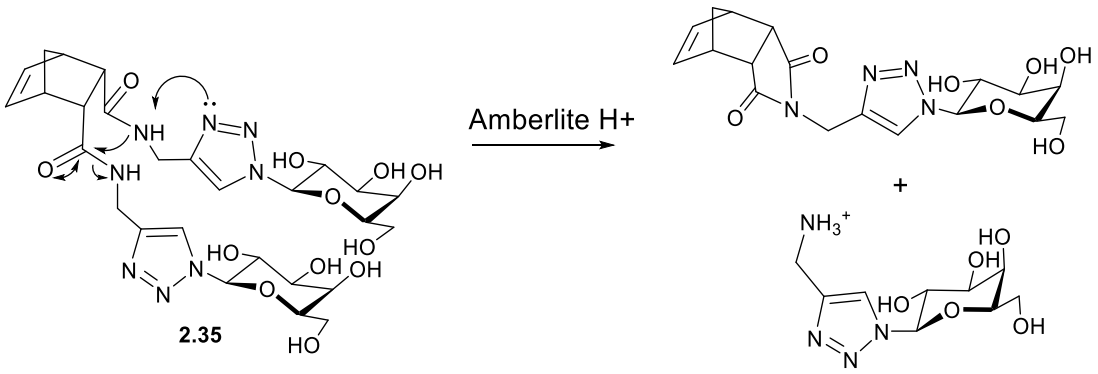

Scheme 2.1: Proposed mechanism for the cyclisation reaction observed in cis-norbornene compound **2.35**.

2.2 Chapter Objectives

This chapter aims to explore the feasibility of using *cis*-NB compounds as pH-responsive anti-fungal prodrugs, since the micro-environmental pH is low at infection sites and biofilms. In order to do this, we have firstly performed the synthesis of a series of NB derivatives, both glycoconjugates and non-glycoconjugates as model compounds to identify the structural requirements for pH sensitivity. We have then carried out the assessment of their abilities to undergo the pH induced cyclisation reaction shown in Scheme 2.1. This is a prerequisite to these compounds acting as prodrug-like compounds against *C. albicans*. While studying these compounds we chose to assess the effect of a number of structural factors, these are:

- Presence/lack of carbohydrate moieties (analogues **2.35**, **2.45** and **2.46**)
- The type of carbohydrate moieties (analogues **2.35** and **2.46**)
- Presence of the 1,2,3-triazole or other heterocycles (analogues **2.35**-**2.55**)

In addition to these compounds, a number of model compounds were prepared which correspond to the products of the potential cyclisation reactions being monitored.

Two additional novel hybrid norbornene compounds **2.80** and **2.81** were prepared, containing Farnesol and Tyrosol moieties respectively. Tyrosol and farnesol are QS compounds known to inhibit the formation of biofilms in *C. albicans* [116]. These molecules would be released in a pH-sensitive manner if these compounds would undergo the cyclisation reaction. The resulting product, compound **2.37**, is also a

moderate inhibitor of fungal adhesion (as discussed in Section **2.1.4**) so hybrid compounds **2.80** and **2.81** could provide "proof-of-principle" for a new class of anti-fungal agents with dual (anti-adhesion and anti-biofilm) mode of action.

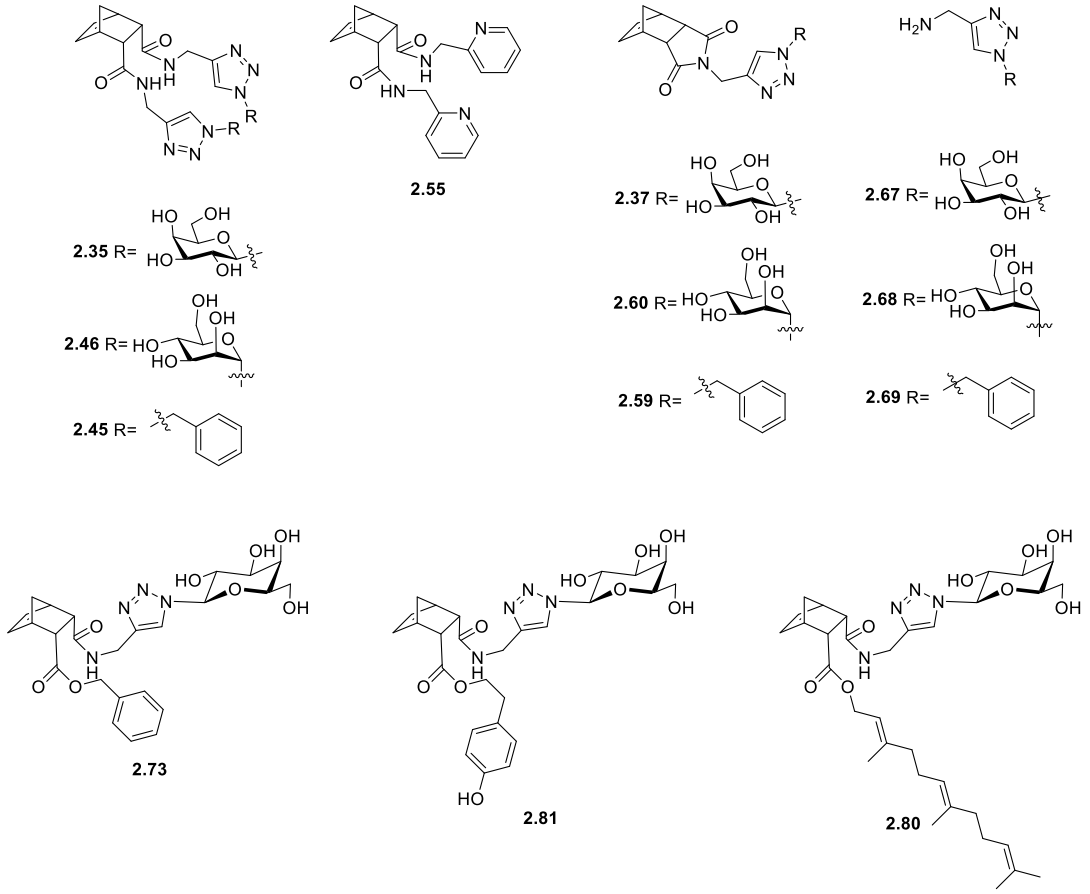

Figure 2.19: Norbornene compounds prepared in this chapter.

2.3 Results and Discussion

2.3.1 Synthesis

2.3.1.1 Synthesis of sugar azides 2.40 and 2.41

All *O*-acetyl sugar azides used in this work were synthesised following well known synthetic routes [117]. Both the galactose and mannose derivatives, **2.40** and **2.41**, were prepared from their corresponding peracetylated precursors, **2.38** and **2.39** (**Scheme 2.2**). The azido functional group was introduced at the anomeric position using $TMSN_3$ and $SnCl_4$, using anhydrous DCM as the solvent. $SnCl_4$ is used as a Lewis acid catalyst which activates the anomeric acetyl group. As a result of neighbouring group participation, the β-anomer **2.40** is obtained from the peracetylated galactose, whereas the α-anomer **2.41** is obtained from peracetylated mannose.

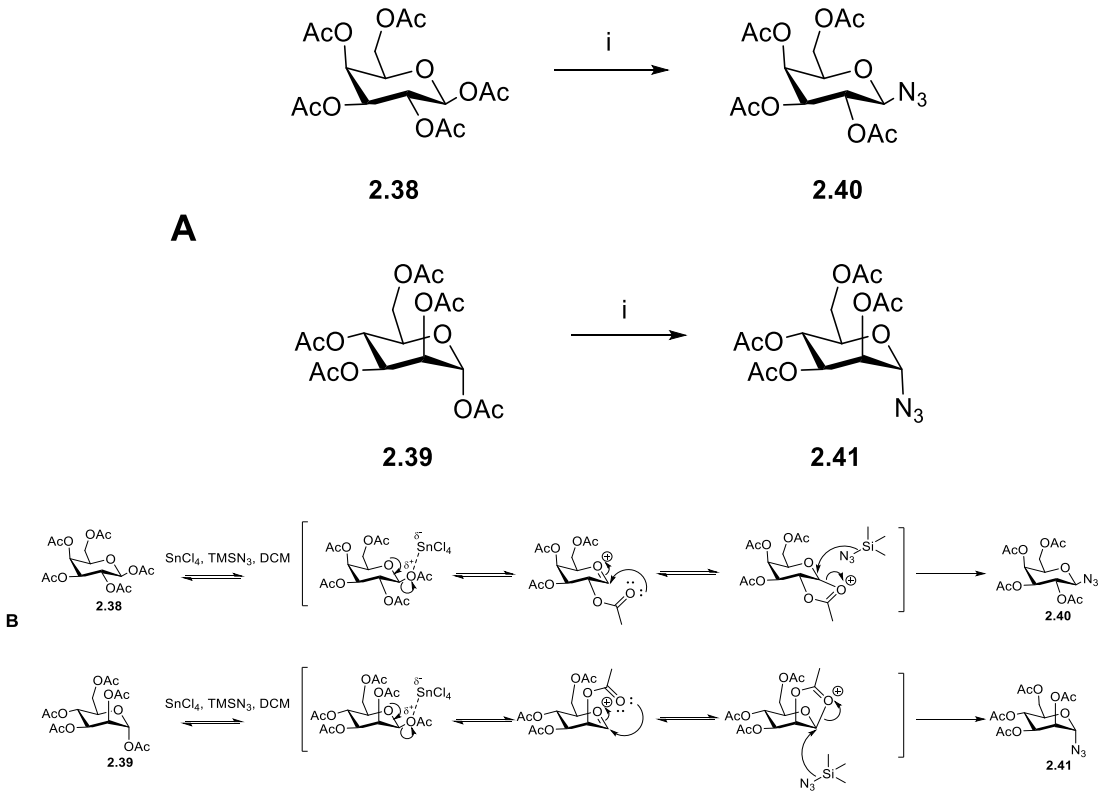

Scheme 2.2: ***A.*** Synthesis of D-sugar azides. *Reagents and conditions*; i) $TMSN_3$, $SnCl_4$, anhydrous DCM, N_2, 16 h, 70-94%; ***B.*** Reaction mechanisms for the synthesis of β-D-galactose azide **2.40** and α-D-mannose azide **2.41**.

2.3.1.2 Synthesis of norbornene compounds 2.35, 2.45 and 2.46 via CuAAC chemistry

Two NB glycoconjugates, **2.43** and **2.44**, were prepared using the corresponding β-D-galactose azide **2.40** and α-D-mannose azide **2.41**, respectively. Copper (I) catalysed azide-alkyne cycloaddition (CuAAC) was employed by reacting the azides with a dialkyne NB compound **2.42**, which was prepared by coupling propargylamine with *cis*-5-norbornene-*endo*-2,3-dicarboxylic acid using TBTU as the coupling agent (**Scheme 2.3**). A catalytic system of copper sulfate pentahydrate and sodium ascorbate was used in these reactions. The CuAAC reaction was performed in the microwave at 100 ^{o}C for typically 30 mins yielding the NB glycoconjugates **2.43** and **2.44**. The final step in the preparation of these compounds was the removal of the acetyl protecting groups in both glycoconjugates under mild basic conditions to give the galactose **2.35** and mannose **2.46** derivatives in high yields (**Scheme 2.3**).

A third NB compound **2.45** was also prepared by reaction of the dialkyne NB **2.42** with benzyl azide (**Scheme 2.3**). This was done in order to test if the presence of carbohydrates was needed for the pH induced cyclisation reaction discussed earlier. The CuAAC reaction involving benzyl azide was carried out at RT for four days (initially, this reaction was done in the microwave at 100 ^{o}C; however, it was found that under these conditions the reaction either failed to go to completion or decomposed, hence the reaction was eventually found to go to completion after four days at RT). This yielded the non-carbohydrate-containing NB compound **2.45**.

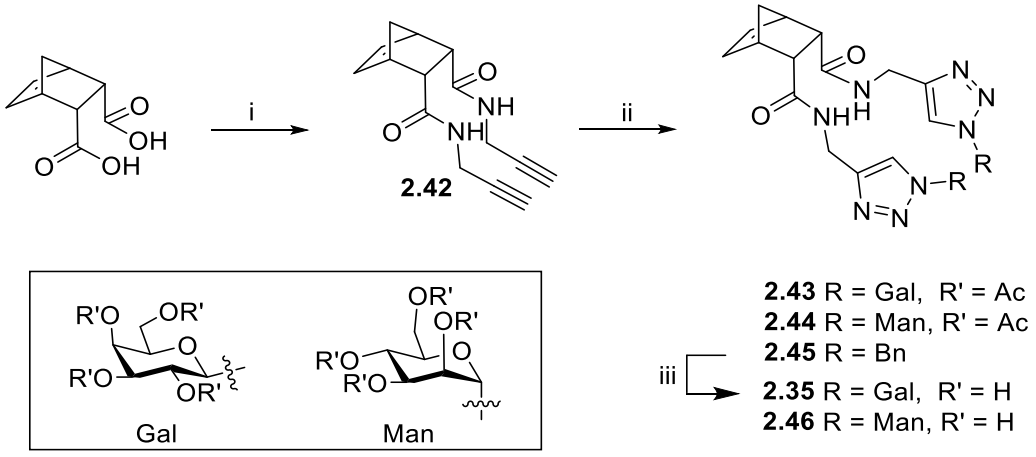

Scheme 2.3: Synthesis of norbornene compounds **2.35**, **2.45** and **2.46**. *Reagents and conditions*; i) Propargylamine, NEt_3, TBTU, DMF, 16 h, 79%; ii) O-acetyl sugar azide **2.40** or **2.41** or Benzyl azide, $CuSO_4.5H_2O$/Na Asc, CH_3CN/H_2O, 30 mins (MW, 100 ^{o}C) or 4 days at RT, 43-91%; iii) MeOH, H_2O, NEt_3, 45 ^{o}C, 6 h for **2.35** and **2.46**, 94-95%.

As mentioned, the synthesis of the above compounds was achieved using Copper (I) catalysed azide-alkyne cycloaddition (CuAAC) chemistry. Under normal uncatalyzed conditions, the Huisgen 1,3-dipolar cycloaddition of organic azides with alkynes tend to be slow, requiring high temperatures and low selectivity yielding an equimolar mixture of 1,4- and 1,5-disubstituted 1,2,3-triazole regioisomers. However, as discovered by the Meldal and Sharpless groups separately in 2002, a 'copper effect' was observed. This effect meant that, in the presence of catalytic amounts of Copper (I), the reaction is both accelerated greatly and the 1,4-disubstituted regioisomer obtained exclusively (**Scheme 2.4**) [66,118,119]. These discoveries have opened exciting avenues in the development of novel medicinal compounds, with enhanced

stability in comparison to its bioisosteres and enhanced binding interactions [120,121].

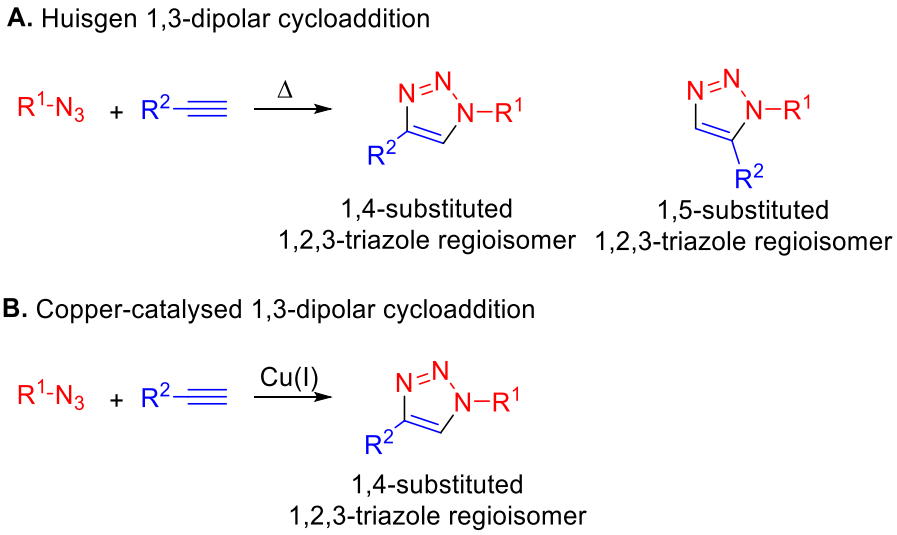

Scheme 2.4: A. Huisgen 1,3-dipolar cycloaddition, **B.** Copper-catalysed 1,3-dipolar cycloaddition [119].

There have been various iterations to the proposed mechanism of the CuAAC reaction, including the initial mechanism proposed by Fokin and Sharpless [66]. The most up-to-date proposed mechanism is shown in Scheme **2.5**. The first step in this mechanism is the formation of σ, π-di(copper) acetylide **2.47**, which is involved in both σ and π bonding with copper (I) (step i). Initial work with this mechanism proposed a single copper (I) atom, however, due to the high activation energy barrier associated with forming metacycle **2.50**, it was then suggested that two copper (I) ion are involved. Addition of a second copper (I) ion to the metacycle structure alleviates some of the ring strain in **2.50**, this lowers the activation energy barrier. Due to the tendency of copper (I) to participate in both σ and π bonding with alkynes, this copper (I) ion is introduced at acetylide **2.47** stage of the catalytic cycle. In the next step acetylide **2.47** forms an azide/alkyne/copper (I) ternary complex **2.48**, by binding to azide **2.49** (step ii). The metacyle **2.50** is formed through the oxidation of one copper (I) to copper (III) (step iii). A reduction ring contraction step yields the copper (I) triazolide **2.51** (step iv), which then deprotonates an alkyne to complete the catalytic cycle and afford **2.52** [122]. Intermediates **2.47** and **2.51** have been isolated, fully characterised and verified as viable intermediates in the catalytic cycle.

However, to date intermediates **2.48** and **2.50** have not, highlighting that these steps are fast steps in the catalytic cycle. Intermediate **2.48** has been detected once via an ion-tagged electron spray ionisation mass spectrometry method. While intermediate **2.50** was found to be involved in a rapid internal rearrangement equilibrium, using a copper isotope labelling experiment [122].

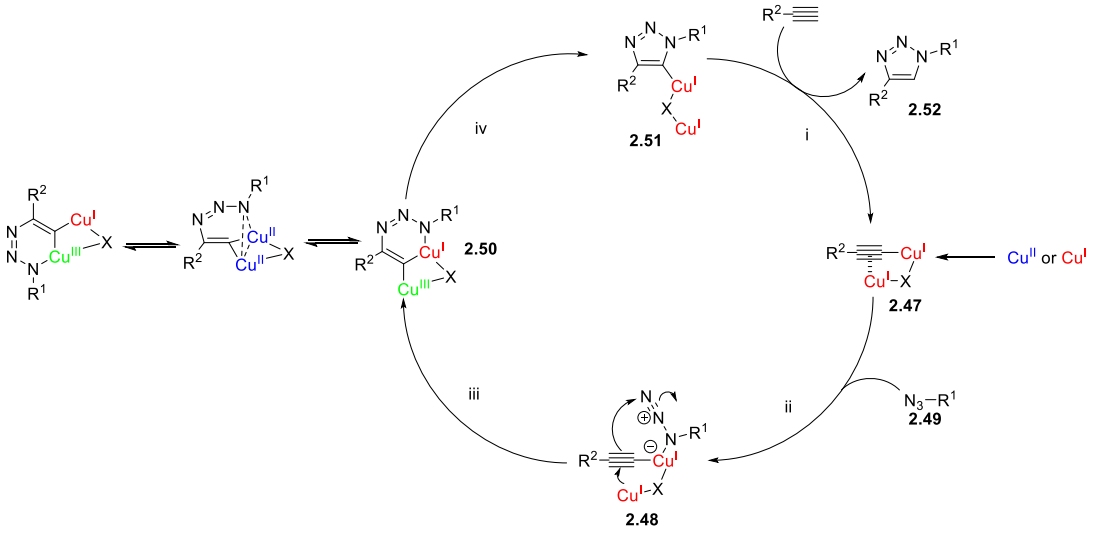

Scheme 2.5: Plausible mechanism for the Cu(I) catalysed reaction between organic azides and terminal [122].

2.3.1.3 Synthesis of Norbornene-Picolylamine diamide 2.55

Previously, NB diamide derivatives **2.53** and **2.54** (**Fig. 2.20**) had been prepared by our research group [123]. The purpose of this was to assess if the presence of 1,2,3-triazole was a structural requirement for NB compounds to undergo the cyclisation reaction discussed earlier (Scheme **2.1**). Thus, by preparing and exposing these compounds to acidic media in the same conditions as the triazolyl-bearing derivatives, it could be deduced whether the lack of a 1,2,3-triazole moiety in **2.53** and **2.54** prevents the cyclisation reaction. It was found that both compounds did not undergo the cyclisation reaction indicating the requirement for a 1,2,3-triazole moiety.

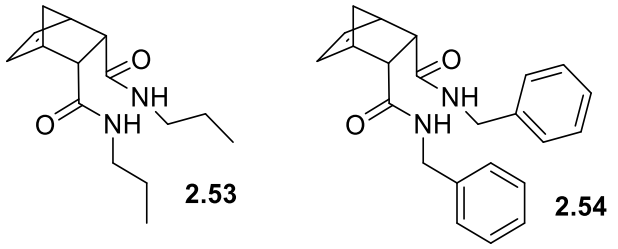

Figure 2.20: Structures of NB diamide compounds **2.53** and **2.54** previously prepared in our group [123].

An additional compound **2.55** was prepared according to Scheme **2.6**, as a means of assessing whether it was necessary for the *cis*-NB compounds to have a triazole ring in order to undergo the cyclisation reaction. It was proposed to investigate the effect of another heterocycle with a weakly basic nitrogen such as pyridine (pK_a of pyridinium 5.2). Thus, derivative **2.55** was prepared using 2-picolylamine. In addition, the distance between the amide functional groups in both NB compounds **2.35** and **2.55** and the corresponding nitrogen atoms is similar, which allows for a more direct comparison.

Compound **2.55** was prepared by the coupling of *cis*-5-norbornene-*endo*-2,3-dicarboxylic to 2-picolylamine using EDCI as the coupling reagent. Though previous coupling reactions using *cis*-5-norbornene-*endo*-2,3-dicarboxylic were found to typically work using TBTU as the coupling reagent, this reaction was found to be unsuccessful using TBTU.

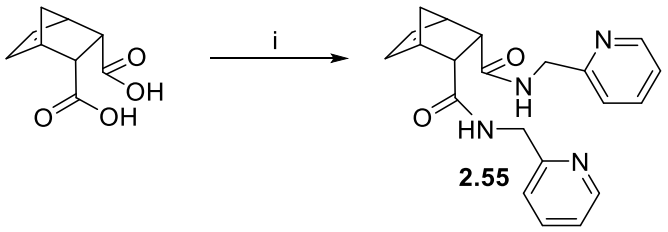

Scheme 2.6: Synthesis of 2-picolylamine coupled norbornene compound **2.55**. *Reagent and conditions*; i) 2-Picolylamine, EDCI, NEt_3, DMF, 16 h, 35%.

The ^1H NMR spectrum of diamide compound **2.55** is shown in Figure **2.21**. The key signals for this compound are the aromatic protons (purple circles) found at 8.43, 7.53 and 7.10 ppm. The newly formed amide proton peak (green circle) is found as a

broad singlet at 7.20 ppm while the methylene protons (blue circle) adjacent to the amide functional group is found as a multiplet at 4.33 ppm.

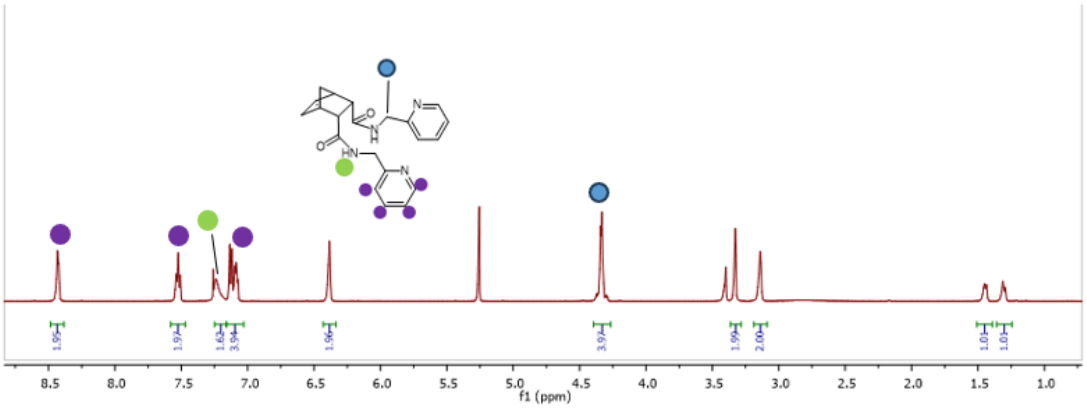

Figure 2.21: ^{1}H NMR spectrum of compound **2.55**.

2.3.1.4 Synthesis of cyclisation reaction product compounds 2.37, 2.59, 2.60, 2.67, 2.68 and 2.69

In order to monitor the proposed cyclisation reactions, a number of standard compounds were synthesised which correspond to the cyclic imide products formed. Cyclic imides **2.37**, **2.59**, and **2.60** and three amino-triazolyl products **2.67**, **2.68** and **2.69** were prepared for each of the three corresponding and previously discussed 1,2,3-triazolyl NB compounds **2.35**, **2.45** and **2.46** respectively. A sample of 2-picolylamine was to be used as possible elimination product from the 2-picolylamine-NB compound **2.55**.

The cyclic imide compounds **2.37**, **2.59** and **2.60** were prepared according to Scheme **2.7** below. Initially, *cis*-5-norbornene-endo-2,3-dicarboxylic anhydride was reacted with propargylamine and triethylamine in anhydrous toluene at 120 ^{o}C overnight. This resulting compound **2.56** was then reacted with the necessary sugar azide **2.40** or **2.41** or benzyl azide, using a catalytic system of copper sulfate pentahydrate and sodium ascorbate in the microwave at 100 ^{o}C for typically 30 minutes. This yielded the acetylated glycoconjugates, **2.57** and **2.58**, and the non-carbohydrate-containing NB compound **2.59**. The final step in the preparation of these compounds was again the deacetylation of the acetyl protecting groups in both glycoconjugates under mild basic conditions to give **2.37** (galactose) and **2.60** (mannose) derivatives.

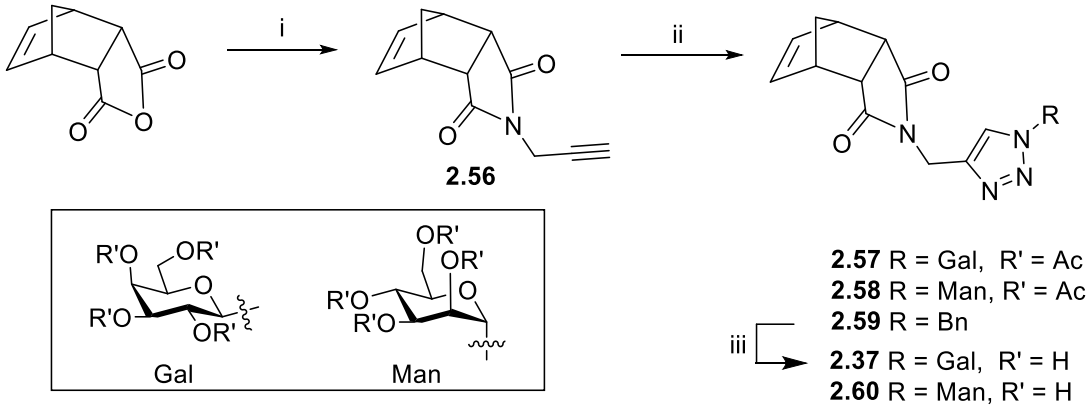

Scheme 2.7: Synthesis of cyclic imide reaction product compounds **2.37**, **2.59** and **2.60**. *Reagent and conditions*; i) Propargylamine, NEt_3, Anhydrous Toluene, 120 °C, 16 h, 99%; ii) O-acetyl sugar azide **2.40** or **2.41** or Benzyl azide, $CuSO_4.5H_2O$/Na Asc, CH_3CN/H_2O, 30 mins (MW, 100 °C), 16-63%; iii) MeOH, H_2O, NEt_3, 45 °C for **2.37** and **2.60**, 66-69%.

The three ammonium-triazolyl product compounds **2.67**, **2.68**, and **2.69** were prepared according to Scheme **2.8**. The first step was the protection of the amine functional group in propargylamine using di-*tert*-butyl dicarbonate and triethylamine in DCM overnight. The resulting *N*-protected alkyne **2.61** was then reacted in a CuAAC reaction using the same conditions as previously described. The removal of the acetyl groups in the galactosyl and mannosyl derivatives **2.62** and **2.63,** respectively, was achieved using mild basic conditions. The final step was the *N*-Boc deprotection using TFA to give compounds **2.67**, **2.68**, and **2.69**.

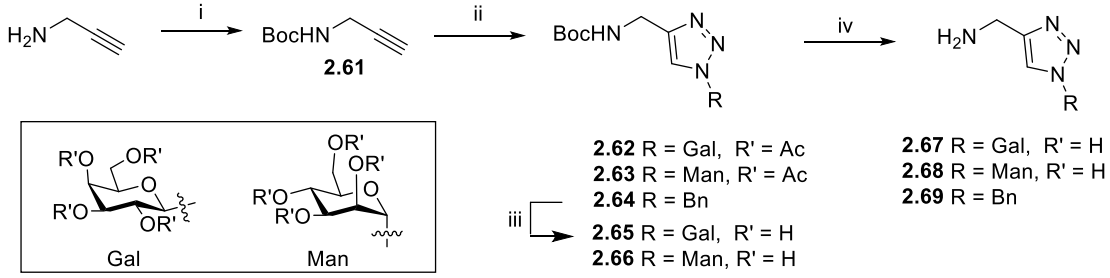

Scheme 2.8: Synthesis of amino-triazolyl reaction product compounds **X**-**X**. *Reagent and conditions*; i) Di-tert-butyl dicarbonate, NEt_3, DCM, 16 h, 71%; ii) O-acetyl sugar azide **2.40** or **2.41** or Benzyl azide, $CuSO_4.5H_2O$/Na Asc, CH_3CN/H_2O, 30 mins (MW, 100 °C), 33-81%; iii) MeOH, H_2O, NEt_3, 45 °C for **2.62** and **2.63**, 92%; iv) TFA, Anhydrous DCM (for **2.64**) or H_2O (for **2.65** and **2.66**), 91-96%.

2.3.1.5 Synthesis of 'Hybrid' norbornene compounds

The asymmetric 'hybrid' *cis*-NB compounds were envisaged to combine a galactose moiety and an antifungal drug. Initially, the target compound **2.70** (**Scheme 2.9**),

containing fluconazole, was to be prepared. Fluconazole, which belongs to the azole family of antifungal drugs, is one of the most commonly used treatments against fungal infections [124].

The first attempt to prepare fluconazole derivative **2.70** involved a ring opening of *cis*-5-norbornene-*endo*-2,3-dicarboxylic anhydride through reaction with fluconazole. However, this reaction was unsuccessful. The reaction was repeated in acetonitrile with triethylamine, in *N,N*-dimethylformamide with sodium hydride and in chloroform with triethylamine. In all cases the desired reaction did not occur. We reconsidered the suitability of fluconazole for the proposed chemistry, as it is a tertiary alcohol, and it suffers from inherently lower nucleophilicity.

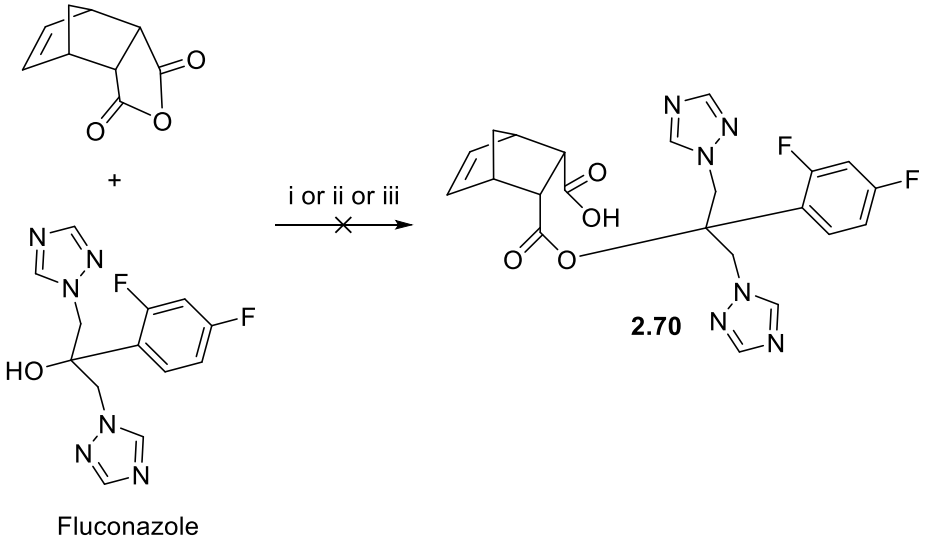

Scheme 2.9: Attempts to synthesise 'Hybrid' norbornene compound **2.70**. *Reagent and conditions*; i) Fluconazole, ACN, 3 days, 45-50 ^{o}C, unsuccessful; or ii) Fluconazole, NaH, DMF, 16 h, RT, unsuccessful; or iii) Fluconazole, NEt_3, Chloroform, 2 days, 45-50 ^{o}C, unsuccessful.

A coupling reaction was investigated using compound **2.71**, prepared from the ring opening of *cis*-5-norbornene-*endo*-2,3-dicarboxylic anhydride with propargyl amine, and fluconazole (**Scheme 2.10**). This reaction was attempted using EDCI as the coupling reagent. However, again it was unsuccessful.

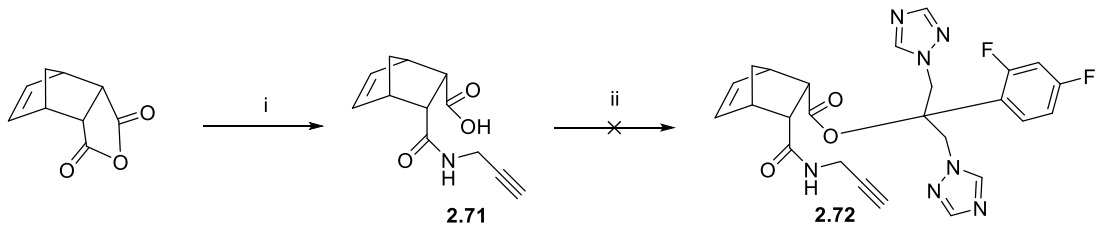

Scheme 2.10: Attempts to synthesise 'Hybrid' norbornene compound **2.72**. *Reagent and conditions*; i) Propargylamine, ACN, 50 mins, 45-50 ^{o}C, reacted on without further purification; ii) Fluconazole, EDCI, NEt_3, DMF, 16 h, RT, unsuccessful.

It was at this point that it was decided to assess the feasibility of preparing such asymmetric *cis*-norbornene compounds. Benzyl alcohol was chosen as a model compound with a primary alcohol. Therefore, benzyl alcohol should have improved nucleophilicity relative to fluconazole. Thus, we set out to prepare derivative **2.73** (**Fig. 2.22**) to determine if such compounds were synthetically feasible.

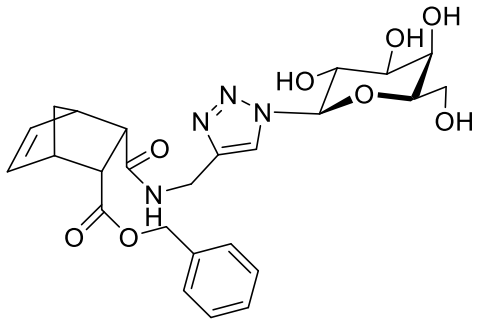

2.73

Figure 2.22: Structure of model compound **2.73**.

In the first attempts to prepare **2.73**, *cis*-5-norbornene-endo-2,3-dicarboxylic anhydride was reacted with propargylamine in acetonitrile; the desired product **2.74** precipitates out of solution once formed and can be isolated via centrifugation. These conditions were adapted from a literature procedure for a very similar reaction [125]. The resulting product **2.74** was reacted on with benzyl alcohol using either TBTU or EDCI in an attempt to prepare **2.75** (**Scheme 2.11**). In both cases, the reaction was unsuccessful.

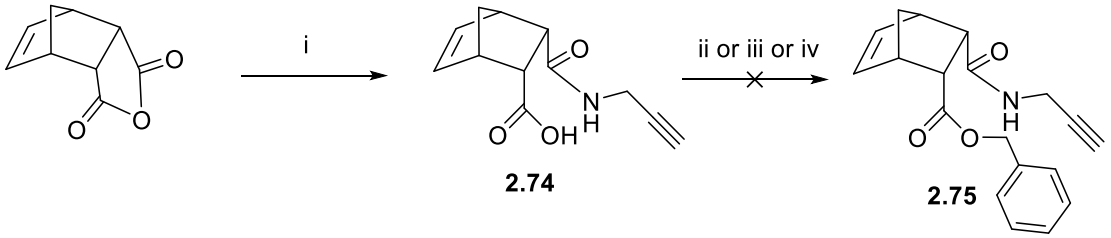

Scheme 2.11: Attempts to synthesise 'Hybrid' norbornene compound **2.75**. *Reagent and conditions*; i) Propargylamine, ACN, 50 mins, 45-50 ^{o}C, reacted on without further purification; ii) Benzyl alcohol, EDCI, NEt_3, DMF, 16 h, RT, unsuccessful; or iii) Benzyl alcohol, TBTU, NEt_3, DMF, 16 h, RT, unsuccessful; or iv) Benzyl alcohol, EDCI, NEt_3, DMAP, DMF, 16 h, RT, unsuccessful.

An alternative reaction pathway was then attempted, firstly by reacting benzyl alcohol with *cis*-5-norbornene-*endo*-2,3-dicarboxylic anhydride (**Scheme 2.12**). The initial conditions using acetonitrile as the reaction solvent were unsuccessful. After screening a number of conditions, compound **2.76** was prepared using chloroform as the solvent and triethylamine (Scheme **2.12**). After purification using flash column chromatography, a coupling reaction between **2.76** and propargylamine using TBTU yielded product **2.77**.

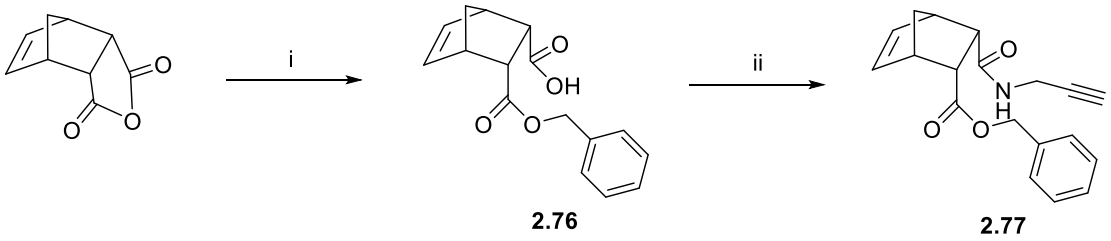

Scheme 2.12: Synthesis of compound **2.77**. *Reagent and conditions*; i) Benzyl alcohol, NEt_3, chloroform, 16 h, RT, 86%; ii) Propargylamine, TBTU, NEt_3, DMF, 16 h, RT, 52%.

The ^{1}H NMR spectrum of intermediate compound **2.76** is shown in Figure **2.23**. The most important signals in this spectrum are the aromatic protons (red circle) found as a multiplet at 7.33 ppm. The alkene protons of the norbornene moiety (green circles) are found as two doublet of doublets at 6.29 and 6.22 ppm respectively. The bridging diastereotopic protons (orange circle) of the norbornene moiety are found as two doublets at 1.49 and 1.33 ppm respectively. Meanwhile, the benzyl methylene protons (blue circle) are found as two doublet peaks at 5.10 and 4.93 ppm respectively. This is due to the asymmetric environment they are in.

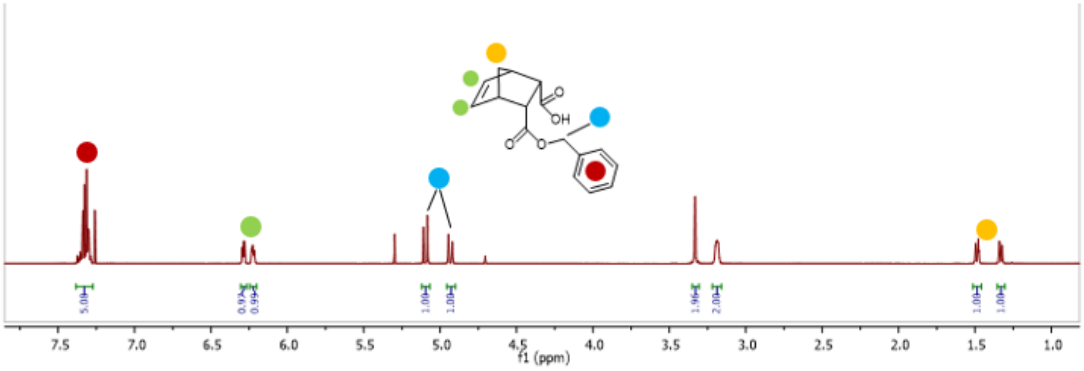

Figure 2.23: ^{1}H NMR spectrum for compound **2.76**.

Secondly, the ^{1}H NMR spectrum of the asymmetric norbornene compound **2.77** is shown in Figure **2.24**. There are a number of important indicative signals for this compound. The aromatic protons peaks (red circle) are found as a multiplet at 7.29 ppm. The newly formed amide proton (green circle) is observed as a broad singlet at 6 ppm. The benzyl methylene protons (blue circle) are found as two doublets at 5.06 and 4.96 ppm respectively. The methylene protons of the propargyl moiety (orange circle) appear as a multiplet at 3.85 ppm. Finally, the alkynyl proton (yellow circle) appears as a triplet at 2.16 ppm.

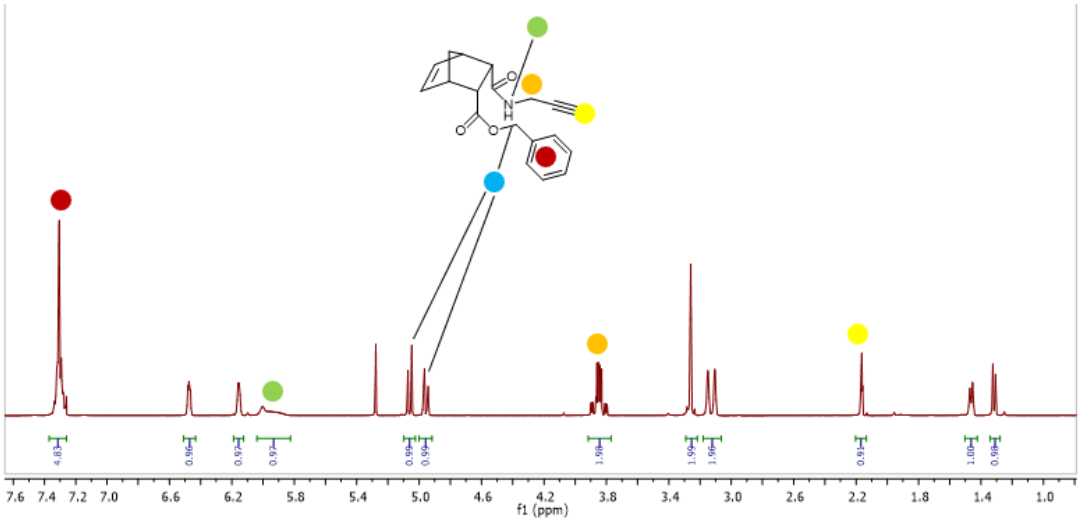

Figure 2.24: ^{1}H NMR spectrum for compound **2.77**.

A CuAAC reaction between **2.77** and the deacetylated sugar azide **2.78** using microwave at 100 °C for 30 mins was then attempted, however, this reaction was unsuccessful (**Scheme 2.13**). Based on NMR analysis of the crude reaction mixture it

appeared that the cyclic imide product **2.37** was formed. Providing further evidence that such *cis*-NB compounds have a tendency to undergo such cyclisation reactions.

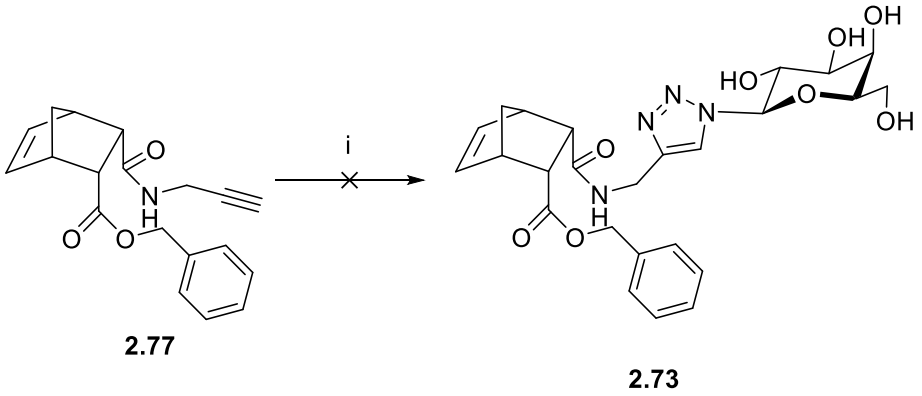

Scheme 2.13: Attempt to synthesise 'Hybrid' norbornene compound **2.73**. *Reagent and conditions*; i) **2.78**, $CuSO_4.5H_2O$, Na asc, ACN/H_2O, (MW, 100 ^oC, 30 mins), unsuccessful.

Attempts made to prepare **2.73** via a ring opening reaction of compound **2.37** with benzyl alcohol were also unsuccessful (**Scheme 2.14**).

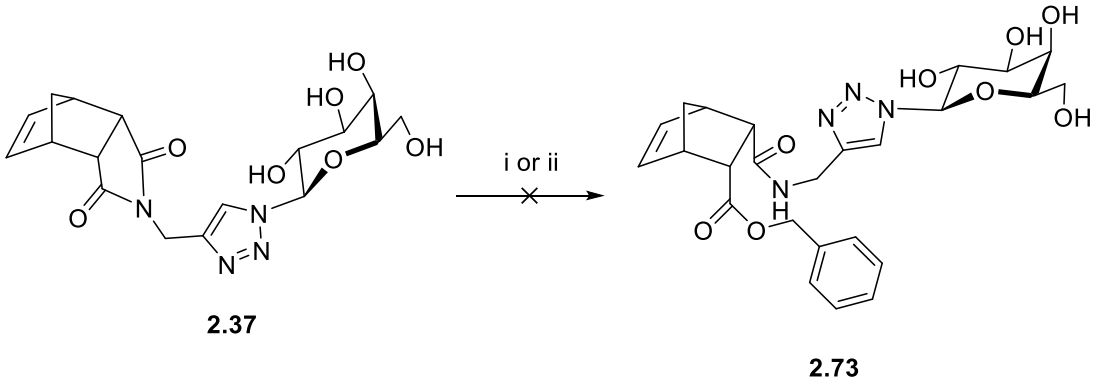

Scheme 2.14: Attempt to synthesise 'Hybrid' norbornene compound **2.73**. *Reagent and conditions*; i) Benzyl alcohol, 60 ^oC, 10 mins, unsuccessful; or ii) Benzyl alcohol, H_2O, 60 ^oC, 15 mins, unsuccessful.

Finally, a successful synthesis for the desired asymmetric *cis*-NB compound **2.73** was achieved (**Scheme 2.15**). Compound **2.76** was coupled with amino-triazolyl **2.67** using TBTU as the coupling reagent. Although compound **2.73** was formed in this reaction, the presence of cyclic imide **2.37** in the resulting reaction mixture was interesting, as it suggests that upon formation of the desired compound **2.73**, this compound may then undergo the previously seen cyclisation reaction to form **2.37** (**Scheme 2.15**). The two compounds were found to be present in a ratio of approximately 1:0.15 (**2.73**:**2.37**). The corresponding 1,2,3-triazole signals in the ^1H

NMR spectrum (**Fig. 2.25**) were found at 8.13 ppm and 8.01 ppm respectively for compounds **2.37** and **2.73**. The ratio of desired product **2.73** to cyclic imide product **2.37** was determined by the peak integrals. The peaks for the anomeric protons in compounds **2.37** and **2.73** were found at 5.61 ppm and 5.57 ppm respectively, again the peak integrals confirmed the ratio of products. HRMS confirmed the presence of both compounds **2.37** and **2.73** (**Fig. 2.26**).

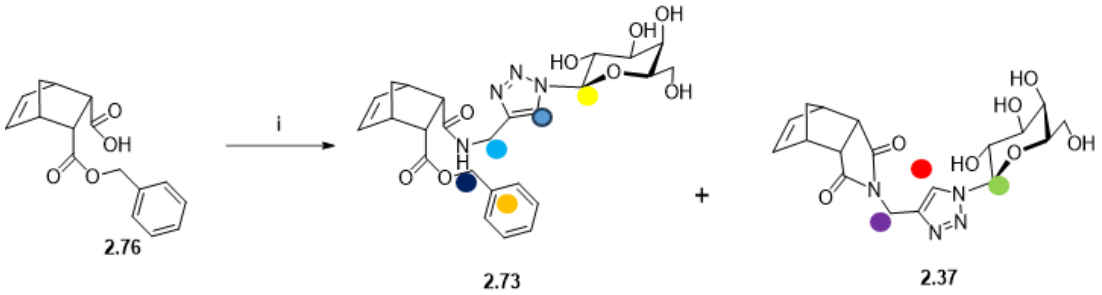

Scheme 2.15: Attempt to synthesise of 'Hybrid' norbornene compound **2.73.** *Reagent and conditions*; i) **2.67**, TBTU, DIPEA, DMF, 1.5 h, RT, mixture of **2.73** and **2.37**, 46%.

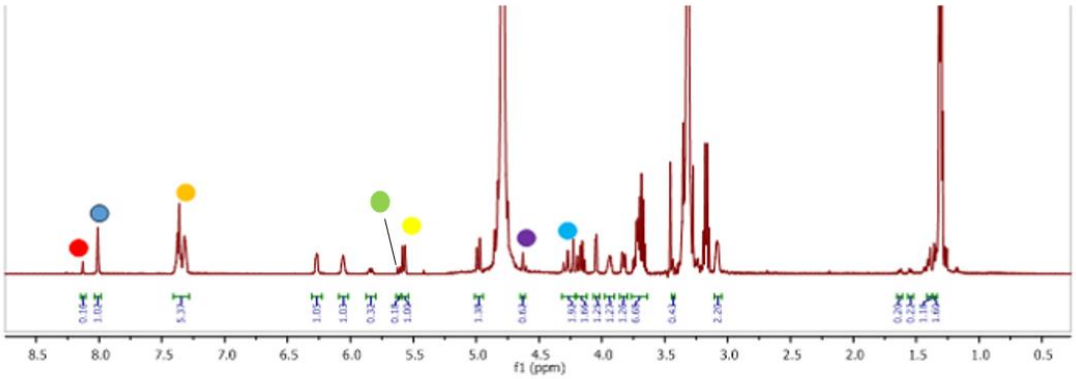

Figure 2.25: ^{1}H NMR of reaction mixture containing **2.37** and **2.73**.

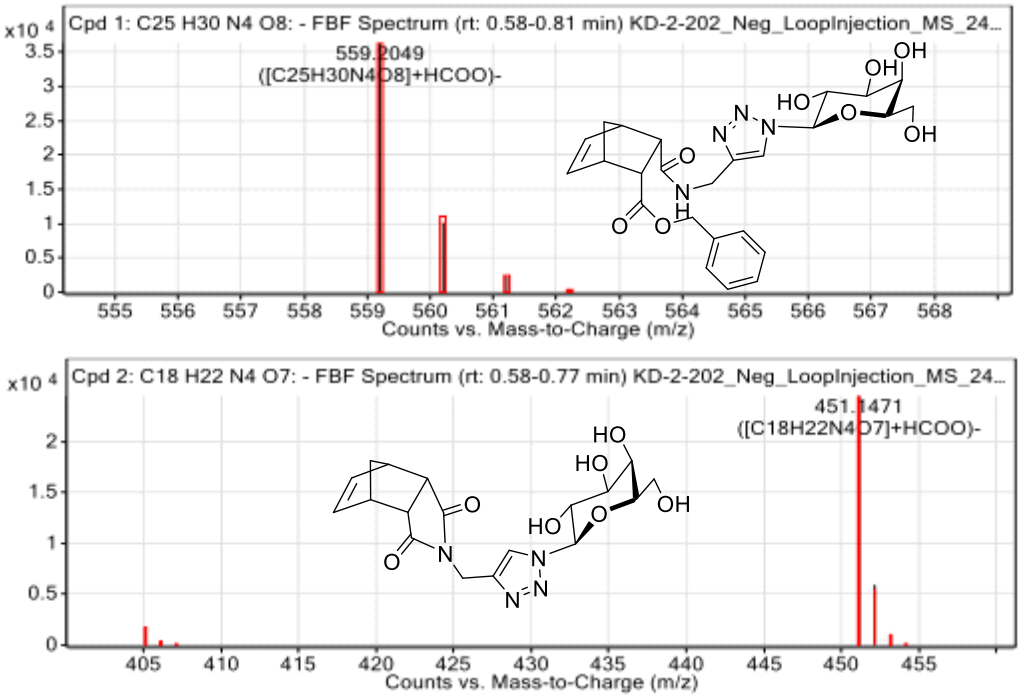

Figure 2.26: Successful HRMS detection of compounds **2.73** and **2.37**.

Once a feasible synthetic approach had been established, the preparation of both asymmetric derivatives **2.80** and **2.81** was undertaken (**Scheme 2.16**). Quorum-sensing (QS) molecules are cell-cell communication compounds and are produced by microogranisms controlling different behaviours. Research has intensified into the use of these QS compounds to treat microbial infections as they control many important infectious processes. Farnesol (**Fig. 2.27**) is a QS compound that blocks the yeast-to-hyphae transition by inducing morphological changes in the yeast cell wall and by suppressing the expression of aspartyl proteinases in *C. albicans*. In addition, Farnesol has been shown to act as an anti-biofilm agent, farnesol effects different stages of biofilm development: cell adhesion to substrates, mature biofilm structure and cell dispersion from the biofilm [116]. Tyrosol (**Fig. 2.27**) is another QS compound and has been reported to inhibit the formation of biofilms in *C. albicans* [116].

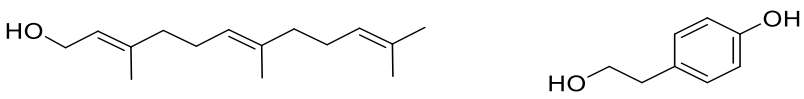

Figure 2.27: Chemical structures of Farnesol (left) and Tyrosol (right).

The reaction of *cis*-5-norbornene-*endo*-2,3-dicarboxylic anhydride with farnesol or tyrosol, and triethylamine in chloroform resulted in intermediate acids **2.78** and **2.79**, respectively (**Scheme 2.16**). Following purification by column chromatography, the second and final step was the coupling of these derivatives with the amino-triazolyl galactoside **2.67**. The coupling conditions for the respective compounds **2.80** or **2.81** were found to be different. Initially both reactions were attempted using TBTU as the coupling reagent. However, it was found that TBTU could successfully be used to prepare the tyrosol derivative **2.81** whereas the synthesis of the farnesol derivative **2.81** was achieved using COMU as the coupling reagent. COMU has an improved reactivity, stability and solubility profile, relative to TBTU, due to the presence of a morpholino group.

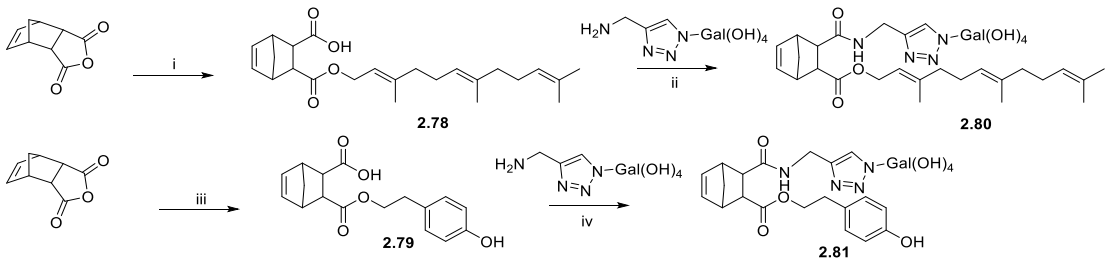

Scheme 2.16: Synthesis of 'Hybrid' NB compounds **2.80** and **2.81**. *Reagent and conditions*; i) Farnesol, NEt_3, Chloroform, 16 h, RT, 19%; ii) COMU, DIPEA, DMF (partially pure, 7 mg, 4%); iii) Tyrosol, NEt_3, Chloroform, 16h, 50 ^oC, 7%; iv) TBTU, DIPEA, DMF, 12%.

The ^1H NMR spectrum for the 'hybrid' norbornene compound **2.81** is shown in Figure **2.28**. Due to the complex, asymmetric nature of this compound there are a number of important signals to highlight. The amide proton (orange circle) is found as a triplet at 8.27 ppm. The triazolyl proton (red circle) is found as a doublet, which is unusual, at 8.06 ppm. The unusual multiplicity of the triazolyl peak may be due to the complex asymmetric chemical environment it exists or perhaps due to the partial double bond character of the amide bond near it. As a result of this there may be a lack of free rotation about this bond, leading to distinct chemical environments. Coupled with the asymmetric nature of **2.81**, due to a lack of a plane of symmetry, this may explain the unusual multiplicity of the triazolyl proton. The aromatic protons (yellow and light green circles) are split into two sets of equivalent proton pairs, both of which appear as doublets at 7.04 and 6.71 ppm respectively. The anomeric proton (dark green circle) appears as a doublet at 5.52 ppm. The methylene protons (light blue circle) adjacent to the amide functional group appear as a multiplet at 4.40 ppm. Lastly, there are two sets of methylene protons (purple and navy/dark blue circles) from the tyrosol-ester moiety. The methylene protons adjacent to the ester functional group (purple circle) appear as diastereotopic protons at 4.14 and 4.01 ppm as multiplets. Note, for both these peaks there are also carbohydrate proton peaks underneath these peaks hence the integration for both peaks are two as opposed to the expected integration of one. Finally, the other set of methylene protons (navy/dark blue circle) adjacent to the aromatic ring appear as a multiplet at 2.75 ppm.

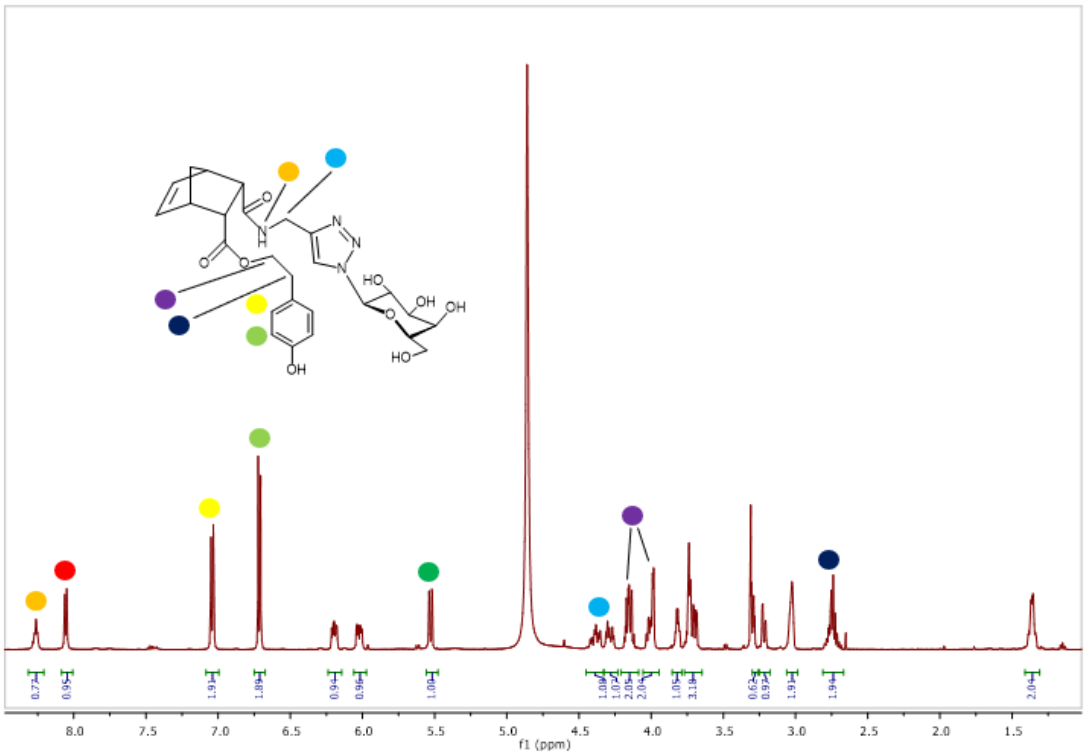

Figure 2.28: ^{1}H NMR spectrum of compound **2.81**. Note: Anomeric proton is assigned as dark green circle while the triazole proton is assigned red circle.

The ^{13}C, HSQC and HMBC NMR spectra in figures **2.29**, **2.30** and **2.31** respectively provide further evidence for the successful preparation of compound **2.81**. Figure **2.29** shows the two distinct carbonyl carbon atoms of compound **2.81** with only a slight difference in the chemical environment of both carbon atoms. These carbon atoms are found at 174.7 ppm and 174.4 ppm.

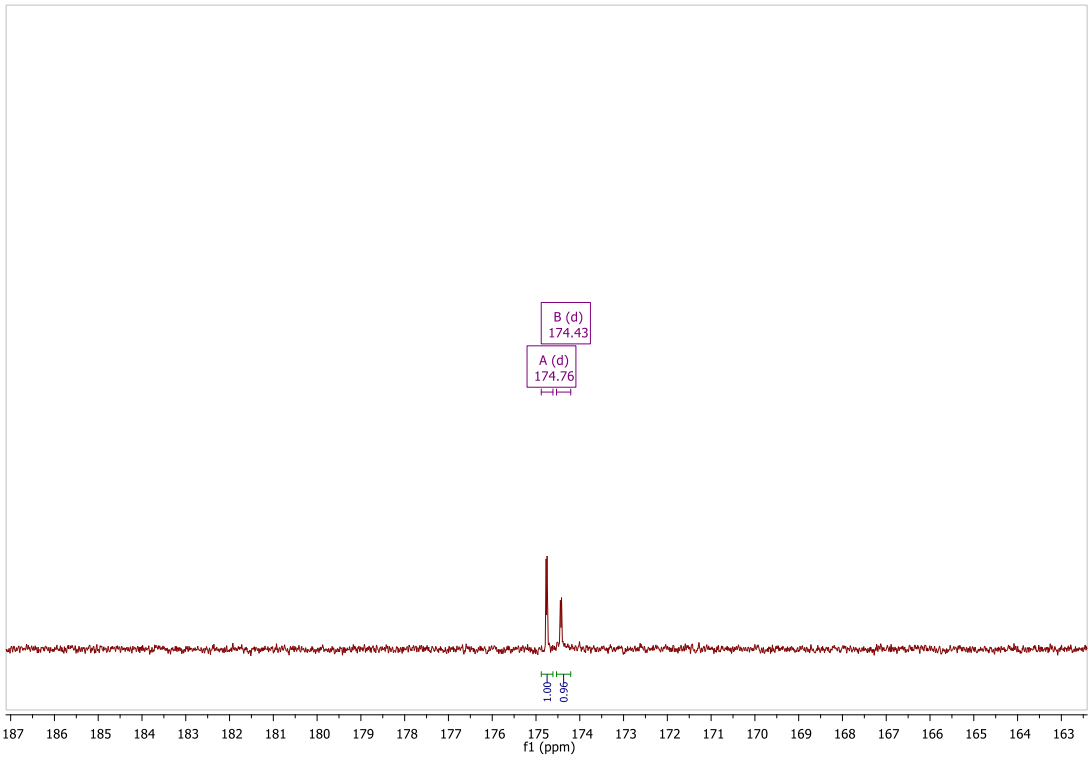

Figure 2.29: ^{13}C NMR spectrum highlighting carbonyl carbon peaks in compound **2.81**.

The HSQC in Figure **2.30** provides evidence of the asymmetric/diastereotopic nature of compound **2.81**. The methylene protons adjacent to the triazolyl moiety appear as two separate signals at 4.41 and 4.30 ppm. Meanwhile, the methylene protons of the tyrosyl moiety nearest the ester moiety are also found as two separate signals at 4.16 and 4.02 ppm.

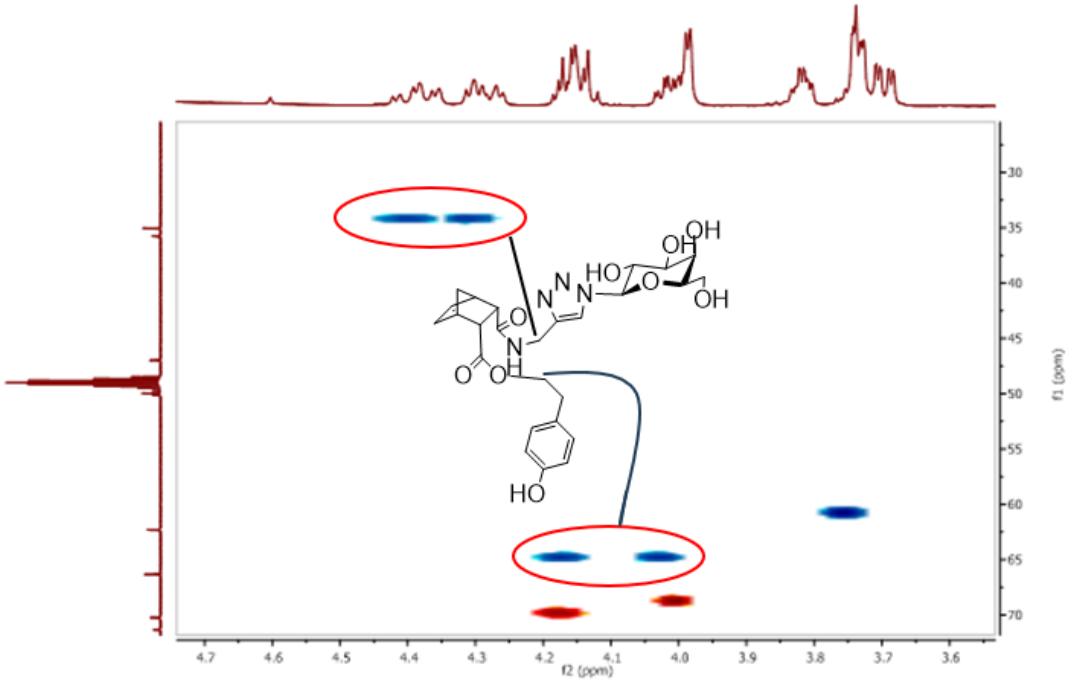

Figure 2.30: HSQC NMR spectrum highlighting methylene protons in compound **2.81**.

Finally, the HMBC shown in Figure **2.31** provides evidence for the successful coupling of **2.67** with **2.79**. The methylene protons adjacent to the triazolyl moiety couple to the carbonyl carbon that is slightly less deshielded at 174.4 ppm, while the methylene protons of the tyrosyl moiety (nearest the ester moiety) couple to the more deshielded carbonyl carbon at 174.7 ppm. HRMS analysis also confirmed successful synthesis of the desired compound **2.81** (**Fig. 2.32**).

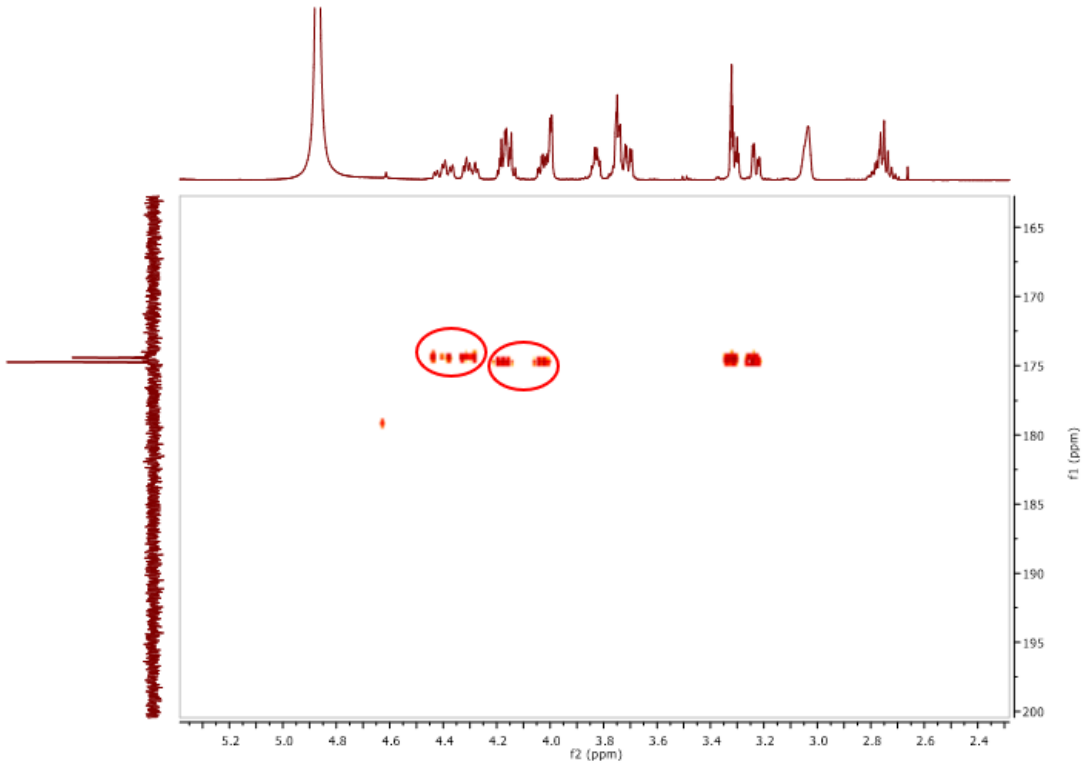

Figure 2.31: HMBC NMR spectrum highlighting coupling of methylene protons to two separate carbonyl carbon atoms in compound **2.81**.

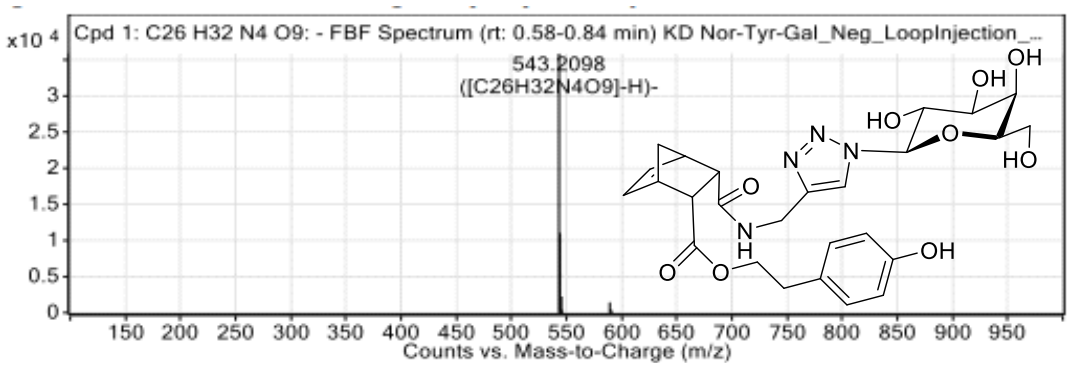

Figure 2.32: Successful HRMS detection of compound **2.81**.

The ^{1}H NMR spectrum for compound **2.80**, which could only be purified partially (see section **2.4**), is shown in Figure **2.33**. The amide proton (orange circle) is observed as a doublet of doublets at 8.26 ppm, the splitting pattern of this peak confirms the diastereotopic nature of the adjacent methylene protons (light blue circle). The triazolyl peak (red circle) is observed as a doublet at 7.96 ppm, also as a result of the asymmetry in this compound, similar to compound **2.81**. The anomeric proton of the galactoside moiety (green circle), H-1, is observed as a doublet at 5.46 ppm. The

alkene proton (purple circle) nearest the ester functional group is found as a multiplet at 5.24 ppm. The methylene protons (yellow circle) adjacent to the ester functional group are also diastereotopic and are found as two separate multiplets at 4.45 and 4.24 ppm respectively. Meanwhile, the methylene protons adjacent to the amide functional group which as mentioned are also diastereotopic are observed as two separate peaks. These are found as a triplet of doublets and a multiplet at 4.33 and 4.11 ppm respectively. Finally, the methyl protons present in the farnesyl moiety are found as two multiplets at 1.65 and 1.57 ppm.

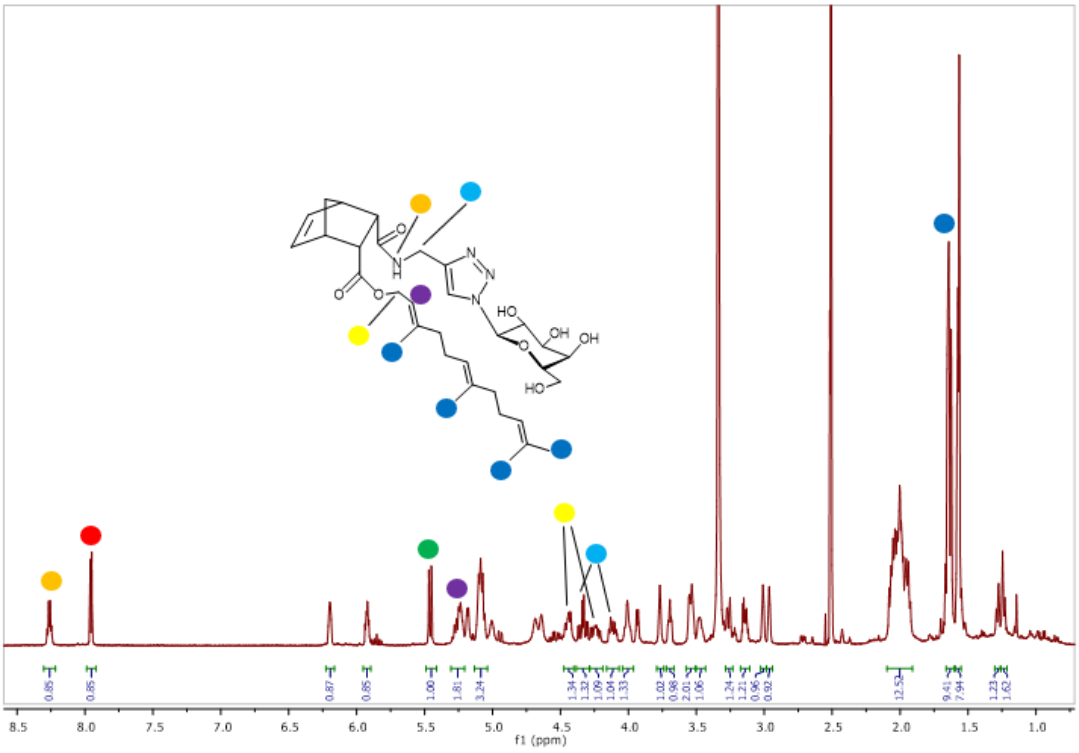

Figure 2.33: ^{1}H NMR spectrum of compound **2.80**. Note: Anomeric proton is assigned as green circle, while the triazolyl proton is assigned as red circle.

The HSQC in Figure **2.34** provides evidence of the asymmetric/diastereotopic nature of compound **2.80**. The methylene protons adjacent to the triazolyl moiety appear as two separate signals at 4.32 and 4.10 ppm. Meanwhile, the methylene protons of the farnesyl moiety nearest the ester moiety are also found as two separate signals at 4.43 and 4.23 ppm. HRMS analysis also confirmed successful synthesis of the desired compound **2.80** (**Fig. 2.35**).

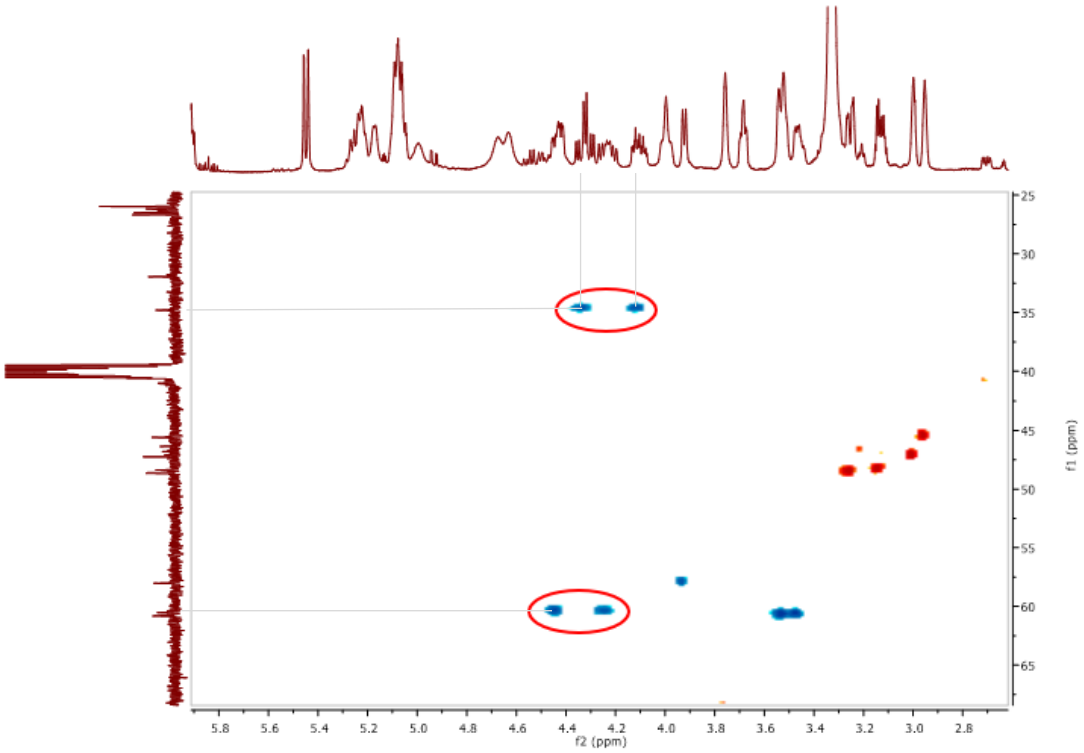

Figure 2.34: HSQC NMR spectrum highlighting methylene protons in compound **2.80**.

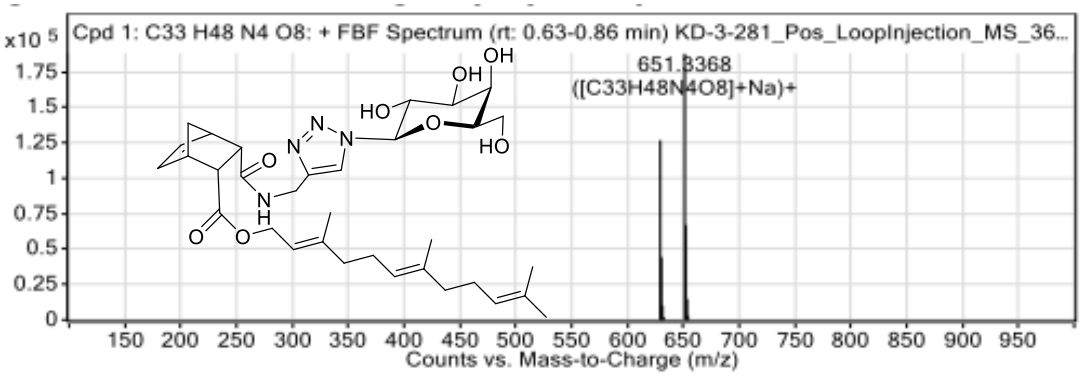

Figure 2.35: Successful HRMS detection of compound **2.80**.

2.3.2 Evaluation of cyclisation/elimination of symmetric NB compounds

In order to elucidate the structural requirements and assess the ability of NB compounds to undergo the cyclisation reaction under acidic conditions as observed by Martin and coworkers [114], these compounds were stirred in either a pH 2 or pH 5 aqueous buffer or treated with Amberlite H^+ resin to replicate the conditions used by Martin *et al.* The reactions were carried out for a time period ranging from 3 h to 7 days.

2.3.2.1 Cyclisation/elimination evaluation of 2.45

Compound **2.45**, which does not feature any carbohydrate moiety, was stirred in MeOH with Amberlite H^+ for a period of 7 days at RT. The progress of the reaction was monitored by HPLC. Figure **2.36** shows the results of this assessment. Analysis of aliquots of the reaction mixtures after 1 day (blue) show the presence of both the starting material, compound **2.45** (retention time (rt) *ca.* 1.9 mins (red)) and the cyclic product **2.59** (rt *ca.* 4.4 mins, green). However, after 7 days (yellow) it appears that all starting material **2.45** has been consumed. This confirms the capability of compound **2.45** to undergo the proposed cyclisation reaction and also indicates that a carbohydrate moiety is not absolutely essential for this reaction to occur. However, it is not yet known if a carbohydrate moiety may influence the rate of such a reaction.

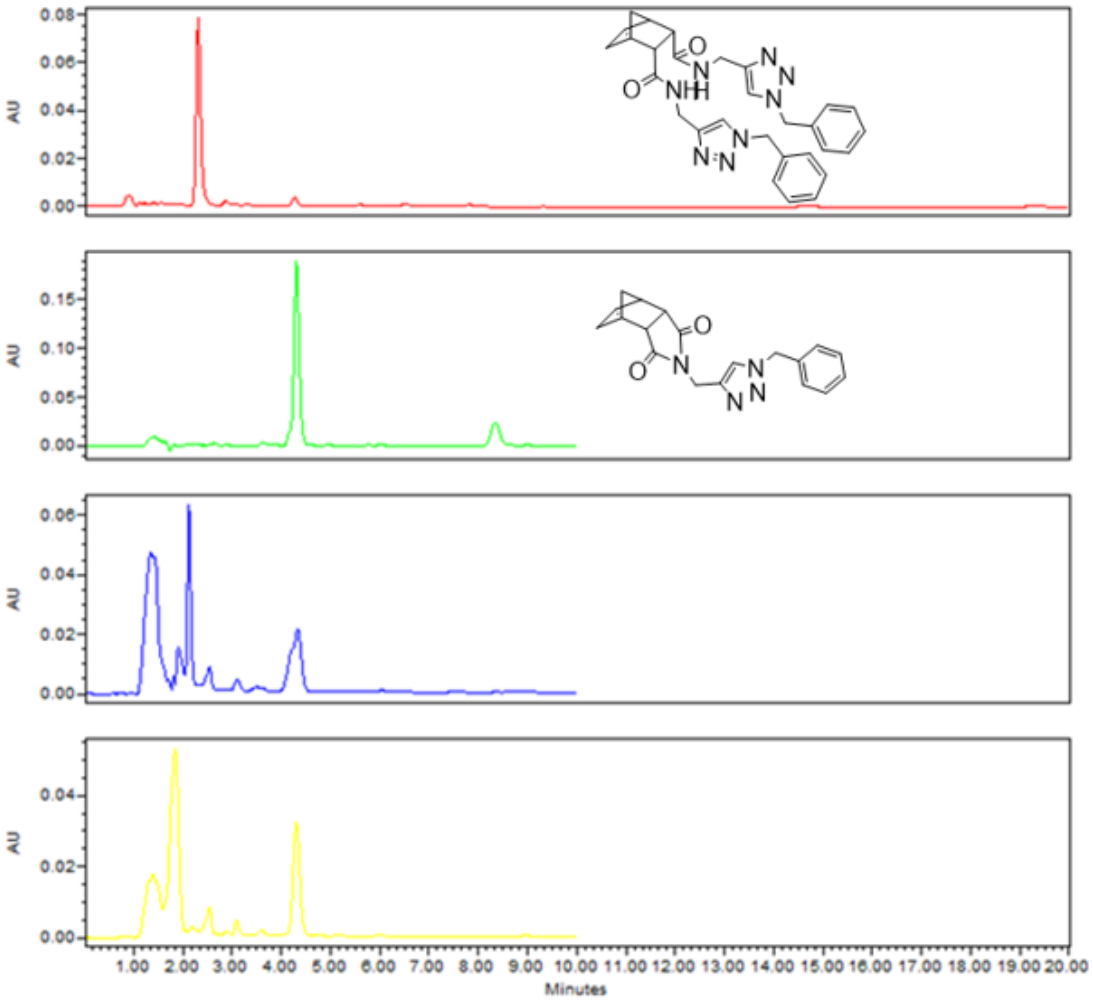

Figure 2.36: Reaction of compound **2.45** at RT with Amberlite H^+ in MeOH: Chromatograms (top to bottom); 1) **2.45**, 2) **2.59**, 3) **2.45** (after 1 day) , 4) **2.45** (after 7 days). HPLC Conditions: 60:40 H_2O:ACN, 1 mL/min, Agilent Eclipse Plus C_{18} column 3 µm, Detector set at 254 nm.

2.3.2.2 Cyclisation/elimination evaluation of 2.55

Picolylamine derivative compound **2.55** was evaluated for its tendencies to undergo cyclisation/elimination by stirring a sample of **2.55** in MeOH with Amberlite H^+ for a period of 7 days at RT. The progress of the reaction was monitored by HPLC. Figure **2.37** shows the results of this assessment. Aliquots of the reaction mixture after 1 and 7 days (green and blue, respectively) still show the presence of starting material, compound **2.55** (rt *ca.* 1.8 mins, red). Another broad peak is observed after 1 day at rt *ca*. 1.4 mins, whose intensity appears to increase after 7 days reaction. It was not possible to establish if this new peak was due to the cyclization or hydrolysis reactions. In any case, it appears that compound **2.55** is less prone to undergo cyclisation when treated with the acidic resin Amberlite H^+ since, after 7 days, there is still a significant amount of starting material **2.55** unreacted. This may indicate that a 1,2,3-triazole ring, which **2.55** lacks, is necessary for such *cis*-5-NB compounds to undergo the proposed cyclisation reaction. This may be due to the 1,2,3-triazole ring possessing the optimal basic character to catalyse this reaction, further work is needed to provide further evidence for this theory.

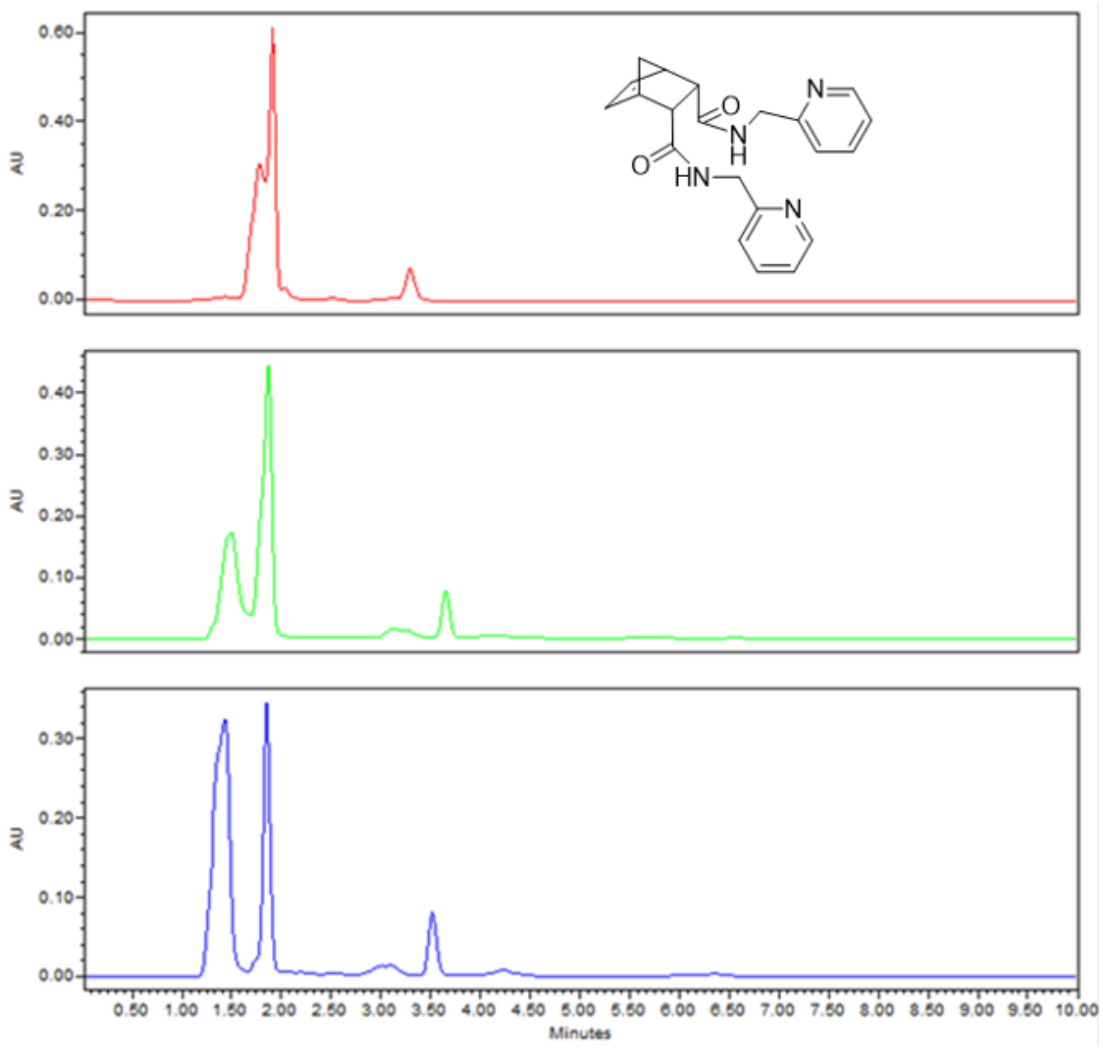

Figure 2.37: Reaction of compound **2.55** at RT with Amberlite H^+ in MeOH: Chromatograms (top to bottom); 1) **2.55**, 2) **2.55** (after 1 day), 3) **2.55** (after 7 days). HPLC conditions: 65:35 H_2O:ACN, 1 mL/min, Agilent Eclipse Plus C_{18} column 3 µm, Detector set at 254 nm.

The reaction with **2.55** in acidic media was also investigated in a 2:1 mixture of MeOH/pH 2 aqueous buffer for a period of 7 days at RT. Note, MeOH was necessary to solubilise **2.55** as it was not soluble in the aqueous pH 2 buffer used. Figure **2.38** shows the results of this assessment by HPLC. Once again, aliquots of the reaction mixtures taken after 1 and 7 days (green and blue, respectively) show the presence of starting material, compound **2.55** (rt *ca*. 1.8 mins, red). Similarly, another broad peak was observed at rt *ca*. 1.4 mins, albeit its increase in intensity was less pronounced after 7 days than when the reaction was carried out in Amberlite H^+. This further indicates that a 1,2,3-triazole moiety may be necessary for such *cis*-5-NB compounds to undergo the proposed cyclisation reactions.

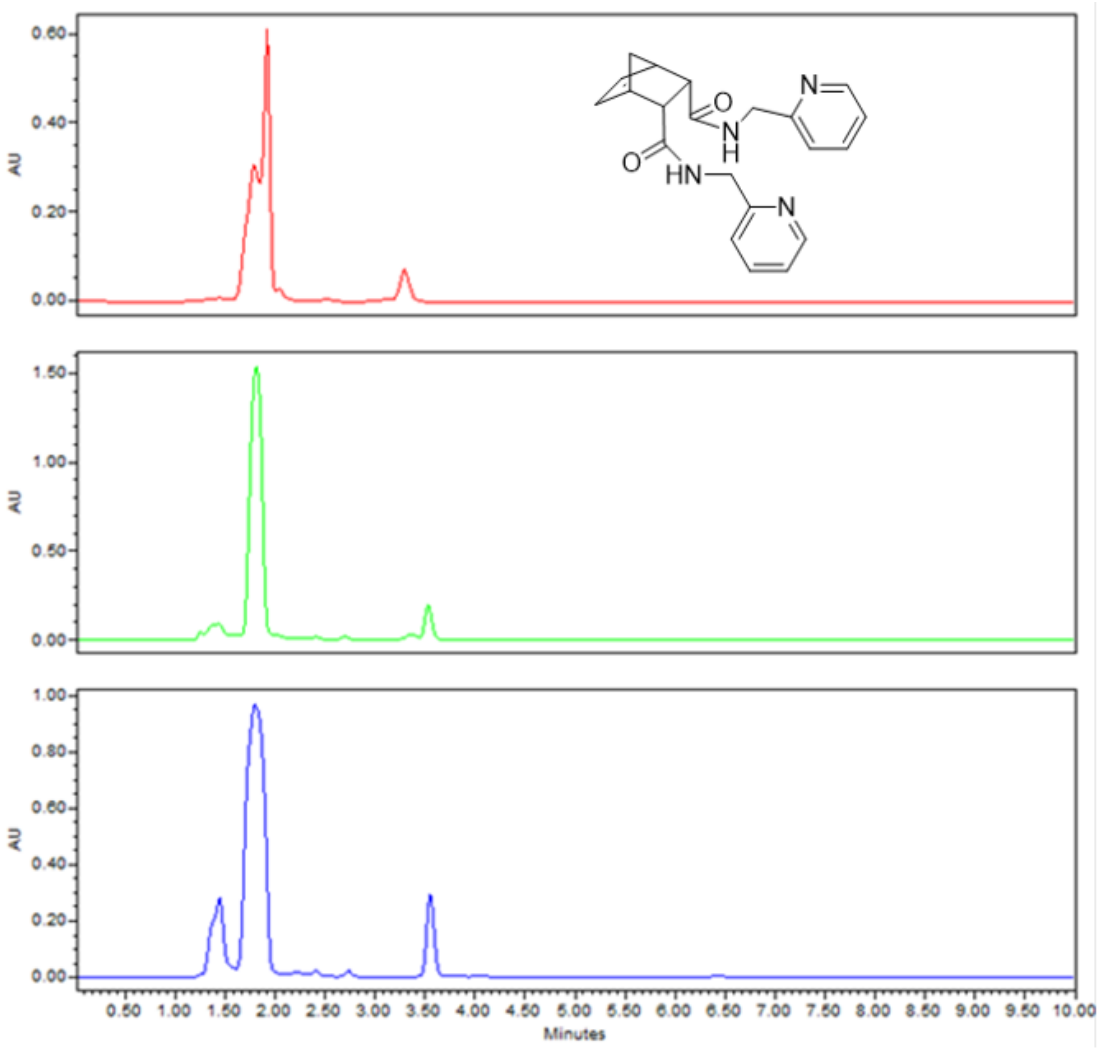

Figure 2.38: Reaction of compound **2.55** at RT in pH 2 buffer in a H_2O/MeOH mixture: Chromatograms (top to bottom); 1) **2.55**, 2) **2.55** (after 1 day), 3) **2.55** (after 7 days). HPLC conditions: 65:35 H_2O:ACN, 1 mL/min, Agilent Eclipse Plus C_{18} column 3 µm, Detector set at 254 nm.

2.3.2.3 Cyclisation/elimination evaluation of galactoside 2.35

Divalent NB-galactoside **2.35,** which was originally observed to undergo the cyclisation/elimination, was evaluated again. A sample of **2.35** in deionised water was stirred in Amberlite H^+ overnight at RT. This reaction was monitored by HPLC analysis. Figure **2.39** shows the results of this assessment. The NB-galactoside **2.35** starting material (red) and the cyclic imide elimination product **2.37** (green) have very similar rt (*c.a* 5.1 and 5 mins, respectively). The reaction mixture (yellow) shows a peak at rt *ca*. 4.5. mins, which could correspond to either the starting material, **2.35**, (red) or the cyclic product **2.37** (green). Interestingly, the reaction mixture (yellow) also shows a peak at rt *ca*. 2.6 mins, possibly corresponding to amino glycoconjugate

2.67 (blue, rt *ca*. 2.3 mins), which would result from the proposed elimination reaction. The discrepancies in rt may be due to the acidic Amberlite H^+ resin altering the pH of the aqueous aliquot taken. These results suggest that compound **2.35** can undergo the proposed cyclisation reaction, however it is not possible to confirm if the reaction has come to completion under these conditions.

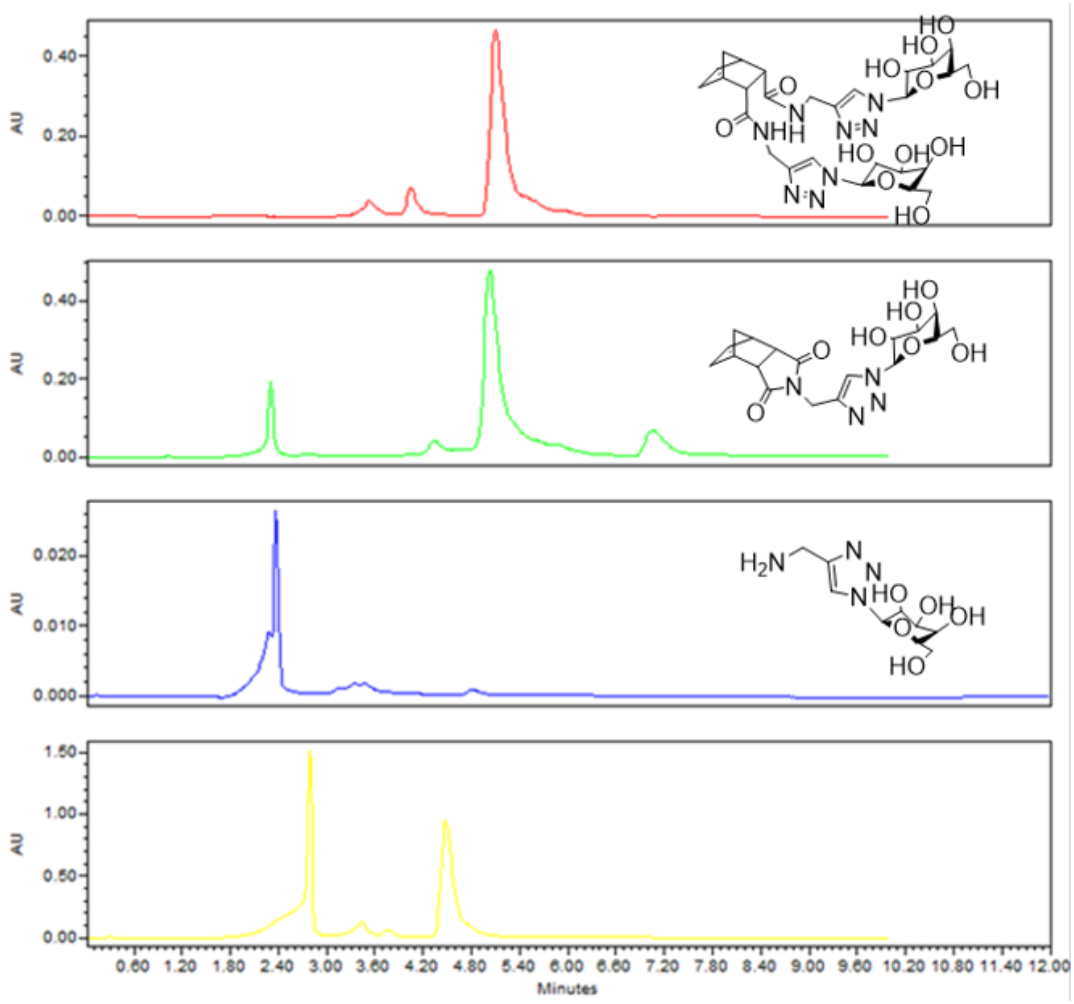

Figure 2.39: Reaction of compound **2.35** at RT with Amberlite H^+ in H_2O: Chromatograms (top to bottom); 1) **2.35**, 2) **2.37**, 3) **2.67**, 4) **2.35** (after 1 day). HPLC conditions: 95:5 H_2O:ACN, 1 mL/min, Phenomenex Luna CN column 5 µm, Detector set at 232 nm.

2.3.2.4 Cyclisation/elimination evaluation of mannoside 2.46

Mannoside compound **2.46** was next evaluated for its tendencies to undergo cyclisation/elimination by stirring a sample of **2.46** in deionised water with Amberlite H^+ overnight at RT. Figure **2.40** shows the results of this assessment. The reaction mixture following overnight (24 h) stirring at RT is shown (blue), showing the complete disappearance of starting material compound **2.46** (red, *ca*. 4.6 mins).

There appears to be solely a peak with rt *ca*. 2.8 mins, which could correspond to amino glycoconjugate **2.68** (green, rt *ca*. 3.1 mins). Once again, slight discrepancies in rt may be due to the acidic Amberlite H^+ resin altering the pH of the aqueous aliquot taken. This appears to confirm the capability of compound **2.46** to undergo the proposed cyclisation reaction discussed, independently of the type of carbohydrate moiety present.

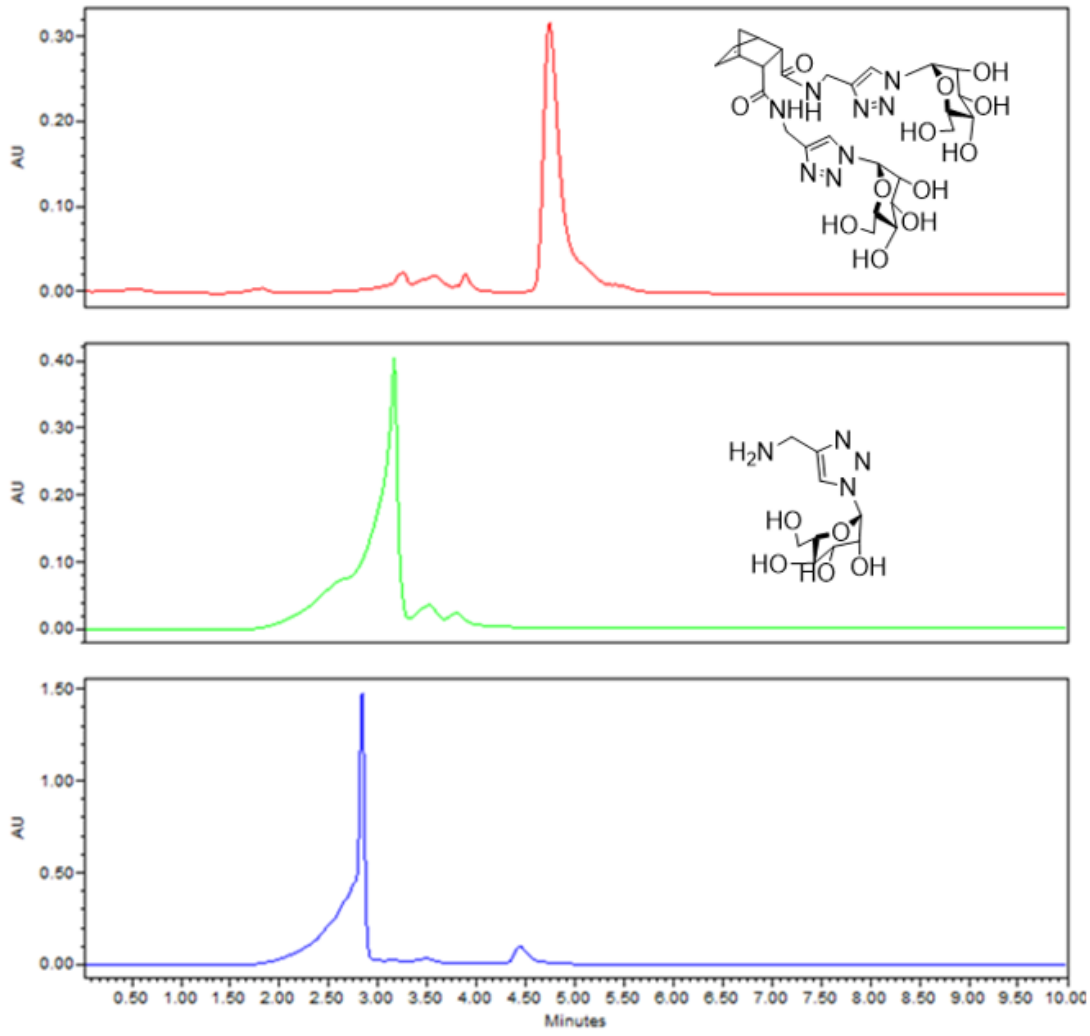

Figure 2.40: Reaction of compound **2.46** at RT with Amberlite H^+ in H_2O: Chromatograms (top to bottom); 1) **2.46**, 2) **2.68**, 3) **2.46** (after 1 day), HPLC conditions: 90:10 H_2O:ACN, 1 mL/min, Phenomenex Luna CN column 5 µm, Detector set at 232 nm.

2.3.3 Evaluation of cyclisation/elimination of asymmetric NB-tyrosol compound 2.81

The initial assessment of the tendencies of asymmetric NB compounds **2.80** and **2.81** to undergo the cyclisation reaction was performed by stirring them in MeOH with Amberlite H^+ at RT for a total of 24 h. Aliquots of these reaction mixtures were taken after 3, 6 and 24 h.

HPLC analysis could not confirm that compound **2.81** underwent the cyclisation reaction as expected. The two potential elimination products for this reaction are tyrosol (green, rt *ca*. 5 mins) and compound **2.37** (blue, rt *ca*. 4.5 mins). Starting material **2.81** (red) appears at rt *ca*. 2.3 mins. The yellow and pink trace in Figure **2.41**

were obtained after 3 and 24 h, respectively; these traces are identical and show a main peak at rt *ca*. 2.6 mins, assigned to starting material **2.81** with the discrepancies in retention times attributed to the acidic Amberlite H^+ resin altering the pH of the aqueous aliquot taken. A second peak at rt *ca*. 2.3-2.4 mins starts to appear, but no peaks are observed matching the rt of tyrosol nor compound **2.37**. Hence, under these conditions compound **2.81** does not appear to undergo the proposed cyclisation reaction.

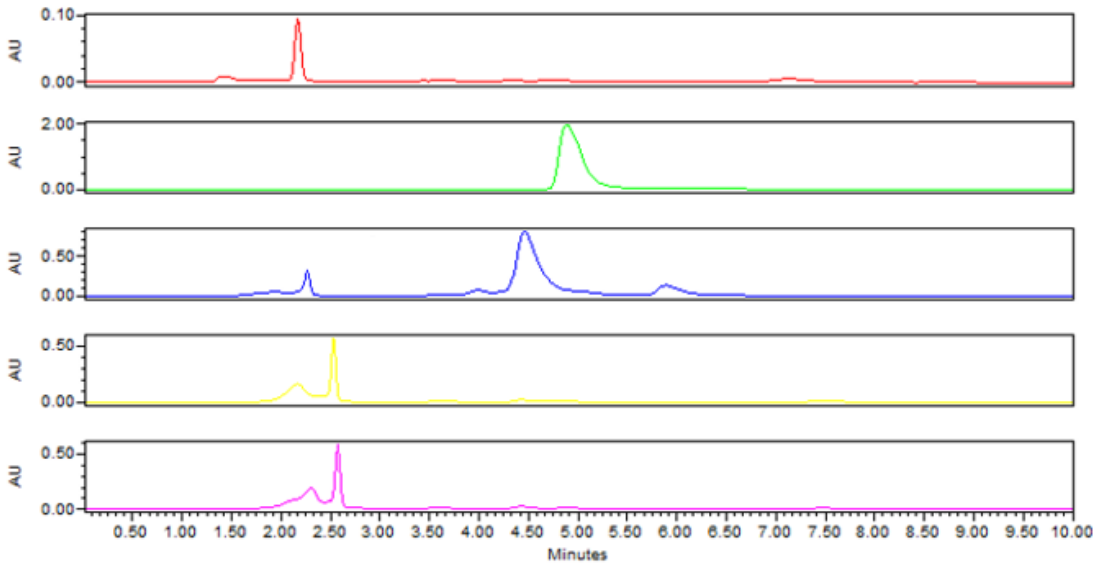

Figure 2.41: Reaction of compound **2.81** at RT with Amberlite H^+ in MeOH: Chromatograms (top to bottom); 1) **2.81**, 2) Tyrosol, 3) **2.37**, 4) **2.81** (after 3 h), 5) **2.81** (after 24 h). HPLC conditions: 90:10 H_2O:ACN, 1 mL/min, Phenomenex Luna CN column 5 µm, Detector set at 232 nm.

Similar results were obtained when a small amount of aq. 1M HCl (2 drops, *c.a* 60 µL) was added to this reaction mixture (pH *c.a* 1.2). Heating at 40 °C for four days, with further heating at 60 °C overnight showed no changes by HPLC analysis.

Next, the pH of the reaction mixture was adjusted to *ca.* 7 using aq. saturated $NaHCO_3$ and heated overnight at 60 °C. However, once again only a peak at rt *ca*. 2.7 mins was observed for the starting compound **2.81** (**Fig. 2.42**, yellow) At this point the pH of the reaction mixture was again adjusted, a pH *ca.* 8-9 with saturated $NaHCO_3$ solution and heated at 60°C for several days. Aliquots were taken after 3 and 5 days (**Fig. 2.42**, pink). Although a broad peak at rt *ca*. 1.6-1.8 mins began to appear, the starting compound **2.81** was still present and no peaks for tyrosol nor cyclization product **2.37** were observed. When the reaction was carried out under harsher

conditions (DMF, aq. NaOMe and heating at 60 °C for 2 days), HPLC analysis (**Fig. 2.42**, light blue) showed the disappearance of the starting compound **2.81** and the presence of a new broad peak at rt *ca*. 3.6-4.7 mins. It was unclear if the elimination had occurred as this broad peak overlapped with tyrosol and cyclic imide **2.37** (green and blue, respectively) and could be due to hydrolysis products. However, none of these species in their various possible ionisation states could be detected by HRMS analysis of the reaction mixture.

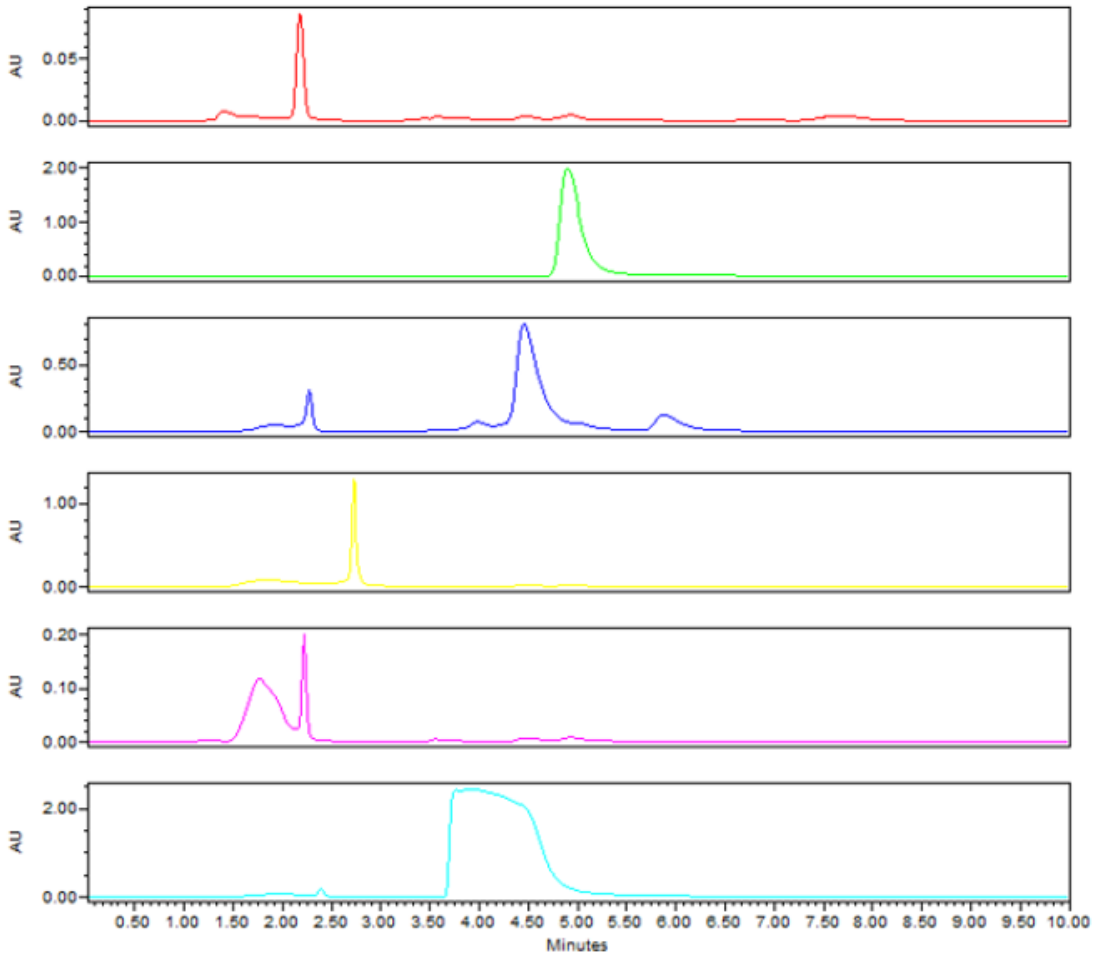

Figure 2.42: Reaction of compound **2.81** at 40-60 °C with in pH 7-9 in MeOH/DMF: Chromatograms (top to bottom); 1) **2.81**, 2) Tyrosol, 3) **2.37**, 4) **2.81** (after 24 h), 5) **2.81** (after 5 days), 6) **2.81** (after 2 days). HPLC conditions: 90:10 H_2O:ACN, 1 mL/min, Phenomenex Luna CN column 5 µm, Detector set at 232 nm.

Finally, the elimination reaction of compound **2.81** was evaluated in aqueous HCl solution (pH *c.a* 1.2) heating at 60 °C over 6 days. HPLC analysis after 24 h (yellow) showed a peak at rt *ca*. 2.5 mins attributed to stating material **2.81** and the

appearance of two new peaks rt *ca*. 4.5 and 5 mins, which could correspond to compound **2.37** and tyrosol, respectively (**Fig. 2.43**).

After 4 days heating at 60 ^{o}C, with further addition of HCl (pink), the peaks for the elimination products seemed to have increased in intensity, however the peak corresponding to starting material **2.81** could still be observed. In addition, a new peak at rt *ca*. 2.8 mins appeared, which could correspond to hydrolysis products. Interestingly, HRMS analysis of the reaction mixture detected compound **2.67**, which could result from the amide hydrolysis reaction of hybrid NB compound **2.81** (**Fig. 2.44**). The reason that only this species was detected may be due to low concentration of the cyclisation products tyrosol and compound **2.37**, together with **2.67** containing an ionisable primary amine which would aid HRMS detection.

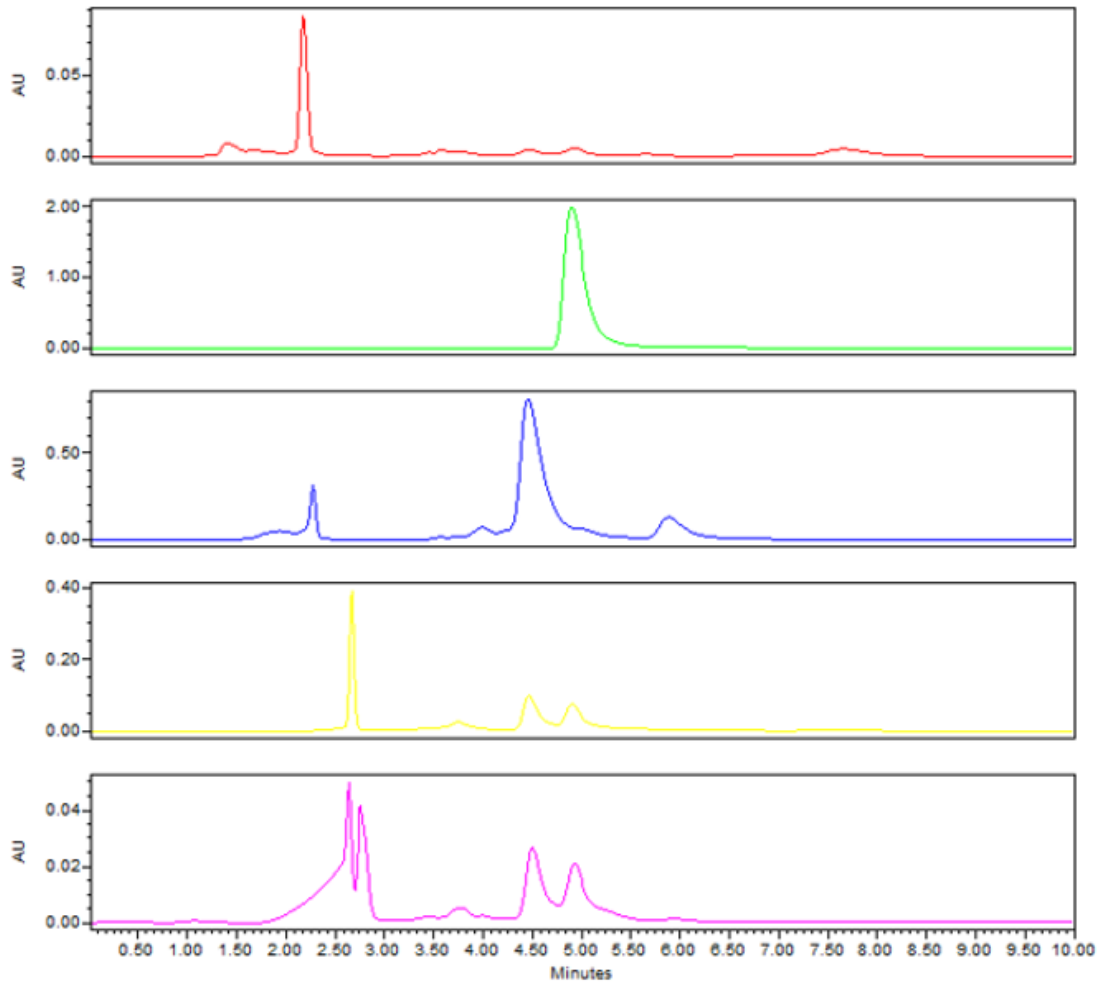

Figure 2.43: Reaction of compound **2.81** at 60 °C with in acidic pH in H_2O: Chromatograms (top to bottom); 1) Compound **2.81**, 2) Tyrosol, 3) Compound **2.37**, 4) **2.81** (after 24 h), 5) **2.81** (after 4 days). HPLC conditions: 90:10 H_2O:ACN, 1 mL/min, Phenomenex Luna CN column 5 µm, Detector set at 232 nm.

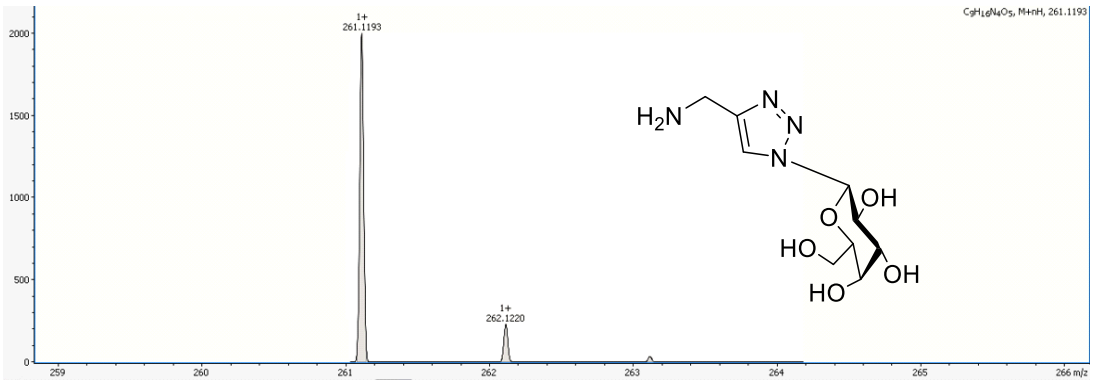

Figure 2.44: Detection of compound **2.67** in the above reaction mixture.

2.3.4 Evaluation of cyclisation/elimination of asymmetric NB-farnesol compound 2.80

Although farnesol-NB hybrid compound **2.80** was not obtained completely pure, initial assessment of the potential for this compound to cyclise was performed. As observed for the tyrosol-NB derivative **2.81**, no cyclisation/elimination occurred stirring with Amberlite H^+ in MeOH and only starting material **2.80** at rt *ca.* 2.6 mins (**Fig. 2.45**, blue) was observed.

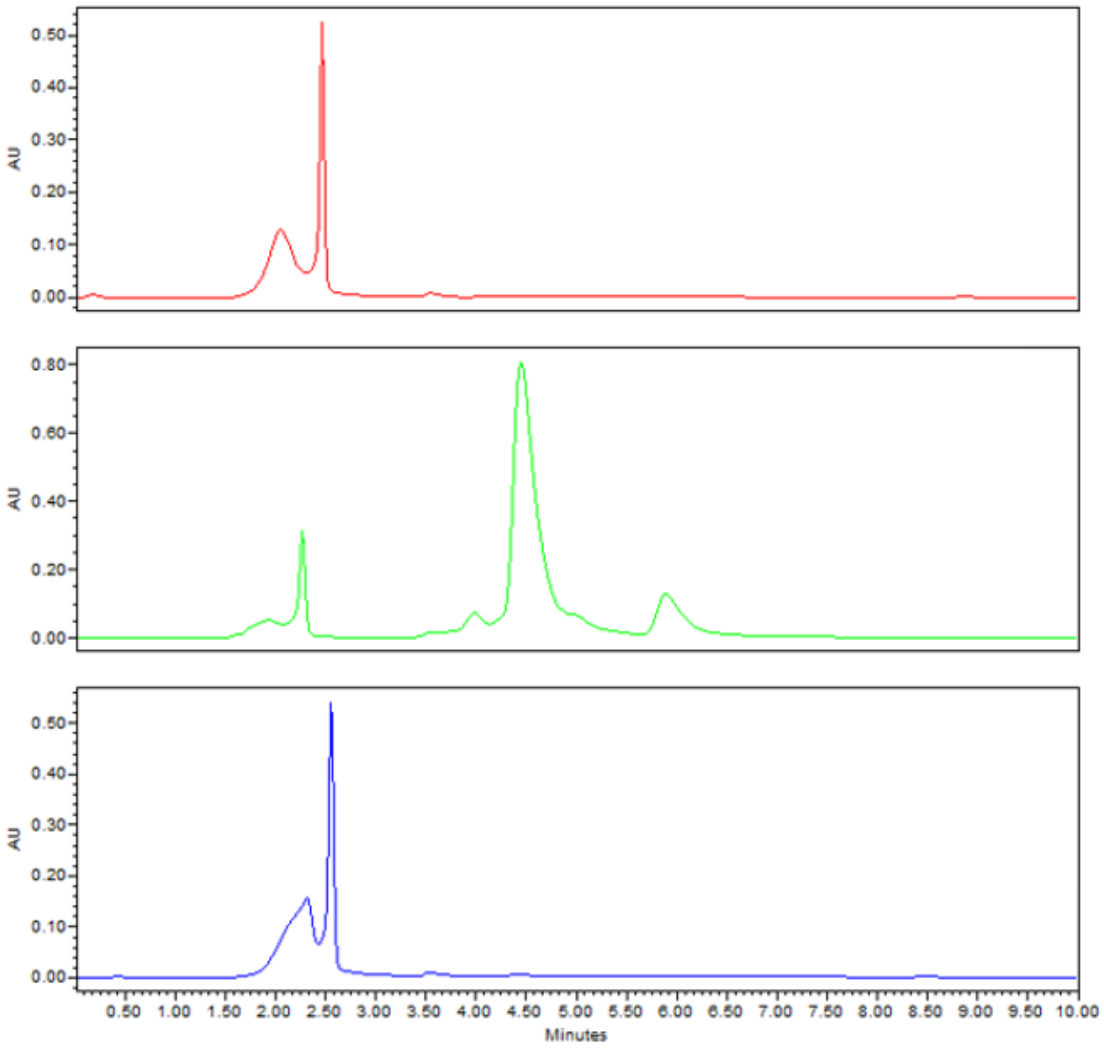

Figure 2.45: Reaction of compound **2.80** at RT with Amberlite H^+ in MeOH: Chromatograms (top to bottom); 1) Compound **2.80** (resolved with Amberlite H^+), 2) **2.37**, 3) **2.80** (after 24 h). HPLC conditions: 90:10 H_2O:ACN, 1 mL/min, Phenomenex Luna CN column 5 µm, Detector set at 232 nm.

When the reaction of compound **2.80** was carried out in aqueous 1M HCl at RT overnight, HPLC analysis (**Fig. 2.46**, blue) did not show the presence of cyclization product **2.37** (green). Disappointingly, no evidence of this reaction taking place could be found after heating for five days at 60 °C (yellow).

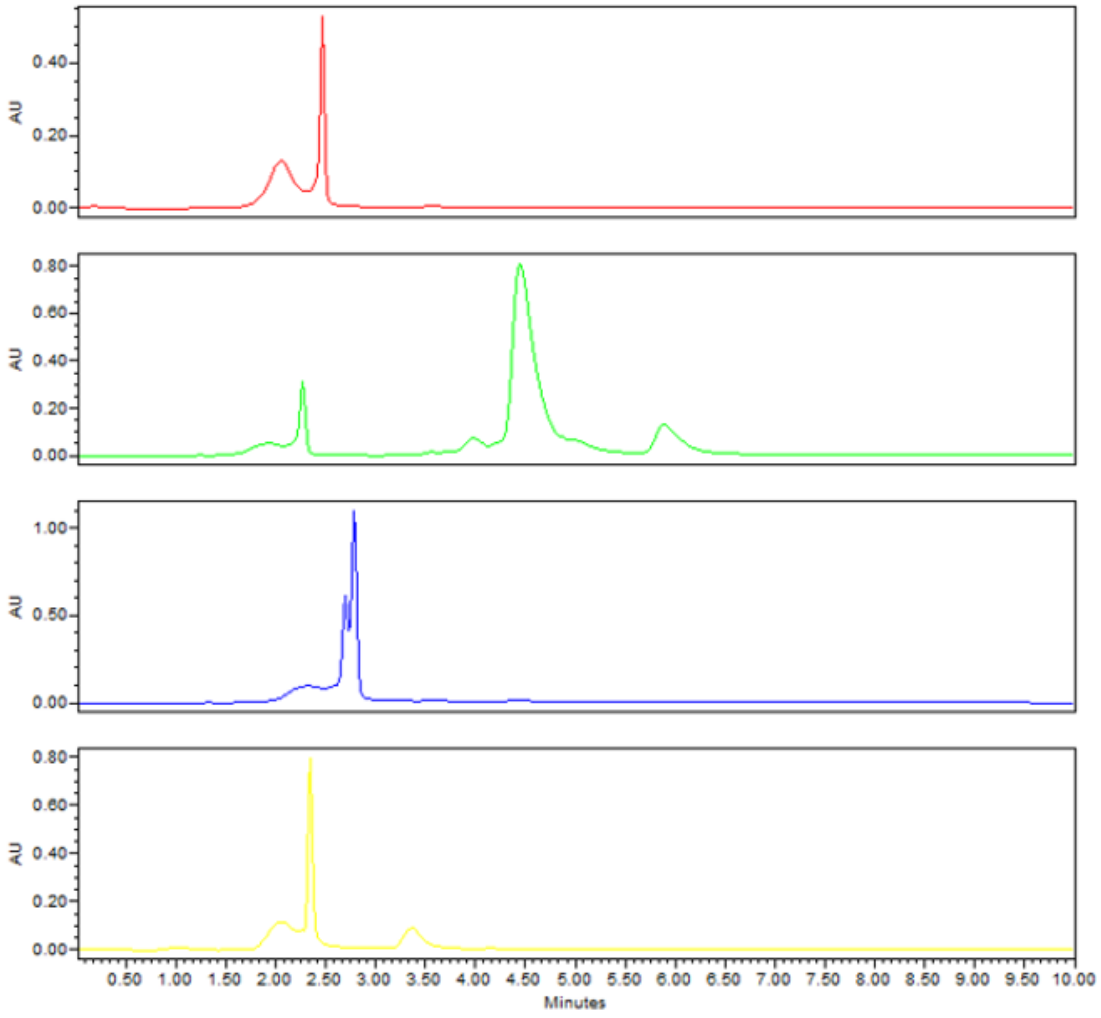

Figure 2.46: Reaction of compound **2.80** at 60 °C with in acidic pH in H_2O: Chromatograms (top to bottom); 1) Compound **2.80** (resolved with Amberlite H^+), 2) **2.37**, 3) **2.80** (after 24 h), 4) **2.80** (after five days). HPLC conditions: 90:10 H_2O:ACN, 1 mL/min, Phenomenex Luna CN column 5 µm, Detector set at 232 nm.

When farnesol derivative **2.80** was heated at 60 °C in aqueous saturated $NaHCO_3$ (pH 8-9) for six days no evidence of cyclisation product **2.37** (**Fig. 2.47**, green) could be found by HPLC analysis, showing instead a peak with rt *c.a* 1.8 mins (blue). When the reaction of farnesol derivative **2.80** was carried out heating at 60 °C in aqueous NaOMe over 10 days (yellow), a broad peak at rt *ca*. 3.6-4.7 mins appeared, which

likely correspond to hydrolysis products. A sample of this reaction mixture was analysed by HRMS. However, none one of the possible elimination products nor the hydrolysis products were detected.

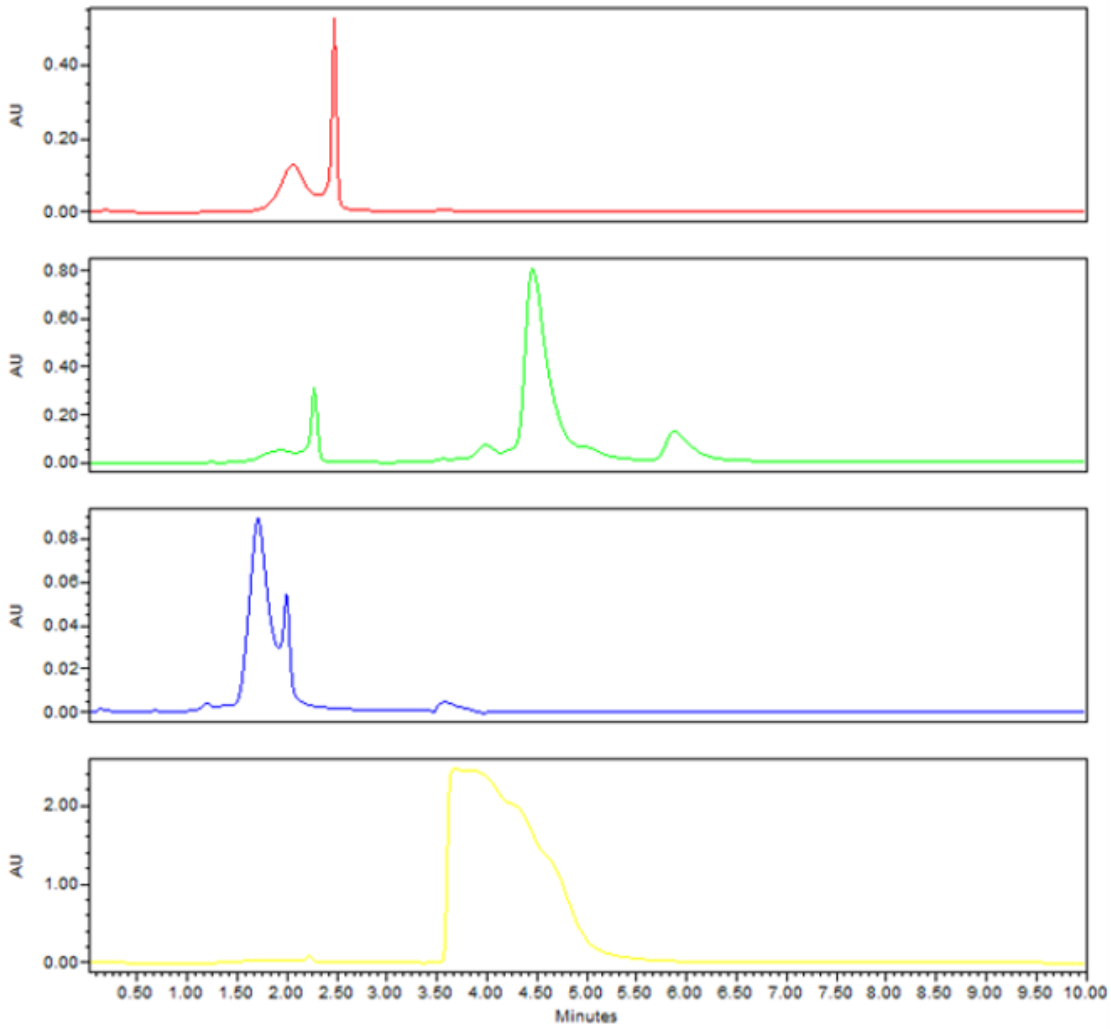

Figure 2.47: Reaction of compound **2.80** at 60 °C with in basic pH in H_2O: Chromatograms (top to bottom); 1) Compound **2.80** (resolved with Amberlite H^+), 2) **2.37**, 3) **2.80** (after 6 days), 4) **2.80** (after 10 days). HPLC conditions: 90:10 H_2O:ACN, 1 mL/min, Phenomenex Luna CN column 5 µm, Detector set at 232 nm.

Finally, compound **2.80** was dissolved in 1:0.15 mixture of aqueous 1M HCl and MeOH (minimum amount required to dissolve it). Following 24 h of heating at 60°C, HPLC analysis showed a very small amount of compound **2.37** (**Fig. 2.48**, blue), indicating that cyclisation may be promoted under these conditions. However, even after 5 days and with further addition of 1M HCl, there was no increase in intensity for the peaks corresponding to cyclization product **2.37** (yellow).

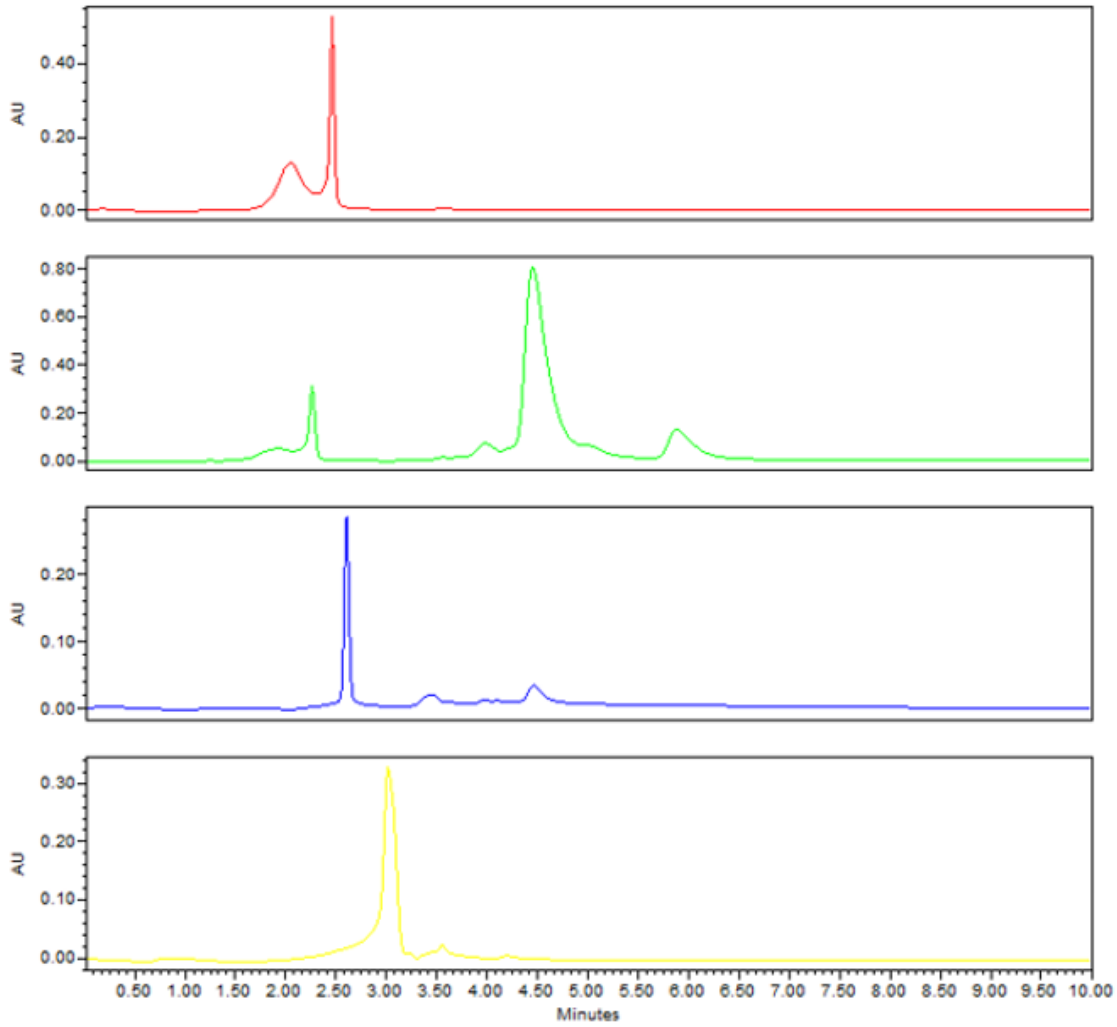

Figure 2.48: Reaction of compound **2.80** at 60 °C with in acidic pH in H_2O: Chromatograms (top to bottom); 1) **2.80** (resolved with Amberlite H^+), 2) **2.37**, 3) **2.80** (after 24 h), 4) **2.80** (after 5 days). HPLC conditions: 90:10 H_2O:ACN, 1 mL/min, Phenomenex Luna CN column 5 µm, Detector set at 232 nm.

HRMS analysis of the reaction mixture could not detect any of the possible elimination products nor the hydrolysis products.

2.4 Conclusion

In conclusion, a series of NB-based compounds have been designed and synthesised to assess different structural requirements for acid-promoted elimination/cyclisation reaction to occur. Additionally, building on this promising chemistry for potential stimuli-responsive compounds, novel asymmetric NB compounds **2.80** and **2.81** were also investigated. The elimination/cyclisation reaction was performed under a range of conditions and monitored using HPLC analysis.

Results from the assessment of the structural requirements indicate that the presence of carbohydrate moieties in the NB compounds is not essential to undergo elimination/cyclization. However, it may influence the rate of the reaction as seen by it going to completion overnight in the cases of the galactoside and mannoside NB derivatives **2.35** and **2.46**, whereas the benzyl NB derivative **2.45** required a period of seven days to reach completion. Whether the different carbohydrate moieties present in the two NB glycoconjugates prepared have different cyclisation rates was not determined. This may require much more frequent aliquoting and HPLC analysis of the corresponding reaction mixtures to pinpoint more accurately reaction completion.

Furthermore, additional evidence has been obtained that the 1,2,3-triazole heterocycle is important for the reaction to occur. The reaction for NB compound **2.55**, containing a pyridyl heterocycle, did not reach completion even after seven days. This suggests that the 1,2,3-triazole heterocycle (pK_a 1.3) is more efficient at promoting the elimination/cyclization reaction than other heterocycles containing basic nitrogen atoms like pyridine (pK_a 5.2).

Mixed results were obtained in the preparation of the novel asymmetric NB compounds. Initial attempts using fluconazole as the anti-fungal agent proved to be quite synthetically challenging. Upon re-evaluation of the proposed strategy using benzyl alcohol as a model compound, it was decided that anti-fungal agents containing primary alcohol groups should be much more synthetically feasible. Farnesol and tyrosol, two compounds with reported anti-fungal properties, were chosen. The synthesis and purification of the resulting NB analogues **2.80** and **2.81** proved very challenging. The tyrosol NB derivative **2.81** was prepared, though with very poor yields of 12%. Further work will be required to optimise the synthesis and efficient purification of this compound. Unfortunately, the farnesol NB derivative **2.80** could only be partially purified. The purification of this compound was especially difficult, which could possibly be attributed to its amphiphilic nature of this compound, conferred by the hydrophilic galactosyl moiety and lipophilic farnesyl tail. Future work to purify this compound fully may involve further column

chromatography using lower flow rates or higher pressure. Additionally, trituration and/or recrystallization may lead to the purified product.

Finally, assessment of the elimination/cyclisation profiles of **2.80** and **2.81** was carried out. Compound **2.81** appeared to undergo the proposed cyclisation reaction under aqueous conditions with an acidic pH, though heat appears to be necessary. Meanwhile, compound **2.80** did not undergo the cyclisation reaction, to any great extent, under the conditions assessed but further screening of different conditions may be required. Another possibility is that due to the high temperature and acidic pHs in which the reactions were assessed hydrolysis/degradation of potential cyclisation products may occur which were not detected by HPLC or HRMS analysis.

Chapter 3

Glycoconjugates as Covalent Inhibitors of Adhesion of Fungal Pathogens of the *Candida* spps

3.1 Introduction

3.1.1 Anti-fungal drug resistance

Emerging drug resistance to many of the traditionally conventional anti-fungal drugs is a global problem. For example, crop-destroying fungi account for yield losses of approximately 20% worldwide and another 10% lost after crop harvesting. In addition, from a medical perspective, mortality rates for fungal diseases exceeds the mortality rates for both breast cancer and malaria and is now comparable to tuberculosis and HIV. This highlights the effect of emerging drug resistance in fungal species and also the urgent need to develop new effective drugs. Worryingly, clinical pathogens with resistance to all licensed systemic antifungals has been reported [126]. Anti-fungal resistance typically occurs due to changes that affect, either directly or indirectly, the drug-target interaction thus rendering a drug ineffective. Changes to the target binding site, overexpression of the drug target, efflux pumps or limiting prodrug activation are all routes through which anti-fungal drug resistance has been reported. In addition to resistance, anti-fungal tolerance allows drug-susceptible cells to continue to grow at drug concentrations above the minimum inhibitory concentration (MIC). Anti-fungal tolerance is yet another way in which the efficacy of currently used anti-fungal drugs has been reduced in recent years [127].

There are roughly nine times more anti-fungal compounds that are available to treat crop diseases than systemic animal diseases. Licensed anti-fungal treatments in humans are limited to four classes of anti-fungal drugs. The first class, polyenes, sequester ergosterol and, in doing so, disrupt the fungal cell membrane. The second class is 5-fluorocytosine, which is a pyrimidine analogue, and this compound blocks pyrimidine metabolism and DNA synthesis. Azoles are the most widely used class and work by inhibiting lanosterol 14-α-demethylase; this results in the inhibition of ergosterol biosynthesis due to accumulation of 14-α-methyl-sterols. This causes changes to membrane stability and permeability and also alters the activity of membrane-bound enzymes. The newest class of anti-fungal drugs is the echinocandins, which inhibit (1,3)-β-D-glucan synthase and also disrupts cell wall biosynthesis [126]. Over 140 substitutions in the azole drug target, lanosterol 14-α-

demethylase, have been reported in different resistant *Candida* strains. In *A. fumigatus* drug target site alterations are the most common reported drug resistance mechanism. Alterations in the uptake of anti-fungal drugs into pathogen cells is another resistance mechanism. Many anti-fungal drugs are reported to utilise permeases to gain entry into the pathogen cell. It is believed that changes in permease expression may facilitate a reduction in drug uptake. Drug efflux is an important drug resistance mechanism, whereby upon entry into a fungal cell, an anti-fungal drug is pumped back out into the extracellular environment. There are two classes of efflux pumps which confer azole resistance in fungal pathogen. These are the ATP-binding cassette (ABC) superfamily and the major facilitator superfamily (MFS). Biofilms, particularly in *Candida* species, is another important mechanism of resistance to a range of anti-fungal drugs. Biofilms consist of a dense three-dimensional network of fungal cells, carbohydrates, proteins and nucleic acids. The susceptibility of *Candida* species to azole drugs is drastically reduced when these cells are embedded within a biofilm. There are a number of factors that reduce the efficacy of these drugs which include induction of drug efflux pumps and also drug sequestration. Biofilms have a thick, viscous consistency which can result in an administered drug becoming trapped (sequestered) in the biofilm without reaching its target. This results in the potency of a given anti-fungal drug drastically increasing or potentially being eliminated completely. There are many other mechanisms of resistance to conventional treatments in fungal diseases, the above mechanisms are examples of some of them [128].

3.1.2 Covalent inhibitors and infection

In recent years there has been a renewed push in the search for novel antimicrobials and in pursuit of such agents, there has been a renewed interest in covalent inhibitors. Covalent inhibitors are a separate class of drug compounds which function through the formation of a stable covalent bond between the drug and drug target. This results in inhibition of the drug target which ultimately leads to the desired biological effect. This is in contrast to drugs which act via non-covalent interactions. These interactions, by their nature, are temporary and exist in an equilibrium between bound drug (drug-target complex) and the dissociated species.

In general, covalent drug inhibitors are designed to contain an electrophilic warhead (**Fig. 3.1)**, which may selectively react with a nucleophilic group on the biomolecule (drug target). Common electrophilic warheads found in covalent inhibitors include epoxides, aziridines, ketones and α,β-unsaturated carbonyls [129]. α,β-unsaturated systems are a very common moiety used as the electrophilic warhead in covalent inhibitors. In biological systems, cysteine thiols have historically been targeted as the nucleophilic groups. Other nucleophilic groups which have more recently been targeted are lysine, which has shown a preference to react with sulfur (VI)-based reactive centres, and histidine, which has shown a preference to react with epoxides[130].

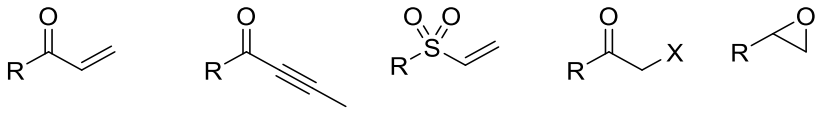

Figure 3.1: Examples of some common electrophilic warheads including acrylamides and other unsaturated systems, α-halocarbonyls and epoxides [129].

Traditionally, covalent inhibitors have been disfavoured due to disadvantages such as off-target reactivity leading to undesired side-effects. However, such is the need for new antimicrobials to combat rapidly emerging antibiotic resistance, further research is being conducted into this class of inhibitor. A good example of successful antimicrobial which acts as a covalent inhibitor is penicillin; the β-lactam moiety contained in penicillin, and its other analogues approved for use in humans, is used to target a serine residue in a transpeptidase enzyme which is important for the integrity of the bacterial cell wall (**Fig. 3.2**)

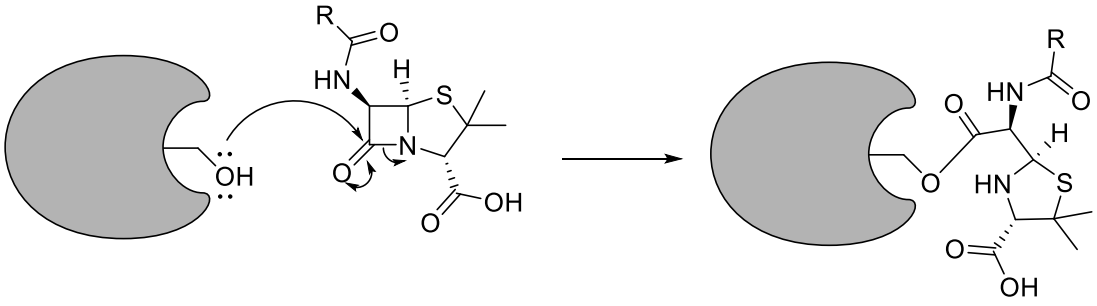

Figure 3.2: Mechanism of action of typical penicillin antibiotic.

However, despite these successes, the threat of immunogenicity (as a result of non-specific covalent drug-protein adducts), means potential covalent inhibitors of infection must be designed in a way that ensures selectivity for the desired target. At the same time, they should contain a suitable electrophilic warhead which will efficiently crosslink, and thus inhibit the target. Considerations must be given to the location of potential nucleophilic residues in the target which may react with the electrophilic group, thus detailed structural information on the target is hugely beneficial in the design of such inhibitors.

There have been some recent successes in the application of covalent inhibition in the prevention of microbial infections. Wagner *et al.* reported the synthesis and evaluation of two epoxide-containing galactosides against the common pathogen *Pseudomonas aeruginosa*. This work is an excellent example of the application of detailed structural knowledge of a target to design a selective and efficient inhibitor of a given target, in this case LecA, which is a key lectin (carbohydrate-binding protein) involved in the adherence of *Pseudomonas aeruginosa* to human cells, subsequently leading to infection. The authors identified a cysteine residue in the binding site of LecA which they were able to selectively target using galactoside **3.1** (**Fig. 3.3**). In addition, compound **3.1** displayed an IC_{50} value of 64 μM for LecA inhibition, while its diastereomer was not recognized. This highlights the high selectivity of compound **3.1** for LecA. The authors were able to show a covalent linkage is formed with the cysteine residue originally targeted, using mass spectrometry, through a ring-opening reaction of the strained epoxide, thus inhibiting LecA [131].

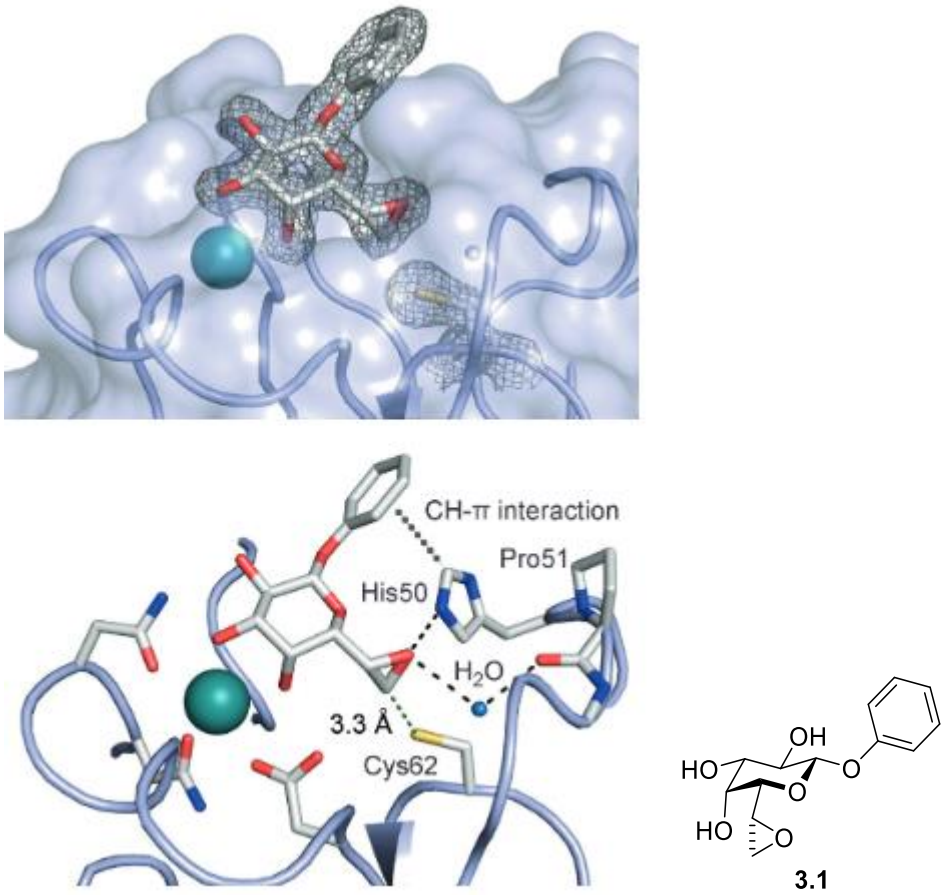

Figure 3.3: Structure of compound **3.1** (right) and crystal structure of **3.1** in complex with LecA (left) [131].

In an effort to exploit the presence of the fructose-1,6-bisphosphate aldolase (FBA) class two (FBA-II) in fungal and bacterial cells only, Wen *et al.* reported the preparation of a series of covalent inhibitors of this enzyme in *C. albicans* (CaFBA). To do this, the authors had to initially identify a covalent binding site within CaFBA. A reactive cysteine residue was identified (C292S) as essential to the catalytic activity of CaFBA. Following a structure activity relationship study (SAR), compound **3.2** (Fig. **3.4**) was identified as a potent inhibitor of CaFBA through covalent bond formation with C292S, as determined by LC-MS. The authors deduced that a covalent bond is formed between the Se atom in **3.2** and the thiol group in C292S, by co-crystallisation of CaFBA and an analogue of compound **3.2**. Compound **3.2** was found to produce an IC_{50} value of 92 nM against CaFBA. This compound also displayed MIC_{80} values ranging from 1 to 4 μg/mL against four *C. albicans* strains, including three azole resistant strains. Finally, **3.2** was capable of near complete biofilm inhibition at a

concentration of 64 μg/mL against *C. albicans* (0304103), which is also an azole resistant strain [132].

MurA (UDP-*N*-acetylglucosamine enolpyruvyl transferase) is a key enzyme involved in peptidoglycan biosynthesis. Peptidoglycan is the major component of the bacterial cell wall in both gram-positive and gram-negative bacteria, thus compounds that can inhibit MurA should pose as effective anti-bacterial agents against both gram-positive and gram-negative bacteria. Following the preparation of a library of chloroacetamide-based compounds, Grabrijan *et al.* identified compound **3.3** (**Fig. 3.4**) as a potent inhibitor of MurA in *E. coli*. Compound **3.3** produced an IC_{50} value of 39 μM for MurA covalent inhibition. **3.3** displayed a time-dependent decrease in IC_{50} with increasing preincubation times, which is characteristic of covalent inhibitors. The authors identified Cys115 as the amino acid residue which reacts and crosslinks to **3.3**, though they noted that there may be other cysteine residues that may react with **3.3** to lesser extents, through LC-MS/MS experiments. Unfortunately, compound **3.3** was found to have no anti-microbial activity against *S. aureus* (ATCC29213) and *E. coli* (ATCC25922), possibly due to poor cell wall penetration or active transport of **3.3** out of the bacterial cell. Another factor may have been the reactive chemical nature of **3.3** resulting in it being sequestered by enzymes or other biomolecules [133].

β-lactamase enzymes are frequently used by gram-negative bacteria to confer resistance to β-lactam drugs. This is highly problematic as many extended-spectrum β-lactamases have emerged over the past two decades. A solution to this problem is to develop β-lactamase inhibitors, which are currently used in combination with β-lactam antibiotics, thus restoring their activity. To this end, Hecker *et al.* set about developing novel boronate-containing β-lactamase inhibitors for *K. pneumoniae* carbapenemase (KPC). This enzyme is important for the persistence of carbapenem-resistant enterobacteriaceae (CRE), with many of the currently used β-lactamase inhibitors being poor inhibitors for it. Initial *in silico* evaluation of **3.4** (**Fig. 3.4**) as an inhibitor of β-lactamase enzymes from three classes (A, B and C) confirmed it formed favourable poses in class A and C enzyme active sites. It was then found that **3.4** produces an MPC_1 of 0.02 μg/mL in combination with biapenem (β-lactam antibiotic)

against KPC-producing *K. pneumoniae*. MPC_1 is the concentration of **3.4** required to reduce the MIC of biapenem from 32 μg/mL to 1 μg/mL. The authors found that **3.4** was active against a broad range of β-lactamase enzymes. The efficacy of **3.4** was illustrated by the lowering of the MICs of biapenem, meropenem, ertapenem and imipenem (all carbapenems) from 16, 64, >64 and 16 μg/mL to 0.25, 1, 2 and 0.25 μg/mL respectively, against *K. pneumoniae* (KP1087). This illustrates that **3.4** can revive the activity of such carbapenem antibiotics which currently, on their own, are ineffective. Crystallography experiments confirmed that the boron atom in **3.4** is covalently bound to the catalytic serine residue in the active site of the corresponding β-lactamase enzyme. This justifies the inclusion of a boronate moiety in **3.4** for selective targeting of serine proteases such as β-lactamase enzymes, as boronates are known to possess high affinity for serine hydrolases in general [134].

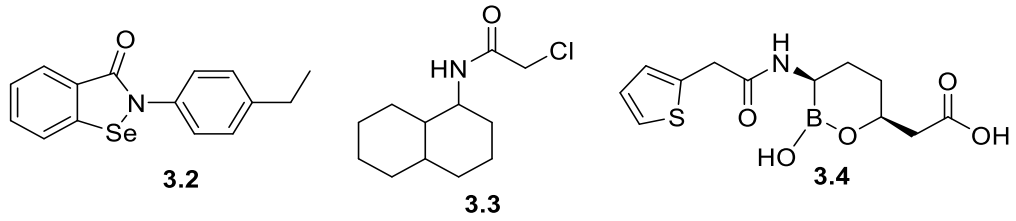

Figure 3.4: Structure of covalent inhibitors **3.2**, **3.3** and **3.4** [132-134].

3.1.3 Bacterial pathogens and adhesion

Coincidently, at the same time as the increase in research into covalent inhibitors, there has been increased interest in developing antimicrobial drugs with novel modes of action, such as anti-adhesion agents [80]. Anti-adhesion agents work by preventing adhesion of pathogens to host cells, and thus prevent infection without killing the targeted pathogen. A key advantage of anti-adhesion agents lies in their lower selective pressure for resistance in comparison to antibiotic-type antimicrobials, which are presently hindered by this problem. There are many examples of pathogens utilising biomolecules, normally proteins, to adhere to carbohydrate structures on host cells. These glycans can be found present as polysaccharides on the host cells or carbohydrate structures attached to proteins or lipids (glycoproteins or glycolipids) [135]. Thus, as the adherence step commonly involves carbohydrates, there has been extensive research into the development of

carbohydrate-based compounds which can selectively bind to the biomolecules used by pathogens to adhere to host cells. These compounds are usually mimics of carbohydrate structures found on the host cell [136].

However, a key challenge with developing glycoconjugates as effective adhesion blockers is overcoming the intrinsically low affinities between the carbohydrate proteins and their mono- or oligosaccharide ligands. The glycoside cluster effect is both an extremely common and highly effective method used to overcome these challenges. The glycoside cluster effect involves the presentation of many copies of the relevant carbohydrate ligand in suitable displays/poses to enhance its affinity for its corresponding carbohydrate binding protein. Many characterised lectins which have multiple carbohydrate-binding sites have been reported. Multivalent glycoconjugates, presenting carbohydrates in the correct orientation to be able to bind multiple binding sites, are key to achieving the most optimal binding affinity over their monovalent counterparts [137].

FimH is a mannose-binding lectin used by uropathogenic *E. coli* to bind to the surface of epithelia cells in the bladder, which leads to urine infections. One of the first effective examples of glycoconjugate inhibitors of pathogen adhesion was *n*-heptyl-α-D-mannoside **3.5** which was found to be a potent inhibitor of FimH (K_d= 5 nM) (**Fig. 3.5**) [135]. Touaibia *et al.* prepared a series of multivalent mannoside dendrimers, with compound **3.6** (**Fig. 3.5**) identified as a potent FimH inhibitor (K_d = 0.45 nM, as determined by Surface plasmon resonance (SPR). This is a greater than ten-fold increase in potency in comparison to compound **3.5** (**Heptyl-Man**), [138]. FimH will be discussed in more detail in Chapter 5.

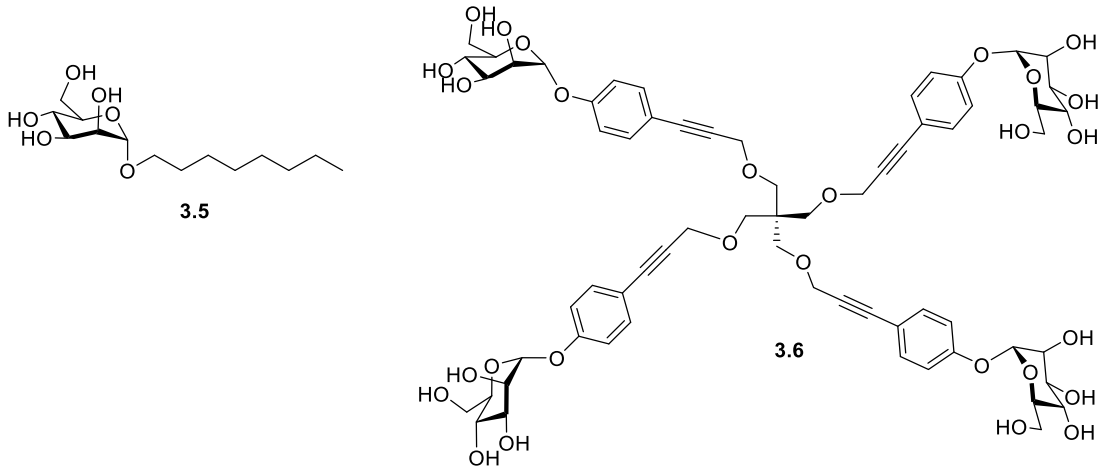

Figure 3.5: Structures of FimH inhibitors **3.5** and **3.6** [135,138].

P. aeruginosa is a common bacterial pathogen involved in diseases such as septicaemia and lung infections in both cystic fibrosis and immunocompromised patients. LecA and LecB are two key lectins with specificities for galactosides and fucosides, respectively [136]. Berthet *et al.* exploited the glycoside cluster effect to achieve low nanomolar affinity for LecB with compound **3.7** (**Fig**. **3.6**), which produced IC_{50} = 0.6 nM in an enzyme-linked lectin assay (ELLA) and K_d = 28 nM as determined by isothermal titration microcalorimetry (ITC) [139].

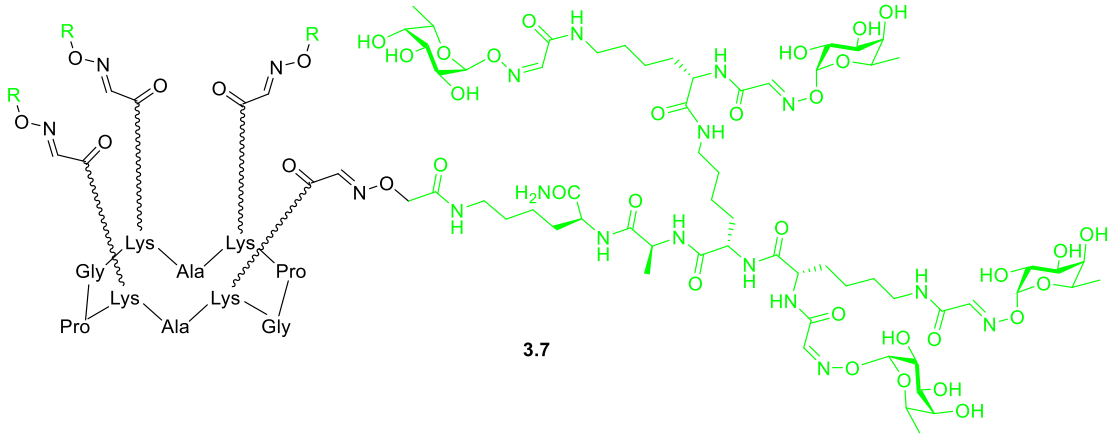

Figure 3.6: Structure of LecB inhibitor **3.7** [139].

Cholera toxin (CT) is a protein toxin produced by *V. cholerae*, which is the causative agent of cholera. CT binds to the galactoside head group in ganglioside GM1, on the surface of human intestinal epithelial cells. Pickens *et. al* reported the synthesis and evaluation of a library of galactosides as potential inhibitors of CT. Compound **3.8** (**Fig. 3.7**) showed K_d = 12 µM through ITC and 6 µM through pulsed ultrafiltration

(PUF) [140]. Similar to previous examples, drastic improvements were seen upon preparation of multivalent glycoconjugate derivatives as inhibitors of CT. Garcia-Hartjes *et al.* reported compound **3.9** (**Fig. 3.7**) as a highly potent inhibitor of CT, with IC_{50} = 450 pM in an ELISA assay, in which its corresponding monovalent analogue produced an IC_{50} = 44 µM. This 100,000-fold increase in potency highlights the importance of the glycoside cluster effect in the design of high affinity anti-adhesion glycoconjugates. [141].

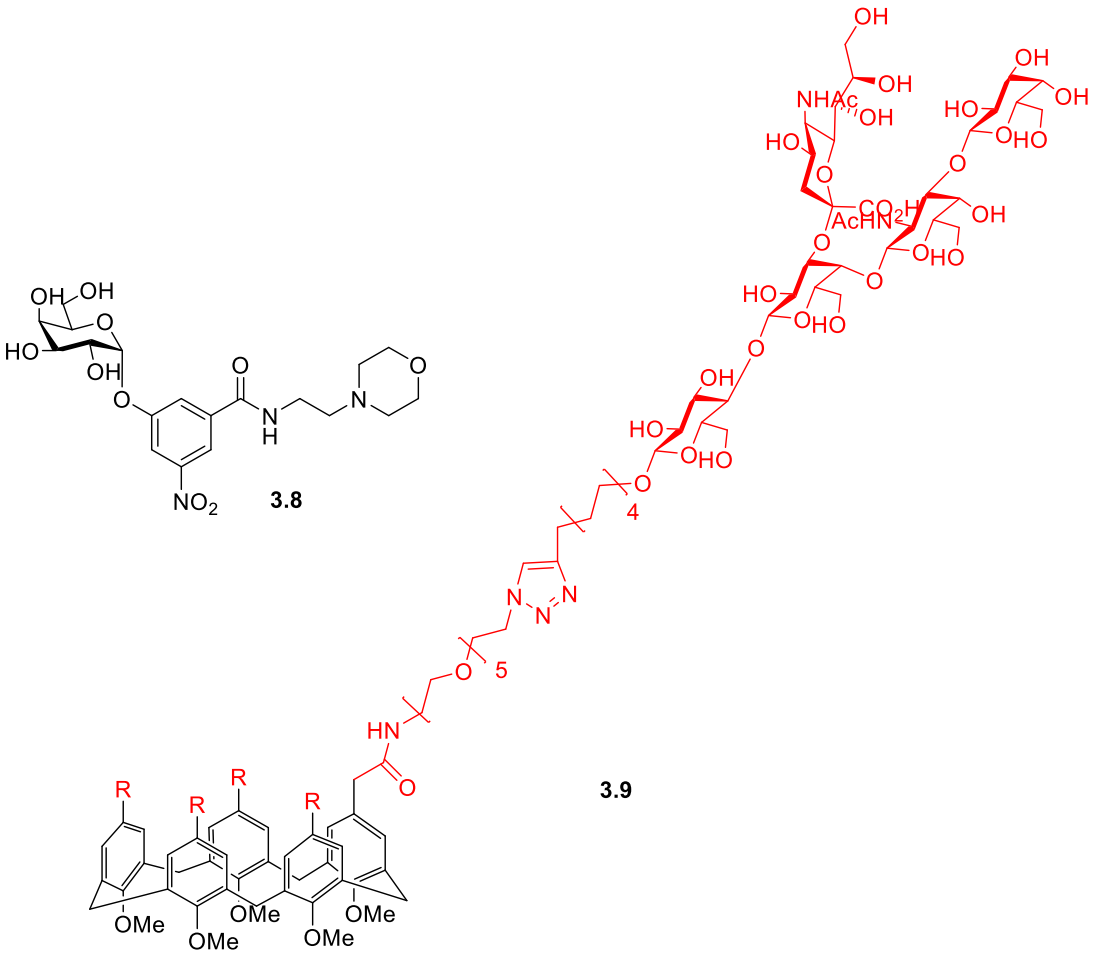

Figure 3.7: Structures of cholera toxin inhibitors **3.8** and **3.9** [140,141].

3.1.4 Fungal pathogens and adhesion

A major challenge in the development of effective anti-adhesion molecules against fungal species in general is that the structural information available on fungal adhesins is limited in comparison to bacterial adhesins [142]. For this reason, most of the work of anti-adhesion antimicrobials have focused on bacterial pathogens,

with fewer examples reported for fungal ones. FleA is an adhesin lectin found in *A. fumigatus,* which is a highly problematic fungal pathogen worldwide. Like many fungal pathogens, treating *A. fumigatus* has become more difficult due to resistance to conventional treatments. FleA is a 32-kDa protein which has specificity for L-fucose, and to a lesser extent, it has some specificity for L-galactose and D-arabinose [143]. FleA has been co-crystallised with methyl-α,L-selenofucoside by Houser *et al.* [144]. With the relevant structural information for FleA in hand, Lehot *et al.* reported the preparation of a series of α-cyclodextrin-functionalised and cubic octameric silsesquioxane-functionalised glycoconjugates. ITC was used to determine the binding affinities of this library of compounds for FleA. The octavalent fucosyl-glycoconjugate **3.10** (**Fig. 3.8**) was the best performing one (K_d = 40 nM). Significantly, it was found that one molecule of **3.10** was bound to more than one protein (FleA), which is indicative of either aggregative or chelate-aggregative binding; this partly explains the high affinity of **3.10** for FleA. [145].

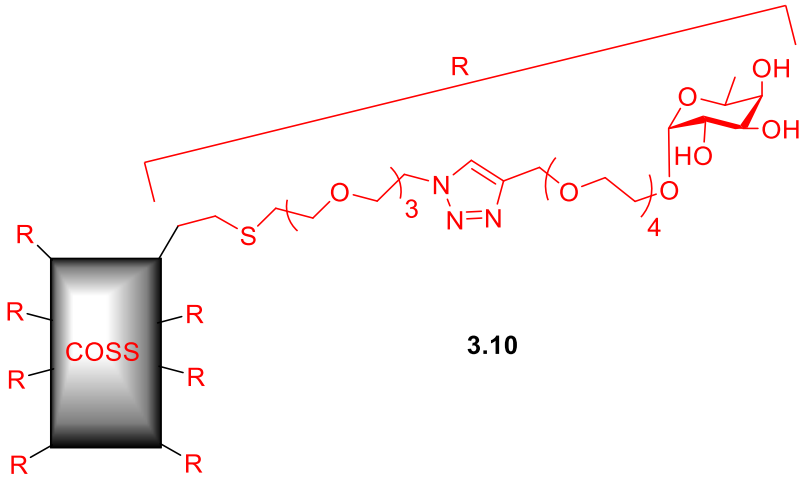

Figure 3.8: Structure of Octavalent glycoconjugate **3.10** [145].

The development of anti-adhesion agents against fungal pathogens has been hindered by a lack of structural information on fungal adhesins (proteins). As discussed previously, *Candida albicans* is the main cause of fungal infections in the world and it is particularly common in nosocomial settings. Due to the increasing prevalence of anti-fungal resistance worldwide, novel treatments must be developed to treat such infections. *C. albicans* must adhere to the host cell surface before subsequently infecting the host organism. In comparison to other pathogens, less is

known about the mechanisms of adherence and the biomolecules involved in *C. albicans* adherence to host cells [21]. The agglutinin-like sequence (ALS) protein family have been extensively studied and characterised as key adhesins used by *C. albicans*. These proteins are found on the cell surface of *C. albicans* and their upregulation can be correlated to disease/infection progression in a rat model of oral infection [146]. This indicates that this family of adhesins is an important virulence factor for *C. albicans*. When the effect of gene deletion of various ALS genes was studied, it was found that adherence to host cells and other ligands was altered. For example, gene deletion of Als1p reduced binding of *C. albicans* by 20%. However, deletion of one ALS gene has been observed to result in increased expression of other ALS genes. For example, the gene deletion of ALS4 resulted in increased expression of ALS2, this is likely to compensate for the loss of adherence, however, it also implies that individual ALS adhesins have overlapping specificities for the same ligands [146]. Thus, anti-adhesion molecules may benefit from an enhancement in activity as a result of the ability to target more than one adhesin. Als proteins bind to a number of structurally unrelated proteins and peptides with very broad specificities, and it has also been postulated that the *N*-terminal part of Als1 protein specifically binds fucose-containing glycans, albeit with low affinity (K_d = 21 mM) [30].

Recent work by Takagi *et al.* has identified synthetic derivatives of mucin *O*-glycans, **3.11**-**3.13** (**Fig. 3.9**) that inhibit filamentation from yeast to the hyphae form in *C. albicans* at potencies comparable to those of native mucins, commonly found across mucosal surfaces. This study highlights the importance of controlling virulence traits without killing the microbe, which may prevent the evolution of drug resistance [147].

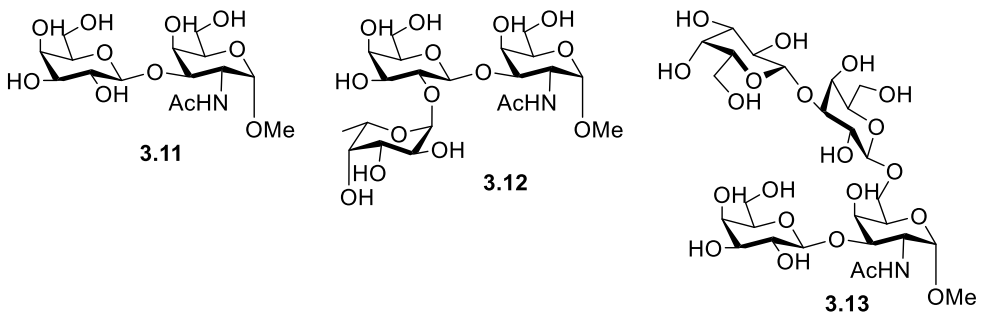

Figure 3.9: Synthetic *O*-glycans inhibitors **3.11**, **3.12** and **3.13** [147].

Thus, the development of new anti-fungal agents to treat *C. albicans* infections will be greatly aided by the elucidation of the structures of key lectins and other biomolecules involved in the different steps of the infection process. Early studies showed that *C. albicans* adhesion to epithelial cells was reduced in the presence of a range of carbohydrates including galactose, *N*-acetylglucosamine, L-fucose and methylmannoside [148]. However, no galactose-binding lectin structure for this fungal pathogen has been elucidated to date. Due to the likelihood of *C. albicans* possessing a variety of lectins with specificities for different carbohydrates, the importance of identifying and structurally characterising them cannot be underestimated for the effective development of anti-adhesion compounds.

In previous work in our group, a library of aromatic glycoconjugates were prepared and assessed as potential novel inhibitors of *C. albicans* adhesion to buccal epithelial cells (BECs). Of this library, compound **1.39** (**Fig. 3.10**), a divalent galactoside, was the best performing compound in several biological assays. In an exclusion assay, which involved incubating *C. albicans* cells with **1.39** prior to exposure to BECs, compound **1.39** produced an 80% reduction in adhered yeast cells in comparison to a control. The control was the level of adherence of the untreated yeast cells to BECs. A competitive assay involved incubating *C. albicans* cells, **1.39** and BECs together with no prior incubation step. Compound **1.39** again performed well in this assay, reducing yeast cell adherence to BECs by 65%. Finally, a displacement assay involved incubation of BECs with *C. albicans* followed by exposure to **1.39**. In this assay, compound **1.39** was capable of reducing adhered *C. albicans* cells by 56% relative to a control in the absence of compound. Evaluation of the anti-adhesion activities of the library of mono-, di- and trivalent aromatic-core glycoconjugates featuring different carbohydrate moieties showed that the divalent presentation of D-galactose moieties was essential for achieving effective anti-adhesion activity [80].

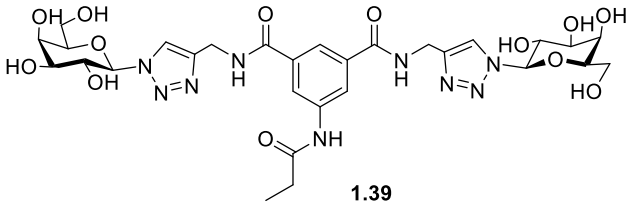

1.39

Figure 3.10: Structure of compound **1.39** [80].

3.2 Chapter Objectives:

In this chapter, the synthesis and evaluation of different glycoconjugates as potential covalent crosslinkers of unknown target lectins is discussed, using compound **1.39** as a lead compound. As discussed above, the binding of lectins/adhesins by anti-adhesion molecules, whether in non-covalent or covalent mode, can significantly inhibit pathogen infection processes. With this in mind, we set about developing a number of glycoconjugates with varying carbohydrate moieties and crosslinking groups.

As mentioned previously, covalent inhibitors have seen a recent resurgence in popularity. In this chapter, we firstly investigate the synthesis of analogues of compound **1.39** with suitable electrophilic moieties to achieve a further enhancement in anti-adhesion activity. We propose acryloyl and vinyl sulfonamide moieties as suitable crosslinking groups to be featured in target compounds **3.25** and **3.27** respectively (**Fig. 3.11**). In the absence of structural information of the target lectin for lead compound **1.39**, it was expected that if nucleophilic amino acids were present in the binding site of said lectin target, they would react with compounds **3.25** and/or **3.27** at these electrophilic sites; this would lead to the crosslinking and permanent inhibition of this lectin upon formation of a stable covalent bond between the compound and lectin.

Furthermore, since L-fucose has also been proposed as an inhibitor of *C. albicans* adhesion [148], divalent fucoside analogues **3.26** and **3.28** (**Fig. 3.11**), featuring the acryloyl and vinyl sulfonamide moieties respectively, were also investigated. I was tasked with the synthesis and characterization of acryloyl derivatives **3.25** and **3.26**, while other members of the group (PhD student Keela Kessie and summer intern Jordan Loughin) completed the synthesis of the vinyl sulfone derivatives **3.27** and **3.28**.

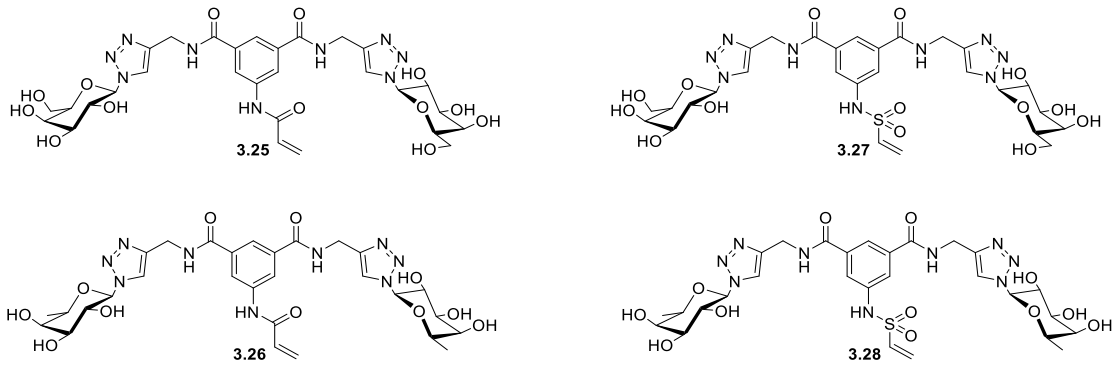

Figure 3.11: Structures of potential covalent crosslinking glycoconjugates **3.25**-**3.28**.

Secondly, the toxicity of a library of compounds, including lead compound **1.39**, target compounds **3.25**-**3.28**, some norbornene derivatives discussed in Chapter 2 and some other compounds previously prepared in the Velasco-Torrijos group, were tested against a number of *Candida* species: *C. albicans*, *C. lusitaniae*, *C. guilliermondii*, *C. parapsilosis*, *C. glabrata* and *C. auris*. This evaluation was carried out in the National Institute of Chemical Physics and Biophysics (NICPB), Estonia.

In addition, the potential for this class of compounds to achieve the proposed covalent crosslinking was evaluated in a series of model experiments with nucleophilic amino acids based on a previously reported protocol and via HRMS analysis [149].

Finally, the inhibition of the adhesion of *C. albicans* to BECs, effected by these analogues, was assessed in collaboration with Prof Kevin Kavanagh (Maynooth University).

3.3 Results and Discussion

3.3.1 Synthesis of glycoconjugates 3.25-3.28

The synthesis of target compounds **3.25**-**3.28** was achieved using reliable reactions commonly employed in the literature. Key to the synthesis of the compounds is the CuAAC reaction that provides the means for joining the sugar azides to the aromatic scaffold through the formation of 1,4-triazolyl linkages. Firstly, the aromatic scaffold **3.15** was prepared (**Scheme 3.1**); the first step involved protecting the amine functional group with a *N*-Boc protecting group using di-*tert*-butyl decarbonate to give **3.14**. Once this was accomplished, the next step was an amide coupling between

the two carboxylic acid groups and propargylamine using TBTU as the coupling agent, which afforded the desired aromatic scaffold **3.15**.

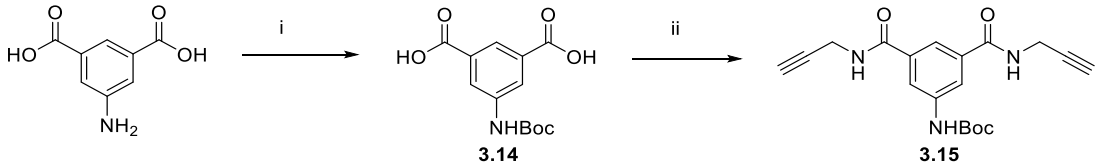

Scheme 3.1: Synthesis of aromatic scaffold **3.15**. Reagents and conditions: i) 1N NaOH, Di-*tert*-butyl dicarbonate, 1.4-dioxane, 16 h, RT, 86%; ii) TBTU, Anhydrous DMF, N_2, Propargylamine, NEt_3, 2 h, RT, 55%.

Fucosyl azide **3.16** was prepared as shown in Scheme **3.2**, using the same conditions as used to prepared **2.40** and **2.41** in Chapter 2.

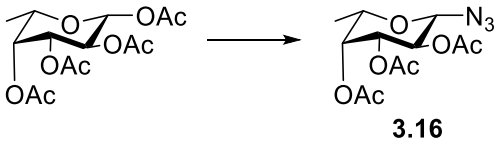

Scheme 3.2: Synthesis of Fucosyl azide **3.16**. Reagents and conditions: i) $TMSN_3$, $SnCl_4$, Dry DCM, 16 h, RT, 76%.

Scaffold **3.15** and sugar azide **2.40** or **3.16** were then used with CuAAC reaction conditions. This reaction is particularly advantageous due to the short reaction times (typically at most 30 mins under microwave irradiation) and the lack of by-products produced, enabling simple purification using flash column chromatography. The reaction of **2.40** or **3.16** with **3.15** yielded **3.17** and **3.18** respectively (**Scheme 3.3**).

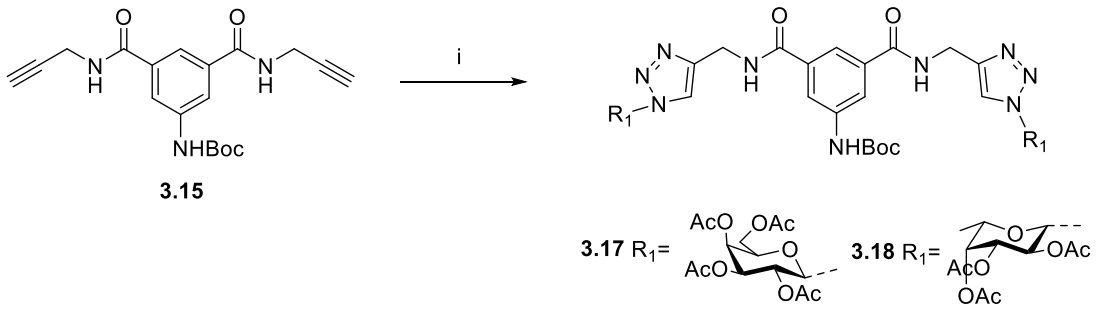

Scheme 3.3: Synthesis of glycoconjugates **3.17** and **3.18**. Reagents and conditions: i) 2,3,4,6-tetra-*O*-acetyl-1-β-azido-galactoside **2.40** or 2,3,4-tri-*O*-acetyl-1-β-azido-fucoside **3.16**, $CuSO_4.5H_2O$/Na Asc, ACN/H_2O, 100 °C in MW, 30 mins, 52-71%.

The *N*-Boc-protected amine group in the resulting products **3.17** and **3.18** was deprotected using TFA to give compounds **3.19** and **3.20** (**Scheme 3.4**). In the next step these amines were reacted with acryloyl chloride to give the desired products **3.21** and **3.22** (**Scheme 3.4**). The vinyl sulfonyl derivatives **3.23** and **3.24** were prepared by fellow group members by reaction of amines **3.19** and **3.20** with 2-chloroethanesulfonyl chloride and NEt_3 (**Scheme 3.4**).

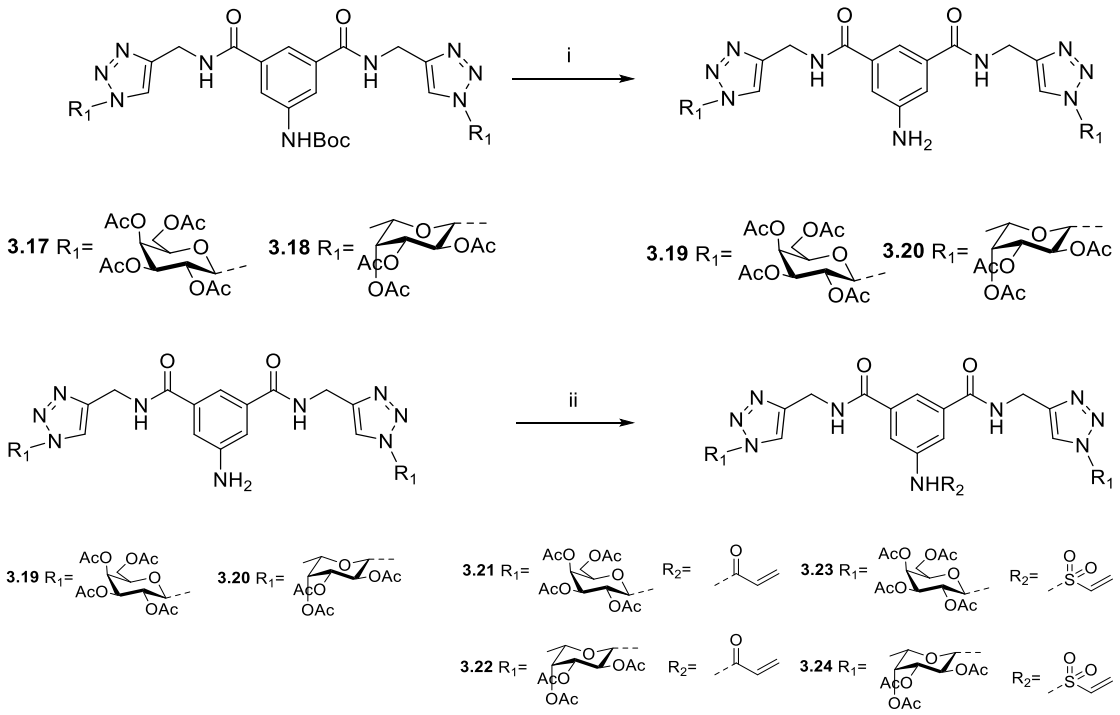

Scheme 3.4: Synthesis of glycoconjugates **3.19**-**3.24**. Reagents and conditions: i) DCM, TFA, 5 h, RT, 38-99%; ii) Acryloyl chloride or 2-chloroethanesulfonyl chloride, NEt_3, DCM, 16 h, RT, 48-73%.

The ^{1}H NMR spectrum for compound **3.21** is shown in Figure **3.12**. The indicative peaks in this spectrum are as follows: the amide proton within the acrylamide moiety (orange circle) is observed as a broad singlet at 9.09 ppm. Two singlet peaks at 8.05 and 7.99 ppm represent the triazolyl protons (dark green circle), amide protons (purple circle) and aromatic protons (yellow circle). A second singlet peak at 7.78 ppm represents another aromatic proton (yellow circle). The alkene protons (light green and blue circles) of the acrylamide moiety are found at as a multiplet at 6.32 ppm and a doublet at 5.67 ppm. Finally, the anomeric proton (red circle) is found at 5.92 ppm as a doublet.

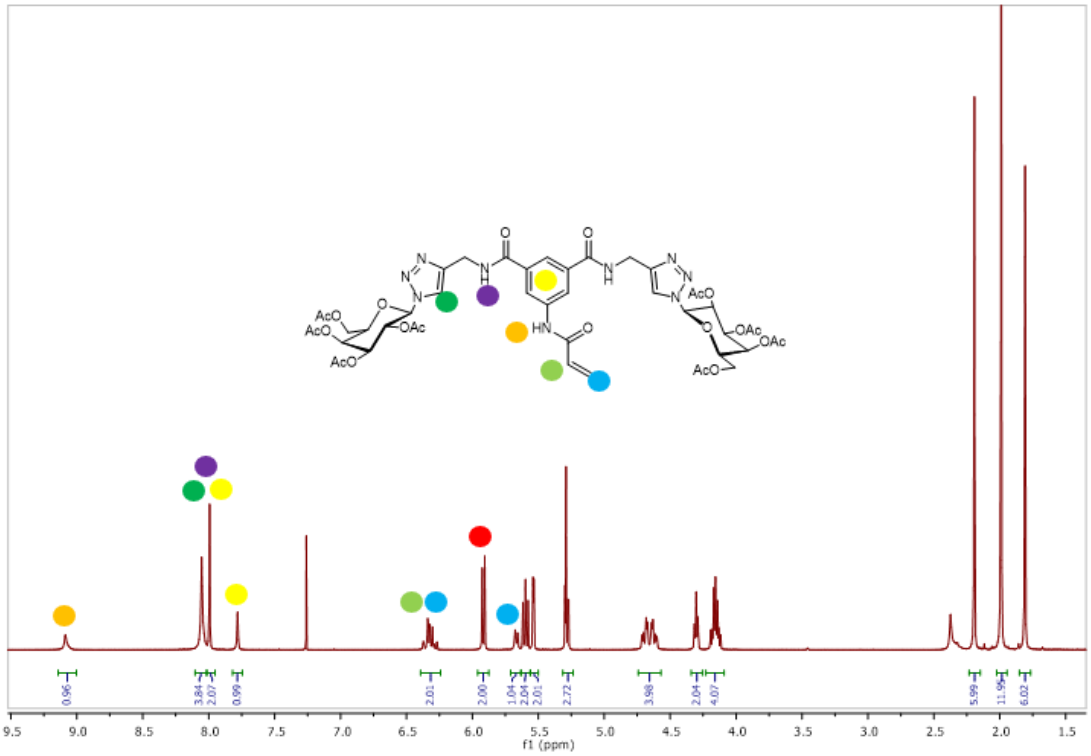

Figure 3.12: ^{1}H NMR spectrum of compound **3.21**. Note: Anomeric proton is assigned as red circle.

These reactions required some optimisation, due to the varied reactivity of acryloyl chloride in comparison to 2-chloroethanesulfonyl chloride. Eventually it was found that 4 equivalents of acryloyl chloride provided a sufficient yield (48-60%) of the desired acryloyl-containing glycoconjugates **3.21** and **3.22** (**Scheme 3.4**). For the vinyl sulfonyl-containing glycoconjugates, it was eventually found that 0.8 equivalents of 2-chloroethansulfonyl chloride and higher dilution were optimal conditions for the synthesis of the corresponding vinyl sulfonyl glycoconjugates. This was required in order to minimize the formation of di-sulfonyl amides. The final step to prepare all four glycoconjugates was deprotection of the acetyl groups on the carbohydrate moieties under mild basic conditions to yield the final desired compounds **3.25**, **3.26**, **3.27**, and **3.28** (**Scheme 3.5**).

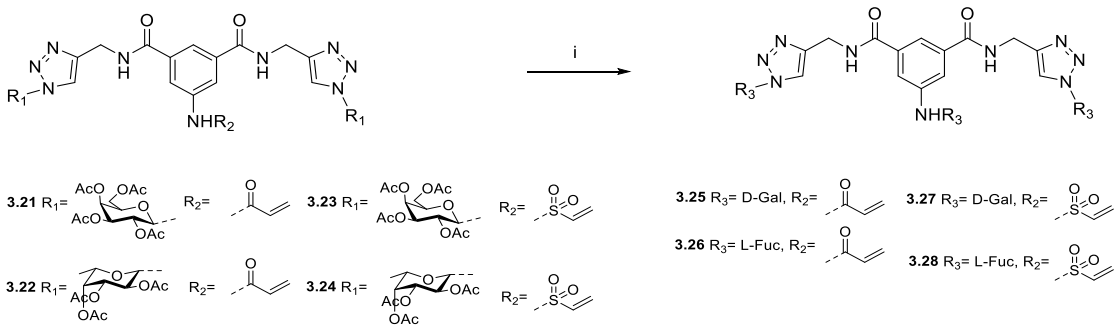

Scheme 3.5: Synthesis of glycoconjugates **3.25**-**3.28**. Reagents and conditions: i) MeOH, H_2O, NEt_3, 45 ^oC, 6 h, 89-96%.

An indicative ^1H NMR for deacetylated compound **3.25** is shown in Figure **3.13**. The triazolyl proton (orange circle) is found as a singlet peak at 8.19 ppm. The aromatic ring protons (green circle) are found as two singlets at 7.76 and 7.68 ppm. The alkene protons of the acrylamide moiety (blue and purple circles) are found as two peaks at 6.19 ppm (doublet) and 5.73 ppm (multiplet), with the two alkene protons bound to the same carbon atom (purple circle) being found as two separate peaks. This indicates that these protons are in different chemical environments. Finally, the anomeric proton of the galactoside moiety (red circle) is found as a doublet at 5.61 ppm.

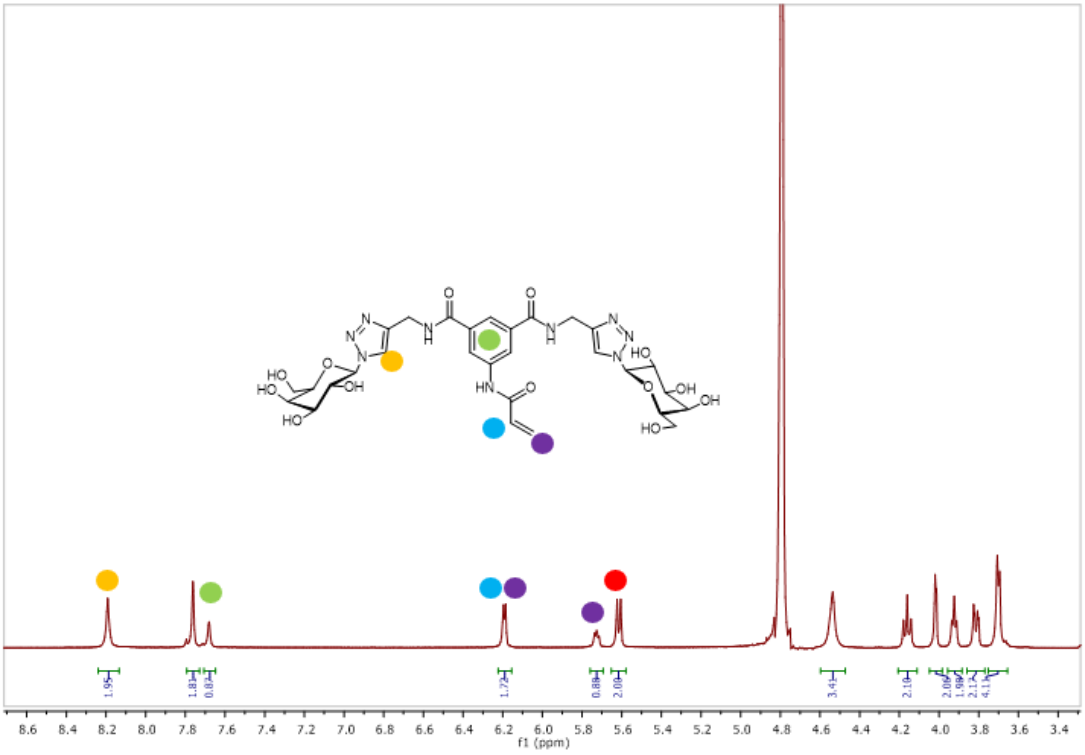

Figure 3.13: ^{1}H NMR spectrum of compound **3.25**. Note: Anomeric proton is assigned as red circle.

An indicative ^{1}H NMR for deacetylated compound **3.26** is shown in Figure **3.14**. The triazolyl proton (orange circle) is found as a singlet peak at 8.23 ppm. The aromatic ring protons (green circle) are found as two singlets at 7.84 and 7.74 ppm. The alkene protons of the acrylamide moiety (blue and purple circles) are found as two peaks at 6.24 ppm (doublet) and 5.78 ppm (multiplet), with the two alkene protons bound to the same carbon atom (purple circle) being found as two separate peaks. This indicates that these protons are in different chemical environments. The anomeric proton of the galactoside moiety (red circle) is found as a doublet at 5.63 ppm. The methyl protons in the fucoside moiety (navy circle) are found as a doublet at 1.22 ppm.

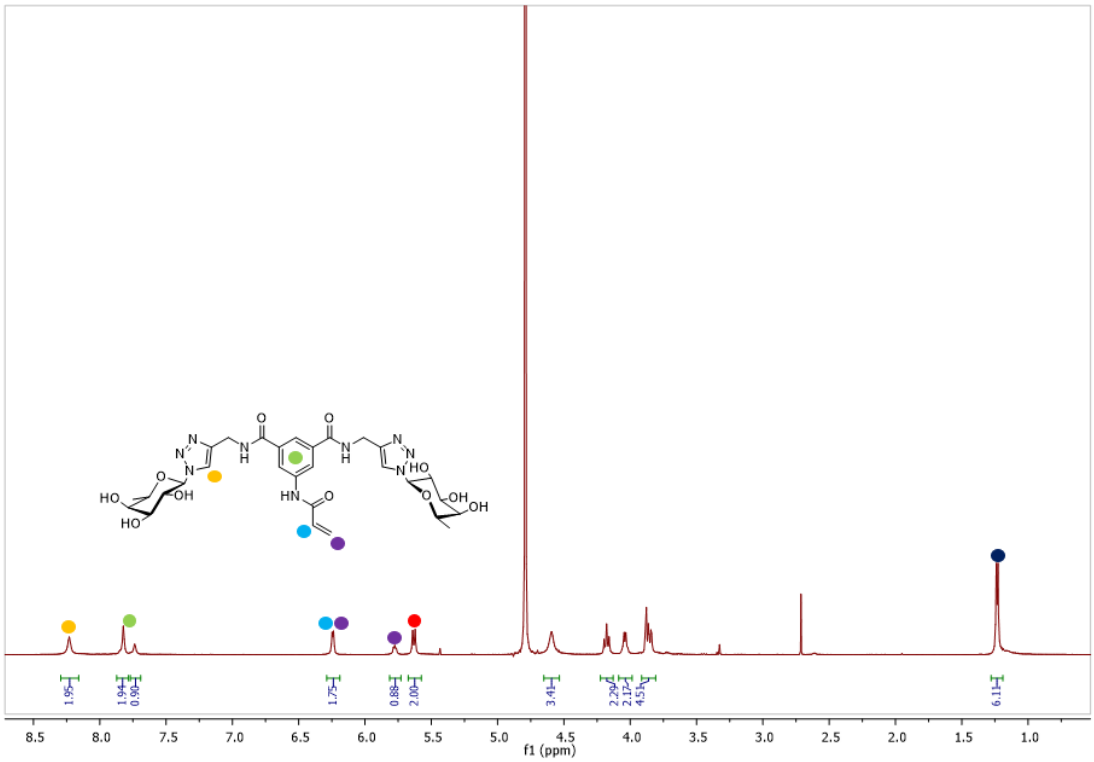

Figure 3.14: ^{1}H NMR spectrum of compound **3.26**. Note: Anomeric proton is assigned as red circle, while the methyl protons of the fucoside are assigned navy circle.

3.3.2 Adhesion inhibition assays against Candida albicans

The ability of the acryloyl glycoconjugates **3.25** and **3.26** to inhibit the adherence of *C. albicans* to BECs was evaluated in the laboratory of Prof. Kevin Kavanagh, Department of Biology (Maynooth University). The adherence assays were performed by (i) treating *C. albicans* with the glycoconjugates, allowing for an incubation period and then exposing the treated yeast cells to the exfoliated BECs (exclusion assay) or (ii) allowing the incubation of yeast cells, BECs and glycoconjugates all together (competition assay). **Figure 3.15** shows the results corresponding to divalent galactoside **3.25** and the original lead compound **1.39** as a positive control. The presence of the acryloyl group did not interfere significantly with the anti-adhesion ability of compound **3.25**, which was comparable in both assays to the lead compound **1.39**.

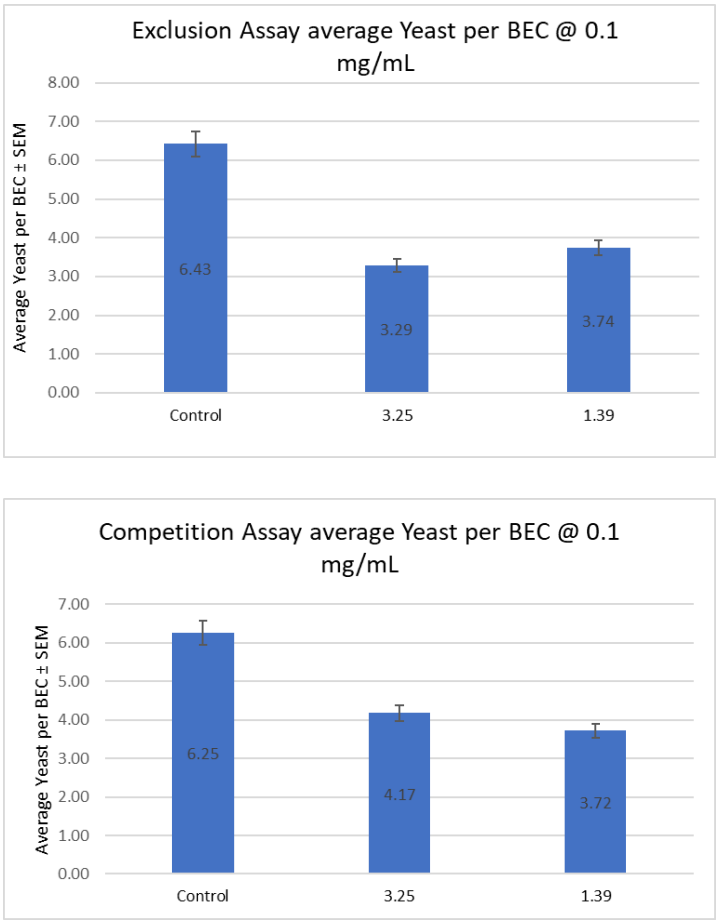

Figure 3.15: Inhibition of adhesion evaluation for compound **3.25.** *Top:* Exclusion assay (0.1 mg/mL) shows a reduction of adhesion of 49% (**3.25**) and 42% (**1.39**) compared to the control (untreated yeast); *Bottom:* competition assay (0.1 mg/mL) shows a reduction of adhesion of 33% (**3.25**) and 40% (**1.39**) compared to the control (untreated yeast).

Next, the ability of the divalent fucoside **3.26** to inhibit the adherence of *C. albicans* to BECs was evaluated. Figures **3.16** and **3.17** show the exclusion and competition assays, respectively, for fucosyl compound **3.26** and lead compound **1.39.** In addition, these compounds were evaluated in combination to probe a potential synergistic effect.

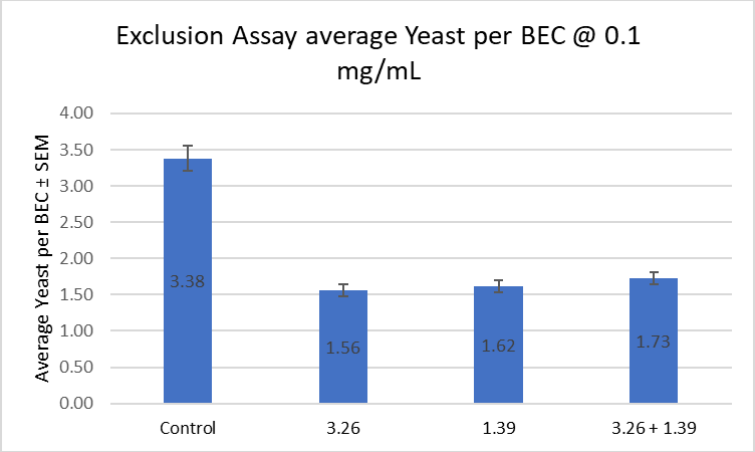

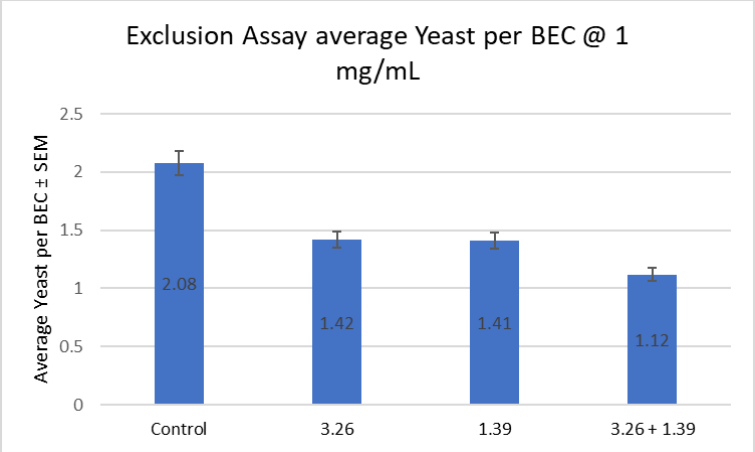

Figure 3.16: Inhibition of adhesion evaluation for compound **3.26.** *Top:* Exclusion assay (0.1 mg/mL) shows a reduction of adhesion of 54% (**3.26**), 52% (**1.39**) and 49% (combination of **3.26** and **1.39** (1:1)) compared to the control (untreated yeast); *Bottom:* Exclusion assay (1 mg/mL) shows a reduction of adhesion of 32% (**3.26**), 32 % (**1.39**) and 46% (combination of **3.26** and **1.39** (1:1)) compared to the control (untreated yeast).

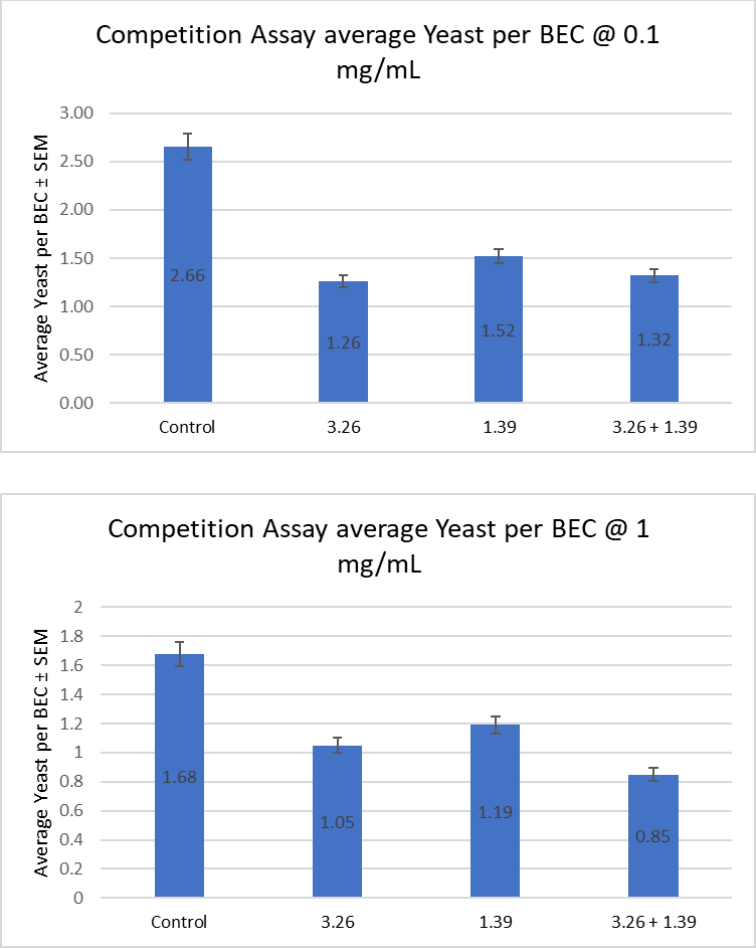

Figure 3.17: Inhibition of adhesion evaluation for compound **3.26.** *Top:* Competition assay (0.1 mg/mL) shows a reduction of adhesion of 52% (**3.26**), 43% (**1.39**) and 50% (combination of **3.26** and **1.39** (1:1)) compared to the control (untreated yeast); *Bottom:* Competition assay (1 mg/mL) shows a reduction of adhesion of 38% (**3.26**), 29% (**1.39**) and 49% (combination of **3.26** and **1.39** (1:1)) compared to the control (untreated yeast).

Interestingly, the divalent fucosyl derivative **3.26** appeared to have comparable activity to lead compound **1.39** in all the assays. It was hypothesised that, since some *C. albicans* adhesins have been reported to bind fucosylated cell surface glycans, treatment with glycoconjugates bearing distinct carbohydrate moieties may enhance the desired anti-adhesion activity, similar to the work by Takagi *et al.* [30,147]. Therefore, it could be possible that galactoside **1.39** and fucoside **3.26** could be interacting with different targets specifically. However, the reduction of adhesion did not change significantly when treating the yeast with the combination of compounds.

Finally, a displacement assay was carried out, involving co-incubation of BECs and *C. albicans*, which allows for adhesion to occur. Following this incubation step, the

glycoconjugate was added and the ability of the compounds to reverse the adherence of the yeast to the BECs was then examined. Two controls were used in this assay: control 1 involved the assessment of the binding of *C. albicans* to BECs prior to compound exposure; control 2 involved BECs and adherent yeast cells being re-incubated in PBS for 90 minutes prior to a second filtration step. (**Fig. 3.18**). It was found that **3.26** and **1.39** had a comparable activity, however, the combination of both compounds reduced adherence by a very promising 59% (compared to the control 2). This surprising result needs to be further validated, but it may open interesting possibilities for the design of mixed/heterovalent glycoconjugates to target fungal adhesion.

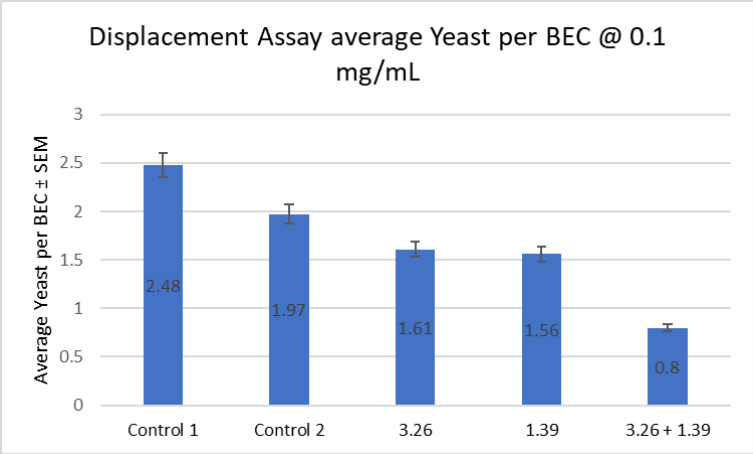

Figure 3.18: Inhibition of adhesion evaluation for compound **3.26.** Displacement assay (0.1 mg/mL) shows a reduction of adhesion of 18% (**3.26**), 20% (**1.39**) and 59% (combination of **3.26** and **1.39** (1:1)) compared to control 2.

3.3.3 Preparation of fluorescently labelled derivatives of 1.39 and 3.26

In light of these interesting results from the combinatorial treatment of **3.26** and **1.39**, two fluorescently labelled derivatives of these compounds were envisaged. Importantly, these derivatives would be labelled with two different fluorescent probes with the hope of visualising, separately, the targets of each individual glycoconjugate. The attempted synthesis of both probes is show in Schemes **3.6** and **3.7**. A low conversion (8%) to desired compound **3.30** was achieved (see below for explanation). Unfortunately, synthesis of fluorescently labelled probe **3.33** was not

successful (**Scheme 3.7**). Therefore, further optimisation is required to prepare compound **3.33.**

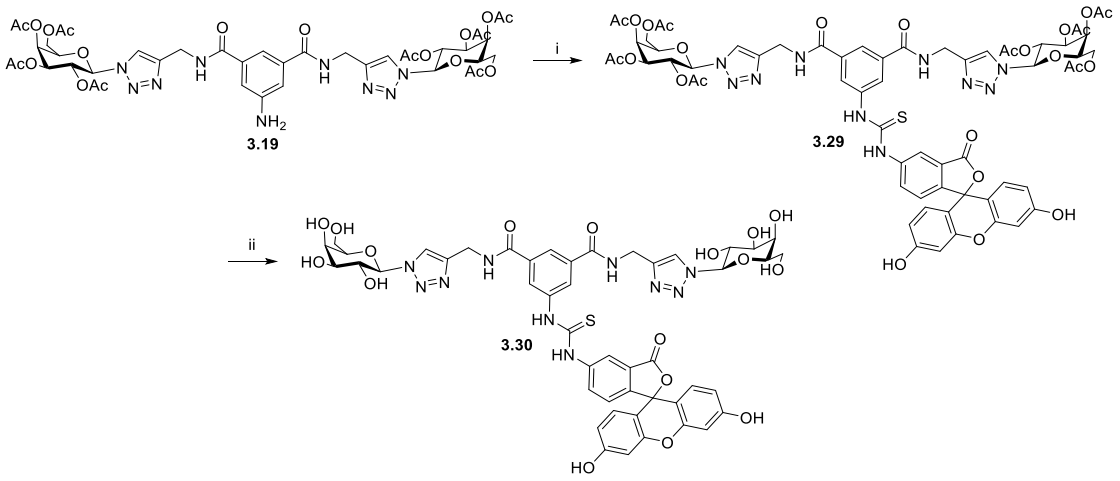

Scheme 3.6: Synthesis of fluorescently-labelled glycoconjugates **3.30**. Reagents and conditions: i) FITC, acetone, 50 ˚C, MW, 1 h, 8%; ii) MeOH, NEt_3, H_2O, 45 ˚C, 6.5 h.

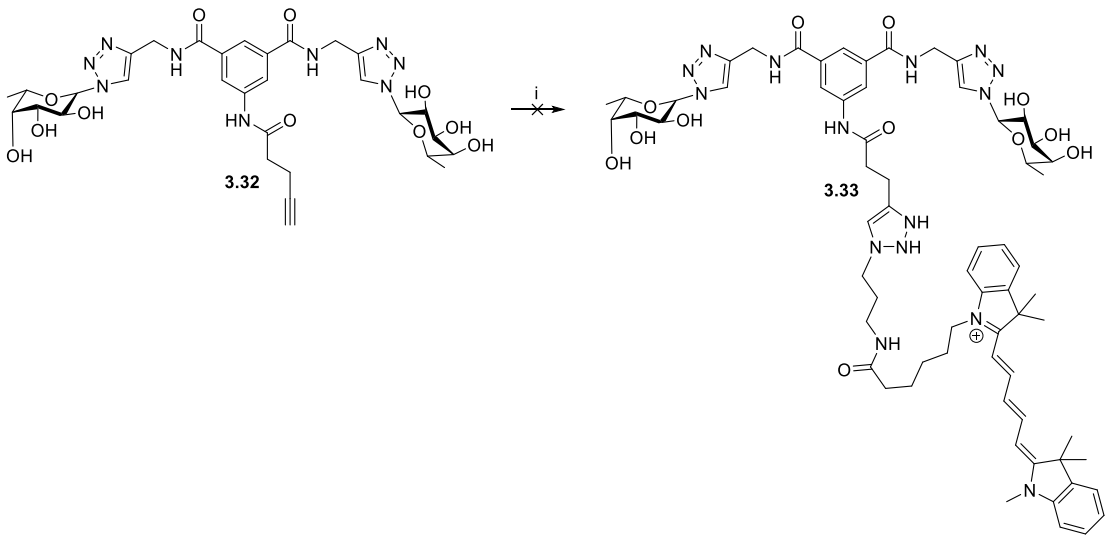

Scheme 3.7: Synthesis of fluorescently-labelled glycoconjugates **3.33**. Reagents and conditions: i) Cyanine 5 azide, $CuSO_4.5H_2O$/Na Asc, ACN/H_2O, 45-50°C, 6 h, unsuccessful.

Unfortunately, a relatively low conversion of 8% was achieved following reaction of **3.19** with fluorescein isothiocyanate (FITC). This can be seen in the ^{1}H NMR spectrum shown in Figure **3.19**, the signal corresponding to the anomeric proton consists of two overlapping doublets. The major doublet, corresponding to the anomeric proton in the unlabelled compound, has a relative integration of 2 whereas the relative integration of the anomeric proton of probe **3.30** is 0.16. Thus, there was an approximate 8% conversion to the fluorescently labelled. As a result of this low

conversion, the desired compound **3.30** was not detected upon HRMS analysis of a sample of this compound. Initial testing of compound **3.30** in the presence of *C. albicans* cells resulted in confocal images of poor resolution. This was attributed to errors in the concentrations of **3.30** that was used and/or the concentration of *C. albicans* used when incubated with **3.30**. Again, further optimisation is currently underway to prepare samples to achieve the desired confocal images. This will involve optimisation of the concentration of **3.30** being incubated with a given quantity of *C. albicans* cells.

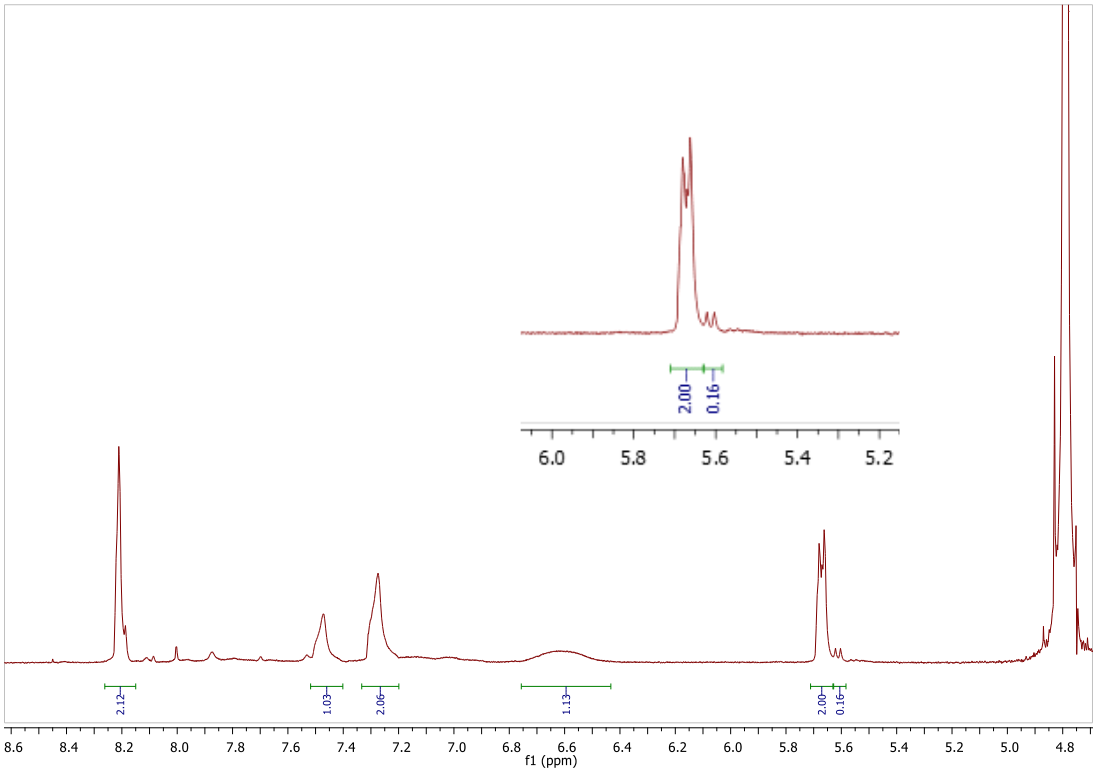

Figure 3.19: ^{1}H NMR of compound **3.30** in D_2O.

3.3.4 Toxicity assays against Candida spps.

The toxicity of compounds **1.39**-**3.42,** alongside several norbornene derivatives discussed in Chapter 2 and compounds previously prepared in the Velasco-Torrijos' research group, were tested against a number of *Candida* species (**Fig. 3.20**).

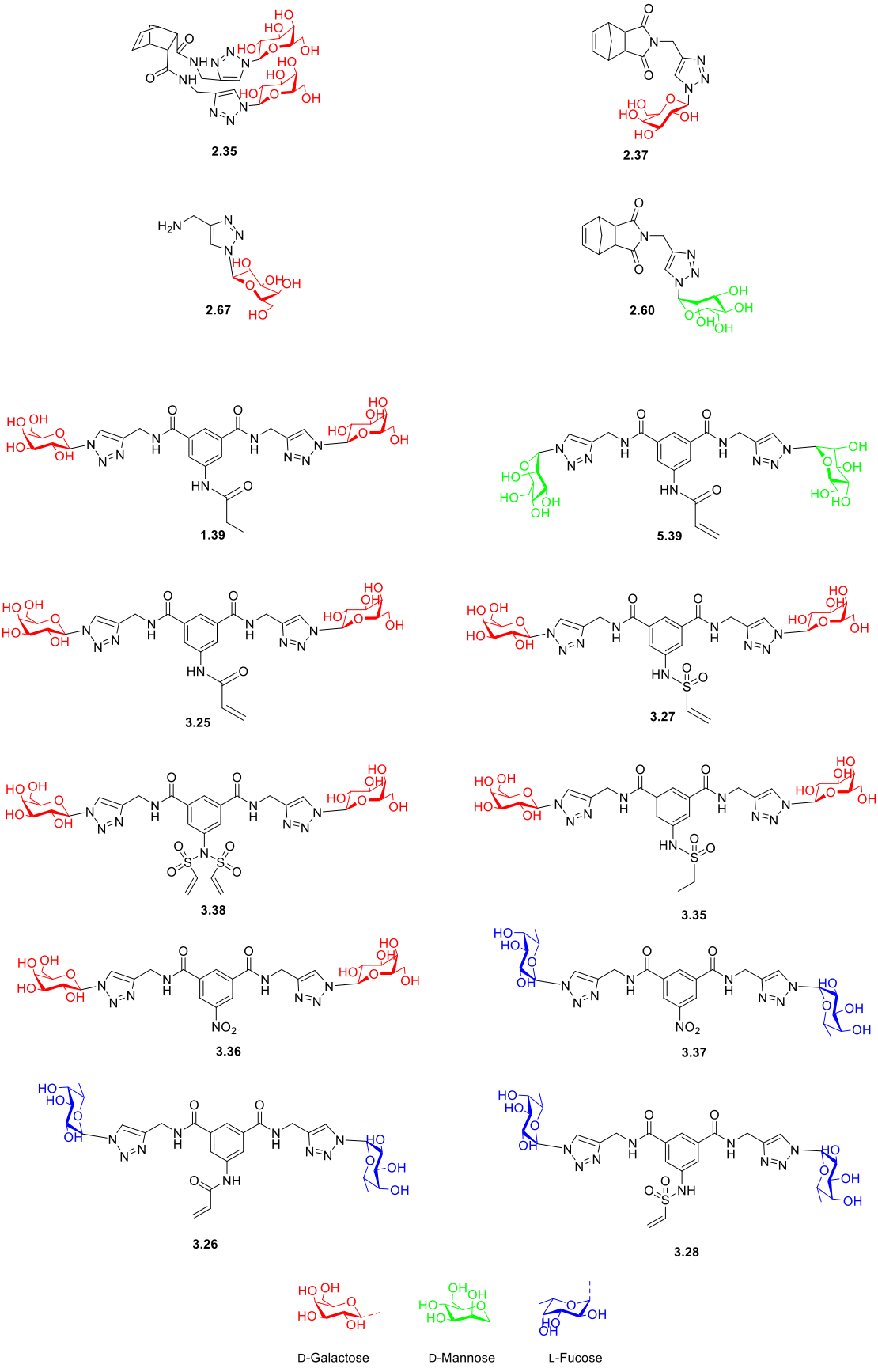

Figure 3.20: Structures of compounds **1.39**-**3.42** evaluated in toxicity testing.

This evaluation was performed in collaboration with Prof Kaja Kasements in the National Institute of Chemical Physics and Biophysics (NICPB), Estonia, through a Short-term Scientific Mission (funded by COST Action 18132 GlycoNanoProbes). The toxicity of the compounds at a range of concentrations was evaluated on *Candida* species which included *C. albicans* (ATCC10231), *C. lusitaniae* (C64), *C. guilliermondii* (C18), *C. parapsilosis* (ATCC22019), *C. glabrata* (ATCC90030) and *C. auris* (CMYA-5001) (**Table 3.1**). Some of these species (*C. albicans, C. auris)* are considered fungal pathogens of critical priority by the World Health Organization, while others (*C. glabrata, C. parapsilosis)* are within the high priority fungal pathogens classification [150,151].

To evaluate the toxicity of these compounds a 'spot test' was performed in NICPB. The relevant *Candida* species were incubated with the compounds at a range of concentrations in a 96-well microplate for 24 h at 30 ^{o}C. Then the cell cultures from each well were transferred onto agar medium plates and incubated at 30 ^{o}C for further 48 h. The growth of cells was then visually evaluated. The minimum biocidal concentration (MBC) was determined as the lowest tested concentration of the compound which completely inhibits the growth of cells (formation of colonies) on agar plates after 24 h exposure in deionised water. The compounds were tested at a concentration of 10-100 mg/mL.

Some of the most encouraging results are shown in Figures **3.21** and **3.22**. Figure **3.21** shows the results of the spot test of the range of compounds mentioned against *C. albicans*. Of note, rows one and two (orange box) show that compound **3.25** is toxic to *C. albicans* at a concentration of 100 mg/mL. Also, rows five and six (red box) show that compound **1.39** is toxic to *C. albicans* at a concentration of 100 mg/mL. Thus, MBCs of 100 mg/mL were determined for both compound **1.39** and **3.25** against *C. albicans*.

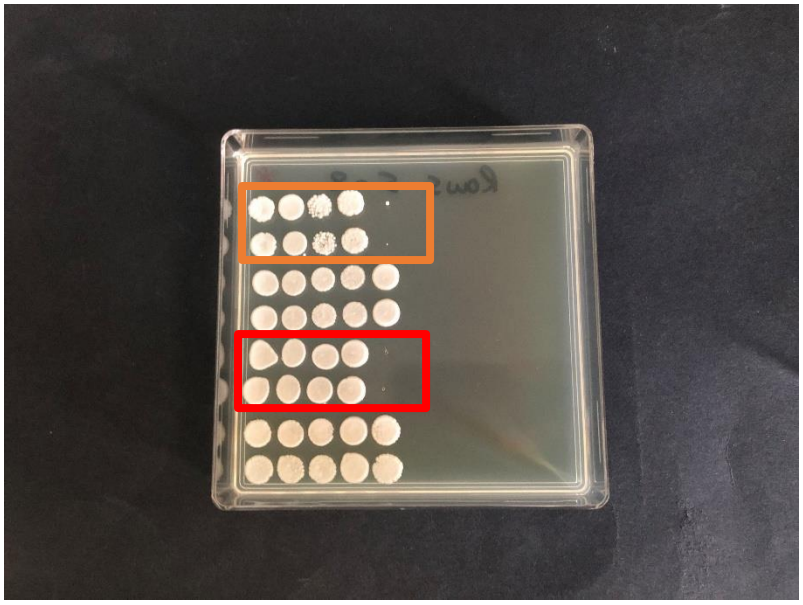

Figure 3.21: Toxicity evaluation of compounds **3.25** (orange box) and **1.39** (red box) against *C. albicans*, concentrations increase from 0 mg/mL (left, control) to 100 mg/mL (right) in each row.

In Figure **3.22** the results of the spot test of the range of compounds mentioned against *C. glabrata* is shown. Of note, rows one and two (orange box) show that compound **3.25** is toxic to *C. glabrata* at a concentration of 100 mg/mL. Also, rows five and six (red box) show that compound **1.39** is toxic to *C. glabrata* at a concentration of 100 and 10 mg/mL. Rows seven and eight (green circle) show that compound **3.27** is toxic to *C. glabrata* at a concentration of 10 mg/mL. Thus, MBCs of 100, 10 and 10 mg/mL were determined for compounds **3.25**, **1.39** and **3.27** against *C. glabrata* respectively.

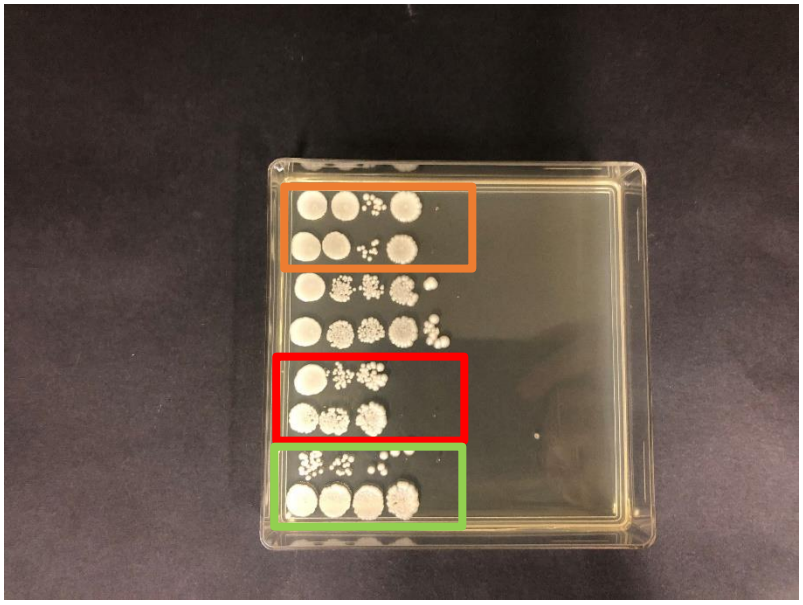

Figure 3.22: Toxicity evaluation of compounds **3.25** (orange box), **1.39** (red box) and **3.27** (green box) against *C. glabrata*, concentrations increase from 0 mg/mL (left, control) to 100 mg/mL (right) in each row.

The results are shown in Table **3.1**. None of the norbornene derivatives **2.35**-**2.67** were found to be toxic at the highest concentrations tested (10 mg/mL) for any of the Candida spps. While all the aromatic-core compounds tested were found to be non-toxic at clinically relevant concentrations, at higher concentrations some toxicity was observed. The lead compound **1.39** showed some toxicity at 100 mg/mL for *C. albicans, C. lusitaniae* and *C. parapsilosis*. This compound also showed toxicity at 10 mg/mL for *C. guilliermondii* and *C. glabrata*. As discussed earlier, this compound has previously been shown to be an effective inhibitor of the adhesion of *C. albicans*, so the observed toxicity may be due to the interaction with yeast adhesins [80]. Interestingly, compound **3.27** was also toxic against *C. guilliermondii* and *C. glabrata*, giving MBC values of 10 mg/mL. *C. glabrata* is known to express Epa adhesins which recognize and bind terminal galactosides in host cells surface glycans [152]. Divalent galactoside derivative **3.25** showed toxicity at high concentration (100 mg/mL) across all the species tested. The corresponding vinyl sulfonamide derivative **3.27** was less toxic than lead compound **1.39** and acryloyl **3.25** for *C. albicans, C. lusitaniae* and *C. parapsilosis* but showed comparable toxicity to lead compound **1.39** at 10 mg/mL for *C. guilliermondii* and *C. glabrata.* Importantly, **3.27** was also toxic at this concentration for *C. auris*, an emerging fungal pathogen of highest concern due to its

multi-drug resistance [153]. On the other hand, ethyl sulfonamide derivative **3.40**, which lacks cross-linking ability, did not show toxicity for any *Candida* spps at the highest concentration tested (>100 mg/mL). However, di-vinyl sulfonamide **3.38** did not show significant toxicity either, which could be due to steric hinderance at the binding site due to the second vinyl sulfone group. The presence of the electrophilic groups in the fucoside derivatives (**3.26** and **3.28**) did not result in toxicity at >10 mg/mL for any of the *Candida* spps evaluated. The only fucoside found to have toxicity at high concentrations (100 mg/mL) for all species was compound **3.42** which features a nitro-substituted aromatic scaffold. The corresponding galactoside compound **3.41** showed similar activity, except for *C. albicans*, for which no toxicity was observed at >100 mg/mL.

Compounds (mg/mL)	**MBC**					
	Yeast (Candida sp)					
	C. albicans ATCC10231	*C. lusitaniae* C64	*C. guilliermondii* C18	*C. parapsilosis* ATCC22019	*C. glabrata* ATCC90030	*C. auris* CMYA-5001
	24-h MBC					
3.25	100	100	100	100	100	n.d*
1.39	100	100	10	100	10	n.d*
3.27	>10	>10	10	>10	10	10
3.40	>100	>100	>100	>100	>100	n.d*
3.42	100	100	100	100	100	100
3.26	>10	>10	>10	>10	>10	>10
2.35	>10	>10	>10	>10	>10	>10
2.37	>10	>10	>10	>10	>10	>10
2.67	>10	>10	>10	>10	>10	>10
2.60	>10	>10	>10	>10	>10	>10
3.37	>10	>10	>10	>10	>10	n.d*
3.38	>10	>10	>10	>10	>10	>10
3.41	>100	100	100	100	100	n.d*
>10mg/mL						
>100mg/mL						
10mg/mL						
100mg/mL						

Table 3.1: Minimum biocidal concentrations for compounds **1.39**-**3.42** against six *Candida sp.*

3.3.5 Model cross-linking experiments

To assess the reactivity of the glycoconjugates featuring electrophilic groups that had shown some toxicity against *Candida* spps, model cross-linking experiments were designed. In these experiments, three model nucleophiles: *N*-α-acetyl-L-lysine, *N*-acetyl-L-histidine and *N*-acetyl-L-cysteine (**Fig. 3.23**, which were considered models of the common reactive sidechains of amino acids found in lectin binding sites) were reacted with compounds **3.25** or **3.27** in either a pH 7.4 or 10.2 buffer. The extent, if any, of the crosslinking between compound **3.25** or **3.27** and each of these nucleophiles was assessed by HPLC and HRMS. The two buffers were chosen as the pH 7.4 buffer corresponds to the blood's pH and the pH 10.2 buffer was chosen based on the protocol from which these model crosslinking experiments were based. A pH 10.2 buffer was chosen to mimic the lowered pK_a of biologically relevant nucleophilic lysine. Based on this procedure, the electrophile (**3.25** or **3.27**) is present in a 1:50 ratio with the nucleophile (*N*-α-acetyl-L-lysine, *N*-acetyl-L-histidine or *N*-acetyl-L-cysteine), ensuring a large excess of nucleophile in the reaction [149].

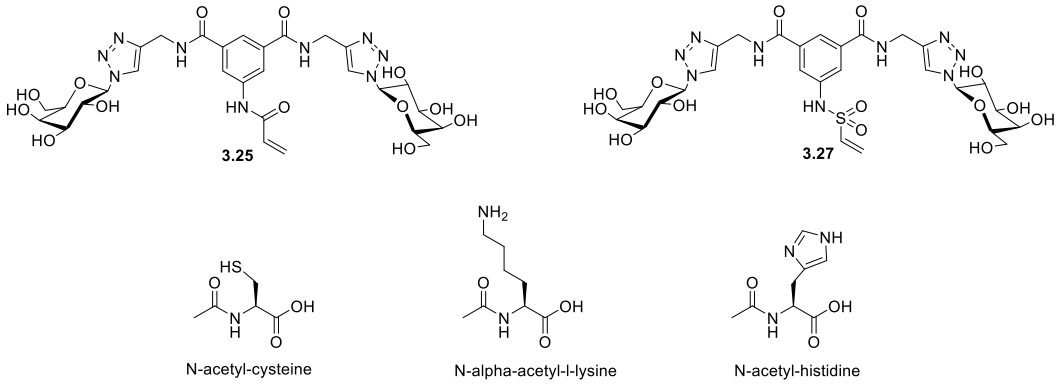

Figure 3.23: Proposed Electrophiles (**3.25** & **3.27**) & Nucleophiles for model crosslinking reactions.

Compounds **3.25** and **3.27** were reacted with three nucleophiles; *N*-α-acetyl-L-lysine, *N*-acetyl-L-histidine and *N*-acetyl-L-cysteine at pH 7.4 and pH 10.2 over the course of 24 h. Aliquots were taken from each reaction after 3 h, 6 h and 24 h and they were analysed by HPLC. Upon analysis of the resulting chromatograms, it was observed that no significant reactions between **3.25** or **3.27** with *N*-acetyl-L-cysteine or *N*-acetyl-L-histidine had occurred at either pH 7.4 or 10.2 (**Fig. 3.24** and **3.25**). In these reactions, a significant amount of starting materials **3.25** or **3.27** and the

corresponding amino acids could still be observed even after 24 h, and no additional novel peaks that could be attributed to cross-linking products were detected.

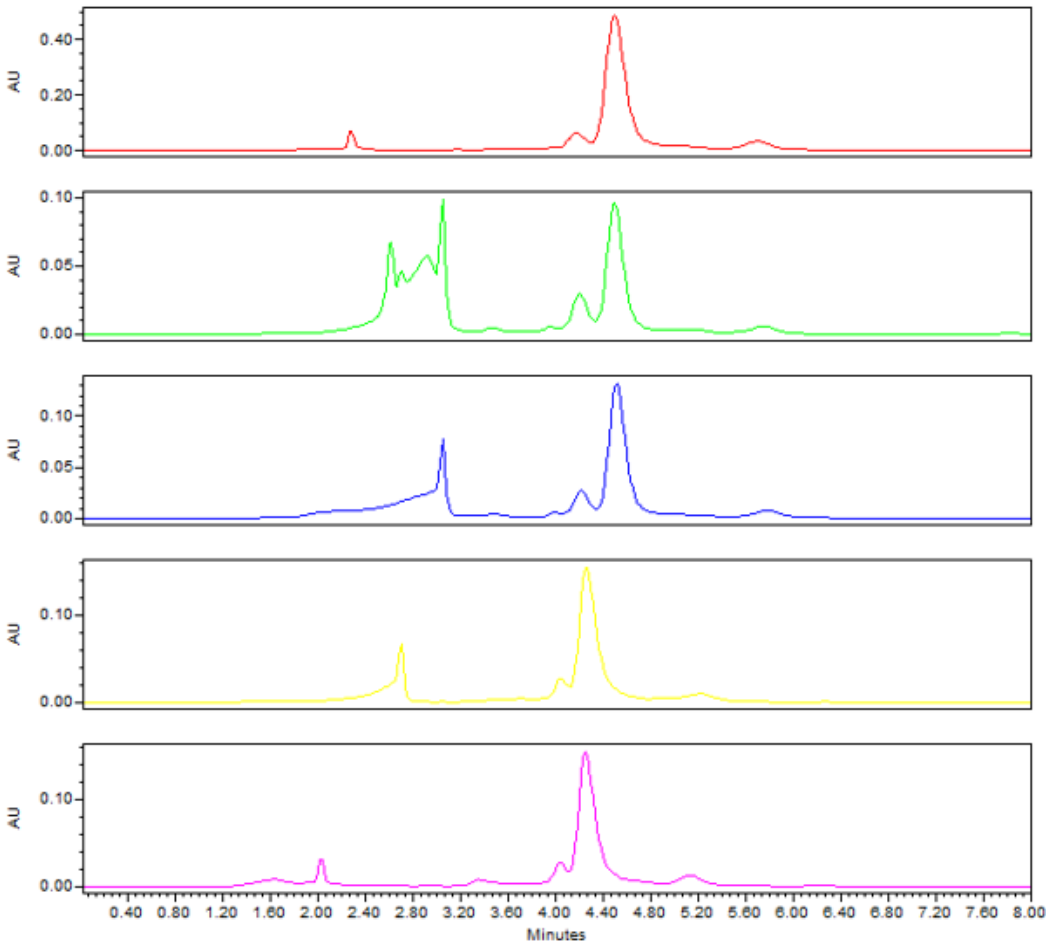

Figure 3.24: Reaction of **3.25** at RT with *N*-acetyl-L-cysteine or *N*-acetyl-L-histidine at pH 7.4 & 10.2 after 24 h: Chromatograms (top to bottom); 1) **3.25**), 2) **3.25** (1 equiv.) following reaction with *N*-acetyl-L-cysteine (50 equiv.) at pH 7.4, 3) **3.25** (1 equiv.) following reaction with *N*-acetyl-L-cysteine (50 equiv.) at pH 10.2, 4) **3.25** (1 equiv.) following reaction with *N*-acetyl-L-histidine (50 equiv.) at pH 7.4, 5) **3.25** (1 equiv.) following reaction with *N*-acetyl-L-histidine (50 equiv.) at pH 10.2.

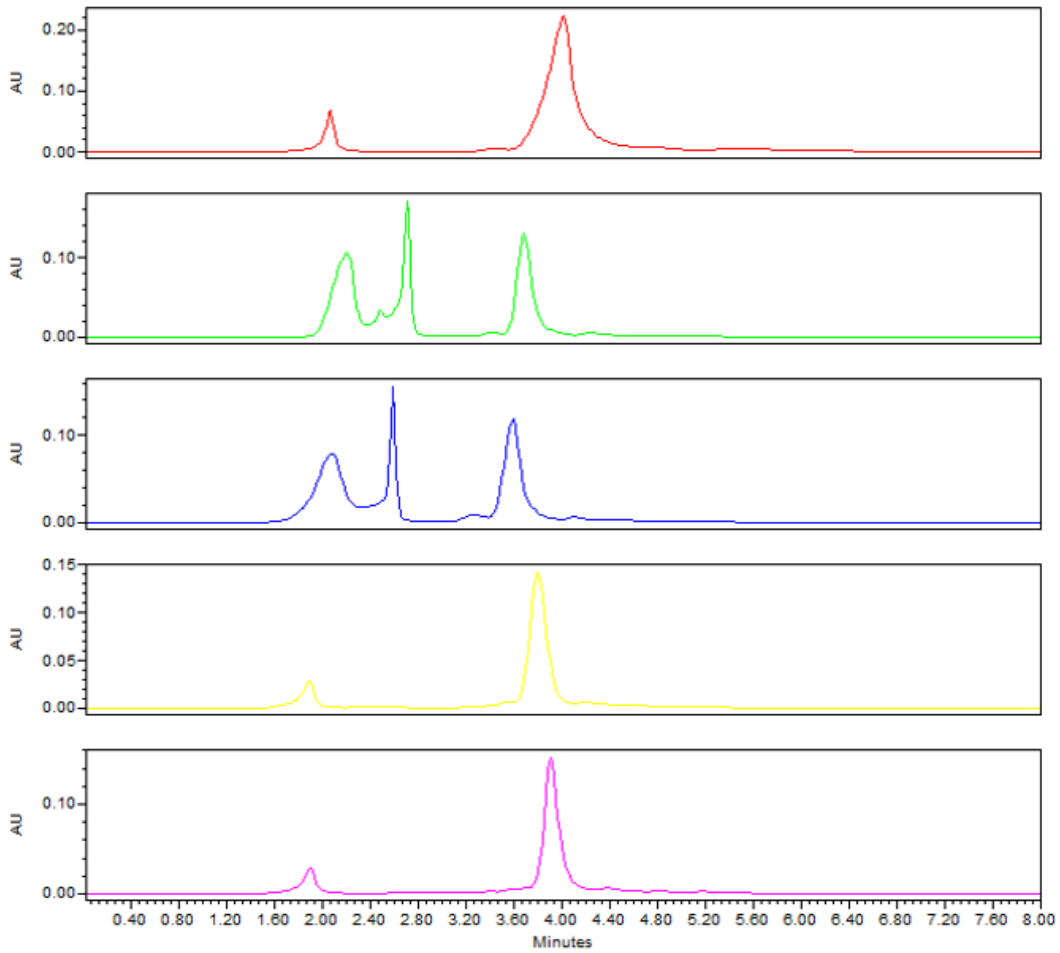

Figure 3.25: Reaction of **3.27** at RT with *N*-acetyl-L-cysteine or *N*-acetyl-L-histidine at pH 7.4 & 10.2 after 24 h: Chromatograms (top to bottom); 1) **3.27**, 2) **3.27** (1 equiv.) following reaction with *N*-acetyl-L-cysteine (50 equiv.) at pH 7.4, 3) **3.27** (1 equiv.) following reaction with *N*-acetyl-L-cysteine (50 equiv.) at pH 10.2, 4) **3.27** (1 equiv.) following reaction with *N*-acetyl-L-histidine (50 equiv.) at pH 7.4, 5) **3.27** (1 equiv.) following reaction with *N*-acetyl-L-histidine (50 equiv.) at pH 10.2.

The results from the reaction of **3.25** and **3.27** with *N*-α-acetyl-L-lysine in pH 7.4 and pH 10.2 are summarized in Table **3.2**.

Electrophile	Peak retention times (rt) following reaction with *N*-α-acetyl-L-lysine after 24 h
3.25 (pH 7.4) (**rt *ca*. 4.5 mins**)	2.53 mins (small peak) and 4.3 mins (likely **3.25**)
3.25 (pH 10.2) (**rt *ca*. 4.5 mins**)	1.46 mins (likely by product/impurity) and 3.6 mins (possible adduct)
3.27 (pH 7.4) (**rt *ca*. 3.9 mins**)	2.58 mins (small peak), 3 mins (possible adduct) and 3.9 mins (likely **3.27**)
3.27 (pH 10.2) (**rt *ca*. 3.9 mins**)	2 mins (small peak), 3.2 mins (possible adduct) and 4 mins (likely **3.27**)

Table 3.2: Model crosslinking reactions results.

It was not clear if the cross-linking reaction between **3.25** with *N*-α-acetyl-L-lysine at pH 7.4 had taken place, as the peaks observed after HPLC analysis of the reaction mixtures had very small differences in rt with the starting material **3.25** (**Fig. 3.26**, **Table 3.2**).

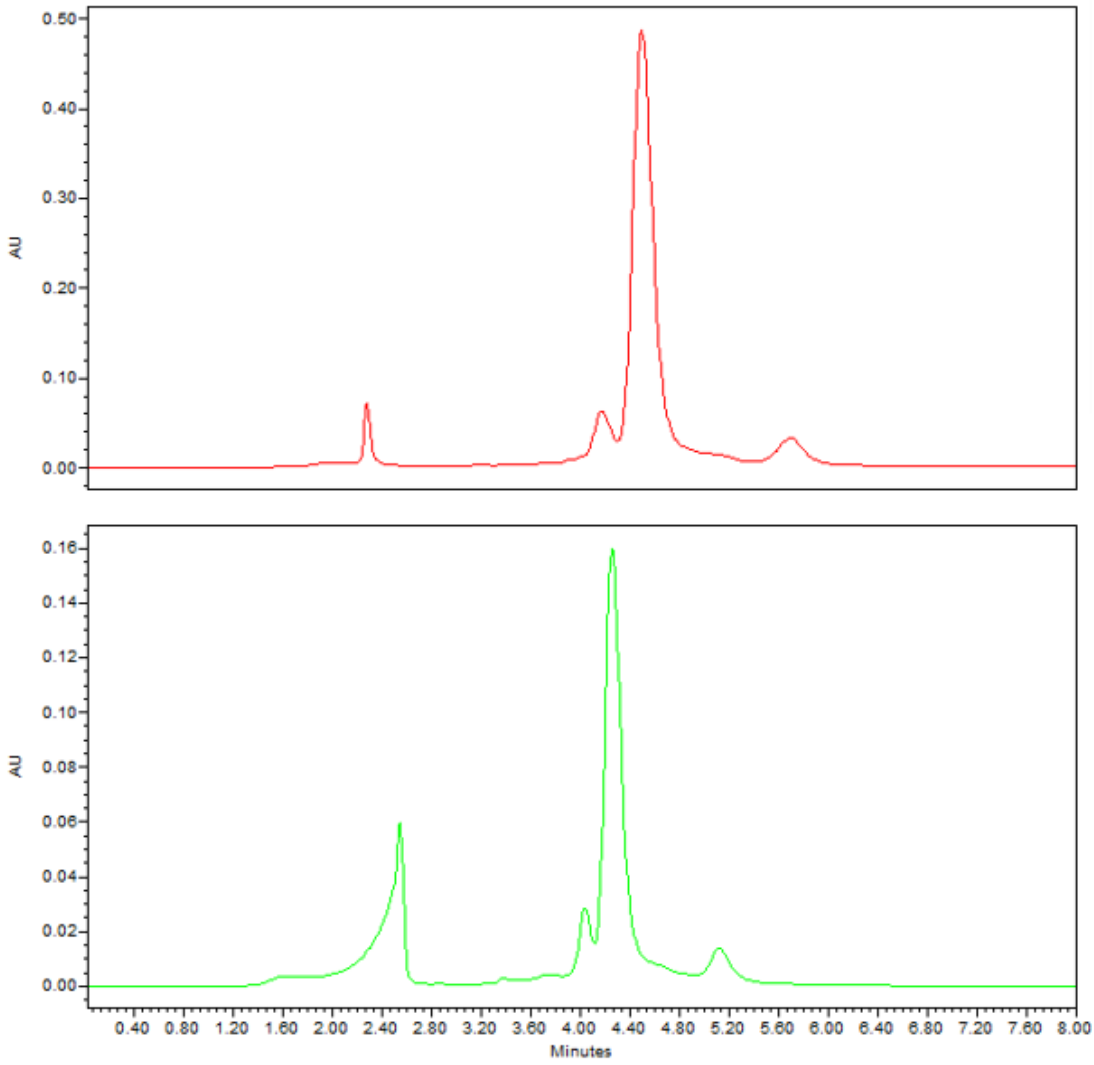

Figure 3.26: Reaction of **3.25** at RT with *N*-α-acetyl-L-lysine at pH 7.4 after 24 h: Chromatograms (top to bottom); 1) **3.25**, 2) **3.25** (1 equiv.) following reaction with *N*-α-acetyl-L-lysine (50 equiv.).

However, at pH 10.2 it was observed that the reaction of **3.25** with *N*-α-acetyl-L-lysine was completed after 3 h (**Fig. 3.27**)**,** according to the change in rt of the major peak from 4.5 mins to 3.6 mins. To confirm the appearance of this new peak, this reaction mixture was spiked with a 1 mg/mL solution of **3.25** (**Fig. 3.27**). This confirmed that the new peak at 3.6 mins may indeed be the crosslinking product formed from the reaction between **3.25** and *N*-α-acetyl-L-lysine.

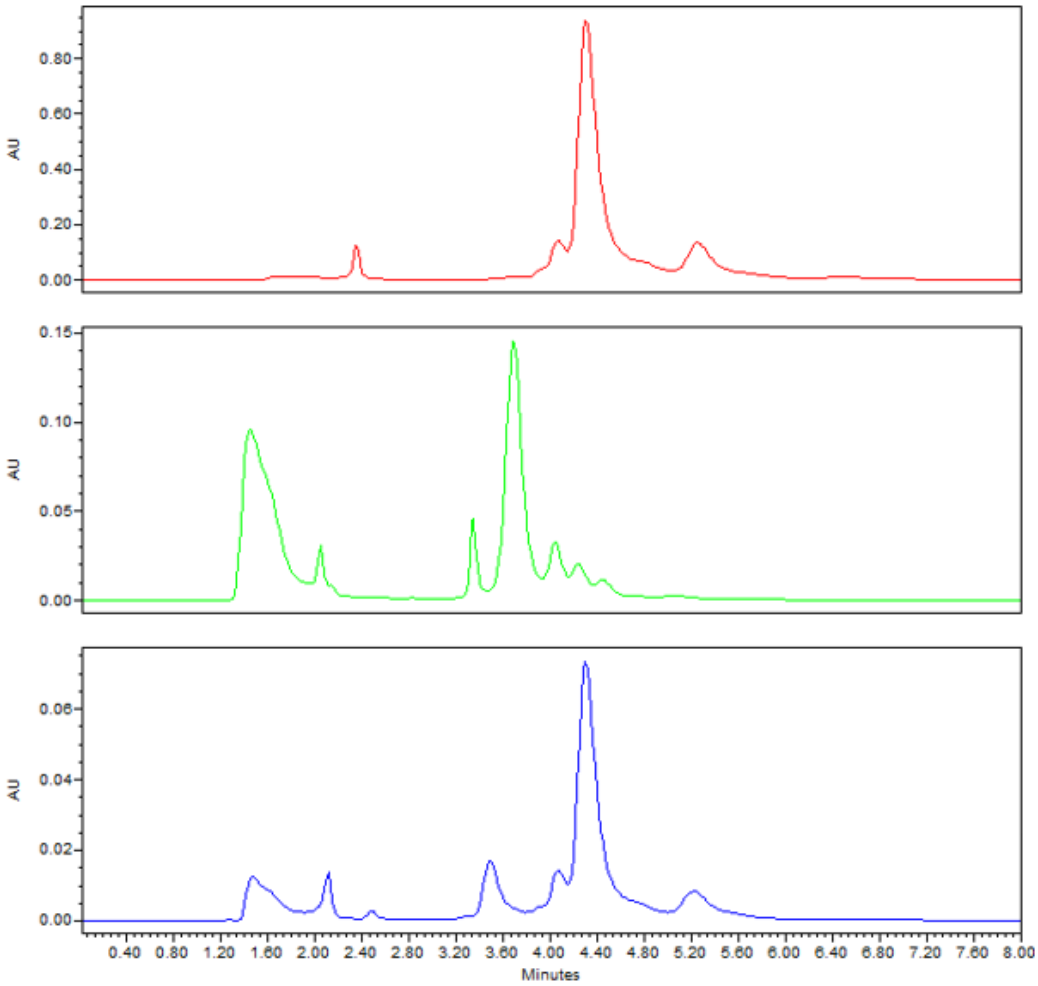

Figure 3.27: Reaction of **3.25** at RT with *N*-α-acetyl-L-lysine at pH 10.2 after 3 h: Chromatograms (top to bottom); 1) **3.25**, 2) **3.25** (1 equiv.) following reaction with *N*-α-acetyl-L-lysine (50 equiv.), 3) **3.25** (1 equiv.) following reaction with *N*-α-acetyl-L-lysine (50 equiv.) spiked with 1 mg/mL **3.25**.

With regard to compound **3.27** in reaction with *N*-α-acetyl-L-lysine at pH 7.4, a new peak with rt *ca*. 3 mins was observed (**Fig. 3.28**). This peak is different to the peak for **3.27**. However, this reaction does not go to completion at pH 7.4. Interestingly, the intensity of the new peak increases when the reaction was performed at pH 10.2 (**Fig. 3.28**). According to literature reports, at this pH the ε-amine of *N*-α-acetyl-L-lysine should be mostly deprotonated, thus enhancing its nucleophilicity [149]. Interestingly, even at the higher pH, a significant amount of vinyl sulfone starting material **3.27** could be observed after 24 h (Fig. **3.28**).

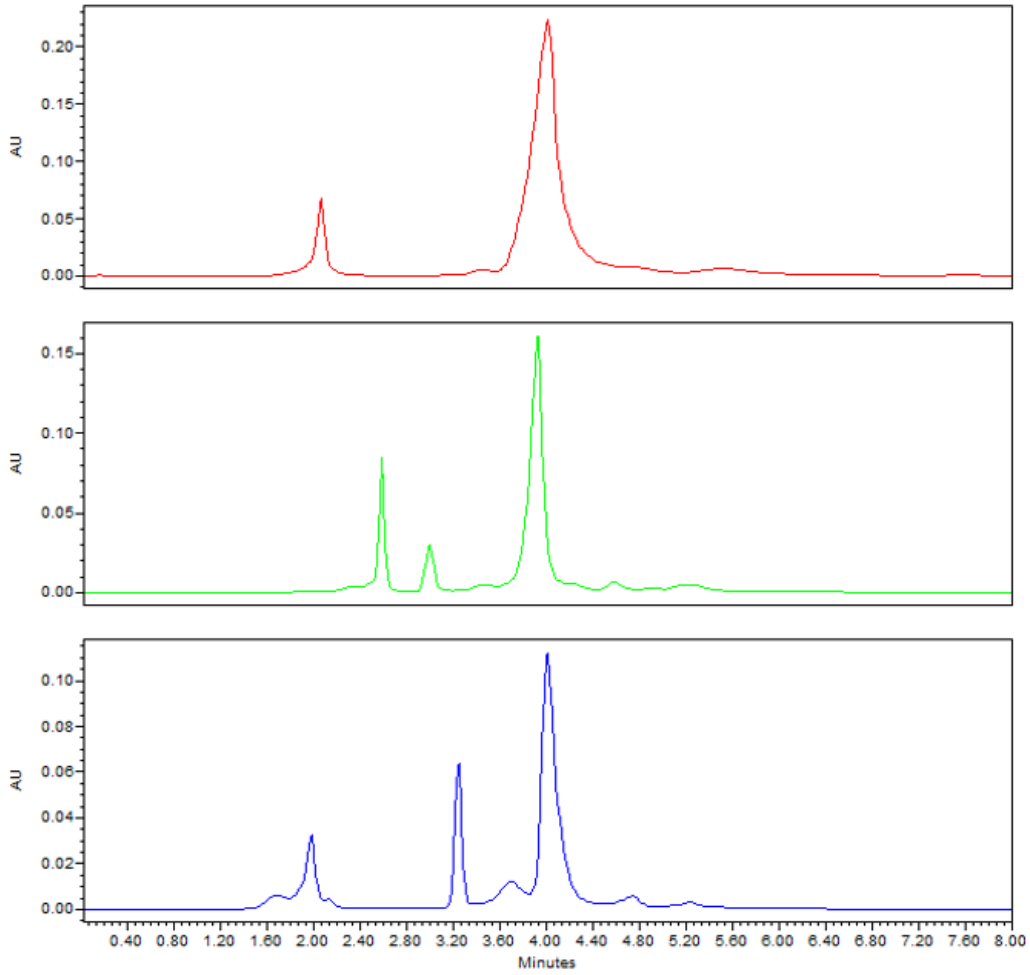

Figure 3.28: Reaction of **3.27** at RT with *N*-α-acetyl-L-lysine at pH 7.4 & 10.2 after 24 h: Chromatograms (top to bottom); 1) **3.27**, 2) **3.27** (1 equiv.) following reaction with *N*-α-acetyl-L-lysine (50 equiv.) at pH 7.4, 3) **3.27** (1 equiv.) following reaction with *N*-α-acetyl-L-lysine (50 equiv.) at pH 10.2.

To confirm the success of the cross-linking reactions, it was necessary to perform MS analysis of the reaction mixtures. Following consideration of the components of the pH 10.2 buffer, it was thought that the PO_4^{3-} ion present in this buffer may interfere with accurate LCMS analysis, which was envisioned to be an ideal method to detect the presence of an adduct formed via the crosslinking of **3.25** or **3.27** with *N*-α-acetyl-L-lysine. Thus, an analogous reaction was performed using **3.25** and **3.27** with *N*-α-acetyl-L-lysine in a pH 10.2 buffer, prepared using only aqueous NaOH which should not affect LCMS analysis. These reactions were run for the same duration (24 h) and monitored by HPLC.

Figure **3.29** shows the successful detection of the adduct **3.34** formed between **3.25** and *N*-α-acetyl-L-lysine by HRMS analysis of the reaction mixture. Thus, the peak observed at rt 3.6 mins in Figure **3.27** may correspond to the proposed product below.

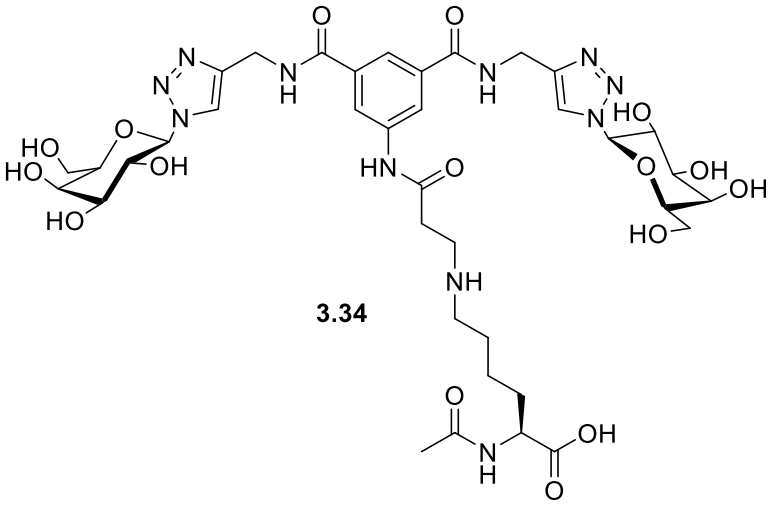

3.34

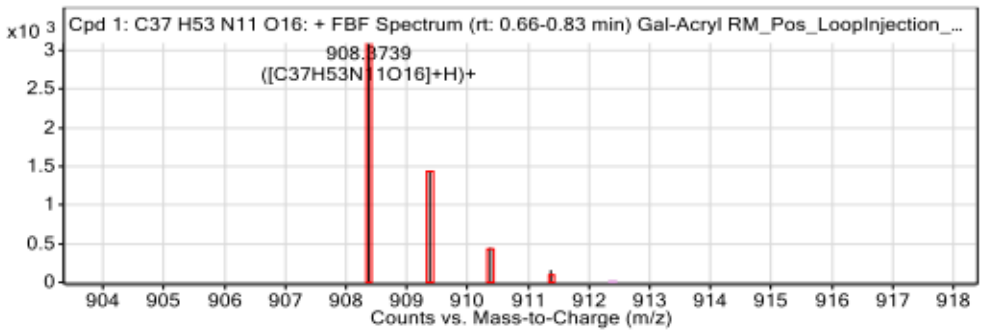

Figure 3.29: HRMS results for **3.25** reaction with *N*-α-acetyl-L-lysine.

Figure **3.30** shows the successful detection of the adduct **3.35** formed between **3.27** and *N*-α-acetyl-L-lysine by HRMS analysis of the reaction mixture. Thus, the peak observed at rt *ca*. 3 mins in Figure **3.28** may correspond to the proposed product below.

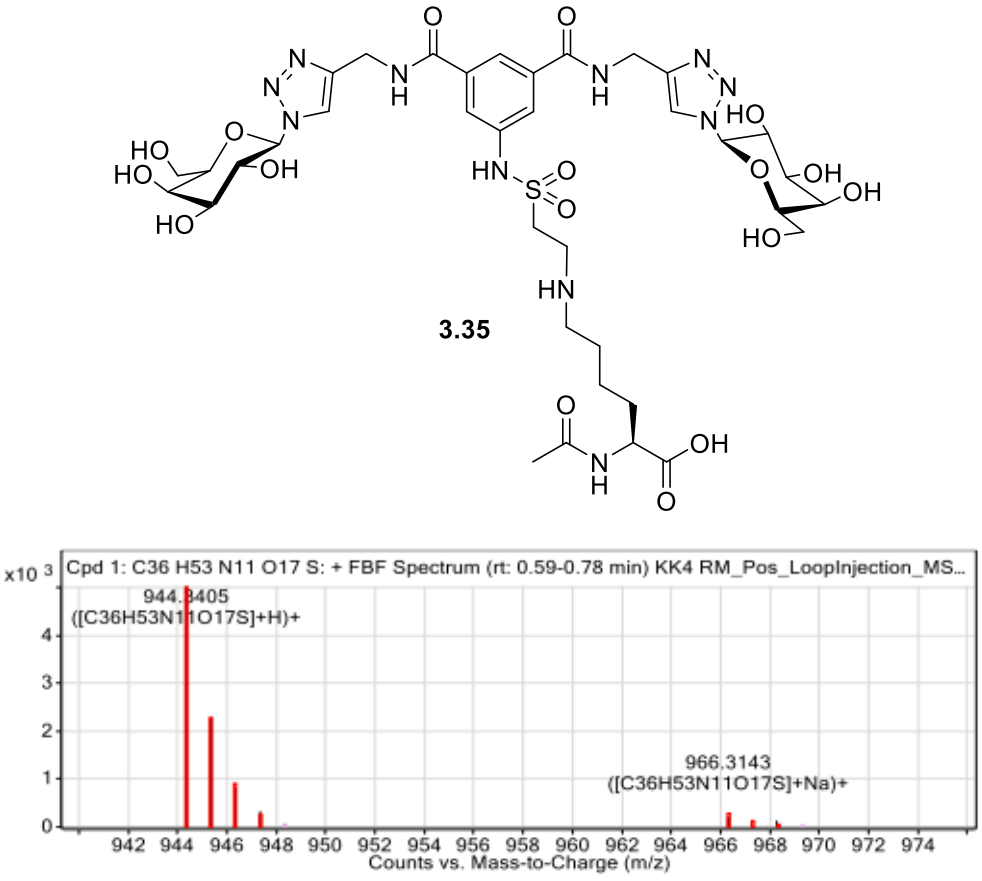

Figure 3.30: HRMS results for **3.27** reaction with *N*-α-acetyl-L-lysine.

3.4 Conclusion

In conclusion, divalent galactoside **3.25** and fucoside **3.26**, analogues of lead compound **1.39** which feature acryloyl substituents, capable of cross-linking and hence, covalent binding, were synthesised and characterized. The ability of these compounds to inhibit the adhesion of C. albicans to BECs was evaluated. Both compound **3.25** and **3.26** performed similarly to the lead compound **1.39**. This compound may be targeting a separate lectin to **1.39**, as hypothesised previously. Interestingly, the use of **1.39** in combination with **3.26** performed quite well; achieving a promising 59% reduction in adherence in *C. albicans* cells already bound to BECs. This highlights the potential of this approach for the development of novel treatments for Candidiasis.

Compounds **3.25** and **3.26** were included in a library of diverse glycoconjugate compounds (previously prepared in the Velasco-Torrijos' group) and assessed for toxicity against 6 *Candida* species. While all compounds tested were found to be non-

toxic at clinically relevant concentrations, at high concentrations some toxicity was observed; vinyl sulfonamide **3.27** showed comparable activity to lead compound **1.39** in some *Candida* species (i.e *C. glabrata, C. auris and C. guilliermondii*). This suggests that these strains may be more susceptible to glycoconjugates with reactive cross-linking moieties. Compound **3.25** showed toxicity at a 10-fold higher concentration than compound **3.27** in these species (note **3.25** was not assessed against *C. auris*). Both nitro derivatives **3.41** and **3.42** showed broad spectrum toxicity at high concentrations of 100 mg/mL against a most of the *Candida* species tested.

From these results, a series of model cross-linking reactions were conducted on two compounds (**3.25** and **3.27**), which had shown toxicity in these *Candida* species, using three *N*-terminal protected amino acids commonly found in the active sites of enzymes and lectins. The model cross-linking reactions revealed the formation of a new species in the cases of the reaction of both **3.25** and **3.27** with *N*-α-acetyl-L-lysine by HPLC. Neither **3.25** or **3.27** formed any new species in reaction with *N*-acetyl-L-cysteine or *N*-acetyl-L-histidine at either of the pHs tested, as assessed by HPLC. Compound **3.25** was found to produce a new species in reaction with *N*-α-acetyl-L-lysine at pH 10.2 but not at pH 7.4, perhaps due to the acrylamide moiety in **3.25** possessing lower intrinsic reactivity than the vinyl sulfonamide moiety in **3.27**. Meanwhile, **3.27** was found to produce a new species in reaction with *N*-α-acetyl-L-lysine at pH 10.2 and pH 7.4, albeit this reaction seems to progress at a slower rate. HRMS analysis of the resulting reaction mixtures revealed the presence of an adduct formed from the cross-linking of *N*-α-acetyl-L-lysine with both **3.25** and **3.27** in each case. Thus, we propose, based on these results, that the observed toxicity induced by **3.25** and **3.27** against a number of *Candida* species may be due to the cross-linking of key amino acids in potentially a target lectin with these compounds.

However, it should be noted that in terms of clinically applicable concentrations, all compounds were found to be non-toxic which was desirable.

Chapter 4

Optimisation of a promising inhibitor of *C. albicans* adhesion through Structure Activity Relationship

4.1 Introduction:

4.1.1 Anti-adhesion compounds to treat microbial infections

As discussed in Chapter 3, section 3.1.1, the increasing number of infections caused by pathogens resistant to traditional antimicrobial drugs calls for new approaches to treat infectious disease and efficient therapies. As noted by Bravo *et al.*, while the development of novel antibiotics is urgently needed, the identification of novel targets and strategies may likely be the best way forward in the long-term, due to the rapid development of resistance to novel 'classical' antibiotics [154]. In a review by Dickey *et al.*, the authors discuss the development of anti-virulence compounds, which act by targeting virulence factors associated with a given pathogen. Virulence factors are molecules that confer a pathogen the ability to infect or damage its host tissues. In contrast to traditional antibiotics, anti-virulence compounds may not have the same selective pressure for resistance, so they may supplement antibiotics. This may lead to increased antibiotic efficacy and less of an impact on host commensal flora. However, this class of compounds may not be effective in all forms of disease caused by the same pathogen, reduced efficacy in comparison to antibiotics and may require the rapid identification of the pathogen to be treated. Another potentially critical disadvantage is that the pathogen may persist once treatment ceases. Nevertheless, in 2016 benzlotoxumab was the first anti-virulence compound approved by the FDA. Its use is indicated to reduce the recurrence of *Clostridium difficile* infections. Benzlotoxumab is a monoclonal antibody which binds to *C. difficile* Toxin B, thus blocking its adhesion to mammalian cells [155].

4.1.2 Carbohydrate-based anti-adhesion compounds in infection

As discussed throughout this thesis, compounds which block the adhesion of pathogens to host cells have become increasingly favoured as a preferred route to novel treatments. In particular, carbohydrate-based (glycoconjugates) anti-adhesion compounds have recently undergone rapid study and development [156]. Lectins are carbohydrate-binding proteins which are commonly used by pathogens to mediate this adhesion step to host cell. Lectins also play important roles in cell-cell recognition and immune defence [131]. Lectins are divided into intracellular lectins, which bind

to core oligosaccharide structures, mediating glycoprotein processing and quality control and extracellular lectins, which bind to terminal carbohydrate epitopes found on other cells and pathogens [157]. Thus, intensive research has been conducted to develop high affinity ligands for these lectins to achieve an effective reduction in pathogen adhesion [158]. Importantly, over 80 microbial lectins have been identified with defined binding specificities, however, many key lectins are yet to be identified [157]. This hampers the effective design of high affinity lectin ligands.

P. aeruginosa utilises LecA and LecB, two extracellular lectins with specificities for D-galactose and L-fucose respectively, as key lectins to cause severe infections. Chronic lung colonisation by *P. aeruginosa* is the major cause of mortality in cystic fibrosis (CF) patients. The X-ray crystal structures of these lectins have been reported, which has prompted the design and evaluation of multiple carbohydrate-based ligands, some of which are capable of high affinity binding (in the nM range) [159]. As an example, Deguise *et al.* described the synthesis of a series of multivalent glycodendrimers presenting both D-galactose and L-fucose simultaneously. The affinity of these glycodendrimers for LecA and LecB were determined using turbidimetric assays. Compound **4.1** (**Fig. 4.1**) was found to effectively bind both LecA and LecB simultaneously, due to specificity of LecA for galactosides and LecB for fucosides. Compound **4.1** formed insoluble complexes with both LecA and LecB within a few minutes, confirming its high binding affinity for the lectins [160].

Another lectin whose structure is very well characterized is FimH, found in uropathogenic *E. coli* (UPEC) and other *E. coli* strains. As discussed in Chapter 5, FimH recognizes mannosides from cell surface glycans in the host cells. FimH is found on type 1 pili and facilitates the adherence of UPEC to host cells, through binding to the uroplakin Ia glycoprotein, within the urinary tract, leading to urinary tract infections (UTIs). Numerous mannose-containing ligands have been designed targeting FimH for the treatment of *E. coli* caused infections [161]. As an example, Klein *et. al.* reported the synthesis of a series of α-D-mannosides as FimH ligands, generated through a series of Structure-Activity Relationship (SAR) studies. A SAR study involves the design and evaluation of a series of derivatives of a lead compound, exploring different structural replacements in order to optimize a given biological activity

[162]. Building on previously reported FimH antagonists, the authors reported **4.2** (**Fig. 4.2**) which in addition to nanomolar affinity for FimH, had suitable pharmacokinetic properties for treating UTIs *via* intravenous and oral delivery. Compound **4.2** produced an IC_{50} value of 4.8 nM in a cell-free competitive binding assay, while in a cell-based aggregation assay it had an IC_{50} value of 9 nM. The authors found that the introduction of a methyl ester drastically improved the oral bioavailability of **4.2** and this compound was stable in gastric fluid. In a mouse UTI model, **4.2** was also found to significantly reduce the amount of culture-forming units (CFUs) [163].

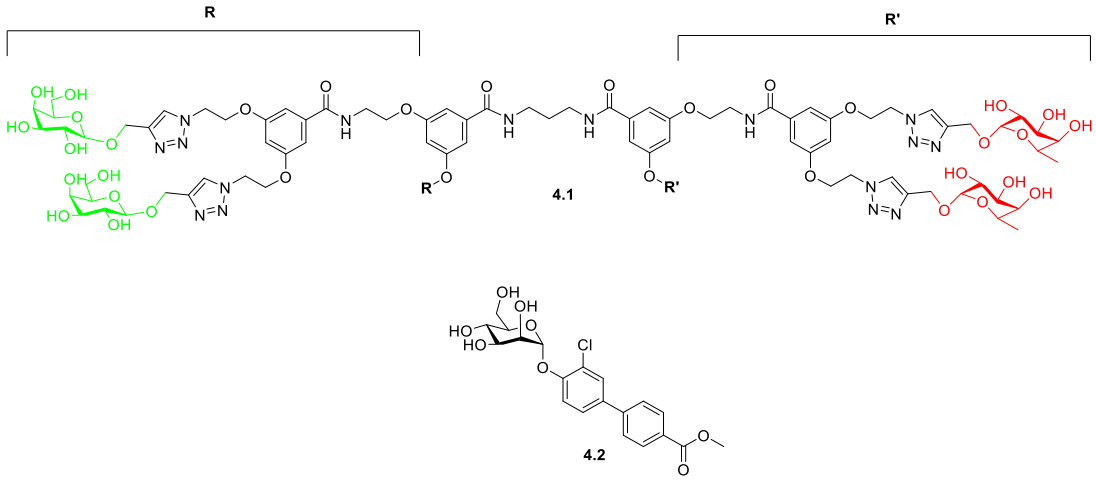

Figure 4.1: Structures of dual LecA and LecB inhibitor **4.1** (D-galactose in green, L-fucose in red) and FimH inhibitor **4.2** [160,163].

4.1.3 Biologically active glycoconjugates containing heterocycles

One common structural replacement carried out in SAR studies is the substitution of aromatic rings and functional groups containing heteroatoms for heterocyclic systems. This strategy has been used in the optimization of many lead compounds. This was the case for the design of glycogen phosphorylase (GP) inhibitors, discussed here as an example. A common target to treat Type 2 Diabetes Mellitus (T2DM) is glycogen phosphorylase (GP), which carries out the phosphorylative degradation of glycogen. Toth *et al.* reported the synthesis and evaluation of a series of C-glycosylated oxadiazoles as GP inhibitors, building on previously reported GP inhibitors, which include *N*-acyl-glucopyranosylamines and *N*-acyl-*N'*-β-D-glucopyranosyl-ureas (**Fig. 4.2**). Of these compounds, 1,2,4-oxadiazoles **4.3** and **4.4**

(**Fig. 4.2**) were the best performing compounds producing K_i values of 8.8 µM and 11.6 µM respectively. Through X-ray crystallography of **4.4** with GP, the authors observed no hydrogen bonding between the 1,2,4-oxadiazole heterocycle and the GP enzyme. However, 11 van der Waals interactions were observed between **4.4** and GP, which likely greatly contribute to the strong binding of **4.4** to GP [164]. In further efforts to develop potent GP inhibitors, Benltifa *et al.* reported the preparation of a series of isoxazoline derivatives which were evaluated as inhibitors of GP. Similar to compound **4.4**, compound **4.5** (**Fig. 4.2**) containing a 2-Naphthyl moiety produced the most efficient inhibition of GP, with a K_i value of 0.63 µM. In X-ray crystallography studies of **4.5** in complex with GP, **4.5** forms 15 hydrogen bonds and 111 van der Waals interactions with GP. Interestingly, 40 of these involved the 2-naphthyl moiety, highlighting the additive effect this moiety has to the binding affinity [165].

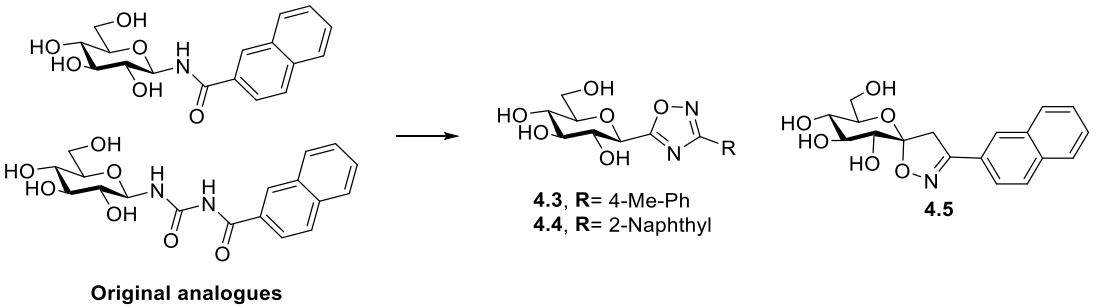

Figure 4.2: Structures of Glycogen phosphorylase inhibitors **4.3**-**4.5** [164,165].

4.1.4 sp^2-Iminosugar derivatives as glycomimetics

Carbohydrate-based molecules pose many challenges for their development as drug molecules. These may be overcome by the design of glycomimetic compounds, which maintain the ability to bind the carbohydrate-recognizing targets with improved pharmacodynamic and pharmacokinetic profiles [157]. sp^2-iminosugar derivatives are an important type of glycomimetic compounds that have been investigated for several biomedical applications, some of which will be discussed as follows.

Glycosidase enzymes catalyse the cleavage of glycosidic bonds in oligosaccharides and glycoconjugates and thus are important in a range of biological processes. Work by Risquez-Cuadro *et al.* aimed to develop novel inhibitors of a number of glycosidases. In an assessment of monovalent and multivalent sp^2-iminosugar

glycoconjugates, compound **4.6** and **4.7** (**Fig. 4.3**) were potent inhibitors of maltase and isomaltase. Compound **4.6** produced K_i values of 2.6 and 5.1 µM against maltase and isomaltase, while compound **4.7** produced K_i values of 5.3 and 2.2 µM against maltase and isomaltase respectively. However, in a multivalent presentation of similar compounds, compounds **4.8** and **4.9** (**Fig. 4.3**) were most active against α-mannase, producing K_i values of 2 µM and 0.81 µM. The authors attributed this switch in enzyme specificities of a given epitope/carbohydrate moiety to changes in the binding mechanisms of each inhibitor to the corresponding enzyme. Compounds **4.6**, **4.7**, **4.8** and **4.9** were then assessed for binding affinity to ConA and PNA, two important lectins. IC_{50} values of 3400 µM, 2580 µM, 21 µM and 7 µM were determined for compounds **4.6**, **4.7**, **4.8** and **4.9** respectively. This highlights the enhancement effect of multivalent presentation in improving binding affinity between target lectin and a given glycoconjugate [166].

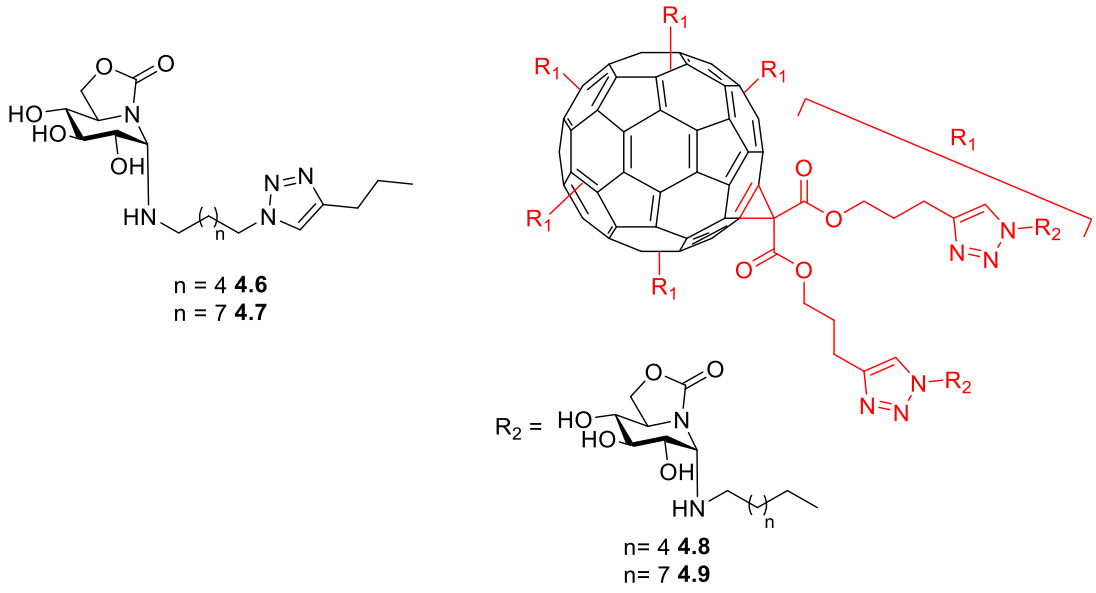

Figure 4.3: Structures of glycosidase inhibitors **4.6**-**4.9** [166].

Previously, a number of iminosugar-based glycosyl hydrolase inhibitors have been reported. These target enzymes, such as α-glucosidases have been implicated in key steps of tumour progression. However, these inhibitors have unfortunately been found to also inhibit lysosomal acid α and β-glucosidases and intestinal glucoamylase, which leads to undesired side effects. In an attempt to improve the selectivity of these inhibitors, Sanchez-Fernandez *et al.* reported the synthesis and evaluation of a

number of sp^2-iminosugar derivatives, in which the anomeric configuration can be controlled by ensuring a high sp^2 hybridisation via the inclusion of an endocyclic nitrogen atom. This leads to a preference for axial (α) configurations at the anomeric carbon atom. Compounds **4.10**, **4.11** and **4.12** (**Fig. 4.4**) were assessed as inhibitors of several glycosidase enzymes. Interestingly, none of them were found to be active against human lysosomal acid α-glucosidase. Thus, these compounds may well produce the desired inhibition without causing undesired side effects through interaction with off-target glucosidases. Next, these compounds were evaluated for cytostatic activities against human breast carcinoma MCF-7 cell line. Compounds **4.11** and **4.12** produced the most pronounced anti-proliferative activity with IC_{50} values of 29 µM and 22 µM respectively, which makes them promising compounds for further development as selective anti-cancer agents [167].

In further work by the same authors, novel sp^2-iminosugar derivatives were prepared and assessed for anti-tumour, anti-leishmanial and anti-inflammatory activities. Compounds **4.13** and **4.14** produced EC_{50} values of 24.55 µM and 27.18 µM, respectively, against the intracellular amastigotes form of *Leishmania donovani*, which is the clinically relevant form of this parasite. However, their activities were modest compared to reference drug used miltefosine (EC_{50} = 0.44 µM) [168]. More recently, these authors have described compound **4.15** (**Fig. 4.4**) with promising anti-tumour, anti-leishmanial and anti-inflammatory agent [169].

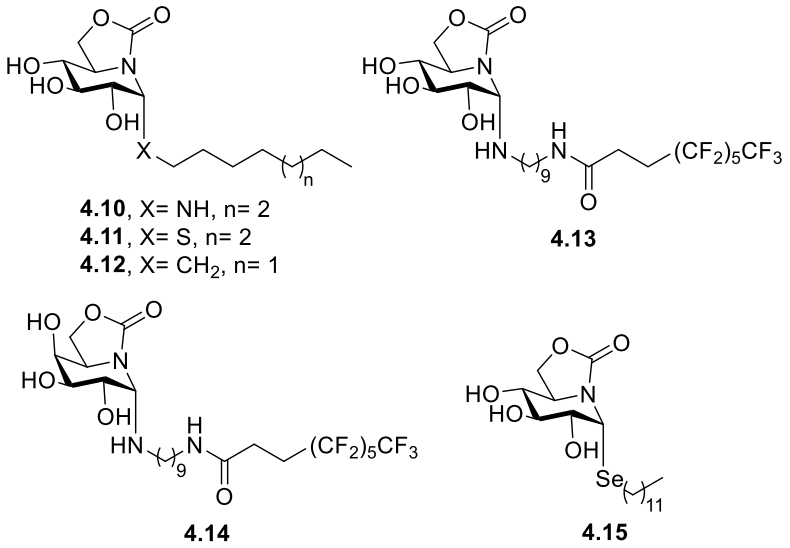

Figure 4.4: Structures of compounds **4.10**-**4.15**, with glycosidase inhibitory, anti-tumour, anti-leishmanial and anti-inflammatory activities [167-169].

4.1.5 Lectins adhesins as targets

The identification and structural characterization of lectin adhesins involved in infection processes greatly aids with the design of effective anti-adhesion glycoconjugates, as discussed previously. In many cases, lectins are identified via genomic analysis of the relevant species, expression of the desired protein (lectin) and subsequent purification and elucidation of binding specificity [170]. Chemical proteomics methods are emerging in attempts to identify the structure and functions of different biomolecules, including lectins. Of those, a relatively recent approach is photoaffinity labelling (PAL). PAL involves the use of small molecules containing a photoreactive label which, when activated via the correct wavelength of light, yields a reactive group which can form covalent bonds with adjacent groups in the target protein. In many cases these groups are adjacent amino acid residues in bound proteins. This method is particularly advantageous for lectins, which typically interact with their carbohydrate ligands with low affinity and hamper traditional methods of purification such as conventional affinity chromatography. Sakurai *et al.* reported the preparation and evaluation of a series of glycoconjugate-based photoaffinity probes for carbohydrate-binding proteins. The authors found that probe **4.16** (**Fig. 4.5**)

produced a relatively high yield of crosslinked protein, in this case peanut agglutinin [171]. Meanwhile, Ota *et al.* reported compound **4.17** (**Fig. 4.5**) which was capable of successfully crosslinking Concanavalin A (ConA), a mannose-binding lectin. Probe **4.17** was capable of this labelling with higher specificity and efficiency than other probes including benzophenone (BP), diazirine (Daz) and aryl azide (AAz) probes [172]. Tsushima *et al.* reported the successful use of magnetic beads functionalised with lactose and ruthenium complexes in tandem with 1-methyl-4-arylurazole (MAUra) to label galectin-1 and galectin-3, which are both lactose-binding proteins. Importantly, the authors were able to successfully label these proteins in cell lysates, highlighting the specificity of these probes in complex mixtures. These probes offer great potential in the identification of carbohydrate-binding proteins which, in many cases, form low affinity interactions. However, the high reactivity of the intermediate radical species can also lead to false positives [173].

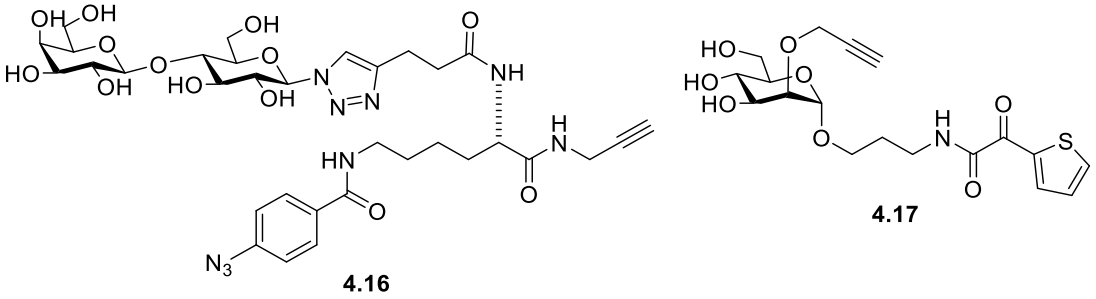

Figure 4.5: Structures of photoaffinity probes **4.16** and **4.17** [171,172].

4.2 Chapter Objectives

As discussed previously in this thesis, work in our research group identified **1.39** (**Fig. 4.6**) as a potent inhibitor of *C. albicans* adhesion to BECs [80]. In the absence of a known target for this compound, the optimization of its biological activity relies on structural modifications to identify the essential structural elements that can be related to anti-adhesion activity. Extensive research has been conducted into developing novel derivatives of **1.39** with improved performance. For example, 1,4-substituted aromatic core, squaramide core, and, as discussed in Chapter 2, *trans*- and *cis*-norbornene core derivatives of **1.39** have been developed and evaluated [114].

This chapter deals with the preparation of additional derivatives of **1.39** through three key modifications:

- Alteration of the aromatic substituents at the *meta*-position: bromo **4.25**, methoxy **4.26** and cyclopropyl **4.27** derivatives were proposed.
- Alteration of the D-galactoside moieties to novel sp^2-iminosugar moieties: galactose derivative **4.42**, as well as the corresponding *O*-ethylene derivatives **4.43** and **4.44**, respectively, were proposed.
- Alteration of the 1,2,3-triazole heterocycle linker to 1,2,4-oxadiazole (**4.55** and **4.58**), isoxazole (**4.59** and **4.60**) or isooxazoline (**4.61**, **4.62** and **4.63**) were proposed.

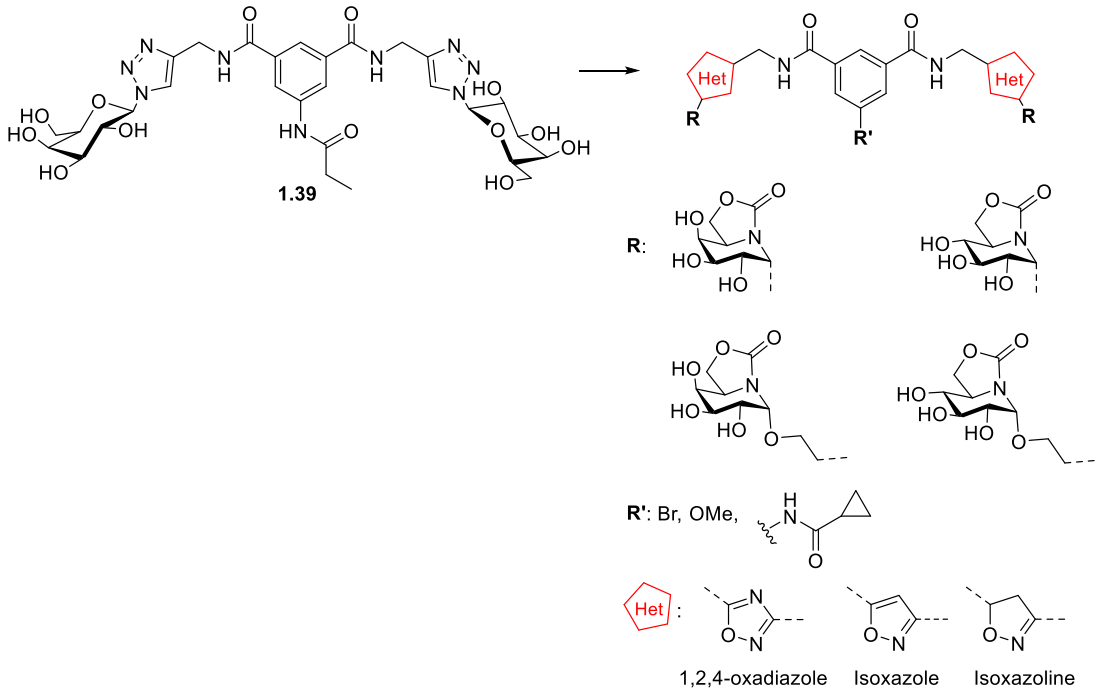

Figure 4.6: Structure Activity Relationship study (SAR) of lead compound **1.39**.

In addition, the preparation of amino-derivative **4.67** is discussed. This compound was envisaged for use in resin modification to identify the lectin and/or protein which **1.39** targets to achieve its anti-adhesion activity. The structural elucidation of this lectin(s) would help greatly with the design of more effective glycoconjugates.

4.3 Results and Discussion

4.3.1 Synthesis of compounds 4.25, 4.26 and 4.27 (variation of substituents at the meta-position of the aromatic core)

To probe the necessity of the propionyl/propionamide group at the *meta*-position in **1.39** for the observed anti-adhesion activity, three derivatives of this compound, **4.25** (-Br), **4.26** (-OMe), and **4.27** (cyclopropenecarboxamide) were prepared. While the bromide substituent has an electron-withdrawing character, the methoxy group is considered as an electron donating group (albeit with an inductive electron withdrawing effect). This different character may influence the electron density distribution in the aromatic core. The synthesis of **4.25** and **4.26** started from the commercially available diacids **4.18** and **4.19**, using propargylamine, TBTU, NEt_3 and DMF for amide coupling reactions to give two novel aromatic scaffolds **4.20** and **4.21** respectively (**Scheme 4.1**).

They were next reacted with galactosyl azide **2.40** in a CuAAC reaction under the typical conditions of 100 ^oC under microwave irradiation, with both reactions going to completion within 30 mins. Both compounds **4.22** and **4.23** were purified using flash column chromatography.

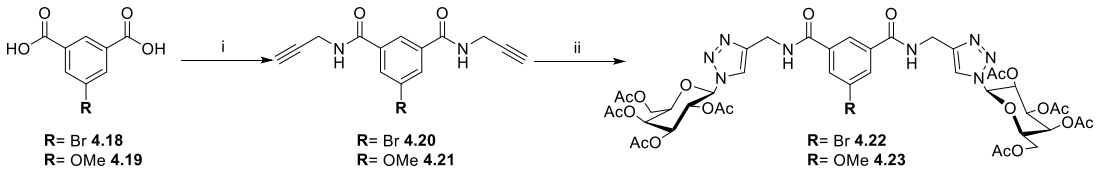

Scheme 4.1: Synthesis of glycoconjugate **4.22** and **4.23**. Reagents and conditions: i) Propargylamine, TBTU, NEt_3, DMF, 16 h, RT, 38% (**4.20**) or 99% (**4.21**), ii) 2,3,4,6- tetra-O-acetyl-1-β-azido-galactoside **2.40**, $CuSO_4.5H_2O$/Na Asc, ACN/H_2O, 100 ^oC in MW, 30 mins, 33% (**4.22**) or 64% (**4.23**).

To prepare the cyclopropenecarboxamide derivative **4.27**, intermediate **3.19** (previously discussed in Chapter 3) was reacted with cyclopropanecarbonyl chloride to yield **4.24** (**Scheme 4.2**). The reaction was determined to have gone to completion by TLC analysis after approximately 22 h with sequential addition of 8 equivalents of cyclopropanecarbonyl chloride overall. This excess suggests that the

aniline in **3.19** is not highly reactive, likely due to donation of its lone pair of election into the aromatic ring.

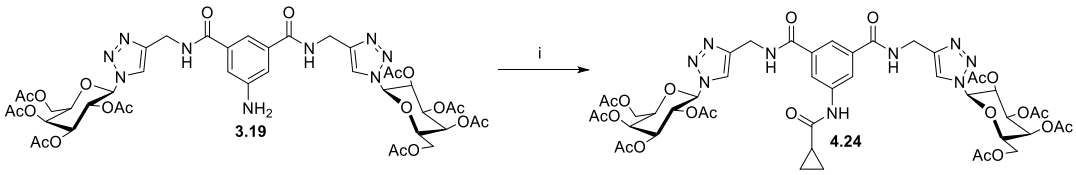

Scheme 4.2: Synthesis of glycoconjugate **4.24**. Reagents and conditions: i) Cyclopropanecarbonyl chloride, NEt_3, DCM, 22 h, RT, 75%.

The ^{1}H NMR spectrum of compound **4.24** is shown in Figure **4.7**. There are a number of key indicative peaks, the first is the amide proton adjacent to the cyclopropyl group (light blue circle) is found as a broad singlet/doublet at 8.79 ppm. The triazolyl proton (orange circle) is found as a singlet at 7.96 ppm. The aromatic ring protons (light green circle) are found as two separate peaks, one singlet at 8.03 ppm and the second is found as part of a broad multiplet at 7.81 ppm. The pair of amide protons (dark green circle) is also found as part of this multiplet at 7.81 ppm. The anomeric proton H-1 (red circle) as a doublet at 5.89 ppm. Finally, the methine proton (purple circle) of the cyclopropyl group is found as a broad singlet at 1.63 ppm, while the methylene protons of the cyclopropyl group (dark blue circle) are found as two separate broad singlets at 1.02 and 0.82 ppm. This indicates that these methylene protons are in two separate chemical environments. This may be due to the partial double bond character displayed by many amides which has the effect of placing the adjacent methylene protons in distinct chemical environments.

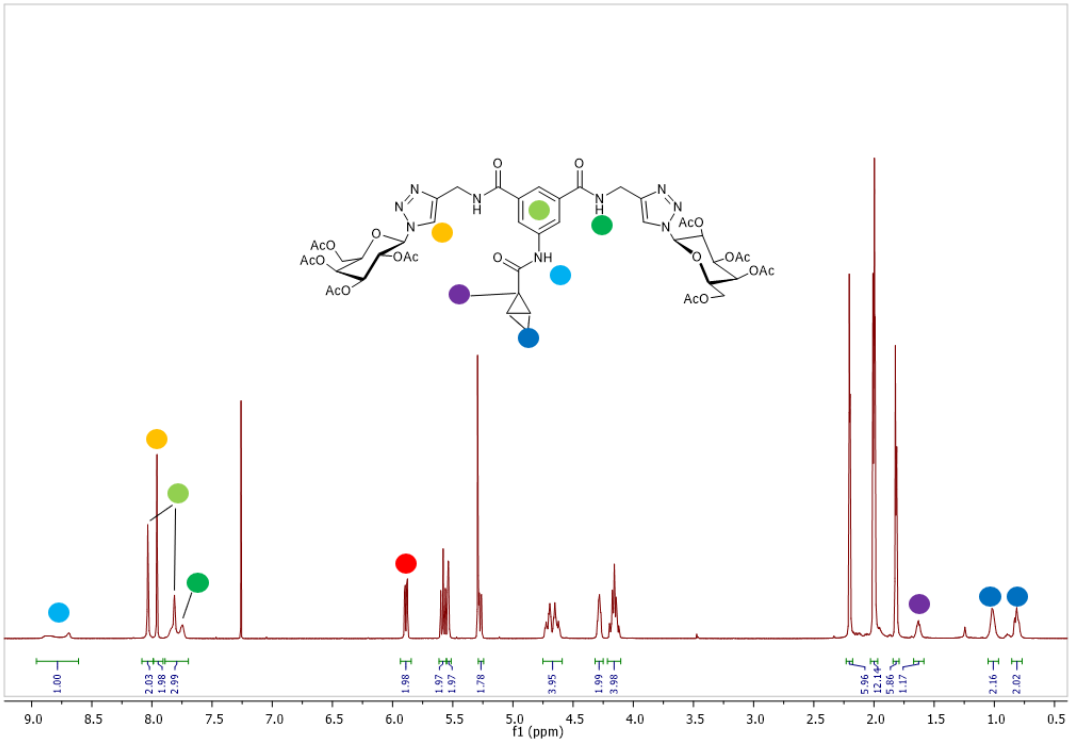

Figure 4.7: ^{1}H NMR spectrum for compound **4.24**. Note: Anomeric proton is assigned as red circle.

The final step in the preparation of all three desired glycoconjugates was the deprotection of the acetyl protecting groups on the carbohydrate moieties under the same mild basic conditions described previously, to yield the final desired compounds **4.25**, **4.26** and **4.27** (**Scheme 4.3**).

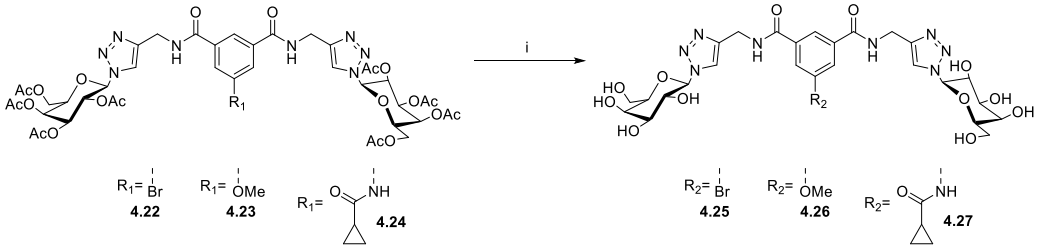

Scheme 4.3: Synthesis of glycoconjugates **4.25**, **4.26** and **4.27**. Reagents and conditions: i) MeOH, H_2O, NEt_3, 45 °C, 6 h, 66% (**4.25**) or 77% (**4.26**) or 89% (**4.27**).

The ^{1}H NMR spectrum of compound **4.26** is shown in Figure **4.8**. The triazolyl proton (blue circle) is found as a singlet at 8.23 ppm. The aromatic ring protons (green circle) are found as two separate peaks, both singlets, at 7.61 and 7.31 ppm respectively. The anomeric proton H-1 (red circle) is found as a doublet at 5.66 ppm. The methylene protons adjacent to the 1,2,3-triazole ring (orange circle) appears as a singlet at 4.63 ppm. Finally, the methyl protons of the methoxy substituent (purple circle) are found as part of a multiplet at 3.76 ppm.

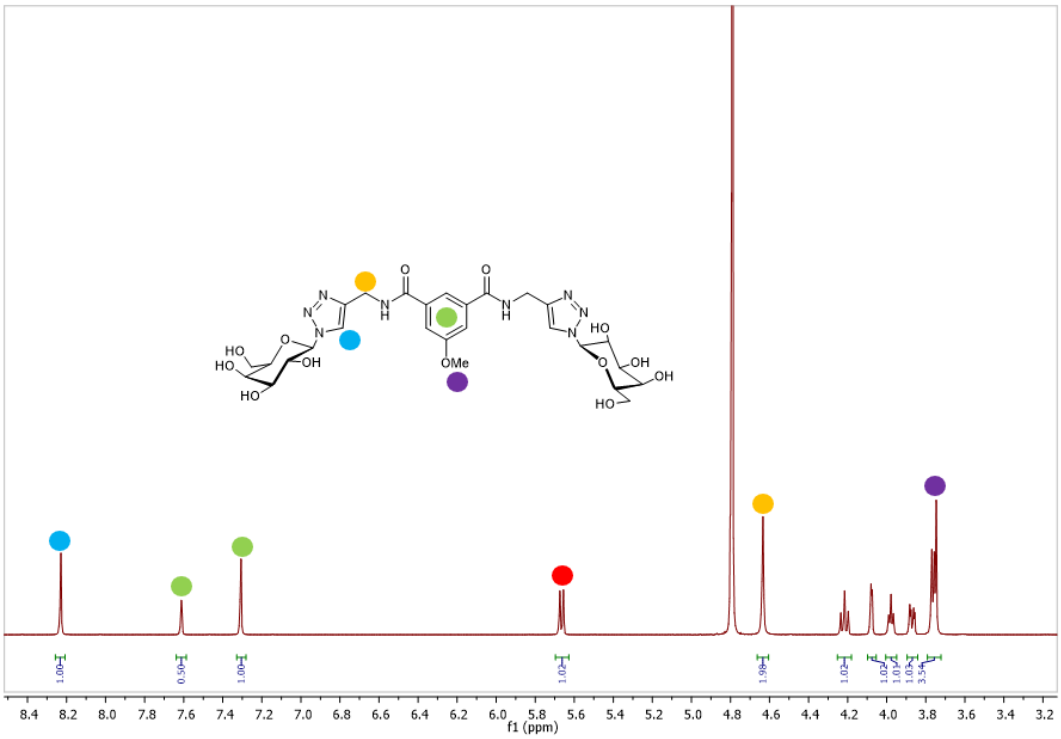

Figure 4.8: ^{1}H NMR spectrum for compound **4.26**. Note: Anomeric proton is assigned as red circle.

4.3.2 Synthesis of sp^2-iminosugar glycocomimetics 4.42, 4.43, and 4.44

4.3.2.1 Synthesis of sp^2-iminosugar azide derivatives 4.32, 4.33, 4.34 and 4.35

The synthesis of **4.32** and **4.33** was achieved using the corresponding tetraacetate derivatives **4.28** and **4.29**, which were obtained from collaborators in the laboratory of Prof. Carmen Ortiz Mellet, University of Sevilla, Spain (**Scheme 4.4**). The first step in the preparation of **4.32** and **4.33** was achieved by the *in-situ* formation of the corresponding glycosyl bromides. This was achieved by reacting **4.28** or **4.29** with HBr (33% HBr in AcOH) in anhydrous DCM. Initially, an iminium ion is formed *via* protonation of the acetyl protecting group, followed by nucleophilic attack by the bromide ion (**Scheme 4.5**) to form **4.30** and **4.31**. Secondly, the bromide ion is a good leaving group, thus, the iminium ion is reformed and then the nucleophilic attack by the azide group takes place to afford **4.32**. Note, the formation of **4.33** involves the same reaction mechanism. Initial attempts for this reaction were stirred for 5 mins on ice, however, these attempts were unsuccessful. It was believed that the intermediate glycosyl bromide was rapidly hydrolysed. Thus, **4.30** and **4.31** were successfully prepared by stirring the corresponding tetraacetate for a shorter period

(3 mins) on ice followed by a quick workup. The crude bromide products were reacted with NaN_3, to yield desired products **4.32** and **4.33** which were purified using flash column chromatography.

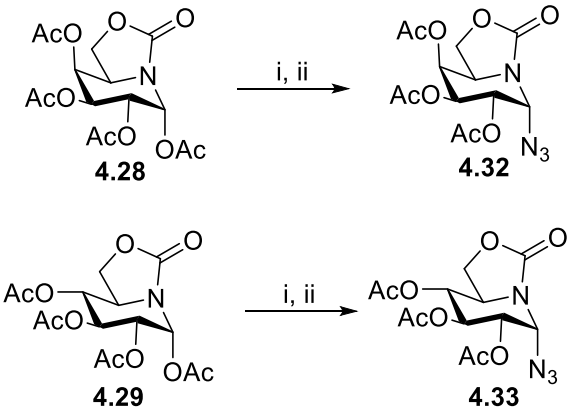

Scheme 4.4: Synthesis of aromatic scaffold **4.32** and **4.33**. Reagents and conditions: i) 33% HBr in AcOH, DCM, 3 mins, 0 ^oC, used without further purification, ii) NaN_3, DMF, 2 hr, RT, 23-51%.

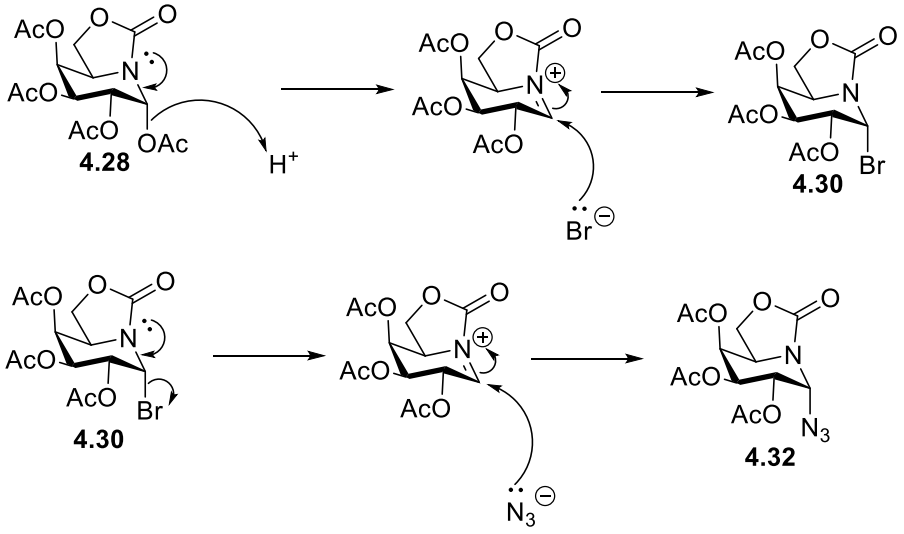

Scheme 4.5: Reaction mechanism for the synthesis of **4.32**.

The synthesis of the *O*-glycosides **4.34** and **4.35** was carried out using the same tetraacetate derivatives **4.28** and **4.29** (**Scheme 4.6**). *O*-Glycosylation reactions were employed using $BF_3.Et_2O$ as a Lewis acid promoter and 2-azidoethanol, which had been prepared by a member of the laboratory of Prof. Carmen Ortiz Mellet, University of Sevilla, Spain. $BF_3.Et_2O$ is used to promote the formation of the iminium ion, which then reacts with 2-azidoethanol to form the desired product in each case (**Scheme 4.7**). Note, the formation of **4.35** involves the same reaction mechanism.

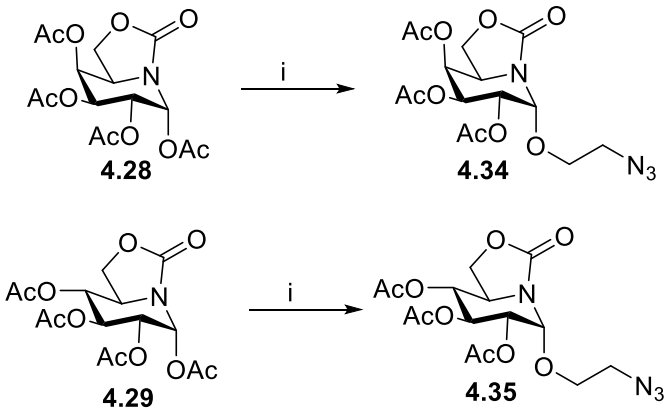

Scheme 4.6: Synthesis of aromatic scaffold **4.34** and **4.35**. Reagents and conditions: i) 2-azidoethanol, $BF_3.Et_2O$, DCM, 30 mins, 0 °C, 68-72%.

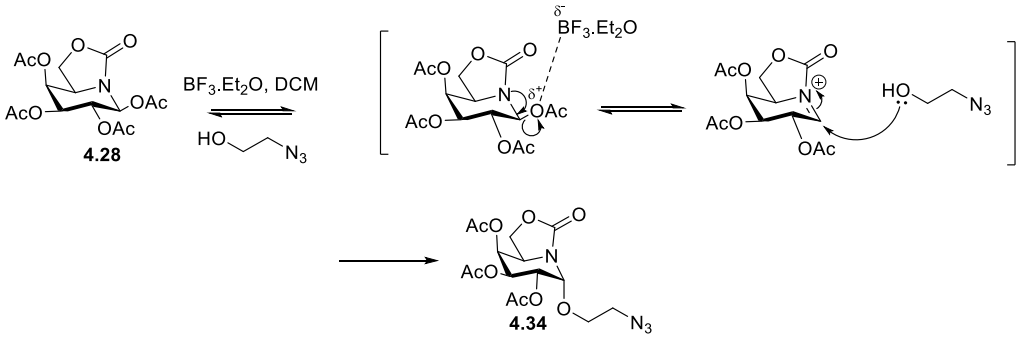

Scheme 4.7: Reaction mechanism for the synthesis of **4.34**.

4.3.2.2 Synthesis of divalent sp²-iminosugar glycomimetics 4.42, 4.43 and 4.44

The synthesis of this series of compounds was achieved using the same synthetic approach as previously used for the preparation of analogues of **1.39**. (**Scheme 4.8**). Firstly, the aromatic scaffold **4.37** was prepared according to literature procedures developed in our research group [80]. *O*- and *N*-glycosidic azides **4.32**, **4.33**, **4.34** and **4.35** were each reacted with this aromatic scaffold **4.37** in a CuAAC reaction under microwave irradiation as described previously. Each crude product was then purified using flash column chromatography (**Scheme 4.8**).

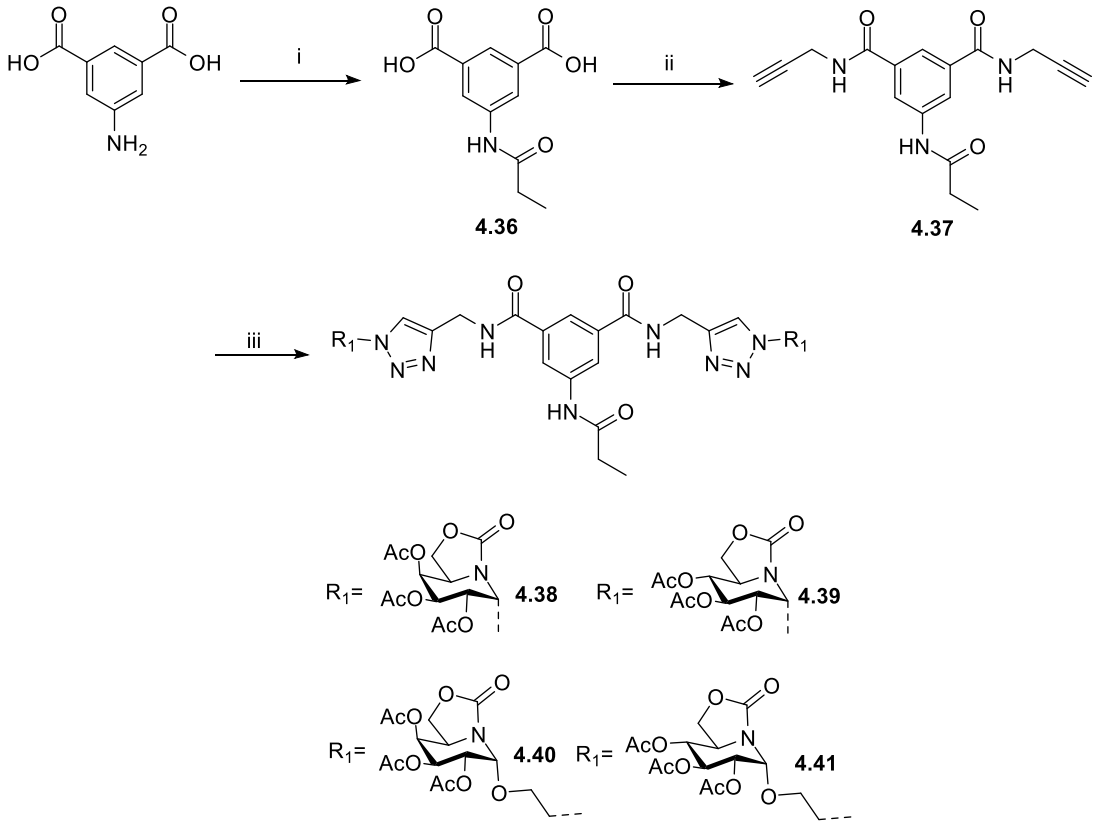

Scheme 4.8: Synthesis of glycoconjugates **4.38**-**4.41**. Reagents and conditions: i) Propionyl chloride, NEt_3, THF, 22 h, RT, used without further purification, ii) Propargylamine, TBTU, NEt_3, DMF, 16 h, RT, 36%, iii) **4.32**/**4.33**/**4.34**/**4.35**, $CuSO_4.5H_2O$/Na Asc, ACN/H_2O, 100 °C in MW, 30 mins, 40-75%.

The ^{1}H NMR spectrum for compound **4.40** is shown in Figure **4.9**. This spectrum is indicative for the other *O*-glycoside derivative **4.41**. The amide proton adjacent to the propionyl group (dark green circle) is found as a broad singlet at 10.11 ppm, while the amide protons adjacent to the 1,2,3-triazole rings (orange circle) are found as a triplet at 8.97 ppm. The aromatic ring protons (light green circle) are found as two separate peaks, one narrow doublet at 8.18 ppm and a singlet at 7.98 ppm. The triazole ring proton (light blue circle) is found as a singlet at 8.01 ppm. The anomeric proton H-1 (red circle) is found as a doublet at 5.31 ppm. The methylene protons adjacent to the 1,2,3-triazole ring (dark blue circle) is found as a multiplet at 4.55 ppm. The methylene protons adjacent to these protons and the *O*-glycosidic oxygen atom (yellow circle) are found as two separate peaks at 4 and 3.82 ppm, both of which are multiplets. The methylene protons adjacent to the carbamate ring of the sp^2 iminosugar (purple circle) are found as multiplets at 4.34 and 4 ppm. The

presence of two separate peaks indicates these protons are diastereotopic, in a similar way to **4.38**.

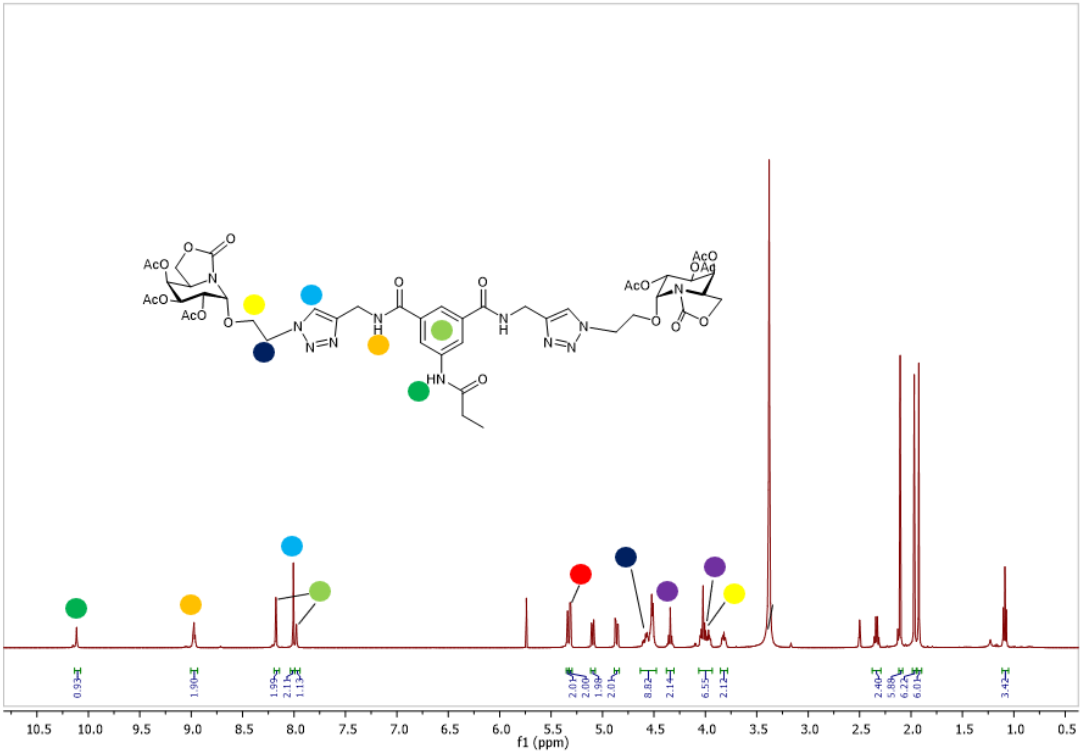

Figure 4.9: ^{1}H NMR spectrum of compound **4.40**. Note: Anomeric proton is assigned as red circle.

The final step in the preparation of all four sp^{2}-iminosugar glycoconjugates was the deprotection of the acetyl groups on the carbohydrate moieties under mild basic conditions. Importantly, the reaction of compound **4.39** under the same mild basic conditions as above over 18 h resulted in the degradation of the product. It is possible that the extended reaction time may have led to possible undesired competing side reactions. Therefore, shorter reaction times and careful monitoring of the hydrolysis reaction yielded the final desired compounds **4.42**, **4.43** and **4.44** (**Scheme 4.9**).

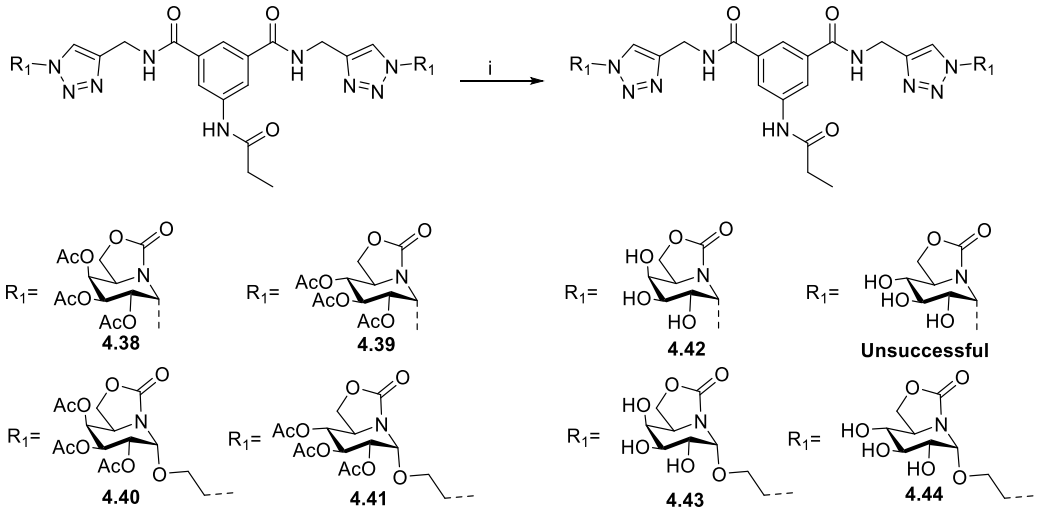

Scheme 4.9: Synthesis of glycoconjugates **4.42**-**4.44**. Reagents and conditions: i) MeOH, H_2O, NEt_3, 45 °C, 6 h, 34-53%.

The ^{1}H NMR spectrum for the deprotected *O*-glycoside compound **4.43** is shown in Figure **4.10**. This spectrum is indicative for the other deprotected *O*-glycoside derivative **4.44**. The triazole ring proton (light blue circle) is found as a singlet at 8.07 ppm. The aromatic ring protons (light green circle) are found as two separate singlet peaks at 8.01 and 7.93 ppm. Interestingly, a mixture of the α and β anomers for this glycoconjugate were obtained following deprotection of the acetyl protecting groups, with the α anomer being the predominant anomer. This was also observed following initial attempts at the deprotection of the acetyl protecting groups on other sp^2-iminosugar glycoconjugates. The anomeric proton H-1 of the minor β anomer (yellow circle) is found as a doublet at 5.43 ppm, while the anomeric proton H-1 of the major α anomer (red circle) is found as a doublet at 5.09 ppm. Finally, the methylene protons of the linker between the sp^2-iminosugar moiety and the aromatic core (green and purple circles) are found as part of a broad singlet/multiplet at 4.67 ppm and a second pair of peaks which are two multiplets at 4.03 and 3.95 ppm.

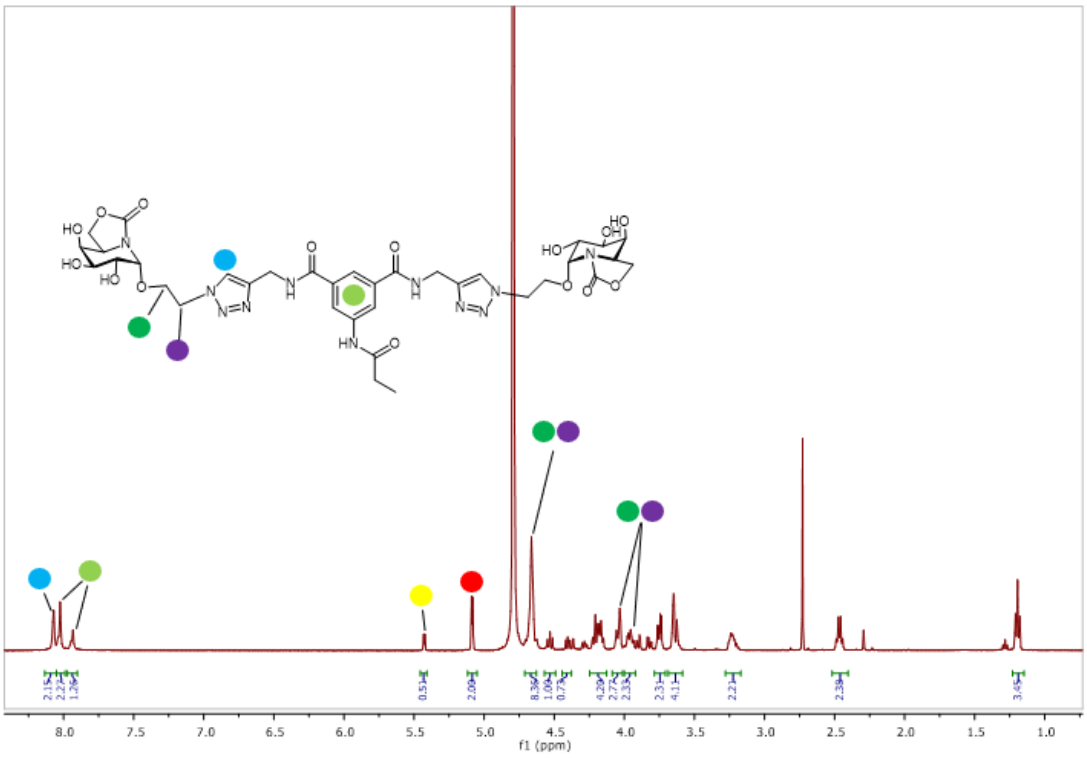

Figure 4.10: ^{1}H NMR spectrum of compound **4.43**. Note: Anomeric α proton is assigned as red circle while the anomeric β proton is assigned as yellow circle.

4.3.3 Synthesis of scaffolds 4.48-4.53 (for variations of the heterocyclic linker)

To prepare derivatives of **1.39** containing alternative heterocyclic linkers to the 1,2,3-triazole ring, several novel aromatic scaffolds **4.48**-**4.53** were prepared. Both aromatic mono- and diacids were used as starting materials for scaffolds to generate mono- and divalent derivatives. Firstly, to prepare the mono-amide scaffolds shown in Scheme **4.10**, 3-aminobenzoic acid was reacted with propionyl chloride to afford the amide **4.45**. Next, the coupling of **4.45** with either allyl amine or aminoacetonitrile hydrochloride using TBTU as the coupling reagent gave monovalent scaffolds **4.46** and **4.47,** respectively. An indicative mechanism for the amide coupling using TBTU is shown in Scheme **4.11**. The first step involves deprotonation of the carboxylic acid to form the corresponding carboxylate, using a mild base. The carboxylate then reacts with TBTU, forming an intermediate acyloxy-aminium/uranium (III) salt which then reacts with $HOBt^{-}$ to form the next intermediate. The final step involves the reaction of this intermediate with the

amine, in this example allylamine, to form the desired amide product and 1-hydroxybenzotriazole (HOBt) as a by-product [174].

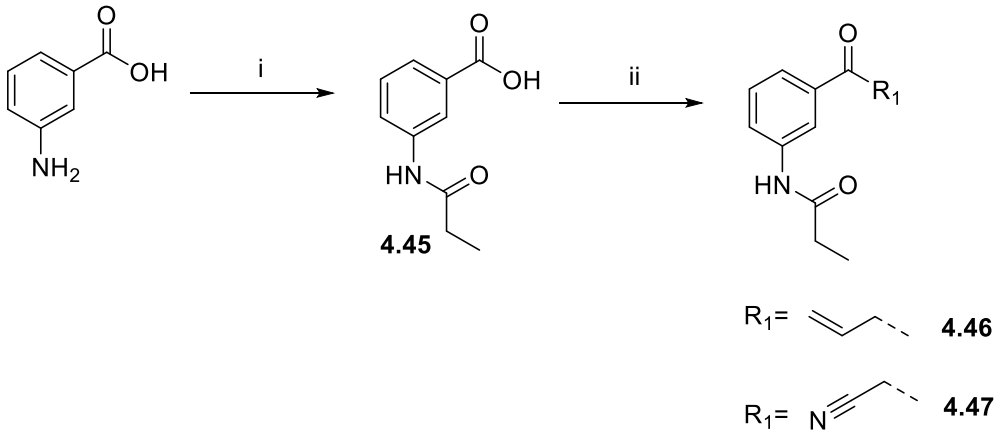

Scheme 4.10: Synthesis of aromatic scaffolds **4.46** and **4.47**. Reagents and conditions: i) Propionyl chloride, NEt_3, THF, 22 h, RT, used without further purification, ii) Allylamine/Aminoacetonitrile, TBTU, NEt_3, DMF, 16 h, RT, 20-45%.

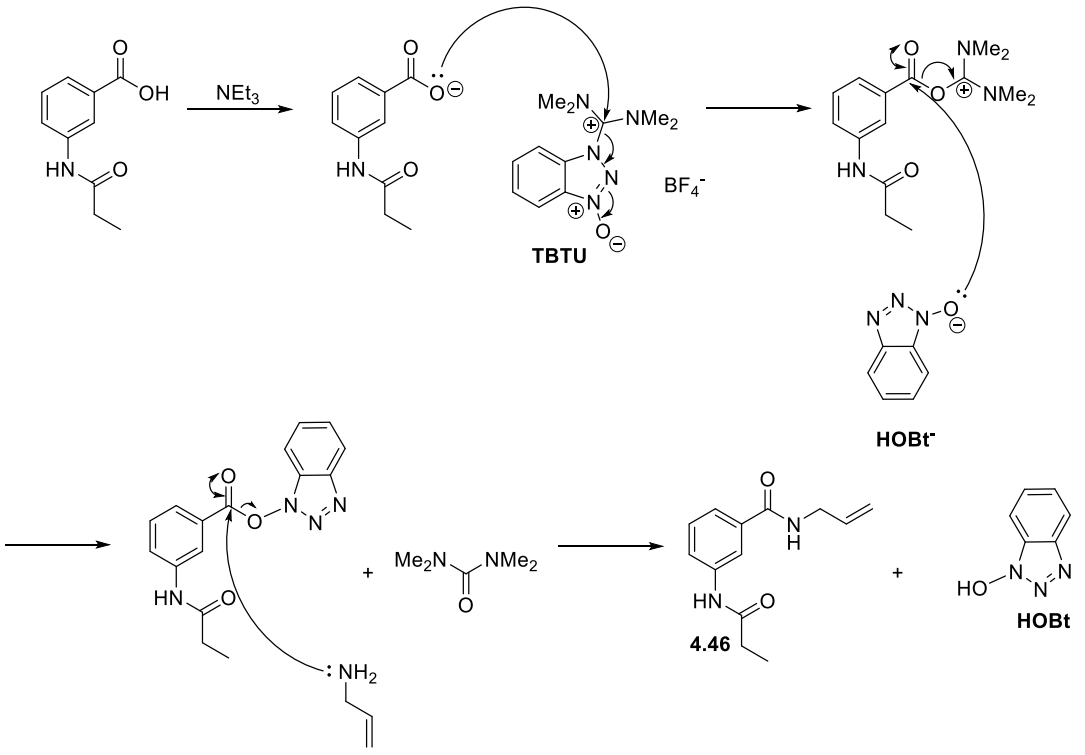

Scheme 4.11: Mechanism of TBTU-mediated amide coupling [174].

The synthesis of the scaffolds for the divalent derivatives, compounds **4.48**-**4.53**, is shown in Scheme **4.12**. Diacid **4.36** or 5-nitro-isophtalic acid were reacted with TBTU

and either allylamine, aminoacetonitrile hydrochloride or propargylamine, to give the corresponding derivatives as shown in Scheme **4.12**.

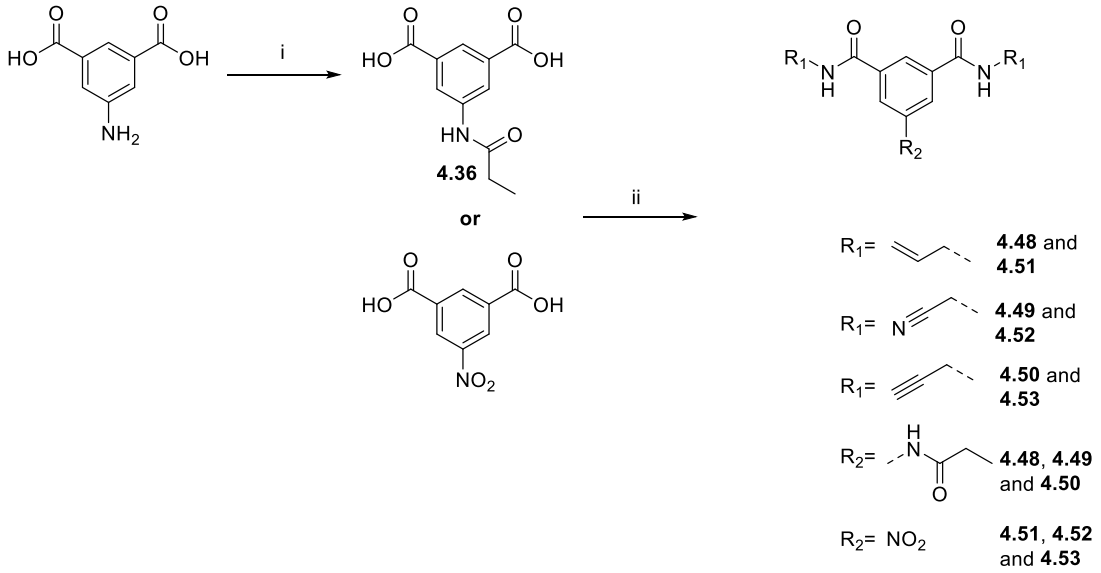

Scheme 4.12: Synthesis of aromatic scaffolds **4.48**-**4.53**. Reagents and conditions: i) Propionyl chloride, NEt_3, THF, 22 h, RT, used without further purification, ii) Allylamine/Aminoacetonitrile hydrochloride/Propargylamine, TBTU, NEt_3, DMF, 16 h, RT, 7-67%.

An indicative ^1H NMR spectrum of compound **4.48** is shown in Figure **4.11**. The amide proton adjacent to the propionyl functional group (light blue circle) is found as a singlet at 10.14 ppm. The second set of amide protons (orange circle) are found as a triplet at 8.66 ppm, while the aromatic protons (green circle) are found as a doublet at 8.18 ppm and a triplet at 7.94 ppm. The alkene protons of the allyl moiety are found as three distinct sets of protons. The singular proton (red circle) is found as a multiplet at 5.9 ppm, while the two diastereotopic protons (purple circle) are found in two slightly different chemical environments, appearing as two multiplets at 5.19 and 5.10 ppm. Lastly, the methylene protons between the allyl and amide functional groups (dark blue circle) are found as a multiplet at 3.9 ppm.

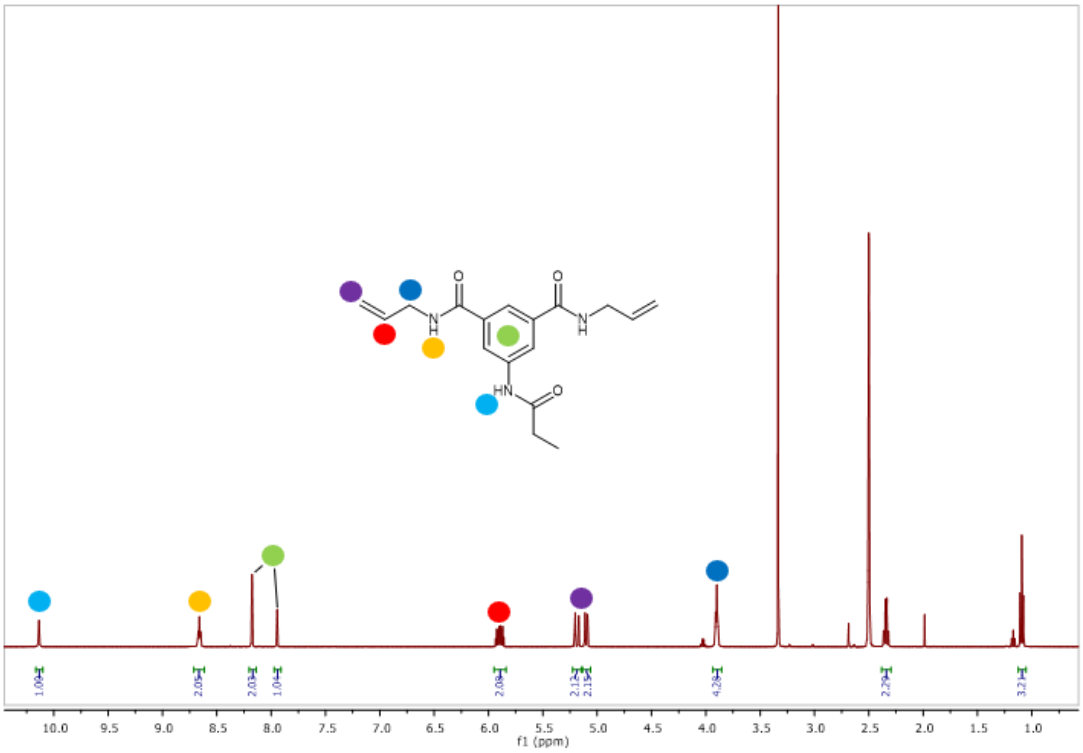

Figure 4.11: ^{1}H NMR spectrum of compound **4.48**.

4.3.3.1 Synthesis of heterocyclic derivatives 4.55, 4.58, 4.59, 4.60, 4.61, 4.62 and 4.63

Once prepared, these scaffolds were sent to the laboratory of Prof. Somsák and Prof. Tóth, University of Debrecen, Hungary for preparation of the novel heterocyclic derivatives. Initially, following several unsuccessful attempts to prepare 1,2,4-oxadiazole derivative **4.55** (**Fig. 4.12**), our collaborators prepared alternative scaffold **4.57** (**Fig. 4.13**).

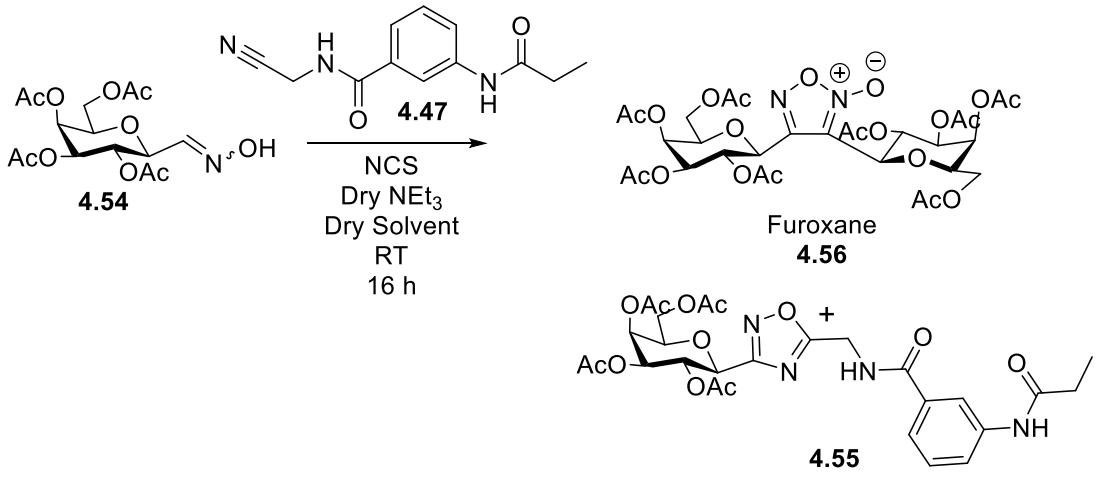

Figure 4.12: Attempted synthesis of 1,2,4-oxadiazole derivative **4.55** by collaborators.

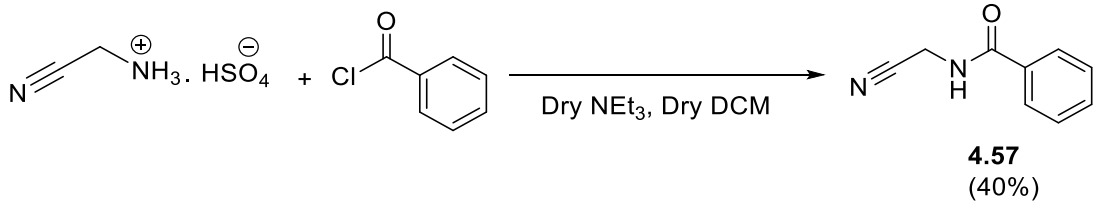

Figure 4.13: Synthesis of alternative scaffold **4.57** for reaction optimisation (see below).

Unfortunately, the desired 1,2,4-oxadiazole derivative **4.58** was not prepared using the alternative scaffold **4.57**, with furoxane **4.56** obtained instead in all cases (**Fig. 4.14**). Thus, further work is required to optimise the preparation of 1,2,4-oxadiazole derivative **4.58**.

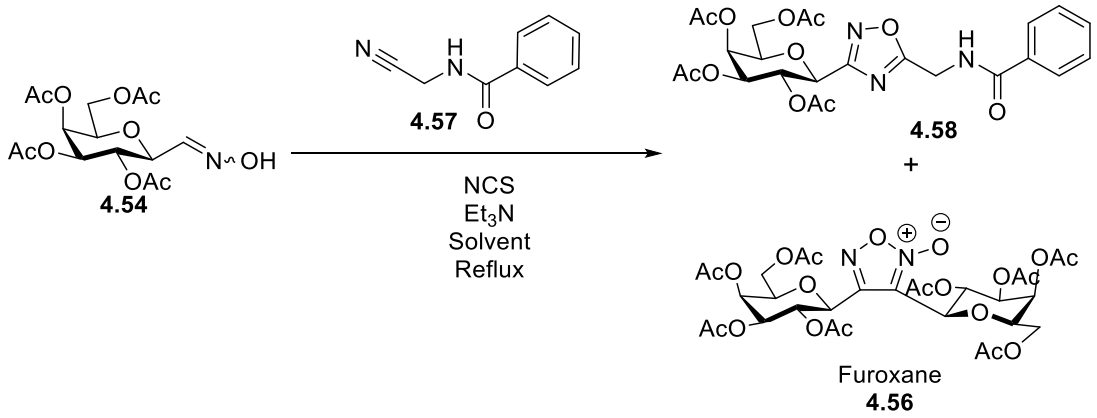

Figure 4.14: Attempted alternative synthesis of 1,2,4-oxadiazole derivative **4.58** by collaborators.

Thankfully, isoxazole derivatives **4.59** and **4.60** were synthesised though with low to moderate yields (19-38%), with the furoxane **4.56** again obtained (**Fig. 4.15**). Further work will be required to optimise the yields/conditions for these compounds, minimising the formation of the furoxane **4.56**.

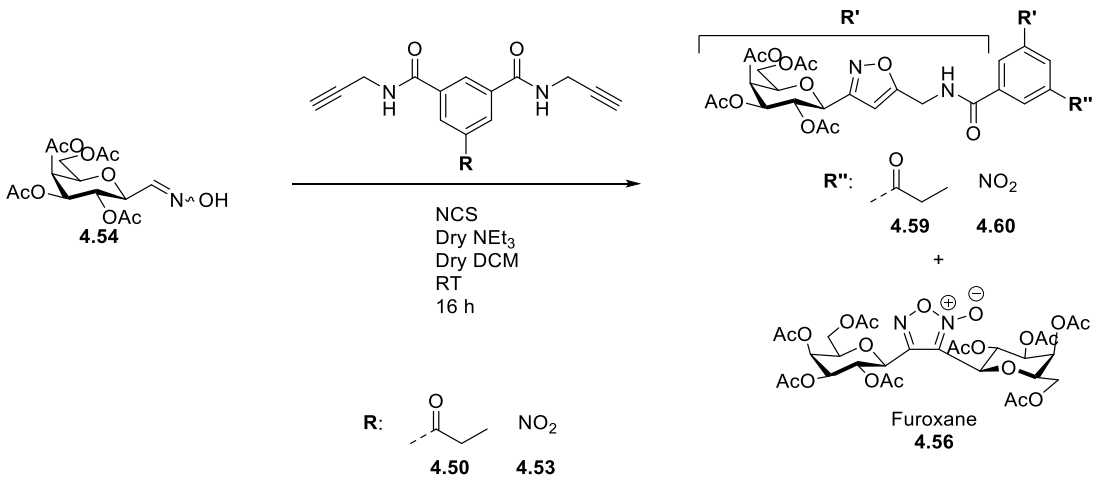

Figure 4.15: Synthesis of Isoxazole derivatives **4.59** and **4.60** by collaborators.

Finally, isoxazoline derivatives **4.61**-**4.63** were obtained as diastereomeric mixture of products, again with low to excellent yields (14-90%), with furoxane **4.56** again being produced (**Fig. 4.16**).

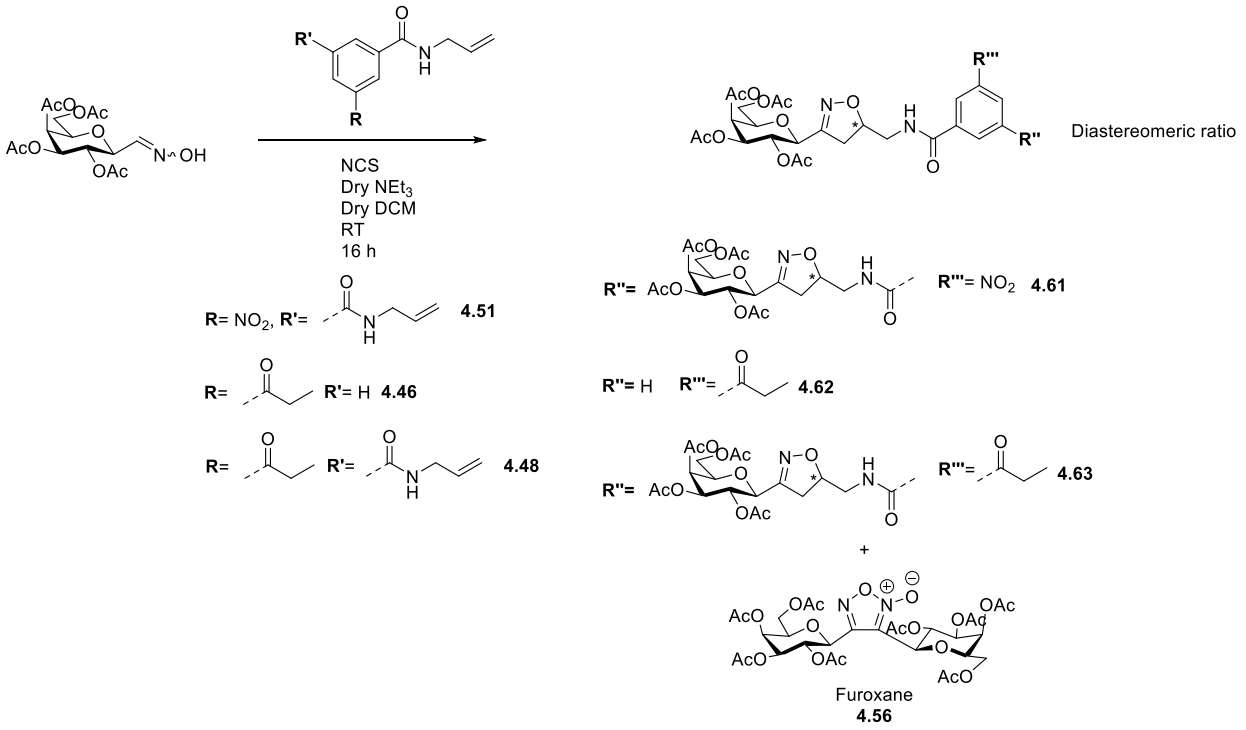

Figure 4.16: Synthesis of Isoxazoline derivatives **4.61**, **4.62** and **4.63** by collaborators.

4.3.4 Synthesis of a derivative of compound 1.39 to identify target lectin(s)

As discussed earlier, the identification and structural characterization of the lectin/protein to which the lead compound **1.39** binds to would be extremely

advantageous for the design of derivatives with improved affinity and ultimately, anti-adhesion activity against *C. albicans*.

To this end, a collaboration was established with the laboratory of Dr Lenka Malinovska in Masaryk University, Czech republic, who are experts in lectin isolation and characterization [175]. A derivative of **1.39**, **4.67**, was prepared and this compound was to be immobilised on a resin in order to isolate the lectins, or proteins, which **1.39** targets to achieve its anti-adhesion activity. This was achieved via reaction of **4.67** with an epoxide-functionalised resin to yield a resin which presents our lead compound **1.39**. This would be used to capture potential target proteins (see ahead). The first step in the synthesis of compound **4.67** was the reaction of intermediate **3.19** with 4-chlorobutyryl chloride (**Scheme 4.13**). Initially, 1.5 equivalents of 4-chlorobutyryl chloride were reacted with **3.19** overnight at RT, however, following TLC analysis a further 2 equivalents of 4-chlorobutyryl chloride were added. The reaction was stirred for a further 3 days at RT. The number of equivalents of 4-chlorobutyryl chloride needed (2.5 equiv.) and time (approximately 4 days) again suggests the low reactivity of the amine functional group in **3.19** as previously discussed. The resulting intermediate compound **4.64** was then reacted with NaN_3 in DMF overnight at RT. The resulting crude product was purified by flash column chromatography to yield **4.65**.

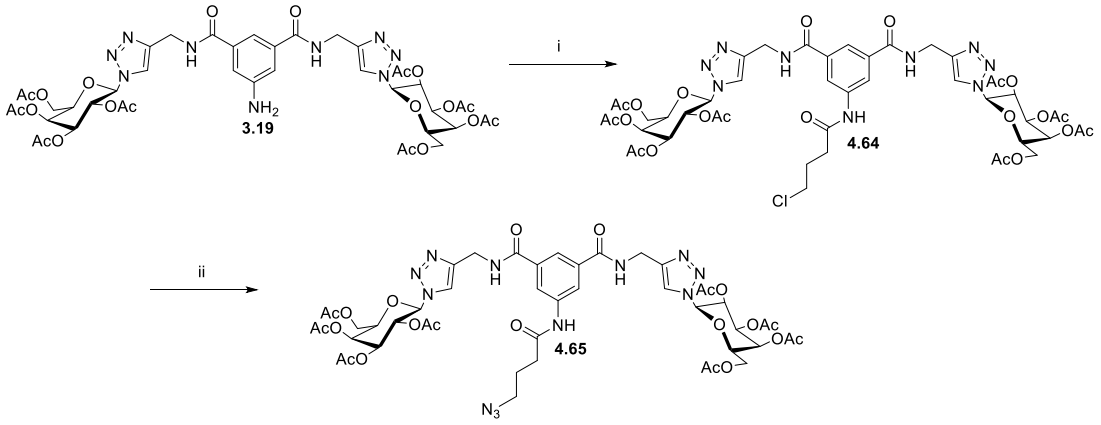

Scheme 4.13: Synthesis of glycoconjugate **4.65**. Reagents and conditions: i) 4-chlorobutyryl chloride, NEt_3, DCM, RT, 4 days, used without further purification, ii) NaN_3, DMF, RT, 20 h, 59%.

In the next step in the synthesis of **4.67**, the acetyl protecting groups were removed from the D-galactoside moieties under the same mild basic conditions as discussed above, to yield **4.66** (**Scheme 4.14**).

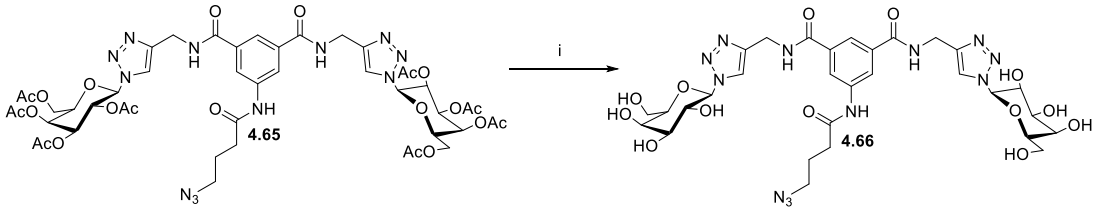

Scheme 4.14: Synthesis of glycoconjugate **4.66**. Reagents and conditions: i) MeOH, H_2O, NEt_3, 45 °C, 6 h, 95%.

The ^{1}H NMR spectrum of compound **4.66** is shown in Figure **4.17**. The triazolyl proton (light blue circle) is found as a singlet at 8.20 ppm, the aromatic ring protons (light green circle) are found as two distinct singlet peaks at 7.81 and 7.75 ppm. The anomeric proton H-1 (red circle) is found as a doublet at 5.61 ppm. The methylene protons adjacent to the 1,2,3-triazole ring (orange circle) is found as a singlet at 4.58 ppm. The three sets of methylene protons from the butyryl moiety appear as three distinct peaks. The most downfield methylene protons are again those adjacent to the azide functional group (dark blue circle) and these are found as a triplet at 3.29 ppm. The methylene protons adjacent to the carbonyl functional group (dark green circle) appear as a triplet at 2.36 ppm, the last set of methylene protons (purple circle) also appear as a triplet at 1.82 ppm.

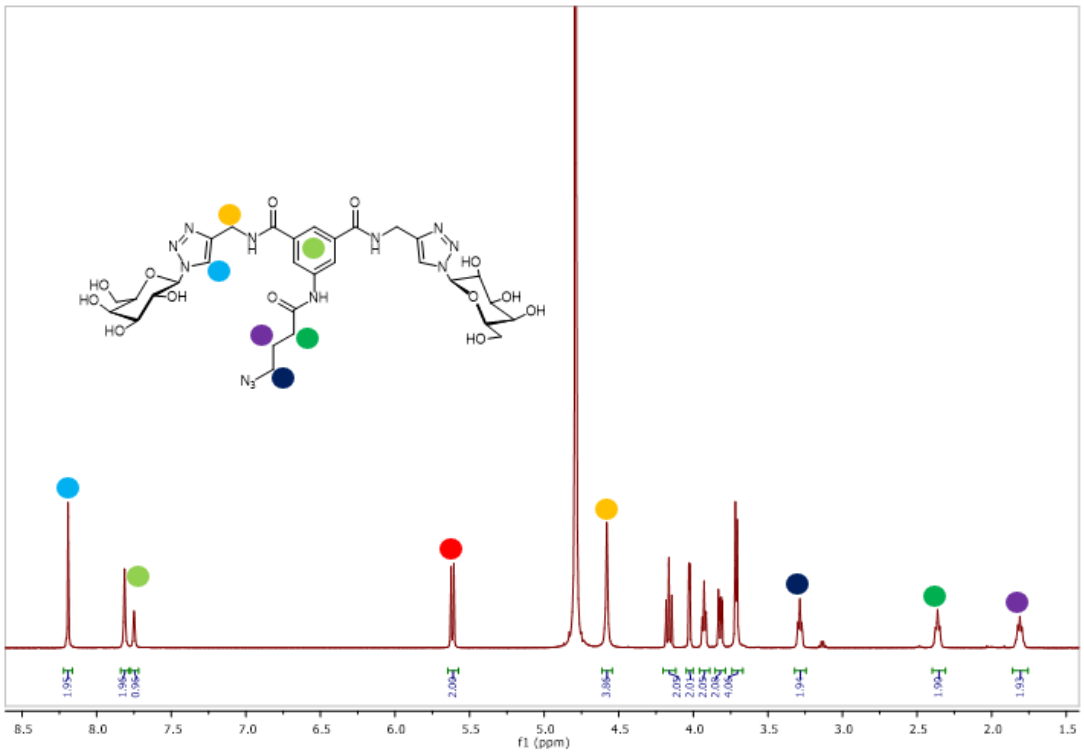

Figure 4.17: ^{1}H NMR spectrum of compound **4.66**. Note: Anomeric proton is assigned as red circle.

Finally, the desired compound **4.67** was prepared *via* the hydrogenation of **4.66** using hydrogen gas and palladium on activated charcoal (**Scheme 4.15**).

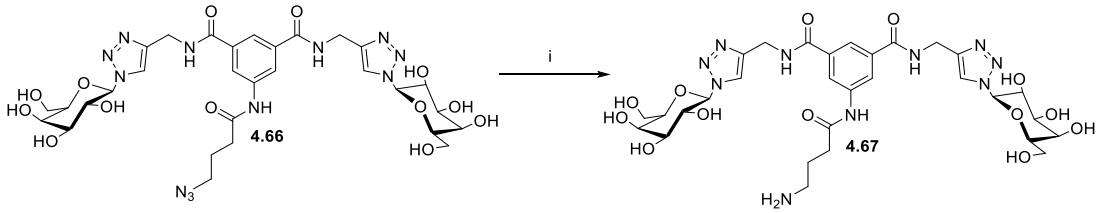

Scheme 4.15: Synthesis of glycoconjugate **4.67**. Reagents and conditions: i) Pd/C, H_2, MeOH, 16 h, RT, 79%.

The ^{1}H NMR spectrum of compound **4.67** is shown in Figure **4.18**. The triazolyl proton (blue circle) is found as a singlet at 8.25 ppm, the aromatic ring protons (light green circle) appear as two separate singlet peaks at 7.95 and 7.87 ppm respectively. The anomeric proton H-1 (red circle) appears as a doublet at 5.69 ppm. The methylene protons adjacent to the newly formed amine functional group (purple circle) are found as a multiplet at 3.10 ppm, while the methylene protons adjacent to the carbonyl functional group (orange circle) appear as a multiplet at 2.57 ppm. The

methylene protons adjacent to both of these sets of methylene protons (dark green circle) appear as a multiplet at 2.05 ppm.

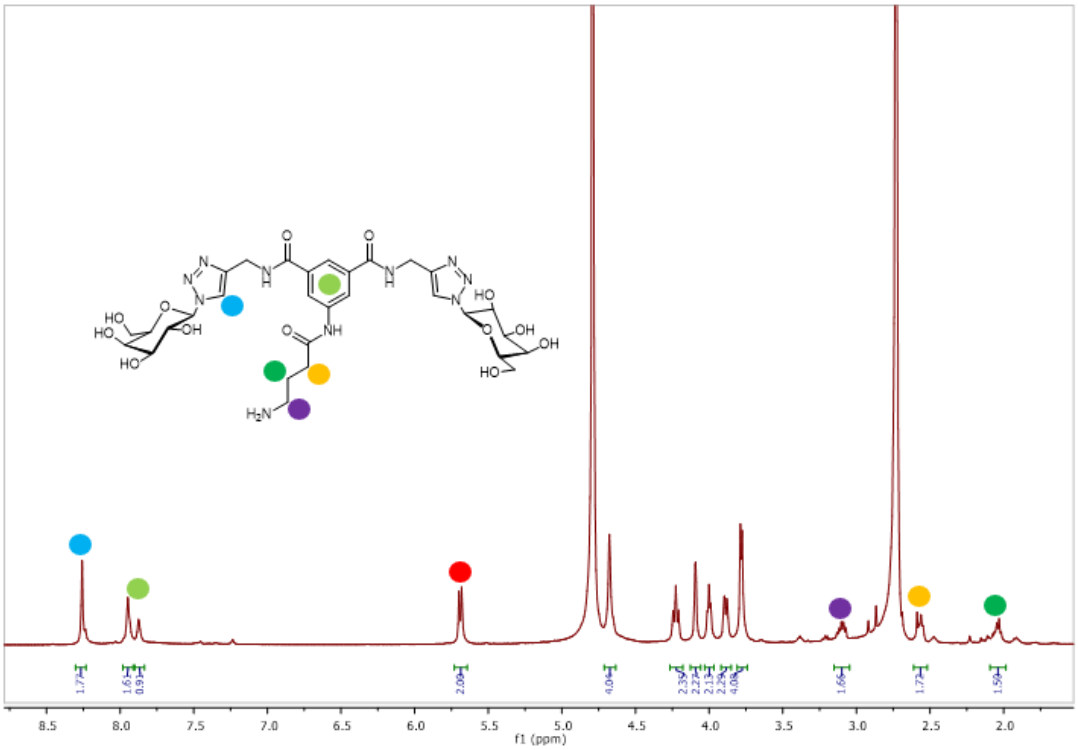

Figure 4.18: ^{1}H NMR spectrum of compound **4.67**. Note: Anomeric proton is assigned as red circle.

Initial work with compound **4.67** was carried out by our collaborators, led by Dr Lenka Malinovska, in Masaryk University, Czech Republic. This involved immobilisation of **4.67** on an epoxy-activated-Sepharose™ 6B resin, as discussed above. *C. albicans* cells were isolated by centrifugation, resuspended in buffer and lysed by sonication. Next, the cell lysate was passed incubated and mixed periodically with a **4.67**-immobilised affinity resin and, separately, with three other resins immobilised with L-fucose, D-mannose and D-galactose which were controls. These were then washed with buffer and any potentially bound proteins were released from the resin through thermal and chemical denaturation. Following SDS-PAGE analysis of the resulting samples, no bound protein was detected.

At this point our collaborators speculated that the potential target lectin may be located on the *C. albicans* cell surface. Thus, the pellet from before, which should contain the cell wall, was incubated with Lyticase from *Arthrobacter luteus*.

Incubation with the series of affinity resins mentioned above was repeated with the resulting sample. Thankfully, an approximate 40 kDa protein was found to bind immobilised **4.67** significantly better than the other control resins. Currently, work is being carried out with mass spectrometry experts to try and identify this protein and to rule out that it is not, in fact, contamination.

4.3.5 Biological evaluation

The anti-adhesion activity of the compounds discussed in this Chapter has been evaluated in the laboratory of our collaborator Prof Kevin Kavanagh (Maynooth University) by Aoife Battersby and Erasmus student Laia Moreno. Derivative **4.27** is currently undergoing biological evaluation. Each assay was performed in duplicate.

4.3.5.1 Exclusion assay

This is the first adherence assay used to evaluate the anti-adhesion activities of the glycoconjugates in this chapter. This assay involves pre-treating *C. albicans* with the glycoconjugate to be tested (incubating) for a defined period of time, followed by exposure of these yeast cells to buccal epithelial cells (BECs). Of the sp^2-iminosugar glycoconjugates tested in this assay, compounds **4.42**, **4.43** and **4.44** were found to reduce adherence by 49, 43 and 59% respectively, at a concentration of 0.1 mg/mL (**Fig. 4.19**).

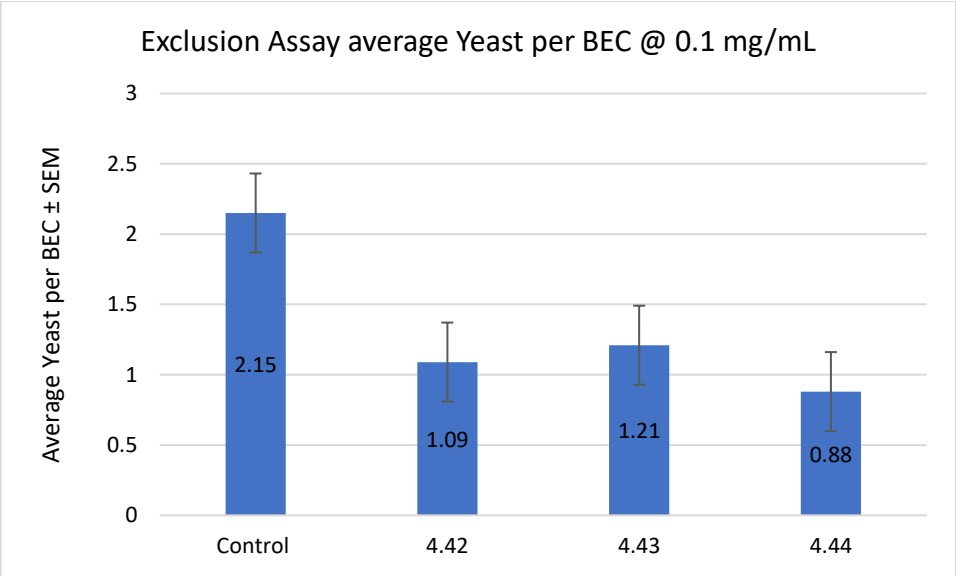

Figure 4.19: Inhibition of adhesion evaluation for compounds **4.42**, **4.43** and **4.44.** Exclusion assay (0.1 mg/mL) shows a reduction of adhesion of 49% (**4.42**), 43% (**4.43**) and 59% (**4.44**) compared to the control (untreated yeast).

Next, the bromo and methoxy analogues **4.25** and **4.26** were assessed. These analogues performed similarly to the lead compound **1.39**, with **4.25** and **4.26** reducing adherence by 23 and 39% respectively in comparison to **1.39** (26%) at a concentration of 0.1 mg/mL (**Fig. 4.20**). The inclusion of an overall electron-donating group such as a methoxy may enhance the activity of our lead compound as suggested by the slight improvement in activity of **4.26** relative to **1.39**.

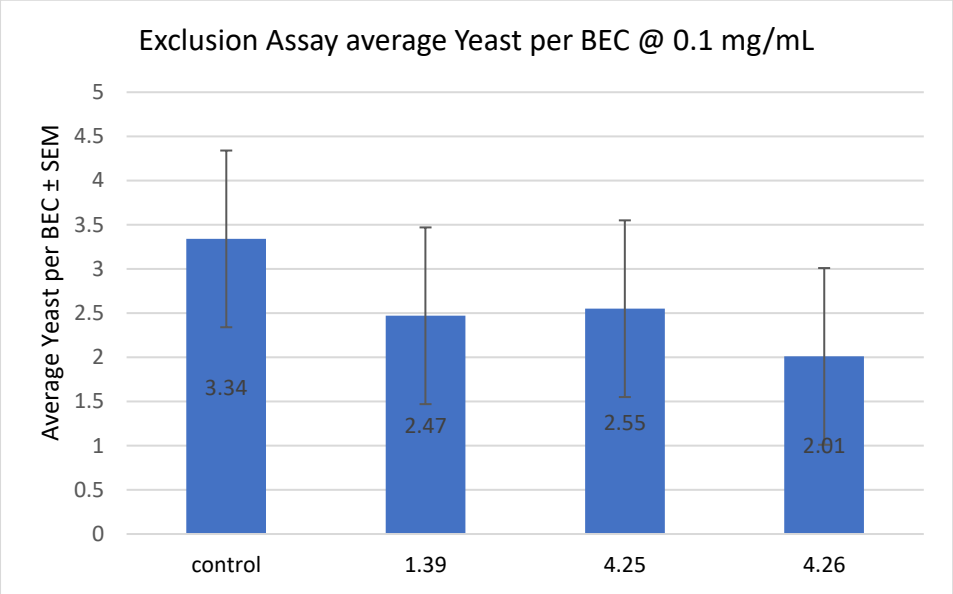

Figure 4.20: Inhibition of adhesion evaluation for compounds **1.39**, **4.25** and **4.26.** Exclusion assay (0.1 mg/mL) shows a reduction of adhesion of 26% (**1.39**), 23% (**4.25**) and 39% (**4.26**) compared to the control (untreated yeast).

4.3.5.2 Competition assay

Next, the compounds were evaluated in a competitive assay, in which their anti-adherence activities are tested in the presence of both *C. albicans* and BECs. Glycoconjugates **4.42**, **4.43** and **4.44** reduced adherence to a lesser extent, though still significant, by 27, 25 and 34% respectively (**Fig. 4.21**).

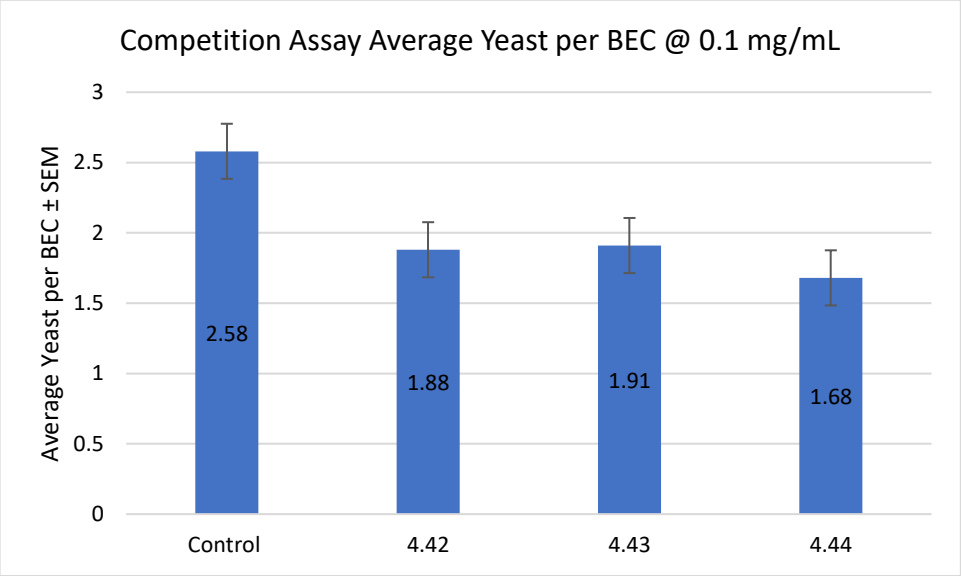

Figure 4.21: Inhibition of adhesion evaluation for compounds **4.42**, **4.43** and **4.44.** Competition assay (0.1 mg/mL) shows a reduction of adhesion of 27% (**4.42**), 25% (**4.43**) and 34% (**4.44**) compared to the control (untreated yeast).

To further assess the performance of **4.25** and **4.26** relative to **1.39**, these compounds were assessed at lower concentrations of 0.05 and 0.005 mg/mL in a competition assay. Interestingly, as seen in Figures **4.22** and **4.23**, compounds **4.25** and **4.26** performed worse than **1.39** at 0.05 mg/mL (**Fig. 4.22**), whereas they performed better at 0.005 mg/mL than **1.39**, our lead compound (**Fig. 4.23**). This suggests an unusual concentration dependent activity for these compounds, possibly due to the tendency to aggregate at higher concentrations. However, in both cases the methoxy derivative **4.26** (55% reduction) was the better performing glycoconjugate in comparison to bromo compound **4.25** (46% reduction).

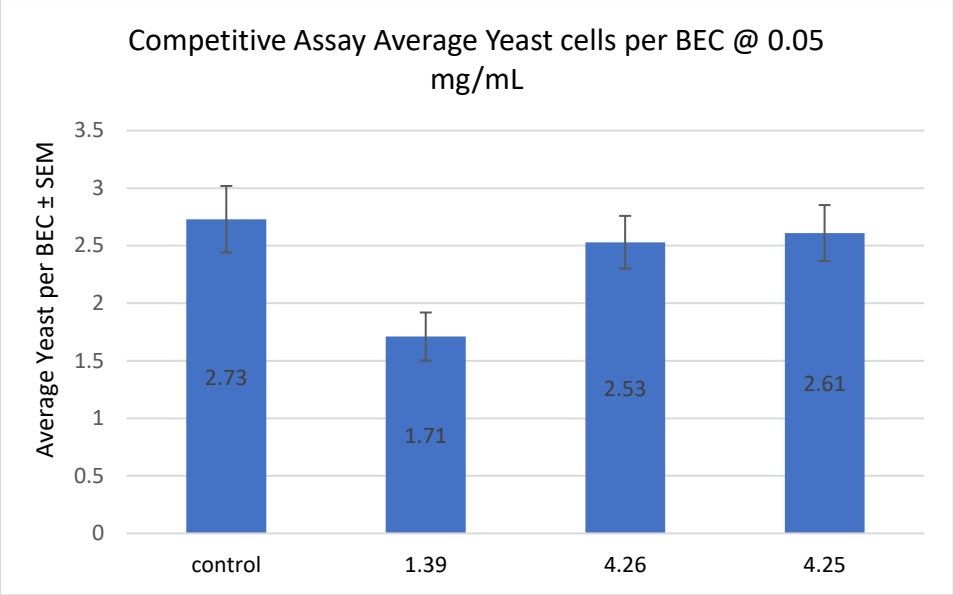

Figure 4.22: Inhibition of adhesion evaluation for compounds **1.39**, **4.25** and **4.26.** Competition assay (0.05 mg/mL) shows a reduction of adhesion of 37% (**1.39**), 7% (**4.25**) and 4% (**4.26**) compared to the control (untreated yeast).

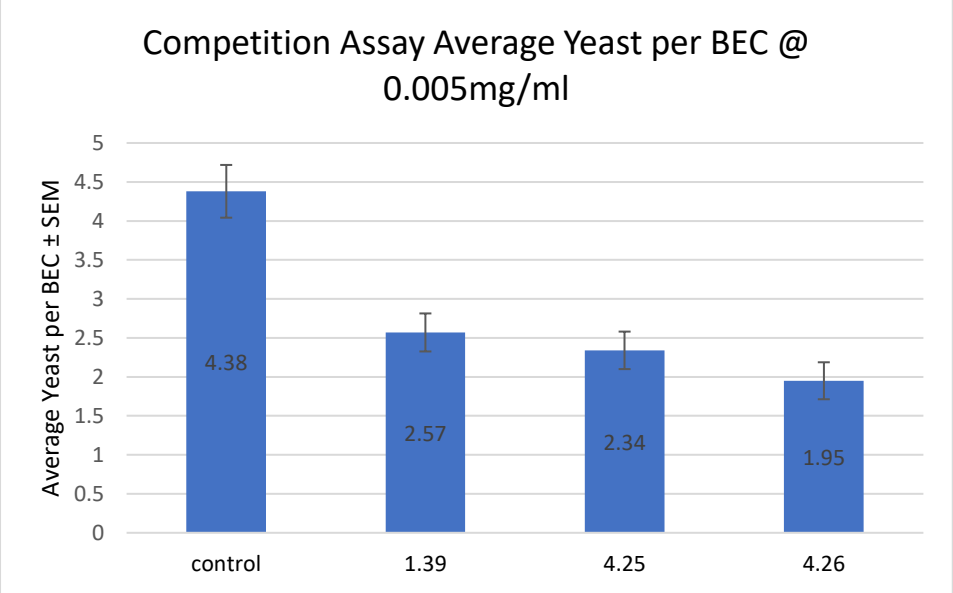

Figure 4.23: Inhibition of adhesion evaluation for compounds **1.39**, **4.25** and **4.26.** Competition assay (0.005 mg/mL) shows a reduction of adhesion of 41% (**1.39**), 46% (**4.25**) and 55% (**4.26**) compared to the control (untreated yeast).

4.3.5.3 Displacement assay

Finally, a displacement assay was carried out on **4.44** as it was the best overall performing sp^2-iminosugar glycoconjugate from the previous two assays. Interestingly, compound **4.44** reduced adhered *C. albicans* cells by 66% relative to

control 2 (**Fig. 4.24**). These are very encouraging results, as the displacement assay resembles best an infection situation in which the yeast cells are already attached to the BECs, highlighting the potential for therapeutic application for these compounds.

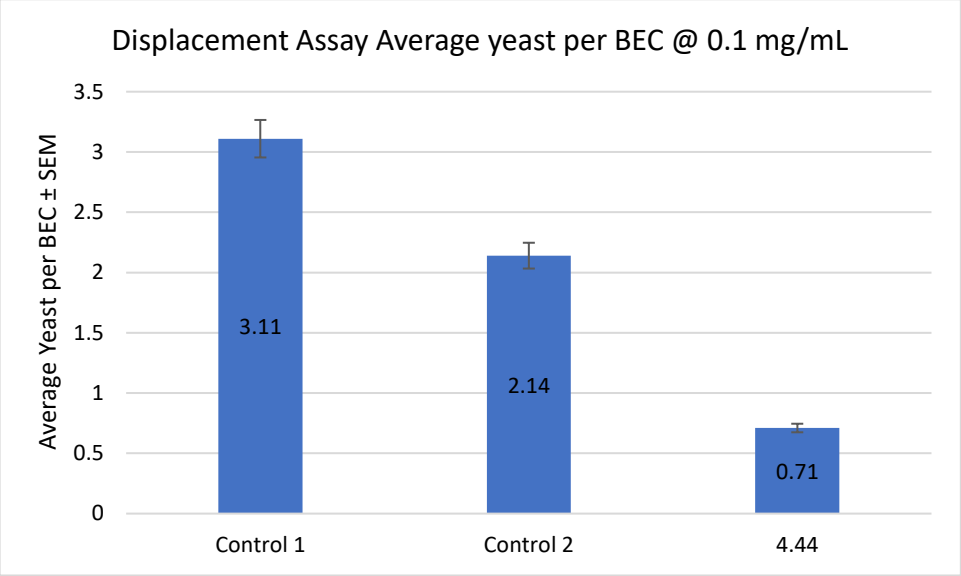

Figure 4.24: Inhibition of adhesion evaluation for compound **4.44.** Displacement assay (0.1 mg/mL) shows a reduction of adhesion of 66% (**4.44**) compared to the control 2 (untreated yeast).

Bromo and methoxy derivatives **4.25** and **4.26** were next assessed in a displacement assay at concentrations of 0.1 and 0.01 mg/mL (**Fig. 4.25** and **4.26**). Interestingly, once again a similar trend was observed whereby both derivatives **4.25** (38%) and **4.26** (43%) performed better than **1.39** (32%) at the lower concentration of 0.01 mg/mL, while our lead compound **1.39** performed better at 0.1 mg/mL.

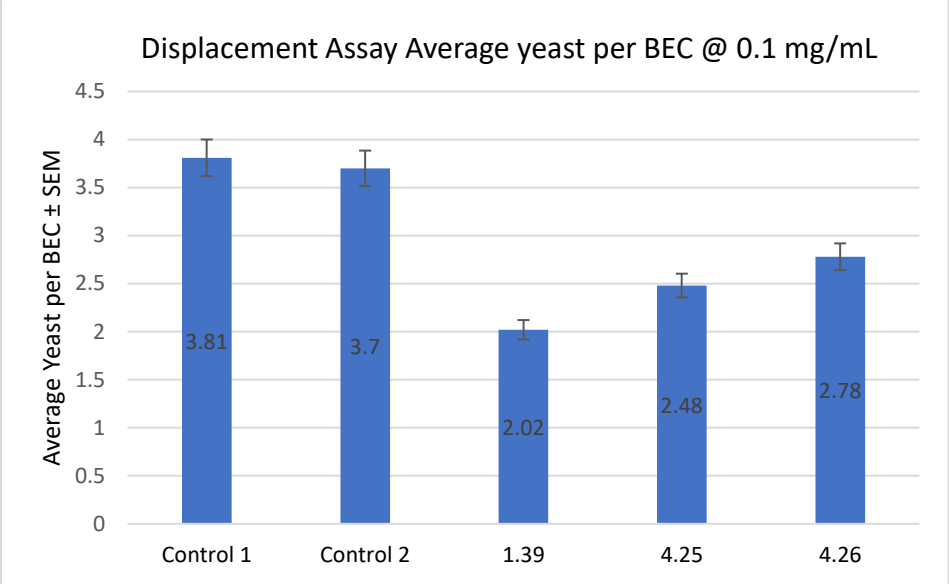

Figure 4.25: Inhibition of adhesion evaluation for compound **1.39**, **4.25** and **4.26.** Displacement assay (0.1 mg/mL) shows a reduction of adhesion of 45% (**1.39**), 32% (**4.25**) and 24% (**4.26**) compared to the control 2 (untreated yeast).

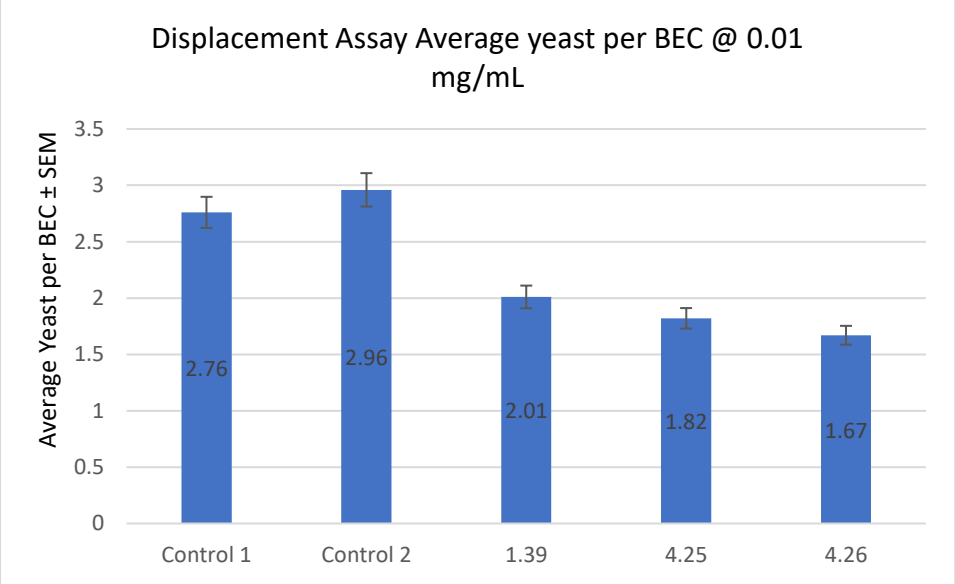

Figure 4.26: Inhibition of adhesion evaluation for compound **1.39**, **4.25** and **4.26.** Displacement assay (0.01 mg/mL) shows a reduction of adhesion of 32% (**1.39**), 38% (**4.25**) and 43% (**4.26**) compared to the control 2 (untreated yeast).

4.4 Conclusion

In conclusion, a small structure-activity-relationship study has been conducted in this chapter of lead compound **1.39**. Three key areas of this compound have been modified to probe their importance for the observed anti-adhesion activity. Firstly,

the *meta* position of the aromatic core in **1.39** was modified to yield three novel derivatives **4.25**, **4.26** and **4.27** and these compounds are currently undergoing biological testing. Initial results for compounds **4.25** and **4.26** suggest that the methoxy derivative **4.26** performs well in preventing adhesion of *C. albicans* to BECs, with bromo derivative **4.25** being less effective. The cyclopropyl derivative **4.27** is currently undergoing assessment at the time of writing. In addition, these and other compounds described in this thesis have been sent for biofilm inhibition assays with a panel of *Candida* spps. in the laboratory of Dr Irene Heredero-Bermejo (Universidad de Alcala de Henares, Madrid).

Secondly, a series of novel derivatives of **1.39** bearing sp^2-iminosugar carbohydrate moieties have been prepared to assess the necessity of a D-galactose moiety in **1.39** to confer anti-adhesion activity. Though overall these compounds **4.42**, **4.43** and **4.44** were not as effective as **1.39**, interestingly, **4.44** produced better anti-adhesion activity than **1.39** in a displacement assay. Since **4.44** contains D-glucose moieties as opposed to D-galactose moieties, this suggests that either a D-galactose moiety is not essential or the lectin target has also affinity for D-glucose derivatives, or even perhaps that **4.44** may target a separate lectin to **1.39**.

The importance of the 1,2,3-triazolyl moiety was next probed via the attempted preparation of novel 1,2,4-oxadiazole, Isoxazole and Isoxazoline derivatives. Following initial preparation of a series of novel mono- and divalent aromatic scaffolds by myself, these compounds were sent to collaborators in University of Debrecen, Hungary. Unfortunately, the desired 1,2,4-oxadiazole derivative was unable to be synthesised. Thankfully, the desired Isoxazole and Isoxazoline derivatives were successfully prepared, though with varying yields, and their syntheses are currently being optimized prior to biological testing.

The final aspect of this chapter was the preparation of **4.67**, which could be used to identify the lectin(s) which **1.39** targets to confer its anti-adhesion activity. Following successful synthesis of this compound, it was sent to collaborators in Masaryk University who are experts in such lectin identification. Initial assessment of this compound immobilised on an affinity resin revealed one 40 kDa protein that appears to bind the resin immobilised with **4.67** better than the other control resins assessed.

At the time of writing our collaborators are working with mass spectrometry experts to try to identify this protein. This would be of great importance to the design of more effective adhesion inhibitors in *C. albicans*, as structural information on the protein will greatly aid with binding optimisation.

Chapter 5

Inhibitors of AMR plasmid conjugation

5.1 Introduction

5.1.1 Antimicrobial resistance

Anti-microbial resistance (AMR) is a major cause for concern in healthcare due to the appearance of increasing numbers of resistant pathogens. Due to the higher mortality rates in patients infected with resistant pathogens, there is an urgent need to develop novel treatments for such infections [176]. Multidrug-resistant (MDR) bacteria pose a particular threat given that, in many cases, infection with such pathogens limits the therapeutic options available, which are often unsuccessful. In hospital settings, a large amount of infections are caused by highly resistant bacteria including methicillin-resistant *Staphylococcus aureus* (MRSA), vancomycin-resistant *enterococci* (VRE) and multidrug-resistant Gram-negative bacteria [177]. The development of novel antibiotics has slowed in the past few decades for a number of reasons, including permeability issues associated with the outer membranes of Gram-negative bacteria and a lack of novel bacterial targets [178]. Many newly developed antibiotics are analogues of previously successful antibiotics and these soon suffer from anti-microbial resistance. Hence, there is a need for both novel bacterial targets for antibiotics and drugs with novel modes of action which may not lead to resistance or to a lesser extent than the current types of antibiotics.

5.1.2 Mechanism of Resistance

In recent times it has become clear that, in addition to antibiotic resistance genes (ARGs) found in clinical pathogens, ARGs found in commensal and environmental bacteria are also important. Altogether, they form part of a larger reservoir of ARGs known as the resistome [179]. AMR is normally acquired either through mutation or horizontal gene transfer (HGT). HGT is considered to be the biggest factor in the current wave of the spread of AMR. There are a number of HGT mechanisms through which AMR can arise, these include conjugation, transformation, transduction and gene transfer agents (**Fig. 5.1**). Once incorporated into the recipient genome, the recipient cell may now demonstrate resistance to current antibiotics through several mechanisms. These mechanisms include reduced antibiotic permeability, active

transport of antibiotics, target modification, antibiotic modification/inactivation and target bypass (**Fig. 5.2**).

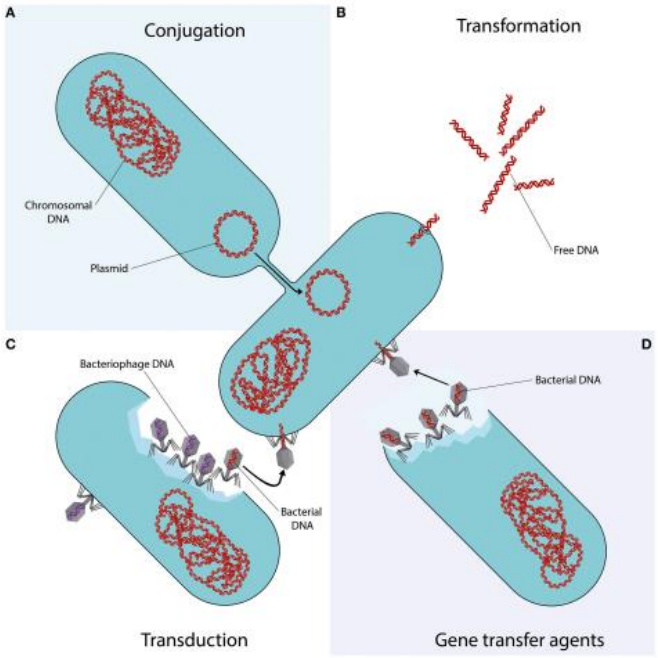

Figure 5.1: Mechanisms of horizontal gene transfer: ***A.*** Conjugation, ***B.*** Transformation, ***C.*** Transduction and ***D.*** Gene transfer agents [179].

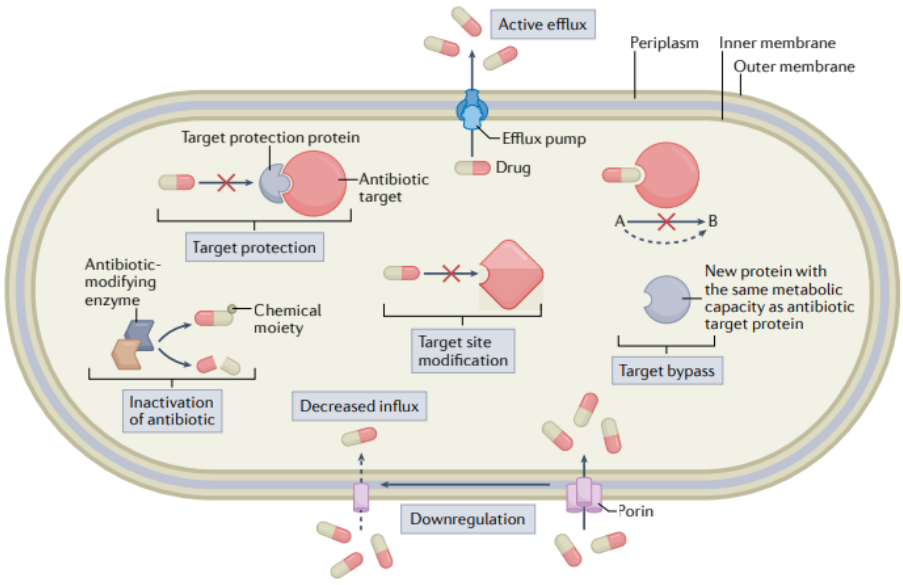

Figure 5.2: Mechanisms of antibiotic resistance [178].

5.1.2.1 Reduced antibiotic permeability

One of the first challenges faced by antibiotic drugs is the ability to cross the bacterial cell membrane in order to exert their antibiotic effect. Gram-negative bacteria

possess a double-membrane which makes this challenge particularly difficult. Porins are β-barrel protein channels which are involved in the transport of hydrophilic compounds with masses less than 600 kDa, which includes many antibiotics. Alterations to porin structure have been identified as a route through which microbes can decrease their susceptibility to different antibiotics. The size, electrical charge and genetic expression of porins may all be modified to ensure antibiotic resistance. Resistant strains of *K. pneumoniae* have been observed to modify certain porins which results in the restriction of porin size, hence limiting carbapenem permeability in this pathogen. MDR *E. coli* isolates obtained from patients have shown the ability to, through mutation, alter the electrical charge within the pore. This also reduces the efficacy of antibiotics used to treat *E. coli* infections. *Enterobacterales* have demonstrated the ability to up or downregulate porin expression in response to different stimuli [178].

Biofilms are also important structures which help to reduce antibiotic permeability. Biofilms may contain a predominant organism or a range of different organisms. Biofilms containing a range of different pathogenic bacteria may be problematic, as biofilms are known to promote HGT as different bacterial cells are placed in close proximity of each other. Biofilms are able to reduce antibiotic permeability as they are composed of a mixture of polysaccharides, proteins and DNA, which gives the biofilm a viscous, sticky consistency. Therefore, in order to confer the same antibiotic effect, higher concentrations of a given antibiotic are required. [180].

5.1.2.2 Active transport of antibiotics

Efflux is a process by which bacteria can actively transport antibiotics back out of the cell upon entering the cell. Efflux pumps are transmembrane proteins which transport a range of compounds out of the cell. This process is energy dependent. In the case of Gram-negative bacteria, the combination of a double membrane and the use of these efflux pumps makes these pathogens especially resistant to a number of antibiotics.

There are six families of efflux pumps: the resistance-nodulation-division (RND) family is of main concern as they confer the most clinically relevant levels of resistance in Gram-negative bacteria. The overexpression of these RND efflux pumps

has been observed to increase MDR in clinical isolates. Many efflux pumps are expressed constitutively, however, the expression of some are induced or overexpressed in response to stimuli or when a particular substrate is present [178]. Gram-positive bacteria are also known to possess efflux pumps, with many having been found to be encoded on their chromosomes while some have been found on bacterial plasmids [180].

5.1.2.3 Target modification

Many bacterial species have shown the ability to modify antibiotic targets which give the antibiotic its ability to limit bacterial growth or cause bacteria death. They achieve this through target alteration or protection. If the target is altered or protected through the attachment of new chemical groups, then the binding of the antibiotic to the target can be significantly impacted to the point that the antibiotic is now rendered ineffective. Typically, target modification involves genetic mutation resulting in the substitution of amino acids in or near the target binding site.

In the cases of enzymes, these alterations can lower the binding affinity of the substrate to its corresponding enzyme, however, they still allow the enzyme to function whilst inhibiting antibiotic binding to the modified enzyme. For example, mutations in genes encoding penicillin-binding proteins (PBPs) lead to increased bacterial resistance to β-lactam antibiotics. This is particularly relevant for Gram-positive bacteria as β-lactam antibiotics are used almost exclusively against this class of bacteria [180]. With regard to target protection, a good example of this route to antibiotic resistance is lipopolysaccharide (LPS). LPS is a component of bacterial cell membranes [181]. Since many of the commonly used antibiotics have become increasingly ineffective due to resistance, older antibiotics are increasingly being used. Clinical isolates demonstrating resistance to these older drugs are less common. Colistin (**5.1**, **Fig. 5.3**) is one such older antibiotic which acts by targeting LPS as part of a complex mode of action. Colistin binding to LPS ultimately leads to membrane damage and eventually cell death. Bacterial species have evolved to decorate LPS with different chemical groups which modify the charge of LPS which limits binding of colistin to LPS. A common modification of LPS is the transfer of phosphoethanolamine (pEtN) from phosphatidylethanolamine to LPS via a pEtN

transferase enzyme, which alters the charge of LPS and hence confers colistin resistance.

Bacterial species have also shown resistance to antibiotics which are capable of binding their target. Fusidic acid-resistant *S. aureus* can express FusB-type proteins. Fusidic acid (**5.2**, **Fig. 5.3**) is often administered to treat *S. aureus* infections as it can bind to elongation factor G. This ultimately inhibits bacterial translation as a protein complex involved in mRNA and tRNA processing cannot dissociate. FusB-type proteins can promote dissociation of this protein complex, hence, limiting the efficacy of Fusidic acid even though it did successfully bind to its target [178].

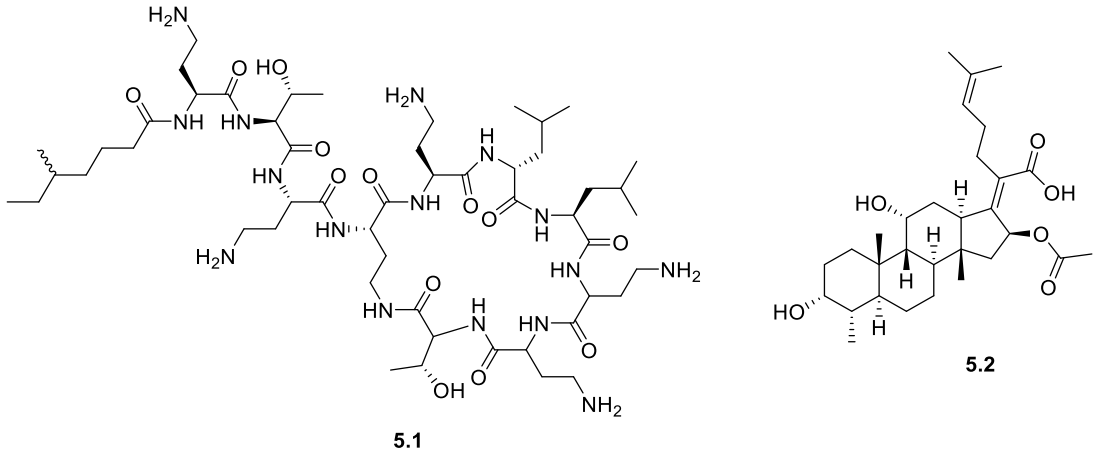

Figure 5.3: Structures of Colistin **5.1** (left) and Fusidic acid **5.2** (right) [178].

5.1.2.4 Antibiotic modification/inactivation

Another effective way by which bacterial species may develop resistance to antibiotics is through modification/inactivation of the antibiotic itself. Modification typically involves the attachment of a chemical group to the antibiotic, whereas inactivation typically involves degradation of the antibiotic. Several antibiotic-modifying enzymes have been identified to date. For example, aminoglycosides such as streptomycin (**5.3**, **Fig. 5.4**) are a common antibiotic class, which may be modified by acetyltransferases, phosphotransferases or nucleotidyltransferases. These enzymes function by altering the hydroxyl or amino groups of the aminoglycoside resulting in decreased affinity of the drug for its target.

Antibiotic inactivation is another effective route to resistance used by bacteria. β-lactamases are prominent enzymes used by bacteria to hydrolyse the amide bond

within the β-lactam ring of β-lactam antibiotics. There are over 7,000 β-lactamases characterised to date, highlighting how widespread these enzymes are in bacterial species. Carbapenems such as meropenem (**5.4**, **Fig. 5.4**) are one of the most recently developed classes of β-lactam antibiotics, as they are amongst the most potent antibiotics currently available, increasing resistance to carbapenems through β-lactamases is of great concern. Of the carbapenemases (β-lactamases), New Delhi metallo-β-lactamase (NDM) eznymes have increased in prevalence hugely in the last decade. These enzymes are encoded on multiple plasmids and as a result are now found globally. NDM enzymes have been shown to confer resistance to all β-lactams except aztreonam, which shows the impact of the spread of plasmids encoding these and other mechanisms of resistance [178].

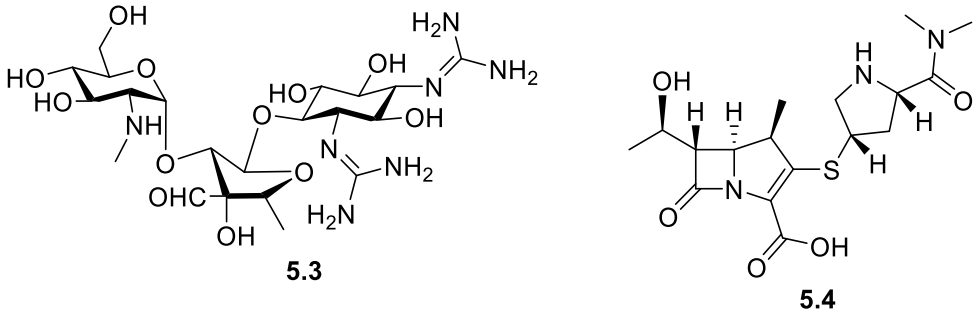

Figure 5.4: Structures of streptomycin **5.3** (left) and meropenem **5.4** (right) [178].

5.1.2.5 Target bypass

The final main strategy through which bacteria achieve antibiotic resistance is target bypass. This involves producing a different cellular pathway which results in the corresponding antibiotic being made redundant. A good example is the development of methicillin-resistant *S. aureus* (MRSA). β-Lactam antibiotics such as methicillin bind to PBPs which inhibits cell wall synthesis. *S*. aureus was able to acquire an exogeneous PBP that is homologous to the original PBP. However, while the new exogenous PBP fulfils the same function as the original, it binds β-lactam antibiotics with much lower affinity. The exogenous PBP is encoded by *mecA* gene which is a mobile genetic element (MGE) encoding methicillin resistance. Hence, the spread of this gene has led to widespread methicillin resistance in *S. aureus*. An alternative to the acquisition of a novel pathway component to confer resistance may also be the

overexpression of the drug target. This has the effect of decreasing the potency of a given antibiotic and also ensuring cell survival [178].

5.1.3 Transmission of AMR

Conjugation is the most extensively studied of the HGT mechanisms. It requires cell to cell contact between bacteria which are called the 'mating pair'. During the conjugation process, the DNA to be transferred between host and recipient cells, is often modified to become single-stranded. This is then processed to become double-stranded DNA by replication machinery in the recipient cell. Integrative and conjugative elements (ICEs) are mobile genetic elements (MGEs) that encode the cellular machinery used in the conjugation process, the regulatory systems needed to control excision from the chromosome and their conjugative transfer. As seen in Figure **5.5**, the typical ICE life cycle begins with excision of the ICE. An Excisionase is an enzyme required for excision in Gram-positive host cells, while it increases the frequency of excision in Gram-negative host cells. Excision results in the formation of a circular DNA molecule which is an extrachromosomal form of this element. For conjugative transfer to occur, further processing of the extrachromosomal ICE DNA is required. For plasmid transfer, a relaxase enzyme must bind to and cause a nick in the plasmid DNA in a region known as the origin of transfer (oriT). This enables initiation of rolling circle replication. Once this is completed, the relaxase enzyme remains bound to the single-stranded plasmid DNA and interacts with a coupling protein, which is usually conjugal transfer protein G. This targets the DNA-enzyme complex to a mating pore which results in transfer of the DNA to the recipient cell.

Bioinformatic analysis suggests that systems similar to type IV secretion systems (T4SSs) are commonly used to transfer this DNA from host to recipient cells. T4SSs is composed of a protein complex that spans the bacterial membrane forming a secretion channel. Many of these type IV secretion systems also contain an extracellular component such as a pilus. Once inside the recipient cell, the single-stranded DNA is targeted by a DNA polymerase which forms a double-stranded circular DNA molecule. The next step to ensure successful uptake of the ARGs is the integration of the relevant genetic information into the recipient cells chromosomes.

An integrase enzyme is used to integrate the double-stranded circular DNA molecular into the recipient chromosome. The integrase enzymes are essential for the proper integration of this important genetic information and some are also involved in the excision process. Once the integration process has been completed, the recipient cell may repeat this process, this time acting as the donor or host cell by transferring this genetic information to a new recipient cell. The process has rapidly increased the prevalence of AMR, to the detriment of current antibiotics [182].

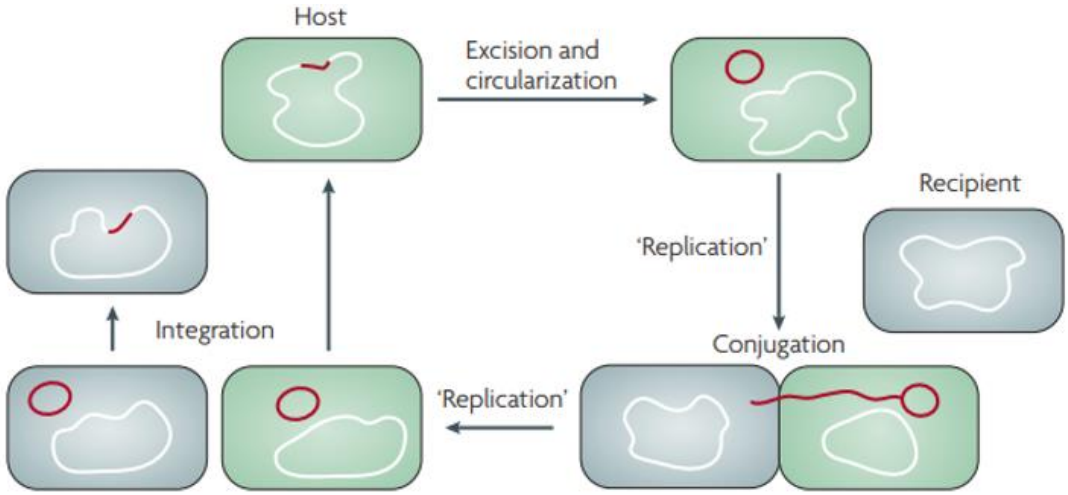

Figure 5.5: Schematic representation of the conjugation process [182].

5.1.4 Conjugation inhibitors

Since conjugation is the main method of HGT between virulent pathogenic species, there is an increasing interest on finding conjugation inhibitors as a means of slowing down the spread of AMR. Interestingly, antibiotic resistance as a result of conjugation may be 10^5 more frequent than spontaneous chromosomal mutations which result in resistance [183]. Thus, chemical compounds demonstrating the ability to inhibit HGT through conjugation would be of important clinical relevance. The frequency of the appearance of new antibiotic resistant strains would be stunted by such compounds. To this end, in recent research compounds such as intercalators, acridine dyes and quinolones were all reported to produce conjugation inhibition [184-187]. However, following further studies it was found that these compounds were active due to their ability to impact bacterial growth or bacterial DNA synthesis

as opposed to specifically affecting the conjugation process. Thus, the search for potential inhibitors of bacterial conjugation continues.

Attempts have been made to develop compounds that target the T4SS secretion system or associated proteins. As discussed earlier, these proteins are important for the transfer of DNA from host to recipient cell. Another promising strategy to prevent conjugation is targeting the conjugative pilus, since these are required for bacteria cell contact which is ultimately needed for the spread of ARGs. Hence, compounds or biomolecules that either prevent the formation of these pili or prevent bacterial cell contact represent promising candidates as conjugation inhibitors [188].

Lin *et al.* observed that conjugation could be inhibited by g3p, a phage minor coat protein, at low nanomolar concentrations. Importantly this inhibition did not affect the growth rate of cells which, in the case of conjugation inhibitors, would have important implications for the development of resistance to these compounds in bacteria [183]. Palencia-Gándara *et al.* reported the *in vivo* assessment of 2-hexadecynoic acid (**5.5**, **Fig. 5.6**): prior to this work the *in vivo* assessment of conjugation inhibitors had not been reported. Compound **5.5** was assessed in two *in vivo* models: a freshwater microcosm and the mouse gut. Due to residual antibiotic concentrations found in waste-water, which provide a selective pressure, water environments are hotspots for antibiotic resistance. Thus, this freshwater microcosm is a realistic model to study conjugation inhibition. The authors found that compound **5.5** was able to inhibit conjugation in the freshwater model system. The conjugation frequency was found to decrease greater than 10-fold when 1.6 μg/mL of **5.5** was fed to the fish in this model system. Importantly, compound **5.5** did not affect the bacterial growth rate. Similarly, an approximate 10-fold decrease in conjugation frequency was observed in the mouse gut model system [189]. Garcia-Cazorla *et al.* reported the assessment of the same compound **5.5** as a non-competitive inhibitor of the traffic ATPase TrwD. This enzyme is a VirB11 homolog. VirB11 is one of a number of proteins which make up a type IV secretion system which is key to the transfer of DNA between bacterial cells during conjugation. The authors found that **5.5** is incorporated into bacterial membranes and replaces palmitic acid as the major component of phospholipids in bacterial membranes, resulting in the inhibition of

bacterial conjugation [190]. Ripoll-Rozada *et al.* had previously identified ATPase TrwD as the molecular target for such compounds [191].

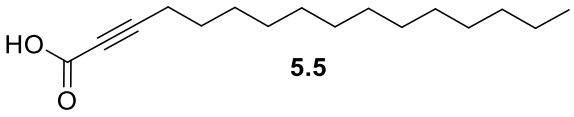

Figure 5.6: Structure of compound **5.5** [189].

Oyedemi *et al* found that rottlerin **5.6** (**Fig. 5.7**) and 'red compound' **5.7** (**Fig. 5.7**), isolated from the plant *Mallotus philippensis,* showed anti-bacterial activity against a range of Gram-positive bacteria, including *E. faecalis*, *S. aureus* and *B. subtilis* as well as MDR *S. aureus*. These both compounds showed poorer activity against Gram-negative bacteria including *E. coli*, *P. aeruginosa* and *K. pneumoniae*. Building on this, the authors found that both compounds **5.6** and **5.7** displayed significant abilities to inhibit conjugative transfer of a range of AMR plasmids between *E. coli* [192]. Additionally, plumbagin **5.8** (**Fig. 5.7**), which is produced by the plant *Plumbago zeylanica*, had been tested and identified as a plasmid conjugation inhibitor [193,194].

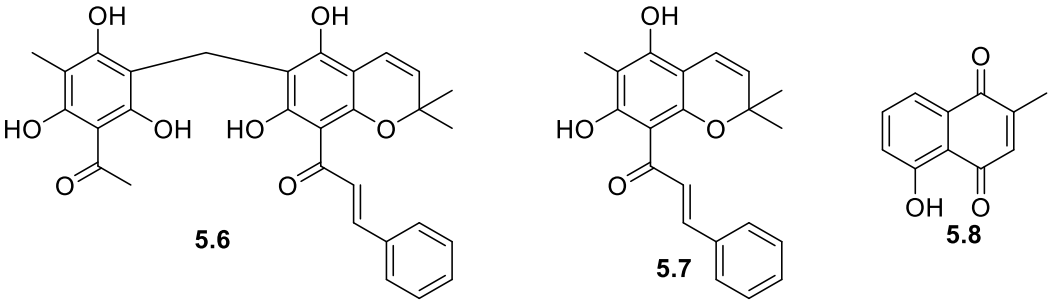

Figure 5.7: Structures of **5.6**, **5.7** and **5.8** [192,193].

Lujan *et al.* hypothesised that inhibition of DNA relaxase, a key enzyme in the conjugative transfer of plasmids between host and recipient, would result in reduced plasmid transfer. The authors believed that, as relaxase enzymes are capable of binding two phospotyrosine within their active site, bisphosphonate derivatives, such as **5.9** and **5.10** (**Fig. 5.8**) could potentially act as inhibitors of these enzymes. The authors envisioned these bisphosphonates binding to the Mg^{2+} metal chelating ion found in the active site. They found that **5.9** and **5.10** were capable of inhibiting conjugative transfer of DNA between F^+ and F^- *E. coli* with EC_{50} values of

approximately 10 µM and 110 nM respectively [195]. Shaffer *et al.* described the effects two compounds, **5.11** and **5.12** (**Fig. 5.8**), had on a number of T4SS-dependent processes in *E. coli* involved in DNA transfer between respective host and recipient cells. The group found that both compounds significantly reduced the DNA conjugation efficiency in *E. coli* and they also did not impair *E. coli* growth [196].

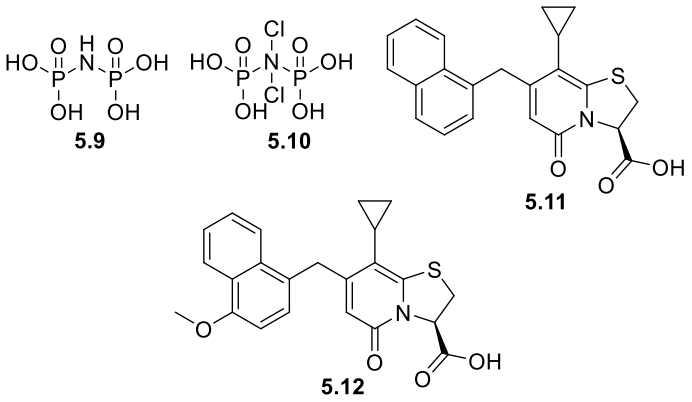

Figure 5.8: Structures of **5.9**, **5.10**, **5.11** and **5.12** [195,196].

In a screen of AQUAc, which is a collection of bioactive compounds isolated from aquatic microorganisms, Getino *et al.* identified two compounds **5.13** and **5.14** (**Fig. 5.9**) as plasmid conjugation inhibitors. Compound **5.14** was able to reduce R388 plasmid conjugation to 2%**,** at a concentration of 0.4 mM in a plate-conjugation assay with a number of donor and recipient *E. coli* strains. Compound **5.14** also inhibited IncW plasmid R388 and IncFII plasmid R100-1 conjugation between *E.* coli cells with a 100-fold inhibition at 0.4 M, while inhibition was observed in several other plasmids to a lesser extent. Meanwhile, compound **5.13** performed similarly to compound **5.14** [197].

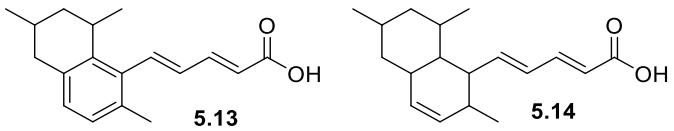

Figure 5.9: Structures of **5.13** and **5.14** [197].

5.1.5 Escherichia coli and FimH

E. coli is a common bacterial pathogen which is involved in urinary tract infections (UTIs). Antibiotic resistance in *E. coli* has made the treatment of UTIs increasingly

difficult, thus the development of conjugation inhibitors against *E. coli* would help to extend the therapeutic use of treatments still effective for UTIs, which are very common.

FimH is an adhesin protein found at the tip of type 1 fimbriae in *E. coli*. Attachment of *E. coli* to host cells is facilitated by the binding of FimH to high mannosylated glycoproteins found on host cell walls via what is known as a 'catch and release mechanism' [161]. FimH shows binding specificity for α-D-mannosides, in addition to aryl and alkyl mannosides. Bouckaert *et al.* assessed the binding of a range of mono- and disaccharides to FimH and observed a trend whereby alkyl mannosides of increasing alkyl chain length had lower binding constants (K_d). The lowest K_d value, 5 nM, was observed for the heptyl-α-D-mannoside **5.15** (**Fig. 5.10**) with an alkyl chain of 7 carbon atoms. The authors believed this high affinity is due to alkyl chain binding to a hydrophobic pocket in FimH, which is found in a region surrounded by Tyrosine 48 and 137 and Isoleucine 52 near the mannose binding pocket. Figure **5.10** shows the interactions of FimH with butyl α-D-mannoside. The mannose ring forms a range of hydrogen bonds between itself and a number of amino acids [198]. Importantly, heptyl-α-D-mannoside **5.15** has also been shown to inhibit biofilm formation by blocking the FimH binding site on type 1 pili. Heptyl-α-D-mannoside **5.15** was capable of decreasing biofilm formation at 10μM [135]. The significance of this is that it is believed that biofilms facilitate conjugation due to the close proximity of bacterial cells within biofilms [180].

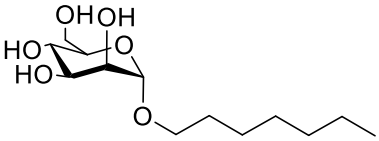

5.15

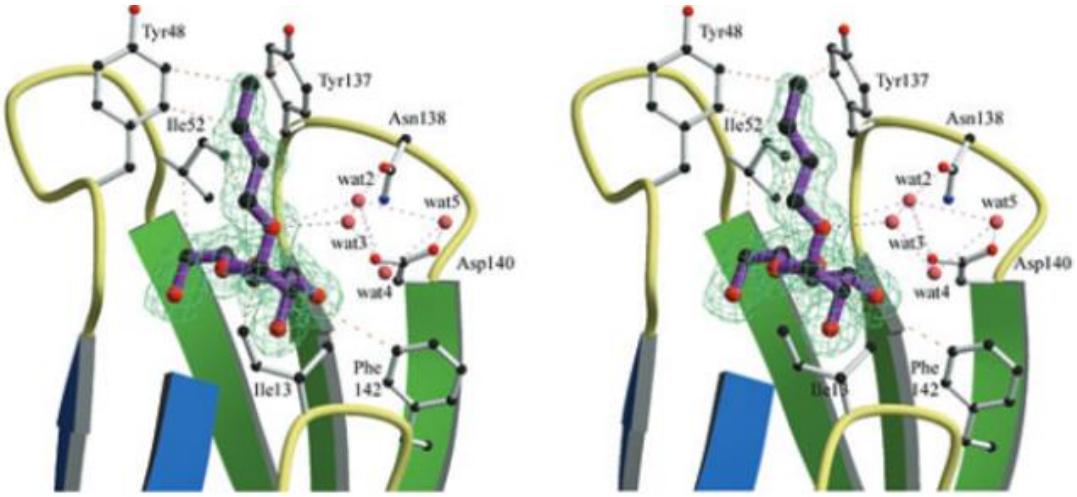

Figure 5.10: *Top:* Structure of **5.15**; *Bottom:* Binding of FimH with butyl α-D-mannoside [198].

In a study assessing the correlation of virulence-associated genes (VAG), including the gene encoding FimH, with the conjugation frequency/potential of a number of strains, Kuznetsova *et al.* found that of the 29 strains assessed 21 (72.4%) strains possessed the FimH gene. This suggests that FimH may play an important role in the conjugation process [199].

5.2 Chapter Objective

Very little is known about the role that carbohydrate-mediated interactions play, if any, in the conjugation process. Since cell-surface carbohydrates are found on essentially every cell type and have been shown to be important in the adherence of pathogens to host cells [200], it is plausible to expect that carbohydrates may also be involved in initial adhesion processes between bacterial cells necessary to initiate plasmid conjugation. As mentioned above, *Escherichia coli* is a common pathogen which utilises the FimH lectin for its adherence to host cells. It was hypothesised that this pathogen may also utilise this lectin during the conjugation process to gain initial proximity and establish cell to cell contact at the earlier stages of the conjugation

process. Taking advantage of the fact that several high affinity ligands for FimH have been identified and are very well characterized, several known and potential FimH antagonists were selected and prepared to test this hypothesis (**Fig. 5.11**). Both the known and potential FimH antagonists share alkyl aglycons.

The objective of this chapter is to investigate if glycoconjugate inhibitors of bacterial adhesins, such as FimH, can also inhibit plasmid conjugation. Heptyl α-D-mannoside **5.15**, (HMan) a well-established high affinity ligand of FimH was chosen as the lead compound in this investigation. A novel triazolyl mannoside derivative **5.19** was prepared as an analogue of **5.15**. In addition, two control galactoside glycoconjugates, heptyl β-D-galactoside **5.23** (HGal) and novel triazolyl **5.18** were prepared as negative controls, as FimH has specificity for mannosides over galactosides. The novel mannoside derivative **5.39** (**Fig. 5.11**) was prepared and assessed as a plasmid conjugative transfer inhibitor. Thus, a difference in plasmid transfer following treatment with either the mannoside- or galactoside-based compounds in *E. coli* could indicate that lectin-related interactions may have a role in conjugative processes. The evaluation of the ability of these compounds to inhibit AMR plasmid conjugation in *E. coli* was carried out by Marwa Alawi, a PhD student of our collaborator Prof Fiona Walsh (Maynooth University).

Finally, fluorescently-labelled derivatives of the best performing glycoconjugates were prepared to aid in the elucidation of the mechanism of action of these compounds for plasmid conjugative transfer inhibition.

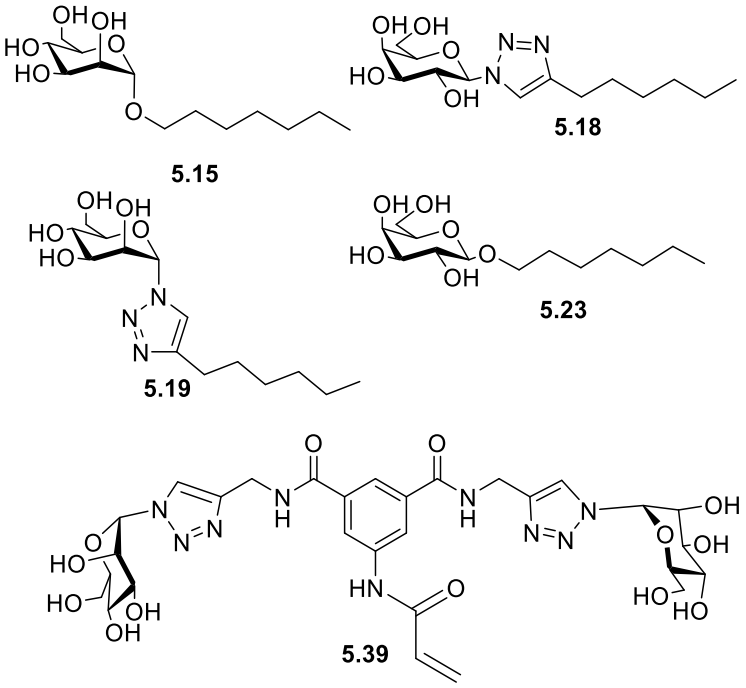

Figure 5.11: Structures of proposed Carbohydrate-based plasmid conjugation inhibitors **5.15**-**5.39.**

5.3 Results and Discussion

5.3.1 Synthesis of Glycoconjugates as AMR plasmid conjugation

5.3.1.1 Synthesis of N-triazolyl glycoconjugates

The synthesis of *N*-mannoside **5.18** and *N*-galactoside **5.19** was achieved through Copper-catalysed azide-alkyne cycloaddition (CuAAC). Reaction of the corresponding sugar azide **2.40** or **2.41** with 1-octyne yielded the acetylated products **5.16** and **5.17** (**Scheme 5.1**). The final desired products **5.18** and **5.19** were prepared by deacetylation under standard conditions (methanol/water with catalytic NEt_3 at 45-50 ^{O}C for 6 h).

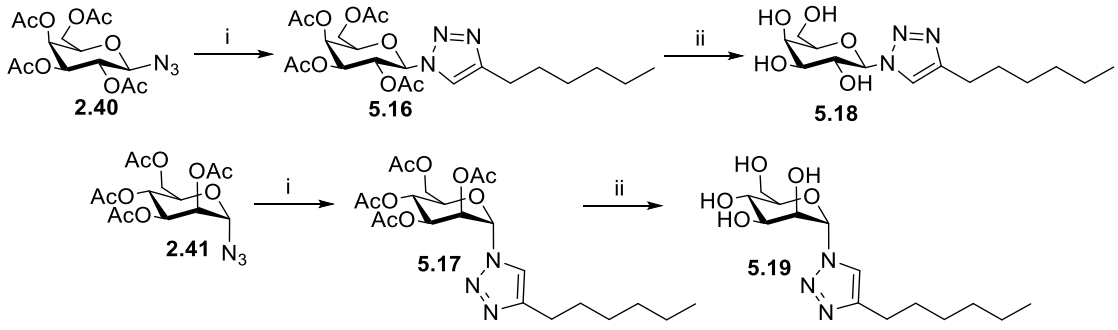

Scheme 5.1: Synthesis of **5.18** and **5.19**. *Reagents and conditions*: i) 1-Octyne, $CuSO_4.5H_2O$, Na Asc, ACN/H_2O, 100 ^{O}C (MW), 30 mins, 14-57%; ii) $MeOH/H_2O$, NEt_3, 45-50 ^{O}C, 6 h, 82-83%.

The ^{1}H NMR for compound **5.16** is shown in Figure **5.12** as a representative example for the *N*-triazolyl glycoconjugates. The 1,2,3-triazole H peak is found at 7.53 ppm as a singlet (red circle). The anomeric proton H-1 is found at 5.8 ppm as a doublet (green circle), while the methylene CH_2 (blue circle) adjacent the 1,2,3-triazole ring is found 2.68 ppm as a multiplet. The acetyl protecting groups (orange circles) are found at 2.19, 2.01, 1.98 and 1.85 ppm as singlets.

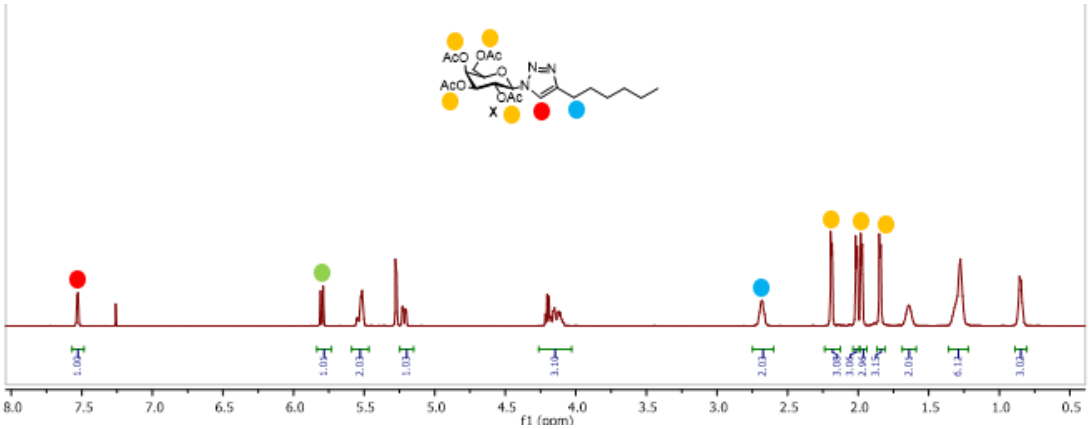

Figure 5.12: ^{1}H NMR spectrum of compound **5.16**. Note: Anomeric proton is assigned as green circle.

5.3.1.2 Synthesis of O-glycosidic glycoconjugates

The synthesis of both the heptyl *O*-mannoside (HMan) **5.15** and heptyl *O*-galactoside (HGal) **5.23** was initially investigated through direct glycosylation from the corresponding manno- or galactosyl pentaacetate and *n*-heptanol, using $BF_3.OEt_2$ as reaction promoter. However, this approach was not successful. We then proceeded to use trichloacetimidates as glycosyl donors to attempt the synthesis of the target compounds (**Scheme 5.2**). The initial step in the preparation of both the mannoside **5.15** and galactoside **5.23** derivatives was the selective deacetylation of the anomeric protecting group. This was achieved using *N,N*-dimethylamine to give mannoside **5.24** and galactoside **5.20** hemiacetals. In the next step, more reactive trichloroacetamidate derivatives **5.21** and **5.25** were formed from the reaction of **5.20** and **5.24** with trichloroacetonitrile and sodium hydride to give glycosyl donors **5.25** (Man) and **5.21** (Gal). Issues were encountered when isolating the product from this step as the paraffin liquid from sodium hydride suspension was quite viscous and difficult to separate from the product. It was found that when the crude reaction mixture, following concentration *in vacuo*, was washed and centrifuged in

chloroform that the desired reaction mixture could be separated from the paraffin liquid. Galactosyl *O*-glycoside **5.22** was formed by reaction of glycosyl donor **5.21** with 1-heptanol and trimethylsilyl trifluoromethanesulfonate (TMSOTf) as a reaction promoter.

However, when attempting these reaction conditions with mannoside tricholoroacetimidate **5.25**, it was found that the orthoester compound **5.27** was also formed (**Scheme 5.2**). This side reaction complicated chromatographic purification and decreased the yield of desired heptyl mannoside **5.26**. The ^{13}C NMR of acetylated HMan **5.26** and orthoester **5.27** are shown in Figure **5.13**. The orthoester quaternary carbon peak appears at 123 ppm (**Fig. 5.13**), while no such peak is observed for **5.26** in the ^{13}C NMR spectrum (**Fig. 5.13**). This confirms the formation of this by product. The mechanism for the formation of the orthoester **5.27** is shown in Scheme **5.3**. The oxycarbenium intermediate is stabilized by the neighbouring C-2 acetyl protecting group to form an intermediate acetal-like compound. Nucleophilic attack of the carbonyl carbon by 1-Heptanol forms the orthoester **5.27**.

The final step was the removal of the *O*-Acetyl protecting groups under standard conditions by heating in a MeOH/H_2O mixture with catalytic NEt_3 to yield **5.15** and **5.23**.

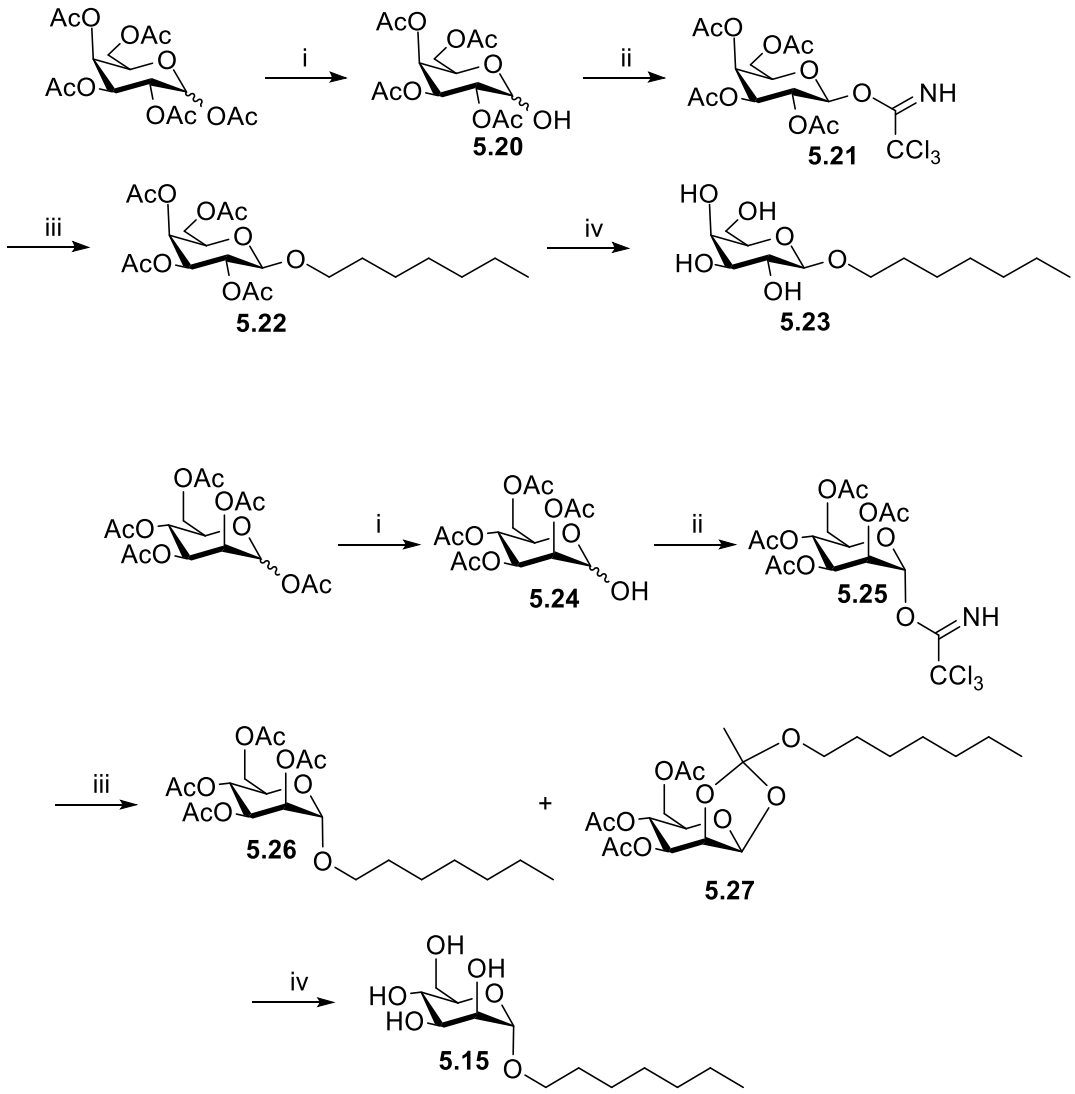

Scheme 5.2: Synthesis of heptyl galactoside **5.23** (HGal, top) and heptyl mannoside **5.15** (HMan, bottom). *Reagents and conditions:* i) *N,N*-dimethylamine, ACN, RT, 24 h, 37-38%; ii) NaH (60% dispersion), Trichloroacetonitrile, Dry DCM, RT, 16 h, 16-34%; iii) 1-Heptanol, Trimethylsilyl trifluoromethanesulfonate, Dry DCM, RT, 16 h, 57-93%; iv) NEt_3, $MeOH/H_2O$, 45-50 ^oC, 5-6 h, 12-91%.

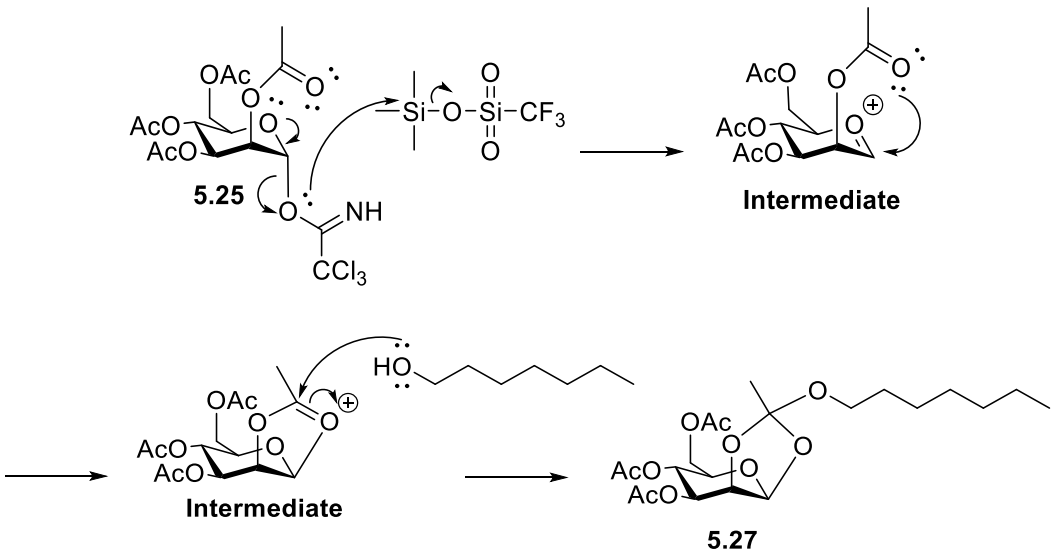

Scheme 5.3: Mechanism for the formation of orthoester **5.27**.

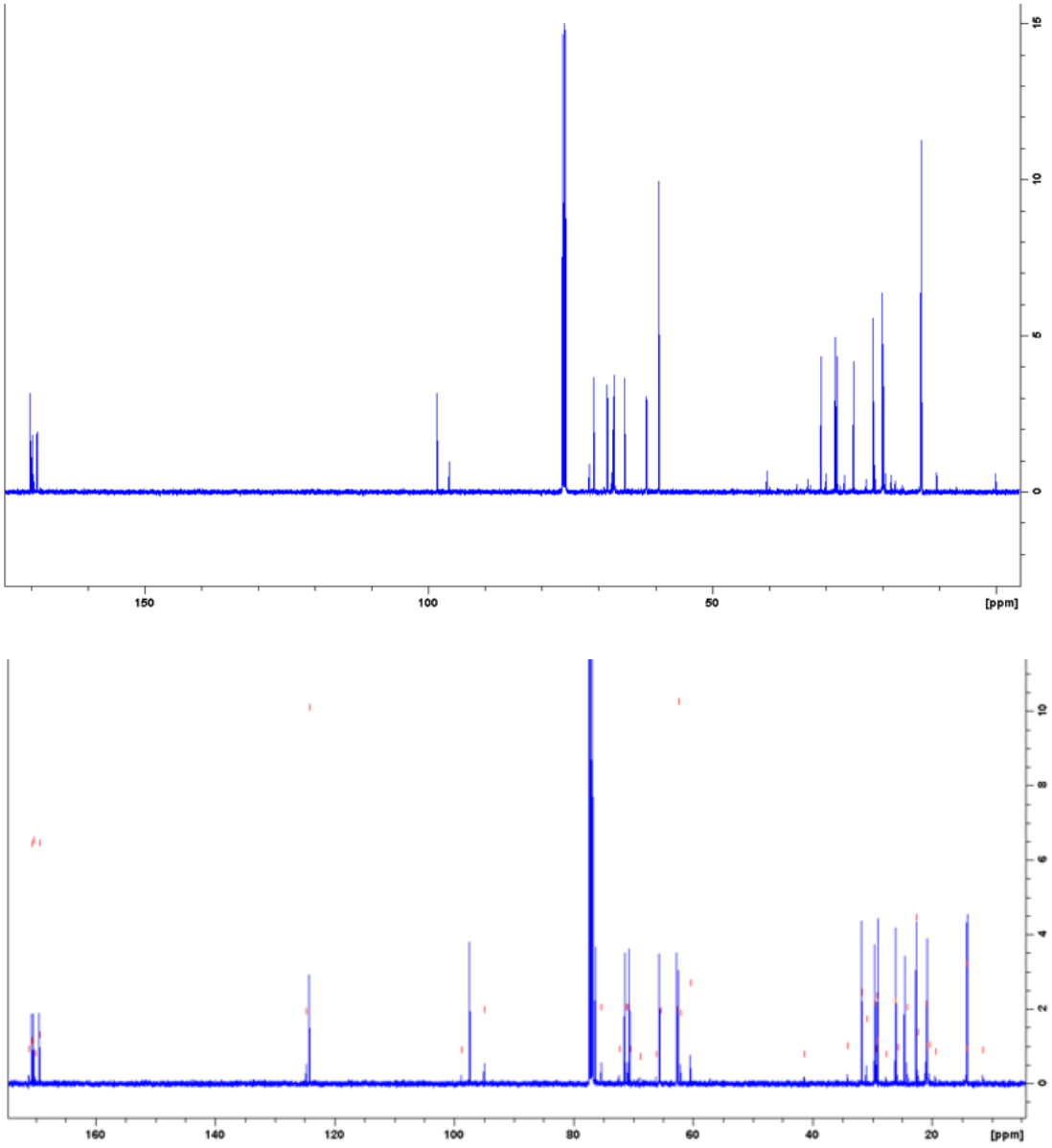

Figure 5.13: *Top:* ^{13}C NMR spectrum of compound **5.26**; *Bottom:* ^{13}C NMR spectrum of orthoester **5.27**.

The ^{1}H NMR for compound **5.23** is shown in Figure **5.14** as a representative example for the *O*-glycosidic glycoconjugates. The characteristic signals for this compound are also highlighted. The doublet peak at 4.31 ppm represents the anomeric H-1 proton (red circle), while the methylene CH_2 adjacent to the glycosidic O atom is found as diastereotopic protons at 3.86 ppm and 3.60 ppm. This data was also in agreement with literature [201].

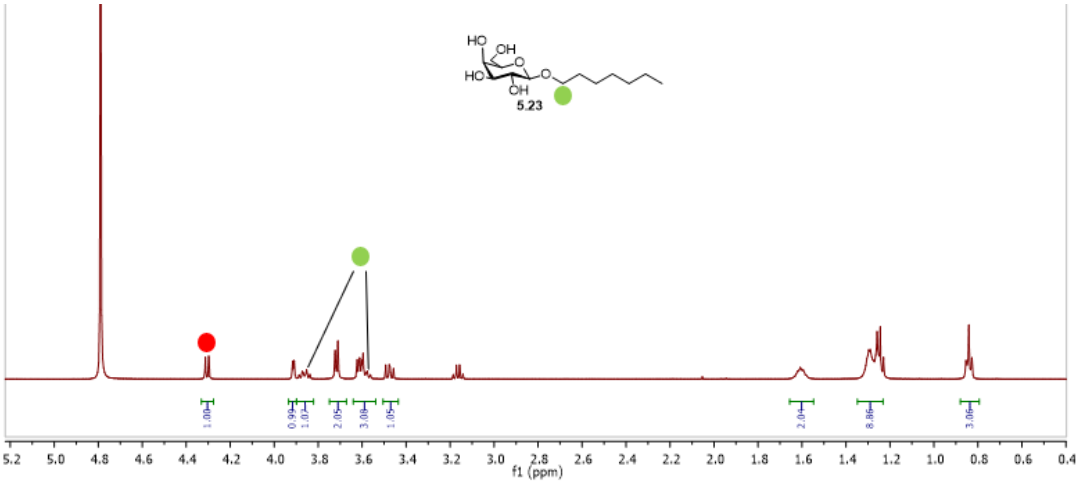

Figure 5.14: ^{1}H NMR spectrum of compound **5.23**. Note: Anomeric proton is assigned as red circle.

To overcome formation of orthoester side-product **5.27**, an alternative synthetic route to HMan **5.15** involving benzoyl protecting groups was investigated (**Scheme 5.4**) [202]. D-mannose was reacted with benzoyl chloride in pyridine to give per-benzoylated compound **5.28**. This was converted to mannosyl bromide **5.29**, which was used as the glycosyl donor. Reaction of bromide **5.29** with 1-heptanol and silver trifluoromethanesulfonate gave desired heptyl tetra-benzoyl-α-D-mannose **5.30**. Removal of the benzoyl protecting groups was achieved under the Zemplen deprotection conditions (sodium methoxide in methanol), to give HMan **5.15** after column chromatography purification.

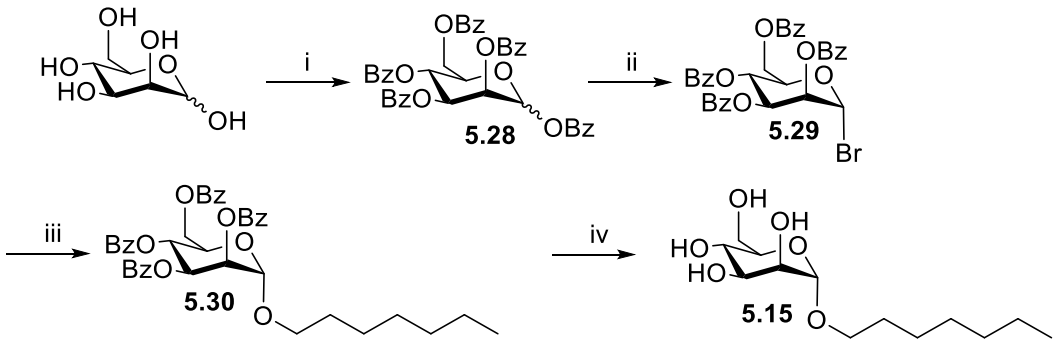

Scheme 5.4: Synthesis of heptyl mannoside **5.15** through benzoyl protected intermediates. *Reagents and conditions:* i) Benzoyl chloride, Pyridine, RT, 18 h, 64%; ii) 33% HBr in AcOH, Dry DCM, 2 h, 96 %; iii) 1-Heptanol, Silver trifluoromethanesulfonate, Dry DCM, RT, 16 h, 20%; iv) NaOMe, MeOH, RT, 16 h, 14%.

5.3.1.3 Synthesis of fluorescently labelled Heptyl α-D mannoside 5.35

A fluorescently labelled derivative of HMan **5.15** was prepared in order to confirm FimH in the bacterial membrane in *E. coli* (but no other cytosolic proteins) was the target/binding site. The fluorescently labelled derivative **5.35** was prepared with the assistance of Anna Suhas, Erasmus student in the group. The synthesis (**Scheme 5.5**) involved firstly the monopropargylation of 1,7-heptanediol, to form compound **5.31**. This was used as glycosyl acceptor with mannosyl bromide **5.29**, reacted with silver trifluoromethanesulfonate to give compound **5.32**. The removal of the benzoyl groups once again using Zemplen conditions gave HMan derivative **5.33** (^{1}H NMR spectrum, **Fig. 5.15**). The propargyl group in this compound was necessary to react with fluorescein azido derivative **5.34** through CuAAC reaction, which gave compound **5.35**. This compound is currently being used in Prof Walsh' laboratory for optimization of conjugation inhibition and imaging conditions.

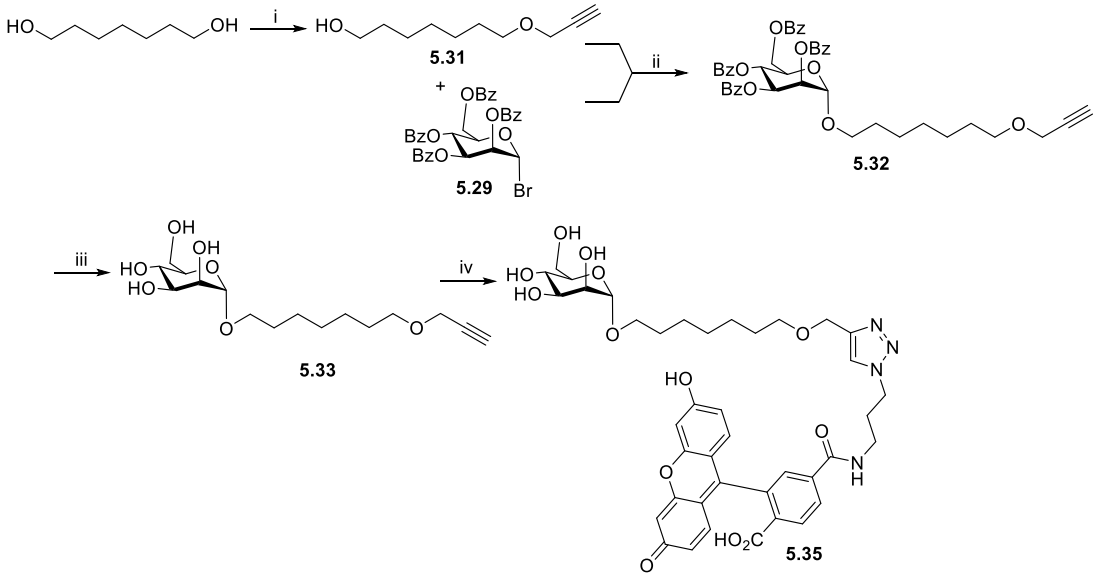

Scheme 5.5: Synthesis of fluorescently-labelled heptyl mannoside **5.35** through benzoyl protected intermediates. *Reagents and conditions:* i) 1,7-heptanediol, Propargyl bromide, NaH, Dry THF, RT, 16 h, 31%; ii) Silver trifluoromethanesulfonate, Dry DCM, RT, 16 h, 55%; iii) NaOMe, MeOH, RT, 16 h, 45%; iv) Fluorescein azide **5.34**, $CuSO_4.5H_2O$, Na Asc, ACN/H_2O, 100 ^OC (MW), 10 mins.

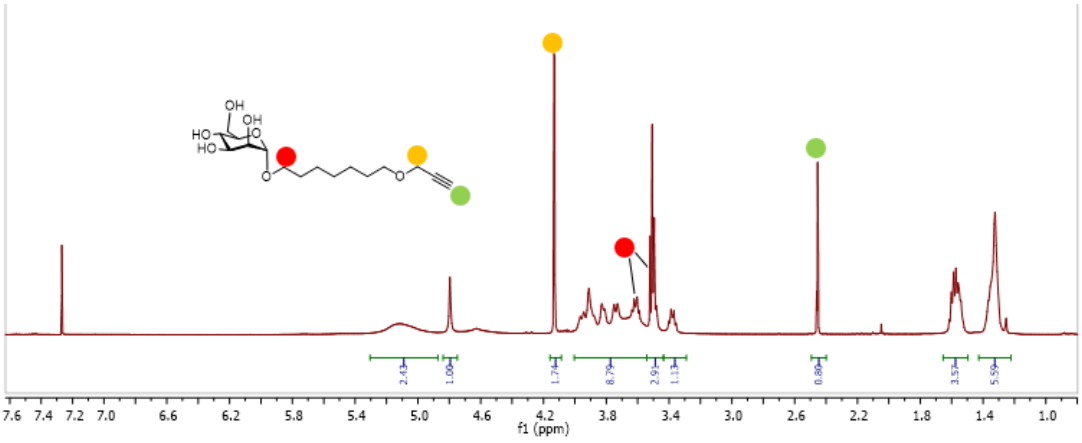

Figure 5.15: ^{1}H NMR spectrum of compound **5.33**.

5.3.1.4 Synthesis of novel mannoside compound 5.39

An additional mannoside compound **5.39** was prepared according to Scheme **5.6**, using the same chemistry as used in section 3.3.1 (Chapter 3). Initially CuAAC chemistry afforded **5.36**, which was *N*-deprotected to give **5.37**. Reaction with acryloyl chloride (as discussed in Chapter 3) afforded **5.38** which upon deprotection gave the desired compound **5.39**.

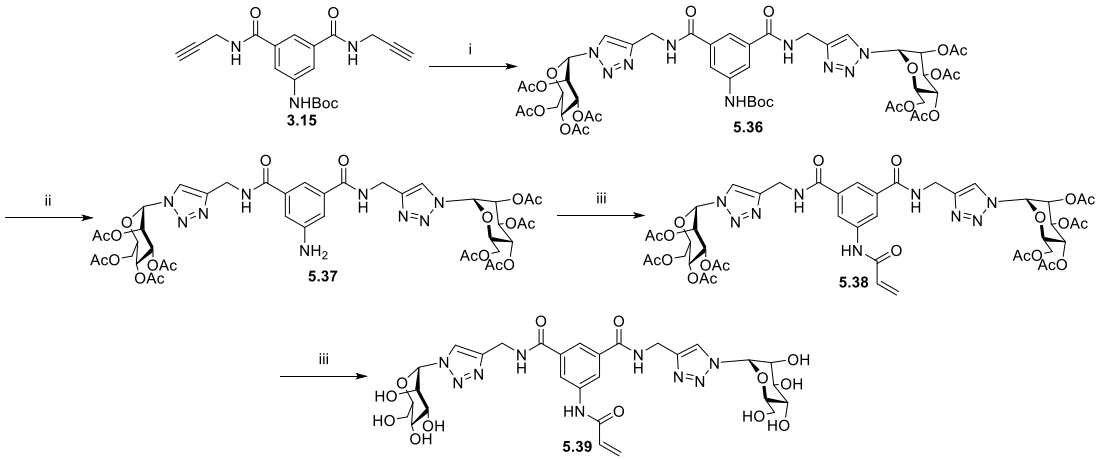

Scheme 5.6: Synthesis of mannoside **5.39**. *Reagents and conditions:* i) 2,3,4,6-tetra-*O*-acetyl-1-α-azido-mannoside **2.41**, $CuSO_4.5H_2O$/Na Asc, ACN/H_2O, 100 °C in MW, 30 mins, 52%; ii) DCM, TFA, 5 h, RT, 95%; iii) Acryloyl chloride, NEt_3, DCM, 16 h, RT, 55%.; iv) MeOH, H_2O, NEt_3, 45 °C, 6 h, 94%.

5.4 Biological Evaluation

5.4.1 Biofilm Inhibition assays of HMan 5.15

The biological evaluation of the target compounds was carried out by Marwa Alawi, a PhD student of our collaborator Prof Fiona Walsh (Maynooth University). As

mentioned earlier, a correlation between HGT and biofilm formation has been suggested, due to the close proximity of bacterial cells in biofilms potentially facilitating HGT [180]. Previous reports had shown that HMan **5.15** was able to reduce biofilm formation of UTI89 *E. coli* (a pathogenic strain isolated from a patient suffering from a urinary tract infection) at concentrations in the μM range [135]. Hence, the ability of the compounds to inhibit biofilm formation in another strain of *E. coli* (NCTC13400 (pEK499)) was assessed first. This strain, which would be used as a donor in the conjugation inhibition experiments, contains the plasmid pEK499, which confers resistance to eight antibiotics, such as Tetracycline [203].

HMan **5.15** was found to decrease biofilm formation (**Fig. 5.16**), with close to a 50% inhibition at a concentration of 16 μg/mL, while at a concentration of 32 μg/mL an approximate 75% inhibition was achieved. These results were particularly encouraging as the *E. coli* strain used (NCTC13400 (pEK499)) is a strong biofilm former. Galactoside derivative HGal **5.23**, on the other hand, did not show inhibition of biofilm formation.

In order to compare the effects of HMan **5.15**, with other *E. coli* strains, with different abilities to form biofilm structures, *E. coli* strain CV601 (a weak biofilm former) was chosen. In addition, this strain would be used as the recipient in the conjugation inhibition experiments. It was treated with **5.15** in the same biofilm inhibition assay. HMan **5.15** reduced the biofilm mass formed and produced the desired effect at a much lower concentration of 1 μg/mL (**Fig. 5.16**). The same effect was first seen with the NCTC13400 (pEK499) strain at a concentration of 16 μg/mL. This suggests that less virulent *E. coli* strains are more susceptible to the desired effects of HMan **5.15**.

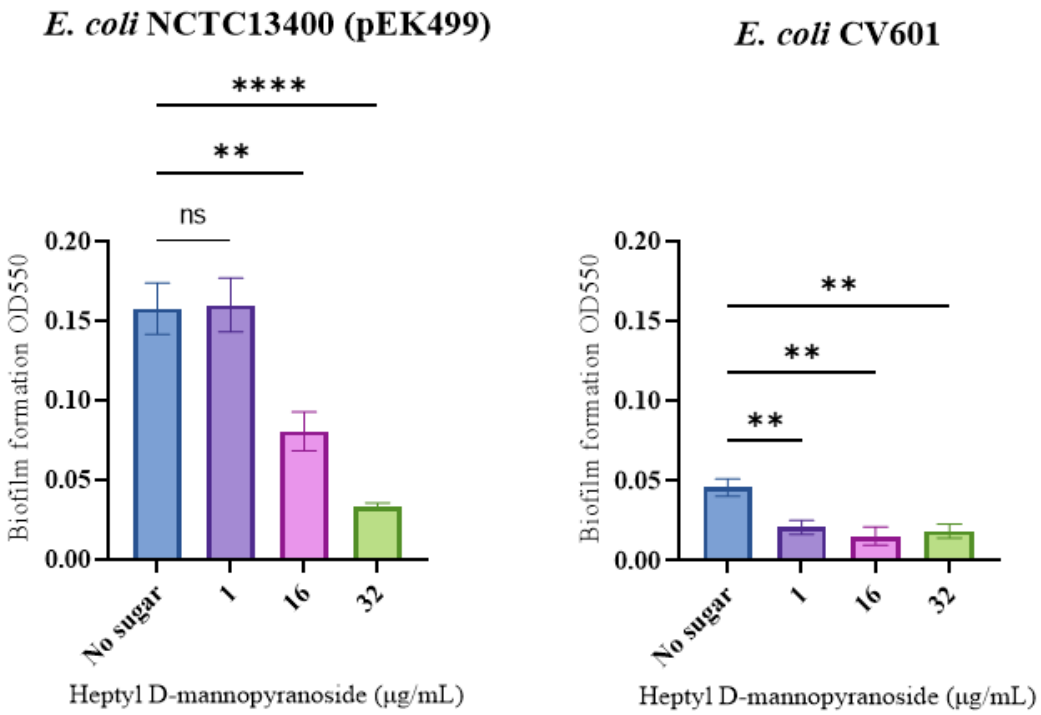

Figure 5.16: Biofilm inbibition assays using **5.15**. *Left: E. coli* NCTC13400 (pEK499); *Right:* and *E. coli* CV601.

5.4.2 Conjugation Inhibition assays of HMan 5.15

Next, the conjugation inhibition ability of HMan **5.15** was assessed. Firstly, the HGT reduction was assessed in liquid mating experiments, where the donor strain NCTC13400 (pEK499 donor) and recipient strain CV601 were incubated in liquid media. When incubation was stopped, the bacteria were spotted in plates containing specific antibiotics (e.g. Tetracycline), that would allow selection of donor and transconjugants. If conjugation failed, the plasmid transferring resistance would not confer protection against the given antibiotic and the recipient bacteria would die. After quantification to measure the colony forming units/mL (cfu/mL) of the donors and transconjugants, the conjugation frequency was calculated as the number of transconjugants formed per donor. It was found that HMan **5.15** caused up to 52% HGT reduction at 32 mg/mL (**Fig. 5.17**).

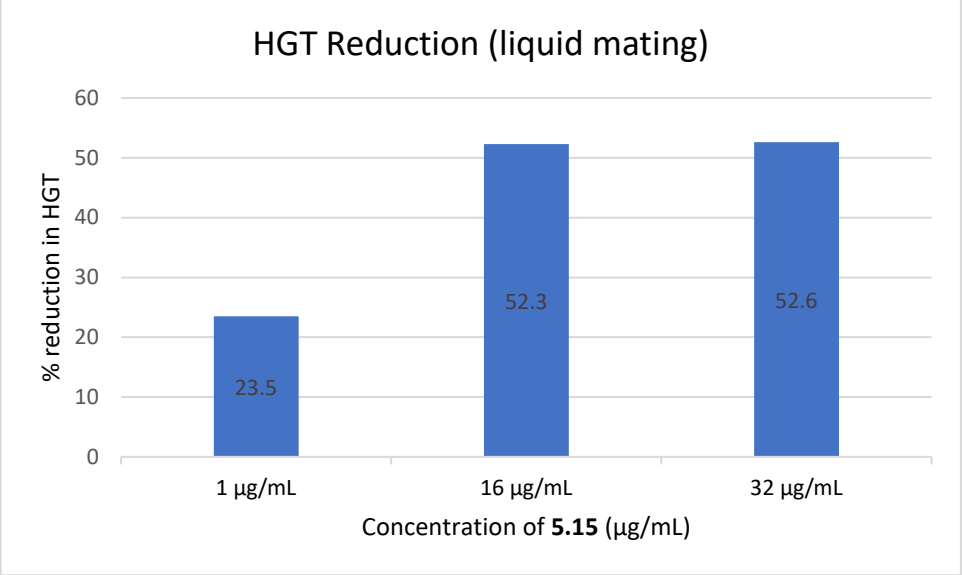

Figure 5.17: % reduction in HGT (conjugation) caused by HMan **5.15** in liquid mating assays between *E. coli* NCTC13400 (pEK499) (donor) and *E. coli* CV601 (recipient).

Then, filter mating experiments were performed where the conjugation of NCTC13400 (pEK499 donor) and recipients took place on the surface of filters (membranes). It has been reported that the conjugation frequency is slightly higher in filter matings than in liquid matings [204]. HMan **5.15** was found to produce a concentration-dependent decrease in conjugation (**Fig. 5.18**). The maximum inhibition level reached, 48%, was observed at a concentration of 32 µg/mL, with significant inhibition of 27% and 34% observed at 1 and 16 µg/mL respectively. All values are relative to the control, which was the untreated *E. coli* strains. These very promising results are currently being investigated in the laboratory of Prof Walsh with further experiments involving different knockout *E. coli* strains.

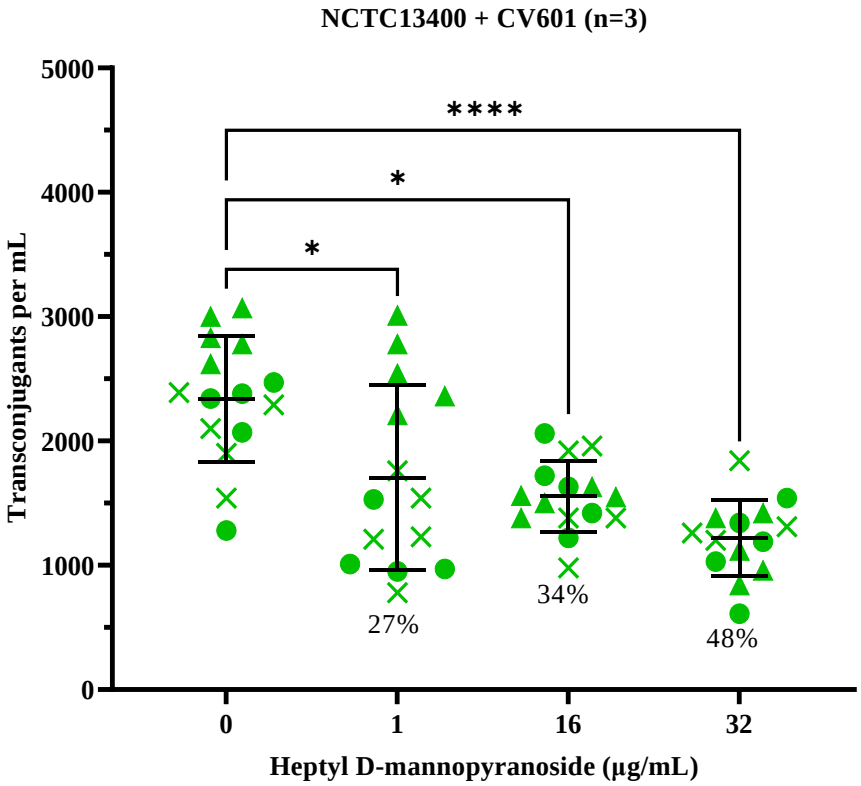

Figure 5.18: % reduction in HGT (conjugation) caused by HMan **5.15** in filter mating assays between *E. coli* NCTC13400 (pEK499) (donor) and *E. coli* CV601 (recipient).

5.4.3 Conjugation Inhibition assays of glycoconjugates 5.18, 5.19 and 5.39

Novel triazolyl glycoconjugates **5.18** and **5.19** and divalent mannoside **5.39** were then evaluated. First, the relationship between bacterial growth (toxicity) and biofilm formation effected by the compounds was determined (**Fig. 5.19**). It was found that none of the triazolyl compounds **5.18** and **5.19** were toxic to either donor or recipient *E. coli* strains investigated at concentrations below 286 mg/mL. While galactoside compound **5.18** had generally little effect on biofilm formation, the mannoside derivative **5.19** had a significant reduction of biofilm formation in donor strain NCTC13400 at concentrations higher than 16 mg/mL. Small increase in biofilm formation in some cases may be due to a given glycoconjugate facilitating agglutination of bacterial cells. This may in turn lead to increased biofilm formation.

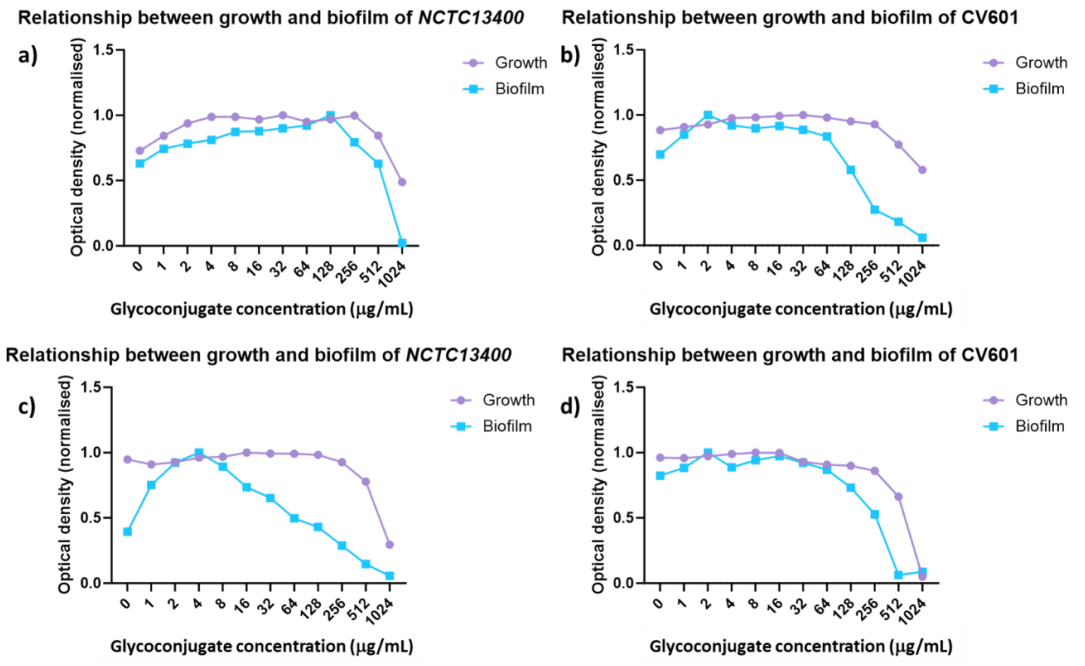

Figure 5.19: Relationship between bacterial growth (toxicity) and biofilm formation effected by: *Top:* galactoside **5.18** in *E. coli* NCTC13400 (pEK499) (**a**) and *E. coli* CV601 (**b**); *Bottom:* mannoside **5.19** in *E. coli* NCTC13400 (pEK499) (**c**), *E. coli* CV601 (**d**).

Interestingly, divalent mannoside **5.39**, which features a covalent cross-linking acryloyl group was found to affect biofilm formation at concentrations higher than 128 mg/mL for donor strain NCTC13400 (**Fig. 5.20**). This effect was more pronounced for the recipient strain CV601: although this strain is worse at forming biofilm, significant reduction was observed at concentrations as low as 2 mg/mL. Increases in biofilm formation, such as at a concentration of 512 µg/mL in the CV601 strain, may come as a result of glycoconjugate-facilitated agglutination of bacterial cells as discussed above.

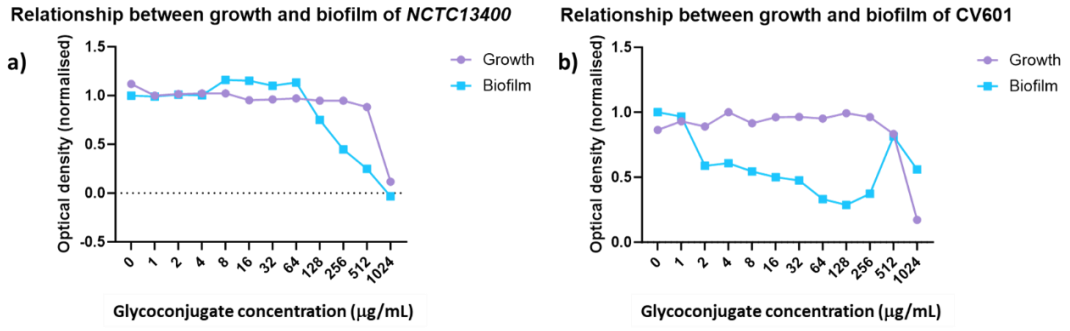

Figure 5.20: Relationship between bacterial growth (toxicity) and biofilm formation effected by divalent mannosidel **5.39** in *E. coli* NCTC13400 (pEK499) (**a**) and *E. coli* CV601 (**b**).

Finally, the ability of mannoside derivatives **5.19** and **5.39** to inhibit plasmid transfer by conjugation was assessed in liquid mating experiments (**Fig. 5.21**). These preliminary results show that while triazolyl mannoside **5.19** does not have any inhibitory effect, the divalent compound **5.39** appears to slightly reduce the conjugation between NCTC13400 (pEK499 donor) and CV601 (recipient) at concentrations as low as 16 µg/mL, relative to the control (untreated *E. coli* strains).

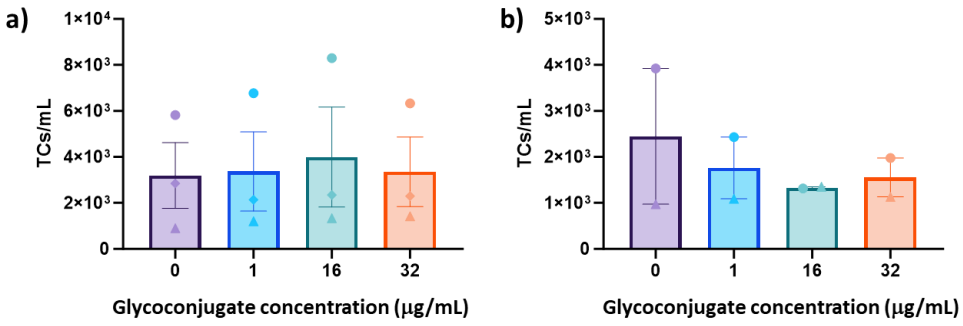

Figure 5.21: % reduction in HGT (conjugation) caused by triazolyl mannoside **5.19** (**a**) and divalent mannoside **5.39** (**b**) in liquid mating assays between *E. coli* NCTC13400 (pEK499) (donor) and *E. coli* CV601 (recipient).

5.5 Conclusion

In conclusion, a small library of *N*- and *O*-glycoconjugates have been prepared and assessed as novel conjugation inhibitors in different *E. coli* strains. As HMan **5.15** had already been reported to bind FimH with high affinity (K_d = 5 nM), this compound was the starting point to test the role of carbohydrate-mediated interactions in bacterial conjugation. With the known specificity of the *E. coli* lectin FimH for mannose derivatives in mind, mannosides **5.15** and **5.19** were prepared as prospective positive controls. We hoped these compounds could inhibit AMR plasmid transfer by conjugation between *E. coli* strains. Additionally, the galactoside analogues of these compounds, **5.23** and **5.18**, were also prepared as prospective negative controls. As FimH does not have binding specificity for galactose, we believed that these should lack the conjugation inhibition abilities we hoped to observe from mannosides **5.15** and **5.19**. The corresponding *N*-glycoside analogue **5.19** was prepared to assess if this derivative had firstly an improved binding affinity

for FimH and secondly, as a result of this improved affinity, an increased conjugation inhibition [198].

The results obtained so far for these compounds regarding inhibition of biofilm formation and conjugation between *E. coli* donor and recipient strains are very promising. Compound **5.15** (HMan) showed effective anti-biofilm and anti-conjugation activities in these assays, at concentrations as low as 16 μg/mL. This represents the first example of a glycoconjugate conjugation inhibitor, opening the door to exploring the role of fimbrial proteins in conjugative transfer.

Chapter 6

Conclusion

6.1 Conclusion

The aim of the research described in this thesis was to develop novel compounds that would be used to combat both bacterial and fungal infection. In particular, *C. albicans* is a pathogen that received much attention to this end. Building on previous work in our research group, novel glycoconjugate derivatives were prepared with the aim of disrupting adherence, conjugation, and biofilm formation processes in a number of pathogenic species.

Chapter 2 describes the design, synthesis and structural evaluation of a series of symmetric and asymmetric *cis*-norbornene derivatives. Following initial observation of an intramolecular cyclisation reaction in these compounds, a study was conducted to determine the structural requirements and reaction conditions necessary for this cyclisation reaction to occur. It was found that the cyclization reaction was favoured in the presence of triazolyl groups and in aqueous acidic conditions. After this study was complete, the synthesis of novel asymmetric *cis*-norbornene compounds, bearing both a carbohydrate and an anti-biofilm agent (i.e tyrosol or farnesol) was probed. It was envisaged that following intramolecular cyclisation in these compounds, the anti-biofilm agents would be released selectively in acidic microenvironments, in which target pathogens are known to reside. Two novel asymmetric *cis*-norbornene compounds were synthesised: tyrosol derivative **2.81** and farnesol derivative **2.80**, obtained partially pure. The cyclisation/release profiles of these compounds were studied by HPLC analysis and revealed the expected cyclisation and release of the anti-biofilm in the case of compound **2.81**, while compound **2.80** did not appear to do the same under the conditions assessed.

In Chapter 3, several analogues of our lead compound **1.39** were prepared, some of which incorporate two reactive crosslinking groups (acryloyl and vinyl sulfonyl) in order to enhance the anti-adhesion activity of these compounds. Following initial toxicity testing against a range of *Candida spp.*, toxicity was observed in a number of compounds, including those containing the reactive crosslinking moieties. Model crosslinking reactions were conducted at pH 7.4 and 10.2 with compounds **3.25** and **3.27**, using three *N*-protected amino acids (*N*-α-acetyl-L-lysine, *N*-α-acetyl-L-histidine and *N*-α-acetyl-L-cysteine), which were chosen due to their known nucleophilic

reactivity in receptors and enzymes. In the case of the reaction of both **3.25** and **3.27** with *N*-α-acetyl-L-lysine at pH 10.2, crosslinked adducts were detected via HRMS analysis for both compounds. Therefore, we propose that the observed toxicity seen in these compounds, may be in part due to the crosslinking of these compounds with fungal proteins.

To advance the SAR study previously conducted in our group on lead compound **1.39**, Chapter 4 details further studies of the structural requirements to optimize anti-adhesion activity. Three features were selected to determine their importance for the observed anti-adhesion activity: (i) the substituents at the *meta* position of the aromatic core in **1.39** were modified; (ii) the D-galactose moieties in **1.39** were also replaced by a number of sp^2-iminosugars (prepared in collaboration with the group of Prof Ortiz-Mellet, University of Seville) and (iii) lastly, the 1,2,3-triazolyl moiety was altered for other novel heterocycles. Promising results were obtained in this work, namely a methoxy derivative of **1.39** performed comparably to the lead compound. Meanwhile, one of the sp^2-iminosugar glycoconjugates (a glucosyl derivative **4.44**) performed well in displacement assays. These derivatives still offer good insight into the structural prerequisites for optimal anti-adhesion activity. Finally, the synthesis of novel 1,2,4-oxadiazole, isoxazole and isoxazoline derivatives was attempted in collaboration with the group of Prof Toth in University of Debrecen. Biological evaluation of these compounds is yet to be conducted. Importantly, a derivative of **1.39** has been prepared, successfully immobilized on a resin and used to capture a protein which is hoped may be the target protein of our lead compound. Mass spectrometry analysis is currently being conducted to identify this protein.

Chapter 5 deals with the synthesis of a small library of *N*- and *O*-glycoconjugates which were assessed as novel conjugation inhibitors in different *E. coli* strains. *E. coli* adhesin FimH mediates its binding to mannosides at the surface of epithelial host cells, causing infections. Many high affinity mannosides targeting FimH have been reported as anti-adhesion compounds, such as heptyl mannoside **5.15**. We hypothesized that these compounds could also prevent bacteria-bacteria interactions and inhibit conjugation between *E. coli* cells. With the mannoside specificity of FimH in mind, mannosides **5.15** and **5.19** were prepared as prospective

positive controls, while the galactoside analogues of these compounds, **5.23** and **5.18**, were also prepared as prospective negative controls (as FimH does not have binding specificity for galactose). Interestingly, initial results indicated that **5.15** was capable of reducing biofilm formation, with a 50% inhibition at 16 μg/mL and 75% inhibition at 32 μg/mL, in an *E. coli* strain which had been characterised as a strong biofilm former. **5.15** was found to reduce the conjugation frequency in two *E. coli* strains, with the maximum inhibition reached being 48% at a concentration of 32 μg/mL. Finally, a fluorescently labelled derivative of **5.15**, **5.35**, was prepared and is currently being used to study the mode of action of **5.15** to help shed light on how this compound achieves its anti-biofilm and anti-conjugation activities.

Finally, looking forward, it will be important to optimise the synthesis and also cyclisation/release profiles of compounds **2.80** and **2.81** to achieve selective release of the discussed anti-biofilm agents to treat fungal infections. Secondly, should our target protein/lectin be identified through mass spectrometry analysis and subsequent structural data obtained for it, the design of highly effective ligands for this protein should proceed. This would achieve highly effective anti-adhesion in *C. albicans* and potentially a breakthrough in the treating its infections through the anti-adhesion approach. Lastly, upon confirmation that our mannoside-based compounds are targeting FimH on *E. coli* cell surfaces, further derivatives of these compounds should be targeted. Ideally these derivatives will improve on the promising anti-biofilm and anti-conjugation activities already observed for these compounds.

Chapter 7

Experimental

7.1 General Procedures and instrumentation

All chemicals purchased were reagent grade and used without further purification, unless stated otherwise. DCM was distilled over CaH_2. Anhydrous DMF was purchased from Sigma Aldrich. Molecular sieves used for glycosylation and coupling were 3 Å and were dried in the oven at 100°C at ambient pressure prior to use. Reactions were monitored using thin layer chromatography (TLC) on Merck Silica Gel F_{254} plates. Detection was effected by visualisation in UV light and/or charring in a mixture of 5% sulphuric acid-EtOH, in a potassium permanganate solution (3 g $KMnO_4$, 20 g K_2CO_3, 5 mL 5% aqueous NaOH and 300 mL H_2O), or in a ninhydrin solution (0.3 g ninhydrin, 3 mL conc. H_2SO_4 and 100 mL n-butanol) or in a mostain solution (5g Ammonium molybdate, 0.1g $Ce(SO_4)_2$, 10% H_2SO_4 in H_2O). Evaporation under reduced pressure was always affected with the bath temperature kept at or below 60°C. NMR spectra were obtained a Bruker Ascend 500 spectrometer operated at 500 MHz for ^1H NMR analysis and 125 MHz for ^{13}C analysis at 293 K, unless otherwise stated. The residual solvent peak was used as an internal standard. Chemical shifts (δ) were reported in ppm. Proton and carbon signals were assigned with the aid of 2D NMR experiments (COSY, HSQC, HMBC, ^{15}N HSQC, ^{15}N HMBC) and DEPT experiments for novel compounds. The following abbreviations were used to explain the observed multiplicities; s (singlet), bs (broad singlet), d (doublet), appd (apparent doublet), t (triplet), appt (apparent triplet), q (quartet), m (multiplet), bs (broad singlet). Flash chromatography was performed with Merck Silica Gel 60. Automated Flash column chromatography was performed using an Interchim PuriFlash 420. Microwave reactions were carried out using a CEM Discover Microwave Synthesizer. Optical rotations were obtained using AA-100 polarimeter. High performance liquid chromatography (HPLC, Waters Alliance 2695) was performed in final compounds and indicated purity of ca. 95%. High resolution mass spectrometry (HRMS) was performed on an Agilent-LC 1200 Series coupled to a 6210 Agilent Time-Of-Flight (TOF) or mass spectrometer equipped with an electrospray source in both positive and negative (ESI +/-) modes. Infrared spectra were obtained as a film on NaCl plates, as KBr disks or via ATR as a solid on a zinc selenide crystal in the region 4000-400 cm^{-1} on a Perkin Elmer Spectrum 100 FT-IR spectrophotometer

or Thermo scientific Nicolet iS50 FT-IR. UV-Vis spectra were recorded in a Perkin Elmer Lambda 365 UV/Vis spectrometer. Compounds were lyophilized on a Labconco FreeZone 1 Freeze Dry system.

7.2 Experimental Procedures

7.2.1 Experimental procedures for Chapter 2

Bicylco[2.2.1]cis-hept-5-ene-2,3-*endo*-2,3-dicarboxamide, *N*-(β-D-galactopyranosyl-1,2,3-triazol-4-ylmethylamino) 2.35

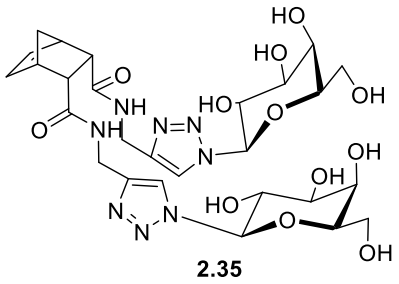

2.35

2.43 (168 mg, 0.16 mmol) was dissolved in a MeOH/H_2O mixture (2.5 mL/1.25 mL) under reflux conditions at 45-50 ^oC and NEt_3 (65 µL) was added. The reaction mixture was stirred for approx. 5 h until the reaction was deemed complete via TLC analysis. The solvent was then removed *in vacuo* and the resulting residue was dried using a Schlenk line to yield the pure product **2.35** as a white fluffy solid (105 mg, 95%).

^1H NMR (500 MHz, D_2O) δ 8.36 (s, 1H, triaz-H), 8.18 (s, 1H, triaz-H), 5.93 – 5.82 (m, 2H, H_e and H_f), 5.75 (d, *J* = 9.2 Hz, 1H, H-1' or H-1'), 5.67 (d, *J* = 9.3 Hz, 1H, H-1 or H-1'), 4.69 (s, 2H, CH_2-triaz), 4.35 (d, *J* = 8.9 Hz, 2H, CH_2-triaz), 4.23 (dt, *J* = 25.4, 9.5 Hz, 2H, H-2 & H-2'), 4.11 (dd, *J* = 7.9, 3.3 Hz, 2H, H-4 & H-4'), 4.02 (dt, *J* = 15.3, 6.2 Hz, 2H, H-5 5 H-5'), 3.89 (ddd, *J* = 17.1, 9.8, 3.2 Hz, 2H, H-3- & H-3'), 3.83 – 3.76 (m, 4H, H-6 & H-6' (x2)), 3.50 (d, *J* = 2.9 Hz, 2H, H_b & H_c), 3.35 (s, 2H, H_a & H_d), 1.68 (d, *J* = 8.9 Hz, 1H, H_g or $H_{g'}$), 1.60 (d, *J* = 8.7 Hz, 1H, H_g or $H_{g'}$).

The NMR data is in agreement with the data recorded in the literature [114].

Bicyclo[2.2.1]cis-hept-5-ene-2,3-di-*exo*-carboximide, *N*-(β-D-galactopyranosyl-1,2,3-triazol-4-ylmethylamino) 2.37

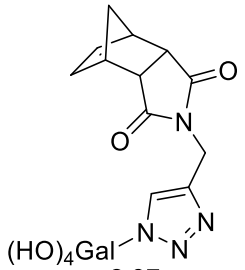

2.37

2.57 (383 mg, 0.66 mmol) was dissolved in MeOH/H_2O (6 mL/3 mL) in a round-bottom flask, a waterless condenser was attached, and stirred in an oil bath at 50-55 ^oC for 5 mins. NEt_3 (0.27 mL) was then added and the reaction mixture was stirred at 50-55 ^oC until the reaction was deemed to be complete by TLC analysis (4.5 h). The solvent was then removed *in vacuo*, the resulting residue was then dissolved in deionised water, Amberlite H^+ was then added and the crude product was stirred for 40 mins. The Amberlite H^+ was then filtered off and the solvent was then removed *in vacuo* to yield the product **2.37** as a yellow/orange solid (178.8 mg, 66%).

^1H NMR (500 MHz, D_2O) δ 8.15 (s, 1H, triaz-H), 5.85 (dt, *J* = 8.0, 4.4 Hz, 2H, H_e &H_f), 5.64 (d, *J* = 9.2 Hz, 1H, H-1), 4.65 (s, 2H, CH_2), 4.17 (t, *J* = 9.5 Hz, 1H, H-2), 4.07 (d, *J* = 3.2 Hz, 1H, H-4), 3.97 (t, *J* = 6.0 Hz, 1H, H-5), 3.84 (dd, *J* = 9.8, 3.3 Hz, 1H, H-3), 3.76 (d, *J* = 6.0 Hz, 2H, H-6 & H-7), 3.46 (s, 2H, H_b & H_c), 3.31 (s, 2H, H_a & H_d), 1.64 (d, *J* = 8.8 Hz, 1H, $H_{g/g'}$), 1.56 (d, *J* = 8.7 Hz, 1H, $H_{g/g'}$). ^{13}C NMR (125 MHz, D_2O) δ 180.7 (CO), 142.2 (C-triaz), 134.2 ($C_{e/f}$), 134.2 ($C_{e/f}$), 123.9 (*C*H-triaz), 87.9 (C-1), 78.2 (C-5), 73.0 (C-3), 69.6 (C-2), 68.5 (C-4), 60.8 (C-6/7), 51.9 ($C_{g/g'}$), 45.6 ($C_{b/c}$), 44.8 ($C_{a/d}$), 32.7 (CH_2). IR (ATR): 3336, 1686, 1428, 1400, 1335, 1229, 1168, 1090, 1050, 1016 cm^{-1}. HRMS (ESI+): m/z calculated for $C_{18}H_{22}N_4O_7$+ Na^+ [M+Na^+]: 429.1386, found 429.1382.

2,3,4,6-tetra-*O*-acetyl-1-β-azido-D-galactopyranoside 2.40

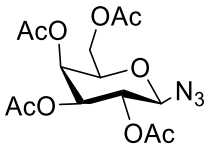

2.40

$TMSN_3$ (1 mL, 7.62 mmol, 1.5 equiv) was added to a solution of β-D-galactose pentaacetate **2.82** (1.99 g, 5.11 mmol) in anhydrous DCM (18 mL). $SnCl_4$ (0.3 mL, 2.56 mmol, 0.5 equiv) was added to this solution and the reaction mixture was stirred at RT for 18 h. Sat. $NaHCO_3$ solution (30 mL) was added and the suspension was extracted with DCM (2 x 30 mL). The combined organic layers were dried over MgSO4, filtered and concentrated in vacuo to afford **2.40** as a white solid which was recrystallized from EtOH giving the pure product **2.40** as white crystals (1.81 g, 95%). ^{1}H NMR (500 MHz, $CDCl_3$) δ 5.34 (d, *J* = 3.3 Hz, 1H, H-4), 5.08 (dd, *J* = 19.3, 9.2 Hz, 1H, H-2), 4.97 (ddd, *J* = 10.4, 3.3, 0.7 Hz, 1H, H-3), 4.56 (d, *J* = 8.7 Hz, 1H, H-1), 4.16 – 4.02 (m, 2H, H-6 & H-6'), 4.02 – 3.92 (m, 1H, H-5), 2.10 (dd, *J* = 7.9, 0.9 Hz, 3H, CH_3 of OAc), 2.03 – 1.99 (m, 3H, CH_3 of OAc), 1.98 (d, *J* = 0.8 Hz, 3H, CH_3 of OAc), 1.91 (dd, *J* = 8.8, 1.7 Hz, 3H, CH_3 of OAc).

The NMR data is in agreement with the data recorded in the literature [117].

2,3,4,6-tetra-*O*-acetyl-1-α-azido-D-mannopyranoside 2.41

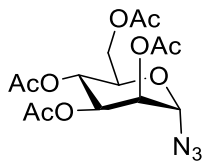

2.41

$TMSN_3$ (3.18 mL, 24.3 mmol, 1.5 equiv) was added to a solution of α-D-mannose pentaacetate **2.83** (6.33 g, 16.2 mmol) in anhydrous DCM (20 mL). $SnCl_4$ (0.94 mL, 8.1 mmol, 0.5 equiv) was added to this solution and the reaction mixture was stirred at RT for 18 h. Sat. $NaHCO_3$ solution (30 mL) was added and the suspension was extracted with DCM (2 x 30 mL). The combined organic layers were dried over MgSO4, filtered and concentrated in vacuo to afford **2.41** as a viscous orange-yellow oil giving the pure product **2.41**. (4.27 g, 71%). ^{1}H NMR (500 MHz, $CDCl_3$) δ 5.38 (m,

1H, H-1), 5.31 – 5.27 (m, 1H, H-4), 5.27 – 5.23 (m, 1H, H-3), 5.14 (dd, *J* = 5.9, 3.9 Hz, 1H, H-2), 4.33 – 4.26 (m, 1H, H-6 or H-6'), 4.15 (ddd, *J* = 10.7, 8.4, 2.3 Hz, 2H, H-6 or H-6' & H-5), 2.16 (s, 3H, CH_3 of OAc), 2.11 (s, 3H, CH_3 of OAc), 2.05 (s, 3H, CH_3 of OAc), 1.99 (s, 3H, CH_3 of OAc).

The NMR data is in agreement with the data recorded in the literature [205].

Bicyclo[2.2.1]cis-hept-5-ene-2,3-*endo*-2,3-dicarboxamide, *N*-(prop-2-yn-1-yl) 2.42

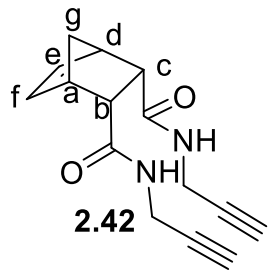

2.42

Cis-5-Norbornene-endo-2,3-dicarboxylic acid (300 mg, 1.65 mmol) and TBTU (1.32 g, 4.12 mmol) were dissolved in anhydrous DMF (15 mL) under N_2. NEt_3 (0.57 mL, 4.12 mmol) and propargylamine (0.22 mL, 3.46 mmol) were added after approx. 10 mins. The reaction was allowed to stir for 48 h at RT. The DMF was removed *in vacuo*, the resulting residue was dissolved in DCM (20 mL) and washed with brine (3 x 20 mL) and sat. NaHCO3 (2 x 20 mL), dried of MgSO4, filtered and concentrated *in vacuo* to yield the crude product. This was then recrystallised using hot DCM to give the pure product **2.42** as a white crystalline solid (334 mg, 79%). Rf=0.08 (1:1 EtOAc:Pet. Ether).

^{1}H NMR (500 MHz, DMSO) δ 7.70 (t, *J* = 5.3 Hz, 2H, N*H*), 6.09 (t, *J* = 1.8 Hz, 2H, H_e and H_f), 3.82 – 3.64 (m, 4H, CH_2CCH), 3.12 – 3.09 (m, 2H, H_b and H_c), 3.04 (t, *J* = 2.5 Hz, 2H, CH_2CC*H*), 2.96 – 2.94 (m, 2H, H_a and H_d), 2.08 (s, 1H), 1.25 – 1.19 (m, 1H). ^{13}C NMR (125 MHz, DMSO) δ 171.5 (CO), 134.9 (C_e and C_f), 81.9 (CH_2*C*CH), 73.2 (CH_2C*C*H), 50.1 (C_b and C_c), 48.9 (C_g), 46.7 (C_a and C_d), 28.4 (*C*H_2CCH). IR (ATR): 3286, 1654, 1525, 1415, 1333, 1278, 1256, 1226, 1098, 1029, 908, 846 cm^{-1}.

The NMR data is in agreement with the data recorded in the literature [114].

Bicylco[2.2.1]cis-hept-5-ene-2,3-*endo*-2,3-dicarboxamide, *N*-(2,3,4,6-tetra-*O*-acetyl-β-D-galactopyranosyl-1,2,3-triazol-4-ylmethylamino) 2.43

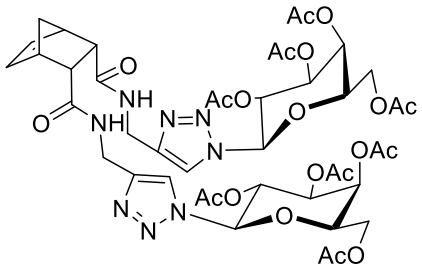

2.43

Copper sulphate pentahydrate (60 mg) and sodium ascorbate (120 mg) were added to a solution of **2.40** (337 mg, 0.9 mmol) and **2.42** (90 mg, 0.35 mmol) in CH_3CN/H_2O (4 mL/ 1mL). The reaction was allowed to stir in the MW at 100°C until deemed complete by TLC analysis (10 mins). The solvent was removed *in vacuo*. The residue was dissolved in DCM (30 mL), washed with water (20 mL x 3), and dried ($MgSO_4$). The mixture was filtered and the solvent was removed *in vacuo* to yield the crude product, which was purified by silica gel column chromatography (DCM:MeOH 98:2-90:10) to give the pure product **2.43** as an off-white solid (200 mg, 57%). R*f*=0.41 (DCM:MeOH 9:1). ^{1}H NMR (500 MHz, $CDCl_3$) δ 7.83 (s, 1H, triaz-H), 7.79 (s, 1H, triaz-H'), 6.97 (t, *J* = 5.5 Hz, 1H, N*H*CH2-triaz), 6.83 (t, *J* = 5.6 Hz, 1H, N*H*CH2-triaz), 6.27 (ddd, *J* = 35.6, 5.3, 3.0 Hz, 2H, H_e and H_f), 5.83 – 5.77 (m, 2H, H-1 and H-1'), 5.52 – 5.46 (m, 4H, H-2, H-2', H-4 and H-4'), 5.24 – 5.18 (m, 2H, H-3 and H-3'), 4.42 – 4.01 (m, 10H, C*H2*-triaz x2, H-5, H-5', H-6, H-6', H-6'' and H-6'''), 3.25 – 3.17 (m, 2H, H_b and H_c), 3.06 (app s, 2H, H_a and H_d), 2.16 (s, 6H, CH_3 of OAc), 2.01 – 1.88 (m, 12H, CH_3 of OAc), 1.80 (s, 6H, CH_3 of OAc), 1.43 – 1.23 (m, 2H, H_g and $H_{g'}$). ^{13}C NMR (125 MHz, $CDCl_3$) δ 171.7 (CO), 171.7 (CO), 169.3 (CO of OAc), 169.3 (CO of OAc), 169.1 (CO of OAc), 168.9 (CO of OAc), 168.8 (CO of OAc), 167.9 (CO of OAc), 167.9 (CO of OAc), 144.6 (*C*-triaz), 144.5 (*C'*-triaz), 134.6 (Ce/f), 134.2 ($C_{e/f}$), 120.4 (*C*H-triaz), 120.2 (*C*H-triaz), 85.1 (C-1), 72.9 (C-5), 69.9 (C-3), 67.0 (C-2/4), 65.9 (C-2/4), 60.2 (C-6), 60.1 (C-6'), 50.5 ($C_{b/c}$), 50.3 ($C_{b/c}$), 48.7 (C_g), 46.1 (C_a and C_d), 33.7 (*C*H2-triaz), 19.7 (CH3 of OAc), 19.6 (CH3 of OAc), 19.6 (CH3 of OAc), 19.5 (CH3 of OAc), 19.2 (CH3 of OAc). IR

(ATR): 3392, 2967, 1746, 1663, 1527, 1368, 1211, 1045, 922 cm^{-1}. The NMR data is in agreement with the data recorded in the literature [114].

Bicylco[2.2.1]cis-hept-5-ene-2-*endo*,3-exo-2,3-dicarboxamide, *N*-(2,3,4,6-tetra-*O*-acetyl-α-D-mannopyranosyl-1,2,3-triazol-4-ylmethylamino) 2.44

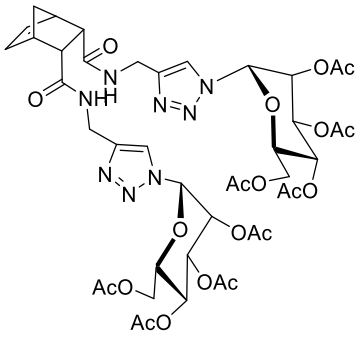

2.44

Copper sulphate pentahydrate (90 mg) and sodium ascorbate (110 mg) were added to a solution of **2.41** (209 mg, 0.56 mmol) and **2.42** (60 mg, 0.23 mmol) in CH_3CN/H_2O (4 mL/1 mL). The reaction was allowed to stir in the MW at 100 ^oC until deemed complete by TLC analysis (30 mins). The solvent was removed *in vacuo*. The residue was dissolved in DCM (30 mL), washed with water (20 mL x 3), and dried ($MgSO_4$). The mixture was filtered and the solvent was removed *in vacuo* to yield the crude product, which was purified by silica gel column chromatography (DCM:MeOH 98:2-90:10) to give the pure product **2.44** as an off-white solid (215 mg, 92%). R*f*=0.41 (DCM:MeOH 9:1).

^1H NMR (500 MHz, $CDCl_3$) δ 7.81 (s, 1H, triaz-H), 7.78 (s, 1H, triaz-H'), 6.48 (dd, J = 13.1, 5.8 Hz, 2H, N*H*CH_2-triaz), 6.35 (t, J = 3.3 Hz, 2H, H_e and H_f), 6.01 (d, J = 2.2 Hz, 1H, H-1), 5.97 (d, J = 3.0 Hz, 1H, H-1'), 5.96 – 5.92 (m, 2H, H-2 and H-2'), 5.88 (ddd, J = 16.2, 9.3, 3.7 Hz, 2H, H-3 and H-3'), 5.39 (td, J = 9.4, 2.1 Hz, 2H, H-4 and H-4'), 4.36 (ddt, J = 18.7, 14.0, 5.5 Hz, 6H, C*H*$_2$-triaz x2, H-6 or H-7 and H-6' or H-7'), 4.05 (ddd, J = 12.6, 5.6, 2.6 Hz, 2H, H-6 or H-7 and H-6' or H-7'), 3.96 – 3.87 (m, 2H, H-5), 3.25 (s, 2H, H_b and H_c), 3.15 (s, 2H, H_a and H_d), 2.18 (s, 6H, CH_3 of OAc), 2.09 (s, 6H, CH_3 of OAc), 2.04 (s, 6H, CH_3 of OAc), 2.02 (s, 6H, CH_3 of OAc), 1.50 (d, J = 8.6 Hz, 1H, H_g), 1.35 (d, J = 8.6 Hz, 1H, $H_{g'}$).

^{13}C NMR (125 MHz, $CDCl_3$) δ 172.6 (CO), 170.6 (CO & CO of OAc), 169.7 (CO of OAc), 169.6 (CO of OAc), 145.4 (C-triaz), 135.2 ($C_{e/f}$), 123.3 (*C*H-triaz), 123.1 (*C*H-triaz), 83.8 (C-1), 71.8 (C-5), 68.9 (C-3), 68.2 (C-2), 65.7 (C-4), 61.6 (C-6/7), 51.1 ($C_{b/c}$), 49.6 (C_g),

46.9 ($C_{a/d}$), 34.6 (*C*H_2-triaz), 20.7 (CH_3 of OAc), 20.7 (CH_3 of OAc), 20.6 (CH_3 of OAc), 20.5 (CH_3 of OAc). IR (ATR): 1741, 1368, 1212, 1123, 1039 cm^{-1}. HRMS (ESI+): m/z calculated for $C_{43}H_{54}N_8O_{20}$ + Na^+ [M+Na^+]: 1025.3352, found 1025.3342.

Bicylco[2.2.1]cis-hept-5-ene-2,3-*endo*-2,3-dicarboxamide, *N*-(1-benzyl-1H-1,2,3-triazol-4-ylmethylamino) 2.45

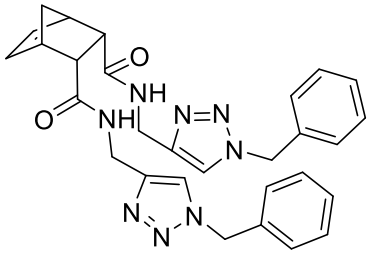

2.45

Copper sulphate pentahydrate (60 mg) and sodium ascorbate (120 mg) were added to a solution of **2.42** (224 mg, 0.87 mmol) and Benzyl azide (5.4 mL, 2.7 mmol (0.5 M solution in DCM)) in CH_3CN/H_2O (4 mL/1 mL). The reaction was allowed to stir at RT for four days. Following TLC analysis, the solvent was removed *in vacuo*. The residue was dissolved in DCM (30 mL), washed with water (20 mL x 3), and dried ($MgSO_4$). The mixture was filtered and the solvent was removed *in vacuo* to yield the pure product **2.45** as an off-white amorphous solid (198 mg, 43%). Rf=0.59 (90:10 DCM:MeOH).

^{1}H NMR (500 MHz, DMSO) δ 7.91 – 7.84 (m, 4H, triaz-H), 7.34 – 7.24 (m, 10H, Ar-H), 6.08 – 6.04 (m, 2H, H_e & H_f), 5.50 (s, 4H, C*H*$_2$Ph), 4.18 – 4.07 (m, 4H, C*H*$_2$-triaz), 3.10 (s, 2H, H_b & H_c), 2.93 (s, 2H, H_a & H_d), 1.26 – 1.18 (m, 2H, H_g).

^{13}C NMR (125 MHz, DMSO) δ 171.9 (CO), 146.1 (C-triaz), 136.4 ($C_{e/f}$), 134.7 ($C_{e/f}$), 129.1 (C_{Ar}), 128.5 (C_{Ar}), 128.4 (C_{Ar}), 123.4 (*C*H-triaz), 53.2 (*C*H_2Ph), 49.9 ($C_{b/c}$), 49.0 (C_g), 46.6 ($C_{a/d}$), 34.8 (*C*H_2-triaz). IR (ATR): 1671, 1551, 1213, 1049 cm^{-1}. HRMS (ESI+): m/z calculated for $C_{29}H_{30}N_8O_2$ + Na^+ [M+Na^+]: 545.2389, found 545.2387.

Bicylco[2.2.1]cis-hept-5-ene-2,3-*endo*-2,3-dicarboxamide, *N*-(α-D-mannopyranosyl-1,2,3-triazol-4-ylmethylamino) 2.46

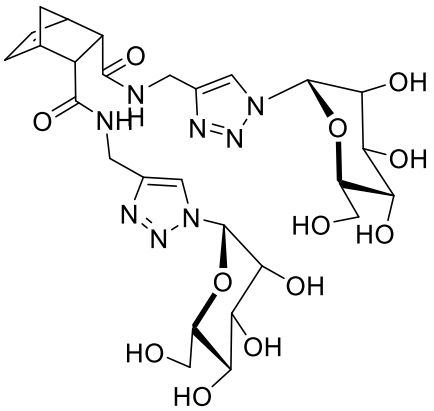

2.46

2.44 (76 mg, 0.07 mmol) was dissolved in a MeOH/H_2O mixture (1 ml/0.5 mL) under reflux conditions and NEt_3 (0.1 mL) was added, the reaction mixture was stirred until deemed complete via TLC analysis (5 h). The solvent was then removed *in vacuo* and the resulting residue was dried using a Schlenk line to yield the pure product as a white fluffy solid (46 mg, 94%). ^{1}H NMR (500 MHz, D_2O) δ 8.21 (s, 1H, triaz-H), 8.07 (s, 1H, triaz-H'), 6.15 (d, *J* = 2.2 Hz, 1H, H-1), 6.10 (d, *J* = 2.1 Hz, 1H, H-1), 5.87 (dt, *J* = 8.1, 5.6 Hz, 2H, H_e & H_f), 4.78 (s, 2H, H-2), 4.67 (s, 4H, C*H*$_2$-triaz), 4.15 (ddd, *J* = 12.6, 11.2, 6.7 Hz, 2H, H-3), 3.88 – 3.73 (m, 6H, H-4, H-6 & H-7), 3.53 – 3.44 (m, 2H, H_b & H_c), 3.40 – 3.29 (m, 3H, H_a & H_d & H-5), 3.24 (ddd, *J* = 9.4, 8.9, 6.6 Hz, 1H, H-5'), 1.68 (d, *J* = 8.9 Hz, 1H, H_g/$H_{g'}$), 1.60 (d, *J* = 8.9 Hz, 1H, H_g/$H_{g'}$).

^{13}C NMR (125 MHz, D_2O) δ 180.8 (CO), 180.7 (CO), 142.3 (qC_{triaz}), 134.2 (C_e/C_f), 134.1 (C_e/C_f), 124.4 (C-triaz), 86.6 (C-1), 76.2 (C-5/C-5'), 76.2 (C-5/C-5'), 70.5 (C-3/C-3'), 70.5 (C-3/C-3'), 68.2 (C-2/C-2'), 68.2 (C-2/C-2'), 66.6 (C-4/C-4'), 66.4 (C-4/C-4'), 60.4 (C-6/C-6'), 60.4 (C-6/C-6'), 51.9 (C_g), 45.7 (C_b/C_c), 44.8 (C_a/C_d), 32.7 (*C*H_2-triaz). IR(ATR): 3334, 1691, 1400, 1335, 1234, 1115, 1083, 1046 cm^{-1}. HRMS (ESI+): m/z calculated for $C_{27}H_{38}N_8O_{12}$ + H^+ [M+H^+]: 667.2687, found 667.2681.

Bicyclo[2.2.1]*cis*-hept-5-ene-2,3-*endo*-2,3-dicarboxamide, *N*-(picolylamine) 2.55

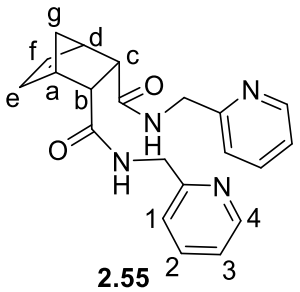

2.55

Cis-5-norbornene-endo-2,3-dicarboxylic acid (300 mg, 1.64 mmol) and EDCI (0.76 g, 4.94 mmol, 3 equiv.) were put under N_2 and dissolved in anhydrous DMF (10 mL) and stirred for 10 mins. 2-picolylamine (0.486 mL, 4.94 mmol) was added followed by NEt_3 (0.69 mL, 4.94 mmol), the reaction mixture was stirred at RT overnight. The solvent was removed *in vacuo* and the resulting residue was dissolved in DCM (30 mL) and extracted using H_2O (3x20 mL), sat. $NaHCO_3$ (2x20 mL), brine (30 mL) and dried ($MgSO_4$). The crude product was purified via flash column chromatography (97:3-90:10 DCM:MeOH) to yield the pure product **2.55** as an orange-yellow solid (209 mg, 35%).

^{1}H NMR (500 MHz, $CDCl_3$) δ 8.43 (d, *J* = 4.6 Hz, 2H, H-4), 7.58 – 7.48 (m, 2H, H-2), 7.24 (s, 2H, N*H*), 7.12 (d, *J* = 6.5 Hz, 2H, H-1), 7.11 – 7.05 (m, 2H, H-3), 6.38 (s, 2H, H_e & H_f), 4.39 – 4.28 (m, 4H, CH_2), 3.33 (s, 2H, H_b & H_c), 3.14 (s, 2H, H_a & H_d), 1.44 (d, *J* = 7.0 Hz, 1H, H_g), 1.30 (d, *J* = 8.2 Hz, 1H, H_g').

^{13}C NMR (125 MHz, $CDCl_3$) δ 172.7 (CO), 156.9 (qC_{Ar}), 148.9 (C-4), 136.6 (C-2), 135.5 ($C_{e/f}$), 122.1 (C-3), 121.7 (C-1), 51.6 ($C_{b/c}$), 49.7 (C_g), 47.1 ($C_{a/d}$), 44.7 (*C*H_2). IR (ATR): 1702, 1654, 1592, 1570, 1540, 1469, 1437, 1414, 1337, 1258, 1229, 1214, 1028 cm^{-1}. HRMS (ESI+): m/z calculated for $C_{21}H_{22}N_4O_2$+ Na^+ [M+Na^+]: 385.1640, found 385.1638.

***N*-Propargyl-bicyclo[2.2.1]cis-hept-5-ene-2,3-di-*exo*-carboximide 2.56**

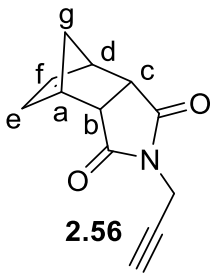

2.56

Cis-5-norbornene-endo-2,3-dicarboxylic anhydride (1 g, 6.1 mmol) was dissolved in anhydrous toluene (30 mL, 3Å molecular sieves), Propargylamine (0.469 mL, 7.3 mmol) and NEt_3 (8.5 mL, 61 mmol) were then added to the reaction mixture. A Dean Stark apparatus was then attached to the round-bottomed flask, along with a waterless condenser. The reaction mixture was then refluxed at 120 ^oC overnight. Following TLC analysis, the solvent was removed in vacuo to yield the product **2.56** as an orange solid (1.21 g, 99%). Rf (3:1 Ethyl Acetate: Petroleum ether)= 0.82

^1H NMR (500 MHz, $CDCl_3$) δ 6.10 (t, *J* = 1.8 Hz, 2H, H_e & H_f), 4.08 (d, *J* = 2.5 Hz, 2H, CH_2), 3.42 (dt, *J* = 4.5, 1.6 Hz, 2H, H_a & H_d), 3.32 – 3.26 (m, 2H, H_b & H_c), 2.13 (t, *J* = 2.5 Hz, 1H, CH_2CCH), 1.73 (dt, *J* = 8.8, 1.7 Hz, 1H, $H_{g/g'}$), 1.54 (dd, *J* = 8.8, 0.5 Hz, 1H, $H_{g/g'}$).

The NMR data is in agreement with the data recorded in the literature [206].

Bicyclo[2.2.1]cis-hept-5-ene-2,3-di-*exo*-carboximide, *N*-(2,3,4,6-tetra-*O*-acetyl-β-D-galactopyranosyl-1,2,3-triazol-4-ylmethylamino) 2.57

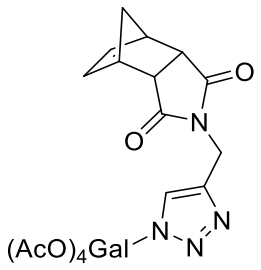

2.57

2.56 (507 mg, 2.52 mmol) and **2.40** (1.16 g, 3.10 mmol) were reacted with sodium ascorbate (150 mg) and copper sulfate pentahydrate (130 mg) in ACN/H_2O (8 mL/2 mL) in a microwave at 100 ^oC until deemed complete by TLC analysis (30 mins). The solvent was then removed *in vacuo* and an extraction of the resulting residue was carried out using DCM and brine. The organic phase was then dried ($MgSO_4$), filtered

and the solvent was removed *in vacuo*. The crude product was then purified by flash column chromatography (1:1-1:4 Pet Ether:Ethyl Acetate) to yield the pure product **2.57** as a colourless oil (922 mg, 64%) Rf (90:10 DCM:MeOH)= 0.68.

^{1}H NMR (500 MHz, $CDCl_3$) δ 7.75 (s, 1H, triaz-H), 5.95 (dt, *J* = 10.0, 5.1 Hz, 1H, $H_{e/f}$), 5.91 (dd, *J* = 5.2, 2.8 Hz, 1H, $H_{e/f}$), 5.79 (d, *J* = 9.3 Hz, 1H, H-1), 5.50 (dd, *J* = 3.3, 0.9 Hz, 1H, H-4), 5.45 (t, *J* = 9.8 Hz, 1H, H-2), 5.21 (dd, *J* = 10.3, 3.4 Hz, 1H, H-3), 4.60 (q, *J* = 14.9 Hz, 2H, C*H*$_2$), 4.22 – 4.04 (m, 3H, H-5, H-6, H-7), 3.35 (s, 2H, H_a & H_d), 3.27 – 3.24 (m, 2H, H_b & H_c), 2.20 (s, 3H, CH_3 of OAc), 2.02 – 1.98 (m, 3H, CH_3 of OAc), 1.96 (s, 3H, CH_3 of OAc), 1.83 (s, 3H, CH_3 of OAc), 1.66 (d, *J* = 8.8 Hz, 1H, $H_{g/g'}$), 1.49 (d, *J* = 8.8 Hz, 1H, $H_{g/g'}$).

^{13}C NMR (125 MHz, $CDCl_3$) δ 176.9 (CO), 170.2 (CO of OAc), 170.0 (CO of OAc), 169.7 (CO of OAc), 168.9 (CO of OAc), 142.9 (C-triaz), 134.4 ($C_{e/f}$), 134.3 ($C_{e/f}$), 121.5 (*C*H-triaz), 86.2 (C-1), 74.0 (C-5), 70.7 (C-3), 67.8 (C-2), 66.8 (C-4), 61.2 (C-6/7), 52.1 ($C_{g/g'}$), 45.8 ($C_{b/c}$), 45.0 ($C_{a/d}$), 33.1 (*C*H$_2$), 21.0 (CH_3 of OAc), 20.7 (CH_3 of OAc), 20.4 (CH_3 of OAc), 20.2 (CH_3 of OAc). IR (ATR): 1746, 1697, 1368, 1211, 1165, 1090, 1043 cm^{-1}. HRMS (ESI+): m/z calculated for $C_{26}H_{30}N_4O_{11}$+ Na^+ [M+Na^+]: 597.1809, found 597.1806.

Bicyclo[2.2.1]cis-hept-5-ene-2,3-di-*exo*-carboximide, *N*-(2,3,4,6-tetra-*O*-acetyl-α-D-mannopyranosyl-1,2,3-triazol-4-ylmethylamino) 2.58

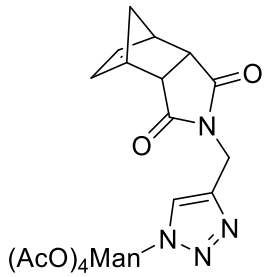

2.58

2.56 (250 mg, 1.24 mmol) and **2.41** (650 mg, 1.74 mmol) were reacted with sodium ascorbate (140 mg) and copper sulfate pentahydrate (100 mg) in ACN/H_2O (8 mL/2 mL) in a microwave at 100 °C until deemed complete by TLC analysis (30 mins). The solvent was then removed *in vacuo* and an extraction of the resulting residue was carried out using DCM and brine. The organic phase was then dried ($MgSO_4$), filtered and the solvent was removed *in vacuo*. The crude product was then purified by flash

column chromatography (1:1-1:4 Pet Ether:Ethyl Acetate) to yield the pure product **2.58** as a colourless oil (119 mg, 17%). Rf (90:10)= 0.66.

^{1}H NMR (500 MHz, $CDCl_3$) δ 7.68 (s, 1H, triaz-H), 6.02 – 5.96 (m, 2H, $H_{e/f}$), 5.94 (d, *J* = 2.5 Hz, 1H, H-1), 5.90 – 5.85 (m, 2H, H-2 & H-3), 5.35 – 5.30 (m, 1H, H-4), 4.70 – 4.61 (m, 2H, CH_2), 4.34 (dd, *J* = 12.5, 5.6 Hz, 1H, $H_{6/7}$), 4.03 (dd, *J* = 12.5, 2.6 Hz, 1H, $H_{6/7}$), 3.85 (ddd, *J* = 8.5, 5.6, 2.6 Hz, 1H, H-5), 3.40 – 3.36 (m, 2H, $H_{a/d}$), 3.29 (dt, *J* = 5.1, 2.5 Hz, 2H, $H_{b/c}$), 2.15 (s, 3H, CH_3 of OAc), 2.08 (s, 3H, CH_3 of OAc), 2.05 (s, *J* = 3.4 Hz, 3H, CH_3 of OAc), 2.03 (s, *J* = 2.5 Hz, 3H, CH_3 of OAc), 1.75 – 1.69 (m, 1H, $H_{g/g'}$), 1.53 (d, *J* = 8.8 Hz, 1H, $H_{g/g'}$). ^{13}C NMR (125 MHz, $CDCl_3$) δ 176.9 (CO), 176.8 (CO), 170.5 (CO of OAc), 169.6 (CO of OAc), 169.2 (CO of OAc), 142.9 (C-triaz), 134.4 ($C_{e/f}$), 134.4 ($C_{e/f}$), 123.3 (*C*H-triaz), 83.4 (C-1), 72.2 (C-5), 68.6 (C-2/3), 68.2 (C-2/3), 66.0 (C-4), 61.5 (C-6/7), 52.2 ($C_{g/g'}$), 45.9 ($C_{b/c}$), 44.9 ($C_{a/d}$), 33.0 (CH_2), 21.0 (CH_3 of OAc), 20.7 (CH_3 of OAc), 20.7 (CH_3 of OAc), 20.5 (CH_3 of OAc). IR (ATR): 1744, 1697, 1368, 1215, 1163, 1122, 1037, 1013 cm^{-1}. HRMS (ESI+): m/z calculated for $C_{26}H_{30}N_4O_{11}$+ Na^+ [M+Na^+]: 597.1809, found 597.1806.

Bicyclo[2.2.1]cis-hept-5-ene-2,3-di-*exo*-carboximide, *N*-(1-benzyl-1H-1,2,3-triazol-4-ylmethylamino) 2.59

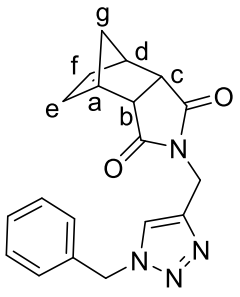

2.59

2.56 (200 mg, 0.994mmol) and Benzyl azide (2.58 mL, 1.29 mmol (0.5M solution in DCM)) were reacted with sodium ascorbate (140 mg) and copper sulfate pentahydrate (100 mg) in ACN/H_2O (8 mL/2 mL) in a microwave at 100 ^{o}C until deemed complete by TLC analysis (30 mins). The solvent was then removed *in vacuo* and an extraction of the resulting residue was carried out using DCM and brine. The organic phase was then dried ($MgSO_4$), filtered and the solvent was removed *in vacuo* to yield the pure product **2.59** as a yellow-green solid (174 mg, 53%).

^{1}H NMR (500 MHz, $CDCl_3$) δ 7.41 – 7.33 (m, 4H, triaz-H & Ar-H), 7.23 (dd, *J* = 7.4, 1.9 Hz, 2H, Ar-H), 5.81 (s, 2H, $H_{e/f}$), 5.47 (s, 2H, C*H*$_2$Ph), 4.60 (s, 2H, CH_2), 3.34 (s, 2H, $H_{a/d}$), 3.27 – 3.22 (m, 2H, $H_{b/c}$), 1.71 – 1.66 (m, 1H, $H_{g/g'}$), 1.50 (d, *J* = 8.8 Hz, 1H, $H_{g/g'}$).
^{13}C NMR (125 MHz, $CDCl_3$) δ 176.9 (CO), 142. (q*C*-triaz), 134.3 ($C_{e/f}$), 129.1 (*C*$_{Ar}$), 128.8 (*C*$_{Ar}$), 128.0 (*C*$_{Ar}$), 122.8 (*C*-triaz), 54.2 (*C*H$_2$Ph), 52.2 ($C_{g/g'}$), 45.8 ($C_{b/c}$), 44.9 ($C_{a/d}$), 33.4 (*C*H$_2$-triaz). IR (ATR): 1693, 1388, 1337, 1327, 1222, 1171, 1158, 1118, 1046 cm^{-1}. HRMS (ESI+): m/z calculated for $C_{19}H_{18}N_4O_2$+ H$^+$ [M+H$^+$]: 335.1508, found 335.1506.

Bicyclo[2.2.1]cis-hept-5-ene-2,3-di-*exo*-carboximide, *N*-(α-D-mannopyranosyl-1,2,3-triazol-4-ylmethylamino) 2.60

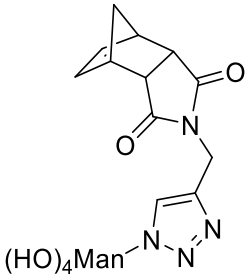

2.60

2.58 (119 mg, 0.21 mmol) was dissolved in MeOH/H_2O (2 mL/1 mL) in a round-bottom flask, a waterless condenser was attached, and stirred in an oil bath at 50-55 ^{o}C for 5 mins. NEt_3 (0.1 mL) was then added and the reaction mixture was stirred at 50-55 ^{o}C until the reaction was deemed to be complete by TLC analysis (4.5 h). The solvent was then removed *in vacuo*, the resulting residue was then dissolved in deionised water, Amberlite H$^+$ was then added and the crude product was stirred for 40 mins. The Amberlite H$^+$ was then filtered off and the solvent was then removed *in vacuo* to yield the product **2.60** as a yellow oil (57.9 mg, 69%).

^{1}H NMR (500 MHz, D_2O) δ 8.06 (d, *J* = 8.9 Hz, 1H, triaz-H), 6.08 (dd, *J* = 11.4, 4.7 Hz, 1H, H-1), 5.90 – 5.80 (m, 2H, $H_{e/f}$), 4.75 (d, *J* = 3.5 Hz, 1H, H-2), 4.68 – 4.61 (m, 2H, CH_2), 4.12 (dt, *J* = 10.0, 5.0 Hz, 1H, H-3), 3.85 – 3.74 (m, 3H, H-4, H-6 & H-7), 3.51 – 3.43 (m, 2H, H_b & H_c), 3.33 (s, 2H, H_a & H_d), 3.26 – 3.19 (m, 1H, H-5), 1.65 (dt, *J* = 12.8, 6.4 Hz, 1H, $H_{g/g'}$), 1.57 (t, *J* = 9.6 Hz, 1H, $H_{g/g'}$). ^{13}C NMR (125 MHz, D_2O) δ 180.7 (CO), 142.4 (C-triaz), 134.3 ($C_{e/f}$), 134.2 ($C_{e/f}$), 124.4 (*C*H-triaz), 86.6 (C-1), 76.2 (C-5), 70.5 (C-3), 68.2 (C-2), 66.5 (C-4), 60.4 (C-6/7), 51.9 ($C_{g/g'}$), 45.7 ($C_{b/c}$), 44.9 ($C_{a/d}$), 32.7 (CH_2). IR (ATR): 3363, 1686, 1399, 1335, 1232, 1169, 1117, 1068, 1048 cm^{-1}. HRMS (ESI+): m/z calculated for $C_{18}H_{22}N_4O_7$+ Na$^+$ [M+Na$^+$]: 429.1386, found 429.1381.

***tert*-butyl prop-2-yn-1-ylcarbamate 2.61**

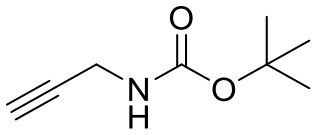

2.61

Di-*tert*-butyl dicarbonate (720 mg, 3.3 mmol) was dissolved in DCM (10 mL) and added over 10 mins to a solution of propargylamine (0.13 mL, 3.6 mmol, 1.1 equiv), NEt_3 (0.46 mL, 3.3 mmol) in DCM (10mL) on ice. The reaction mixture was stirred overnight at RT. Following TLC analysis, the solvent was removed *in vacuo*, to yield the product **2.61** as a yellow solid (367 mg, 72%). R_f = 0.92 (pet ether:EtOAc 1:1) ^{1}H NMR (500 MHz, $CDCl_3$) δ 4.83 (bs, 1H, N*H*), 3.87 (s, 2H, CH_2), 2.17 (t, *J* =2.5 Hz, 1H, C*H*), 1.40 (s, 9H, C(CH_3)$_3$).

The NMR data is in agreement with the data recorded in the literature [207].

***tert*-butyl-(*N*-(2,3,4,6-tetra-*O*-acetyl-β-D-galactopyranosyl-1,2,3-triazol-4-yl)methyl)carbamate 2.62**

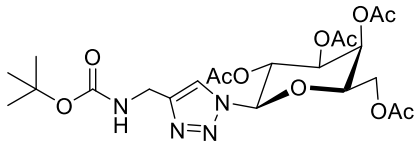

2.62

Copper sulphate pentahydrate (60 mg) and sodium ascorbate (120 mg) were added to a solution of **2.40** (571 mg, 1.53 mmol) and **2.61** (136 mg, 0.87 mmol) in CH_3CN/H_2O (6 mL/ 3 mL). The reaction was allowed to stir in the MW at 100 ^oC until deemed complete by TLC analysis (30 mins). The solvent was removed *in vacuo*. The residue was dissolved in DCM (30 mL), washed with water (20 mL x 3), and dried ($MgSO_4$). The mixture was filtered and the solvent was removed *in vacuo* to yield the crude product, which was purified by silica gel column chromatography (DCM:MeOH 99:1-95:5) to give the pure product **2.62** as a white crystalline solid (379 mg, 81%). Rf=0.43 (90:10 DCM:MeOH).

^{1}H NMR (500 MHz, $CDCl_3$) δ 7.79 (s, 1H, triaz-H), 5.81 (d, *J* = 9.3 Hz, 1H, H-1), 5.55 – 5.45 (m, 2H, H-2 & H-4), 5.24 – 5.19 (m, 1H, H-3), 5.18 (s, 1H, NH), 4.41 – 4.30 (m, 2H, CH_2), 4.21 (t, *J* = 6.4 Hz, 1H, H-5), 4.17 – 4.05 (m, 2H, H-6 & H-7), 2.18 (dd, *J* = 5.8, 3.5

Hz, 3H, CH_3 of OAc), 2.02 – 1.98 (dd, 3H, CH_3 of OAc), 1.98 – 1.93 (dd, 3H, CH_3 of OAc), 1.84 (dd, *J* = 5.1 Hz, 3H, CH_3 of OAc), 1.40 (s, 9H, $C(CH_3)_3$).

^{13}C NMR (125 MHz, $CDCl_3$) δ 170.3 (CO of OAc), 170.0 (CO of OAc), 169.8 (CO of OAc), 168.9 (CO of OAc), 155.7 (*C*O(O)$(CH_3)_3$), 146.0 (C-triaz), 120.5 (*C*H-triaz), 86.1 (C-1), 79.7 (*C*$(CH_3)_3$), 73.9 (C-5), 70.7 (C-3), 67.8 (C-2/C-4), 66.8 (C-2/C-4), 61.2 (C-6/7), 36.0 (*C*H_2), 28.3 (C(*C*$H_3)_3$), 20.6 ((CO)*C*H_3), 20.5 ((CO)*C*H_3), 20.2 ((CO)*C*H_3). IR (ATR): 1743, 1718, 1366, 1218, 1163, 1107, 1038 cm^{-1}. HRMS (ESI+): m/z calculated for $C_{22}H_{32}N_4O_{11}$ + H^+ [M+H^+]: 529.2146, found 529.2143.

tert-butyl-(_N_-(2,3,4,6-tetra-_O_-acetyl-α-D-mannopyranosyl-1,2,3-triazol-4-yl)methyl)carbamate 2.63

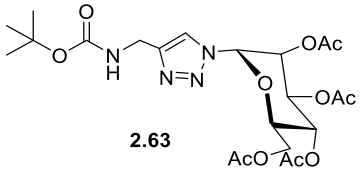

2.63

2.61 (339 mg, 2.18 mmol) and **2.41** (1.338 g, 3.58 mmol) were dissolved in a ACN/H_2O (6 mL/2 mL), sodium ascorbate (173 mg) and copper sulfate pentahydrate (109 mg) were added and the reaction mixture was stirred at 100 °C in the MW until deemed complete via TLC analysis (30 mins). The solvent was removed *in vacuo* and the resulting residue was extracted using DCM (30 mL) and brine (3x20 mL) and dried ($MgSO_4$). The crude product was purified using flash column chromatography (2:1-2:1 Petroleum ether: Ethyl acetate) to yield the pure product **2.63** as a white solid (510 mg, 44%). Rf=0.46 (90:10 DCM:MeOH).

^{1}H NMR (500 MHz, $CDCl_3$) δ 7.71 (s, 1H, triaz-H), 5.97 (s, 1H, H-1), 5.96 – 5.94 (m, 1H, H-2), 5.91 (dd, *J* = 8.9, 3.6 Hz, 1H, H-3), 5.36 (t, *J* = 9.0 Hz, 1H, H-4), 5.12 (s, 1H, N*H*), 4.43 (t, *J* = 6.8 Hz, 2H, C*H*$_2$), 4.37 (dd, *J* = 12.5, 5.3 Hz, 1H, H-6/7), 4.04 (dd, *J* = 12.5, 2.5 Hz, 1H, H-6/7), 3.90 – 3.84 (m, 1H, H-5), 2.18 (s, 3H, CH_3 of OAc), 2.09 (s, 3H, CH_3 of OAc), 2.04 (dd, *J* = 10.1, 7.3 Hz, 6H, CH_3 of OAc x2), 1.44 (s, 9H, $C(CH_3)_3$).

^{13}C NMR (125 MHz, $CDCl_3$) δ 170.5 (CO of OAc), 169.6 (CO of OAc), 169.3 (CO of OAc), 155.8 (*C*O(O)$(CH_3)_3$), 146.2 (C-triaz), 122.3 (*C*H-triaz), 83.5 (C-1), 79.7 (*C*$(CH_3)_3$) 72.0 (C-5), 68.7 (C-3), 68.2 (C-2), 66.0 (C-4), 61.5 (C-6/7), 35.9 (*C*H_2), 28.3 (C(*C*$H_3)_3$), 21.0 ((CO)*C*H_3), 20.6 ((CO)*C*H_3), 20.5 ((CO)*C*H_3). IR (ATR): 1746, 1708, 1367, 1216, 1164,

1120, 1039 cm^{-1}. HRMS (ESI+): m/z calculated for $C_{22}H_{32}N_4O_{11}$ + Na^+ [M+Na^+]: 551.1965, found 551.1961.

***tert*-butyl-((1-benzyl-1H-1,2,3-triazol-4-yl)methyl)carbamate 2.64**

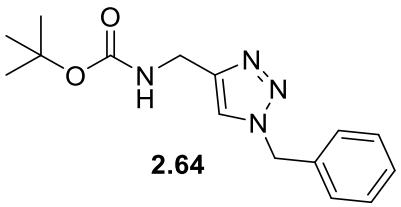

2.64

Copper sulphate pentahydrate (100 mg) and sodium ascorbate (140 mg) were added to a solution of **2.61** (129 mg, 0.83 mmol) and Benzyl azide (0.12 mL, 0.99 mmol, 1.2 equiv) in CH_3CN/H_2O (4 mL/ 1mL). The reaction was allowed to stir in the MW at 100 ^oC for 30 mins, copper sulfate pentahydrate (60 mg), sodium ascorbate (120 mg) and benzyl azide (0.1 mL) were then added. The reaction mixture was transferred to a round-bottomed flask, copper sulfate pentahydrate (60 mg), sodium ascorbate (120 mg) was added and the reaction mixture was stirred for five days at RT. The solvent was removed *in vacuo*. The residue was dissolved in DCM (30 mL), washed with water (20 mL x 3), and dried ($MgSO_4$). The mixture was filtered and the solvent was removed *in vacuo* to yield the crude reaction mixture. The reaction mixture was dissolved in THF-*tert*-butanol-H_2O (3 mL: 3 mL: 3 mL), sodium ascorbate (150 mg), copper sulfate pentahydrate (100 mg) and benzyl azide (0.1 mL) were added and the reaction mixture was stirred overnight at RT. Benzyl azide (0.1 mL) was added the following day and the reaction mixture was stirred overnight at RT again. The solvent was removed *in vacuo*. The residue was dissolved in DCM (30 mL), washed with water (20 mL x 3), and dried ($MgSO_4$). The mixture was filtered and the solvent was removed *in vacuo* to yield the product **2.64** (80 mg, 33%).

^1H NMR (500 MHz, $CDCl_3$) δ 7.48 – 7.39 (s, 1H, triaz-H), 7.39 – 7.29 (m, 3H, Ar_H), 7.24 (d, *J* = 7.2 Hz, 2H, Ar_H), 5.47 (s, 2H, CH_2), 5.18 (s, 1H, N*H*), 4.34 (d, *J* = 5.6 Hz, 2H, CH_2), 1.40 (s, 9H, Boc-CH_3).

The NMR data is in agreement with the data recorded in the literature [208].

***tert*-butyl-(*N*-(β-D-galactopyranosyl-1,2,3-triazol-4-yl)methyl)carbamate 2.65**

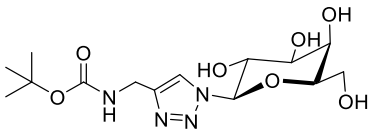

2.65

2.62 (37 mg, 0.72 mmol) was dissolved in a MeOH/H_2O (4 mL/2 mL) under reflux conditions, NEt_3 (0.22 mL) was added, and the reaction mixture was stirred until deemed complete via TLC analysis (approx. 6 h). The solvent was removed *in vacuo* and the crude reaction mixture was dissolved in deionised water and treated with amberlite H^+ by stirring for 30-40 mins, the reaction was then filtered using vacuum filtration and the solvent was removed *in vacuo* to give the pure product **2.65** as a colourless oil (237 mg, 92%).

^{1}H NMR (500 MHz, D_2O) δ 8.08 (s, 1H, triaz-H), 5.60 (d, *J* = 9.1 Hz, 1H, H-1), 4.24 (s, 2H, CH_2), 4.14 (t, *J* = 9.2 Hz, 1H, H-2), 4.02 (d, *J* = 2.8 Hz, 1H, H-4), 3.91 (t, *J* = 5.8 Hz, 1H, H-5), 3.83 – 3.76 (m, 1H, H-3), 3.69 (t, *J* = 9.4 Hz, 2H, H-6 & H-7), 1.30 (s, 9H, $C(CH_3)_3$).

^{13}C NMR (125 MHz, D_2O) δ 157.6 (CO), 146.1 (C-triaz), 122.5 (*C*H-triaz), 88.0 (C-1), 81.0 (*C*$(CH_3)_3$), 78.2 (C-5), 72.8 (C-3), 69.7 (C-2), 68.4 (C-4), 60.7 (C-6/7), 35.2 (*C*H_2), 27.7 (C(*C*$H_3)_3$). IR (ATR): 3321, 2977, 2931, 1685, 1522, 1453, 1392, 1365, 1274, 1249, 1163, 1091, 1050, 1016 cm^{-1}. HRMS (ESI+): m/z calculated for $C_{14}H_{24}N_4O_7$ + Na^+ [M+Na^+]: 383.1543, found 383.1537.

(1-β-D-galactopyranosyl-1,2,3-triazol-4-yl)methanamine 2.67

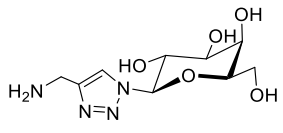

2.67

2.65 (39 mg, 0.1 mmol) was dissolved in deionised water (5 mL) and TFA (0.25 mL, 3.27 mmol) and the reaction mixture was stirred at RT until deemed complete via TLC analysis (6:3.5:0.5, DCM:MeOH:H_2O) (5 h). The solvent was then removed *in vacuo* and the product was dried using a schlenk line to yield a white fluffy solid **2.67** (26 mg, 96%).

^{1}H NMR (500 MHz, D_2O) δ 8.31 (s, 1H, triaz-H), 5.66 (d, *J* = 9.2 Hz, 1H, H-1), 4.32 (s, 2H, C*H*$_2$), 4.18 (t, *J* = 9.5 Hz, 1H, H-2), 4.02 (d, *J* = 4.3 Hz, 1H, H-4), 3.96 (t, *J* = 6.0 Hz, 1H, H-5), 3.83 (dd, *J* = 10.0, 5.0 Hz, 1H, H-3), 3.72 (d, *J* = 8.4 Hz, 2H, H-6 & H-7). ^{13}C NMR (125 MHz, D_2O) δ 140.1 (C-triaz), 124.5 (*C*H-triaz), 88.0 (C-1), 78.3 (C-5), 72.8 (C-3), 69.6 (C-2), 68.6 (C-4), 60.8 (C-6/7), 33.9 (*C*H$_2$). IR (ATR): 3264, 1673, 1200, 1128, 1089, 1051 cm^{-1}. HRMS (ESI+): m/z calculated for $C_9H_{16}N_4O_5$ + H^+ [M+H$^+$]: 261.1199, found 261.1198.

(1-α-D-mannopyranosyl-1,2,3-triazol-4-yl)methanamine 2.68

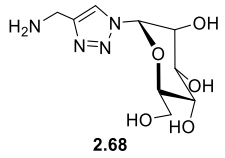

2.68

2.63 (265 mg, 0.501 mmol) was dissolved in a MeOH/H_2O mixture (3 mL/1 mL) under reflux conditions, NEt_3 (0.15 mL) was added and the reaction mixture was refluxed until the reaction was deemed complete via TLC analysis (6 h). The solvent was removed *in vacuo*, the resulting residue was dissolved in H_2O and treated with Amberlite H^+ by stirring for 30-40 mins. The reaction mixture was then filtered using vacuum filtration, the solvent was then removed *in vacuo* to yield the pure product **2.66** as a colourless oil (160 mg, 89%), this was dissolved in deionised water (20 mL), TFA (1 mL, 13 mmol) was added and the reaction mixture was stirred at RT until the reaction as deemed complete via TLC analysis (mobile phase= DCM:MeOH:H_2O, 6:3.5:0.5) (5 h). The solvent was then removed *in vacuo* and the product was dried on the Schlenk line, to yield the pure product **2.68** as a white fluffy solid (108 mg, 94%).

^{1}H NMR (500 MHz, D_2O) δ 8.31 (s, 1H, triaz-H), 6.16 (d, *J* = 2.3 Hz, 1H, H-1), 4.84 – 4.80 (m, 1H, H-2), 4.42 – 4.37 (m, 2H, CH_2), 4.17 (dd, *J* = 9.0, 3.5 Hz, 1H, H-3), 3.88 – 3.78 (m, 3H, H-4, H-6 & H-7), 3.37 – 3.31 (m, 1H, H-5).

^{13}C NMR (125 MHz, D_2O) δ 140.2 (C-triaz), 125.1 (*C*H-triaz), 86.7 (C-1), 76.2 (C-5), 70.5 (C-3), 68.2 (C-2), 66.5 (C-4), 60.4 (C6/7), 34.0 (*C*H$_2$). IR (ATR): 1663, 1390, 1192, 1133, 1059, 1038, 1018 cm^{-1}. HRMS (ESI+): m/z calculated for $C_9H_{16}N_4O_5$+ H^+ [M+H$^+$]: 261.1199, found 261.1194.

(1-Benzyl-1H-1,2,3-triazol-4-yl)methanamine 2.69

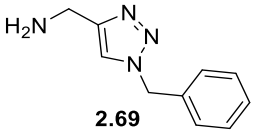

2.69

2.64 (80 mg, 0.27 mmol) was placed under N_2 and dissolved in anhydrous DCM (0.7 mL), TFA (0.23 mL, 3 mmol) was added and the reaction mixture was stirred at RT until deemed complete via TLC analysis (35 mins), NaOH (1 N, 10 mL) was added to the reaction mixture and it was extracted using DCM (20 mL), brine (3x20 mL) and dried ($MgSO_4$), the solvent was removed *in vacuo* to yield the pure product **2.69** as a yellow oil (47 mg, 91%).

^{1}H NMR (500 MHz, DMSO) δ 7.92 (s, 1H, triaz-H), 7.40 – 7.26 (m, 5H, Ar_H), 5.55 (s, 2H, CH_2), 3.72 (s, 2H, CH_2).

The NMR data is in agreement with the data recorded in the literature [208].

2-*endo*-*N*-(β-D-galactopyranosyl-1,2,3-triazol-4-ylmethylamino)-3-*endo*-benzyloxycarbonyl-bicyclo[2.2.1]hept-5-ene-2-*endo*-carboxamide-3-*endo*-carboxylic acid benzyl ester 2.73

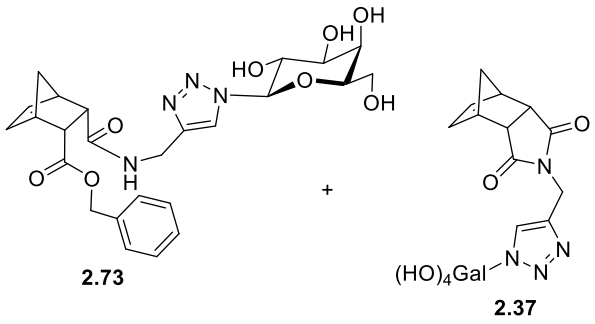

2.73 + **2.37**

2.76 (48.6 mg, 0.17 mmol, 1.5 equiv.) and TBTU (42 mg, 0.13 mmol, 1.1 equiv.) were placed under N_2 and dissolved in anhydrous DMF (2 mL) and stirred for 15 mins. N,N-DIPEA (approx. 31 µL, 0.17 mmol, 1.5 equiv.) was then added to the reaction mixture, which was then stirred for 15 mins. **2.67** (31 mg, 0.12 mmol, 1 equiv.) had been placed under N_2 and dissolved in anhydrous DMF (1 mL), this was then added to the reaction mixture via a cannula. After one h of stirring at RT, the solvent was removed *in vacuo*. The crude residue was then extracted using deionised water and DCM. The crude product was then purified using flash column chromatography (90:10

DCM:MeOH), the purified mixture appeared to contain a 0.15:1 mixture of the **2.37**:**2.73** (**A**= **2.37** & **B**= **2.73**) (28 mg, 46%)).

^{1}H NMR (500 MHz, D_2O) δ 8.13 (s, 0.16H, triaz-H(**A**)), 8.01 (s, 1H, triaz-H(**B**)), 7.43 – 7.27 (m, 5H, Ar_H(**B**)), 6.27 (d, *J* = 2.3 Hz, 1H, H_e/H_f (**B**)), 6.06 (s, 1H, H_e/H_f (**B**)), 5.84 (dd, *J* = 7.2, 2.6 Hz, 0.32H, H_e/H_f (**A**)), 5.61 (d, *J* = 9.3 Hz, 0.17H, H-1 (**A**)), 5.58 (d, *J* = 9.2 Hz, 1H, H-1 (**B**)), 4.98 (d, *J* = 12.2 Hz, 1H, C*H*$_2$Ph (**B**)), 4.87 – 4.83 (m, 1H, C*H*$_2$Ph (**B**)), 4.63 (s, 0.61H, C*H*$_2$-triaz (**A**)), 4.25 (dd, *J* = 37.8, 16.4 Hz, 2H, C*H*$_2$-triaz (**B**)), 4.15 (t, *J* = 9.3 Hz, 1H, H-2 (**B**)), 4.05 (d, *J* = 3.0 Hz, 1H, H-4 (**B**)), 3.97 – 3.90 (m, 1H, H-5 (**B**)), 3.82 (dt, *J* = 12.3, 6.0 Hz, 1H, H-3 (**B**)), 3.77 – 3.62 (m, 3H, H-6 & H-6' (**B**)), 3.43 (dd, *J* = 11.5, 1.6 Hz, 0.47H, $H_{b/c}$ (**A**)), 3.27 (dd, *J* = 7.1, 1.9 Hz, 1H, $H_{b/c}$ (**B**)), 3.12 – 3.04 (m, 2H, $H_{a/d}$ (**B**)), 1.63 (d, *J* = 8.6 Hz, 0.2H, $H_{g/g'}$ (**A**)), 1.55 (d, *J* = 8.9 Hz, 0.23H, $H_{g/g'}$ (**A**)), 1.37 (dd, *J* = 24.1, 8.0 Hz, 2H, $H_{g/g'}$ (**B**)).

^{13}C NMR (125 MHz, D_2O) δ 180.6 (s, *C*O of **A**), 175.1 (s, *C*OOCH$_2$Ph (**B**)), 174.3 (s, *C*ONHtriaz (**B**)), 145.1 (s, qC_{triaz} (**B**)), 142.2 (s, qC_{triaz} (**A**)), 135.7 (s, $C_{e/f}$ (**B**)), 134.2 (s, $C_{e/f}$ (**B**)), 128.6 (s, C_{Ar} (**B**)), 128.4 (s, C_{Ar} (**B**)), 128.3 (s, C_{Ar} (**B**)), 122.7 (s, C-triaz (**B**)), 88.0 (s, C-1 (**B**)), 78.1 (s, C-5 (**B**)), 72.9 (s, C-3 (**B**)), 69.6 (s, C-2 (**B**)), 68.4 (s, C-4 (**B**)), 66.6 (s, *C*H$_2$Ph (**B**)), 60.7 (s, C-6 (**B**)), 49.0 (s, C_g (**B**)), 47.0 (s, $C_{a/d}$ (**B**)), 45.5 (s, $C_{a/d}$ (**B**)), 44.8 (s, $C_{b/c}$ (**B**)), 34.2 (s, *C*H$_2$-triaz (**B**)).

HRMS (ESI+): m/z calculated for $C_{18}H_{22}N_4O_7$ + $HCOO^-$ [M+$HCOO^-$]: 451.1471, found 451.1471 (**2.37**). HRMS (ESI+): m/z calculated for $C_{25}H_{30}N_4O_8$ + $HCOO^-$ [M+$HCOO^-$]: 559.2046, found 559.2049 (**2.73**).

3-*endo*-benzyloxycarbonyl-bicyclo[2.2.1]cis-hept-5-ene-2-*endo*-carboxylic acid 2.76

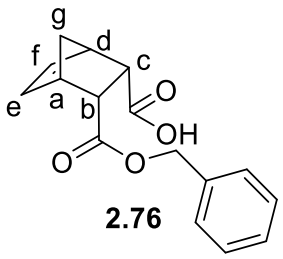

2.76

Benzyl alcohol (0.14 mL, 1.37 mmol, 1.5 equiv) was added to a round bottom flask along with chloroform (8 mL) and stirred, NEt_3 (0.19 mL, 1.37 mmol, 1.5 equiv) was then added to the round bottom flask and it was stirred for 15 mins. *Cis*-5-norbornene-endo-2,3-dicarboxylic anhydride (150 mg, 0.91 mmol) was then added

and the reaction mixture was stirred overnight at RT. Following TLC analysis, the solvent was removed in vacuo. The resulting solid was purified via flash column chromatography (99:1-90:10 DCM:MeOH) to yield the pure product **2.76** as a white solid (213 mg, 86%). Rf=0.44 (90:10 DCM:MeOH).

^{1}H NMR (500 MHz, $CDCl_3$) δ 7.41 – 7.27 (m, 5H, Ar_H), 6.29 (dd, *J* = 5.6, 3.0 Hz, 1H, H_e or H_f), 6.22 (dd, *J* = 5.6, 2.9 Hz, 1H, H_e or H_f), 5.10 (d, *J* = 12.3 Hz, 1H, C*H*$_2$Ph), 4.93 (d, *J* = 12.3 Hz, 1H, C*H*$_2$Ph), 3.33 (dd, *J* = 6.8, 5.6 Hz, 2H, H_b & H_c), 3.23 – 3.14 (m, 2H, H_a & H_d), 1.49 (dt, *J* = 8.7, 1.8 Hz, 1H, H_g or $H_{g'}$), 1.33 (d, *J* = 8.7 Hz, 1H, H_g or $H_{g'}$).

The NMR data is in agreement with the data recorded in the literature [209].

2-*endo*-*N*-(prop-2-yn-1-yl)- 3-*endo*-benzyloxycarbonyl-bicyclo[2.2.1]hept-5-ene-2-*endo*-carboxamide-3-*endo*-carboxylic acid benzyl ester 2.77

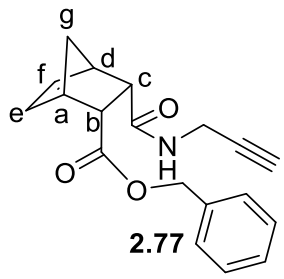

2.77

2.76 (0.202 mg, 0.74 mmol) and TBTU (357 mg, 1.11 mmol, 1.5 equiv.) were placed under N_2, dissolved in anhydrous DMF (8 mL) and stirred for 30 mins. Propargylamine (0.05 mL, 0.82 mmol, 1.1 equiv.) and NEt_3 (0.156mL, 1.11 mmol, 1.5 equiv.) were added and the reaction mixture was stirred overnight at RT. Following TLC analysis, propargylamine (0.05 mL, 0.82 mmol, 1.1 equiv.) was added and the reaction mixture was stirred. 6 h later, following TLC analysis, the solvent was removed *in vacuo*. The resulting residue was dissolved in DCM and extracted using cold deionised water, sat. $NaHCO_3$ solution and brine, the organic phase was dried ($MgSO_4$) filtered and the solvent was removed in vacuo. The crude product was then purified via flash column chromatography (DCM, 99:1-93:7 DCM:MeOH) to yield the pure product **2.77** as a white solid (118.8 mg, 52%). Rf=0.71 (90:10 DCM:MeOH)

^{1}H NMR (500 MHz, $CDCl_3$) δ 7.35 – 7.26 (m, 5H, Ar-H), 6.47 (dd, *J* = 5.3, 2.8 Hz, 1H, $H_{e/f}$), 6.15 (dd, *J* = 5.2, 2.8 Hz, 1H, $H_{e/f}$), 6.00 (s, 1H, N*H*), 5.06 (d, *J* = 12.3 Hz, 1H, C*H*$_2$Ph), 4.95 (d, *J* = 12.3 Hz, 1H, C*H*$_2$Ph), 3.92 – 3.78 (m, 2H, NHC*H*$_2$CCH), 3.30 – 3.23 (m, 2H, H_b & H_c), 3.15 (s, 1H, $H_{a/d}$), 3.11 (s, 1H, $H_{a/d}$), 2.16 (t, *J* = 2.1 Hz, 1H, CH_2CCH), 1.48 – 1.43 (m, 1H, $H_{g/g'}$), 1.32 (d, *J* = 8.6 Hz, 1H, $H_{g/g'}$). ^{13}C NMR (125 MHz, $CDCl_3$) δ

172.7 (*C*OOBn), 171.4 (*C*O), 136.5 ($C_{e/f}$), 133.6 ($C_{e/f}$), 128.4 (C_{Ar}), 128.4 (C_{Ar}), 128.1 (C_{Ar}), 79.9 ($NHCH_2CCH$), 71.2 (s, $NHCH_2CCH$), 66.4 (CH_2Ph), 49.8 ($C_{b/c}$), 49.1 ($C_{b/c}$), 49.0 (C_g), 47.3 ($C_{a/d}$), 45.7 ($C_{a/d}$), 29.0 ($NHCH_2CCH$). IR (ATR): 3271, 1726, 1644, 1542, 1340, 1329, 1260, 1219, 1183, 1149, 1038 cm^{-1}. HRMS (ESI+): m/z calculated for $C_{19}H_{19}NO_3$+ Na^+ [M+Na^+]: 332.1263, found 332.1263.

3-*endo*-farnesylcarbonyl-bicyclo[2.2.1]cis-hept-5-ene-2-*endo*-carboxylic acid 2.78

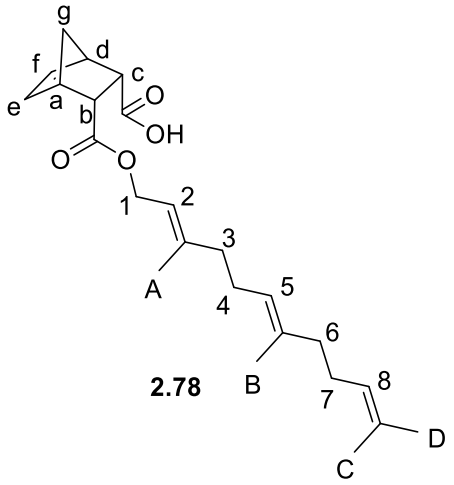

2.78

Farnesol (1.25 mL, 4.98 mmol) and chloroform (8 mL) were placed in a round-bottomed flask and stirred for 5 mins, NEt_3 (0.86 mL, 6.16 mmol) was added and the reaction mixture was then stirred for 25 mins. *Cis*-5-norbornene-2,3-endo-dicarboxylic acid anhydride (550 mg, 3.35 mmol) was added and the reaction was stirred overnight at RT. Following TLC analysis, the solvent was removed *in vacuo*. The crude product was purified by flash column chromatography (1:1 Petroleum ether: Ethyl acetate-3:1 Ethyl acetate: Petroleum ether) to yield **2.78** as a colourless oil (252 mg, 19%).

^{1}H NMR (500 MHz, $CDCl_3$) δ 6.28 (dd, *J* = 5.3, 2.8 Hz, 1H, $H_{e/f}$), 6.21 (dd, *J* = 5.3, 2.8 Hz, 1H, $H_{e/f}$), 5.29 (t, *J* = 7.1 Hz, 1H, H_2), 5.13 – 5.04 (m, 2H, $H_{5/8}$), 4.62 – 4.52 (m, 1H, $H_{1/1'}$), 4.42 (dd, *J* = 12.3, 7.1 Hz, 1H, $H_{1/1'}$), 3.34 – 3.21 (m, 2H, $H_{b/c}$), 3.15 (d, *J* = 9.7 Hz, 2H, $H_{a/d}$), 2.13 – 1.90 (m, 8H, $H_{3/3'/4/4'/6/6'/7/7'}$), 1.69 – 1.63 (m, 7H, CH_3(A,B,C,D)), 1.62 – 1.55 (m, 5H, CH_3(A,B,C,D)), 1.47 – 1.41 (m, 1H, $H_{g/g'}$), 1.34 – 1.27 (m, 1H, $H_{g/g'}$).

^{13}C NMR (125 MHz, $CDCl_3$) δ 178.0 (s, CO), 172.4 (s, CO), 142.1 (s, CH_3(A)-q*C*), 135.4 (s, $C_{e/f}$), 134.4 (s, $C_{e/f}$), 131.5 (s, CH_3(B/C)-q*C*), 131.3 (s, CH_3(B/C)-q*C*), 124.4 (s, C-5/8), 123.7 (s, C-5/8), 118.3 (s, C-2), 61.3 (s, C-1), 48.7 (s, $C_{b/c/g}$), 48.3 (s, $C_{b/c/g}$), 48.1 (s, $C_{b/c/g}$), 46.5 (s, $C_{a/d}$), 46.2 (s, $C_{a/d}$), 39.7 (s, C-3/4/6/7), 31.9 (s, C-3/4/6/7), 26.6 (s, C-

3/4/6/7), 26.1 (s, C-3/4/6/7), 25.7 (s, *C*H_3(A/B/C/D)), 23.3 (s, *C*H_3(A/B/C/D)), 17.6 (s, *C*H_3(A/B/C/D)), 16.3 (s, *C*H_3(A/B/C/D)), 16.0 (s, *C*H_3(A/B/C/D)). IR (ATR): 2916, 1732, 1446, 1376, 1338, 1252, 1171, 1144, 1074, 1014 cm^{-1}. HRMS (ESI+): m/z calculated for $C_{24}H_{34}O_4$ - H $[M-H]^-$: 385.2384, found 385.2389.

3-*endo*-tyrosollcarbonyl-bicyclo[2.2.1]cis-hept-5-ene-2-*endo*-carboxylic acid 2.79

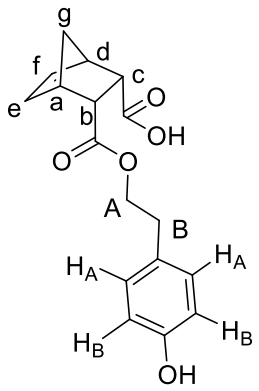

2.79

Tyrosol (2-(4-hydroxyphenyl)ethanol) (330 mg, 2.4 mmol, 0.8 equiv.) was placed in chloroform (25 mL) and refluxed at 50°C (grind up Tyrosol before reflux), NEt_3 (0.63 mL, 4.5 mmol, 1.5 equiv) was added and the reaction mixture was stirred for 25 mins. *Cis*-5-norbornene-endo-2,3,dicarboxylic acid anhydride (500 mg, 3 mmol, 1 equiv.) was then added and the reaction mixture was stirred overnight at 50 °C, following TLC analysis (90:10 DCM:MeOH) the solvent was removed in vacuo.. The crude product was purified via column chromatography, initially flash column chromatography was attempted (95:5-88:12 DCM:MeOH), however, co-elution occurred. Repeat flash column chromatography was attempted (95:5-94:6 DCM:MeOH) leading to the pure product **2.79** as a colourless oil (62.3 mg, 7%).

^{1}H NMR (500 MHz, DMSO) δ 7.04 – 6.95 (m, 2H, Ar_H), 6.71 – 6.64 (m, 2H, Ar_H), 6.10 – 6.02 (m, 2H, H_e & H_f), 4.02 (ddt, *J* = 41.1, 10.7, 7.1 Hz, 2H, C*H*$_2$(A)), 3.29 – 3.18 (m, 2H, H_b & H_c), 3.03 (s, 1H, H_a & H_d), 2.97 (s, 1H, H_a & H_d), 2.74 – 2.66 (m, 2H, C*H*$_2$(B)), 1.32 (d, *J* = 8.2 Hz, 1H, H_g or $H_{g'}$), 1.29 – 1.22 (m, 1H, H_g or $H_{g'}$).

^{13}C NMR (125 MHz, DMSO) δ 173.6 (s, *C*OOH), 172.4 (s, *C*OOCH$_2$), 156.2 (s, qC_{Ar}), 135.3 (s, C_e or C_f), 134.8 (s, C_e or C_f), 130.1 (s, C_{Ar}), 128.4 (s, qC_{Ar}), 115.5 (s, C_{Ar}), 64.8 (s, *C*H$_2$(A)), 49.0 (s, C_g), 48.5 (s, C_b or C_c), 47.7 (s, C_b or C_c), 46.3 (s, C_a or C_d), 46.0 (s, C_a or C_d), 33.9 (s, *C*H$_2$(B)). IR (ATR): 3222, 2979, 1718 1613, 1565, 1514, 1449, 1388,

1346, 1245, 1171, 1105, 1043 cm^{-1}. HRMS (ESI+): m/z calculated for $C_{17}H_{18}O_5$ + Na $[M+Na]^+$: 325.1052, found 325.1045.

2-*endo*-*N*-(β-D-galactopyranosyl-1,2,3-triazol-4-ylmethylamino)-3-*endo*-farnesylcarbonyl-bicyclo[2.2.1]hept-5-ene-2-*endo*-carboxamide-3-*endo*-carboxylic acid farnseyl ester 2.80

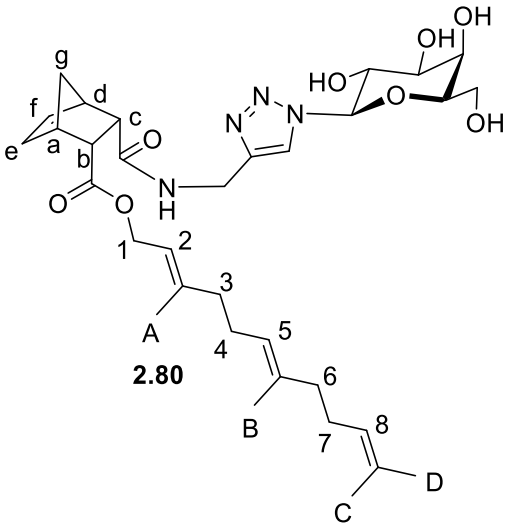

2.78 (106 mg, 0.27 mmol, 1 equiv.) and COMU (235 mg, 0.54 mmol, 2 equiv.) were placed under N_2 in a round-bottomed flask and dissolved in anhydrous DMF (5 mL), **2.67** (143 mg, 0.54 mmol, 2 equiv.) was placed under N_2 in a separate round-bottomed flask and dissolved in anhydrous DMF (2 mL). The RBF containing **2.78** was stirred for 30 mins after which N,N-DIPEA (0.1 mL, 0.54 mmol, 2 equiv.) was added and this was stirred for 30 mins. The **2.67** solution was then added via a cannula to the reaction mixture over the course of approx. 5 mins. The reaction mixture was stirred overnight at RT, following TLC analysis (90:10 DCM:MeOH) the solvent was removed *in vacuo*, with the water bath set to 40°C. The crude mixture was ran through the puriflash automated column chromatography using lambda max of 242nm in a gradient of 100:0 DCM:MeOH to 0:100 DCM:MeOH. Following this fractions that appeared to contain product (R_f (MeOH)= 0.77) were then washed with deionised water. When the product was attempted to be analysed by NMR in MeOD, a precipitate appeared in the NMR tube so the sample was washed with MeOH to separate product **2.80** from precipitate. (partially pure, 7 mg, 4%).

^{1}H NMR (500 MHz, DMSO) δ 8.26 (dd, *J* = 10.8, 5.3 Hz, 1H, N*H*), 7.96 (d, *J* = 5.8 Hz, 1H, triaz-H), 6.20 (s, 1H, $H_{e/f}$), 5.92 (ddd, *J* = 17.1, 10.1, 7.3 Hz, 1H, $H_{e/f}$), 5.46 (dd, *J* = 9.2,

1.0 Hz, 1H, H-1), 5.32 – 5.14 (m, H_2), 5.14 – 5.03 (m, H_5 & H_8), 4.48 – 4.38 (m, 1H, $H_1/_{1'}$), 4.33 (td, *J* = 14.9, 6.0 Hz, 1H, NHC*H*$_2$), 4.29 – 4.18 (m, 1H, $H_1/_{1'}$), 4.16 – 4.05 (m, 1H, NHC*H*$_2$), 4.01 (s, 1H, H-2), 3.77 (s, 1H, H-4), 3.70 (t, *J* = 4.8 Hz, 1H, H-5), 3.54 (d, *J* = 9.2 Hz, 2H, H-3 & H-6/6'), 3.47 (s, 1H, H-6/6'), 3.29 – 3.22 (m, 1H, $H_{b/c}$), 3.14 (ddd, *J* = 12.5, 7.9, 4.5 Hz, 1H, $H_{b/c}$), 3.01 (s, 1H, $H_{a/d}$), 2.96 (s, 1H, $H_{a/d}$), 2.12 – 1.89 (m, 12H, H_3 & $H_{3'}$, H_4 & $H_{4'}$, H_6 & $H_{6'}$, H_7 & $H_{7'}$), 1.65 (dt, *J* = 10.3, 8.0 Hz, 10H, CH_3(A-D)), 1.59 – 1.53 (m, 8H, CH_3(A-D)), 1.25 (dt, *J* = 15.0, 7.4 Hz, 3H, $H_{g/g'}$).

^{13}C NMR (125 MHz, DMSO) δ 172.6 (s, *C*OOCH$_2$), 171.3 (s, NH*C*O), 145.4 (s, qC_{triaz}), 140.8 (s, qC next to CH_3 (A-D)), 135.1 (s, $C_{e/f}$), 134.0 (s, $C_{e/f}$), 131.1 (s, qC next to CH_3 (A-D)z), 124.5 (d, *J* = 2.0 Hz, C_5 & C_8), 121.7 (s, C_{triaz}), 119.5 (s, C_2), 88.5 (s, C-1), 78.7 (s, C-5), 74.2 (s, C-3), 69.8 (s, C-2), 68.8 (s, C-4), 60.8 (s, C-6), 60.5 (s, C_1), 48.6 (s, C_g), 48.3 (s, $C_{b/c}$), 47.2 (s, $C_{a/d}$), 45.5 (s, $C_{a/d}$), 39.3 (s, $C_{6/7}$), 34.8 (s, *C*H$_2$NH), 31.9 (s, $C_{6/7}$), 26.6 (s, $C_{6/7}$), 26.4 (s, CH_3 (A-D)), 23.6 (s, CH_3 (A-D)), 18.0 (s, CH_3 (A-D)), 16.2 (s, CH_3 (A-D)). HRMS (ESI+): m/z calculated for $C_{33}H_{48}N_4O_8$ + Na $[M+Na]^+$: 651.3370, found 651.3368.

2-*endo*-*N*-(β-D-galactopyranosyl-1,2,3-triazol-4-ylmethylamino)- 3-*endo*-tyrosolcarbonyl-bicyclo[2.2.1]hept-5-ene-2-*endo*-carboxamide-3-*endo*-carboxylic acid tyrosol ester 2.81

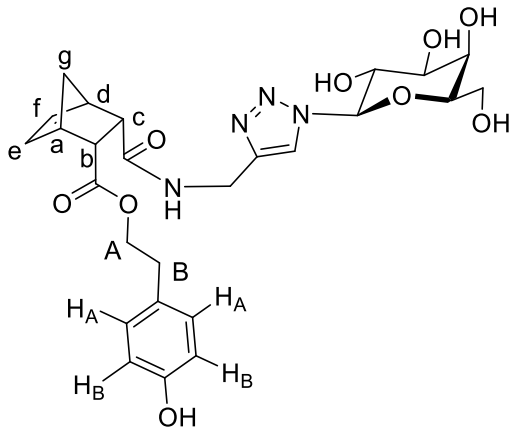

2.81

2.79 (50 mg, 0.16 mmol, 1 equiv.) and TBTU (79 mg, 0.24 mmol, 1.5 equiv.) were placed under N_2 in a round-bottomed flask and dissolved in anhydrous DMF (4 mL), **2.67** (64 mg, 0.24 mmol, 1.5 equiv.) was placed under N_2 in a separate round-bottomed flask and dissolved in anhydrous DMF (2 mL). The RBF containing **2.79** was stirred for 30 mins after which N,N-DIPEA (14.4 µL, 0.08 mmol, 0.5 equiv.) was added and this was stirred for 30 mins. The solution of **2.67** was then added via a cannula

to the reaction mixture over the course of approx. 5 mins. The reaction mixture was stirred overnight at RT, following TLC analysis (90:10 DCM:MeOH) the solvent was removed *in vacuo*, with the water bath set to 40°C. The reaction was rerun using TBTU (105 mg, 0.32 mmol, 2 equiv.), **2.67** (60 mg, 2.2 mmol), N,N-DIPEA (30 µL) using the same procedure as used previously. Following the same workup and NMR analysis, the reaction was put back on again using the same procedure and the following reagents: TBTU (210 mg, 4 equiv.), N,N-DIPEA (30 µL). Following stirring overnight at RT and TLC analysis, the solvent was removed in vacuo (water bath at 40°C) and the crude mixture was washed 3 times with MeOH and centrifuged, recovering the supernatant each time. This was then stirred in DCM for 1 h and the solid formed (precipitate) was then washed many times with DCM and centrifuged. The resulting crude mixture was ran through the puriflash automated column chromatography using lambda max of 228 nm in a gradient of 100:0 DCM:MeOH to 0:100 DCM:MeOH. Following this, fractions that appeared to contain product (R_f(MeOH)= 0.8) were then washed with DCM . When the product was attempted to be analysed by NMR in MeOD, a precipitate appeared in the NMR tube, so the sample was washed with MeOH to separate product from precipitate. The supernatant was collected, solvent removed *in vacuo* to yield the product **2.81** as a colourless oil (10 mg, 12%). R_f (MeOH)= 4.5/5.6= 0.8.

^{1}H NMR (500 MHz, MeOD) δ 8.27 (dd, *J* = 10.5, 5.4 Hz, 1H, N*H*), 8.06 (d, *J* = 6.9 Hz, 1H, triaz-H), 7.04 (d, *J* = 7.9 Hz, 2H, H_A), 6.75 – 6.67 (m, 2H, H_B), 6.19 (ddd, *J* = 10.3, 5.5, 3.0 Hz, 1H, $H_{e/f}$), 6.07 – 5.98 (m, 1H, $H_{e/f}$), 5.53 (dt, *J* = 4.9, 3.8 Hz, 1H, H_1), 4.40 (ddd, *J* = 18.9, 11.9, 4.7 Hz, 1H, C*H*$_2$-triaz), 4.29 (dt, *J* = 12.0, 5.3 Hz, 1H, C*H*$_2$-triaz), 4.20 – 4.09 (m, 2H, H_2 & CH_2(A)), 4.05 – 3.95 (m, 2H, H_4 & CH_2(A)), 3.86 – 3.78 (m, 1H, H_5), 3.77 – 3.72 (m, 2H, $H_{6/7}$), 3.69 (ddd, *J* = 10.9, 6.7, 4.2 Hz, 1H, H_3), 3.30 – 3.26 (m, 1H, $H_{b/c}$), 3.25 – 3.18 (m, 1H, $H_{b/c}$), 3.09 – 2.99 (m, 2H, $H_{a/d}$), 2.81 – 2.67 (m, 2H, CH_2(B)), 1.41 – 1.31 (m, 2H, $H_{g/g'}$).

^{13}C NMR (125 MHz, MeOD) δ 174.7 (s, CO), 174.4 (s, *C*ONH), 156.85 (s, qC_{Ar}), 146.6 (s, qC_{triaz}), 136.5 (s, $C_{e/f}$), 134.8 (s, $C_{e/f}$), 130.9 (s, qC_{Ar}), 130.4 (s, *C*H_A), 123.1 (s, C_{triaz}), 116.1 (s, *C*H_B), 90.1 (s, C-1), 79.8 (s, C-5), 75.2 (s, C-3), 71.3 (s, C-2), 70.2 (s, C-4), 66.3 (s, *C*H_2(A)), 62.3 (s, $C_{6/7}$), 50.1 (s, $C_{b/c}$), 49.9 (s, $C_{b/c}$), 46.9 (d, *J* = 2.3 Hz, $C_{a/d}$), 35.7 (s, NH*C*H_2), 35.0 (s, *C*H_2(B)). IR (ATR): 3303, 1715, 1651, 1515, 1453, 1335, 1223, 1184,

1091, 1053 cm^{-1}. HRMS (ESI+): m/z calculated for $C_{26}H_{32}N_4O_9$ - H $[M-H]^-$: 543.2097, found 543.2098.

7.2.2 Experimental procedures for Chapter 3

5-[[(1,1-Dimethylethoxy)carbonyl]amino]-1,3-benzenedicarboxylic acid 3.14

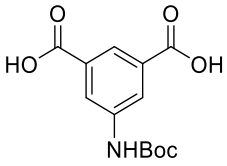

3.14

5-Aminoisophthalic acid (1 g, 5.5 mmol) was dissolved in aqueous NaOH (1 N, 10 mL) at 0 ^oC. Di-*tert*-butyl dicarbonate (1.32 g, 6.05 mmol) was dissolved in 1,4-dioxane (12 mL), which was added dropwise to the other solution over 2 h. The reaction mixture was stirred at 0-5 ^oC for 3 h, and then left to stir overnight at RT. The reaction mixture was evaporated to half it's original volume *in vacuo* and then cooled in an ice-bath. The solution was acidified to pH 5 with HCl 1 M solution. The precipitated was filtered and washed with water. The product was allowed to anhydrous in the fumehood overnight to give the pure product **3.14** as an off-white solid (1.34 g, 86%). ^1H NMR (500 MHz, DMSO) δ 9.79 (s, 1H, NH), 8.30 (appd, *J* = 1.5 Hz, 2H, Ar-H), 8.08 (appt, *J* = 1.6 Hz, 1H, Ar-H), 1.48 (s, 9H, $C(CH_3)_3$).

The NMR data is in agreement with the data reported in the literature [210].

***N,N'*-di(prop-2-yn-1-yl)-5-[[(1,1-Dimethylethoxy)carbonyl]amino]isophthalamide 3.15**

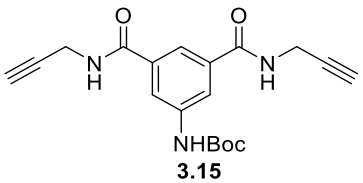

3.15

3.14 (3 g, 12 mmol) and TBTU (8 g, 25 mmol) were suspended in anhydrous DMF (22 mL) under N_2. After 10 mins, Propargylamine (1.60 mL, 25 mmol) was added dropwise followed by triethylamine (3.70 mL, 26 mmol). The solution was left to stir for 2 h at RT. The resulting solution was poured over ice and sat. Sat. $NaHCO_3$ solution (100 mL) and stirred until the ice melted, a creamy white precipitate formed readily. This was filtered on a sintered glass funnel and dried on a Schlenk line to give **3.15** as

a white solid (2.34 g, 55%). ^{1}H NMR (500 MHz, DMSO) δ 9.65 (s, 1H, N*H*Boc), 8.90 (t, *J* = 5.6 Hz, 2H, N*H*CH_2CCH), 8.02 (s, 2H, Ar-H), 7.83 (s, 1H, Ar-H), 4.04 (dd, *J* = 5.6, 2.5 Hz, 4H, C*H*$_2$CCH), 3.11 (t, *J* = 2.5 Hz, 2H, CH_2CC*H*), 1.48 (s, 9H, C(C*H*$_3$)$_3$).

The NMR data is in agreement with the data reported in the literature [210].

2,3,4-tri-*O*-acetyl-1-β-azido-L-fucopyranoside 3.16

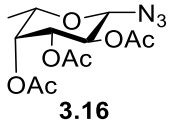

3.16

$TMSN_3$ (1.23 mL, 9.35 mmol, 1.45 equiv) was added to a solution of β-L-fucose tetraaacetate (2.13 g, 6.41 mmol) in anhydrous DCM (20 mL). $SnCl_4$ (0.37 mL, 3.16 mmol, 0.5 equiv) was added to this solution and the reaction mixture was stirred at RT for 18 h. Sat. $NaHCO_3$ solution (30 mL) was added and the suspension was extracted with DCM (2 x 30 mL). The combined organic layers were dried over $MgSO_4$, filtered and concentrated in vacuo to afford **3.16** as an off-white solid which recrystallised using hot ethanol, to yield **3.16** as a white solid (1.54 g, 76%).

^{1}H NMR (500 MHz, $CDCl_3$) δ 5.26 (dd, *J* = 3.4, 1.0 Hz, 1H, H-4), 5.14 (dd, *J* = 10.4, 8.7 Hz, 1H, H-2), 5.03 (dd, *J* = 10.3, 3.4 Hz, 1H, H-3), 4.58 (d, *J* = 8.7 Hz, 1H, H-1), 3.90 (qd, *J* = 6.4, 1.1 Hz, 1H, H-5), 2.19 (s, 6H, CH_3 of OAc), 2.08 (s, 6H, CH_3 of OAc), 1.99 (s, 6H, CH_3 of OAc), 1.57 (s, 3H, C-6 CH_3).

The NMR data is in agreement with the data reported in the literature [117].

***N,N'*-di-(2,3,4,6-tetra-*O*-acetyl-β-D-galactopyranosyl-1,2,3-triazol-4-ylmethylamide)-*N''*-*tert*-butoxycarbonyl-5-aminobenzene-1,3-dicarboxamide 3.17**

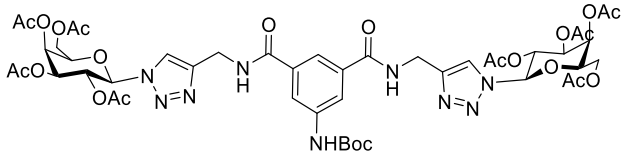

3.17

Copper sulphate pentahydrate (60 mg) and sodium ascorbate (120 mg) were added to a solution of **2.40** (1.27 g, 3.39 mmol) and **3.15** (570 mg, 1.62 mmol) in acetone/H_2O (4 mL/ 2mL). The reaction was allowed to stir at 100 ^{o}C in the MW until deemed complete by TLC analysis (30 mins). The solvent was removed *in vacuo*. The residue was dissolve in DCM (30 mL), washed with water (20 mL x 3), and dried ($MgSO_4$). The mixture was filtered and the solvent was removed *in vacuo* to yield the

crude product, which was purified by silica gel column chromatography (DCM:MeOH 98:2-93:7) to give the pure product **3.17** as a white solid (1.25 g, 71%). R_f = 0.38 (DCM:MeOH 9:1).

^{1}H NMR (500 MHz, $CDCl_3$): δ 8.08 (s, 2H, Ar-H), 7.98 – 7.84 (m, 4H, triaz-H and N*H*CH_2-triaz), 7.81 (bs, 2H, Ar-H and N*H*Boc), 5.95 (d, *J* = 9.2 Hz, 2H, H-1), 5.48 (t, *J* = 9.7 Hz, 4H, H-2 and H-4), 5.27 (dd, *J* = 10.3, 3.1 Hz, 2H, H-3), 4.63 (dd, *J* = 15.0, 5.1 Hz, 4H, C*H*$_2$-triaz), 4.31 (t, *J* = 6.4 Hz, 2H, H-5), 4.09 (dd, *J* = 11.5, 6.4 Hz, 4H, H-6 and H-6'), 2.14 (s, 6H, OAc), 1.92 (overlapping of 2 s, 12H, OAc x2), 1.72 (s, 6H, OAc), 1.41 (s, 9H, Boc). ^{13}C NMR (125 MHz, $CDCl_3$): δ 170.3 (CO of OAc), 170.1 (CO of OAc), 169.8 (CO of OAc), 169.0 (CO of OAc), 166.7 (*C*ONHCH$_2$-triaz), 152.8 (CO of Boc), 145.5 (*C*-triaz), 139.9 (Ar-C), 134.9 (Ar-C), 121.8 (CH_2-triaz), 120.5 (Ar-CH), 119.3 (Ar-CH), 86.0 (C-1), 73.8 (C-5), 70.8 (C-3), 68.1 (C-2), 67.0 (C-4), 61.2 (C-6), 35.3 (*C*H_2-triaz), 28.2 (CH_3 of Boc), 20.6 (CH_3 of OAc), 20.8 (CH_3 of OAc), 20.5 (CH_3 of OAc), 20.1 (CH_3 of OAc). IR (film on NaCl): 3434, 2106, 1752, 1648, 1558 cm^{-1}. HRMS (ESI+): *m/z* calcd for $C_{47}H_{59}N_9O_{22}$ + H^+ $[M+H]^+$ 1102.3853, found 1102.3847.

***N,N'*-di-(2,3,4-tri-O-acetyl-β-D-fucopyranosyl-1,2,3-triazol-4-ylmethylamide)-*N''*-*tert*-butoxycarbonyl-5-aminobenzene-1,3-dicarboxamide 3.18**

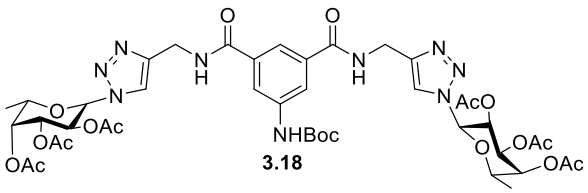

3.18

3.15 (640 mg, 1.8 mmol), **3.16** (1.25 g, 3.96 mmol), Copper sulfate pentahydrate (200 mg) and sodium ascorbate (250 mg) were dissolved in ACN/H_2O (12 mL/3 mL) and reacted in the microwave at 100 ^{o}C until the reaction was deemed complete by TLC analysis (90:10 DCM:MeOH). The solvent was then removed in vacuo and the resulting residue was extracted using DCM and brine, the organic phase was dried ($MgSO_4$), filtered and the solvent was removed *in vacuo*. The product was purified by flash column chromatography (99:1-95:5 DCM:MeOH) to give **3.18** as a white solid (1.26 g, 71%).

^{1}H NMR (500 MHz, $CDCl_3$) δ 8.02 (s, 2H, Ar_H), 7.96 (s, 2H, triaz-H), 7.85 (s, 1H, Ar_H), 7.67 (s, 2H, N*H*), 7.16 (s, 1H, N*H*Boc), 5.86 (d, *J* = 9.2 Hz, 2H, H-1), 5.52 – 5.44 (m, 2H,

H-2), 5.38 (dd, *J* = 3.4, 0.8 Hz, 2H, H-4), 5.25 (dd, *J* = 10.3, 3.4 Hz, 2H, H-3), 4.76 (dd, *J* = 15.2, 5.8 Hz, 2H, C*H*$_2$), 4.63 (dd, *J* = 15.1, 5.6 Hz, 2H, C*H*$_2$), 4.16 (q, *J* = 6.4 Hz, 2H, H-5), 2.23 (s, 6H, CH_3 of OAc), 1.99 (s, 6H, CH_3 of OAc), 1.82 (s, 6H, CH_3 of OAc), 1.50 (s, 9H, Boc C*H*$_3$), 1.24 (d, *J* = 6.4 Hz, 6H, C-6 CH_3).

^{13}C NMR (125 MHz, $CDCl_3$) δ 170.5 (s, CO of OAc), 169.9 (s, CO of OAc), 169.2 (s, CO of OAc), 166.5 (s, *C*ONH), 145.3 (s, qC-triaz), 139.6 (s, qC_{Ar}), 135.0 (s, qC_{Ar}), 121.5 (s, C-triaz), 120.4 (s, C_{Ar}), 119.4 (s, C_{Ar}), 86.2 (s, C-1), 72.6 (s, C-5), 71.1 (s, C-3), 69.8 (s, C-4), 68.2 (s, C-2), 35.3 (s, CH_2), 28.2 (s, Boc *C*H$_3$), 20.7 (s, CH_3 of OAc), 20.5 (s, CH_3 of OAc), 20.2 (s, CH_3 of OAc), 16.0 (s, C-6). IR (ATR): 1747, 1367, 1213, 1156, 1092, 1061 cm^{-1}. HRMS (ESI+): m/z calcd for $C_{43}H_{56}N_9O_{18}$ + H^+ [M+H$^+$]: 986.3743, found 986.3767.

***N, N'*-di-(2,3,4,6-tetra-*O*-acetyl-β-D-galactopyranosyl-1,2,3-triazol-4-ylmethylamide)-5-aminobenzene-1,3-dicarboxamide 3.19**

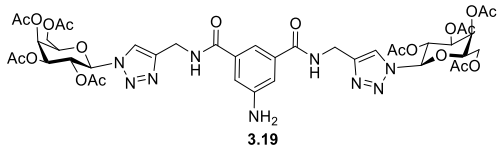

3.19

Compound **3.17** (725 mg, 0.66 mmol) was dissolved in DCM (5 mL) and was cooled to 0 ^{o}C in an ice-bath. TFA (1.5 mL) was added and the reaction mixture was stirred at RT for 2 h. DCM (40 mL) was added to the reaction mixture, it was washed with sat. $NaHCO_3$ (40 mL) and brine (40 mL), and dried ($MgSO_4$). The mixture was filtered and the solvent was removed *in vacuo* to yield the product **3.19** which was used without further purification: pale yellow solid (689 mg, 99%). R_f = 0.53 (DCM:MeOH 9:1).

^{1}H NMR (500 MHz, $CDCl_3$): δ 7.95 (s, 4H, triaz-H, N*H*CH_2-triaz), 7.43 (s, 1H, Ar-H), 7.17 (s, 2H, Ar-H), 5.96 (d, *J* = 9.2 Hz, 2H, H-1), 5.50 (m, 4H, H-2 and H-4), 5.29 (dd, *J* = 10.3, 3.3 Hz, 2H, H-3), 4.59 (dd, *J* = 15.1, 5.6 Hz, 4H, C*H*$_2$-triaz), 4.32 (t, *J* = 6.5 Hz, 2H, H-5), 4.23 – 4.00 (m, 4H, H-6 and H-6'), 2.16 (s, 6H, OAc), 1.94 (s, 12H, OAc), 1.73 (s, 6H, OAc). ^{13}C NMR (125 MHz, d_6-DMSO) δ 170.5 (CO of OAc), 170.4 (CO of OAc), 169.9 (CO of OAc), 169.0 (CO of OAc), 167.1 (*C*ONHCH_2-triaz), 146.1 (C-triaz), 135.6 (Ar-C), 122.8 (CH-triaz), 115.7 (Ar-CH) 113.8 (Ar-CH) 84.7 (C-1), 73.4 (C-5), 71.0 (C-3), 68.1 (C-2), 67.8 (C-4), 62.0 (C-6), 35.1 (*C*H_2NH), 21.0 (CH_3 of OAc), 20.9 (CH_3 of OAc), 20.8 (CH_3 of OAc), 20.5 (CH_3 of OAc). IR (film on NaCl): 3434, 2103, 1751, 1642, 1534 cm^{-1}. HRMS (ESI+): *m/z* calcd for $C_{42}H_{51}N_9O_{20}$ + H^+ [M+H]$^+$ 1002.3329, found 1002.3323.

***N, N'*-di-(2,3,4-tri-O-acetyl-β-D-fucopyranosyl -1,2,3-triazol-4-ylmethylamide)-5-aminobenzene-1,3-dicarboxamide 3.20**

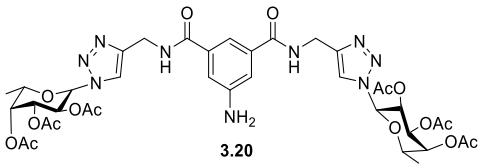

3.20

3.18 (1.26 g, 1.28 mmol) was dissolved in DCM (12 mL) and placed on ice, TFA (2.6 mL) was then gradually added and the reaction mixture was stirred at RT until deemed complete via TLC analysis (90:10 DCM:MeOH) (5 h). Sat. $NaHCO_3$ (40 mL) was then gradually added to the reaction mixture and stirred for 2-3mins, an extraction was then carried out using DCM and brine. The organic phase was dried ($MgSO_4$), filtered and the solvent was removed *in vacuo* to yield the pure product **3.20** as a white solid (715 mg, 63%).

^{1}H NMR (500 MHz, DMSO) δ 8.82 (t, *J* = 5.7 Hz, 2H, N*H*), 8.06 (s, 2H, triaz-H), 7.44 (s, 1H, Ar_H), 7.16 (s, 2H, Ar_H), 6.16 (d, *J* = 9.3 Hz, 2H, H-1), 5.57 (t, *J* = 9.7 Hz, 2H, H-2), 5.45 (s, 2H, NH_2), 5.39 (dd, *J* = 10.2, 3.5 Hz, 2H, H-3), 5.25 (d, *J* = 3.2 Hz, 2H, H-4), 4.48 (d, *J* = 5.6 Hz, 4H, CH_2), 4.37 (q, *J* = 6.2 Hz, 2H, H-5), 2.19 (s, 6H, CH_3 of OAc), 1.95 (s, 6H, CH_3 of OAc), 1.80 (s, 6H, CH_3 of OAc), 1.10 (d, *J* = 6.4 Hz, 6H, C-6 CH_3).

^{13}C NMR (125 MHz, DMSO) δ 170.7 (s, CO of OAc), 169.9 (s, CO of OAc), 169.0 (s, CO of OAc), 167.0 (s, CO), 149.2 (s, qC_{Ar}), 145.9 (s, qC-triaz), 135.6 (s, qC_{Ar}), 122.6 (s, C-triaz), 115.7 (s, C_{Ar}), 113.7 (s, C_{Ar}), 84.7 (s, C-1), 71.8 (s, C-5), 71.3 (s, C-3), 70.3 (s, C-4), 68.1 (s, C-2), 35.1 (s, CH_2), 20.9 (s, CH_3 of OAc), 20.8 (s, CH_3 of OAc), 20.5 (s, CH_3 of OAc), 16.0 (s, C-6). IR (ATR): 1745, 1367, 1212, 1092, 1061, 1042, 1020 cm^{-1}. HRMS (ESI+): m/z calcd for $C_{38}H_{48}N_9O_{16}$ + H^+ [M+H^+]: 886.3219, found 886.3210.

***N*, *N*'-di-(2,3,4,6-tetra-*O*-acetyl-β-D-galactopyranosyl-1,2,3-triazol-4-ylmethylamide)-N''-(1-oxo-2-propen-1-yl)-5-aminobenzene-1,3-dicarboxamide 3.21**

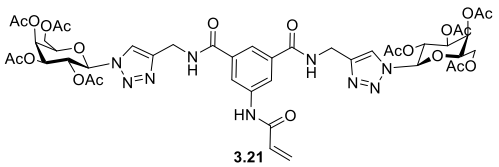

3.21

3.19 (391 mg, 0.39 mmol) was placed under N_2 and dissolved in anhydrous DCM (20 mL), after stirring for 5 mins NEt_3 (65 µL, 0.47 mmol, 1.2 equiv) was added and the reaction mixture was stirred for 5 mins. Acryloyl chloride (37.5 µL, 0.47 mmol, 1.2 equiv) was added and the reaction mixture was stirred overnight at RT. Following TLC analysis (90:10), the solvent was removed *in vacuo*, the crude residue was dissolved in DCM and extracted using deionised water, 1M HCl, sat. $NaHCO_3$ solution and brine. The organic phase was dried (Na_2SO_4), filtered and concentrated *in vacuo*. The crude product was then purified by flash column chromatography (99:1-95:5 DCM:MeOH) to yield the pure product **3.21** as a white solid (246 mg, 60%).

^{1}H NMR (500 MHz, $CDCl_3$) δ 9.08 (s, 1H, N*H*COCHCH$_2$), 8.13 – 7.89 (m, 6H, H$_{Ar}$, C*H*-triaz & N*H*), 7.77 (s, 1H, H$_{Ar}$), 6.31 (q, *J* = 16.8 Hz, 2H, COC*H*CH$_2$ & COCHC*H*$_2$), 5.92 (d, *J* = 9.2 Hz, 2H, H-1), 5.65 (d, *J* = 10.0 Hz, 1H, COCHC*H*$_2$), 5.60 (t, *J* = 9.7 Hz, 2H, H-2), 5.53 (d, *J* = 2.6 Hz, 2H, H-4), 4.65 (dd, *J* = 36.0, 10.8 Hz, 4H, C*H*$_2$-triaz), 4.30 (t, *J* = 6.0 Hz, 2H, H-5), 4.15 (qd, *J* = 11.5, 6.6 Hz, 4H, H-6/7), 2.16 (d, *J* = 17.1 Hz, 6H, CH_3 of OAc), 1.98 (s, 12H, CH_3 of OAc), 1.79 (s, 6H, CH_3 of OAc).

^{13}C NMR (125 MHz, $CDCl_3$) δ 170.3 (s, CO of OAc), 170.1 (s, CO of OAc), 169.8 (s, CO of OAc), 169.2 (s, CO of OAc), 166.7 (s, CO), 164.1 (s, CO-acryloyl), 145.5 (s, qC-triaz), 139.0 (s, qC$_{Ar}$), 134.8 (s, qC$_{Ar}$), 131.0 (s, C$_e$), 128.1 (s, C$_f$), 121.6 (s, C$_{Ar}$ & C-triaz), 121.4 (s, C$_{Ar}$ & C-triaz), 121.0 (s, C$_{Ar}$), 86.1 (s, C-1), 73.9 (s, C-5), 70.8 (s, C-3), 68.0 (s, C-2), 66.9 (s, C-4), 61.1 (s, C-6), 35.4 (s, CH_2), 20.6 (s, CH_3 of OAc), 20.6 (s, CH_3 of OAc), 20.4 (s, CH_3 of OAc), 20.2 (s, CH_3 of OAc). IR (ATR): 1744, 1367, 1208, 1091, 1044 cm^{-1}. HRMS (ESI+): m/z calcd for $C_{45}H_{53}N_9O_{21}$ + Na^+ [M+Na]: 1078.3254, found 1078.3253.

***N*, *N*'-di-(2,3,4-tri-O-acetyl-β-D-fucopyranosyl -1,2,3-triazol-4- ylmethylamide)-N''-(1-oxo-2-propen-1-yl)-5-aminobenzene-1,3-dicarboxamide 3.22**

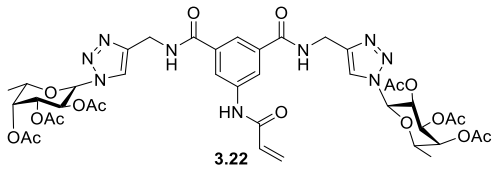

3.22

3.20 (81 mg, 0.09 mmol) was placed under N_2 and dissolved in anhydrous DCM (14 mL), after stirring for 5 mins NEt_3 (15 µL, 0.11 mmol, 1.2 equiv) was added and the reaction mixture was stirred for 5 mins. Acryloyl chloride (30 µL, 0.36 mmol) was added and the reaction mixture was stirred overnight at RT. Following TLC analysis (90:10), the solvent was removed *in vacuo*, the crude residue was dissolved in DCM and extracted using deionised water, 1M HCl, sat. $NaHCO_3$ solution and brine. The organic phase was dried (Na_2SO_4), filtered and concentrated *in vacuo*. The crude product was then purified by flash column chromatography (95:5-92:8 DCM:MeOH) to yield the pure product **3.22** as a white solid (41 mg, 48%).

^{1}H NMR (500 MHz, $CDCl_3$) δ 9.32 (s, 1H, N*H*), 8.19 (t, *J* = 5.4 Hz, 2H, N*H*), 8.00 (s, 2H, Ar_H), 7.97 (s, 2H, triaz-H), 7.78 (s, 1H), 6.38 – 6.24 (m, 2H, COC*H*CH_2 & COCHC*H*$_2$), 5.82 (d, *J* = 9.2 Hz, 2H, H-1), 5.65 (dd, *J* = 9.1, 2.5 Hz, 1H, COCHC*H*$_2$), 5.54 (dd, *J* = 10.1, 9.4 Hz, 2H, H-2), 5.39 – 5.34 (m, 2H, H-4), 5.27 – 5.21 (m, 2H, H-3), 4.64 (qd, *J* = 15.4, 5.6 Hz, 4H, CH_2), 4.17 – 4.10 (m, 2H, H-5), 2.20 (s, 6H, CH_3 of OAc), 1.98 (s, 6H, CH_3 of OAc), 1.83 (s, 6H, CH_3 of OAc), 1.22 (d, *J* = 6.4 Hz, 6H, C-6 CH_3).

^{13}C NMR (125 MHz, $CDCl_3$) δ 169.2 (s, CO of OAc), 168.4 (s, CO of OAc), 168.2 (s, CO of OAc), 165.5 (s, *C*ONHCH$_2$triaz), 163.0 (s, *C*OCHCH$_2$), 144.0 (s, qC-triaz), 137.5 (s, qC$_{Ar}$), 133.4 (s, qC$_{Ar}$), 129.6 (s, C$_e$), 126.8 (s, C$_f$), 120.1 (s, C$_{Ar}$ & C-triaz), 119.9 (s, C$_{Ar}$), 84.9 (s, C-1), 71.4 (s, C-5), 69.8 (s, C-3), 68.5 (s, C-4), 66.8 (s, C-2), 34.0 (s, CH_2), 19.3 (s, CH_3 of OAc), 19.2 (s, CH_3 of OAc), 19.0 (s, CH_3 of OAc), 14.7 (s, C-6). IR (ATR): 1746, 1367, 1212, 1092, 1061, 1042 cm^{-1}. HRMS (ESI+): m/z calcd for $C_{41}H_{49}N_9NaO_{17}$ + Na^+ [M+Na^+]: 962.3144, found 962.3124.

***N'*,*N''*-di-(2,3,4,6-tetra-O-acetyl-β-D-galactopyranosyl)-1H-1,2,3-triazol-4-yl)methyl))-5-(vinylsulfonamido)isophthalamide 3.23**

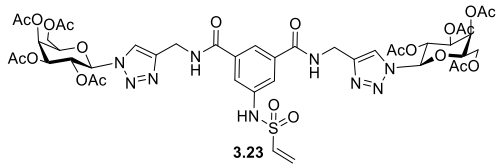

3.19 (303 mg, 0.30 mmol) was dissolved in dry DCM (15 mL). NEt_3 (84 µL, 0.61 mmol) was added to this solution. 2-chloroethanesulfonyl chloride (0.038 mL, 0.36 mmol) was dissolved in dry DCM (15 mL) in a separate round-bottom flask. The first solution was added to the second dropwise via a cannula and the resulting reaction mixture was allowed to stir for 16 h. The reaction mixture was washed with water (20 mL), HCl (1 N, 20 mL), sat. $NaHCO_3$ solution (20 mL), followed by brine (20 mL). The organic phase was dried ($MgSO_4$), and the solvent was removed in vacuo to obtain the crude product which was purified via column chromatography (97:3 – 9:1 DCM: MeOH) to give the pure product **3.23** as a brown, sticky solid (158 mg, 48%). R_f= 0.28 (Ethyl acetate). ^{1}H NMR: ^{1}H NMR (500 MHz, $CDCl_3$) δ 8.04 (s, 2H, CH-triaz), 7.96 (s, 1H, Ar-H), 7.94 (s, 2H, Ar-H), 7.87 (s, 2H, N*H*CO), 6.56 (dd, *J* = 16.5, 9.9 Hz, 1H, *H*C=CH_2), 6.26 (d, *J* = 16.5 Hz, 1H, C=C*H*$_2$), 5.96 (d, *J* = 9.2 Hz, 2H, H-1), 5.93 (d, *J* = 9.9 Hz, 1H, C=C*H*$_2$), 5.57 – 5.54 (m, 4H, H-2 & H-4), 5.32 – 5.30 (m, 2H, H-3), 4.82 – 4.61 (m, 4H, $NHCH_2$-triaz), 4.32 (t, *J* = 6.6 Hz, 2H, H-5), 4.20 – 4.13 (m, 4H, H-6 and H-6'), 2.22 (s, *J* = 5.1 Hz, 6H, OAc), 2.01 (d, *J* = 4.6 Hz, 12H OAc x 2), 1.84 (s, 6H, OAc).^{13}C NMR (125 MHz, $CDCl_3$) δ 170.4 (s, CO of OAc), 170.1 (s, CO of OAc), 169.8 (s, CO of OAc), 169.2 (s, CO of OAc), 166.1 (s, *C*O$NHCH_2$), 145.1 (s, qC_{triaz}), 135.4 (s, qC_{Ar}), 135.1 (s, SO_2*C*HCH_2), 128.8 (s, SO_2CH*C*H_2), 122.1 (s, C-triaz), 121.7 (s, C_{Ar}), 121.2 (s, C_{Ar}), 86.1 (s, C-1), 73.9 (s, C-5), 70.7 (s, C-3), 68.1 (s, C-2), 66.8 (s, C-4), 61.1 (s, C-6), 53.4 (s, DCM), 35.2 (s, NH*C*H_2-triaz), 20.7 (s, CH_3 of OAc), 20.6 (s CH_3 of OAc), 20.5 (s CH_3 of OAc), 20.2 (s, CH_3 of OAc). IR (ATR): 2965, 2918, 1746, 1655, 1533, 1432, 1368, 1329, 1210, 1157, 1045 cm^{-1}. HRMS (ESI+): m/z calcd for $C_{44}H_{53}N_9O_{22}S$ + H^+ $(M+H)^+$ 1091.30, found 1092.3089.

***N'*,*N''*-di-(2,3,4-tri-O-acetyl-β-D-fucopyranosyl-1,2,3-triazol-4-ylmethylamide)-1H-1,2,3-triazol-4-yl)methyl))-5-(vinylsulfonamido)isophthalamide 3.24**

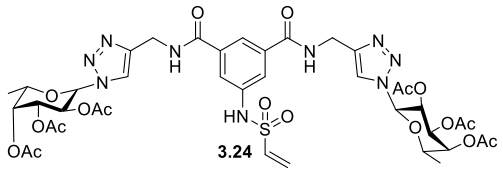

3.20 (124 mg, 0.15 mmol) was dissolved in dry DCM (10 mL). NEt_3 (50 µL, 0.34 mmol) was added to this solution. 2-chloroethanesulfonyl chloride (25 µL, 0.23 mmol) was dissolved in dry DCM (10 mL) in a separate round-bottom flask. The first solution was added to the second dropwise via a cannula and the resulting reaction mixture was allowed to stir for 16 h at RT. The reaction mixture was washed with water (20 mL), HCl (1 N, 20 mL), sat. $NaHCO_3$ solution (20 mL), followed by brine (20 mL). The organic phase was dried ($MgSO_4$), and the solvent was removed in vacuo to obtain the crude product which was purified via column chromatography (99:1 – 9:1 DCM: MeOH) to give the pure product **3.24** as a white solid (107 mg, 73%). ^{1}H NMR (500 MHz, $CDCl_3$) δ 8.87 (s, 1H, N*H*SO_2CHCH_{2z}), 8.00 (s, 2H, triaz-H), 7.94 (s, 2H, Ar_H), 7.88 (s, 3H, Ar_H & N*H*CH_2), 6.56 (dd, *J* = 16.5, 9.9 Hz, 1H, SO_2CHCH_2), 6.27 (d, *J* = 16.5 Hz, 1H, SO_2CHCH_2), 5.91 (m, 3H, SO_2CHCH_2 & H-1), 5.50 (dd, *J* = 18.9, 9.6 Hz, 2H, H-2), 5.39 (d, *J* = 3.1 Hz, 2H, H-4), 5.28 (dd, *J* = 10.3, 3.4 Hz, 2H, H-3), 4.79 (dd, *J* = 15.1, 5.7 Hz, 2H, CH_2-triaz), 4.64 (dd, *J* = 15.2, 5.4 Hz, 2H, CH_2-triaz), 4.23 – 4.14 (m, 2H, H-5), 2.27 – 2.20 (m, 6H, CH_3 of OAc), 2.03 – 1.96 (m, 6H, CH_3 of OAc), 1.83 (s, 6H, CH_3 of OAc), 1.26 (dd, *J* = 13.2, 4.1 Hz, 6H, C-6 CH_3).

^{13}C NMR (125 MHz, $CDCl_3$) δ 170.5 (s, CO), 169.9 (s, CO), 169.3 (s, CO), 166.1 (s, *C*ONHCH_2), 145.1 (s, qC_{Ar}), 135.4 (s, qC_{Ar}), 135.2 (s, SO_2CHCH_2), 128.8 (s, SO_2CHCH_2), 122.0 (s, C_{Ar}), 121.6 (s, C_{triaz}), 121.1 (s, C_{Ar}), 86.3 (s, C-1), 72.7 (s, C-5), 71.1 (s, C-3), 69.8 (s, C-4), 68.2 (s, C-2), 35.2 (s, CH_2-triaz), 20.7 (s, CH_3 of OAc), 20.5 (s, CH_3 of OAc), 20.3 (s, CH_3 of OAc), 16.0 (s, C-6).

***N*, *N*'-di-(β-D-galactopyranosyl-1,2,3-triazol-4- ylmethylamide)-N''-(1-oxo-2-propen-1-yl)-5-aminobenzene-1,3-dicarboxamide 3.25**

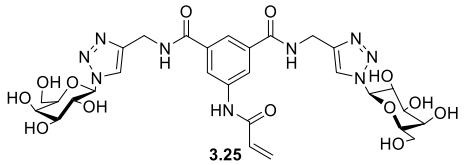

3.21 (174 mg, 0.16 mmol) was dissolved in MeOH/H_2O (10 mL/5 mL) and refluxed at 45-50 ^oC for 5 mins, NEt_3 (0.37 mL, 2.65 mmol) was then added and the reaction mixture was refluxed at 45-50 ^oC until the reaction was deemed complete by TLC analysis (90:10 DCM:MeOH) (5 h). The solvent was removed *in vacuo*, the residue was dissolved in water and treated with Amberlite H^+ for 1 h, this was then filtered and the solvent was removed *in vacuo* to yield the pure product **3.25** as a yellow fluffy solid (114 mg, 97%).

^1H NMR (500 MHz, D_2O) δ 8.26 (s, 2H, triaz-H), 8.07 (s, 2H, Ar-H), 7.94 (s, 1H, Ar-H), 6.47 – 6.33 (m, 2H, H_e & H_f COC*H*CH_2 & COCHC*H*$_2$), 5.91 (d, *J* = 10.2 Hz, 1H, COCHC*H*$_2$), 5.70 (d, *J* = 9.1 Hz, 2H, H-1), 4.72 (s, 4H, C*H*$_2$), 4.23 (t, *J* = 9.5 Hz, 2H, H-2), 4.10 (d, *J* = 2.9 Hz, 2H, H-4), 4.01 (t, *J* = 6.1 Hz, 2H, H-5), 3.89 (dd, *J* = 9.8, 3.3 Hz, 2H, H-3), 3.79 (d, *J* = 6.0 Hz, 4H, H-6/7).

^{13}C NMR (125 MHz, D_2O) δ 168.1 (s, CO), 166.2 (s, CO), 138.0 (s, qC_{Ar}), 134.0 (s, qC_{triaz}), 129.9 (s, C_{alkene}), 129.0 (s, C_{alkene}), 123.1 (s, C-triaz), 122.0 (s, C_{Ar}), 121.8 (s, C_{Ar}), 88.0 (s, C-1), 78.2 (s, C-5), 72.8 (s, C-3), 69.7 (s, C-2), 68.5 (s, C-4), 60.8 (s, C-6), 34.9 (s, CH_2). IR (ATR): 3266, 1644, 1538, 1287, 1211, 1090, 1052, 1015 cm^{-1}. HRMS (ESI+): m/z calcd for $C_{29}H_{37}N_9O_{13}$ + Na^+ $[M+Na]^+$ 742.2409, found 742.2399.

***N*, *N*'-di-(β-D-fucopyranosyl -1,2,3-triazol-4- ylmethylamide)-N''-(1-oxo-2-propen-1-yl)-5-aminobenzene-1,3-dicarboxamide 3.26**

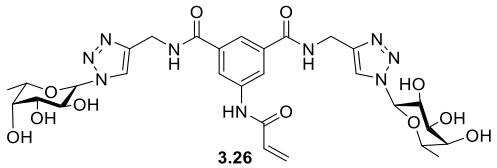

3.22 (179 mg, 0.19 mmol) was dissolved in MeOH/H_2O (10 mL/5 mL) and refluxed at 45-50 ^oC for 5 mins, NEt_3 (0.5 mL) was then added and the reaction mixture was refluxed at 45-50 ^oC until the reaction was deemed complete by TLC analysis (90:10 DCM:MeOH) (5 h). The solvent was removed *in vacuo*, the residue was dissolved in water and treated with Amberlite H^+ for 1 h, this was then filtered and the solvent was removed *in vacuo* to yield the pure product **3.26** as a yellow solid (76 mg, 95%)

^1H NMR (500 MHz, D_2O) δ 8.23 (s, 2H, triaz-H), 7.84 (s, 2H, Ar_H), 7.74 (s, 1H, Ar_H), 6.24 (d, *J* = 5.2 Hz, 2H, H_e & H_f), 5.78 (m, 1H, H_f), 5.63 (d, *J* = 9.1 Hz, 2H, H-1), 4.65 – 4.55 (m, 4H, CH_2), 4.18 (t, *J* = 9.3 Hz, 2H, H-2), 4.04 (d, *J* = 6.5 Hz, 2H, H-5), 3.91 – 3.81 (m, 4H, H-3 & H-4), 1.21 (dd, *J* = 19.7, 6.0 Hz, 6H, C-6 CH_3).

^{13}C NMR (125 MHz, $CDCl_3$) δ 167.1 (s, CO), 165.1 (s, CO-acryloyl), 137.1 (s, qC_{Ar}), 133.1 (s, qC_{Ar}), 129.0 (s, C_e), 128.1 (s, C_f), 122.2 (s, C-triaz), 120.9 (s, C_f), 87.1 (s, C-1), 73.4 (s, C-5), 72.2 (s, C-3/4), 70.2 (s, C-3/4), 68.5 (s, C-2), 34.1 (s, CH_2), 14.6 (s, C-6). IR (ATR): 3271, 1651, 1596, 1538, 1445, 1423, 1339, 1285, 1211, 1158, 1091 cm^{-1}. HRMS (ESI+): m/z calcd for $C_{29}H_{37}N_9NaO_{11}$ + Na^+ [M+Na^+]: 710.2510, found 710.2488.

***N*',*N*''-di-((β-D-galactopyranosyl)-1H-1,2,3-triazol-4-yl)methyl)-5-(vinylsulfonamido)isophthalamide 3.27**

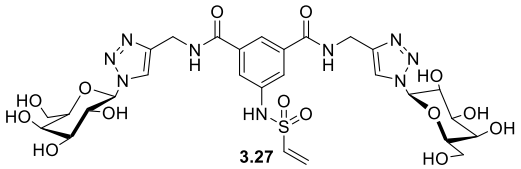

Compound **3.23** (122 mg, 0.11 mmol) was dissolved in MeOH/water (2:1 ratio). NEt_3 (0.1 mL) was added, and the reaction mixture was allowed to stir at 45 ^oC until completion (typically 6-18 h). The solution was cooled to RT, Amberlite H^+ was added

and the mixture was allowed to stir for 30 mins. The solution was filtered, and the solvent was removed in the rotatory evaporator and the residue was dried under high vacuum or lyophilized to give the deprotected glycoconjugate **3.27** (75 mg, 89%).

^{1}H NMR (500 MHz, D_2O) δ 8.22 (s, 2H, Triaz-H), 7.87 (d, *J* = 1.1 Hz, 1H, Ar-H), 7.62 (s, 2H, Ar-H), 6.69 (ddd, *J* = 16.5, 10.0, 1.0 Hz, 1H, SOC*H*), 6.20 (d, *J* = 16.5 Hz, 1H, HC=C*H*$_2$), 6.07 – 6.04 (m, 1H, HC=C*H*$_2$), 5.66 (d, *J* = 9.2 Hz, 2H, H-1), 4.64 (s, 4H, $NHCH_2$), 4.21 (t, *J* = 9.5 Hz, 2H, H-2), 4.08 (d, *J* = 3.2 Hz, 2H, H-4), 3.98 (t, *J* = 6.0 Hz, 2H, H-5), 3.87 (m, 2H, H-3), 3.76 (d, *J* = 5.9 Hz, 4H, H-6 &H-6'). ^{13}C NMR (125 MHz, D_2O) δ 168.4 (s, *C*ONH), 144.8 (s, qC_{triaz}), 137.3 (s, C_{Ar}), 136.1 (s, C_{Ar}), 135.0 (s), 134.7 (s), 133.7 (s,SO_2*C*HCH_2), 130.1 (s,SO_2CH*C*H_2), 123.5 (s, C_{triaz}), 123.4 (s, C_{Ar}), 122.9 (s, C_{Ar}), 122.3 (s, C_{triaz}), 88.0 (s, C-1), 78.2 (s, C-5), 72.9 (s, C-3), 69.7 (s, C-2), 68.5 (s, C-4), 60.8 (s, C-6), 35.0 (s, *C*H_2NH.) IR: 2962, 1720, 1645, 1596, 1541, 1405, 1331, 1288, 1203, 1135, 1092, 1051 cm^{-1}. HRMS (ESI+): m/z calcd for $C_{28}H_{37}N_9O_{14}S$ +H^+ $(M+H)^+$ 755.21, found 756.2264.

***N*',*N*''-di-(β-D-fucopyranosyl-1,2,3-triazol-4-ylmethylamide)-1H-1,2,3-triazol-4-yl)methyl))-5-(vinylsulfonamido)isophthalamide 3.28**

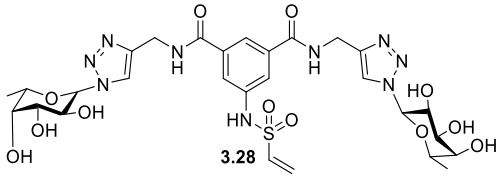

Compound **3.24** (117 mg, 0.12 mmol) was dissolved in MeOH/water (2:1 ratio). NEt_3 (0.1 mL) was added, and the reaction mixture was allowed to stir at 45 ^{o}C until completion (typically 6-18 h). The solution was cooled to RT, Amberlite H^+ was added and the mixture was allowed to stir for 30 mins. The solution was filtered, and the solvent was removed in the rotatory evaporator and the residue was dried under high vacuum or lyophilized to give the deprotected glycoconjugate **3.28** (74 mg, 89%). ^{1}H NMR (500 MHz, D_2O) δ 8.14 (s, 2H, triaz-H), 7.75 (s, 1H, Ar_H), 7.53 (s, 2H, Ar_H), 6.59 (dt, *J* = 24.3, 12.1 Hz, 1H, SO_2C*H*CH_2), 6.11 (d, *J* = 16.5 Hz, 1H, SO_2CHC*H*$_2$), 5.94 (t, *J* = 9.3 Hz, 1H, SO_2CHC*H*$_2$), 5.55 (d, *J* = 9.1 Hz, 2H, H-1), 4.57 (s, 4H, CH_2-triaz), 4.09 (t, *J* = 9.4 Hz, 2H, H-2), 3.96 (d, *J* = 6.3 Hz, 2H, H-5), 3.78 (dd, *J* = 14.8, 5.1 Hz, 4H, H-3 & H-4), 1.23 – 1.09 (m, 6H, C-6 CH_3). ^{13}C NMR (125 MHz, D_2O) δ 168.2 (s, CO),

145.2 (s, qC_{triaz}), 137.9 (s, qC_{Ar}), 134.9 (s, qC_{Ar}), 133.9 (s, SO_2CHCH_2), 129.7 (s, SO_2CHCH_2), 122.6 (s, C_{Ar} & C-triaz), 121.9 (s, C_{Ar}), 87.9 (s, C-1), 74.3 (s, C-5), 73.0 (s, C-3/4), 71.1 (s, C-3/4), 69.4 (s, C-2), 35.0 (s, CH_2-triaz), 15.5 (s, C-6).

N, N'-di-(β-D-galactopyranosyl-1,2,3-triazol-4-ylmethylamide)-5-(fluoresceinthiourea)-benzene-1,3-dicarboxamide 3.30

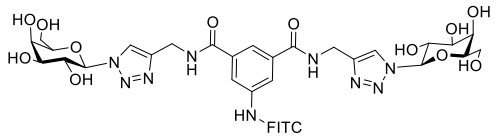

3.30

Compound **3.19** (102 mg, 0.1 mmol) was dissolved in acetone (11 mL). FITC (79 mg, 0.2 mmol) was added, and the reaction mixture was heated in the MW at 50 °C for 1 h. Following TLC analysis, the solvent was removed *in* vacuo to give the crude product **3.29**. Rf = 0.47 (DCM:MeOH 8.5:1.5). The crude product was then deprotected. It was dissolved in MeOH/H_2O (4 mL/2 mL). NEt_3 (0.1 mL) was added, and the reaction mixture was allowed to stir at 45 °C for 6.5 h. The solvent was removed in vacuo. Crude product was then triturated with chloroform to give product **3.30**. ^1H NMR analysis (Figure **X**) showed that ~8% of the product was fluorescently labelled with FITC. HRMS analysis was unable to detect **3.30**, likely due to the low conversion of **3.29** to fluorescently labelled derivative **3.30**.

***N,N'*-di-(2,3,4-tri-O-acetyl-β-D-fucopyranosyl-1,2,3-triazol-4-ylmethylamide)-*N''*-pent-4-ynoylamino-5-aminobenzene-1,3-dicarboxamide 3.31**

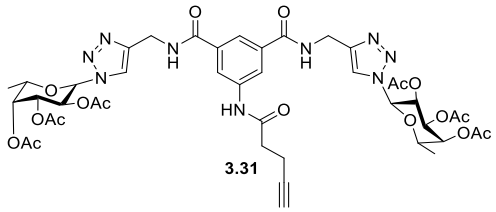

3.31

4-pentynoic acid (10.5 mg, 0.11 mmol), TBTU (34 mg, 0.11 mmol) and NEt_3 (15 µL, 0.11 mmol) were placed under N_2 and dissolved in anhydrous DMF (2 mL) and stirred for 20 mins. **3.20** (79 mg, 0.09 mmol, 1 equiv.) was placed under N_2 and dissolved in anhydrous DMF (4 mL) in a separate round-bottom flask. After 20 mins, the **3.20** solution was added via a cannula to the reaction mixture over a 10 min period. The reaction was stirred overnight at RT. Following TLC analysis, 4-pentynoic acid (31.5 mg, 3 equiv.) was added, after 2 h of stirring and TLC analysis, TBTU (57 mg, 2 equiv.)

and NEt_3 (24.8 µL, 2 equiv.) were added. Following TLC analysis, the solvent was removed *in vacuo*. The crude residue was dissolved in DCM and washed with sat. $NaHCO_3$ (x2) and brine (x1), the organic phase was dried (Na_2SO_4) and concentrated *in vacuo* to yield a colourless oil **3.31** (58 mg, 67%).

^{1}H NMR (500 MHz, $CDCl_3$) δ 8.88 (d, *J* = 16.0 Hz, 1H), 8.08 – 8.00 (m, 2H), 7.99 (s, 2H), 7.92 (s, 2H), 7.69 (s, 1H), 5.85 (d, *J* = 9.2 Hz, 2H), 5.56 (t, *J* = 9.7 Hz, 2H), 5.40 – 5.33 (m, 2H), 5.25 (dd, *J* = 10.3, 3.4 Hz, 2H), 4.65 (qd, *J* = 15.4, 5.4 Hz, 4H), 4.19 – 4.09 (m, 2H), 2.64 – 2.56 (m, 2H), 2.56 – 2.49 (m, 2H), 2.21 (d, *J* = 1.4 Hz, 6H), 2.01 (dd, *J* = 5.2, 3.1 Hz, 1H), 1.99 (d, *J* = 1.3 Hz, 6H), 1.82 (d, *J* = 1.6 Hz, 6H), 1.29 – 1.13 (m, 7H).

^{13}C NMR (125 MHz, $CDCl_3$) δ 170.5 (s, CO of OAc), 169.9 (s, CO of OAc), 169.4 (s, CO of OAc), 166.7 (s, *C*ONH), 145.5 (s, qC_{triaz}), 138.8 (s, qC_{Ar}), 134.8 (s, qC_{Ar}), 121.4 (s, C_{triaz}), 121.2 (s, C_{Ar}), 120.6 (s, C_{Ar}), 86.2 (s, C-1), 72.7 (s, C-5), 71.2 (s, C-3), 69.8 (s, C-4), 69.5 (s, CH_2CH_2C*C*H), 68.1 (s, C-2), 35.7 (s, *C*H_2CH_2CCH), 35.4 (s, *C*H_2NH), 20.7 (s, CH_3 of OAc), 20.5 (s, CH_3 of OAc), 20.3 (s, CH_3 of OAc), 16.0 (s, C-6), 14.4 (s, *C*H_2CCH). IR (ATR): 1745, 1651, 1533, 1367, 1212, 1159, 1092, 1060 cm^{-1}. HRMS (ESI+): m/z calculated for $C_{43}H_{51}N_9O_{17}$ + Na^+ [M+Na^+]: 988.3301, found 988.3333.

***N,N'*-di-(β-D-fucopyranosyl-1,2,3-triazol-4-ylmethylamide)-*N''*-pent-4-ynoylamino-5-aminobenzene-1,3-dicarboxamide 3.32**

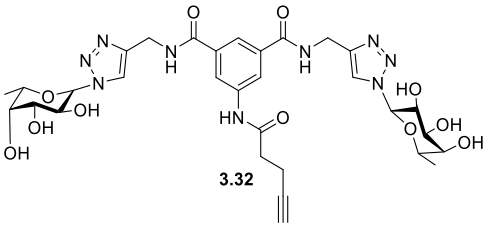

3.31 (33 mg, 0.03 mmol) was dissolved in a mixture of MeOH/H_2O (4 mL/2 mL) and refluxed at 45-50 °C, NEt_3 (0.1 mL) was then added and the mixture was refluxed until the reaction was deemed complete by TLC analysis (approx. 16 h). The solvent was then removed *in vacuo*, the crude residue was then dissolved in deionised water and stirred with Amberlite H^+ for one h, this was then filtered, concentrated *in vacuo* and freeze dried to yield the pure product **3.32** as a white solid (17.5 mg, 73%).

^{1}H NMR (500 MHz, D_2O) δ 8.17 (s, 1H, triaz-H), 7.81 (d, *J* = 1.5 Hz, 2H, Ar_H), 7.77 – 7.70 (m, 1H, Ar_H), 5.57 (d, *J* = 9.2 Hz, 2H, H-1), 4.57 (s, 4H, C*H*$_2$NH), 4.10 (t, *J* = 9.4 Hz, 2H, H-2), 4.02 – 3.94 (m, 2H, H-5), 3.81 (dd, *J* = 3.3, 0.7 Hz, 2H, H-4), 3.78 (dd, *J* = 9.7, 3.3

Hz, 2H, H-3), 2.51 (dd, *J* = 10.5, 4.0 Hz, 2H, NHCOC*H*$_2$CH$_2$), 2.43 (ddd, *J* = 8.2, 3.3, 1.9 Hz, 2H, CH$_2$C*H*$_2$CCH), 2.29 (t, *J* = 2.6 Hz, 1H, CH$_2$CH$_2$CC*H*), 1.21 – 1.11 (m, 6H, C-6 CH$_3$). ^{13}C NMR (125 MHz, D$_2$O) δ 173.1 (s, *C*OCH$_2$CH$_2$CCH), 168.5 (s, *C*ONHCH$_2$), 144.9 (s, qC$_{triaz}$), 137.9 (s, qC$_{Ar}$), 134.4 (s, qC$_{Ar}$), 122.8 (s, C-triaz), 122.4 (s, C$_{Ar}$), 122.0 (s, C$_{Ar}$), 88.0 (s, C-1), 83.4 (s, CH$_2$CH$_2$*C*CH), 74.3 (s, C-5), 73.0 (s, C-3), 71.2 (s, C-4), 70.1 (s, CH$_2$CH$_2$C*C*H), 69.3 (s, C-2), 35.0 (s, CH$_2$-triaz & CO*C*H$_2$CH$_2$), 15.5 (s, C-6), 14.1 (s, CH$_2$*C*H$_2$CCH). IR (ATR): 3282, 1647, 1597, 1541, 1446, 1339, 1282, 1161, 1090 cm^{-1}. HRMS (ESI+): m/z calculated for $C_{31}H_{39}N_9O_{11}$ + Na$^+$ [M+Na$^+$]: 736.2667, found 736.2702.

***N,N'*-di-(β-D-fucopyranosyl-1,2,3-triazol-4-ylmethylamide)-*N''*-pent-4-(cyanine-5)-1H-1,2,3-triazol-4-yl)amino-5-aminobenzene-1,3-dicarboxamide 3.33**

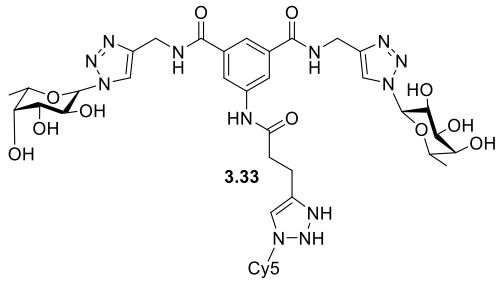

3.32 (approx. 3 mg, 0.0045 mmol) and Cyanine 5 azide (approx. 2 mg, 0.003 mmol) were dissolved in ACN/H$_2$O (2 mL/1 mL) in a round bottom flask wrapped in tin foil. Copper sulfate pentahydrate (5 mg) and sodium ascorbate (5 mg) were added and the reaction mixture was refluxed at 45-50 ^{o}C for 6 h. Following TLC analysis, the solvent was removed *in vacuo*, the resulting crude mixture was dissolved in deionised water (3 mL) and stirred in the presence of chelex resin for 20 mins. The solution was then removed via a syringe into a round bottom flask wrapped in tin foil and the solvent was removed *in vacuo*. The crude mixture was then triturated 3 times with chloroform, the remaining residue was dried *in vacuo*. Unfortunately, this reaction was unsuccessful.

5-(ethylsulfonamido)-*N*',*N*''-di-(((2,3,4,6-tetra-*O*-acetyl-β-D-galactopyranosyl)-1H-1,2,3-triazol-4-yl)methyl)isophthalamide 3.34

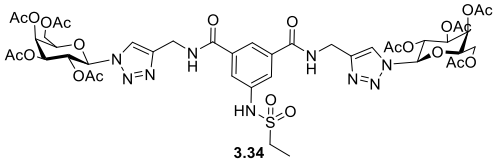

3.34

3.19 (200 mg, 0.19 mmol) was dissolved in dry DCM (20 mL). NEt_3 (0.033 mL, 0.24 mmol) was added to this solution. Ethanesulfonyl chloride (19 µL, 0.19 mmol) was dissolved in dry DCM (5 mL) in a separate round-bottom flask. The first solution was added to the second dropwise via a cannula and the resulting reaction mixture was allowed to stir for 16 h at RT. The reaction mixture was washed with water (20 mL), HCl (1 N, 20 mL), sat. $NaHCO_3$ solution (20 mL), followed by brine (20 mL). The organic phase was dried ($MgSO_4$), and the solvent was removed in vacuo to obtain the crude product which was purified via column chromatography (97:3 – 9:1 DCM: MeOH) to give the pure product **3.34** as a brown, sticky solid (169 mg, 77%). R_f 0.2 (98:2 DCM: MeOH).^{1}H NMR (500 MHz, $CDCl_3$) δ 8.38 (s, 2H N*H*CH_2-triaz,), 8.21 (s, 1H, NH-S), 8.04 (d, *J* = 1.3 Hz, 2H, triaz-H), 8.00 (s, 2H, Ar-H), 7.91 (d, *J* = 1.0 Hz, 1H, Ar-H), 6.00 (d, *J* = 9.2 Hz, 2H, H-1), 5.58 – 5.55 (m, 4H, H-2 and H-4), 5.33 (dd, *J* = 6.1, 4.2 Hz, 2H, H-3), 4.77 – 4.61 (m, 4H, CH_2-triaz), 4.35 (t, *J* = 6.8 Hz, 2H, H-5), 4.23 (m, 2H, H-6 and H-6',), 3.56 (m, 2H, S-CH_2), 2.23 (s, 6H, OAc), 2.04 (s, 6H, OAc), 2.01 (s, 6H, OAc), 1.85 (s, 6H, OAc), 1.43 (t, *J* = 7.4 Hz, 3H, CH_3).^{13}C NMR (125 MHz, d_6-DMSO) δ 170.5 (CO of OAc), 170.4 (CO of OAc), 169.9 (CO of OAc), 169.0 (CO of OAc), 167.1 (*C*ONHCH_2-triaz), 146.1 (Triaz-C), 135.6 (Ar-C), 122.8 (triaz-CH), 115.7 (Ar-CH) 113.8 (Ar-CH) 84.7 (C-1), 73.4 (C-5), 71.0 (C-3), 68.1 (C-2), 67.8 (C-4), 62.0 (C-6), 50.3 (S-CH_2), 35.1 (*C*H_2NH), 21.0 (CH_3 of OAc), 20.9 (CH_3 of OAc), 20.8 (CH_3 of OAc), 20.5 (CH_3 of OAc), 7.6 (SCH_2*C*H_3).HRMS (ESI+): *m/z* calcd for $C_{44}H_{55}N_9O_{22}$ + H^+ $[M+H]^+$ 1093.3182, found 1094.3270.

5-(ethylsulfonamido)-*N*',*N*''-di-((β-D-galactopyranosyl)-1H-1,2,3-triazol-4-yl)methyl)isophthalamide 3.35

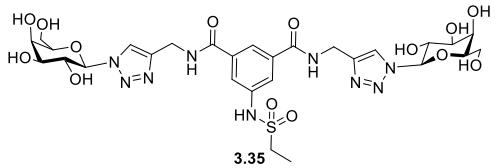

3.35

3.34 (169 mg, 0.15 mmol) was dissolved in MeOH/water (2:1 ratio). NEt_3 (0.1 mL) was added, and the reaction mixture was allowed to stir at 45 ^oC until completion (typically 6-18 h). The solution was cooled to RT, Amberlite H^+ was added and the mixture was allowed to stir for 30 mins. The solution was filtered, and the solvent was removed in the rotatory evaporator and the residue was dried under high vacuum or lyophilized to give the deprotected glycoconjugate **3.35** (95 mg, 82%). R_f: Baseline (9:1 DCM: MeOH). ^1H NMR: (500 MHz, D_2O) δ 8.14 (s, 2H, Ar-H), 7.82 (s, 1H, Ar-H), 7.64 (s, 2H, Triaz-H), 5.57 (d, *J* = 9.1 Hz, 2H, H-1), 4.58 (s, 4H, CH_2-Triaz), 4.10 (t, *J* = 9.4 Hz, 2H, H-2), 3.97 (m, 2H, H-4), 3.89 (t, *J* = 5.9 Hz, 2H, H-3), 3.77 (dd, *J* = 9.8, 3.1 Hz, 2H, H-5), 3.67 (d, *J* = 6.0 Hz, 4H, H-6 & H-6'), 3.18 (m, 2H S-CH_2), 2.80 (q, *J* = 7.4 Hz, 2H, CH_3). ^{13}C NMR: (125 MHz, D_2O) δ 168.6 (CONH), 137.8 (Triaz-C), 135.2 (qC_{Ar}), 122.3 (Ar-CH), 122.2 (Ar-CH), 88.0 (C-1), 78.2 (C-3), 72.8 (C-5), 69.7 (C-2), 68.5 (C-4), 60.8 (C-6), 46.0 (S-CH_2), 45.8 (CH_3), 35.0 (CH_2-triaz). IR: 3295, 2927, 2884 1641, 1539, 1437, 1402, 1321, 1285, 1235, 1138, 1091, 1051 cm^{-1}. HRMS (ESI+): *m/z* calcd for $C_{28}H_{39}N_9O_{14}$ $[M+Na]^+$ 757.2337, found 780.2227.

Toxicity assays against *Candida spps.*

Spot test (*Candida sp*)

Test environment:

Deionised water (DI, Milli-Q, Millipore), sterilised by autoclaving (121 ^oC, 20 mins).

Yeast-Extract-Peptone-Dextrose medium (YPD):

Yeast extract 1%, peptone 2%, glucose 2%, sterilised by autoclaving (121 ^{o}C, 20 mins). Glucose was autoclaved separately (20% or 40% glucose) and added after autoclaving (e.g 40 mL 20% glucose + 360 mL YPD). Agar media was prepared by adding 2% agar.

Overnight culture:

Some colonies (2-3) were transferred with sterile inoculation loop from the master plates to 3 mL of sterile YPD medium (Falcon 14 mL round-bottom polypropylene culture tube) and incubated at 30 ^{o}C on an orbital shaker at 200 rpm overnight.

Mid-exponential growth phase culture:

The OD_{600nm} of the overnight culture was measured (dilute the overnight culture 50-times- 40 µL culture + 1960 µL YPD). The overnight culture was then diluted in 20 mL YPD media in a 100 mL conical flask, which had been sterilised, such that the OD_{600nm} of the culture was 0.25. The conical flask was then incubated at 30 ^{o}C on an orbital shaker at 200 rpm until the cells had reached the mid-exponential growth phase (3-5.5 h for *Candida sp*). Note: the OD_{600nm} of the yeast culture at the mid-exponential phase should be ~1.

Toxicity test (cell viability test in deionised water)

Cell culture in DI: Cells from the mid-exponential growth phase were then harvested by centrifugation (6500 rpm for 5 mins), the yeast culture was transferred to a 50 mL falcon after the OD_{600nm} was checked (400 µL culture + 1600 µL YPD) and found to be ~1. The supernatant was discarded and approximately 20 mL of deionised water was added. The cells were washed twice with 20 mL of deionised water (centrifugation repeated twice). The cells were then resuspended in 10 mL deionised water, vortexing to ensure the suspension is homogenous. The cell culture was then diluted in a new 50 mL falcon tube with deionised water so that the OD_{600nm} was 1.2.

Exposure experiment: 70 µL of the tested compound(s) (including dilutions) were transferred into a 96-well polystyrene microplate (BD falcon) and 70 µL of the cell

culture (OD_{600nm}=1.2) in deionised water was also added into the wells (140 µL total). As a control, 70 µL of deionised water was also added into the 96-well plate and 70 µL of the cell culture was also added into these well (140 µL total).

Incubation of cells: The 96-well microplate was then incubated for 24 h at 30 ^{o}C in the dark without shaking. To avoid/reduce evaporation during this experiment, the 96-well microplate edges were wrapped in Parafilm.

'Spotting': After 24 h of exposure, 5 µL of the cell culture from each well was pipetted onto agar medium plates and incubated at 30 ^{o}C for 48 h in the dark without shaking. The growth of cells was then visually evaluated.

Minimum biocidal concentration (MBC): MBC was determined as the lowest tested concentration of the compound which completely inhibits the growth of cells (formation of colonies) on agar plates after 24 h exposure in deionised water.

Model crosslinking reactions:

250 µL of a stock 20 mM solution of the electrophile (Compound **3.25** or **3.27**) was placed under N_2, 4.5 mL of the Nucleophile (N-α-acetyl-l-lysine, N-acetyl-histidine and N-acetyl-cysteine) dissolved in either the pH 7.4 or pH 10.2 buffer (55.5 mM stock solution) was then added. After 3 h a small aliquot was taken, and this was repeated after 6 h and 24 h after which the reaction mixtures were placed on the freeze-drier. Following on from this, within 24 h of taking the final aliquot (24 h), these aliquots were analysed by HPLC using a 90:10 H_2O:ACN isocratic gradient with a Phenomenex Luna CN column 5 µm (detector set at 254 nm), along with samples of the electrophile (**3.25** or **3.27**) and nucleophile (N-α-acetyl-l-lysine, N-acetyl-histidine and N-acetyl-cysteine). If any new peaks were observed in the resulting chromatograms, i.e not corresponding to the electrophile or nucleophile, a sample was submitted for High-resolution mass spectrometry to detect the presence of any electrophile-nucleophile adducts.

7.2.3 Experimental procedures for Chapter 4

N,N'-di(prop-2-yn-1-yl)-5-bromo-isophthalamide 4.20

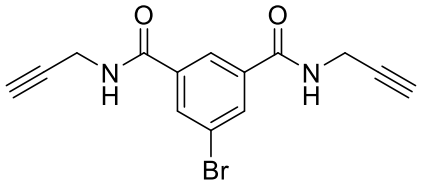

4.20

4.18 (1 g, 4.08 mmol) and TBTU (3.14 g, 9.79 mmol) were placed under N_2 and dissolved in anhydrous DMF (10 mL), after 10 mins of stirring propargylamine (0.63 mL, 9.79 mmol) was added, followed by anhydrous NEt_3 (1.36 mL, 9.79 mmol). The reaction was then stirred overnight at RT. Ice and 100 mL of saturated $NaHCO_3$ were placed in a large beaker and the reaction mixture was then gradually poured into the beaker and stirred. The precipitate formed was isolated using vacuum filtration to obtain the purified product **4.20** as a white solid (500 mg, 39%).

^{1}H NMR (500 MHz, DMSO) δ 9.26 (s, 2H, NH), 8.35 (s, 1H, Ar_H), 8.19 (d, *J* = 1.4 Hz, 2H, Ar_H), 4.07 (dd, *J* = 5.4, 2.5 Hz, 4H, CH_2), 3.16 (t, *J* = 2.5 Hz, 2H, CH_2CCH). ^{13}C NMR (125 MHz, DMSO) δ 164.5 (s, CO), 136.5 (s, *C*-Br), 133.0 (s, C_{Ar}/qC_{Ar}), 126.1 (s, C_{Ar}), 122.2 (s, qC_{Ar}), 81.3 (s, CH_2CCH), 73.6 (s, CH_2CCH), 29.2 (s, CH_2). IR (ATR): 3306, 3258, 1637, 1532, 1449, 1426, 1358, 1319, 1290, 1265, 1097, 1066, 1052, 1012 cm^{-1}. HRMS (ESI+): m/z calcd for $C_{14}H_{11}BrN_2O_2$ + H^+ $[M+H]^+$ 318.0004, found 319.0076.

N,N'-di(prop-2-yn-1-yl)-5-methoxy-isophthalamide 4.21

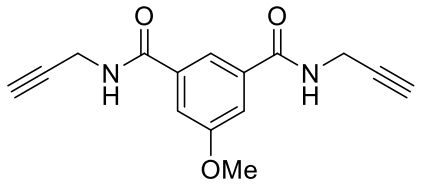

4.21

4.19 (400 mg, 2.04 mmol) and TBTU (1.57 g, 4.89 mmol) were placed under N_2 and dissolved in anhydrous DMF (10 mL), after 10 mins of stirring propargylamine (0.31 mL, 4.89 mmol) was added, followed by anhydrous NEt_3 (0.68 mL, 4.89 mmol). The reaction was then stirred overnight at RT. Ice and 100 mL of saturated $NaHCO_3$ were placed in a large beaker and the reaction mixture was then gradually poured into the

beaker and stirred. The precipitate formed was isolated using vacuum filtration to obtain the purified product **4.21** as a white solid (549 mg, 99%).

^{1}H NMR (500 MHz, DMSO) δ 9.04 (t, *J* = 5.5 Hz, 2H, NH), 7.94 (dd, *J* = 4.7, 3.2 Hz, 1H, Ar_H), 7.54 (d, *J* = 1.4 Hz, 2H, Ar_H), 4.07 (dd, *J* = 5.5, 2.5 Hz, 4H, CH_2), 3.86 (s, 3H, OCH_3), 3.14 (t, *J* = 2.5 Hz, 2H, CH_2CCH). ^{13}C NMR (125 MHz, DMSO) δ 165.7 (s, CO), 159.6 (s, $COCH_3$), 135.9 (s, qC_{Ar}), 119.2 (s, C_{Ar}), 115.9 (s, C_{Ar}), 81.6 (s, CH_2CCH), 73.4 (s, CH_2CCH), 56.1 (s, OCH_3), 29.0 (s, CH_2). IR (ATR): 3329, 3255, 1636, 1603, 1532, 1451, 1416, 1321, 1291, 1266, 1250, 1145, 1069. HRMS (ESI+): m/z calcd for $C_{15}H_{14}N_2O_3$ + Na^+ $[M+Na]^+$ 293.0902, found 293.0899.

***N,N'*-di-(2,3,4,6-tetra-*O*-acetyl-β-D-galactopyranosyl-1,2,3-triazol-4-ylmethylamide)-N''-propyl-5-bromobenzene-1,3-dicarboxamide 4.22**

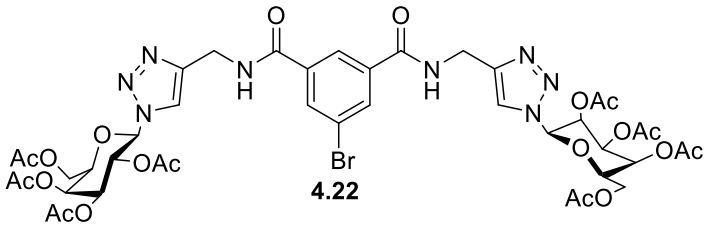

4.22

4.20 (300 mg, 0.94 mmol), **2.40** (774 mg, 2.07 mmol), Copper sulfate pentahydrate (120 mg) and sodium ascorbate (150 mg) were dissolved in ACN/H_2O (10 mL/2 mL) and reacted in the microwave at 100 ^{o}C until the reaction was deemed complete by TLC analysis (90:10 DCM:MeOH) (30 mins). The solvent was then removed in vacuo and the resulting residue was extracted using DCM and brine, the organic phase was dried ($MgSO_4$), filtered and the solvent was removed *in vacuo*. The product was purified by flash column chromatography (99:1-94:6 DCM:MeOH) as a white solid **4.22** (335 mg, 33%).

^{1}H NMR (500 MHz, $CDCl_3$) δ 8.13 (s, 3H, Ar-H), 8.00 (s, 2H, triaz-H), 7.86 – 7.79 (t, 2H, N*H*), 5.98 (d, *J* = 9.2 Hz, 2H, H-1), 5.56 (dd, *J* = 3.4, 1.0 Hz, 2H, H-4), 5.49 (dt, *J* = 15.2, 7.6 Hz, 2H, H-2), 5.33 – 5.25 (m, 2H, H-3), 4.76 (dd, *J* = 15.2, 5.9 Hz, 2H, CH_2), 4.60 (dd, *J* = 15.1, 5.6 Hz, 2H, CH_2), 4.35 – 4.29 (m, 2H, H-5), 4.20 (dd, *J* = 11.5, 6.1 Hz, 2H, H-6/7), 4.14 (dd, *J* = 11.5, 6.8 Hz, 2H, H-6/7), 2.23 (s, 6H, CH_3 of OAc), 2.03 (s, 6H, CH_3 of OAc), 2.00 (s, 6H, CH_3 of OAc), 1.83 (s, 6H, CH_3 of OAc).

^{13}C NMR (125 MHz, $CDCl_3$) δ 170.3 (s, CO of OAc), 170.0 (s, CO of OAc), 169.8 (s, CO of OAc), 169.1 (s, CO of OAc), 165.3 (s, *C*ONHCH$_2$), 145.2 (s, qC-triaz), 135.9 (s, qC-Ar), 133.9 (s, qC-Ar & C-Ar), 123.4 (s, C-Ar), 121.7 (s, C-triaz), 86.2 (s, C-1), 74.0 (s, C-5), 70.6 (s, C-3), 68.2 (s, C-2), 66.8 (s, C-4), 61.2 (s, C-6), 35.2 (s, *C*H$_2$), 20.7 (s, *C*H$_3$ of OAc), 20.6 (s, *C*H$_3$ of OAc), 20.5 (s, *C*H$_3$ of OAc), 20.2 (s, *C*H$_3$ of OAc). IR (ATR): 1744, 1367, 1208, 1090, 1043, 922 cm^{-1}. HRMS (ESI+): m/z calcd for $C_{42}H_{49}BrN_8O_{20}$ + H$^+$ [M+H]$^+$ 1065.2325, found 1067.2303.

***N*,*N*'-di-(2,3,4,6-tetra-*O*-acetyl-β-D-galactopyranosyl-1,2,3-triazol-4-ylmethylamide)-N''-propyl-5-methoxybenzene-1,3-dicarboxamide 4.23**

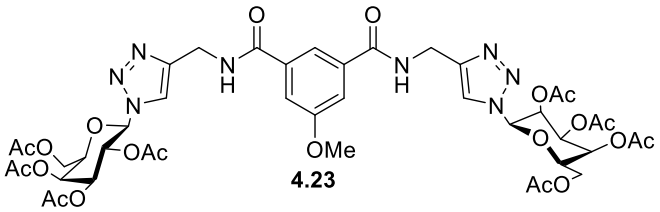

4.23

4.21 (400 mg, 1.48 mmol), **2.40** (1.21 g, 3.26 mmol), Copper sulfate pentahydrate (110 mg) and sodium ascorbate (150 mg) were dissolved in ACN/H_2O (10 mL/2 mL) and reacted in the microwave at 100 ^{o}C until the reaction was deemed complete by TLC analysis (90:10 DCM:MeOH) (30 mins). The solvent was then removed in vacuo and the resulting residue was extracted using DCM and brine, the organic phase was dried ($MgSO_4$), filtered and the solvent was removed *in vacuo*. The product was purified by flash column chromatography (99:1-94:6 DCM:MeOH) as a white solid **4.23** (965 mg, 64%).

^{1}H NMR (500 MHz, $CDCl_3$) δ 7.99 (s, 2H, triaz-H), 7.75 (s, 1H, Ar-H), 7.71 (t, *J* = 5.6 Hz, 2H, NH), 7.54 (d, *J* = 1.3 Hz, 2H, Ar-H), 5.97 (d, *J* = 9.2 Hz, 2H, H-1), 5.55 (dd, *J* = 3.4, 1.0 Hz, 2H, H-4), 5.50 (dd, *J* = 10.2, 9.3 Hz, 2H, H-2), 5.28 (d, *J* = 3.4 Hz, 2H, H-3), 4.77 (dd, *J* = 15.2, 5.9 Hz, 2H, CH_2), 4.61 (dd, *J* = 15.1, 5.6 Hz, 2H, CH_2), 4.34 – 4.28 (m, 2H, H-5), 4.20 (dd, *J* = 11.5, 6.1 Hz, 2H, H-6/H-7), 4.13 (dd, *J* = 11.5, 6.8 Hz, 2H, H-6/H-7), 3.85 (s, 3H, OMe), 2.23 (s, 6H, CH_3 of OAc), 2.02 (d, *J* = 3.7 Hz, 6H, CH_3 of OAc), 2.00 (s, 6H, CH_3 of OAc), 1.82 (s, 6H, CH_3 of OAc).

^{13}C NMR (125 MHz, $CDCl_3$) δ 170.3 (s, CO of OAc), 170.0 (s, CO of OAc), 169.8 (s, CO of OAc), 169.1 (s, CO of OAc), 166.5 (s, CO), 160.2 (s, qC_{Ar}), 145.4 (s, qC_{triaz}), 135.6 (s, qC_{Ar}), 121.6 (s, C_{triaz}), 116.7 (s, C_{Ar}), 116.5 (s, C_{Ar}), 86.2 (s, C-1), 74.0 (s, C-5), 70.6 (s, C-

3), 68.1 (s, C-2), 66.8 (s, C-4), 61.2 (s, C-6), 55.7 (s, O*C*H$_3$), 35.2 (s, *C*H$_2$), 20.7 (s, *C*H$_3$ of OAc), 20.6 (s, *C*H$_3$ of OAc), 20.5 (s, *C*H$_3$ of OAc), 20.2 (s, *C*H$_3$ of OAc). IR (ATR): 1745, 1367, 1209, 1090, 1043, 922 cm^{-1}. HRMS (ESI+): m/z calcd for $C_{43}H_{52}N_8O_{21}$ + Na^+ $[M+Na]^+$ 1039.3145, found 1039.3132.

_N_,_N_'-di-(2,3,4,6-tetra-_O_-acetyl-β-D-galactopyranosyl-1,2,3-triazol-4-ylmethylamide)-N''-propyl-5-(cyclopropanecarbonylamino)benzene-1,3-dicarboxamide 4.24

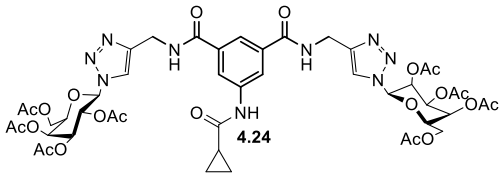

3.19 (145 mg, 0.14 mmol) was placed under N_2 and dissolved in anhydrous DCM (8 mL), NEt_3 (20 µL, 0.14 mmol) was added and the mixture was stirred. Cyclopropanecarbonyl chloride (26 µL, 0.29 mmol) was added and the reaction mixture was stirred overnight at RT. Following TLC analysis, more Cyclopropanecarbonyl chloride (52 µL) was added and the reaction mixture was stirred. Following further TLC analysis more Cyclopropanecarbonyl chloride (30 µL) was added. Following TLC analysis (90:10), the solvent was removed *in vacuo*, the crude residue was dissolved in DCM and extracted using deionised water, 1M HCl, sat. $NaHCO_3$ solution and brine. The organic phase was dried (Na_2SO_4), filtered and concentrated *in vacuo*. The crude product was then purified by flash column chromatography (97:3-95:5 DCM:MeOH) to yield the pure product **4.24** as a white solid (117 mg, 76%).

^{1}H NMR (500 MHz, $CDCl_3$) δ 8.79 (m, 1H), 8.03 (s, 2H, Ar_H), 7.96 (s, 2H, triaz-H), 7.86-7.71 (m, 3H, Ar_H & N*H*CH_2), 5.89 (dd, *J* = 9.2, 3.1 Hz, 2H, H-1), 5.58 (t, *J* = 9.7 Hz, 2H, H-2), 5.55 – 5.51 (m, 2H, H-4), 5.29 – 5.24 (m, 2H, H-3), 4.76 – 4.58 (m, 4H, C*H*$_2$-triaz), 4.32 – 4.25 (m, 2H, H-5), 4.21 – 4.10 (m, 4H, H-6 & H-6'), 2.23 – 2.16 (m, 6H, CH_3 of OAc), 2.00 (dd, *J* = 5.5, 3.3 Hz, 12H, CH_3 of OAc), 1.82 (d, *J* = 5.7 Hz, 6H, CH_3 of OAc), 1.63 (dd, *J* = 7.2, 4.8 Hz, 1H, C*H* of cyclopropyl), 1.02 (d, *J* = 4.3 Hz, 2H, C*H*$_2$ of cyclopropyl), 0.82 (d, *J* = 8.3 Hz, 2H, C*H*$_2$ of cyclopropyl).

^{13}C NMR (125 MHz, $CDCl_3$) δ 170.3 (s, CO of OAc), 170.1 (s, CO of OAc), 169.8 (s, CO of OAc), 169.2 (s, CO of OAc), 166.6 (s, CO of carbamate), 145.4 (s, qC_{triaz}), 139.1 (s,

qC_{Ar}), 134.9 (s, qC_{Ar}), 121.4 (s, C_{triaz}), 121.2 (s, C_{Ar}), 120.7 (s, C_{Ar}), 86.1 (s, C-1), 73.9 (s, C-5), 70.8 (s, C-3), 68.0 (s, C-2), 66.8 (s, C-4), 61.1 (s, C-6), 35.4 (s, *C*H_2-triaz), 20.6 (s, CH_3 of OAc), 20.6 (s, CH_3 of OAc), 20.5 (s, CH_3 of OAc), 20.2 (s, CH_3 of OAc), 15.4 (s, *C*H of cyclopropyl), 8.2 (s, *C*H_2 of cyclopropyl). IR (ATR): 1746, 1367, 1211, 1107, 1043 cm^{-1}. HRMS (ESI+): m/z calculated for $C_{46}H_{55}N_9O_{21}$ + Na^+ [M+Na^+]: 1092.3410, found 1092.3405.

***N,N'*-di-(β-D-galactopyranosyl-1,2,3-triazol-4-ylmethylamide)-N''-propyl-5-bromobenzene-1,3-dicarboxamide 4.25**

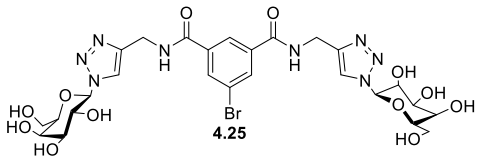

4.25

4.22 (222 mg, 0.21 mmol) was dissolved in MeOH/H_2O (4 mL/2 mL) and refluxed at 45-50 ^oC for 5 mins, NEt_3 (0.25 mL, 1.79 mmol) was then added and the reaction mixture was refluxed at 45-50^oC until the reaction was deemed complete by TLC analysis (90:10 DCM:MeOH) (6 h). The solvent was removed *in vacuo*, the residue was dissolved in water and treated with Amberlite H^+ for 1 h, this was then filtered and the solvent was removed *in vacuo* to yield the pure product **4.25** as an off-white solid (101 mg, 67%).

^{1}H NMR (500 MHz, D_2O) δ 8.25 (s, 2H, triaz-H), 8.04 (s, 1H, Ar_H), 8.02 (s, 2H, Ar), 5.71 – 5.66 (m, 2H, H-1), 4.70 (d, *J* = 10.2 Hz, 4H, CH_2), 4.22 (t, *J* = 9.5 Hz, 2H, H-2), 4.09 (s, 2H, H-4), 4.00 (t, *J* = 6.0 Hz, 2H, H-5), 3.88 (dd, *J* = 10.1, 1.5 Hz, 2H, H-3), 3.79 (t, *J* = 8.7 Hz, 4H, H-6/7).

^{13}C NMR (125 MHz, D_2O) δ 167.9 (s, CO), 144.9 (s, qC-triaz), 135.4 (s, qC-Ar), 133.3 (s, C_{Ar}), 124.7 (s, C_{Ar}), 122.9 (s, C-triaz), 122. (s, qC-Ar), 88.04 (s, C-1), 78.2 (s, C-5), 72.9 (s, C-3), 69.7 (s, C-2), 68.5 (s, C-4), 60.8 (s, C-6), 35.0 (s, *C*H_2). IR (ATR): 3302, 1647, 1534, 1282 cm^{-1}. HRMS (ESI+): m/z calcd for $C_{26}H_{33}BrN_8O_{12}$ + Na^+ [M+Na]$^+$ 751.1299, found 751.1276.

***N*,*N*'-di-(β-D-galactopyranosyl-1,2,3-triazol-4-ylmethylamide)-N''-propyl-5-methoxybenzene-1,3-dicarboxamide 4.26**

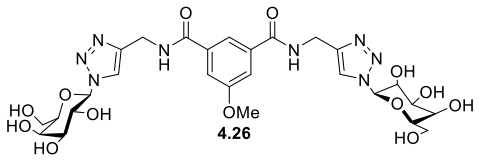

4.26

4.23 (610 mg, 0.6 mmol) was dissolved in MeOH/H_2O (10 mL/5 mL) and refluxed at 45-50 ^oC for 5 mins, NEt_3 (0.5 mL, 3.58 mmol) was then added and the reaction mixture was refluxed at 45-50^oC until the reaction was deemed complete by TLC analysis (90:10 DCM:MeOH) (6 h). The solvent was removed *in vacuo*, the residue was dissolved in water and treated with Amberlite H^+ for 1 h, this was then filtered and the solvent was removed *in vacuo* to yield the pure product **4.26** as an off-white solid (315 mg, 77%).

^1H NMR (500 MHz, D_2O) δ 8.23 (s, 2H, triaz-H), 7.61 (s, 1H, Ar-H), 7.31 (s, 2H, Ar-H), 5.66 (d, *J* = 9.2 Hz, 2H, H-1), 4.63 (s, 4H, CH_2), 4.22 (t, *J* = 9.5 Hz, 2H, H-2), 4.08 (d, *J* = 3.1 Hz, 2H, H-4), 3.98 (t, *J* = 6.0 Hz, 2H, H-5), 3.87 (dd, *J* = 9.7, 2.8 Hz, 2H, H-3), 3.80 – 3.72 (m, 7H, H-6/7 & OMe).

^{13}C NMR (125 MHz, D_2O) δ 168.7 (s, CO), 159.1 (s, qC_{Ar}), 144.9 (s, qC-triaz), 134.8 (s, qC_{Ar}), 122.9 (s, C-triaz), 118.2 (s, C_{Ar}), 116.0 (s, C_{Ar}), 88.0 (s, C-1), 78.2 (s, C-5), 72.9 (s, C-3), 69.7 (s, C-2), 68.5 (s, C-4), 60.8 (s, C-6), 55.6 (s, O*C*H_3), 34.9 (s, *C*H_2). IR (ATR): 3292, 1643, 1592, 1534, 1455, 1425, 1337, 1286 cm^{-1}. HRMS (ESI+): m/z calcd for $C_{27}H_{36}N_8O_{13}$ + H^+ $[M+H]^+$ 681.2480, found 681.2466.

***N*,*N*'-di-(β-D-galactopyranosyl-1,2,3-triazol-4-ylmethylamide)-N''-propyl-5-(cyclopropanecarbonylamino)benzene-1,3-dicarboxamide 4.27**

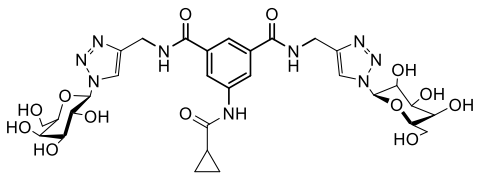
4.27

4.24 (53 mg, 0.05 mmol) was dissolved in a mixture of MeOH/H_2O (6 mL/3 mL) and refluxed at 45-50^oC, NEt_3 (0.1 mL) was then added and the mixture was refluxed until the reaction was deemed complete by TLC analysis (approx. 5 h). The solvent was

then removed *in vacuo*, the crude residue was then dissolved in deionised water and stirred with Amberlite H^+ for one h, this was then filtered, concentrated *in vacuo* and freeze dried to yield the pure product **4.27** as a white solid (32 mg, 89%).

^{1}H NMR (500 MHz, D_2O) δ 8.23 (s, 2H, triaz-H), 7.79 (s, 2H, Ar_H), 7.73 (s, 1H, Ar_H), 5.66 (d, *J* = 9.2 Hz, 2H, H-1), 4.61 (s, 4H, CH_2-triaz), 4.21 (t, *J* = 9.5 Hz, 2H, H-2), 4.07 (d, *J* = 3.2 Hz, 2H, H-4), 3.97 (t, *J* = 6.1 Hz, 2H, H-5), 3.86 (dd, *J* = 9.8, 3.3 Hz, 2H, H-3), 3.75 (d, *J* = 6.0 Hz, 4H, H-6), 1.68 – 1.57 (m, 1H, Ch of cyclopropyl), 0.87 (d, *J* = 5.3 Hz, 4H, CH_2 of cyclopropyl).

^{13}C NMR (125 MHz, D_2O) δ 175.5 (s, CO of cyclopropyl), 168.4 (s, CO), 144.6 (s, qC_{triaz}), 138.3 (s, qC_{Ar}), 134.1 (s, qC_{Ar}), 123.0 (s, C_{triaz}), 121.9 (s, C_{Ar}), 121.3 (s, C_{Ar}), 88.0 (s, C-1), 78.2 (s, C-5), 72.9 (s, C-3), 69.7 (s, C-2), 68.5 (s, C-4), 60.8 (s, C-6), 35.0 (s, *C*H_2-triaz), 14.8 (s, CH of cyclopropyl), 7.9 (s, CH_2 of cyclopropyl). IR (ATR): 3266, 1640, 1540, 1445, 1423, 1338, 1286, 1200, 1091, 1054, 1015 cm^{-1}. HRMS (ESI+): m/z calculated for $C_{30}H_{39}N_9O_{13}$ + Na^+ [M+Na^+]: 756.2565, found 756.2573.

1-Azido-2,3,4-tri-*O*-acetyl-1-deoxy-5*N*,6*O*-oxomethylidenegalactojirimycin 4.32

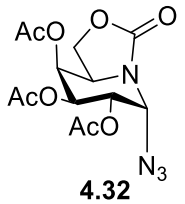

4.32

4.28 (100 mg, 0.26 mmol) was dissolved in anhydrous DCM (5 mL) and cooled to 0 ^oC, 33% HBr in AcOH (0.18 mL) was slowly added to the reaction mixture. The reaction mixture was stirred for 3 mins, after which the solution was diluted with DCM (10 mL) and quickly extracted using sat. $NaHCO_3$ (x2) solution and brine (x1), the organic phase was dried (Na_2SO_4), filtered and concentrated *in vacuo*. The crude product was placed on the schlenk line for 30 mins before NaN_3 (26 mg, 0.4 mmol) was added and this was placed under argon and dissolved in anhydrous DMF (6.6 mL). The reaction mixture was stirred at RT for 2 h after which the reaction progress was checked by TLC analysis. The solvent was removed *in vacuo* and an extraction was carried out using ethyl acetate, deionised H_2O (x1) and brine (x1), the organic phase was dried (Na_2SO_4), filtered and concentrated *in vacuo*. The crude product was purified by flash

column chromatography (1:1 Ethyl acetate: Cyclohexane) to yield the pure product **4.32** as a colourless oil (22 mg, 23%).

^{1}H NMR (500 MHz, $CDCl_3$) δ 5.39 (s, 1H, H-4), 5.23 – 5.13 (m, 1H, H-2), 4.99 (ddd, *J* = 9.9, 3.0, 1.3 Hz, 1H, H-3), 4.75 (d, *J* = 8.6 Hz, 1H, H-1), 4.39 – 4.31 (m, 1H, H-6/H-6'), 4.14 – 4.04 (m, 1H, H-5), 3.94 (ddd, *J* = 8.5, 6.3, 2.4 Hz, 1H, H-6/H-6'), 2.17 (m, 3H, CH_3 of OAc), 2.13 – 2.06 (m, 3H, CH_3 of OAc), 1.99 – 1.94 (m, 3H, CH_3 of OAc). ^{13}C NMR (75.5 MHz, $CDCl_3$) δ 168.7 (CO (OAc)), 156.5 (CO of carbamate), 72.7 (C-3/4), 71.8 (C-2), 68.4 (C-5), 67.6 (C-6), 52.6 (C-1), 20.6 (CH_3 of OAc). HRMS (ESI+): m/z = 379.1 [M+Na^+]. Anal. calcd. for $C_{13}H_{16}N_4O_8$: C 43.82, H 4.53, N 15.73. Found C 43.89, H 4.60, N 15.57.

1-Azido-2,3,4-tri-*O*-acetyl-1-deoxy-5*N*,6*O*-oxomethyleneglucojirimycin 4.33

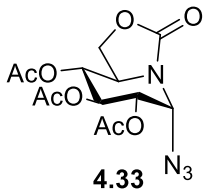

4.33

4.29 (100 mg, 0.26 mmol) was dissolved in anhydrous DCM (5mL) and cooled to 0 °C, 33% HBr in AcOH (0.18 mL) was slowly added to the reaction mixture. The reaction mixture was stirred for 3 mins, after which the solution was diluted with DCM (10 mL) and quickly extracted using sat. $NaHCO_3$ (x2) solution and brine (x1), the organic phase was dried (Na_2SO_4), filtered and concentrated *in vacuo*. The crude product was placed on the schlenk line for 30 mins before NaN_3 (26 mg, 0.4 mmol) was added and this was placed under argon and dissolved in anhydrous DMF (6.6mL). The reaction mixture was stirred at RT for 2 h after which the reaction progress was checked by TLC analysis. The solvent was removed *in vacuo* and an extraction was carried out using ethyl acetate, deionised H_2O (x1) and brine (x1), the organic phase was dried (Na_2SO_4), filtered and concentrated *in vacuo*. The crude product was purified by flash column chromatography (1:1 Ethyl acetate: Cyclohexane) to yield the pure product **4.33** as a white amorphous solid (49 mg, 52%).

^{1}H NMR (500 MHz, $CDCl_3$) δ 5.27 (dd, *J* = 4.1, 0.7 Hz, 1H, H-1), 5.20 (dd, *J* = 10.7, 6.8 Hz, 1H, H-4), 5.09 (ddd, *J* = 6.8, 3.3, 0.8 Hz, 1H, H-3), 5.07 – 5.03 (m, 1H, H-2), 4.48

(dd, *J* = 8.9, 7.8 Hz, 1H, H-6/H-6'), 4.23 (t, *J* = 9.1 Hz, 1H, H-6/H-6'), 3.97 (ddd, *J* = 10.6, 9.1, 7.8 Hz, 1H, H-5), 2.14 (s, 3H, CH_3 of OAc), 2.10 (s, 3H, CH_3 of OAc), 2.08 (s, 3H, CH_3 of OAc).

2-Azidoethyl-2,3,4-tri-*O*-acetyl-1-deoxy-5*N*,6*O*-oxomethylidenegalactojirimycin 4.34

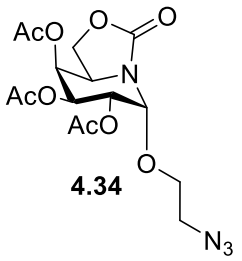

4.34

4.28 (100 mg, 0.26 mmol) was dissolved in anhydrous DCM (5 mL) and cooled to 0 ^oC, $BF_3.Et_2O$ (165 µL, 1.34 mmol) and 2-azidoethanol (29 µL, 0.4 mmol) were added and the reaction mixture was stirred for 30 mins. Following TLC analysis, the reaction mixture was diluted with DCM (10 mL) and an extraction was carried out using sat. $NaHCO_3$ solution (2x10 mL), the organic phase was dried (Na_2SO_4), filtered and concentrated *in vacuo*. The crude product was purified by flash column chromatography (1:1 Ethyl acetate: Cyclohexane) to yield the pure product **4.34** as a colourless oil (73 mg, 68%). R_f= 0.42 (3:2 Ethyl Acetate:Cyclohexane). ^1H NMR (500 MHz, $CDCl_3$) δ 5.50 (d, *J* = 3.0 Hz, 1H, H-1), 5.45 (s, 1H, H-4), 5.33 (ddd, *J* = 10.9, 2.4, 1.4 Hz, 1H, H-3), 5.15 – 5.07 (m, 1H, H-2), 4.45 – 4.37 (m, 1H, H-6/H-6'), 4.29 (ddd, *J* = 8.0, 5.8, 1.8 Hz, 1H, H-5), 4.06 – 3.99 (m, 1H, H-6/H-6'), 3.81 – 3.73 (m, 1H, OC*H*$_2$CH$_2$N$_3$), 3.71 – 3.64 (m, 1H, OC*H*$_2$CH$_2$N$_3$), 3.47 – 3.33 (m, 2H, OCH$_2$C*H*$_2$N$_3$), 2.19 – 2.14 (m, 3H, CH_3 of OAc), 2.11 – 2.07 (m, 3H, CH_3 of OAc), 2.00 – 1.95 (m, 3H, CH_3 of OAc). ^{13}C NMR (125 MHz, $CDCl_3$) δ 170.2 (s, CO of OAc), 170.1 (s, CO of OAc), 169.9 (s, CO of OAc), 155.8 (s, CO of carbamate), 79.5 (s, C-1), 68.0 (s, C-4/C-3/ OCH_2CH$_2$N$_3$), 67.9 (s, C-4/C-3/ OCH_2CH$_2$N$_3$), 67.8 (s, C-4/C-3/ OCH_2CH$_2$N$_3$), 67.1 (s, C-2), 63.0 (s, C-6), 50.5 (s, C-5), 50.2 (s, OCH$_2$CH_2N$_3$), 20.6 (s, CH_3 of OAc), 20.6 (s, CH_3 of OAc), 20.6 (s, CH_3 of OAc). HRMS (ESI+): m/z calculated for $C_{15}H_{20}N_4O_9$ + Na^+ [M+Na+]: 423.112, found 423.11.

2-Azidoethyl-2,3,4-tri-*O*-acetyl-1-deoxy-5*N*,6*O*-oxomethylideneglucojirimycin 4.35

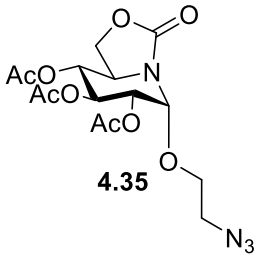

4.29 (100 mg, 0.26 mmol) was dissolved in anhydrous DCM (5 mL) and cooled to 0 ^{o}C, $BF_3.Et_2O$ (165 µL, 1.34 mmol) and 2-azidoethanol (29 µL, 0.4 mmol) were added and the reaction mixture was stirred for 30 mins. Following TLC analysis, the reaction mixture was diluted with DCM (10 mL) and an extraction was carried out using sat. $NaHCO_3$ solution (2x10 mL), the organic phase was dried (Na_2SO_4), filtered and concentrated *in vacuo*. The crude product was purified by flash column chromatography (1:1 Ethyl acetate: Cyclohexane) to yield the pure product **4.35** as a colourless oil (77 mg, 72%). R_f= 0.43 (3:2 Ethyl acetate:Cyclohexane). ^{1}H NMR (500 MHz, $CDCl_3$) δ 5.52 (td, *J* = 10.0, 1.9 Hz, 1H, H-3), 5.40 (d, *J* = 3.8 Hz, 1H, H-1), 4.96 (t, *J* = 9.6 Hz, 1H, H-4), 4.92 – 4.86 (m, 1H, H-2), 4.44 (ddd, *J* = 9.7, 8.3, 1.6 Hz, 1H, H-6/H-6'), 4.25 (tt, *J* = 12.5, 6.3 Hz, 1H, H-6/H-6'), 4.00 (td, *J* = 9.3, 1.5 Hz, 1H, H-5), 3.78 – 3.64 (m, 2H, OC*H*$_2$$CH_2N_3$), 3.46 – 3.31 (m, 2H, OCH_2C*H*$_2$$N_3$), 2.07 – 2.04 (m, 3H, CH_3 of OAc), 2.04 – 2.01 (m, 3H, CH_3 of OAc), 2.01 – 1.98 (m, 3H, CH_3 of OAc). ^{13}C NMR (125 MHz, $CDCl_3$) δ 170.1 (s, CO of OAc), 170.0 (s, CO of OAc), 169.6 (s, CO of OAc), 155.7 (s, CO of carbamate), 79.0 (s, C-1), 72.5 (s, C-4), 70.2 (s, C-2), 68.9 (s, C-3), 68.1 (s, O*C*$H_2$$CH_2N_3$), 66.8 (s, C-6), 51.6 (s, C-5), 50.2 (s, OCH_2*C*$H_2$$N_3$), 20.5 (s, CH_3 of OAc), 20.5 (bs, CH_3 of OAc (x2)). HRMS (ESI+): m/z calculated for $C_{15}H_{20}N_4O_9$ + Na^+ [M+Na+]: 423.112, found 423.11.

***N*,*N*'-di(prop-2-yn-1-yl)-5-propionamido-isophthalamide 4.37**

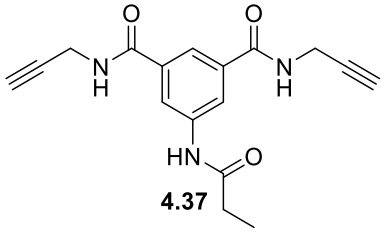

5-aminoisophathalic acid (5 g, 27.6 mmol) was dissolved in anhydrous THF (60 mL) under N_2 and propionyl chloride (2.7 mL, 30.4 mmol) was added dropwise. The mixture was allowed to stir for 5 min and NEt_3 (5 mL, 35.8 mmol) was added slowly. The reaction was left to stir for 22 h at RT. The solvent was removed under reduced pressure, and the residue was dissolved in hot MeOH. The insoluble material was filtered off and the filtrate was concentrated in vacuo to give **4.36**, which was used without further purification (5.03 g, 77%). **4.36** (1 g, 4.22 mmol) and TBTU (4 g, 12.6 mmol) were dissolved in anhydrous DMF (18 mL) under N_2. After 10 min, propargylamine (1.08 mL, 16.8 mmol) and NEt_3 (1.18 mL, 8.44 mmol) were added. It was left to stir at RT for 16 h. The reaction mixture was poured into ice/water (30 mL) and the precipitate formed, which was then filtered and dried *in vacuo* to give **4.37** as a white amorphous solid (478 mg, 36%).

^{1}H NMR (500 MHz, DMSO) δ 10.19 (s, 1H, NH), 8.97 (d, *J* = 5.0 Hz, 2H, N*H*CH_2), 8.17 (s, 2H, Ar_H), 7.92 (s, 1H, Ar_H), 4.05 (d, *J* = 2.8 Hz, 4H, NHC*H*$_2$), 3.12 (s, 2H, $NHCH_2CCH$), 2.34 (q, *J* = 7.4 Hz, 2H, C*H*$_2CH_3$), 1.09 (t, *J* = 7.5 Hz, 3H, CH_2CH_3).

The NMR data is in agreement with the literature [80].

***N*,*N*'-di-(2,3,4-tri-*O*-acetyl-1-deoxy-5*N*,6*O*-oxomethylidenegalactojirimycin-1,2,3-triazol-4-ylmethylamide)-N''-propyl-5-aminobenzene-1,3-dicarboxamide 4.38**

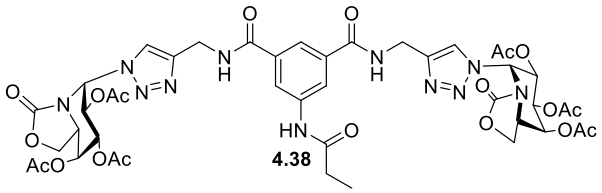

4.37 (32 mg, 0.1 mmol, 1 equiv.), **4.32** (81 mg, 0.22 mmol, 2.2 equiv.), Copper sulfate pentahydrate (100 mg) and sodium ascorbate (150 mg) were dissolved in ACN/H_2O (12 mL/4 mL) and reacted in the microwave at 100 ^oC until the reaction was deemed

complete by TLC analysis (90:10 DCM:MeOH) (30 mins). The solvent was then removed in vacuo and the resulting residue was extracted using DCM and brine, the organic phase was dried ($MgSO_4$), filtered and the solvent was removed *in vacuo*. The product was purified by flash column chromatography (95:5-90:10 DCM:MeOH) as an off-white oil **4.38** (76 mg, 41%).

^{1}H NMR (500 MHz, DMSO) δ 10.16 (s, 1H, N*H*), 9.02 (t, *J* = 5.8 Hz, 2H, N*H*CH_2), 8.17 (d, *J* = 1.2 Hz, 2H, Ar_H), 8.02 (s, 2H, triaz-H), 7.95 (d, *J* = 21.5 Hz, 1H, Ar_H), 6.22 (d, *J* = 9.2 Hz, 2H, H-1), 5.68 – 5.58 (m, 2H, H-2), 5.46 – 5.38 (m, 2H, H-4), 5.31 – 5.22 (m, 2H, H-3), 4.54 – 4.42 (m, 6H, H-5 & CH_2(x2)), 4.40 – 4.30 (m, 2H, H-6/H-6'), 3.98 – 3.89 (m, 2H, H-6/H-6'), 2.30 (dt, *J* = 10.6, 6.1 Hz, 2H, C*H*$_2$$CH_3$), 2.17 (s, 6H, CH_3 of OAc), 1.90 (s, 6H, CH_3 of OAc), 1.77 (s, 6H, CH_3 of OAc), 1.05 (t, *J* = 7.6 Hz, 3H, CH_2C*H*$_3$).
^{13}C NMR (125 MHz, DMSO) δ 172.7 (s, CO of *C*OCH_2CH_3), 170.5 (s, CO of OAc), 169.9 (s, CO of OAc), 168.8 (s, CO of OAc), 166.3 (s, CONH), 154.4 (s, CO of carbamate), 145.1 (s, qC_{triaz}), 139.9 (s, qC_{Ar}), 135.4 (s, qC_{Ar}), 124.1 (s, C_{triaz}), 121.3 (s, C_{Ar}), 120.8 (s, C_{Ar}), 71.4 (s, C-3), 68.7 (s, C-1), 68.6 (s, C-2), 65.8 (s, C-4), 62.9 (s, C-6), 55.7 (s, C-5), 35.2 (s, CH_2), 29.9 (s, *C*H_2CH_3), 21.0 (s, CH_3 of OAc), 20.7 (s, CH_3 of OAc), 20.3 (s, CH_3 of OAc), 10.0 (s, CH_2*C*H_3). IR (ATR): 1746, 1369, 1208, 1018 cm^{-1}. HRMS (ESI+): m/z calculated for $C_{43}H_{49}N_{11}O_{19}$ + H^+ [M+H^+]: 1024.3284, found 1024.3295.

_N_,_N_'-di-(2,3,4-tri-_O_-acetyl-1-deoxy-5_N_,6_O_-oxomethylideneglucojirimycin-1,2,3-triazol-4-ylmethylamide)-N''-propyl-5-aminobenzene-1,3-dicarboxamide 4.39

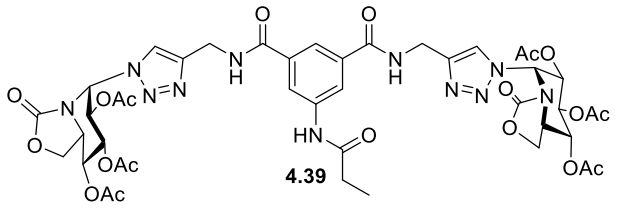

4.39

4.37 (18 mg, 0.05 mmol, 1 equiv.), **4.33** (46 mg, 0.12 mmol, 2.2 equiv.), Copper sulfate pentahydrate (100 mg) and sodium ascorbate (150 mg) were dissolved in ACN/H_2O (12 mL/4 mL) and reacted in the microwave at 100 °C until the reaction was deemed complete by TLC analysis (90:10 DCM:MeOH) (30 mins). The solvent was then removed in vacuo and the resulting residue was extracted using DCM and brine, the organic phase was dried ($MgSO_4$), filtered and the solvent was removed *in vacuo*. The

product was purified by flash column chromatography (98:2-90:10 DCM:MeOH) as an off-white oil **4.39** (58 mg, 53%).

^{1}H NMR (500 MHz, DMSO) δ 10.16 (s, 1H, NH), 9.00 (t, *J* = 5.9 Hz, 2H, N*H*CH_2), 8.25 (s, 2H, triaz-H), 8.21 (d, *J* = 1.2 Hz, 2H, Ar_H), 8.01 (d, *J* = 9.7 Hz, 1H, Ar_H), 6.29 (d, *J* = 8.3 Hz, 2H, H-1), 5.64 (t, *J* = 8.4 Hz, 2H, H-2), 5.35 (dt, *J* = 22.1, 9.0 Hz, 4H, H-3 & H-4), 4.58 – 4.45 (m, 6H, H-6/H-6' & CH_2(x2)), 4.26 (td, *J* = 9.6, 7.5 Hz, 2H, H-5), 4.11 – 4.01 (m, 2H, H-6/H-6'), 2.34 (q, *J* = 7.5 Hz, 2H, C*H*$_2$$CH_3$), 2.02 (s, 6H, CH_3 of OAc), 1.94 (s, 6H, CH_3 of OAc), 1.82 (s, 6H, CH_3 of OAc), 1.09 (t, *J* = 7.6 Hz, 3H, CH_2C*H*$_3$).
^{13}C NMR (125 MHz, DMSO) δ 172.7 (s, CO of *C*OCH_2CH_3), 170.2 (s, CO of OAc), 169.7 (s, CO of OAc), 168.8 (s, CO of OAc), 166.1 (s, CONH), 154.4 (s, CO of carbamate), 145.5 (s, qC_{triaz}), 139.9 (s, qC_{Ar}), 135.3 (s, qC_{Ar}), 123.1 (s, C_{triaz}), 121.4 (s, C_{Ar}), 120.7 (s, C_{Ar}), 71.9 (s, C-3/4), 71.5 (s, C-2), 70.3 (s, C-3/4), 68.5 (s, C-1), 66.3 (s, C-6), 55.7 (s, C-5), 35.2 (s, CH_2), 29.9 (s, *C*H_2CH_3), 20.8 (s, CH_3 of OAc), 20.6 (s, CH_3 of OAc), 20.3 (s, CH_3 of OAc), 10.0 (s, CH_2*C*H_3). IR (ATR): 1747, 1369, 1205, 1023, 952 cm^{-1}. HRMS (ESI+): m/z calculated for $C_{43}H_{49}N_{11}O_{19}$ + H^+ [M+H^+]: 1024.3284, found 1024.3294.

_N_,_N_'-di-[2-O-(2,3,4-tri-_O_-acetyl-1-deoxy-5_N_,6_O_-oxomethylidenegalactojirimycin)-ethyl-1,2,3-triazol-4-ylmethylamide)]-N''-propyl-5-aminobenzene-1,3-dicarboxamide 4.40

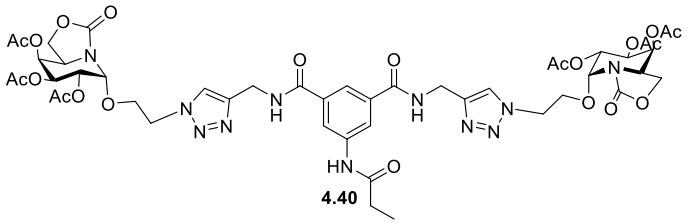

4.37 (29 mg, 0.09 mmol, 1 equiv.), **4.34** (84 mg, 0.21 mmol, 2.2 equiv.) Copper sulfate pentahydrate (100 mg) and sodium ascorbate (150 mg) were dissolved in ACN/H_2O (12 mL/4 mL) and reacted in the microwave at 100 ^{o}C until the reaction was deemed complete by TLC analysis (90:10 DCM:MeOH) (30 mins). The solvent was then removed in vacuo and the resulting residue was extracted using DCM and brine, the organic phase was dried ($MgSO_4$), filtered and the solvent was removed *in vacuo*. The product was purified by flash column chromatography (97:3-92:8 DCM:MeOH) as a colourless oil **4.40** (80 mg, 76%).

^{1}H NMR (500 MHz, DMSO) δ 10.11 (s, 1H, NH), 8.97 (t, *J* = 5.7 Hz, 2H, N*H*CH_2), 8.18 (d, *J* = 1.2 Hz, 2H, Ar_H), 8.01 (s, 2H, triaz-H), 7.98 (s, 1H, Ar_H), 5.34 (d, *J* = 2.3 Hz, 2H, H-4), 5.31 (d, *J* = 4.1 Hz, 2H, H-1), 5.09 (dd, *J* = 10.9, 2.8 Hz, 2H, H-3), 4.86 (dd, *J* = 10.8, 4.1 Hz, 2H, H-2), 4.63 – 4.47 (m, 8H, OCH_2CH_2 & CH_2NH), 4.38 – 4.30 (m, 2H, H-6/H-6'), 4.06 – 3.92 (m, 6H, H-5, H-6/H-6' & OCH_2CH_2), 3.87 – 3.78 (m, 2H, OCH_2CH_2), 2.34 (dt, *J* = 12.1, 5.4 Hz, 2H, CH_2CH_3), 2.11 (s, 6H, CH_3 of OAc), 2.00 – 1.95 (s, 6H, CH_3 of OAc), 1.92 (s, 6H, CH_3 of OAc), 1.09 (td, *J* = 7.5, 2.7 Hz, 3H, CH_2CH_3).

^{13}C NMR (125 MHz, DMSO) δ 172.7 (s, $COCH_2CH_3$), 170.4 (s, CO of OAc), 170.3 (s, CO of OAc), 169.9 (s, CO of OAc), 166.2 (s, CONH), 156.0 (s, CO of carbamate), 145.2 (s, qC_{triaz}), 139.8 (s, qC_{Ar}), 135.3 (s, qC_{Ar}), 123.6 (s, C_{triaz}), 121.4 (s, C_{Ar}), 120.7 (s, C_{Ar}), 78.7 (s, C-1), 68.6 (s, C-4), 67.8 (s, C-3), 67.2 (s, C-2), 66.4 (s, OCH_2CH_2), 63.7 (s, C-6), 50.3 (s, C-5), 49.2 (s, OCH_2CH_2), 35.3 (s, CH_2NH), 29.9 (s, CH_2CH_3), 20.8 (s, CH_3 of OAc), 20.8 (s, CH_3 of OAc), 20.8 (s, CH_3 of OAc), 10.0 (s, CH_2CH_3). IR (ATR): 1743, 1370, 1215, 1118, 1046, 1020, 952 cm^{-1}. HRMS (ESI+): m/z calculated for $C_{47}H_{57}N_{11}O_{21}$ + Na^+ [M+Na^+]: 1134.3628, found 1134.3631,

N,N'-di-[2-O-(2,3,4-tri-O-acetyl-1-deoxy-5N,6O-oxomethylideneglucojirimycin)-ethyl-1,2,3-triazol-4-ylmethylamide)]-N''-propyl-5-aminobenzene-1,3-dicarboxamide 4.41

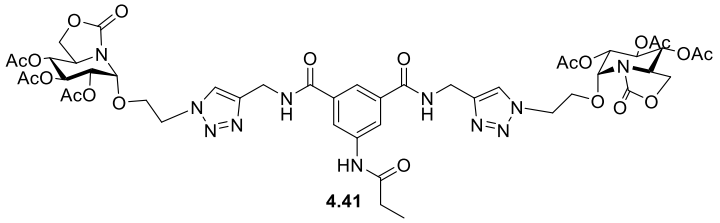

4.37 (26 mg, 0.08 mmol, 1 equiv.), **4.35** (74 mg, 0.18 mmol, 2.2 equiv.) Copper sulfate pentahydrate (100 mg) and sodium ascorbate (150 mg) were dissolved in ACN/H_2O (12 mL/4 mL) and reacted in the microwave at 100 °C until the reaction was deemed complete by TLC analysis (90:10 DCM:MeOH) (30 mins). The solvent was then removed in vacuo and the resulting residue was extracted using DCM and brine, the organic phase was dried ($MgSO_4$), filtered and the solvent was removed *in vacuo*. The product was purified by flash column chromatography (97:3-92:8 DCM:MeOH) as a colourless oil **4.41** (80 mg, 76%).

^{1}H NMR (500 MHz, DMSO) δ 10.13 (s, 1H, NH), 8.94 (t, *J* = 5.7 Hz, 2H, N*H*CH$_2$), 8.20 (dd, *J* = 9.7, 1.5 Hz, 2H, Ar$_H$), 8.01 – 7.99 (m, 2H, triaz-H), 7.98 (t, *J* = 1.4 Hz, 1H, Ar$_H$), 5.26 (d, *J* = 3.7 Hz, 2H, H-1), 5.23 (d, *J* = 10.1 Hz, 2H, H-3), 5.15 (t, *J* = 9.5 Hz, 2H, H-4), 4.97 (dd, *J* = 10.3, 4.0 Hz, 2H, H-2), 4.60 (ddd, *J* = 14.3, 6.9, 3.9 Hz, 2H, OCH$_2$C*H*$_2$), 4.56 – 4.48 (m, 6H, OCH$_2$C*H*$_2$ & C*H*$_2$NH), 4.43 (t, *J* = 8.5 Hz, 2H, H-6/H-6'), 4.14 (dd, *J* = 8.7, 6.8 Hz, 2H, H-6/H-6'), 3.94 (ddd, *J* = 10.9, 7.0, 3.9 Hz, 2H, OC*H*$_2$CH$_2$), 3.85 – 3.78 (m, 2H, OC*H*$_2$CH$_2$), 3.71 (td, *J* = 8.5, 6.9 Hz, 2H, H-5), 2.37 – 2.30 (m, 2H, C*H*$_2$CH$_3$), 1.97 (s, 12H, CH$_3$ of OAc), 1.96 (s, 6H, CH$_3$ of OAc), 1.10 (td, *J* = 7.5, 2.4 Hz, 3H, CH$_2$C*H*$_3$).

^{13}C NMR (125 MHz, DMSO) δ 172.7 (s, NH*C*OCH$_2$CH$_3$), 170.2 (s, CO of OAc), 170.1 (s, CO of OAc), 169.9 (s, CO of OAc), 166.2 (s, CONHCH$_2$), 155.7 (s, CO of carbamate), 145.1 (s, qC$_{triaz}$), 139.9 (s, qC$_{Ar}$), 135.4 (s, qC$_{Ar}$), 123.7 (s, C$_{triaz}$), 121.3 (s, C$_{Ar}$), 120.7 (s, C$_{Ar}$), 78.3 (s, C-1), 72.0 (s, C-4), 69.8 (s, C-2), 69.0 (s, C-3), 66.8 (s, C-6), 66.4 (s, OCH$_2$CH$_2$), 51.3 (s, C-5), 49.0 (s, OCH$_2$*C*H$_2$), 35.3 (s, *C*H$_2$NH), 29.9 (s, *C*H$_2$CH$_3$), 20.8 (s, CH$_3$ of OAc), 20.8 (s, CH$_3$ of OAc), 20.7 (s, s, CH$_3$ of OAc), 10.0 (s, CH$_2$*C*H$_3$). IR (ATR): 1748, 1216, 1022, 952 cm^{-1}. HRMS (ESI+): m/z calculated for $C_{47}H_{57}N_{11}O_{21}$ + Na$^+$ [M+Na$^+$]: 1134.3628, found 1134.3630.

_N_,_N_'-di-(1-deoxy-5_N_,6_O_-oxomethylidenegalactojirimycin-1,2,3-triazol-4-ylmethylamide)-N''-propyl-5-aminobenzene-1,3-dicarboxamide 4.42

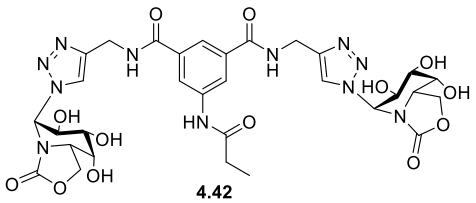

4.42

4.38 (67 mg, 0.06 mmol) was dissolved in MeOH/H$_2$O (4 mL/2 mL) and refluxed at 45-50 ^{o}C for 5 mins, NEt$_3$ (0.1 mL) was then added and the reaction mixture was refluxed at 45-50 ^{o}C until the reaction was deemed complete by TLC analysis (90:10 DCM:MeOH) (6 h). The solvent was removed *in vacuo*, the residue was dissolved in water and treated with Amberlite H$^+$ for 1 h, this was then filtered and the solvent was removed *in vacuo* to yield the pure product **4.42** as a white fluffy solid(26 mg, 53%).

^{1}H NMR (500 MHz, DMSO) δ 10.15 (s, 1H, NH), 9.01 (t, *J* = 5.6 Hz, 2H, N*H*CH$_{2z}$), 8.20 (s, 2H, Ar$_H$), 7.98 (m, 1H, Ar$_H$), 7.70 (m, 2H, triaz-H), 5.06 (d, *J* = 4.0 Hz, 2H, H-1), 4.54

(d, *J* = 5.6 Hz, 4H, C*H*$_2$NH), 4.29 – 4.13 (m, 4H, H-6 & H-6'), 4.01 – 3.91 (m, 2H, H-5), 3.67 (t, *J* = 9.3 Hz, 2H, H-4), 3.62 – 3.55 (m, 2H, H-3), 3.51 (dd, *J* = 9.9, 4.0 Hz, 2H, H-2), 2.34 (dd, *J* = 15.1, 7.5 Hz, 2H, C*H*$_2$CH$_3$), 1.09 (td, *J* = 7.5, 0.7 Hz, 3H, CH$_2$C*H*$_3$).

^{13}C NMR (125 MHz, DMSO) δ 172.8 (s, *C*OCH$_2$CH$_3$), 166.4 (s, CO), 156.2 (s, CO of carbamate), 144.1 (m, qC$_{triaz}$), 139.9 (s, qC$_{Ar}$), 135.4 (s, qC$_{Ar}$), 126.3 (s, C-triaz), 121.3 (s, C$_{Ar}$), 120.7 (s, C$_{Ar}$), 75.4 (s, C-1), 69.5 (s, C-3), 69.2 (s, C-4), 68.2 (s, C-2), 63.4 (s, C-6), 52.8 (s, C-5), 34.8 (s, *C*H$_2$NH), 29.9 (s, *C*H$_2$CH$_3$), 10.0 (s, CH$_2$*C*H$_3$). IR (ATR): 3273, 1731, 1647, 1541, 1422, 1239, 1075, 1046, 1021, 991 cm^{-1}. HRMS (ESI+): m/z calculated for C$_{31}$H$_{37}$N$_{11}$O$_{13}$ + H$^+$ [M+H$^+$]: 772.2651, found 772.2630.

_N_,_N_'-di-[2-O-1-deoxy-5_N_,6_O_-oxomethylidenegalactojirimycin)-ethyl-1,2,3-triazol-4-ylmethylamide)]-N''-propyl-5-aminobenzene-1,3-dicarboxamide 4.43

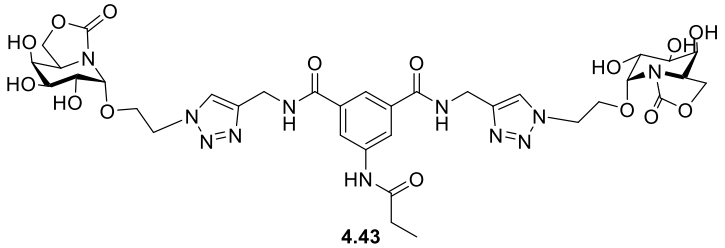

4.43

4.40 (57 mg, 0.05 mmol) was dissolved in MeOH/H$_2$O (4 mL/2 mL) and refluxed at 45-50 ^{o}C for 5 mins, NEt$_3$ (0.1 mL) was then added and the reaction mixture was refluxed at 45-50 ^{o}C until the reaction was deemed complete by TLC analysis (90:10 DCM:MeOH) (5 h). The solvent was removed *in vacuo*, the residue was dissolved in water and treated with Amberlite H$^+$ for 1 h, this was then filtered and the solvent was removed *in vacuo* to yield the pure product **4.43** as a white fluffy solid (17 mg, 50%).

^{1}H NMR (500 MHz, D$_2$O) δ 8.09 (s, 2H, triaz-H), 8.01 (s, 2H, Ar$_H$), 7.92 (bs, 1H, Ar$_H$), 5.43 (d, *J* = 4.2 Hz, 0.5H, H-1 anomer), 5.09 (d, *J* = 4.3 Hz, 2H, H-1), 4.70 – 4.62 (m, 8H, C*H*$_2$NH (x2) & OC*H*$_2$CH$_2$triaz or OCH$_2$C*H*$_2$triaz), 4.53 (t, *J* = 9.1 Hz, 1H, H-6 & H-6' anomer), 4.44 – 4.35 (m, 1H, H-6 & H-6' anomer), 4.32 – 4.24 (m, 0.8H, H-5 anomer), 4.19 (dt, *J* = 14.9, 8.9 Hz, 4H, H-6 & H-6'), 4.09 – 4.00 (m, 3H, OC*H*$_2$CH$_2$triaz or OCH$_2$C*H*$_2$triaz & H-4 anomer), 3.99 – 3.92 (m, 2H, OC*H*$_2$CH$_2$triaz or OCH$_2$C*H*$_2$triaz), 3.92 – 3.85 (m, 0.76H, H-3 anomer), 3.82 (dd, *J* = 10.3, 4.2 Hz, 0.66H, H-2 anomer),

3.75 (dd, *J* = 9.9, 4.3 Hz, 2H, H-2), 3.64 (dd, *J* = 12.2, 1.9 Hz, 4H, H-3 & H-4), 3.27 – 3.17 (m, 2H, H-5), 2.46 (q, *J* = 7.6 Hz, 2H, CH_2CH$_3$), 1.19 (t, *J* = 7.6 Hz, 3H, CH_2CH_3). ^{13}C NMR (125 MHz, D_2O) δ 176.7 (s, *C*OCH$_2$CH$_3$), 168.4 (s, *C*ONH), 158.1 (s, CO of carbamate), 138.4 (s, qC$_{Ar}$), 134.5 (s, qC$_{Ar}$/qC$_{triaz}$), 124.1 (s, C$_{triaz}$), 122.7 (s, C$_{Ar}$), 121.8 (s, C$_{Ar}$), 81.5 (s, C-1), 74.5 (s, C-1 anomer), 69.2 (s, C-3/C-4), 69.1 (s, C-3/C-4 anomer), 68.7 (s, C-3/C-4 anomer), 68.6 (s, C-3/C-4), 67.5 (s, C-2 anomer), 67.1 (s, C-2), 66.8 (s, O*C*H$_2$CH$_2$ or OCH$_2$*C*H$_2$), 64.3 (s, C-6/C-6 anomer), 64.2 (s, C-6/C-6 anomer), 52.6 (s, C-5 anomer), 52.3 (s, C-5), 50.1 (s, O*C*H$_2$CH$_2$ or OCH$_2$*C*H$_2$), 34.8 (s, *C*H$_2$NH), 29.8 (s, *C*H$_2$CH$_3$), 9.1 (s, CH$_2$*C*H$_3$). IR (ATR): 3274, 1730, 1651, 1538, 1423, 1332, 1234, 1121, 1066, 1010, 948 cm^{-1}. HRMS (ESI+): m/z calculated for $C_{35}H_{45}N_{11}O_{15}$ + H^+ [M+H$^+$]: 860.3175, found 860.3169.

***N*,*N*'-di-[2-O-1-deoxy-5*N*,6*O*-oxomethylideneglucojirimycin)-ethyl-1,2,3-triazol-4-ylmethylamide)]-N''-propyl-5-aminobenzene-1,3-dicarboxamide 4.44**

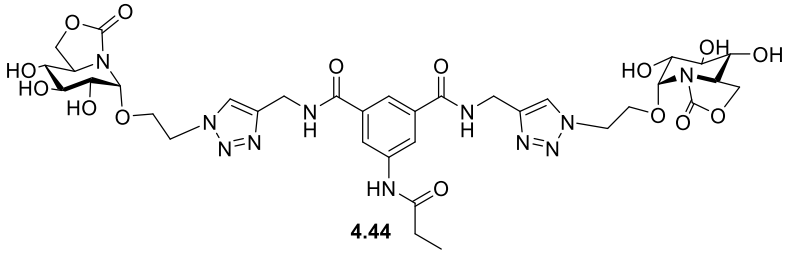

4.44

4.41 (43 mg, 0.04 mmol) was dissolved in MeOH/H_2O (4 mL/2 mL) and refluxed at 45-50 ^{o}C for 5 mins, NEt_3 (0.1 mL) was then added and the reaction mixture was refluxed at 45-50 ^{o}C until the reaction was deemed complete by TLC analysis (90:10 DCM:MeOH) (6 h). The solvent was removed *in vacuo*, the residue was dissolved in water and treated with Amberlite H^+ for 1 h, this was then filtered and the solvent was removed *in vacuo* to yield the pure product **4.44** as a white fluffy solid (11 mg, 35%).

^{1}H NMR (500 MHz, D_2O) δ 8.09 (s, 2H, triaz-H), 8.00 (s, 2H, Ar$_H$), 7.91 (s, 1H, Ar$_H$), 5.38 (d, *J* = 4.0 Hz, 0.09H, H-1 anomer), 5.05 (d, *J* = 3.6 Hz, 2H, H-1), 4.66 (dd, *J* = 14.7, 8.8 Hz, 8H, C*H*$_2$NH (x2) & OC*H*$_2$CH$_2$triaz or OCH$_2$C*H*$_2$triaz), 4.33 (dt, *J* = 13.6, 4.5 Hz, 2H, H-6 & H-6'), 4.15 (m, 2H, H-6 & H-6'), 4.05 (m, 2H, OC*H*$_2$CH$_2$triaz or OCH$_2$C*H*$_2$triaz), 3.98 (m, 2H, OC*H*$_2$CH$_2$triaz or OCH$_2$C*H*$_2$triaz), 3.52 (m, 4H, H-2 & H-3), 3.39 (dd, *J* = 12.0,

6.1 Hz, 2H, H-4), 3.05 – 2.97 (m, 2H, H-5), 2.46 (m, 2H, CH_2CH$_3$), 1.19 (t, *J* = 7.6 Hz, 3H, CH$_2$CH_3).

^{13}C NMR (125 MHz, D$_2$O) δ 176.6 (s, *C*OCH$_2$CH$_3$), 168.9 (s, *C*ONHCH$_2$), 157.8 (s, CO of carbamate), 138.2 (s, qC$_{Ar}$), 134.5 (s, qC$_{Ar}$ & qC$_{triaz}$), 124.3 (s, C-triaz), 122.7 (s, C$_{Ar}$), 121.9 (s, C$_{Ar}$), 81.4 (s, C-1), 73.2 (s, C-4), 72.3 (s, C-2/3), 70.6 (s, C-2/3), 67.3 (s, C-6), 66.8 (s, O*C*H$_2$CH$_2$ or OCH$_2$*C*H$_2$), 52.8 (s, C-5), 50.1 (s, O*C*H$_2$CH$_2$ or OCH$_2$*C*H$_2$), 34.9 (s, *C*H$_2$NH), 29.8 (s, *C*H$_2$CH$_3$), 9.1 (s, CH$_2$*C*H$_3$). IR (ATR): 1743, 1541, 1420, 1258, 1062, 1027, 994 cm^{-1}. HRMS (ESI+): m/z calculated for C$_{35}$H$_{45}$N$_{11}$O$_{15}$ + Na$^+$ [M+Na$^+$]: 882.2994, found 882.2989.

***N*-(allyl)-3-propionamidobenzamide 4.46**

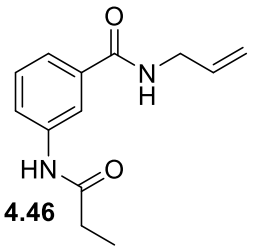

4.46

3-aminobenzoic acid (2 g, 14.6 mmol) was placed under N$_2$ and dissolved in anhydrous THF (15 mL). Propionyl chloride (3.19 mL, 36.5 mmol) was then added very slowly over the course of 30 mins and the reaction mixture was stirred for 10 mins at RT. NEt$_3$ (6.1 mL, 43.8 mmol) was then added over the course of 30 mins. A further 10 mL anhydrous THF was added and the reaction mixture was stirred overnight at RT. The solvent was removed *in vacuo*, an extraction was then carried out using ethyl acetate and 1M HCl aqueous solution. The organic phase was dried (Na$_2$SO$_4$), filtered and concentrated *in vacuo* to yield crude **4.45**. The crude product was dissolved in hot MeOH, the insoluble material was filtered off and the filtrate was concentrated *in vacuo*, the crude product was then recrystallised using ethyl acetate/diethyl ether (1:1) to yield **4.45** which was used without further purification. **4.45** (250 mg, 1.29 mmol) and TBTU (497 mg, 1.548 mmol) were placed under N$_2$ and dissolved in DMF (5 mL). NEt$_3$ (0.22 mL, 1.55 mmol) was added followed by allylamine (0.12 mL, 1.6 mmol), the reaction mixture was stirred overnight at RT. Following TLC analysis, the solvent was removed *in vacuo* and an extraction was carried out using ethyl acetate, sat. NaHCO$_3$ and brine. The organic phase was dried (Na$_2$SO$_4$), filtered and concentrated *in vacuo* to yield the pure product **4.46** as a white solid (135 mg, 45%).

^{1}H NMR (500 MHz, DMSO) δ 10.00 (s, 1H, NH), 8.61 (t, *J* = 5.6 Hz, 1H, N*H*CH_2CHCH_2), 8.02 (s, 1H, Ar_H), 7.77 (dd, *J* = 7.8, 1.6 Hz, 1H, Ar_H), 7.50 (d, *J* = 7.8 Hz, 1H, Ar_H), 7.36 (t, *J* = 7.9 Hz, 1H, Ar_H), 5.88 (ddt, *J* = 17.1, 10.4, 5.2 Hz, 1H, $NHCH_2CHCH_2$), 5.16 (dq, *J* = 17.2, 1.7 Hz, 1H, $NHCH_2CHCH_2$), 5.11 – 5.01 (m, 1H, $NHCH_2CHCH_2$), 3.94 – 3.83 (m, 2H, $NHCH_2CHCH_2$), 2.36 – 2.27 (m, 2H, $COCH_2CH_3$), 1.08 (t, *J* = 7.6 Hz, 3H, $COCH_2CH_3$). ^{13}C NMR (125 MHz, DMSO) δ 172.6 (s, $COCH_2CH_3$), 166.5 (s, $CONHCH_2CHCH_2$), 139.8 (s, qC_{Ar}), 135.9 (s, $NHCH_2CHCH_2$), 135.6 (s, qC_{Ar}), 129.0 (s, C_{Ar}), 122.0 (s, C_{Ar}), 121.7 (s, C_{Ar}), 118.8 (s, C_{Ar}), 115.5 (s, $NHCH_2CHCH_2$), 41.9 (s, $NHCH_2CHCH_2$), 29.9 (s, $COCH_2CH_3$), 10.1 (s, $COCH_2CH_3$). IR (ATR): 3260, 1664, 1634, 1592, 1529, 1476, 1459, 1415, 1432, 1378, 1348, 1307, 1276, 1252, 1208 cm^{-1}. HRMS (ESI+): m/z calcd for $C_{13}H_{16}N_2O_2$ + Na^+ $[M+Na]^+$ 255.1109, found 255.1109.

***N*-(aminoacetonitrile)-3-propionamidobenzamide 4.47**

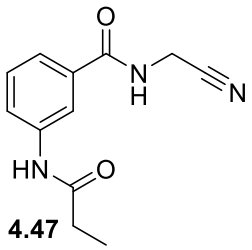

4.47

3-aminobenzoic acid (2 g, 14.6 mmol) was placed under N_2 and dissolved in anhydrous THF (15 mL). Propionyl chloride (3.19 mL, 36.5 mmol) was then added very slowly over the course of 30 mins and the reaction mixture was stirred for 10 mins at RT. NEt_3 (6.1 mL, 43.8 mmol) was then added over the course of 30 mins. A further 10 mL anhydrous THF was added and the reaction mixture was stirred overnight at RT. The solvent was removed *in vacuo*, an extraction was then carried out using ethyl acetate and 1M HCl aqueous solution. The organic phase was dried (Na_2SO_4), filtered and concentrated *in vacuo* to yield crude **4.45**. The crude product was dissolved in hot MeOH, the insoluble material was filtered off and the filtrate was concentrated *in vacuo*, the crude product was then recrystallised using ethyl acetate/diethyl ether (1:1) to yield **4.45** which was used without further purification. **4.45** (1 g, 5.18 mmol) and TBTU (1.99 g, 6.21 mmol) were placed under N_2 and dissolved in DMF (10 mL). NEt_3 (0.87 mL, 6.21 mmol) was added followed by aminoacetonitrile hydrochloride (0.58 g, 6.21 mmol), which had been placed under N_2 in a separate round-bottom flask and dissolved in DMF (3 mL) and added via a cannula to the reaction mixture.

The reaction mixture was stirred overnight at RT. Following TLC analysis, the solvent was removed *in vacuo* and an extraction was carried out using ethyl acetate, sat. $NaHCO_3$ and brine. The organic phase was dried (Na_2SO_4), filtered and concentrated *in vacuo* to yield the pure product **4.47** as a white solid (250 mg, 21%).

^{1}H NMR (500 MHz, DMSO) δ 10.05 (s, 1H, N*H*COCH$_2$CH$_3$), 9.16 (s, 1H, CON*H*CH$_2$CCN), 8.11 (s, 1H, Ar$_H$), 7.78 (dd, *J* = 8.1, 1.1 Hz, 1H, Ar$_H$), 7.54 – 7.45 (m, 1H, Ar$_H$), 7.41 (t, *J* = 7.9 Hz, 1H, Ar$_H$), 4.29 (d, *J* = 3.8 Hz, 2H, C*H*$_2$CCN), 2.39 – 2.28 (m, 2H, COC*H*$_2$CH$_3$), 1.09 (t, *J* = 7.6 Hz, 3H, COCH$_2$C*H*$_3$). ^{13}C NMR (125 MHz, DMSO) δ 172.7 (s, *C*OCH$_2$CH$_3$), 167.1 (s, *C*ONHCH$_2$CCN), 140.0 (s, qC$_{Ar}$), 133.9 (s, qC$_{Ar}$), 129.3 (s, C$_{Ar}$), 122.7 (s, C$_{Ar}$), 121.9 (s, C$_{Ar}$), 118.7 (s, C$_{Ar}$), 118.1 (s, CH$_2$*C*CN), 29.9 (s, CO*C*H$_2$CH$_3$), 28.2 (s, NH*C*H$_2$CCN), 10.0 (s, COCH$_2$*C*H$_3$). IR (ATR): 3262, 1664, 1646, 1596, 1524, 1476, 1460, 1434, 1415, 1309, 1278, 1253, 1208 cm^{-1}. HRMS (ESI+): m/z calcd for $C_{12}H_{13}N_3O_2 + H^+$ $[M+H]^+$ 232.1086, found 232.1082.

***N,N'*-di(allyl)-5-[[(1,1-Dimethylethoxy)carbonyl]amino]isophthalamide 4.48**

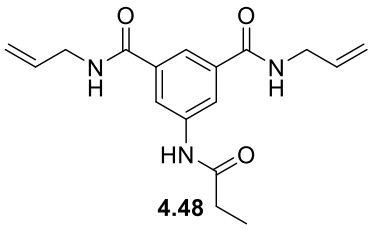

4.48

5-aminoisophathalic acid (5 g, 27.6 mmol) was dissolved in anhydrous THF (60 mL) under N_2 and propionyl chloride (2.7 mL, 30.4 mmol) was added dropwise. The mixture was allowed to stir for 5 min and NEt_3 (5 mL, 35.8 mmol) was added slowly. The reaction was left to stir for 22 h at RT. The solvent was removed under reduced pressure, and the residue was dissolved in hot MeOH. The insoluble material was filtered off and the filtrate was concentrated in vacuo to give **4.36**, which was used without further purification (5.03 g, 77%). **4.36** (500 mg, 2.11 mmol) and TBTU (1.49 g, 4.64 mmol) were placed under N_2 and dissolved in DMF (10 mL). NEt_3 (0.65 mL, 4.64 mmol) was added and the reaction mixture was stirred for 15 mins. Allylamine (0.35 mL, 4.64 mmol) was added and the reaction mixture was stirred overnight at RT. Following TLC analysis, the solvent was removed *in vacuo* and an extraction was carried out using ethyl acetate, sat. $NaHCO_3$ and brine. The organic phase was dried

(Na_2SO_4), filtered and concentrated *in vacuo*. The crude product was triturated in ethyl acetate by dissolving in a minimum amount of ethyl acetate and adding in diethyl ether to encourage precipitation, this yielded the product **4.48** as a pale yellow solid (400 mg, 60%).

^{1}H NMR (500 MHz, DMSO) δ 10.14 (s, 1H, NH), 8.66 (t, *J* = 5.7 Hz, 2H, NH), 8.18 (d, *J* = 1.4 Hz, 2H, Ar_H), 7.94 (t, *J* = 1.4 Hz, 1H, Ar_H), 5.90 (ddt, *J* = 17.1, 10.4, 5.3 Hz, 2H, CH_2CHCH_2), 5.24 – 5.14 (m, 2H, CH_2CHCH_2), 5.11 (ddd, *J* = 10.3, 4.4, 1.6 Hz, 2H, CH_2CHCH_2), 3.93 – 3.85 (m, 4H, CH_2CHCH_2), 2.39 – 2.26 (m, 2H, $COCH_2CH_3$), 1.09 (t, *J* = 7.6 Hz, 3H, $COCH_2CH_3$).

^{13}C NMR (125 MHz, DMSO) δ 172.7 (s, $COCH_2CH_3$), 166.3 (s, CO), 139.9 (s, qC_{Ar}), 135.8 (s, qC_{Ar}), 135.7 (s, CH_2CHCH_2), 121.1 (s, C_{Ar}), 120.5 (s, C_{Ar}), 115.7 (s, CH_2CHCH_2), 42.0 (s, CH_2), 29.9 (s, CH_2CH_3), 10.0 (s, CH_2CH_3). IR (ATR): 1636, 1605, 1567, 1530, 1444, 1417, 1331, 1310, 1267, 1208 cm^{-1}. HRMS (ESI+): m/z calcd for $C_{17}H_{21}N_3O_3$ + H^+ $[M+H]^+$ 316.1661, found 316.1657.

***N,N'*-di(aminoacetonitrile)-5-[[(1,1-Dimethylethoxy)carbonyl]amino]isophthalamide 4.49**

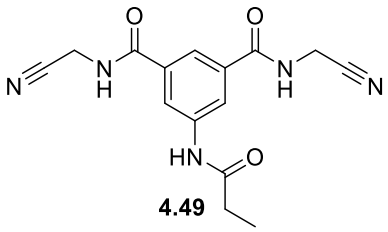

4.49

5-aminoisophathalic acid (5 g, 27.6 mmol) was dissolved in anhydrous THF (60 mL) under N_2 and propionyl chloride (2.7 mL, 30.4 mmol) was added dropwise. The mixture was allowed to stir for 5 min and NEt_3 (5 mL, 35.8 mmol) was added slowly. The reaction was left to stir for 22 h at RT. The solvent was removed under reduced pressure, and the residue was dissolved in hot MeOH. The insoluble material was filtered off and the filtrate was concentrated in vacuo to give **4.36**, which was used without further purification (5.03 g, 77%). **4.36** (500 mg, 2.11 mmol) and TBTU (1.49 g, 4.64 mmol) were placed under N_2 and dissolved in DMF (10 mL). NEt_3 (0.65 mL, 4.64 mmol) was added and the reaction mixture was stirred for 15 mins. Aminoacetonitrile hydrochloride (0.43 mL, 4.64 mmol) was added and the reaction

mixture was stirred overnight at RT. Following TLC analysis, the solvent was removed *in vacuo* and an extraction was carried out using ethyl acetate, sat. $NaHCO_3$ and brine. The organic phase was dried (Na_2SO_4), filtered and concentrated *in vacuo*. The crude product was triturated in ethyl acetate by dissolving in a minimum amount of ethyl acetate and adding in petroleum ether to encourage precipitation, this yielded the product **4.49** as a brown/yellow solid (50 mg, 8%).

^{1}H NMR (500 MHz, DMSO) δ 10.23 (s, 1H, NH), 9.36 – 9.27 (t, *J* = 5.5 Hz, 2H, N*H*CH_2), 8.26 (d, *J* = 1.3 Hz, 2H, Ar_H), 7.98 (s, 1H, Ar_H), 4.35 – 4.27 (m, 4H, CH_2NH), 2.40 – 2.31 (m, 2H, CH_2), 1.09 (dd, *J* = 10.9, 3.9 Hz, 3H, CH_3).
^{13}C NMR (125 MHz, DMSO) δ 172.9 (s, *C*OCH_2CH_3), 166.7 (s, CONH), 140.3 (s, qC_{Ar}), 134.4 (s, qC_{Ar}), 121.7 (s, C_{Ar}), 120.9 (s, C_{Ar}), 29.9 (s, *C*H_2CH_3), 28.3 (s, CH_2NH), 9.9 (s, CH_2*C*H_3). IR (ATR): 3326, 1701, 1651, 1599, 1557, 1531, 1446, 1419, 1355, 1272, 1192, 1077, 1026 cm^{-1}. HRMS (ESI+): m/z calcd for $C_{15}H_{15}N_5O_3$ + Na^+ $[M+Na]^+$ 336.1073, found 336.1069.

***N*,*N*'-di(allyl)-5-nitro-isophthalamide 4.51**

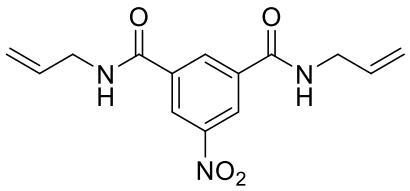

4.51

5-nitroisopthalic acid (500 mg, 2.37 mmol) and TBTU (1.67 g, 5.21 mmol) were placed under N_2 and dissolved in DMF (10 mL). NEt_3 (0.72 mL, 5.21 mmol) was added followed by allylamine (0.39 mL, 5.21 mmol), the reaction mixture was stirred overnight at RT. Following TLC analysis, the solvent was removed *in vacuo* and an extraction was carried out using ethyl acetate, sat. $NaHCO_3$ and brine. The organic phase was dried (Na_2SO_4), filtered and concentrated *in vacuo* to yield the pure product **4.51** as a pale yellow solid (415 mg, 61%).

^{1}H NMR (500 MHz, DMSO) δ 9.16 (t, *J* = 5.5 Hz, 2H, NH), 8.82 (d, *J* = 1.5 Hz, 2H, Ar_H), 8.79 (t, *J* = 1.6 Hz, 1H, Ar_H), 5.92 (ddt, *J* = 17.1, 10.5, 5.3 Hz, 2H, $NHCH_2C$*H*CH_2), 5.21 (dq, *J* = 17.2, 1.7 Hz, 2H, CH_2CHC*H*$_2$), 5.12 (ddd, *J* = 10.3, 3.0, 1.4 Hz, 2H, $NHCH_2CHC$*H*$_2$), 3.98 – 3.91 (m, 4H, NHC*H*$_2CHCH_2$).

^{13}C NMR (125 MHz, DMSO) δ 163.9 (s, CO), 148.3 (s, qC$_{Ar}$), 136.5 (s, qC$_{Ar}$), 135.3 (s, NHCH$_2$*C*HCH$_2$), 132.8 (s, C$_{Ar}$), 124.7 (s, C$_{Ar}$), 116.1 (s, NHCH$_2$CH*C*H$_2$), 42.3 (s, NH*C*H$_2$CHCH$_2$). IR (ATR): 3346, 3287, 1637, 1582, 1536, 1442, 1420, 1341, 1325, 1276 cm^{-1}. HRMS (ESI+): m/z calcd for $C_{14}H_{15}N_3O_4$ + H$^+$ [M+H]$^+$ 290.1141, found 290.1137.

***N*,*N*'-di(aminoacetonitrile)-5-nitro-isophthalamide 4.52**

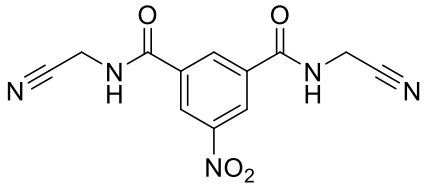

4.52

5-nitroisopthalic acid (500 mg, 2.37 mmol) and TBTU (1.67 g, 5.21 mmol) were placed under N_2 and dissolved in DMF (10 mL). NEt_3 (0.72 mL, 5.21 mmol) was added followed by aminoacetonitrile hydrochloride (0.48 g, 5.21 mmol), which had been placed under N_2 in a separate round-bottom flask and dissolved in DMF (2 mL) and added via a cannula to the reaction mixture. The reaction mixture was stirred overnight at RT. Following TLC analysis, the solvent was removed *in vacuo* and an extraction was carried out using ethyl acetate, sat. $NaHCO_3$ and brine. The organic phase was dried (Na_2SO_4), filtered and concentrated *in vacuo* to yield the pure product **4.52** as brown needle-like crystalline solid (150 mg, 22%).

^{1}H NMR (500 MHz, DMSO) δ 9.79 (s, 2H, NH), 8.87 (d, *J* = 1.5 Hz, 2H, Ar$_H$), 8.81 (t, *J* = 1.5 Hz, 1H, Ar$_H$), 4.41 (s, 4H, CH$_2$).

^{13}C NMR (125 MHz, DMSO) δ 164.5 (s, CO), 148.5 (s, qC$_{Ar}$), 135.1 (s, qC$_{Ar}$), 133.0 (s, C$_{Ar}$), 125.5 (s, C$_{Ar}$), 117.7 (s, CH$_2$*C*CN), 28.4 (s, CH$_2$). IR (ATR): 3298, 1648, 1539, 1410, 1354, 1324, 1286, 1203, 1094, 1068 cm^{-1}. HRMS (ESI+): m/z calcd for $C_{12}H_9N_5O_4$ + Na$^+$ [M+Na]$^+$ 310.0552, found 310.0546.

***N*,*N*'-di(prop-2-yn-1-yl)-5-nitro-isophthalamide 4.53**

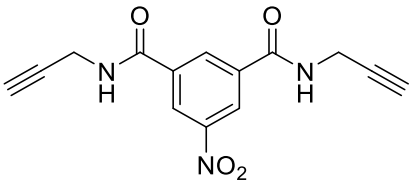

4.53

5-nitroisopthalic acid (500 mg, 2.37 mmol) and TBTU (1.67 g, 5.21 mmol) were placed under N_2 and dissolved in DMF (10 mL). NEt_3 (0.72 mL, 5.21 mmol) was added followed by propargylamine (0.33 mL, 5.21 mmol), the reaction mixture was stirred overnight at RT. Following TLC analysis, the solvent was removed *in vacuo* and an extraction was carried out using ethyl acetate, sat. $NaHCO_3$ and brine. The organic phase was dried (Na_2SO_4), filtered and concentrated *in vacuo* to yield the pure product **4.53** as a pale yellow solid (454 mg, 67%).

^{1}H NMR (500 MHz, DMSO) δ 9.48 (t, *J* = 5.3 Hz, 2H, NH), 8.83 (d, *J* = 1.5 Hz, 2H, Ar_H), 8.78 (t, *J* = 1.6 Hz, 1H, Ar_H), 4.12 (dd, *J* = 5.4, 2.5 Hz, 4H, CH_2), 3.20 (t, *J* = 2.5 Hz, 2H, CH_2CCH).

^{13}C NMR (125 MHz, DMSO) δ 163.9 (s, CO), 148.4 (s, qC_{Ar}), 135.9 (s, qC_{Ar}), 132.9 (s, C_{Ar}), 125.0 (s, C_{Ar}), 73.8 (s, $CH_2C\mathit{C}H$), 29.3 (s, CH_2). IR (ATR): 3283, 1639, 1533, 1346, 1325, 1280 cm^{-1}. HRMS (ESI+): m/z calcd for $C_{14}H_{11}N_3O_4$ + Na^+ $[M+Na]^+$ 308.0647, found 308.0641.

***N*,*N*'-di-(2,3,4,6-tetra-*O*-acetyl-β-D-galactopyranosyl-1,2,3-triazol-4-ylmethylamide)-N''-propyl-5-(4-azido-butyrylamino)benzene-1,3-dicarboxamide 4.65**

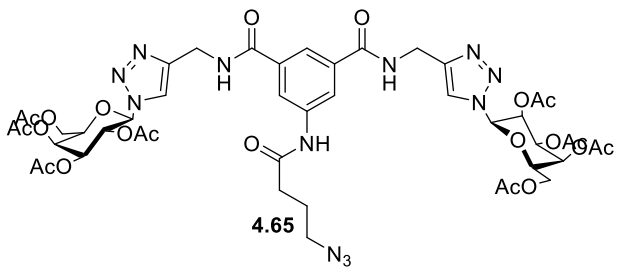

4.65

3.19 (505 mg, 0.5 mmol) was placed under N_2 and 4-chlorobutyryl chloride (84 µL, 0.75 mmol, 1.5 equiv.) was placed under N_2 in a separate round-bottom flask, these were dissolved in anhydrous DCM (10 mL & 5 mL respectively). NEt_3 (0.14 mL, 1 mmol, 2 equiv.) was added to the round bottom flask containing **3.19** and this was

placed on ice. The 4-chlorobutyryl chloride solution was gradually added to the other solution via a cannula, this was stirred overnight (16 h) at RT. Following TLC analysis, 4-chlorobutyryl chloride (56 µL, 1 equiv.) was dissolved in anhydrous DCM under N_2 and gradually added to the reaction flask. Following further TLC analysis after another 3 days stirring at RT, the crude mixture was extracted using DCM, sat. $NaHCO_3$ solution and brine. The organic phase was dried (Na_2SO_4), filtered and concentrated *in vacuo* to yield the product **4.64** as a yellow-orange solid (555 mg, 99%) which was used without further purification. Compound **4.64** (555 mg, 0.5 mmol) and NaN_3 (65 mg, 1 mmol, 2 equiv.) were placed under N_2 and dissolved in anhydrous DMF (12 mL) and stirred overnight (16 h) at RT. Following TLC analysis, NaN_3 (65 mg, 1 mmol) was added. Following further TLC analysis, the solvent was removed *in vacuo* and the crude mixture was extracted using DCM and brine, the organic phase was dried (Na_2SO_4), filtered and concentrated *in vacuo* to yield the crude product, which was purified by flash column chromatography (97:3-96:4 DCM:MeOH) to yield the pure product **4.65** as a white solid (335 mg, 60%).

^{1}H NMR (500 MHz, $CDCl_3$) δ 8.92 (s, 1H, NH), 8.06 – 7.94 (m, 4H, N*H*CO (x2)& triaz-H (x2)), 7.93 (s, 2H, Ar-H), 7.76 (s, 1H, Ar-H), 5.90 (d, *J* = 9.2 Hz, 2H, H-1), 5.59 (t, *J* = 9.7 Hz, 2H, H-2), 5.54 (t, *J* = 4.5 Hz, 2H, H-4), 5.27 – 5.23 (m, 2H, H-3), 4.75 – 4.58 (m, 4H, CH_2 (x2)), 4.29 (t, *J* = 6.5 Hz, 2H, H-5), 4.20 – 4.10 (m, 4H, H-6 & H-7), 3.40 – 3.32 (m, 2H, CH_2), 2.49 (d, *J* = 3.9 Hz, 2H, CH_2), 2.20 (dd, *J* = 6.3, 3.8 Hz, 6H, CH_3 of OAc), 1.99 (t, *J* = 2.8 Hz, 12H, CH_3 of OAc), 1.95 (m, 2H, CH_2), 1.81 (d, *J* = 3.0 Hz, 6H, CH_3 of OAc). ^{13}C NMR (125 MHz, $CDCl_3$) δ 170.4 (s, CO of OAc), 170.1 (s, CO of OAc), 169.9 (s, CO of OAc), 169.3 (s, CO of OAc), 166.6 (s, *C*ONH), 145.4 (s, qC-triaz), 138.8 (s,qC_{Ar}), 134.8 (s,qC_{Ar}), 121.5 (s, C_{Ar}/C-triaz), 121.3 (s, C_{Ar}/C-triaz), 120.9 (s, C_{Ar}), 86.1 (s, C-1), 73.9 (s, C-5), 70.8 (s, C-3), 68.0 (s, C-2), 66.8 (s, C-4), 61.1 (s, C-6), 50.7 (s, CH_2), 35.4 (s, *C*H_2NH), 33.7 (s, CH_2), 24.4 (s, CH_2), 20.6 (s, CH_3 of OAc), 20.5 (s, CH_3 of OAc), 20.2 (s, CH_3 of OAc). IR(ATR): 2099, 1746, 1652, 1598, 1531, 1443, 1367, 1210, 1090, 1045, 951 cm^{-1}. HRMS (ESI+): m/z calcd for $C_{46}H_{56}N_{12}O_{21}$ + Na^+ $[M+Na]^+$ 1135.3581, found 1135.3586.

***N*,*N*'-di-(β-D-galactopyranosyl-1,2,3-triazol-4-ylmethylamide)-N''-propyl-5-(4-azido-butyrylamino)benzene-1,3-dicarboxamide 4.66**

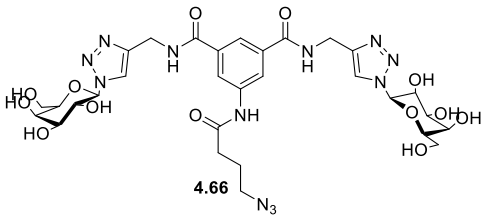

4.65 (250 mg, 0.22 mmol) was dissolved in a mixture of MeOH/H_2O (12 mL/6 mL) and refluxed at 55-60 ^oC, NEt_3 (0.3 mL) was then added and the mixture was refluxed until the reaction was deemed complete by TLC analysis (approx. 5 h). The solvent was then removed *in vacuo*, the crude residue was then dissolved in deionised water and stirred with Amberlite H^+ for one h, this was then filtered, concentrated *in vacuo* and freeze dried to yield the pure product **4.66** as a white solid (167 mg, 96%).

^{1}H NMR (500 MHz, D_2O) δ 8.20 (d, *J* = 5.9 Hz, 2H, triaz-H), 7.81 (d, *J* = 0.8 Hz, 2H, Ar-H), 7.75 (s, 1H, Ar-H), 5.61 (d, *J* = 9.2 Hz, 2H, H-1), 4.58 (s, 4H, C*H*$_2$NH), 4.16 (t, *J* = 9.5 Hz, 2H, H-2), 4.03 (d, *J* = 3.1 Hz, 2H, H-4), 3.93 (t, *J* = 6.0 Hz, 2H, H-5), 3.81 (dt, *J* = 18.9, 9.4 Hz, 2H, H-3), 3.71 (d, *J* = 6.0 Hz, 4H, H-6 &H-6'), 3.29 (t, *J* = 6.5 Hz, 2H, $CH_2CH_2CH_2N_3$), 2.36 (t, *J* = 7.2 Hz, 2H, $CH_2CH_2CH_2N_3$), 1.82 (dd, *J* = 13.8, 6.8 Hz, 2H, $CH_2CH_2CH_2N_3$).

^{13}C NMR (125 MHz, D_2O) δ 174.1 (s, *C*O$(CH_2)_3N_3$), 168.3 (s, *C*ONH), 144.8 (s, qC-triaz), 138.0 (s, qC_{Ar}), 134.2 (s, qC_{Ar}), 123.0 (s, C-triaz), 122.3 (s, C_{Ar}), 121.8 (s, C_{Ar}), 88.0 (s, C-1), 78.2 (s, C-5), 72.9 (s, C-3), 69.7 (s, C-2), 68.5 (s, C-4), 60.8 (s, C-6), 50.4 (s, $CH_2CH_2CH_2N_3$), 34.9 (s, *C*H_2NH), 33.6 (s, *C*$H_2CH_2CH_2N_3$), 24.2 (s, $CH_2CH_2CH_2N_3$). IR (ATR): 3277, 2101, 1644, 1596, 1538, 1446, 1339, 1285, 1090, 1052, 1016 cm^{-1}. HRMS (ESI+): m/z calcd for $C_{30}H_{40}N_{12}O_{13}$ + H^+ $[M+H]^+$ 777.2916, found 777.2924.

***N*,*N*'-di-(β-D-galactopyranosyl-1,2,3-triazol-4-ylmethylamide)-N''-propyl-5-(4-aminobutanoylamino)benzene-1,3-dicarboxamide 4.67**

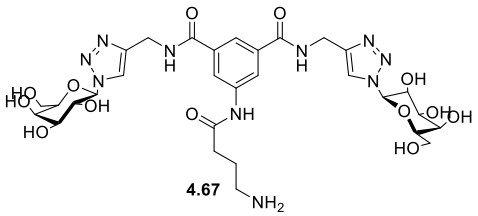

4.66 (83 mg, 0.1 mmol) and Palladium on activated charcoal (40 mg (approx.), 50% w/w) was placed under N_2 and dissolved in anhydrous MeOH (10 mL), while stirring H_2 was bubbled through the suspension, a balloon of H_2 was then attached to the round-bottom flask and the suspension was stirred overnight (16 h) at RT. The suspension was then filtered through celite, concentrated *in vacuo* and freeze-dried to yield the pure product **4.67** as a white solid (64 mg, 80%).

^{1}H NMR (500 MHz, D_2O) δ 8.25 (s, 2H, triaz-H), 7.95 (s, 2H, Ar_H), 7.87 (s, 1H, Ar_H), 5.69 (d, *J* = 9.1 Hz, 2H, H-1), 4.68 (s, 4H, CH_2 (x2)), 4.23 (t, *J* = 9.3 Hz, 2H, H-2), 4.09 (s, 2H, H-4), 4.00 (t, *J* = 5.7 Hz, 2H, H-5), 3.89 (d, *J* = 7.3 Hz, 2H, H-3), 3.78 (d, *J* = 5.8 Hz, 4H, H-6/H-6'), 3.15 – 3.03 (m, 2H, $COCH_2CH_2C\mathit{H}_2N_3$), 2.57 (dd, *J* = 13.5, 6.6 Hz, 2H, $COC\mathit{H}_2CH_2CH_2N_3$), 2.05 (dt, *J* = 14.6, 10.0 Hz, 2H, $COCH_2C\mathit{H}_2CH_2N_3$).

^{13}C NMR (125 MHz, D_2O) δ 173.1 (s, $\mathit{C}OCH_2CH_2CH_2N_3$), 168.2 (s, $\mathit{C}ONH$), 144.9 (s, qC_{triaz}), 138.1 (s, qC_{Ar}), 134.3 (s, qC_{Ar}), 123.0 (s, C-triaz), 122.3 (s, C_{Ae}), 121.8 (s, C_{Ar}), 88.0 (s, C-1), 78.2 (s, C-5), 72.9 (s, C-3), 69.7 (s, C-2), 68.6 (s, C-4), 60.9 (s, C-6), 38.8 (s, $COCH_2CH_2\mathit{C}H_2N_3$), 35.0 (s, CH_2), 33.1 (s, $CO\mathit{C}H_2CH_2CH_2N_3$), 22.5 (s, $COCH_2\mathit{C}H_2CH_2N_3$). IR (ATR): 3285, 1644, 1596, 1538, 1446, 1339, 1286, 1091, 1052 cm^{-1}. HRMS (ESI+): m/z calcd for $C_{30}H_{42}N_{10}O_{13}$ + H^+ $[M+H]^+$ 751.3011, found 751.3003.

7.2.4 Experimental procedures for Chapter 5

4-[1-(2,3,4,6-tetra-*O*-acetyl-β-D-galactopyranosyl)-1H-1,2,3-triazol-4-yl]-hexane 5.16

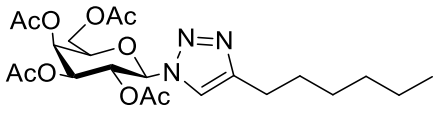

5.16

2.40 (260 mg, 0.69 mmol) and 1-octyne (approx. 0.09 mL, 0.63 mmol), Copper sulfate pentahydrate (60 mg) and sodium ascorbate (100 mg) were dissolved in ACN/H_2O (8 mL/2 mL) and reacted in the microwave at 100 ^oC until the reaction was deemed complete by TLC analysis (90:10 DCM:MeOH) (30 mins). The solvent was then removed in vacuo and the resulting residue was extracted using DCM and brine, the organic phase was dried ($MgSO_4$), filtered and the solvent was removed *in vacuo*. The product was purified by flash column chromatography (96:4 DCM:MeOH) to yield **5.16** as a white amorphous solid (175 mg, 57%).

^{1}H NMR (500 MHz, $CDCl_3$) δ 7.53 (s, 1H, triaz-H), 5.80 (d, *J* = 9.3 Hz, 1H, H-1), 5.54 (ddd, *J* = 9.1, 3.9, 2.0 Hz, 2H, H-2 & H-4), 5.22 (dd, *J* = 10.3, 2.5 Hz, 1H, H-3), 4.23 – 4.07 (m, 3H, H-5, H-6 & H-7), 2.68 (d, *J* = 2.4 Hz, 2H, C*H*$_2$), 2.19 (dd, *J* = 3.5, 1.9 Hz, 3H, CH_3 of OAc), 2.01 (dd, *J* = 3.8, 2.1 Hz, 3H, CH_3 of OAc), 1.98 (dd, *J* = 3.6, 1.9 Hz, 3H, CH_3 of OAc), 1.85 (dd, *J* = 3.7, 2.0 Hz, 3H, CH_3 of OAc), 1.68 – 1.59 (m, 2H, C*H*$_2$), 1.25 (d, *J* = 25.6 Hz, 6H, C*H*$_2$x3), 0.85 (dd, *J* = 3.7, 2.0 Hz, 3H, C*H*$_3$).

^{13}C NMR (125 MHz, $CDCl_3$) δ 170.3 (s, CO of OAc), 169.9 (s, CO of OAc), 169.8 (s, CO of OAc), 169.0 (s, CO of OAc), 149.1 (s, qC-triaz), 118.8 (s, C-triaz), 86.1 (s, C-1), 73.9 (s, C-5), 70.8 (s, C-3), 67.7 (s, C-2), 66.9 (s, C-4), 61.2 (s, C-6), 31.5 (s, *C*H_2), 29.1 (s, *C*H_2), 28.7 (s, *C*H_2), 25.6 (s, *C*H_2), 22.5 (s, *C*H_2), 20.6 (s, CH_3 of OAc), 20.4 (s, CH_3 of OAc), 20.2 (s, CH_3 of OAc), 14.0 (*C*H_3). IR (ATR): 1735, 1248, 1215, 1108, 1078, 1043, 1017, 929 cm^{-1}. HRMS (ESI+): m/z calcd for $C_{22}H_{33}N_3O_9$ + Na^+ $[M+Na]^+$ 506.2114, found 506.2106.

4-[1-(2,3,4,6-tetra-*O*-acetyl-α-D-mannopyranosyl)-1H-1,2,3-triazol-4-yl]-hexane 5.17

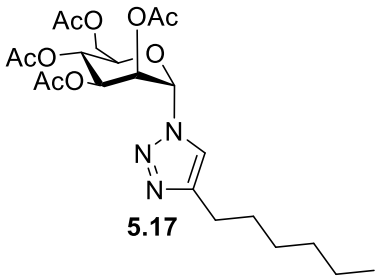

5.17

2.41 (957 mg, 2.56 mmol) and 1-octyne (approx. 0.34 mL, 2.33 mmol), Copper sulfate pentahydrate (150 mg) and sodium ascorbate (200 mg) were dissolved in ACN/H_2O (8 mL/2 mL) and reacted in the microwave at 100 ^oC until the reaction was deemed complete by TLC analysis (90:10 DCM:MeOH) (30 mins). The solvent was then removed in vacuo and the resulting residue was extracted using DCM and brine, the organic phase was dried ($MgSO_4$), filtered and the solvent was removed *in vacuo*. The product was purified by flash column chromatography (3:1-1:1 Petroleum ether: Ethyl acetate) to yield **5.17** as a yellow solid (165 mg, 15%).

^1H NMR (500 MHz, $CDCl_3$) δ 7.44 (s, 1H, triaz-H), 5.93 (dd, *J* = 3.7, 2.0 Hz, 3H, H-1, H-2 & H-3), 5.40 – 5.31 (m, 1H, H-4), 4.33 (dd, *J* = 12.5, 5.3 Hz, 1H, H-6 or H-7), 4.04 (dd, *J* = 12.5, 2.1 Hz, 1H, H-6 or H-7), 3.90 – 3.79 (m, 1H, H-5), 2.72 (q, *J* = 7.7 Hz, 2H, CH_2), 2.19 – 2.13 (m, 3H, CH_3 of OAc), 2.08 – 2.06 (m, 3H, CH_3 of OAc), 2.05 – 2.04 (m, 3H, CH_3 of OAc), 2.04 – 2.02 (m, 3H, CH_3 of OAc), 1.71 – 1.60 (m, 2H, CH_2), 1.39 – 1.24 (m, 6H, CH_2 (x3)), 0.93 – 0.78 (m, 3H, CH_3).

^{13}C NMR (125 MHz, $CDCl_3$) δ 169.5 (s, CO), 168.8 (s, CO), 168.7 (s, CO), 168.4 (s, CO), 148.3 (s, qC_{triaz}), 119.9 (s, C-triaz), 82.5 (s, C-1), 71.0 (s, C-5), 67.9 (s, C-2/C-3), 67.5 (s, C-2/C-3), 65.2 (s, C-4), 60.7 (s, C-6), 30.6 (s, CH_2), 28.2 (s, CH_2), 27.9 (s, CH_2), 24.6 (s, CH_2), 21.6 (s, CH_2), 19.8 (s, CH_3 of OAc), 19.7 (s, CH_3 of OAc), 19.6 (s, CH_3 of OAc), 13.1 (s, CH_3). IR (ATR): 1743, 1368, 1213, 1122, 1037, 1013 cm^{-1}. HRMS (ESI+): m/z calcd for $C_{22}H_{33}N_3O_9 + H^+$ $[M+H]^+$ 484.2295, found 484.2290.

4-[1-(β-D-galactopyranosyl)-1H-1,2,3-triazol-4-yl]-hexane 5.18

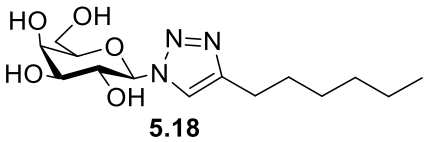

5.18

5.16 (98 mg, 0.2 mmol) was dissolved in MeOH/H_2O (2 mL/1 mL) and refluxed at 45-50 ^oC for 5 mins, NEt_3 (0.1 mL) was then added and the reaction mixture was refluxed at 45-50 ^oC until the reaction was deemed complete by TLC analysis (90:10 DCM:MeOH) (5 h). The solvent was removed *in vacuo*, the residue was dissolved in water and treated with Amberlite H^+ for 1 h, this was then filtered and the solvent was removed *in vacuo* to yield the pure product **5.18** as a white fluffy solid (52 mg, 83%).

^1H NMR (500 MHz, DMSO) δ 7.85 (s, 1H, triaz-H), 5.30 (d, *J* = 8.9 Hz, 1H. H-1), 5.13 (d, *J* = 4.7 Hz, 1H, C-2 OH), 5.00 (s, 1H, C-3 OH), 4.68 (s, 1H, C-6 OH), 4.63 (d, *J* = 3.6 Hz, 1H, C-4 OH), 3.90 (d, *J* = 5.4 Hz, 1H, H-2), 3.67 (s, 1H, H-4), 3.57 (s, 1H, H-5), 3.42 (m, 2H, H-3 & H-6/6'), 3.37 – 3.33 (m, 1H, H-6/6'), 2.42 (d, *J* = 19.6 Hz, 2H, CH_2), 1.48 (d, *J* = 6.4 Hz, 2H, CH_2), 1.18 (s, 6H, 3xCH_2), 0.76 (s, 3H, CH_3).

^{13}C NMR (125 MHz, DMSO) δ 147.3 (s, qC-triaz), 120.9 (s, C-triaz), 88.4 (s, C-1), 78.7 (s, C-5), 74.2 (s, C-3), 69.8 (s, C-2), 68.6 (s, C-4), 60.7 (s, C-6), 31.5 (s, CH_2), 29.3 (s, CH_2), 28.8 (s, CH_2), 25.4 (s, CH_2), 22.5 (s, CH_2), 14.4 (s, CH_3). IR (ATR): 3331, 1092, 1047, 1022, 1006 cm^{-1}. HRMS (ESI+): m/z calcd for $C_{14}H_{25}N_3O_5$ + Na^+ $[M+H]^+$ 338.1692, found 338.1688.

4-[1-(α-D-mannopyranosyl)-1H-1,2,3-triazol-4-yl]-hexane 5.19

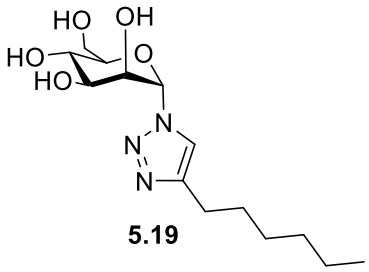

5.19

5.17 (121 mg, 0.25 mmol) was dissolved in MeOH/H_2O (3 mL/1 mL) and refluxed at 45-50 ^oC for 5 mins, NEt_3 (0.1 mL) was then added and the reaction mixture was refluxed at 45-50 ^oC until the reaction was deemed complete by TLC analysis (90:10 DCM:MeOH) (5 h). The solvent was removed *in vacuo*, the residue was dissolved in water and treated with Amberlite H^+ for 1 h, this was then filtered and the solvent was removed *in vacuo* to yield the pure product **5.19** as a white fluffy solid (83 mg, 83%).

^{1}H NMR (500 MHz, DMSO) δ 7.95 (s, 1H, triaz-H), 5.84 (s, 1H, H-1), 4.37 (s, 1H, H-2), 3.81 (d, *J* = 7.3 Hz, 1H, H-3), 3.61 (d, *J* = 11.9 Hz, 1H, H-6 or H-7), 3.54 (dd, *J* = 17.6, 10.1 Hz, 2H, H-6 or H-7 &), 3.31 – 3.23 (m, 1H, H-5), 2.62 (t, *J* = 7.6 Hz, 2H, CH_2), 1.58 (dd, *J* = 14.1, 7.0 Hz, 2H, CH_2), 1.28 (s, 6H, CH_2), 0.86 (dd, *J* = 6.8, 4.5 Hz, 3H, CH_3).
^{13}C NMR (125 MHz, DMSO) δ 147.3 (s, qC_{triaz}), 121.9 (s, C-triaz), 86.0 (s, C-1), 78.5 (s, C-5), 71.6 (s, C-3), 68.6 (s, C-2), 67.9 (s, C-4), 61.2 (s, C-6), 31.4 (s, CH_2), 29.3 (s, CH_2), 28.7 (s, CH_2), 25.4 (s, CH_2), 22.5 (s, CH_2), 14.4 (s, CH_3). IR (ATR): 3059, 2925, 1463, 1403, 1357, 1258, 1233, 1206, 1105, 1084, 1073, 1055, 1031 cm^{-1}. HRMS (ESI+): m/z calcd for $C_{14}H_{25}N_3O_5$ + H^+ $[M+H]^+$ 316.1872, found 316.1872.

2,3,4,6-tetra-*O*-acetyl-β-D-galactopyranose 5.20

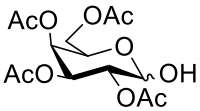

5.20

1,2,3,4,6-penta-*O*-acetyl-β-D-galactopyranose (2.5 g, 6.4 mmol) was dissolved in acetonitrile (40 mL), N,N-dimethylamine (6.4 mL, 12.8 mmol, 2N solution in MeOH) was gradually added to the solution and the reaction mixture stirred overnight at RT. Following TLC analysis, the solvent was removed *in vacuo*, the crude residue was

dissolved in DCM and an extraction was carried out using 1M HCl (x2), sat. $NaHCO_3$ solution (x2) and brine. The organic phase was dried (Na_2SO_4), filtered and concentrated *in vacuo*. The crude product was purified using flash column chromatography (1:1 Petroleum ether: Ethyl acetate) to yield **5.20** as a viscous yellow oil (859 mg, 39%).

^{1}H NMR (500 MHz, $CDCl_3$) δ 5.49 (t, *J* = 3.6 Hz, 1H, H-1α), 5.45 (dd, *J* = 3.3, 1.3 Hz, 1H, H-4α), 5.42 – 5.37 (m, 1H, H-3α & H-4β), 5.13 (ddd, *J* = 10.8, 3.6, 0.9 Hz, 1H, H-2α), 5.07 – 5.04 (m, H-3β, H-2β), 4.71 – 4.66 (m, H-1β), 4.45 (td, *J* = 6.6, 0.9 Hz, 1H, H-5α), 4.15 – 4.04 (m, 3H, H-6α & H-6β), 3.96 (ddd, *J* = 11.8, 7.9, 5.0 Hz, H-5β), 2.12 (s, 3H, CH_3 of OAc), 2.08 (s, 3H, CH_3 of OAc), 2.03 (s, 3H, CH_3 of OAc), 1.97 (s, 3H, CH_3 of OAc)

The NMR data is in agreement with the data reported in the literature [211].

2,3,4,6-tetra-*O*-acetyl-α-galactopyranosyl trichloroacetimidate 5.21

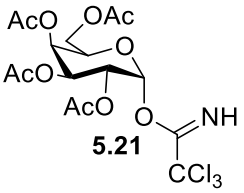

5.21

5.20 (805 mg, 2.31 mmol) was placed under N_2 in the presence of molecular sieves (4 Å) and dissolved in anhydrous dcm. Trichloroacetonitrile (0.69 mL, 6.88 mmol) was added followed by NaH (110 mg, 2.73 mmol (60% dispersion)), the round-bottom was then flushed with N_2 again. The reaction mixture was stirred at RT overnight. Following TLC analysis, the solvent was removed *in vacuo*. the crude product was dissolved in chloroform and centrifuged, the supernatant was removed and the solvent was removed *in* vacuo. The crude product was purified via flash column chromatography (1:1 Petroleum ether: Ethyl acetate) to give **5.21** as a yellow oil (392 mg, 35%).

^{1}H NMR (500 MHz, $CDCl_3$) δ 8.66 (s, 1H, NH), 6.59 (d, *J* = 3.5 Hz, 1H, H-1), 5.54 (dt, *J* = 7.0, 3.5 Hz, 1H, H-4), 5.43 – 5.32 (m, 2H, H-3 & H-2), 4.45 – 4.39 (m, 1H, H-5), 4.18 – 4.02 (m, 2H, H-6 & H-7), 2.15 (s, 3H, CH_3 of OAc), 2.04 – 2.02 (s, 3H, CH_3 of OAc), 2.02 – 2.01 (s, 3H, CH_3 of OAc), 2.00 (s, 3H, CH_3 of OAc)

The NMR data is in agreement with the data reported in the literature [211].

heptyl 2,3,4,6-tetra-*O*-acetyl-β-D-galactopyranoside 5.22

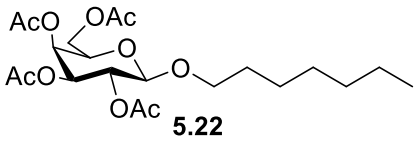

5.22

5.21 (211 mg, 0.45 mmol) was placed under N_2 in the presence of molecular sieves (4 Å) and dissolved in anhydrous dcm (20 mL). 1-Heptanol (approx. 0.19 mL, 1.35 mmol) was then added and the reaction mixture was stirred for 20 mins and it was placed on ice. Trimethylsilyl triflate (approx. 0.12 mL, 0.67 mmol) was placed under N_2 in a separate round-bottom flask and anhydrous dcm was added (8 mL), this was then gradually added to the reaction mixture via a cannula. The reaction mixture was stirred overnight at RT. Following TLC analysis, $NaHCO_3$ (400 mg) was added to the reaction mixture, which was then filtered and concentrated *in vacuo*. The crude product was purified by flash column chromatography (3:1 Petroleum ether: Ethyl acetate), to give the pure product **5.22** as a colourless oil (188 mg, 94%).

^{1}H NMR (500 MHz, $CDCl_3$) δ 5.38 (dd, *J* = 3.4, 1.0 Hz, 1H, H-4), 5.19 (dd, *J* = 10.5, 8.0 Hz, 1H, H-2), 5.01 (dd, *J* = 10.5, 3.4 Hz, 1H, H-3), 4.44 (d, *J* = 8.0 Hz, 1H, H-1), 4.15 (ddd, *J* = 31.4, 11.2, 6.7 Hz, 2H, H-6 & H-7), 3.93 – 3.84 (m, 2H, H-5 & CH_2), 3.46 (dt, *J* = 9.6, 6.9 Hz, 1H, CH_2), 2.14 (s, 3H, CH_3 of OAc), 2.04 (d, *J* = 1.5 Hz, 6H, CH_3 of OAc), 1.97 (d, *J* = 3.7 Hz, 3H, CH_3 of OAc), 1.62 – 1.47 (m, 2H, CH_2), 1.35 – 1.21 (m, 8H, 4xCH_2), 0.91 – 0.83 (m, 3H, CH_3).

The NMR data is in agreement with the data reported in the literature [201].

heptyl β-D-galactopyranoside 5.23

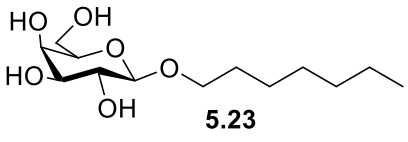

5.23

5.22 (97 mg, 0.21 mmol) was dissolved in MeOH/H_2O (2 mL/1 mL) and refluxed at 45-50 ^oC for 5 mins, NEt_3 (0.1 mL) was then added and the reaction mixture was refluxed at 45-50 ^oC until the reaction was deemed complete by TLC analysis (90:10 DCM:MeOH) (5 h). The solvent was removed *in vacuo*, the residue was dissolved in water and treated with Amberlite H^+ for 1 h, this was then filtered and the solvent

was removed *in vacuo* to yield the pure product **5.23** as a white fluffy solid (53 mg, 91%)

^{1}H NMR (500 MHz, D_2O) δ 4.31 (d, *J* = 7.9 Hz, 1H, H-1), 3.91 (d, *J* = 3.4 Hz, 1H, H-4), 3.86 (dt, *J* = 9.7, 7.2 Hz, 1H, OCH_2), 3.75 – 3.68 (m, 2H, H-6 & H-7), 3.60 (ddd, *J* = 16.6, 7.6, 5.4 Hz, 3H, H-3, H-5 & OCH_2), 3.48 (dd, *J* = 9.8, 7.9 Hz, 1H, H-2), 1.66 – 1.54 (m, 2H, CH_2), 1.35 – 1.23 (m, 8H, CH_2 (x4)), 0.84 (t, *J* = 6.8 Hz, 3H, CH_3).
The NMR data is in agreement with the data reported in the literature [212].

2,3,4,6-tetra-*O*-acetyl-α-D-mannopyranose 5.24

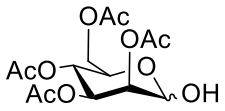

5.24

1,2,3,4,6-penta-*O*-acetyl-α-D-mannopyranose (2.9 g, 7.43 mmol) was dissolved in acetonitrile (45 mL), N,N-dimethylamine (7.43 mL, 14.86 mmol, 2N solution in MeOH) was gradually added to the solution and the reaction mixture stirred overnight at RT. Following TLC analysis, the solvent was removed *in vacuo*, the crude residue was dissolved in DCM and an extraction was carried out using 1M HCl (x2), sat. $NaHCO_3$ solution (x2) and brine. The organic phase was dried (Na_2SO_4), filtered and concentrated *in vacuo*. The crude product was purified using flash column chromatography (2:1-1:1 Petroleum ether: Ethyl acetate) to yield **5.24** as an amber brown oil (957 mg, 37%).

^{1}H NMR (500 MHz, $CDCl_3$) δ 5.47 – 5.36 (m, 1H), 5.29 – 5.18 (m, 3H), 4.30 – 4.18 (m, 2H), 4.16 – 4.08 (m, 1H), 2.93 (s, 1H), 2.15 (s, 3H), 2.09 (s, 3H), 2.04 (s, 3H), 1.99 (s, 3H).
The NMR data is in agreement with the data reported in the literature [213].

2,3,4,6-tetra-*O*-acetyl-α-mannopyranosyl trichloroacetimidate 5.25

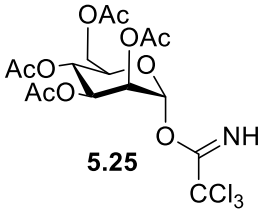

5.25

5.24 (957 mg, 2.75 mmol) was placed under N_2 in the presence of molecular sieves (4 Å) and dissolved in anhydrous DCM. Trichloroacetonitrile (1 mL, 9.97 mmol) was added followed by NaH (250 mg, 6.2 mmol (60% dispersion)), the round-bottom was then flushed with N_2 again. The reaction mixture was stirred at RT overnight. Following TLC analysis, the solvent was removed *in vacuo*. the crude product was dissolved in chloroform and centrifuged, the supernatant was removed and the solvent was removed *in* vacuo. The crude product was purified via flash column chromatography (1:1 Petroleum ether: Ethyl acetate) (217 mg, 16%) to give **5.25** as an orange/yellow oil.

^{1}H NMR (500 MHz, $CDCl_3$) δ 8.78 (s, 1H), 6.27 (d, *J* = 1.8 Hz, 1H), 5.53 – 5.23 (m, 3H), 4.34 – 3.97 (m, 3H), 2.16(s, 3H), 2.08 (s, 3H), 2.06 (s, 3H), 2.03 (s, 3H)
The NMR data is in agreement with the data reported in the literature [214].

heptyl 2,3,4,6-tetra-*O*-acetyl-α-D-mannopyranoside 5.26

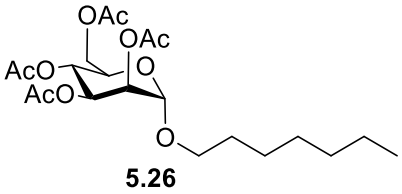

5.26

5.25 (217 mg, 0.44 mmol) was placed under N_2 in the presence of molecular sieves (4 Å) and dissolved in anhydrous DCM (20 mL). 1-Heptanol (approx. 0.19 mL, 1.35 mmol) was then added and the reaction mixture was stirred for 20 mins and it was placed on ice. Trimethylsilyl triflate (approx. 0.12 mL, 0.67 mmol) was placed under N_2 in a separate round-bottom flask and anhydrous DCM was added (8 mL), this was then gradually added to the reaction mixture via a cannula. The reaction mixture was stirred overnight at RT. Following TLC analysis, $NaHCO_3$ (400 mg) was added to the reaction mixture, which was then filtered and concentrated *in vacuo*. The crude

product was purified by flash column chromatography (3:1 Petroleum ether: Ethyl acetate), to give the pure product **5.26** as a white solid (112 mg, 57%).

^{1}H NMR (500 MHz, $CDCl_3$) δ 5.35 (dd, *J* = 10.0, 3.5 Hz, 1H, H-3), 5.31 – 5.24 (m, 1H, H-4), 5.23 (dd, *J* = 3.4, 1.8 Hz, 1H, H-2), 4.80 (d, *J* = 1.7 Hz, 1H, H-1), 4.33 – 4.25 (m, 1H, H-6/7), 4.11 (dd, *J* = 12.2, 2.4 Hz, 1H, H-6/7), 4.02 – 3.95 (m, 1H, H-5), 3.67 (dt, *J* = 9.6, 6.8 Hz, 1H, OC*H*$_2$CH$_2$), 3.49 – 3.42 (m, 1H, OC*H*$_2$CH$_2$), 2.16 (s, 3H, CH_3 of OAc), 2.10 (s, 3H, CH_3 of OAc), 2.04 (s, 3H, CH_3 of OAc), 2.00 (s, 3H, CH_3 of OAc), 1.64 – 1.56 (m, 2H, CH_2), 1.38 – 1.23 (m, 8H, CH_2 (x4)), 0.89 (t, *J* = 7.0 Hz, 3H, CH_2C*H*$_3$).

^{13}C NMR (125 MHz, $CDCl_3$) δ 170.69 (s, CO of OAc), 170.13 (s, CO of OAc), 169.93 (s, CO of OAc), 169.79 (s, CO of OAc), 97.58 (s, C-1), 69.76 (s, C-2), 69.17 (s, C-3), 68.59 (s, O*C*H$_2$CH$_2$), 68.38 (s, C-5), 66.30 (s, C-4), 62.55 (s, C-6), 31.74 (s, CH_2), 29.27 (s, CH_2), 29.02 (s, CH_2), 26.04 (s, CH_2), 22.61 (s, CH_2), 20.7 (m, CH_3 of OAc), 14.08 (s, CH_2*C*H$_3$). IR (ATR): 1742, 1368, 1223, 1132, 1039 cm^{-1}. HRMS (ESI+): m/z calcd for $C_{21}H_{34}O_{10}$ + Na^+ $[M+Na]^+$ 469.2050, found 469.2045.

heptyl α-D-mannopyranoside 5.15

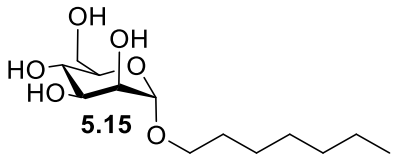

5.26 (197 mg, 0.44 mmol) was dissolved in MeOH (10 mL) and placed on ice. NaOMe (50 mg) was added and the reaction mixture was left to stir at RT until the reaction was deemed to be complete via TLC analysis (90:10 DCM:MeOH) (3.5 h). The solvent was removed *in vacuo*, the residue was dissolved in water and treated with Amberlite H^+ for 1 h, this was then filtered and the solvent was removed *in vacuo* to yield the pure product **5.15** as a white fluffy solid (15 mg, 12%).

^{1}H NMR (500 MHz, D_2O) δ 4.83 (d, *J* = 10.0 Hz, 1H, H-1), 3.96 – 3.90 (m, 1H, H-2), 3.87 – 3.66 (m, 5H, H-3, H-4, H-6/7 & OCH_2), 3.55 (ddd, *J* = 17.3, 10.3, 5.2 Hz, 1H, H-6/7), 3.47 (dt, *J* = 9.6, 6.6 Hz, 1H, H-5), 1.61 (d, *J* = 6.3 Hz, 2H, CH_2), 1.42 – 1.22 (m, 8H, CH_2 (x4)), 0.94 – 0.82 (m, 3H, CH_3).

The NMR data is in agreement with the data reported in the literature [215].

1,2,3,4,6-penta-*O*-benzoyl-α-D-mannopyranose 5.28

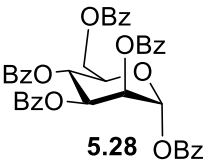

5.28

Benzoyl chloride (48.3 mL, 0.42 mol, 5.5 equiv.) was added dropwise to a solution of D-mannose (13.64 g, 75.7 mmol) in pyridine (120 mL) at 0 °C under N_2, over a period of 30 mins. The reaction mixture was allowed warm to RT and stirred for 18 h. Ice water (200 mL) was added to the reaction mixture and stirred for 1 h. The solvent was concentrated *in vacuo*. The crude product was purified by flash column chromatography (hexane/EtOAc 2:1) to yield the pure α-anomer **5.28** (33.9 g, 64%) as a white solid.

The NMR data is in agreement with the data reported in the literature [216].

2,3,4,6-tetra-*O*-benzoyl-1-bromo-α-D-mannopyranose 5.29

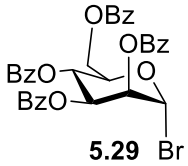

5.29

33% HBr in AcOH (20 mL, 335 mmol, 27 equiv) was slowly added to 1,2,3,4,6-penta-*O*-benzoyl-α-galactopyranose **5.28** (8.72 g, 12.4 mmol) in dry DCM at 0 °C under N_2. After 2 h, the reaction mixture was then diluted with DCM (50 mL), washed with ice-water (40 mL) and aqueous sodium bicarbonate (40 mL). The organic layer was dried using $MgSO_4$, filtered and concentrated *in vacuo* to yield the crude α-anomer **5.29** as a white solid (7.82 g, 96%, crude yield).

The NMR data is in agreement with the data reported in the literature [216].

heptyl α-D-mannopyranoside 5.15

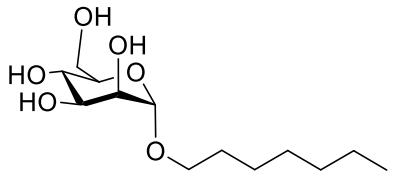

5.15

5.29 (3.47 g, 5.27 mmol, 1 equiv.) was placed under N_2 in the presence of molecular sieves (4 Å) and dissolved in anhydrous DCM (18 mL). 1-Heptanol (approx. 1.64 mL, 11.59 mmol) was then added and the reaction mixture was stirred for 20 mins and it was placed on ice. Silver triflate (approx. 1.88 g, 7.22 mmol) was placed under N_2 in a separate round-bottom flask and anhydrous toluene was added (10 mL), this was then gradually added to the reaction mixture via a cannula. The reaction mixture was stirred overnight at RT. Following TLC analysis, the reaction mixture was filtered through celite and concentrated *in vacuo*. The crude reaction mixture was purified via flash column chromatography (3:1 Pet Ether: EtOAc) to yield the intermediate compound **5.30** (750 mg, 20%). This was dissolved in MeOH (8 mL) and NaOMe in MeOH (0.2 mL) was added, the reaction was stirred overnight at RT. Following TLC analysis, the product was purified via flash column chromatography (EtOAc- 10:1 EtOAc:MeOH) to yield the product **5.15** as a white fluffy solid (189 mg, 13.5%).

The NMR data is in agreement with the data reported in the literature [215].

8-oxaundec-10-yn-1-ol 5.31

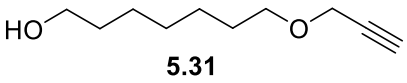

5.31

1,7-heptanediol (1.06 g, 8 mmol) was dissolved in anhydrous THF (10 mL) under N_2 and cooled to 0 ^{o}C. NaH (107 mg, (60% dispersion)) was added portion wise and the reaction mixture was stirred for 20 mins, allowing it to warm to RT. Propargyl bromide (0.29 mL) was added dropwise and the reaction was stirred overnight at RT. Following TLC analysis, the crude product as purified via flash column chromatography (3:1 Pet Ether:EtOAc-EtOAc) to yield the pure product **5.31** (257 mg, 31%).

The NMR data is in agreement with the data reported in the literature [217].

8-oxaundec-10-yn-1-α-D-mannopyranose 5.33

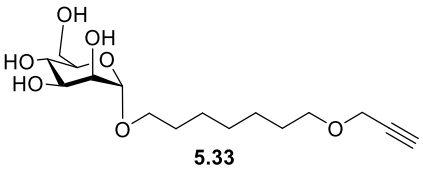

5.33

5.31 (134 mg, 0.787 mmol) and **5.29** (350 mg, 0.525 mmol) were placed under N_2 and dissolved in anhydrous DCM (2 mL) in the presence of molecular sieves (4 Å) and stirred at 0 ^oC. Silver triflate (150 mg, 0.578 mmol) was placed under N_2 in a separate round bottom flask and dissolved in toluene (2 mL), this was gradually added to the reaction mixture via a cannula. The reaction was stirred overnight at RT. Following TLC analysis, the crude product was purified via flash column chromatography (3:1 Pet Ether: EtOAc) to yield the pure product **5.32** (190 mg, 55%). This was reacted on without further purification. **5.32** (204 mg, 0.25 mmol) was dissolved in MeOH (4 mL), NaOMe in MeOH (0.1 mL) was added and the reaction was stirred at room temperature until deemed complete by TLC (2.5 h). The solvent was then removed *in vacuo*, the crude residue was then dissolved in deionised water and stirred with Amberlite H^+ for one h, this was then filtered, concentrated *in vacuo* and freeze dried to yield the pure product **5.33** as a white solid (37 mg, 45%). ^1H NMR (500 MHz, $CDCl_3$) δ 4.80 (s, 1H, H-1), 4.13 (d, *J* = 2.4 Hz, 2H, C*H*$_2$CCH), 3.95 (dd, *J* = 23.8, 12.6 Hz, 3H, H-2, H-4 & H-6/7), 3.82 (d, *J* = 8.3 Hz, 1H, H-3), 3.74 (d, *J* = 11.1 Hz, 1H, H-6/7), 3.61 (dd, *J* = 16.1, 6.8 Hz, 1H, C*H*$_2$), 3.50 (q, *J* = 6.6 Hz, 3H, H-5 & C*H*$_2$), 3.38 (dd, *J* = 15.9, 6.6 Hz, 1H, C*H*$_2$), 2.45 (t, *J* = 2.4 Hz, 1H, CH$_2$CC*H*), 1.63 – 1.51 (m, 4H, C*H*$_2$ (x2)), 1.40 – 1.28 (m, 6H, C*H*$_2$ (x3)). ^{13}C NMR (125 MHz, $CDCl_3$) δ 100.0 (s, C-1), 80.0 (s, qC_{alkyne}), 74.2 (s, CH$_2$C*C*H), 72.2 (s, C-5), 71.4 (s, C-2/3/4), 70.8 (s, C-2/3/4), 70.1 (s, CH$_2$), 67.8 (s, CH$_2$), 66.0 (s, C-2/3/4), 60.7 (s, C-6), 58.0 (s, *C*H$_2$CCH), 29.4 (s, CH$_2$), 29.3 (s, CH$_2$), 29.2 (s, CH$_2$), 26.0 (s, CH$_2$). HRMS (ESI+): m/z calcd for $C_{16}H_{28}O_7$ + Na^+ $[M+Na]^+$ 355.1733, found 355.1727.

***N*-(Fluorescein)-*O*-8-oxaundec-10-yn-1-α-D-mannopyranose 5.35**

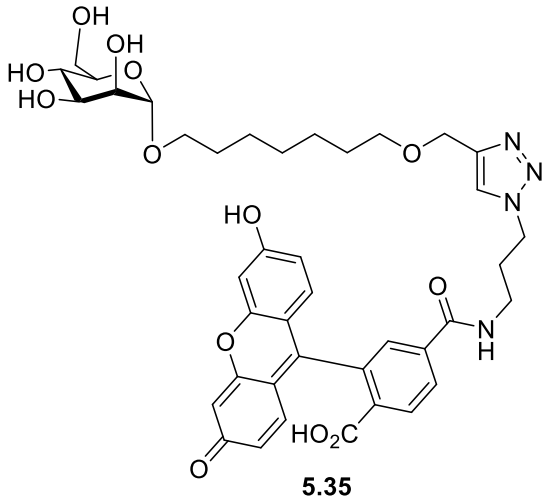

5.35

5.33 (10 mg, 0.03 mmol) and Fluorescein azide **5.34** (6.5 mg, 0.015 mmol), Copper sulfate pentahydrate (1 mg) and sodium ascorbate (1 mg) were dissolved in ACN/H_2O (2 mL/0.5 mL) and reacted in the microwave at 100 ^oC until the reaction was deemed complete by TLC analysis (90:10 DCM:MeOH) (10 mins). The solvent was then removed in vacuo and the resulting residue was extracted using DCM and deionised water, the organic phase was dried ($MgSO_4$), filtered and the solvent was removed *in vacuo* to give **5.35**. HRMS (ESI+): m/z calcd for $C_{40}H_{46}N_4O_{13}$ + H^+ $[M+H]^+$ 791.3140, found 791.3123.

***N,N'*-di-(2,3,4,6-tetra-*O*-acetyl-α-D-mannopyranosyl-1,2,3-triazol-4-ylmethylamide)-*N''*-tert-tbutoxycarbonyl-5-aminobenzene-1,3-dicarboxamide 5.36**

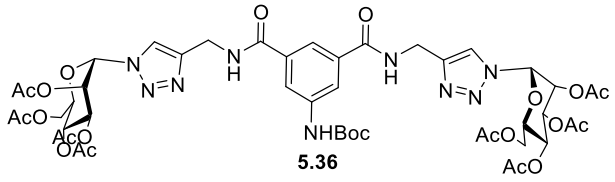

5.36

Copper sulphate pentahydrate (60 mg) and sodium ascorbate (120 mg) were added to a solution of **3.15** (95 mg, 0.27 mmol) and **2.41** (220 mg, 0.59 mmol) in acetonitrile/H_2O (4 mL/ 2mL). The reaction was allowed to stir at 100 ^oC in the MW until deemed complete by TLC analysis (30 mins). The solvent was removed *in vacuo*. The residue was dissolved in DCM (30 mL), washed with water (20 mL x 3), and dried ($MgSO_4$). The mixture was filtered and the solvent was removed *in vacuo* to yield the crude product, which was purified by silica gel column chromatography (DCM:MeOH

99:1-93:7) to give the pure product **5.36** white solid (154 mg, 52%). R_f = 0.38 (DCM:MeOH 9:1).

^{1}H NMR (500 MHz, $CDCl_3$) δ 7.96 (s, 4H, triaz-H (x2) & N*H*CH_2 (x2)), 7.71 (s, 2H, Ar_H), 7.39 (s, 2H, Ar_H & N*H*Boc), 6.10 (d, *J* = 12.5 Hz, 2H, H-1), 6.05 (d, *J* = 9.6 Hz, 2H, H-2), 5.92 – 5.85 (m, 2H, H-3), 5.37 (td, *J* = 9.6, 3.4 Hz, 2H, H-4), 4.59 (td, *J* = 14.8, 4.6 Hz, 4H, C*H*$_2$-triaz), 4.23 (m, 2H, H-6/7), 4.01 (ddd, *J* = 14.2, 7.2, 4.7 Hz, 2H, H-6/7), 3.98 – 3.92 (m, 2H, H-5), 2.18 – 2.12 (m, 6H, CH_3 of OAc), 2.03 (m, 6H, CH_3 of OAc), 2.02 – 1.99 (m, 6H, CH_3 of OAc), 1.99 – 1.94 (m, 6H, CH_3 of OAc), 1.49 – 1.42 (m, 9H, CH_3 of Boc).

^{13}C NMR (125 MHz, $CDCl_3$) δ 171.5 (s, CO of OAc), 170.0 (s, CO of OAc), 169.7 (s, CO of OAc), 169.6 (s, CO of OAc), 166.2 (s, CO), 145.5 (s, qC_{triaz}), 139.1 (s, qC_{Ar}), 134.5 (s, qC_{Ar}), 123.5 (s, C-triaz), 120.2 (s, C_{Ar}), 118.7 (s, C_{Ar}), 84.2 (s, C-1), 71.6 (s, C-5), 69.1 (s, C-3), 68.3 (s, C-2), 65.7 (s, C-4), 61.7 (s, C-6), 35.1 (s, *C*H_2NH), 28.2 (s, Boc *C*H_3 (x3)), 20.9 (s, CH_3 of OAc), 20.7 (s, CH_3 of OAc), 20.6 (s, CH_3 of OAc). IR (ATR): 1743, 1367, 1214, 1155, 1122, 1039 cm^{-1}. HRMS (ESI+): *m/z* calcd for $C_{47}H_{59}N_9O_{22}$ + H^+ $[M+H]^+$ 1102.3853, found 1102.3842.

***N*, *N*'-di-(2,3,4,6-tetra-*O*-acetyl-α-D-mannopyranosyl-1,2,3-triazol-4-ylmethylamide)-N''-(1-oxo-2-propen-1-yl)-5-aminobenzene-1,3-dicarboxamide 5.38**

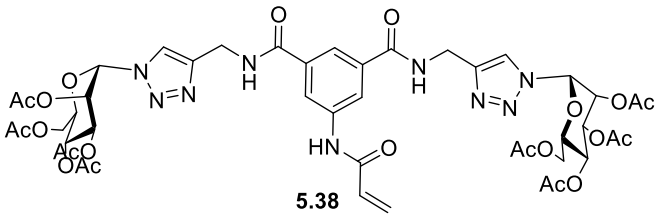

5.38

5.36 (255 mg, 0.23 mmol) was dissolved in DCM (4 mL) and was cooled to 0 ^{o}C in an ice-bath. TFA (0.6 mL) was added and the reaction mixture was stirred at RT for 2 h. DCM (40 mL) was added to the reaction mixture, it was washed with sat. $NaHCO_3$ (40 mL) and brine (40 mL), and dried ($MgSO_4$). The mixture was filtered and the solvent was removed *in vacuo* to yield the product **5.37** which was used without further purification: pale yellow solid (218 mg, 95%). **5.37** (218 mg, 0.22 mmol) was placed under N_2 and dissolved in anhydrous DCM (10 mL), after stirring for 5 mins NEt_3 (36 µL, 0.26 mmol, 1.2 equiv) was added and the reaction mixture was stirred for 5 mins.

Acryloyl chloride (70 µL, 0.87 mmol, 1.2 equiv) was added and the reaction mixture was stirred overnight at RT. Following TLC analysis (90:10), the solvent was removed *in vacuo*, the crude residue was dissolved in DCM and extracted using deionised water, 1M HCl, sat. $NaHCO_3$ solution and brine. The organic phase was dried (Na_2SO_4), filtered and concentrated *in vacuo*. The crude product was then purified by flash column chromatography (97:3-90:10 DCM:MeOH) to yield the pure product **5.38** as a white solid (127 mg, 55%).

^{1}H NMR (500 MHz, $CDCl_3$) δ 9.19 (d, *J* = 23.8 Hz, 1H, NH), 8.21 (s, 2H, N*H*CH_2), 7.97 (s, 2H, triaz-H), 7.86 (s, 2H, Ar_H), 7.59 (s, 1H, Ar_H), 6.33 (dd, *J* = 15.2, 10.1 Hz, 2H, COC*H*CH_2), 6.12 (d, *J* = 1.3 Hz, 2H, H-1), 6.02 (s, 2H, H-2), 5.91 (dd, *J* = 9.6, 3.6 Hz, 2H, H-3), 5.68 (s, 1H, COCHCH_2), 5.42 (t, *J* = 9.7 Hz, 2H, H-4), 4.62 (qd, *J* = 15.6, 5.7 Hz, 4H, CH_2-triaz), 4.28 (dd, *J* = 12.5, 4.7 Hz, 2H, H-6/7), 4.11 – 4.02 (m, 2H, H-6/7), 3.99 (dd, *J* = 5.2, 2.6 Hz, 2H, H-5), 2.18 (s, 6H, CH_3 of OAc), 2.07 (s, 6H, CH_3 of OAc), 2.01 (s, 6H, CH_3 of OAc), 2.00 (s, 6H, CH_3 of OAc).

^{13}C NMR (125 MHz, $CDCl_3$) δ 170.7 (s, CO of OAc), 170.0 (s, CO of OAc), 169.9 (s, CO of OAc), 169.7 (s, CO of OAc), 166.4 (s, CO), 164.3 (s, *C*OCHCH_2), 145.5 (s, qC_{triaz}), 134.4 (s, qC_{Ar}), 131.0 (s, CO*C*HCH_2), 128.0 (s, COCH*C*H_2), 123.5 (s, C-triaz), 121.6 (s, C_{Ar}), 120.4 (s, C_{Ar}), 84.1 (s, C-1), 71.8 (s, C-5), 69.3 (s, C-3), 68.3 (s, C-2), 65.5 (s, C-4), 61.7 (s, C-6), 35.1 (s, *C*H_2NH), 20.8 (s, CH_3 of OAc), 20.7 (s, CH_3 of OAc), 20.6 (s, CH_3 of OAc), 20.6 (s, CH_3 of OAc). IR (ATR): 1479, 1370, 1219, 1041 cm^{-1}. HRMS (ESI+): *m/z* calcd for $C_{45}H_{53}N_9O_{21}$ + H^+ $[M+H]^+$ 1056.3434, found 1056.3423.

***N*, *N*'-di-(α-D-mannopyranosyl-1,2,3-triazol-4- ylmethylamide)-N''-(1-oxo-2-propen-1-yl)-5-aminobenzene-1,3-dicarboxamide 5.39**

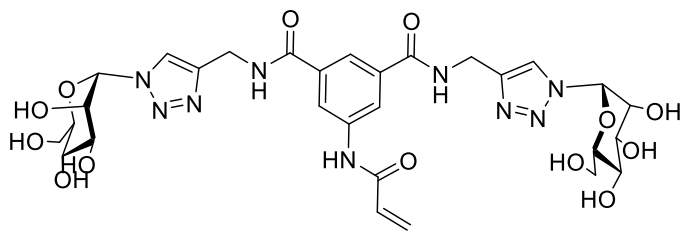

5.39

5.38 (80 mg, 0.07 mmol) was dissolved in MeOH/H_2O (4 mL/2 mL) and refluxed at 45-50 °C for 5 mins, NEt_3 (0.1 mL) was then added and the reaction mixture was refluxed at 45-50 °C until the reaction was deemed complete by TLC analysis (90:10

DCM:MeOH). The solvent was removed *in vacuo*, the residue was dissolved in water and treated with Amberlite H^+ for 1 h, this was then filtered and the solvent was removed *in vacuo* to yield the pure product **5.39** as a white fluffy solid (47 mg, 94%). ^{1}H NMR (500 MHz, D_2O) δ 8.10 (s, 2H, triaz-H), 7.83 (d, *J* = 1.4 Hz, 2H, Ar_H), 7.73 (s, 1H, Ar_H), 6.27 – 6.22 (m, 2H, COC*H*CH_2 & COCHC*H*$_2$), 6.04 (d, *J* = 2.2 Hz, 2H, H-1), 5.81 – 5.74 (m, 1H, COCHC*H*$_2$), 4.72 (dd, *J* = 3.4, 2.4 Hz, 2H, H-2), 4.57 (s, 4H, CH_2-triaz), 4.10 (dd, *J* = 9.1, 3.5 Hz, 2H, H-3), 3.81 – 3.68 (m, 6H, H-4, H-6 & H-7), 3.30 – 3.23 (m, 2H, H-5). ^{13}C NMR (125 MHz, D_2O) δ 168.3 (s, *C*ONHCH$_2$), 166.3 (s, *C*OCHCH$_2$), 144.5 (s, qC_{triaz}), 138.0 (s, qC_{Ar}), 134.2 (s, qC_{Ar}), 130.0 (s, CO*C*HCH$_2$), 129.0 (s, COCH*C*H$_2$), 123.6 (s, C-triaz), 122.1 (s, Ar_H), 121.8 (s, Ar_H), 86.6 (s, C-1), 76.1 (s, C-5), 70.4 (s, C-3), 68.2 (s, C-2), 66.4 (s, C-4), 60.4 (s, C-6), 34.9 (s, *C*H$_2$-triaz). IR (ATR): 3272, 1648, 1541, 1445, 1424, 1340, 1266, 1207, 1046 cm^{-1}. HRMS (ESI+): *m/z* calcd for $C_{29}H_{37}N_9O_{13}$ + Na^+ $[M+Na]^+$ 742.2409, found 742.2401.

Bibliography

1 Hawksworth, D.L. (2001) The magnitude of fungal diversity: the 1.5 million species estimate revisited. *Mycological Research* 105, 1422-1432
2 Brown, G.D. et al. (2012) Tackling Human Fungal Infections. *Science* 336 (6082), 647-647
3 Denning, D.W. and Bromley, M.J. (2015) How to bolster the antifungal pipeline. *Science* 347 (6229), 1414-1416
4 Reddy, G.K.K. et al. (2022) Fungal infections: Pathogenesis, antifungals and alternate treatment approaches. *Current Research in Microbial Sciences* 3
5 Ma, L. et al. (2016) Genome analysis of three Pneumocystis species reveals adaptation mechanisms to life exclusively in mammalian hosts. *Nature Communications* 7
6 Hernandez-Chavez, M.J. et al. (2017) Fungal Strategies to Evade the Host Immune Recognition. *Journal of Fungi* 3 (4)
7 Heinsbroek, S.E.M. et al. (2005) Dectin-1 escape by fungal dimorphism. *Trends in Immunology* 26 (7), 352-354
8 Marcos, C.M. et al. (2016) Anti-Immune Strategies of Pathogenic Fungi. *Frontiers in Cellular and Infection Microbiology* 6
9 Chrisman, C.J. et al. (2011) Phospholipids Trigger Cryptococcus neoformans Capsular Enlargement during Interactions with Amoebae and Macrophages. *Plos Pathogens* 7 (5)
10 Meiller, T.F. et al. (2009) A Novel Immune Evasion Strategy of Candida albicans: Proteolytic Cleavage of a Salivary Antimicrobial Peptide. *Plos One* 4 (4)
11 Szafranski-Schneider, E. et al. (2012) Msb2 Shedding Protects Candida albicans against Antimicrobial Peptides. *Plos Pathogens* 8 (2)
12 Swidergall, M. et al. (2013) Candida albicans Mucin Msb2 Is a Broad-Range Protectant against Antimicrobial Peptides. *Antimicrobial Agents and Chemotherapy* 57 (8), 3917-3922
13 Donlan, R.M. and Costerton, J.W. (2002) Biofilms: Survival mechanisms of clinically relevant microorganisms. *Clinical Microbiology Reviews* 15 (2), 167
14 Ning, Y. et al. (2013) Candida albicans survival and biofilm formation under starvation conditions. *International Endodontic Journal* 46 (1), 62-70
15 Chandra, J. et al. (2007) Interaction of Candida albicans with adherent human peripheral blood mononuclear cells increases C-albicans biofilm formation and results in differential expression of pro- and anti-inflammatory cytokines. *Infection and Immunity* 75 (5), 2612-2620
16 Tits, J. et al. (2020) Combination Therapy to Treat Fungal Biofilm-Based Infections. *International Journal of Molecular Sciences* 21 (22)
17 Zhou, Y.B. et al. (2012) In Vitro Interactions between Aspirin and Amphotericin B against Planktonic Cells and Biofilm Cells of Candida albicans and C. parapsilosis. *Antimicrobial Agents and Chemotherapy* 56 (6), 3250-3260
18 Pfaller, M.A. et al. (2006) Invasive fungal pathogens: Current epidemiological trends. *Clinical Infectious Diseases* 43, S3-S14
19 Spampinato, C. and Leonardi, D. (2013) Candida Infections, Causes, Targets, and Resistance Mechanisms: Traditional and Alternative Antifungal Agents. *Biomed Research International* 2013
20 Mayer, F.L. et al. (2013) Candida albicans pathogenicity mechanisms. *Virulence* 4 (2), 119-128
21 Martin, H. et al. (2021) Targeting adhesion in fungal pathogen Candida albicans. *Future Medicinal Chemistry* 13 (3), 313-334

22 Berman, J. and Sudbery, P.E. (2002) Candida albicans: A molecular revolution built on lessons from budding yeast. *Nature Reviews Genetics* 3 (12), 918-930
23 Saville, S.P. et al. (2003) Engineered control of cell morphology in vivo reveals distinct roles for yeast and filamentous forms of Candida albicans during infection. *Eukaryotic Cell* 2 (5), 1053-1060
24 Garcia, M.C. et al. (2011) A Role for Amyloid in Cell Aggregation and Biofilm Formation. *Plos One* 6 (3)
25 Verstrepen, K.J. and Klis, F.M. (2006) Flocculation, adhesion and biofilm formation in yeasts. *Molecular Microbiology* 60 (1), 5-15
26 Naglik, J.R. et al. (2011) Candida albicans interactions with epithelial cells and mucosal immunity. *Microbes and Infection* 13 (12-13), 963-976
27 Dalle, F. et al. (2010) Cellular interactions of Candida albicans with human oral epithelial cells and enterocytes. *Cellular Microbiology* 12 (2), 248-271
28 Phan, Q.T. et al. (2007) Als3 is a Candida albicans invasin that binds to cadherins and induces endocytosis by host cells. *Plos Biology* 5 (3), 543-557
29 Chaffin, W.L. et al. (1998) Cell wall and secreted proteins of Candida albicans: Identification, function, and expression. *Microbiology and Molecular Biology Reviews* 62 (1), 130
30 Donohue, D.S. et al. (2011) The N-terminal part of Als1 protein from Candida albicans specifically binds fucose-containing glycans. *Molecular Microbiology* 80 (6), 1667-1679
31 Ielasi, F.S. et al. (2016) Lectin-Glycan Interaction Network-Based Identification of Host Receptors of Microbial Pathogenic Adhesins. *Mbio* 7 (4)
32 Fanning, S. and Mitchell, A.P. (2012) Fungal Biofilms. *Plos Pathogens* 8 (4)
33 Uppuluri, P. et al. (2010) Dispersion as an Important Step in the Candida albicans Biofilm Developmental Cycle. *Plos Pathogens* 6 (3)
34 Wachtler, B. et al. (2012) Candida albicans-Epithelial Interactions: Dissecting the Roles of Active Penetration, Induced Endocytosis and Host Factors on the Infection Process. *Plos One* 7 (5)
35 Mavor, A.L. et al. (2005) Systemic fungal infections caused by Candida species: Epidemiology, infection process and virulence attributes. *Current Drug Targets* 6 (8), 863-874
36 Gacser, A. et al. (2007) Lipase 8 affects the pathogenesis of Candida albicans. *Infection and Immunity* 75 (10), 4710-4718
37 Murray, C.J.L. et al. (2022) Global burden of bacterial antimicrobial resistance in 2019: a systematic analysis. *Lancet* 399 (10325), 629-655
38 Dorhoi, A. et al. (2011) For better or for worse: the immune response against Mycobacterium tuberculosis balances pathology and protection. *Immunological Reviews* 240, 235-251
39 Koul, A. et al. (2004) Interplay between mycobacteria and host signalling pathways. *Nature Reviews Microbiology* 2 (3), 189-202
40 Smith, R.S. and Iglewski, B.H. (2003) P-aeruginosa quorum-sensing systems and virulence. *Current Opinion in Microbiology* 6 (1), 56-60
41 Webb, S.A.R. and Kahler, C.M. (2008) Bench-to-bedside review: Bacterial virulence and subversion of host defences. *Critical Care* 12 (6)
42 Hall-Stoodley, L. and Stoodley, P. (2009) Evolving concepts in biofilm infections. *Cellular Microbiology* 11 (7), 1034-1043
43 Lewis, K. (2005) Persister cells and the riddle of biofilm survival. *Biochemistry-Moscow* 70 (2), 267
44 Allesen-Holm, M. et al. (2006) A characterization of DNA release in Pseudomonas aeruginosa cultures and biofilms. *Molecular Microbiology* 59 (4), 1114-1128

45 Bagge, N. et al. (2004) Pseudomonas aeruginosa biofilms exposed to imipenem exhibit changes in global gene expression and beta-lactamase and alginate production. *Antimicrobial Agents and Chemotherapy* 48 (4), 1175-1187
46 Hoffman, L.R. et al. (2005) Aminoglycoside antibiotics induce bacterial biofilm formation. *Nature* 436 (7054), 1171-1175
47 Halstead, F.D. et al. (2015) The Antibacterial Activity of Acetic Acid against Biofilm-Producing Pathogens of Relevance to Burns Patients. *Plos One* 10 (9)
48 Halstea, F.D. et al. (2016) Antibacterial Activity of Blue Light against Nosocomial Wound Pathogens Growing Planktonically and as Mature Biofilms. *Applied and Environmental Microbiology* 82 (13), 4006-4016
49 Hughes, G. and Webber, M.A. (2017) Novel approaches to the treatment of bacterial biofilm infections. *British Journal of Pharmacology* 174 (14), 2237-2246
50 Tenaillon, O. et al. (2010) The population genetics of commensal Escherichia coli. *Nature Reviews Microbiology* 8 (3), 207-217
51 Sarowska, J. et al. (2019) Virulence factors, prevalence and potential transmission of extraintestinal pathogenic Escherichia coli isolated from different sources: recent reports. *Gut Pathogens* 11
52 Cassels, F.J. and Wolf, M.K. (1995) Colonization factors of Diarrheagenic Escherichia-coli and their intestinal receptors. *Journal of Industrial Microbiology* 15 (3), 214-226
53 Eto, D.S. et al. (2007) Integrin-mediated host cell invasion by type 1-piliated uropathogenic Escherichia coli. *Plos Pathogens* 3 (7), 949-961
54 Pakbin, B. et al. (2021) Virulence Factors of Enteric Pathogenic Escherichia coli: A Review. *International Journal of Molecular Sciences* 22 (18)
55 Johnson, T.J. et al. (2012) Associations Between Multidrug Resistance, Plasmid Content, and Virulence Potential Among Extraintestinal Pathogenic and Commensal Escherichia coli from Humans and Poultry. *Foodborne Pathogens and Disease* 9 (1), 37-46
56 Erb, A. et al. (2007) Prevalence of antibiotic resistance in Escherichia coli: overview of geographical, temporal, and methodological variations. *European Journal of Clinical Microbiology & Infectious Diseases* 26 (2), 83-90
57 Poirel, L. et al. (2012) Genetic support and diversity of acquired extended-spectrum beta-lactamases in Gram-negative rods. *Infection Genetics and Evolution* 12 (5), 883-893
58 Paul, M. and Leibovici, L. (2009) Combination Antimicrobial Treatment Versus Monotherapy: The Contribution of Meta-analyses. *Infectious Disease Clinics of North America* 23 (2), 277
59 Rasko, D.A. and Sperandio, V. (2010) Anti-virulence strategies to combat bacteria-mediated disease. *Nature Reviews Drug Discovery* 9 (2), 117-128
60 Keller, M.A. and Stiehm, E.R. (2000) Passive immunity in prevention and treatment of infectious diseases. *Clinical Microbiology Reviews* 13 (4), 602
61 Lowy, I. et al. (2010) Treatment with Monoclonal Antibodies against Clostridium difficile Toxins. *New England Journal of Medicine* 362 (3), 197-205
62 Dehbanipour, R. and Ghalavand, Z. (2022) Anti-virulence therapeutic strategies against bacterial infections: recent advances. *Germs* 12 (2), 262-275
63 Cascioferro, S. et al. (2014) Sortase A: An ideal target for anti-virulence drug development. *Microbial Pathogenesis* 77, 105-112
64 Suree, N. et al. (2009) Discovery and structure-activity relationship analysis of Staphylococcus aureus sortase A inhibitors. *Bioorganic & Medicinal Chemistry* 17 (20), 7174-7185

65 Tiwari, V.K. et al. (2016) Cu-Catalyzed Click Reaction in Carbohydrate Chemistry. *Chemical Reviews* 116 (5), 3086-3240
66 Rostovtsev, V.V. et al. (2002) A stepwise Huisgen cycloaddition process: Copper(I)-catalyzed regioselective "ligation" of azides and terminal alkynes. *Angewandte Chemie-International Edition* 41 (14), 2596
67 Kolb, H.C. et al. (2001) Click chemistry: Diverse chemical function from a few good reactions. *Angewandte Chemie-International Edition* 40 (11), 2004
68 Meldal, M. and Tornoe, C.W. (2008) Cu-catalyzed azide-alkyne cycloaddition. *Chemical Reviews* 108 (8), 2952-3015
69 Hu, J. et al. (2016) Using carbohydrate-based biomaterials as scaffolds to control human stem cell fate. *Organic & Biomolecular Chemistry* 14 (37), 8648-8658
70 He, X.P. et al. (2016) Carbohydrate CuAAC click chemistry for therapy and diagnosis. *Carbohydrate Research* 429, 1-22
71 Lo Conte, M. et al. (2010) Modular Approach to Triazole-Linked 1,6-alpha-D-Oligomannosides to the Discovery of Inhibitors of Mycobacterium tuberculosis Cell Wall Synthetase. *Journal of Organic Chemistry* 75 (19), 6326-6336
72 Hu, X.L. et al. (2015) Triazole-Linked Glycolipids Enhance the Susceptibility of MRSA to beta-Lactam Antibiotics. *Acs Medicinal Chemistry Letters* 6 (7), 793-797
73 Gouin, S.G. et al. (2009) Synthetic Multimeric Heptyl Mannosides as Potent Antiadhesives of Uropathogenic Escherichia coli. *Chemmedchem* 4 (5), 749-755
74 Morsy, H.A. et al. (2020) Click Synthesis of 1,2,3-Triazole Nucleosides Based on Functionalized Nicotinonitriles. *Russian Journal of Organic Chemistry* 56 (1), 143-147
75 Thanh, N.D. et al. (2019) Efficient click chemistry towards novel 1H-1,2,3-triazole-tethered 4H-chromene-D-glucose conjugates: Design, synthesis and evaluation of in vitro antibacterial, MRSA and antifungal activities. *European Journal of Medicinal Chemistry* 167, 454-471
76 Tachallait, H. et al. (2018) Concise synthesis and antibacterial evaluation of novel 3-(1,4-disubstituted-1,2,3-triazolyl)uridine nucleosides. *Archiv Der Pharmazie* 351 (11)
77 Mohammed, A.I. et al. (2017) Synthesis and antibacterial activity of 1-N-(beta-D-glucopyranosyl)-4-((1-substituted-1H-1,2,3-triazol-4-yl)etho xymethyl)-1,2,3-triazoles. *Arabian Journal of Chemistry* 10, S3508-S3514
78 Ay, K. et al. (2017) Synthesis and antimicrobial evaluation of sulfanilamide- and carbohydrate-derived 1,4-disubstitued-1,2,3-triazoles via click chemistry. *Medicinal Chemistry Research* 26 (7), 1497-1505
79 Collins-Lech C et al. (1984) Inhibition by sugars of Candida albicans adherence to human buccal mucosal cells and corneocytes in vitro. (Vol. 46), pp. 831-834
80 Martin, H. et al. (2018) Inhibition of adherence of the yeast Candida albicans to buccal epithelial cells by synthetic aromatic glycoconjugates. *European Journal of Medicinal Chemistry* 160, 82-93
81 Pertici, F. et al. (2013) Optimizing Divalent Inhibitors of Pseudomonas aeruginosa Lectin LecA by Using A Rigid Spacer. *Chemistry-a European Journal* 19 (50), 16923-16927
82 Pertici, F. and Pieters, R.J. (2012) Potent divalent inhibitors with rigid glucose click spacers for Pseudomonas aeruginosa lectin LecA. *Chemical Communications* 48 (33), 4008-4010
83 Yu, G.Y. et al. (2019) Assembly of Divalent Ligands and Their Effect on Divalent Binding to Pseudomonas aeruginosa Lectin LecA. *Journal of Organic Chemistry* 84 (5), 2470-2488

84 Freichel, T. et al. (2019) Effects of linker and liposome anchoring on lactose-functionalized glycomacromolecules as multivalent ligands for binding galectin-3. *Rsc Advances* 9 (41), 23484-23497

85 Nagao, M. et al. (2019) Quantitative preparation of multiblock glycopolymers bearing glycounits at the terminal segments by aqueous reversible addition-fragmentation chain transfer polymerization of acrylamide monomers. *Journal of Polymer Science Part a-Polymer Chemistry* 57 (8), 857-861

86 Otsubo, T. et al. (2019) An Alternating Glycopolymer Composed of Carbohydrate-carrying Maleimide and OH-functionalized Vinyl Ether -A New Synthetic Strategy for Glycosaminoglycan Mimics. *Chemistry Letters* 48 (5), 465-467

87 Liu, M.N. et al. (2020) Precise synthesis of heterogeneous glycopolymers with well-defined saccharide motifs in the side chain via post-polymerization modification and recognition with lectin. *Journal of Polymer Science* 58 (15), 2074-2087

88 Ehrmann, S. et al. (2018) A toolbox approach for multivalent presentation of ligand-receptor recognition on a supramolecular scaffold. *Journal of Materials Chemistry B* 6 (25), 4216-4222

89 Saha, S. et al. (2020) Smart Glycopolymeric Nanoparticles for Multivalent Lectin Binding and Stimuli-Controlled Guest Release. *Biomacromolecules* 21 (6), 2356-2364

90 Ye, J.T. and Lautens, M. (2015) Palladium-catalysed norbornene-mediated C-H functionalization of arenes. *Nature Chemistry* 7 (11), 863-870

91 Lin, C.C. et al. (2015) Thiol-Norbornene Photoclick Hydrogels for Tissue Engineering Applications. *Journal of Applied Polymer Science* 132 (8)

92 Sutthasupa, S. et al. (2009) ROMP of Norbornene Monomers Carrying Nonprotected Amino Groups with Ruthenium Catalyst. *Macromolecules* 42 (5), 1519-1525

93 Pfeffer, F.M. and Russell, R.A. (2003) Strategies and methods for the attachment of amino acids and peptides to chiral n polynorbornane templates. *Organic & Biomolecular Chemistry* 1 (11), 1845-1851

94 Miyamoto, Y. et al. (2004) Synthesis of homopolymers and multiblock copolymers by the living ring-opening metathesis polymerization of norbornenes containing acetyl-protected carbohydrates with well-defined ruthenium and molybdenum initiators. *Journal of Polymer Science Part a-Polymer Chemistry* 42 (17), 4248-4265

95 Mortell, K.H. et al. (1996) Recognition specificity of neoglycopolymers prepared by ring-opening metathesis polymerization. *Journal of the American Chemical Society* 118 (9), 2297-2298

96 Li, Z.H. et al. (2021) pH-responsive hydrogel loaded with insulin as a bioactive dressing for enhancing diabetic wound healing. *Materials & Design* 210

97 Reddy, O.S. and Lai, W.F. (2021) Development of a composite film fabricated from carboxymethyl chitosan and magnetite nanoparticles for pH-responsive bioactive agent release. *Biointerphases* 16 (2)

98 Wang, Q.M. et al. (2014) Hybrid polymeric micelles based on bioactive polypeptides as pH-responsive delivery systems against melanoma. *Biomaterials* 35 (25), 7008-7021

99 Li, S.Y. et al. (2014) A pH-responsive prodrug for real-time drug release monitoring and targeted cancer therapy. *Chemical Communications* 50 (80), 11852-11855

100 Chen, J.J. et al. (2015) Polyion complex micelles with gradient pH-sensitivity for adjustable intracellular drug delivery. *Polymer Chemistry* 6 (3), 397-405

101 Cheng, H. et al. (2015) Activable Cell-Penetrating Peptide Conjugated Prodrug for Tumor Targeted Drug Delivery. *Acs Applied Materials & Interfaces* 7 (29), 16061-16069

102 Zhou, Z.X. et al. (2009) Charge-Reversal Drug Conjugate for Targeted Cancer Cell Nuclear Drug Delivery. *Advanced Functional Materials* 19 (22), 3580-3589

103 Suh, J. and Baek, D.J. (1981) Intramolecular catalysis of amide hydrolysis by carboxyl and metal ion-proton agents: I. Intramolecular reactions of imidazole or pyridine-derivatives of maleamic acid. *Bioorganic Chemistry* 10 (3), 266-276

104 Suh, J.H. (1990) Model studies of Carboxypeptidase-A. *Bioorganic Chemistry* 18 (3), 345-360

105 Sim, Y.L. et al. (2006) Intramolecular carboxylic group-assisted cleavage of N-(2-hydroxyphenyl)-phthalamic acid (7) and N-(2-methoxyphenyl)-phthalamic acid (8): Absence of intramolecular general acid catalysis due to 2-OH in 7. *International Journal of Chemical Kinetics* 38 (12), 746-758

106 Khan, M.N. (1998) Unexpected rate enhancement in the intramolecular carboxylic Acid-catalyzed cleavage of o-carboxybenzohydroxamic acid. *Journal of Physical Organic Chemistry* 11 (3), 216-222

107 Cheong, M.Y. et al. (2008) Effects of mixed H2O-CH3CN and H2O-HCONMe2 solvents on the rate of cleavage of N-benzylphthalamic acid. *Progress in Reaction Kinetics and Mechanism* 33 (2), 167-190

108 Moriconi, E.J. and Crawford, W.C. (1968) The Reaction of Chlorosulfonyl Isocyanate with Bridged Bi- and Tricyclic Olefins. The Journal of Organic Chemistry (Vol. 33), pp. 370-378

109 Park, H. et al. (1999) Ab initio studies of the intramolecular amide hydrolysis in N-methylmaleamic acids. *Journal of Molecular Structure-Theochem* 490, 47-54

110 Kim, H. et al. (2002) Analogues of aspartic proteases synthesized by densely covering silica gel with carboxyl groups. *Bioorganic & Medicinal Chemistry Letters* 12 (19), 2663-2666

111 Hickey, S.M. et al. (2015) Synthesis and evaluation of cationic norbornanes as peptidomimetic antibacterial agents. *Organic & Biomolecular Chemistry* 13 (22), 6225-6241

112 Hickey, S.M. et al. (2015) Synthesis of norbornane bisether antibiotics via silver-mediated alkylation. *Rsc Advances* 5 (36), 28582-28596

113 Hickey, S.M. et al. (2018) Norbornane-based cationic antimicrobial peptidomimetics targeting the bacterial membrane. *European Journal of Medicinal Chemistry* 160, 9-22

114 Martin, H. et al. (2020) Scaffold diversity for enhanced activity of glycosylated inhibitors of fungal adhesion. *Rsc Medicinal Chemistry* 11 (12)

115 Schulze, B. and Schubert, U.S. (2014) Beyond click chemistry - supramolecular interactions of 1,2,3-triazoles. *Chemical Society Reviews* 43 (8), 2522-2571

116 Sebaa, S. et al. (2019) Effects of tyrosol and farnesol on Candida albicans biofilm. *Molecular Medicine Reports* 19 (4), 3201-3209

117 Badia, C. et al. (2012) Sugar-Oligoamides: Synthesis of DNA Minor Groove Binders. *Journal of Organic Chemistry* 77 (23), 10870-10881

118 Tornoe, C.W. et al. (2002) Peptidotriazoles on solid phase: 1,2,3 -triazoles by regiospecific copper(I)-catalyzed 1,3-dipolar cycloadditions of terminal alkynes to azides. *Journal of Organic Chemistry* 67 (9), 3057-3064

119 Haldon, E. et al. (2015) Copper-catalysed azide-alkyne cycloadditions (CuAAC): an update. *Organic & Biomolecular Chemistry* 13 (37), 9528-9550

120 Kolb, H.C. and Sharpless, K.B. (2003) The growing impact of click chemistry on drug discovery. *Drug Discovery Today* 8 (24), 1128-1137

121 Tornoe, C.W. et al. (2004) Combinatorial library of peptidotriazoles: Identification of 1,2,3 -triazole inhibitors against a recombinant Leishmania mexicana cysteine protease. *Journal of Combinatorial Chemistry* 6 (3), 312-324

122 Zhu, L. et al. (2016) On the Mechanism of Copper(I)-Catalyzed Azide-Alkyne Cycloaddition. *Chemical Record* 16 (3), 1501-1517
123 Martin, H. (2019) The Synthesis and Biological Evaluation of Anti-Adhesion Glycoconjugates Against Opportunistic Pathogenic Candida albicans. (Vol. PhD), National University of Ireland Maynooth
124 Sohnle, P.G. and Hahn, B.L. (2002) Effect of prolonged fluconazole treatment on Candida albicans in diffusion chambers implanted into mice. *Antimicrobial Agents and Chemotherapy* 46 (10), 3175-3179
125 Alcock, L.J. et al. (2018) Norbornene probes for the study of cysteine oxidation. *Tetrahedron* 74 (12), 1220-1228
126 Fisher, M.C. et al. (2018) Worldwide emergence of resistance to antifungal drugs challenges human health and food security. *Science* 360 (6390), 739-742
127 Fisher, M.C. et al. (2022) Tackling the emerging threat of antifungal resistance to human health. *Nature Reviews Microbiology* 20 (9), 557-571
128 Cowen, L.E. et al. (2015) Mechanisms of Antifungal Drug Resistance. *Cold Spring Harbor Perspectives in Medicine* 5 (7)
129 Ghosh, A.K. et al. (2019) Covalent Inhibition in Drug Discovery. *Chemmedchem* 14 (9), 889-906
130 Dalton, S.E. and Campos, S. (2020) Covalent Small Molecules as Enabling Platforms for Drug Discovery. *Chembiochem* 21 (8), 1080-1100
131 Wagner, S. et al. (2017) Covalent Lectin Inhibition and Application in Bacterial Biofilm Imaging. *Angewandte Chemie-International Edition* 56 (52), 16559-16564
132 Wen, W.Q. et al. (2022) Structure-Guided Discovery of the Novel Covalent Allosteric Site and Covalent Inhibitors of Fructose-1,6-Bisphosphate Aldolase to Overcome the Azole Resistance of Candidiasis. *Journal of Medicinal Chemistry* 65 (3), 2656-2674
133 Grabrijan, K. et al. (2022) Covalent inhibitors of bacterial peptidoglycan biosynthesis enzyme MurA with chloroacetamide warhead. *European Journal of Medicinal Chemistry* 243
134 Hecker, S.J. et al. (2015) Discovery of a Cyclic Boronic Acid beta-Lactamase Inhibitor (RPX7009) with Utility vs Class A Serine Carbapenemases. *Journal of Medicinal Chemistry* 58 (9), 3682-3692
135 Wellens, A. et al. (2008) Intervening with Urinary Tract Infections Using Anti-Adhesives Based on the Crystal Structure of the FimH-Oligomannose-3 Complex. *Plos One* 3 (4)
136 Cecioni, S. et al. (2015) Glycomimetics versus Multivalent Glycoconjugates for the Design of High Affinity Lectin Ligands. *Chemical Reviews* 115 (1), 525-561
137 Lundquist, J.J. and Toone, E.J. (2002) The cluster glycoside effect. *Chemical Reviews* 102 (2), 555-578
138 Touaibia, M. et al. (2007) Mannosylated G(0) dendrimers with nanomolar affinities to Escherichia coli FimH. *Chemmedchem* 2 (8), 1190-1201
139 Berthet, N. et al. (2013) High Affinity Glycodendrimers for the Lectin LecB from Pseudomonas aeruginosa. *Bioconjugate Chemistry* 24 (9), 1598-1611
140 Pickens, J.C. et al. (2002) Anchor-based design of improved cholera toxin and E-coli heat-labile enterotoxin receptor binding antagonists that display multiple binding modes. *Chemistry & Biology* 9 (2), 215-224
141 Garcia-Hartjes, J. et al. (2013) Picomolar inhibition of cholera toxin by a pentavalent ganglioside GM1os-calix 5 arene. *Organic & Biomolecular Chemistry* 11 (26), 4340-4349
142 Lipke, P.N. (2018) What We Do Not Know about Fungal Cell Adhesion Molecules. *Journal of Fungi* 4 (2)

143 Kuboi, S. et al. (2013) Molecular characterization of AfuFleA, an -fucose-specific lectin from Aspergillus fumigatus. *Journal of Infection and Chemotherapy* 19 (6), 1021-1028

144 Houser, J. et al. (2013) A Soluble Fucose-Specific Lectin from Aspergillus fumigatus Conidia - Structure, Specificity and Possible Role in Fungal Pathogenicity. *Plos One* 8 (12)

145 Lehot, V. et al. (2018) Multivalent Fucosides with Nanomolar Affinity for the Aspergillus fumigatus Lectin FleA Prevent Spore Adhesion to Pneumocytes. *Chemistry-a European Journal* 24 (72), 19243-19249

146 Chaffin, W.L. (2008) Candida albicans cell wall proteins. *Microbiology and Molecular Biology Reviews* 72 (3), 495

147 Takagi, J. et al. (2022) Mucin O-glycans are natural inhibitors of Candida albicans pathogenicity. *Nature Chemical Biology* 18 (7), 762

148 Alonso, R. et al. (2001) Different adhesins for type IV collagen on Candida albicans: identification of a lectin-like adhesin recognizing the 7S(IV) domain. *Microbiology-Sgm* 147, 1971-1981

149 Dahal, U.P. et al. (2016) Intrinsic reactivity profile of electrophilic moieties to guide covalent drug design: N-alpha-acetyl-L-lysine as an amine nucleophile. *Medchemcomm* 7 (5), 864-872

150 Parums, D. (2022) Editorial: The World Health Organization (WHO) Fungal Priority Pathogens List in Response to Emerging Fungal Pathogens During the COVID-19 Pandemic. Med Sci Monit

151 Hoenigl, M. et al. (2022) COVID-19-associated fungal infections. *Nature Microbiology* 7 (8), 1127-1140

152 Willaert, R.G. (2018) Adhesins of Yeasts: Protein Structure and Interactions. *Journal of Fungi* 4 (4)

153 Mishra, S.K.e.a. (2023) *Candida auris*: an emerging antimicrobial-resistant organism with the highest level of concern. (Vol. 4), pp. 482-483

154 Bravo, A. et al. (2018) When Humans Met Superbugs: Strategies to Tackle Bacterial Resistances to Antibiotics. (Vol. 9), pp. 216-226, Biomolecular Concepts

155 Orth, P. et al. (2014) Mechanism of Action and Epitopes of Clostridium difficile Toxin B-neutralizing Antibody Bezlotoxumab Revealed by X-ray Crystallography. *Journal of Biological Chemistry* 289 (26), 18008-18021

156 Sattin, S. and Bernardi, A. (2016) Glycoconjugates and Glycomimetics as Microbial Anti-Adhesives. *Trends in Biotechnology* 34 (6), 483-495

157 Ernst, B. and Magnani, J.L. (2009) From carbohydrate leads to glycomimetic drugs. *Nature Reviews Drug Discovery* 8 (8), 661-677

158 Bernardi, A. et al. (2013) Multivalent glycoconjugates as anti-pathogenic agents. *Chemical Society Reviews* 42 (11), 4709-4727

159 Wojtczak, K. and Byrne, J.P. (2022) Structural Considerations for Building Synthetic Glycoconjugates as Inhibitors for Pseudomonas aeruginosa Lectins. *Chemmedchem* 17 (12)

160 Deguise, I. et al. (2007) Synthesis of glycodendrimers containing both fucoside and galactoside residues and their binding properties to Pa-IL and PA-IIL lectins from Pseudomonas aeruginosa. *New Journal of Chemistry* 31 (7), 1321-1331

161 Mousavifar, L. and Roy, R. (2021) Recent development in the design of small 'drug-like' and nanoscale glycomimetics against Escherichia coli infections. *Drug Discovery Today* 26 (9), 2124-2137

162 Benigni, R. (2005) Structure-activity relationship studies of chemical mutagens and carcinogens: Mechanistic investigations and prediction approaches. *Chemical Reviews* 105 (5), 1767-1800
163 Klein, T. et al. (2010) FimH Antagonists for the Oral Treatment of Urinary Tract Infections: From Design and Synthesis to in Vitro and in Vivo Evaluation. *Journal of Medicinal Chemistry* 53 (24), 8627-8641
164 Toth, M. et al. (2009) Synthesis and structure-activity relationships of C-glycosylated oxadiazoles as inhibitors of glycogen phosphorylase. *Bioorganic & Medicinal Chemistry* 17 (13), 4773-4785
165 Benltifa, M. et al. (2009) Glucose-based spiro-isoxazolines: A new family of potent glycogen phosphorylase inhibitors. *Bioorganic & Medicinal Chemistry* 17 (20), 7368-7380
166 Risquez-Cuadro, R. et al. (2013) Fullerene-sp(2)-Iminosugar Balls as Multimodal Ligands for Lectins and Glycosidases: A Mechanistic Hypothesis for the Inhibitory Multivalent Effect. *Chemistry-a European Journal* 19 (49), 16791-16803
167 Sanchez-Fernandez, E.M. et al. (2010) Synthesis of N-, S-, and C-glycoside castanospermine analogues with selective neutral alpha-glucosidase inhibitory activity as antitumour agents. *Chemical Communications* 46 (29), 5328-5330
168 Sanchez-Fernandez, E.M. et al. (2019) Synthesis of polyfluoroalkyl sp(2)-iminosugar glycolipids and evaluation of their immunomodulatory properties towards anti-tumor, anti-leishmanial and anti-inflammatory therapies. *European Journal of Medicinal Chemistry* 182
169 Sanchez-Fernandez, E.M. et al. (2021) Synthesis of sp(2)-Iminosugar Selenoglycolipids as Multitarget Drug Candidates with Antiproliferative, Leishmanicidal and Anti-Inflammatory Properties. *Molecules* 26 (24)
170 Mu, L.L. et al. (2017) Identification and characterization of a mannose-binding lectin from Nile tilapia (Oreochromis niloticus). *Fish & Shellfish Immunology* 67, 244-253
171 Sakurai, K. et al. (2014) Comparison of the Reactivity of Carbohydrate Photoaffinity Probes with Different Photoreactive Groups. *Chembiochem* 15 (10), 1399-1403
172 Ota, E. et al. (2018) Thienyl-Substituted alpha-Ketoamide: A Less Hydrophobic Reactive Group for Photo-Affinity Labeling. *Acs Chemical Biology* 13 (4), 876-880
173 Tsushima, M. et al. (2019) Catalyst-proximity protein chemical labelling on affinity beads targeting endogenous lectins. *Chemical Communications* 55 (88), 13275-13278
174 Saeed, B. et al. (2008) 2-(1H-benzotriazole-1-yl)-1,1,3,3-tetramethyluronium tetrafluoro borate (TBTU) as an efficient coupling reagent for the esterification of carboxylic acids with alcohols and phenols at room temperature. *Chinese Journal of Chemistry* 26 (6), 1141-1144
175 Le, S.T. et al. (2019) Investigation of the Binding Affinity of a Broad Array of l-Fucosides with Six Fucose-Specific Lectins of Bacterial and Fungal Origin. *Molecules* 24 (12)
176 Lode, H.M. (2009) Clinical impact of antibiotic-resistant Gram-positive pathogens. *Clinical Microbiology and Infection* 15 (3), 212-217
177 Chellat, M.F. et al. (2016) Targeting Antibiotic Resistance. *Angewandte Chemie-International Edition* 55 (23), 6600-6626
178 Darby, E.M. et al. (2023) Molecular mechanisms of antibiotic resistance revisited. *Nature Reviews Microbiology* 21 (5), 280-295
179 von Wintersdorff, C.J.H. et al. (2016) Dissemination of Antimicrobial Resistance in Microbial Ecosystems through Horizontal Gene Transfer. *Frontiers in Microbiology* 7

180 Reygaert, W.C. (2018) An overview of the antimicrobial resistance mechanisms of bacteria. *Aims Microbiology* 4 (3), 482-501
181 Sabnis, A. et al. (2021) Colistin kills bacteria by targeting lipopolysaccharide in the cytoplasmic membrane. *Elife* 10
182 Wozniak, R.A.F. and Waldor, M.K. (2010) Integrative and conjugative elements: mosaic mobile genetic elements enabling dynamic lateral gene flow. *Nature Reviews Microbiology* 8 (8), 552-563
183 Lin, A. et al. (2011) Inhibition of Bacterial Conjugation by Phage M13 and Its Protein g3p: Quantitative Analysis and Model. *Plos One* 6 (5)
184 Molnar, J. et al. (1992) Mechanism of Chlorpromazine binding by Gram-positive and Gram-negative bacteria. *Antonie Van Leeuwenhoek International Journal of General and Molecular Microbiology* 62 (4), 309-314
185 Mazel, D. and Davies, J. (1999) Antibiotic resistance in microbes. *Cellular and Molecular Life Sciences* 56 (9-10), 742-754
186 Nash, R.P. et al. (2012) Investigating the impact of bisphosphonates and structurally related compounds on bacteria containing conjugative plasmids. *Biochemical and Biophysical Research Communications* 424 (4), 697-703
187 Hahn, F.E. and Ciak, J. (1976) Elimination of resistance determinants from R-factor R1 by intercalative compounds. *Antimicrobial Agents and Chemotherapy* 9 (1), 77-80
188 Cabezon, E. et al. (2017) Conjugation Inhibitors and Their Potential Use to Prevent Dissemination of Antibiotic Resistance Genes in Bacteria. *Frontiers in Microbiology* 8
189 Palencia-Gandara, C. et al. (2021) Conjugation Inhibitors Effectively Prevent Plasmid Transmission in Natural Environments. *Mbio* 12 (4)
190 Garcia-Cazorla, Y. et al. (2018) Conjugation inhibitors compete with palmitic acid for binding to the conjugative traffic ATPase TrwD, providing a mechanism to inhibit bacterial conjugation. *Journal of Biological Chemistry* 293 (43), 16923-16930
191 Ripoll-Rozada, J. et al. (2016) Type IV traffic ATPase TrwD as molecular target to inhibit bacterial conjugation. *Molecular Microbiology* 100 (5), 912-921
192 Oyedemi, B.O.M. et al. (2016) Novel R-plasmid conjugal transfer inhibitory and antibacterial activities of phenolic compounds from Mallotus philippensis (Lam.) Mull. Arg. *Journal of Global Antimicrobial Resistance* 5, 15-21
193 Lakshmi, V.V. et al. (1987) Elimination of multidrug-resistant plasmid in bacteria by plumbagin. *Current Microbiology* 16 (3), 159-161
194 Bharathi, A. and Polasa, H. (1991) Elimination of broad-host range plasmid vectors in Escherichia coli by curing agents. *Fems Microbiology Letters* 84 (1), 37-40
195 Lujan, S.A. et al. (2007) Disrupting antibiotic resistance propagation by inhibiting the conjugative DNA relaxase. *Proceedings of the National Academy of Sciences of the United States of America* 104 (30), 12282-12287
196 Shaffer, C.L. et al. (2016) Peptidomimetic Small Molecules Disrupt Type IV Secretion System Activity in Diverse Bacterial Pathogens. *Mbio* 7 (2)
197 Getino, M. et al. (2016) Tanzawaic Acids, a Chemically Novel Set of Bacterial Conjugation Inhibitors. *Plos One* 11 (1)
198 Bouckaert, J. et al. (2005) Receptor binding studies disclose a novel class of high-affinity inhibitors of the Escherichia coli FimH adhesin. *Molecular Microbiology* 55 (2), 441-455
199 Kuznetsova, M.V. et al. (2022) Differences in recipient ability of uropathogenic Escherichia coli strains in relation with their pathogenic potential. *Infection Genetics and Evolution* 97

200 Sharon, N. (2006) Carbohydrates as future anti-adhesion drugs for infectious diseases. *Biochimica Et Biophysica Acta-General Subjects* 1760 (4), 527-537

201 Konstantinovic, S. et al. (2002) Synthesis of C-7-C-16-alkyl glycosides: Part III - Synthesis of alkyl D-galactopyranosides in the presence of tin(IV) chloride as a Lewis acid catalyst. *Indian Journal of Chemistry Section B-Organic Chemistry Including Medicinal Chemistry* 41 (3), 598-603

202 Oscarson, S. and Tiden, A.K. (1993) Synthesis of the octyl and tetradecyl glycosides of 3,6-di-O-alpha-deuterium-mannopyranosyl-alpha-deuterium-mannopyranose and of 3,4-di-O-alpha-deuterium-mannopyranosyl-alpha-deuterium-mannopyranose - A new way for 2,4-di-O-protection of mannopyranosides. *Carbohydrate Research* 247, 323-328

203 Margalit, A. et al. (2022) Global protein responses of multidrug resistance plasmid-containing Escherichia coli to ampicillin, cefotaxime, imipenem and ciprofloxacin. *Journal of Global Antimicrobial Resistance* 28, 90-96

204 Alderliesten, J.B. et al. (2020) Effect of donor-recipient relatedness on the plasmid conjugation frequency: a meta-analysis. *Bmc Microbiology* 20 (1)

205 Kang, B. et al. (2015) Carbohydrate-Based Nanocarriers Exhibiting Specific Cell Targeting with Minimum Influence from the Protein Corona. *Angewandte Chemie-International Edition* 54 (25), 7436-7440

206 Daniel, K.B. et al. (2016) Dual-responsive nanoparticles release cargo upon exposure to matrix metalloproteinase and reactive oxygen species. *Chemical Communications* 52 (10), 2126-2128

207 Molander, G.A. and Cadoret, F. (2011) Synthesis of the stereogenic triad of the halicyclamine A core. *Tetrahedron Letters* 52 (17), 2199-2202

208 Inthong, J. et al. (2020) Dinickel(II) complexes with pyridine-substituted bis(triazolylmethyl) amine ligands: Structures and magnetic properties. *Polyhedron* 191

209 Manzano, R. et al. (2010) Synthesis of both Enantiomers of Hemiesters by Enantioselective Methanolysis of Meso Cyclic Anhydrides Catalyzed by alpha-Amino Acid-Derived Chiral Thioureas. *Journal of Organic Chemistry* 75 (15), 5417-5420

210 Martin, H. et al. (2021) Multivalent Presentations of Glycomimetic Inhibitor of the Adhesion of Fungal Pathogen Candida albicans to Human Buccal Epithelial Cells. *Bioconjugate Chemistry* 32 (5), 971-982

211 Zhu, Z.Y. et al. (2016) Efficient synthesis and activity of beneficial intestinal flora of two lactulose-derived oligosaccharides. *European Journal of Medicinal Chemistry* 114, 8-13

212 Chen, G.Y. et al. (2016) Synthesis and Properties of Alkyl beta-D-Galactopyranoside. *Journal of Surfactants and Detergents* 19 (6), 1095-1105

213 Kim, S. and Nagorny, P. (2022) Electrochemical Synthesis of Glycosyl Fluorides Using Sulfur(VI) Hexafluoride as the Fluorinating Agent. *Organic Letters* 24 (12), 2294-2298

214 Rintelmann, C.L. et al. (2019) Design and synthesis of multivalent alpha-1,2-trimannose-linked bioerodible microparticles for applications in immune response studies of Leishmania major infection. *Beilstein Journal of Organic Chemistry* 15, 623-632

215 Touaibia, M. et al. (2017) Sites for Dynamic Protein-Carbohydrate Interactions of O- and C-Linked Mannosides on the E. coli FimH Adhesin. *Molecules* 22 (7)

216 Doyle, L.M. et al. (2017) Stereoselective Epimerizations of Glycosyl Thiols. *Organic Letters* 19 (21), 5802-5805

217 Wang, D.L. et al. (2022) Enantioselective Synthesis of Planar-Chiral Macrocycles through Asymmetric Electrophilic Aromatic Amination. *Angewandte Chemie-International Edition* 61 (22)